IMPERIAL INSTITUTE

OF

AGRICULTURAL RESEARCH, PUSA

PROCEEDINGS

OF THE

ROYAL SOCIETY OF LONDON

SERIES A

CONTAINING PAPERS OF A MATHEMATICAL AND PHYSICAL CHARACTER.

VOL. CXXXVII

CONTENTS.

SERIES A. VOL. CXXXVII.

No. A831.—July 1, 1932.

v

The Lunar Diurnal Variation of Atmospheric Temperature at Batavia, 1866–1928.

By S. Chapman, F.R.S.

Introduction.

The existence of a lunar tide in the earth's atmosphere is now a well-established fact.* It is indicated by a lunar semidiurnal variation of barometric pressure, found at every station for which the necessary reductions have been made. Now a variation of pressure in a gas is in general accompanied by a variation of temperature. The amount of this variation depends on the rate at which heat can flow in the gas, from a region of compression to one of ·rarefaction, or from the earth or ocean to or from the gas. The maximum variation of temperature corresponds to adiabatic changes of pressure, while if the heat flow can be very rapid, the temperature variation may be reduced almost to zero, corresponding to isothermal changes of pressure.

I have shown† that the lunar tidal changes of pressure will be almost adiabatic so far as concerns heat flow *in the gas*, between regions of compression and of rarefaction. The long time available for equalisation of temperature, viz., a quarter of a lunar day, or about 6 hours, is in fact ineffective because of the long wave-length of the tide, the distance between the regions of highest or

---

* Sabine, 'Phil. Trans.,' vol. 137, p. 45 (1847); S. Chapman with E. Falshaw, M. Hardman, 'Quart. J. R. Met. Soc.,' vol. 44, p. 271 (1918); vol. 45, p. 113 (1919); vol. 48, p. 246 (1922); vol. 50, p. 99 (1924); vol. 57, p. 163 (1931), also 'Mem. R. Met. Soc.,' vol. 2, p. 153 (1928) and other papers not yet published; J. Bartels, 'Veröff. preuss. met. Inst.,' vol. 5, No. 9 (1927).

† 'Quart. J. R. Met. Soc.,' vol. 50, p. 165 (1924).

lowest pressure in any latitude being a quarter of the circumference of the circle of latitude. The temperature variation might be reduced below the adiabatic value if vertical flow of heat, between the air and the ground or ocean, is sufficiently rapid. This point will be discussed in another paper;[*] the conclusion reached is that the vertical flow of heat is unlikely to be important over the *land*. Hence a temperature variation approaching the adiabatic value is likely to be associated with the lunar atmospheric tide at a land station.

The amplitude of the tide predicted by *theory* depends greatly on whether the pressure changes are adiabatic, isothermal, or intermediate between these. Consequently it seemed to me desirable to put the matter to the direct test of observation, by determining the lunar diurnal variation of atmospheric temperature for some station at which a long series of hourly values of the air temperature are available.

The accomplishment of this task promised to be greatly facilitated by the kindness of the British Automatic Tabulating Machine Company. Early in 1930 the Company agreed that in the autumn of that year they would place a set of Hollerith punching, sorting and tabulating machines at the disposal of the Department of Mathematics and Mechanics in the Imperial College of Science and Technology, for use in teaching and research. Such machines are of particular value in dealing with the great masses of data that must be employed when the aim, as in the present case, is to determine a very small periodic variation of a quantity that is subject to much larger periodic and accidental changes.

Other things being equal, the station most likely to yield a satisfactory determination of the lunar diurnal variation of temperature is Batavia, in Java,

<p align="center">Latitude 6·2° S , Longitude 106·8° E.,</p>

where the tidal change of pressure has the greatest known amplitude. At this station the annual mean lunar semidiurnal change of pressure is given by

$$\delta p = 0 \cdot 064 \sin (2t + 65°), \text{ in millimetres of mercury,} \qquad (1)$$

where t denotes lunar time reckoned from local transit, at the rate of 360° per lunar day. This is the determination from the 40 years 1866–1905 made at the observatory. An independent determination made by myself, from the years 1866–1895, is

$$\delta p = 0 \cdot 062 \sin (2t + 68°), \qquad (2)$$

in close agreement with the former. No lunar diurnal component of other

---

* 'Mem. R. Met. Soc.' (in course of publication).

frequency can be detected, and this is in accordance with expectation from tidal theory.

The corresponding maximum (adiabatic) lunar diurnal variation of temperature at Batavia is given by the formula

$$\frac{\delta T}{T} = \frac{\gamma - 1}{\gamma} \frac{\delta p}{p}, \tag{3}$$

where δp and δT denote corresponding variations of the mean pressure p (759 mm.) and the (absolute) mean temperature T (299° C.), and γ denotes the ratio of the specific heats of air : $\gamma = 1 \cdot 40$ approximately. Hence the (adiabatic) lunar daily temperature variation is

$$\delta T = 0 \cdot 0072 \sin (2t + 65°), \text{ in degrees Centigrade}, \tag{4}$$

being purely semidiurnal, and in phase with the pressure variation.

The solar diurnal variations of pressure (in millimetres) and temperature (in degrees Centigrade) at Batavia are given by the harmonic formulæ[*]

$$0 \cdot 63 \sin (\theta + 25°) + 1 \cdot 00 \sin (2\theta + 160°)$$
$$+ 0 \cdot 04 \sin (3\theta + 22°) + 0 \cdot 01 \sin (4\theta + 97°) \tag{5}$$

$$2 \cdot 84 \sin (\theta + 232°) + 0 \cdot 85 \sin (2\theta + 70°)$$
$$+ 0 \cdot 23 \sin (3\theta + 331°) + 0 \cdot 16 \sin (4\theta + 120°). \tag{6}$$

The ratio of the amplitude of δT, given by (4), to that of the solar semidiurnal term in (6), is

$$0 \cdot 0085 \quad \text{or} \quad 1/118, \tag{7}$$

whereas the corresponding ratio for the pressure – from (1) and (5) —is

$$0 \cdot 064 \quad \text{or} \quad 1/16. \tag{8}$$

Since in both cases the solar semidiurnal variation is much larger than the lunar one, but of nearly equal period, its elimination constitutes one of the main difficulties in determining the lunar variation. It is clear from (7) and (8) that the difficulty in the case of δT is distinctly greater than for δp, *i.e.*, about eight times so far as this elimination is concerned. Nevertheless it seemed likely, on consideration, that if the tidal pressure-changes occur adiabatically, the temperature variation δT, then given by (4), should be determinable from the long series of hourly values of temperature available at

[*] These are derived from the 60-year mean diurnal inequalities given in Batavia *Observations*, vol. 48, pp. 76, 80.

Batavia. Plans were therefore prepared for the execution of this work, by methods appropriate to the Hollerith computing machines.

At this stage I discovered that my friend Professor J. Bartels, of the Förstliche Hochschule, Eberswalde, was already engaged on a similar reduction of part of the Batavia material, using different methods. After discussion we agreed that it was well that I should proceed independently with my plans, particularly since they were of larger scope, thanks to the availability of the Hollerith installation. In such investigations of small periodic phenomena, independent determinations by different methods are of decided value.

2 *Description of the Data.*

The hourly values of temperature tabulated in the volumes of Batavia Observations are eye-readings derived from the Batavia standard thermometer, Kew No 323, Fahrenheit scale. They refer to an epoch 2 minutes before the exact hour of local mean time. The readings are given to $0 \cdot 1°$ in Fahrenheit degrees from 1866–1908 inclusive, and in Centigrade degrees in and from 1909. No Sunday observations are available for the first 10 years, 1866–1875 ; these were the only missing values throughout the whole series. The observations are tabulated in rows, for each day, containing the values from 1 h. (1 a.m.) to 24 h. (midnight), and the printed daily means are the means of these 24 hourly values

The printed volumes are published for the period 1866–1926 ; the hourly data for the period 1927–1930 inclusive were very kindly supplied to me, on request, in manuscript form, by Dr. J. Boerema, Director of the Batavia Observatory. Part of these unpublished data, up to the end of 1928, were used in the main part of the present investigation, while the remainder are entered on Hollerith cards for the purpose of a future extension of the work at a later date.

3. *The Data Entered upon the Hollerith Cards.**

On the Hollerith cards numbers are recorded by punching holes in any desired column. As each hole is punched, the carriage holding the card is carried forward as in a typewriter. In each column there are 12 possible positions for the hole, the lower 10 being numbered 0 to 9, while the two upper ones are

called X and Y. In general only one hole is punched in one column, but sometimes it is convenient to double-punch a column, as in entering the day of the month (see below).

Here and in later sections of the paper only those details concerning the Hollerith cards, equipment and methods will be noted that are of special application to the present work, and particularly those which relate to the possible errors that must be guarded against.*

Since the lunar day extends over nearly 25 solar hours, 25 hourly values of T were tabulated for each day. As they were expressed by numbers each of three digits (to $0 \cdot 1°$) this involved 75 digits. Hollerith machines and cards of 80 columns are now made, but as the installation available to me was of the 45 column type, these 75 digits required the use of two cards for each day. On each card the last 39 columns were devoted to 13 hourly 3-digit values, 1 h. to 13 h. on one set of (plain) cards, and 13 h. to 25 h. (*i.e*, 1 h. of the next day) on a second set of (blue-edged) cards ; it was considered desirable to duplicate one hourly value (for 13 h) on the two cards for each day, for checking and other purposes.

The remaining (first) six columns on each card were used as follows :—

(1) The number of the year in its decade or group.

(2) The number of the month in the year 1 to 12, using the two upper rows on the cards as well as the lower 10 (10, 11, 12, in rows 0, X, Y).

(3) The day of the month ; the rows usually numbered X, Y, 0, 1, .., 9 were in this third column numbered 30, 20, 10, 1, . .., 9, and for days after the tenth in the month (other than the 20th and 30th) the card was double-punched, in one of the three upper, and one of the nine lower rows.

(4, 5) The civil time of upper lunar transit at *Greenwich*, on the given date, or rather in the period from 1 h. of that date to 1 h. of the next day ; they were taken to the nearest whole hour, from the Nautical Almanac. These numbers ranged from 1 to 25. They were entered in two columns on the cards.

(6) A number 1, 2, 3 or 4, for classification of the days according to the moon's distance from the earth The day of apogee, and the three days before and after, were included in group 1, and in group 3 those similarly related to perigee ; group 2 included the days after group 1 and before

group 3, when the moon was nearing the earth; group 4 similarly included those between perigee and apogee, when the moon was receding from the earth. In the later sections of this paper, the groups 1, 2, 3, 4 will be referred to as groups A, N, P, R (apogee, nearing, perigee, receding).

The entries in columns 1 to 6 were, of course, made on both cards for each day. In addition, on each card one or more holes were punched in rows X, Y as an index to the decade in which each day occurred. The index numbers were as follows :—

Decade	Column.	Row.	Decade.	Column	Row.
1860–69	7	X	1900–09	7, 8	XY
1870–79	7	Y	1910–19	7, 8	YY
1880–89	7, 8	XX	1920–29	7, 8, 9	XXX
1890–99	7, 8	YX	1930–39	7, 8, 9	YXX

On the Saturday cards for these earlier years, where no observation for 1 a.m. on Sunday was available, the value used in its stead was the midnight value for Saturday, plus the difference between the 1 a.m. value on Saturday and the 12 p.m value on Friday.

The last hourly value on the last card for the year 1908 was the value, converted into Fahrenheit, for 1 a.m. January 1, 1909, which as printed was in Centigrade degrees.

4. *Verification of the Entries on the Cards.*

After the cards had been punched by one operator, the entries for the index number, year and month were checked by " needling " (*i.e.*, passing a needle through the pack of cards for each decade, year or month), and the rest of the entries were verified by a second operator using a verifying punch. Even this, however, did not preclude the possibility of errors, particularly errors of double punching, which had to be found by other methods, to be described elsewhere.

In the subsequent work it was necessary to form sums of the hourly data for various groups of days, chosen according to the values of the data entered in columns 1 to 6. For any such group G, the hourly sums were usually 5 or 6 figure numbers. The available adding machine was one possessing three banks of nine adding wheels, and two of six adding wheels (together with other wheels for adding shillings and pence, which were of no use for the present purpose); hence 5 hourly " fields " of three columns each could be added up

at the same time, and each set of cards, containing 13 hourly fields was put through the machine three times; the 25 hourly fields for each day, on the plain and blue-edged cards, thus required to be passed through the tabulator six times in each process of summation. This yielded 30 sets of sums, five being in duplicate ; the latter were of value in checking the working of the machine.

Each single month (m) yielded a set of 25 hourly sums m_s, one for each hour s. The cards were again passed through the machine, to form a set of hourly sums Y_s for each year Y. These values were divided by the number of days (n_y) in the year, giving annual *mean hourly values*, which were compared with the printed annual mean hourly values given (to $0 \cdot 01°$) in the Batavia volumes for each year. The occasional discrepancies found were further investigated, by forming the *monthly* mean hourly values, from the sums m_s, for the hours in question, and comparing these means with the printed means for each month. The errors were thus tracked down, sometimes to double-punching on the cards, sometimes to a temporary fault in the adding mechanism, and sometimes to errors in the printed means.

5. *The Classification and Summing of the Cards.*

The cards were throughout kept in six separate decade (D) groups, each of 10 years, except the first, which contained 13 years. The groups were therefore as follows :—

1866–78		13 years	$=$	4227	days
79–88	.	10 ,,	$=$	3653	,,
89–98		10 ,,	$=$	3652	,,
99–08		10 ,,	$=$	3652	,,
1909–18	. . .	10 ,,	$=$	3652	,,
19–28	.	10 ,,	$=$	3653	,,
Total	.	63 ,,	$=$	22489	

This choice was made so that the change from Fahrenheit to Centigrade values for the hourly readings, at the end of 1908, should coincide with the break between decades. The first group thus had to include 13 years, but owing to the absence of Sunday data during the first 10 years the number of days in " decade " 1 was equivalent only to about $11\frac{1}{2}$ complete years.

The following operations were then performed on each decade (D) set of cards :—

(a) The cards were sorted " on " columns 4, 5, so as to group together all the cards relating to days of the same transit-time t. These 25 Dt groups of cards were then summed, controlling on column t, giving 25 sets each of 25 Dt_s sums, for the 25 solar hours s.

(b) The cards were then re-sorted " on " column 2, for the month, and the 12 DM sets of cards thus obtained were combined into three seasonal sets (DS), called DJ, DE or DD, for groups of months as follow :—

J $=$ May, June, July, August.

E $=$ March, April, September, Octobe1.

D $=$ November, December, January, February.

The pack of DS sets, in order, was then sorted according to the lunar distance d, giving 12 DSd sets for the decades, and these again were sorted according to the transit time t, giving 300 DSdt sets of cards, containing about 12 cards each. Hourly sums DSdt_s were formed for each group, controlling on column t.

(c) Another summation was made without taking account of the subdivision into t groups, by controlling on column d, thus giving 12 sets of DSd_s hourly sums. By ordinary addition these were combined to give three seasonal sets of DS$_s$ hourly sums, and one set D$_s$ for the whole decade.

It was desired to obtain mean hourly sums according to solar and lunar time for the following groups of the data : (a) for each D group, (b) for each DS group (three for each D). It was desired also to have sums according to *lunar* time (only) for each Dd group (four for each D). Thus solar sums were required for 6 (D) $\times$ (1 $+$ 3) or 24 groups, and lunar sums for 6 $\times$ (1 $+$ 3 $+$ 4) $=$ 48 groups.

The solar series D$_s$ and DS$_s$ were obtained by operation (c). To obtain the lunar sums, however, a more elaborate process was necessary, because the tabulating machine can add numbers from different cards only if these are in the same columns, whereas in different t groups of cards the lunar hours occur at different solar times, and therefore in different columns.

6. *The Formation of the Lunar Sums.*

On the cards on which the lunar transit time t is 1, the hourly entries for solar time s refer to lunar hour $s - 1$; likewise on the group of cards for

transit time t, the solar hour s corresponds to the lunar hour $l = s - t$. It is desired to combine the sums Gt_s from the 25 sets (Gt) of cards in any group G^* of data (ordered according to the value of t) so that the sums corresponding to the same lunar hours shall be brought together. Thus from each set t we wish to take the solar hourly sum $s = t + l$, where l in turn will be given the values 0 to 24. The equation $s = t + l$ is here to be regarded as a congruence with modulus 25, the lunar sums (G_l) being supposed periodic in 25 hours.

This method of summation corresponds to forward-sloping summation effected upon a cylinder on which, in 25 columns ($s = 1$ to $s = 25$), surrounding the cylinder and lying along the generators, the Gt_s sums are entered in 25 rows.

The actual method employed was a slight modification of one suggested to me by Dr. Comrie.

As a preliminary, 25 strips of paper were prepared (actually by printing on the Hollerith tabulator) so that the entries should have the same vertical spacing as the series of Gt_s sums formed from the cards These strips were headed $s = 1$, or $s = 2$, and so on, up to 25. Below were printed 25 numbers l_t^s as follows :—

$s =$	1	2	. . . .	. .	25
$l_t^s =$	1	2			25
	25	1			24
	24	25			23
	2	3			1

Thus

$$l_t^s = s + 1 - t \pmod{25}, \qquad (9)$$

for $t = 1, 2, \ldots, 25$ in order, so that the lunar hour l in the series Gt_s corresponds to the solar hours given by

$$s = l_t^s - 1. \qquad (10)$$

Strip s is then pinned alongside the sth column of the 25 series of sums Gt_s for $t = 1$ to $t = 25$, and the 25 columns of sums are pinned together to form a single column of 625 rows, with the 625 l_t^s numbers against the 625 sums Gt_s. These sums were in general 5-figure numbers (6-figure in the case when $G = D$). Actually the 625 sums Gt_s for eight groups G were placed alongside one another,

---

* Here G is used to represent any group, whether D, DS, DSd, or otherwise.

in eight long columns, with the strips s to the left of all.   An index number was assigned to the set of eight groups G.*

A set of 625 Hollerith cards was then punched with the index number in column 1, the number s in columns 2, 3, the number l_t^s in columns 4, 5, and the eight 5-figure numbers Gt_s in the remaining 40 columns.   Thus each of the 625 cards contains the data on one row of the long 625-row column formed as just described.

In this manner the sums Gt_s for the 12 DSdt sets and 1 Dt set, for each of the six decade groups, were entered on (several) sets of 625 cards ; these sets may be called l_t^s sets

After punching, these cards were placed in the tabulator, controlling on the numbers s (control on column 3 being sufficient) ; the numbers s and l_t^s were listed, and the columns l_t^s and the numbers Gt_s were added.   The sums Σl_t^s for each s-group should equal 325, and this provided one check on the punching of columns 4 and 5.   The sums for the later sets of five columns represented G_s, and were checked against the G_s sums (where $G = D$ or $G = DSd$) already formed (§ 6, c).   Any discrepancies indicate errors in the punching of the Gt_s values, and the 25 sums Gt_s ($t = 1$ to 25) for any hourly column s involving an error were then examined.   The number l_t^s corresponding to the wrongly punched card was noted so that the corresponding correction could afterwards be applied to that l total.

Each l_t^s pack was then sorted according to the number l_t^s, and tabulated, controlling on column 5, thus producing lunar hourly totals G_l.   The 12 sets of DSd_l sums were next combined into four Dd_l sets and 3 DS$_l$ sets.   The accuracy of the additions and tabulations was checked by the final agreement of $\underset{d}{\Sigma}$Dd_l, ΣDS$_l$, and D$_l$ (for $l = 1, 2, ..., 25$).

7. The Harmonic Analysis.

The various sequences G_s, G_l, each consisting of 25 solar or lunar hourly sums, were then harmonically analysed, to determine the second harmonic (only).   The corresponding sequences of numbers of cards (n_{Gt}) for each value of t in each G set, as printed during the formation of the G_s totals (or as found by combination of the n_{DSdt} values, into n_{Dst} and n_{Ddt}) were also analysed in like manner ; this was for the purpose of eliminating the effect of residual solar diurnal variation from the second harmonic of the G_l sequences, according

* For example, one set of eight groups was DJ1, DJ2, DJ3, DJ4, DE1, ..., DE4.

to the method given (in principle, though not in detail for the present mode of tabulation) in a recent paper.*

Thus, let

$$a_{Gl} = \sum_{t=1}^{25} G_{lt} \cos\{2(t-1)\pi/25\}, \qquad b_{Gl} = \sum_{t=1}^{25} G_{lt} \sin\{2(t-1)\pi/25\}, \quad (11)$$

$$a_{Gs} = \sum_{t=1}^{25} G_{st} \cos\{2(t-1)\pi/25\}, \qquad b_{Gs} = \sum_{t=1}^{25} G_{st} \sin\{2(t-1)\pi/25\}, \quad (12)$$

$$a_{Gn} = \sum_{t=1}^{25} n_{Gt} \cos\{2(t-1)\pi/25\}, \qquad b_{Gn} = \sum_{t=1}^{25} n_{Gt} \sin\{2(t-1)\pi/25\}, \quad (13)$$

and

$$N_G = \sum_{t=1}^{25} n_{Gt}. \tag{14}$$

Then the determination of the lunar semidiurnal variation of temperature afforded by group G, corrected for residual solar diurnal variation, and expressed in the form

$$\left. \begin{aligned} \delta T &= L \sin(2\tau + \lambda') \\ &= L'_a \sin 2\tau + L'_b \cos 2\tau, \end{aligned} \right\}, \tag{15}$$

(where τ denotes lunar time measured in angle at the rate 2π per lunar day) is given, apart from certain small phase corrections, by

$$L'_a = \frac{2}{25 N_G} [b_{Gl} - b_{Gs} a_{Gn} + a_{Gs} b_{Gn}], \tag{16}$$

$$L'_b = \frac{2}{25 N_G} [a_{Gl} - b_{Gs} b_{Gn} - a_{Gs} a_{Gn}] \tag{17}$$

The true phase λ is equal to λ' plus certain corrections, of which the main is to allow for the use of Greenwich instead of Batavian transit times t. This correction is $-2L°/29$, where L denotes the (easterly) longitude of Batavia; since $L° = 106·8°$, the correction is $-7·4°$. In addition, the fact that the hourly readings of temperature were made 2 minutes before the exact local hour necessitates a further correction $+1·0°$.

The amplitudes L, L'_a, L'_G, were converted into Centigrade degrees where necessary.

8. *The Main Results.*

The central result of this work is the annual mean value of the lunar semi-

---

* Chapman, 'Z. Geophysik,' vol. 6, p. 396 (1930).

diurnal variation of temperature at Batavia, determined from the whole 63 years or 22,489 days.   This is

$$0 \cdot 0086 \sin (2t + 67°) ° C., \qquad (18)$$

which agrees well in phase, and moderately well in amplitude, with (4), derived from the observed tidal change of pressure, on the adiabatic assumption. The " observed " value of δT is, in fact, even greater than the value calculated from δp ; the discrepancy is, as will be seen later, in § 9, within the limits of the probable error of the present determination of δT.

The determinations of the annual mean value of δT from the separate decade-groups of years are as follows.   The significance of the columns headed ΔL will be explained in § 9.

Table III.

	Decade Group	Number of days	Amplitude L, unit 10^{-4} ° C.	Phase.	ΔL
				°	
a	1866–1878	4227	119	97	62
b	1879–1888	3653	164	32	103
c	1889–1898	3652	59	33	55
d	1899–1908	3652	88	98	49
e	1909 1918	3652	64	77	25
f	1919–1928	3653	88	68	3
M	All	22489	86	67	49

Here the phase angles have an extreme range of 66°, and the amplitudes of $105 \cdot 10^{-4}$ ° C.   These results show that the probable error of a 10-year determination of δT is a considerable fraction of δT itself, and suggest, as will later be proved, that the 63-year mean is liable to error sufficiently to permit the difference between (18) and (4) to be regarded as merely accidental.

This being the case, the seasonal mean results, and the mean results for the lunar-distance groups of data (A, N, P, R, cf. § 3 (6)), being derived from still smaller amounts of material, may be expected to be scattered rather widely about the mean results.   The determinations are as follows, the amplitudes being expressed in terms of 10^{-4} ° C. as unit.

In deriving the results of Table V the solar diurnal variation, which was eliminated in the final stages of the analysis (cf. § 7), was separately removed from each seasonal section of the distance groups, before forming the final result for the group ; that is, the seasonal change in the solar diurnal variation was allowed for in the elimination.

Table IV.—Seasonal Mean Results for δT; Unit 10^{-4} ° C.

Decade group		J — May–August			E — March, April, September, October.			D — November-February.		
		No of days	L	l	No of days	L	l	No of days	L	l	ΔL.

Decade group		No of days	L	l	ΔL.	No of days	L	l	ΔL	No of days	L	l	ΔL.
a	1866–1878	1423	116	101	76	1392	148	109	67	1412	104	75	41
b	1879–1888	1230	225	40	150	1220	172	29	148	1203	93	19	52
c	1889–1898	1230	50	42	34	1220	184	118	112	1202	227	334	220
d	1899–1908	1230	108	159	150	1220	58	34	75	1202	192	87	130
e	1909–1918	1230	65	22	51	1220	184	94	82	1202	23	259	105
f	1919–1928	1230	138	32	76	1220	39	236	130	1203	207	89	148
M	Mean	7573	84	60	89	7492	97	88	102	7424	87	52	116

The significance of these results will be discussed after the probable errors of the determination have been considered.

9. *The Probable Errors.*

The results given in § 8 may with advantage be represented graphically, by vectors drawn from some origin, of length L (on some assigned scale), and making the angle $l°$ with a chosen initial line. If a suitable time-scale be marked round the circumference of the figure, the time at which the harmonic term $L \sin (2t + l°)$ attains its maximum value is also indicated by the diagram, and for this reason I have called such a diagram an harmonic dial; a different time-scale is needed for each harmonic term, according to its frequency. For semidiurnal terms the angular time-scale is the same as in an ordinary clock-face, which is traversed twice daily.

It is not necessary to draw the vectors themselves, which are sufficiently indicated by their end-points.

Fig. 1 shows the results of Table III. The vector points for the six decade-groups *a–f* are widely scattered round the mean point M. The scale is indicated by the arrow along the direction of the initial line; the arrow is of length representing 0·01° C. The distances of the group-points from M will be denoted by ΔL, and are given in the last column of Table III in the same units as for L itself; the mean ΔL, 49, is over half the mean value of L itself. The values of ΔL afford a rough determination of the probable error of the determination of δT from the decades *a* to *f*, and from the whole period. If we ignore the fact that group (*a*) has 1·16 times as many days as groups *b* to *f*,

Table   Val   δT for Groups   Days   ffe   na   §3(6   Unit 10^{-4} °C.

Decade.	No. of days	L	l	ΔL	No of days.	L	l	ΔL	No. of days	L	l	ΔL	No. of days.	L	l	ΔL
			°				°				°				°	
a 1866–1878	1074	140	126	54	1042	44	105	75	1072	188	96	120	1039	134	63	42
b 1879–1888	928	205	33	224	903	84	19	60	927	170	29	95	895	193	40	87
c 1889–1898	929	66	69	101	895	40	16	29	928	229	2	187	900	109	154	176
d 1899–1908	926	74	152	111	908	128	101	159	931	87	75	42	887	103	83	66
e 1909–1918	931	242	108	95	895	192	289	169	924	203	108	148	902	138	358	103
f 1919–1928	924	364	123	228	903	161	307	130	931	84	53	42	895	207	23	116
M All	5712	147	104	135	5546	42	333	104	5713	122	61	106	5518	109	47	98

N

and treat all as of equal weight, the probable error of δT determined from any one group is $0 \cdot 94$ times the mean value of ΔL, *i.e.*, $0 \cdot 0047°$ C. ; the probable error of the mean determination M is $0 \cdot 0047/\sqrt{6}$ or $0 \cdot 0019°$ C. These probable errors are, however, rather rough, being found from only six independent
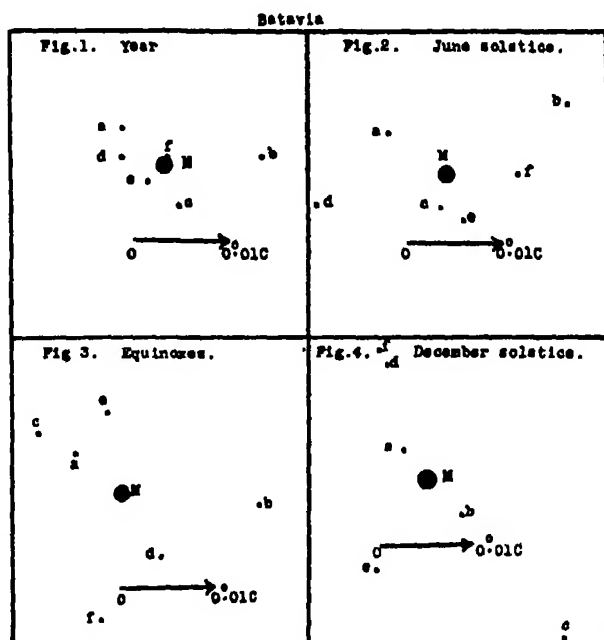
Figs 1–4.

determinations. We shall see that the probable error is likely to be rather larger than the above.

The results contained in Tables IV and V are likewise illustrated in figs. 2–4, and 5, on the same scale as in fig. 1. The scatter of the points is notably greater than in fig. 1, as is natural in view of the greater subdivision of the material. The values of ΔL measured from the mean of each set are given in Tables IV and V. The corresponding probable errors for each of the decade-season or decade-distance determinations of δT are given, in terms of 10^{-4} ° C. as unit, in the first line of the following table · —

	E	D		N	P	R
Probable error for group	84	96	109	127	98	100	92
Decade probable error	48	55	63	63	49	50	46

The second line gives the group probable error divided by $\sqrt{3}$, or by 2, and represents the probable error inferred from these group determinations for respectively 3 and 4 times the amount of material, equal to the number of days in a whole decade. The results are fairly accordant with, though on the whole larger than, the determination made from fig. 1, *i.e.*, 47 units.

There is no reason to anticipate any real difference of probable error between the four A, N, P, R sets of determinations of δT, but the differences between the probable errors for the three seasonal sets of determinations of δT may be real.

In order to investigate the probable errors more closely, the 25 sequences Dt_s (for $t = 1, 2, \ldots, 25$) of hourly sums, for the decade 1909–18, were separately analysed for the semidiurnal component. The semidiurnal component thus obtained is mainly the solar semidiurnal component, though the analysis was made as if the period was 25 hours. The results give S_t and σ_t in the formula $S_t \sin(2\theta + \sigma_t)$, where θ denotes time reckoned from 1 a.m. at the rate 2π per 25 hours. The values of S_t and σ_t for each value of t are represented by the 25 points (P_t) in fig. 6 ; the origin is far outside the figure, in the direction indicated by the downward arrow drawn from the mean (M) of the 25 points ; the scale of the figure is two-fifths of that of figs. 1–5. The radii from M to the 25 points illustrate the " scatter " or variability of the solar semidiurnal variation, even when determined from as many as 145 days , but since these groups of days D_t are classified according to the lunar transit time, the scatter should not be wholly at random, but should be partly determined by the lunar semidiurnal variation.

The radii from M to the various points give, in fact, the semidiurnal component of the sums Dt_s after the mean solar semidiurnal variation has been removed from them. But in combining the Dt_s results according to lunar time, the phases of the vectors MP_t are altered ; the alteration is equivalent to turning the radius MP_t forward through the angle $4\pi(t-1)/25$. If the scatter in fig. 6 were solely due to the lunar influence, the radii MP'_t, when thus rotated, should coincide with one another. Fig. 7 shows their actual distribution , they are nearly at random, as in fig. 6, showing that the scatter there was mainly due to accidental error. But the centroid of the points P'_t is no longer at M, but at an adjacent point P, and the vector MP (after making certain small phase-corrections referred to in § 7) represents the part of the scatter that is not random, but due to lunar influence. Fig. 7 well shows how much the accidental variation in the semidiurnal temperature variation exceeds the component due to the lunar influence, and illustrates the difficulty

of averaging out these much larger accidental variations of T to obtain the very small lunar variation.

The true accidental part of the semidiurnal component of the variation of T is not the vector MP_t of fig. 6, which includes the lunar variation, but the vector PP'_t of fig. 7. The mean magnitude of PP'_t in fig. 7 is $416 . 10^{-4} \,^{\circ}$C. ;
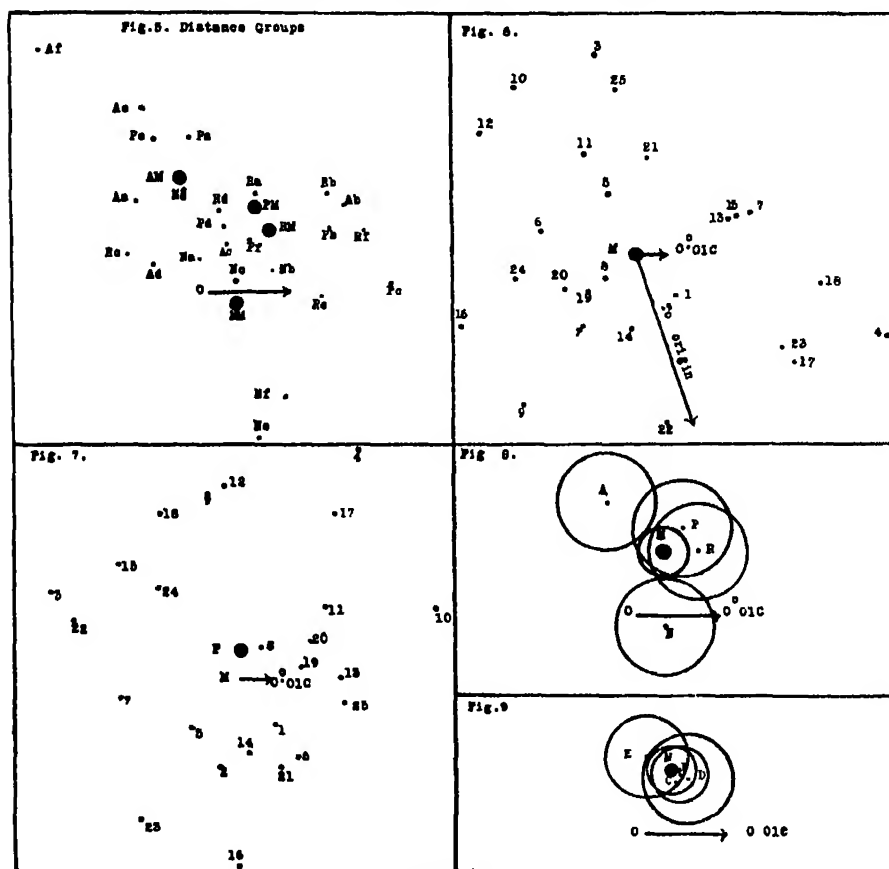
FIGS. 5-9.

treating the points P'_t as being determined from equal numbers of days (which is sufficiently near the truth for our present purpose), the probable error of a single point P'_t in fig. 7 is 390 units, and of the mean point P is $390/\sqrt{25}$ or 78 units. This is distinctly larger than the estimates of the probable error of the mean δT for a decade, already derived from figs. 1-5, which range from 46 to 60 units.

Similar scatter-diagrams were constructed by analyses of the separate

transit-time sequence Gt_s for the various sub-groups G (*i.e.*, J, E, D and A, N, P, R) of the decade 1909–18. The corresponding mean values of ΔL were found to be, in order, 460, 690, 750, 800, 820, 670, and 790 units. The corresponding determinations of the probable errors for each group as a whole, and for an extended group equal in length to a decade, are as follows :—

		D			N		
Probable error for group	86	130	141	150	154	126	149
Decade probable error	50	75	81	75	77	63	74

The mean of the last four is 73 units, and this value will be adopted as the best estimate of the probable error of δT derived from 3650 days (1 decade) drawn nearly equally from all seasons. Likewise the estimates 50, 75 and 81 will be adopted for the seasonal groups J, E, D.

The probable errors of δT for the whole period, and for the whole of the separate seasons J, E, D, and the distance groups A, N, P, R, will therefore be 73/$\sqrt{6}$, (50, 75, 81) $\times$ $\sqrt{3}/\sqrt{6}$, and 73 ($\sqrt{4}/\sqrt{6}$), *i.e.*,

Whole		J	E	D		A, N, P, R
30		35	53	57		60

The corresponding probable error of the determination of δT from a single day is 73$\sqrt{(3650)}$. 10^{-4} or $0.44°$ C.

In figs. 8, 9 the determinations of δT for the whole, and for these sub-groups of the material, are indicated by points, round each of which is drawn a circle of which the radius represents the estimated probable error on the same scale. The calculated value of δT given by (4), on the assumption of adiabatic lunar tidal changes of pressure, is also shown, in fig. 9, by the vector-point C.

It will be seen that C lies within the error-circle round M, indicating that the difference between the points M and C is within the limits of probable error of the determination.

Inspection of figs. 8, 9 suggests that no reliable determination of the change in δT with the changing lunar distance, or even with the changing season, has been achieved ; but the goal is more nearly approached in the latter than in the former case. The mean value of δT for the whole period, however, is fairly well determined, and implies that the lunar tidal changes of

pressure at Batavia take place nearly adiabatically; the present work does not make it possible to exclude a deviation of (say) 20 per cent. from the adiabatic value.

10. *Possible Improvements in the Method of Calculation.*

Two additional calculations were made in order to throw light on possible improvements in future investigations of the present kind The object in one case (*a*) was to ascertain how the results would be affected if the last figure of the printed hourly data, giving the temperature to $0 \cdot 1°$, had been omitted ; in the other case (*b*) the object was to determine the effect of using only alternate hourly values, instead of every hourly value.   In case (*a*) the labour of punching and verifying the cards would have been reduced by one-third, and in case (*b*) by nearly one-half. The combined reduction would be by two-thirds. Much of the later work would also have been considerably reduced, though not to the same extent.

The decade 1909–18 was chosen as the material for the discussion of case (*a*).   Values of δT, corrected for the solar diurnal variation, were obtained for the whole decade and for the groups J, E, D and A, N, P, R, ignoring the decimals of a degree in all the hourly readings. The elimination of the solar diurnal variation was made as before, but this was practically unaffected by the omission of the decimals of degrees   The results for δT are shown in fig. 11, by the points M′, J′, ..., and the differences between them and the corresponding results for this decade, using the decimals of degrees, are shown by the lines joining M′, J′, ., and M, J, ..., respectively. The differences appear to be accidental , if this be so, the corresponding addition to the probable error can easily be estimated. In units 10^{-4} ° C. the magnitudes of the differences are as follows .—

J — J′	E — E′	D — D′	A — A′	N — N′	P — P′	R — R′	M — M′
58	50	74	24	70	24	45	14

The mean of the differences for the seven sub-groups is 49, treating them all as of equal weight, which is roughly true. The corresponding probable error for the decade is $0 \cdot 94 \times 49 \div \sqrt{3}$, or 27. This is larger than M — M′, but agreement was, of course, not to be expected. The accidental error due to the omission of decimals of degrees, added to the errors otherwise involved, raises the decade probable error from 73 (as previously estimated) to $\sqrt{(73^2 + 27^2)}$ or 78. These estimates are naturally rough, but it would seem that the gain of accuracy involved in taking account of the decimals of degrees is hardly

worth the labour involved in their inclusion. This, however, is mainly because the other sources of error are so potent in the present work; in similar investigations where the remaining accidental errors were distinctly smaller, the omission of the decimals might not be advisable.

Fig.10.

Fig.11.
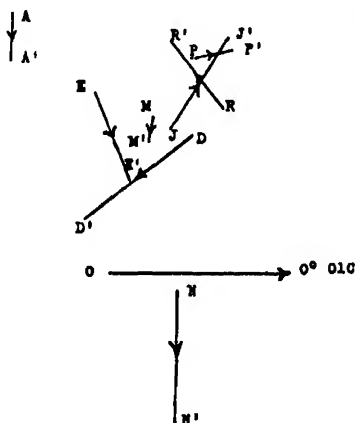
FIGS. 10–11

Case (*b*) was considered by using the D_l sequences of sums (§ 6) for each of the first five decades. Let $a_1, a_2, \ldots, a_{25}$ denote the members of any such sequence If alternate hours had been used, and if these had been the odd hours of lunar time (though this would be a little troublesome to arrange, in practice), we should have obtained the sequence $a_1, a_3, \ldots, a_{25}$; likewise if the even lunar hours had been used, the result would have been $a_2, a_4, \ldots, a_{24}$. Suppose we had interpolated in each case, to obtain values for the missing hours; the results would have been

$$a_1, \quad \tfrac{1}{2}(a_1 + a_3), \quad a_3, \quad \tfrac{1}{2}(a_3 + a_5), \quad \quad , \quad a_{25},$$

and

$$\tfrac{1}{2}(a_{25} + a_2), \quad a_2, \quad \tfrac{1}{2}(a_2 + a_4), \quad . \ , \quad a_{24}, \quad \tfrac{1}{2}(a_{24} + a_1),$$

there being some doubt as to the extrapolation at the two ends of the latter (even) sequence. By subtracting one sequence from the other, we get

$$a_1 - \tfrac{1}{2}(a_{25} + a_2), \quad \tfrac{1}{2}(a_1 + a_3) - a_2, \quad a_3 - \tfrac{1}{2}(a_2 + a_4), \quad \ldots,$$

which is analysed for the second harmonic ; the result is taken to represent twice the difference between δT as actually determined, and as would have been determined if only the odd lunar hours had been considered ; if the even hours only had been taken, the difference would have the opposite sign.

The results are represented graphically in fig. 10 ; the lines are centred at the points representing the determinations given in Table III, and their lengths and directions represent the difference between δT as determined from the odd and even hours respectively. The lengths are as follows, in terms of 10^{-4} ° C. as unit :—

Decade ...	.	a	b	c	d	e	Mean (1866–1918)
Length .	.	30	12	5	34	28	7

The corresponding mean additional probable error for one decade, due to using alternate hours, is therefore about $10 \cdot 10^{-4}$ ° C., slightly less than in case (*b*). It raises the decade probable error from 73 to 74, if the decimals of degrees are omitted also, the total probable error for a decade-mean is raised to 79. The corresponding rise in the probable error for the mean result from the whole period would be from 30 to 32.

This rise is not a serious one, and it would therefore seem that in the present investigation the computing work could have been advantageously reduced by using every second hourly value instead of every value, and by ignoring the decimals of a degree. In any future work of this kind, relating to the lunar variation of atmospheric temperature, careful consideration should be given to these possible improvements in the work. Whether they are advisable or not depends upon the degree of variability of the second harmonic derived from a single day's data, or, what is equivalent, it depends upon the decade probable error as determined in § 9. At a station where this was much less than that for Batavia, it might be best to use the full data, as has been done in the present work. It must be remembered, however, that the temperature variation to be determined is likely to be less at any other station than it is at Batavia, where the lunar atmospheric tide is unusually great ; hence it can only be determined with great difficulty, and from a long series of data, *unless* the decade probable error, as determined in § 9, is much less than that for Batavia. The first thing to be done, therefore, in considering an investiga-

tion at any further station would be to examine the variability of the solar diurnal variation derived from individual days, and to compare the decade probable error inferred from this with the expected magnitude of the lunar diurnal variation of temperature, and with the additional probable error due to contractions (a) and (b); the decision whether to adopt the latter could then be made, and would depend on the number of years' data available, and on the accuracy desired in the final result. If, for example, it were expected that the tidal pressure changes at the station would be nearly isothermal, the expected temperature variation would be much less than the adiabatic value, and the allowable probable error in the result would be correspondingly reduced.

11. *Determination of the Lunar Temperature Variation from Rainless Days only.*

A further possible improvement in method would be by the use of selected days of temperature variability smaller than the average (just as, in determining the lunar atmospheric tide at Greenwich, I used only the days of pressure range less than 0·1 inch). At my request, Mr. J. C. P. Miller investigated the influence of various factors—sunshine, cloud, rainfall—upon the course of the daily temperature variation at Batavia. It appeared that the most important factor was the rainfall, particularly since its effect depended so greatly upon the time at which it occurred. Rain at night was relatively unimportant compared with rain by day, which rapidly lowered the temperature to about the night value. If the rain occurred before noon, the maximum temperature would be that just beforehand, the normal increase towards noon being suppressed. Thus on rainless days the solar diurnal range of temperature is greater than the average, but it is more constant from day to day. It was therefore hoped that a determination of the lunar diurnal variation of temperature from these days would give a result having a smaller probable error than that derived from all days, the reduced variability of the daily temperature variation more than compensating for the reduction in the number of days.

The Batavia volumes fortunately give detailed tables of rainfall, and from these it was easy to pick out the rainless days. The corresponding Hollerith cards were picked out by hand, and dealt with as in the previous investigation of all days, except that, on account of the reduced amount of material, the whole period was divided into two sub-periods only, 1866–1898, and 1899–1926. Each of these was divided up into the three seasons, but no subdivision depending on the moon's distance was made. The work on the period

1899–1926 was initially done in two parts, for the years up to and after 1908, on account of the change in unit from Fahrenheit to Centigrade.

The results obtained are as follows :—

Batavia.

Period.	Season.	No of days.	L. unit 10^{-4} ° C.	$l°$
				°
1866–1898	J	2944	83	83
	E	2303	74	69
	D	1402	204	72
	Total	6649	105	75
1899–1926	J	2429	126	91
	E	1911	133	69
	D	1104	204	70
	Total	5444	142	78
1866–1926	J	5373	102	87
	E	4214	101	69
	D	2506	204	72
	Total	12093	121	77

The above table shows that the number of rainless days was slightly more than 50 per cent. of all days ; the proportion was much greater in the J season (May to August) than in the D season (November to February). The values of L found from the various sub-groups of rainless days are scattered somewhat widely about their mean, which itself is distinctly larger (121) than the mean L found from all days (86). The phases l for the sub-groups of rainless days show a relatively small scatter, while their mean, 77°, is somewhat larger than that (67°) from all days.

The probable errors of the various determinations in the above table were determined from the inequalities for the separate transit-time sets of data in each group. It was thus found that the mean probable error in the semi-diurnal component of the temperature variation on rainless days was 0·32° C., as against 0·44° C. from all days (§ 9). The reduction for rainless days is less than was anticipated, and barely compensates for the reduction in the number of days used. The probable error of the mean determination from all the rain-less days used is $29 . 10^{-4}$ ° C., practically identical with that found in § 9 for the mean result for all days. The vector difference between the two deter-minations has a magnitude $45 \ 10^{-4}$ ° C., or $1\frac{1}{2}$ times the estimated probable error of either result ; the probable error circles round each mean result thus

intersect, but each mean is outside the probable error circle surrounding the other. It would, however, in my opinion, be unsafe to conclude on the present evidence that there is a real difference between the lunar diurnal temperature variation on all days and on rainless days. The work on the rainless days should be regarded as affording further confirmation of the approximate magnitude and phase of the lunar temperature variation previously found from all days, without insisting on the difference between the two determinations. It was, however, somewhat disappointing that the use of rainless days only did not result in a reduction of the final probable error. This work suggests that there is little hope of a materially improved determination of L and *l* from Batavia (and *a fortiori* from any other observatory) within the next 50 years, the accumulation of a much longer series of data being the primary condition.

The Homogeneous Catalysis of Gaseous Reactions.—The Catalytic Decomposition of Nitrous Oxide by Halogens.

By F. F. Musgrave and C. N. Hinshelwood, F.R S.

It was recently discovered[*] that iodine exerts a pronounced catalytic influence on the thermal decomposition of nitrous oxide. Bromine and chlorine have now been found to have similar effects.

The reactions are of the first order with respect to the nitrous oxide and there appears to be little doubt that decomposition into a nitrogen molecule and an oxygen atom occurs under the influence of the halogen. The balance of evidence is in favour of the hypothesis that the effective catalyst is the free halogen atom. Whether the oxygen atom from the nitrous oxide remains attached to the halogen for a finite time cannot be definitely stated.

The most remarkable thing about the reaction with iodine is that it attains a definite limiting rate as the concentration of the catalyst is increased—a type of behaviour of which examples suitable for quantitative study are not common. There are indications that a limiting rate may exist with the other halogens, but, if so, it is not so quickly reached as with iodine.

Kinetics of the Catalytic Reactions.

The method of experiment has been described in previous papers,[†] and the only detail to which reference need now be made is the method of introducing small quantities of iodine into the reaction vessel. This was done by allowing isopropyl iodide vapour to decompose in the vessel itself and then adding enough air to burn the hydrocarbons formed. This has the great advantage that no iodine comes into contact with the mercury of the manometer. Special experiments, to be referred to later, showed that none of the substances present had an influence even remotely comparable with that of the iodine.

The catalytic reaction yields nitrogen and oxygen, no appreciable quantity of nitric oxide being produced. It is of the first order with respect to the nitrous oxide, the time of half change, τ, being independent of the initial

[*] 'Proc. Roy. Soc.,' A, vol. 135, p. 23 (1932).

[†] *E.g.*, 'Proc. Roy. Soc.,' A, vol. 128, p. 75 (1930).

pressure of the gas, and the course of the reaction for a given initial pressure being expressible by the usual unimolecular equation. The results found with iodine are given in Tables I and II.

Table I.

Temperature 700° C. Iodine, 0·032 mm.			Temperature 700° C. Iodine, 1·4 mm.		
Time.	Amount changed	k (unimol.).	Time.	Amount changed.	k (unimol.).
seconds			seconds		
7	10	0 00521	12	25	0·0083
15	20	0·00508	17	35	0 0087
23	30	0 00524	22	45	0·0091
34	40	0·00496	29	55	0·0090
44	50	0·00508	37	65	0·0089
57	60	0 00503	47	75	0·0088
72	70	0 00502	73	95	0·0090
92	80	0 00490	∞	122	—
163	105	0 00500			
∞	124	—			

Table II.

Temperature 675° C.   Catalyst, 6 mm.

Initial pressure of nitrous oxide.	Time of half change, τ.
mm.	seconds
482	81
337	82
126	87
78	93

The reaction is homogeneous, τ being almost exactly the same in an unpacked silica bulb and in one packed with spheres of silica, the area/volume ratio of which was about 16 times greater.

Catalyst (mm)	τ, unpacked vessel.	τ, packed vessel.
0·84	43	40
23	25	29

The influence of the iodine concentration is shown in Tables III and IV.

The figures for the partial pressures of molecular and atomic iodine are calculated from the equation $2C_3H_7I = C_3H_6 + C_3H_8 + I_2$ and from the measurements of Bodenstein and Starck* on the dissociation of iodine, which

* 'Z. Elektrochem.,' vol. 16, p. 961 (1910).

Table III.

Temperature 700° C.   Initial pressure of nitrous oxide, 300–400 mm.

Total pressure of decomposed isopropyl iodide.	Partial pressure of iodine atoms.	Partial pressure of iodine molecules.	Half life.
mm.	mm.	mm.	seconds
0	—	—	1079
0·095	0 045	0 001	60
0 22	0 10	0·007	52
0·89	0 34	0·07	43
1·95	0 61	0·24	40
4·3	1·06	0 73	34
6·2	1 34	1·17	31
23	3 0	5 7	25

Table IV.

Temperature 650° C.

Total pressure of decomposed isopropyl iodide	Half life.
mm.	seconds
0	5600
0 49	262
2 7	211
4 7	168
23	137

by a small extrapolation give $2·07 \times 10^{-3}$ for p_I^2/p_{I_2} at 700° C., the unit being the atmosphere.   A slight inaccuracy is caused by the decomposition of the hydrocarbons, but this is of no importance and does not appreciably affect the relative values of p_I and p_{I_2}.   It will be seen that at the lower pressures of the catalyst the iodine is present predominantly in the form of atoms.   This at once raises the question whether the atom or the molecule is the effective agent.   The problem should be soluble in principle by studying the form of the curve relating τ and the concentration of the catalyst, but the results with iodine are not very well adapted to this purpose, because the concentrations at which measurements can be made conveniently are already in the region of saturation.   With chlorine and bromine the conditions are more favourable.

Two series of experiments were made with bromine : in the first free bromine was used, the mercury in the manometer being protected from attack by a buffer of 50 mm. air, while in the second series the bromine was produced in

the reaction vessel by decomposing propyl bromide, the hydrogen bromide formed being oxidised by air before the nitrous oxide was added. The similarity of the two sets of results shows that the action of the other substances present is negligible compared with that of the halogen. In fig. 2 all the results are plotted on one curve, taking the bromine pressure to be one-fifth of that of the total decomposition products of the propyl bromide.

Table V.

Temperature 722° C   Initial pressure of nitrous oxide, 280–310 mm.

Pressure of bromine	Partial pressure of bromine atoms	Half life
mm	mm	seconds
0	0	650
0 20	0 048	220
0 40	0 071	225
1 04	0 119	161
1 1	0 122	150
2 4	0 180	127
4 7	0 252	102
11	0 39	66
16	0 47	62
27	0 60	52

The partial pressures of bromine atoms are calculated by extrapolation of the data of Bodenstein,[*] K_p at 722° C being approximately 2×10^{-5} (atmospheres).

Table VI.

Temperature 722° C   Initial pressure of nitrous oxide, 300–310 mm.

Pressure of decomposed propyl bromide (before oxidation)	Half life
mm	seconds
0	650
0 5	327
3	222
6	178
11	133
15	119
33	97
50	104

With bromine, as with iodine, the reaction is of the first order. For example, with a constant bromine pressure of 2 mm. the half life values at 705° C. for

* ' Z. Elektrochem.,' vol. 22, p. 327 (1916).

34, 110, 261 and 433 mm. nitrous oxide were 226, 237, 275 and 230 seconds respectively.

Experiments were made with free chlorine, the manometer being protected as before by a buffer of about 50 mm. air.

Table VII.

Temperature 722° C. Initial pressure of nitrous oxide, 300 mm.

Pressure of chlorine.	Partial pressure of chlorine atoms.	Half life.
mm	mm	seconds
0	0	650
1·5	0 0114	435
3 2	0 0166	390
4·75	0 0203	309
7·1	0 0248	264
11 2	0 0311	216
18 9	0 0404	195
100	0 093	115

The partial pressures of atomic chlorine are calculated from the data of Wohl,[*] which by extrapolation to 722° C. give for K_p the value $1·15 \times 10^{-7}$ (atmospheres).

Table VIII

Temperature 680° C. Initial pressure of nitrous oxide, 200 mm.

Pressure of chlorine.	Half life.
mm.	seconds
0	2460
14	825
32	644
58	516
103	384
261	237

Discussion of the Results

With iodine the rate of reaction reaches a limiting value as the concentration of catalyst increases; the first impression given by an inspection of the Tables V to VIII is that similar limits exist with chlorine and bromine, but more careful consideration shows that the matter is not easy to decide.

Iodine exerts a marked influence under conditions where it is present

[*] ' Z. Elektrochem.,' vol. 30, p. 36 (1924).

predominantly in the atomic form. This suggests that the atom may be the effective catalyst. When the velocity constants of the various reactions ($k = \log_e 2/\tau$) are plotted against the actual concentrations of free atoms, the tendency to reach a limiting value is seen still to be clearly marked with iodine, but much less definite with bromine, though the curve is distinctly convex to the rate axis. With chlorine the maximum atomic concentration employed is still so small that there is little sign of departure from a straight line relation. Thus with chlorine and bromine it is hard to come to a definite conclusion about the existence of the limiting rate, though fig. 1 shows that there is no reason to believe that it might not be reached as with iodine, and indeed with bromine there are positive indications of this.

If the halogen molecule were assumed to be the catalyst, then the existence of the limiting rate would be beyond doubt since in fig. 1 we should have to
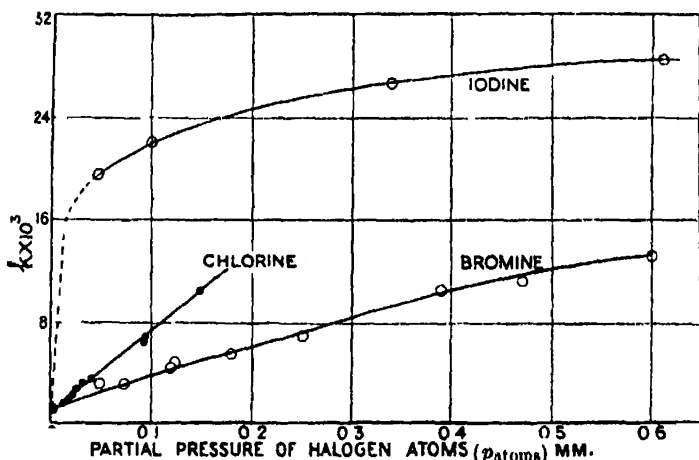
Fig. 1.—Catalysis of the Decomposition of Nitrous Oxide by Halogens. The results for iodine are corrected to a temperature of 722° to make them comparable with those for bromine and chlorine. The two points for the highest chlorine concentration are scaled up from a lower temperature.

plot the rates against the actual pressures of the chlorine and bromine instead of against what is virtually the square root of the pressure. All the curves would then bend round quite sharply.

Several kinds of mechanism may be postulated to explain the tendency of a homogeneous reaction to reach a limiting rate.

1. The catalyst may act in virtue of its ability to communicate the activation energy effectively to molecules which would only acquire it much more slowly in the absence of the catalyst. These decompose or react, not at the moment

of the activating collision, but after a finite interval of time during which they are exposed to the risk of deactivation. Molecules of the catalyst are themselves able to cause deactivation.

2. The molecules of the reacting gas may be activated independently of the catalyst, but require the co-operation of the catalyst before their final transformation can be completed. In the meantime they are exposed to deactivation by such influences as collisions with their own kind. As soon as thé concentration of the catalyst becomes high enough to ensure that all the activated molecules have a reasonable chance of meeting a catalyst molecule, before being deactivated, the rate of reaction begins to approach a limiting value.

3. The catalyst may activate the molecules of the reacting substance and remain temporarily associated with them in the form of a complex, which undergoes the completed decomposition after a certain lapse of time unless it has been previously resolved into its constituents again by further collisions with catalyst molecules.

4. There may be a chain reaction in which the catalyst plays the dual rôle of starting and stopping chains.

It is easily shown that mechanism 2 gives a reaction of the second order with respect to the nitrous oxide ; mechanisms 1 and 3 give first order reactions with velocity constants proportional to $b\,[\text{Catalyst}]/(1 + b'\,[\text{Catalyst}])$. The limiting rate given by mechanism 1 is the same for all catalysts (compare the influence of certain inert gases on quasi-unimolecular reactions), while that given by 3 varies with the catalyst. It is hardly possible from the experimental results to decide conclusively between 1 and 3. On the whole, we are inclined to regard 3 as the most probable, and the possibility of a chain mechanism must also be borne in mind.

The following facts render probable the conclusion that the effective catalyst is the halogen atom ; firstly, iodine is active under conditions where it is predominantly in the atomic form, and secondly, with chlorine and bromine k plotted against the square root of the halogen concentration gives an approximation to a straight line over the range indicated in fig. 1. If there is no need to assume the existence of a limiting rate, the latter fact proves without further discussion that reaction depends upon collisions between nitrous oxide molecules and atoms of chlorine or bromine. With the existence of a limit the square root relation might be of no particular significance, but even here detailed calculation shows the results to be in better accord with the atomic than with the molecular hypothesis. To see this we proceed as follows. From the

equation $k = b[X]/(1 + b'[X])$, where X is the concentration of the catalyst, it follows that τ plotted against the reciprocal of [X] should give a straight line. Fig. 3 shows τ for bromine plotted against $1/[Br_2]$ and against $1/\sqrt{[Br_2]}$, *i.e.*, against $1/[Br]$. It will be seen that there are clear indications of a limiting rate corresponding to $\tau = 32$, and also that the square root relation is the appropriate one. The equation given above neglects the rate of the un-catalysed reaction in comparison with that of the catalytic, an approximation which ceases to be valid when the bromine concentration is small. A better approximation is

$$k_{\text{total}} = k_0 + \frac{b\sqrt{[Br_2]}}{1 + b'\sqrt{[Br_2]}},$$

which is simply transformed into

$$\tau = \tau_\infty + \frac{c}{\sqrt{[Br_2]}}\left(1 - \frac{\tau}{\tau_0}\right),$$

τ_0 being the half life in the absence of the catalyst and τ_∞ that corresponding to the limiting rate. In fig. 2 the continuous line is drawn from the equation

$$\tau = 32 + \frac{186}{\sqrt{[Br_2]}}\left(1 - \frac{\tau}{\tau_0}\right)$$

while the points are the experimental values (those indicated by circles referring to experiments made with propyl bromide).
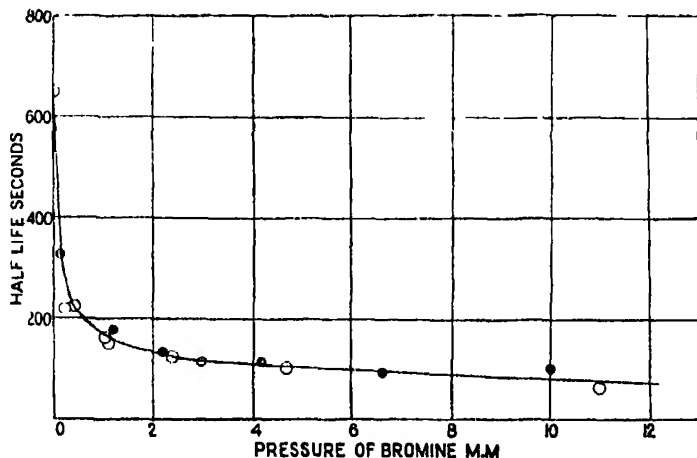
FIG. 2.—The open circles represent experiments with free bromine, the shaded circles those with an equivalent of oxidised propyl bromide. The continuous line is the theoretical curve.

The marked differences in the catalytic efficiency of the various halogens are largely accounted for by the differences in the dissociation constants. For a given atomic concentration fig. 1 shows the order of magnitude of the various influences to be the same, though iodine is still considerably more effective than the other two halogens. This may well be connected with the greater ease of formation of iodine oxides, for even at high temperatures this may reveal itself in the greater ability of iodine to assist the removal of the oxygen atom from the molecule of nitrous oxide. Whether, however, a definite chain of reactions is set up in which various transitory iodine oxides play a part is a matter for speculation; it is suggested by the mechanism of the catalysis of the decomposition of ozone by halogens, where apparently several different oxides of chlorine and bromine are involved. The extreme instability of halogen oxides at high temperatures is not a serious objection, since their life need not be supposed to exceed the time between two collisions of the chemical type necessary to form and destroy them. The stability of the oxygen atom in N_2O at 700° C is about the same as that of the odd oxygen of ozone at ordinary temperatures, so that the molecular forces may well be of the right magnitude to allow the iodine atom to combine with it.

The inverted order of chlorine and bromine in the series in fig. 1 is probably not of much significance. The differences may possibly be explained by the fact that with chlorine there is always a great preponderance of molecules present, and that these may be expected to exert an effect of their own is evident from the catalytic activity of such gases as nitric oxide. At an atomic partial pressure of 0·1 mm. under the conditions shown in fig. 1 the partial pressures of the molecules are respectively 0·007 for iodine, 0·66 for bromine and 114 for chlorine.

Temperature Coefficient of the Reaction Velocity.

The determination of the temperature coefficient is complicated by the changing degree of dissociation of the halogens. The plan adopted was to make measurements at different temperatures with a relatively high constant pressure of the halogen, and to calculate the actual pressure of atoms present at each. For one temperature data are available for plotting rate against atomic partial pressure; over not too large a range this curve may be used to correct the results at each temperature to a constant concentration of atoms. From the data corrected in this way the energy of activation may be calculated.

In all experiments the initial pressure of nitrous oxide was 300 mm. The bromine pressure was 4 mm., chlorine pressure 13 mm., while for iodine 6 mm.

of decomposed isopripyl iodide were used. T is the Centigrade temperature, τ the observed half life, and τ' that corrected to a constant partial pressure of atoms.
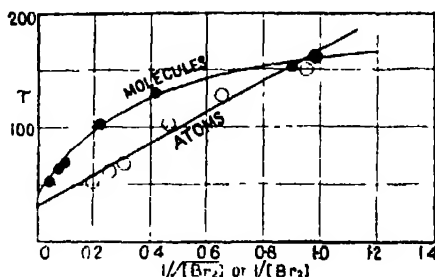
FIG. 3.

Table IX.

Iodine.			Bromine.			Chlorine.		
T.	τ	τ'	T	τ.	τ'.	T.	τ.	τ'.
700	31	31	745	51	62	744	123	137
675	82	75 5	722	112	112	722	210	210
650	158	136	700	220	181	702	448	368
625	433	349	680	443	315	682	820	524
E = 51,500 cal			E = 48,500 cal.			E = 46,500 cal.		

The values of E are given to the nearest 500 calories Having regard to the possible errors we may consider the differences between them unimportant ; indeed, for theoretical calculations it would probably be best to assume a standard value equal to the average, 49,000 This, as might be expected, is appreciably lower than that of the uncatalysed reaction. If the halogen molecules were assumed to be the catalysts, then the changing dissociation would not have to be taken into account in this way, and the values of E would be 59,000, 63,000 and 59,000 for chlorine, bromine and iodine respectively. These are improbably high, which lends some indirect support to the view that the atom is the catalyst. The corrected values are naturally subject to greater uncertainty than they would have been had a more direct method of determination been possible. If the rate of reaction had been a strict linear function of the atomic concentration, then it is easily shown that the correction to be applied is half the heat of dissociation of the halogen molecule. This would make the corrected value for bromine about 40,000 calories. The actual value lies between this and the uncorrected value, since the rate of reaction is rather

less than directly proportional to the atomic concentration. The value of E which would allow the observed rate of reaction, with 0·2 mm. catalyst and 300 mm. nitrous oxide at 722° C., to be accounted for with activation in two square terms only is about 35,000 calories. Thus either several degrees of freedom of the system N_2O–Br are involved in the process, or some kind of chain mechanism operates, or the collisions between the halogen atoms and N_2O are associated with an "abnormal diameter."

Photochemical Experiments.

If the decomposition is catalysed by the halogen atom, it should be possible to accelerate it photochemically, though the effect may be difficult to detect on account of the intensity of the light source required to produce a concentration of atoms comparable with that due to the thermal dissociation at 700°. It is, of course, useless to seek an effect at low temperatures, since the reaction has a high heat of activation. Experiments were made between 600° and 700° in a silica bulb with an optically worked quartz plate fused to one end, contained in a horizontal electric furnace also provided with an optically worked quartz window through which the bulb could be illuminated. The source of light was a 1000 candle-power tungsten lamp. The light was filtered through copper sulphate solution and cooled and concentrated by passage through a globe containing running water. With iodine it was useless to seek any effect at 700° since the limiting rate is too nearly reached at any convenient concentration, but at 600° an appreciable acceleration was observed. With chlorine no acceleration could be detected, probably because of the unfavourable extinction coefficients, but with bromine a small definite effect was found. The best conditions for observing it were with about 0·5 mm. bromine and 300 mm. nitrous oxide at 650. The method of observation was to take the times required for the pressure in the reaction vessel to increase by successive amounts of 10 mm. with the light alternately on and off. The relative shortening of the intervals by illumination is shown in fig. 4. At higher concentrations of bromine the relative acceleration by light is less marked.

Summary.

The thermal decomposition of nitrous oxide is markedly catalysed by halogens. It is probable that the free halogen atom is the effective catalyst. With iodine, and possibly with bromine and chlorine, the rate reaches a limiting value as the concentration of the catalyst increases. The reactions are homogeneous
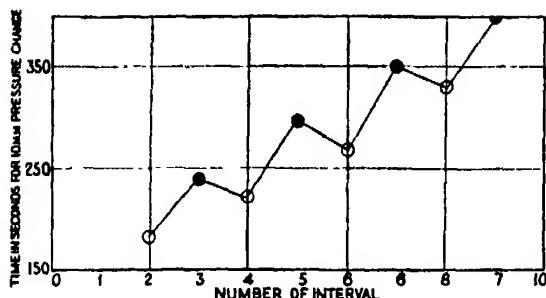
FIG. 4.—Acceleration ,by light of the decomposition of the bromine-catalysed nitrous
oxide. Shaded circles refer to dark intervals, open circles to illuminated intervals.

and are unimolecular with respect to the nitrous oxide. The mechanism of
the process is discussed.

We are indebted to the Royal Society and to Imperial Chemical Industries
for grants with which apparatus for this investigation was purchased.

Some Measurements of Upper-Atmospheric Ionisation.

By E. V. APPLETON, F.R.S., and R. NAISMITH, A.M.I.E.E.

1. *Introduction.*

In the wireless exploration of the electrical structure of the upper atmosphere
a considerable simplification in the interpretation of the experimental results
is effected if the emitting and receiving stations are placed very close together.
In such a case it can be assumed that the waves have travelled to and from
the reflecting region approximately along the same track, and, if care is taken
that the emitting station radiates appreciably in an upward direction, we may
further assume that reflection from the upper-atmospheric layer takes place at
normal incidence. The advantages of such a simplification arise as follows.
The two quantities which can, in general, be measured in the type of wireless
experiments we are considering are (a) the group-time for a signal to traverse
the atmospheric ray track, and (b) the angle of incidence θ_0 of the waves at the
lower boundary of the ionised region. From (a) we can deduce the equivalent
path of the waves in their overhead journey. Also since $\sin \theta_0$ is equal to μ,

the refractive index at the highest point of the wave track, and since the relation between refractive index and ionisation is known, we can find from (b) the maximum ionisation content experienced by the waves It is therefore clear that, in the case of experiments at normal incidence, it is not necessary to supplement the measurements of group-time by measurements of angle of incidence, since it may be assumed that the waves have been reflected at a region where the refractive index has been reduced to zero. Another advantage arises from the fact that the very complicated expressions for the refractive indices of the two component waves which travel in an ionised medium which is subject to the influence of the earth's magnetic field, yield easily calculable values of the ionisation content in terms of the wave frequency for the particular conditions $\mu^2 = 0$.

As a result of the investigations* carried out within the last few years it has been shown that there exist in the upper atmosphere two ionised regions from which wireless waves are reflected. The lower of these two regions is the Kennelly-Heaviside layer, the existence of which was inferred by Kennelly and Heaviside more than a quarter of a century ago to account for successful communication by long waves over long distances. The upper region has been shown to be richer in ionisation than the lower, so that when waves penetrate the Kennelly-Heaviside layer they may still be reflected by the upper region. If, therefore, we project vertically upwards waves of gradually increasing frequency (and therefore gradually shorter wave-length) we find that, at a certain critical frequency, the Kennelly-Heaviside layer is just penetrated and reflection begins to take place from the upper region. Since, as has been stated above, we assume that reflection at vertical incidence takes place at a place where the refractive index tends to zero and since the expression for the refractive index, in terms of N the ionisation content and f the frequency of the waves, is known, the maximum value of N is evidently determined by the critical penetration frequency of the waves.

The penetration frequency of the lower region is more easily found than the penetration frequency of the upper region, since the former is indicated by a discontinuity in the curve in which equivalent height is plotted against frequency, while the latter can only be inferred from the absence of downcoming waves in the case of frequencies higher than a certain value. The present communication is confined chiefly to observations on the critical penetration

---

* ' Nature,' vol. 120, p. 330 (1927) ; ' Proc Roy. Soc.,' A, vol. 126, p. 542 (1930) ; ' Proc. Roy. Soc ,' A, vol. 128, p. 133 (1930) , ' Proc. Roy. Soc.,' A, vol. 128, p. 159 (1930)

frequency of the lower region with special reference to its diurnal variation and to its significance as a measure of the maximum ionisation content of the lower region.

2. *Upper-atmospheric Reflection of Wireless Waves at Vertical Incidence.*

Experiments carried out at the Peterborough Radio Research Station in 1929 showed that it was possible to reduce the distance between the sending and receiving stations to 1 mile and yet obtain evidence of the interference phenomena from which we are able to measure equivalent heights. Later, at the Radio Research Station, Slough, these experiments were continued and the distance in question reduced to 180 yards. The detection of downcoming waves under such conditions was found to be facilitated by the use of an emitting aerial with a long horizontal portion, which ensured appreciable upward radiation, and also of a loop aerial at the receiving station turned so as to be in the " minimum " position for the reception of the direct ground transmission between the two stations It was clear from the experiments that the chief difficulty in working at short distances could be attributed to the excessive strength of the direct ground signal relative to that of the downcoming waves. We were, however, able to make enough measurements, particularly on the shorter wave-lengths, to be able to demonstrate satisfactorily that there is no detectable difference between the values of equivalent height measured at a distance of 180 yards and those measured at greater distances up to 9 miles.

Since, in the determinations of the critical penetration frequency of the Kennelly-Heaviside layer, it was necessary to extend observations to wave-lengths as long as 500 metres, in which case the low attenuation of the ground waves make it quite impossible to detect downcoming waves at very short distances, the measurements detailed in this paper were carried out at a distance of 9 miles from the emitting station. Even at this distance, however, we know that the angle of incidence was never greater than, and usually very much less than 6 degrees. Working at this distance we were able to make measurements of the equivalent height of reflection for a range of wave-lengths from 500 to 50 metres ; that is, for a range of frequencies from $0 \cdot 6 \times 10^6$ cycles per second to $6 \cdot 0 \times 10^6$ cycles per second. We believe that the data obtained would not have been materially different had the distance between the emitting and receiving stations been a few hundred yards.

3. *The Relation between Equivalent Height and Frequency.*

The measurements of equivalent height given below were all made using the frequency-change method, In the present stage of our technique we are able to make a reliable measurement for a single mean frequency in 10 minutes so that a set of comparison measurements on six different frequencies can be made in an hour.   For sunrise and sunset conditions, however, the ionisation in the Kennelly-Heaviside layer is altering so rapidly that the measurements made on, say, 12 frequencies during a run of 2 hours, are hardly strictly comparable.   But round about noon the ionisation, as will be shown below, reaches a maximum and a comparable set of observations is possible between say, 11 a.m. and 1 p.m.

In fig. 1 is exhibited a series of equivalent height measurements, for a wide range of frequencies, made during the 2 hours round noon on October 9, 1931.
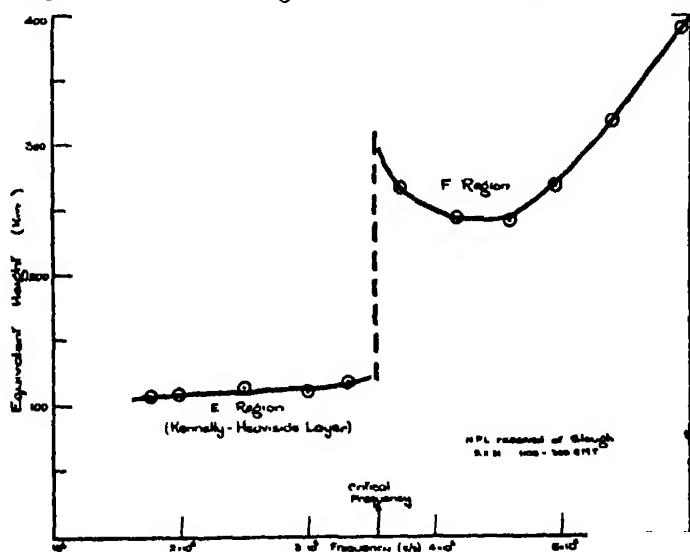
Fig. 1.

This curve is typical for magnetically-undisturbed days at this time of year. It will be seen that for frequencies up to $3 \cdot 33 \times 10^6$ cycles per second (90 metres wave-length) deviation took place at the Kennelly-Heaviside layer, Region E, the equivalent height increasing slightly with increase of frequency. For frequencies of $3 \cdot 75 \times 10^6$ cycles per second (80 metres wave-length) and over deviation took place at the upper reflecting region, Region F. Here the equivalent height is at first reduced but afterwards increased with increase of frequency.

The measurements exhibited in fig. 1 show that on the day in question the critical penetration frequency lay between $3 \cdot 33 \times 10^6$ cycles per second and $3 \cdot 75 \times 10^6$ cycles per second, and we accept the mean value $3 \cdot 54 \times 10^6$ cycles per second as an example of the nearest approach to the noon value of critical frequency we can obtain with our present technique.

The interesting decrease of equivalent height with increase of frequency for frequencies slightly higher than the critical value is just such a phenomenon as may be expected* in the case of a true discontinuity in the nature of the path of the atmospheric waves. The equivalent path, P′, of the atmospheric waves, from which the equivalent height is deduced for such measurements as we are considering, is equal to $\left(P + f\dfrac{dP}{df}\right)$, where P is the optical path of the atmospheric waves. Now, if for a certain frequency, reflection ceases from the lower region and takes place at a higher level there will be a discontinuity in the optical path and therefore an infinity in the relation between P′ and f. Actually, of course, no such infinity is observed in practice for the reasoning given above is based on a ray treatment and it is in just such problems as this that such a treatment breaks down and has to be replaced by the wave treatment of Hartree.†

In fig. 2 is exhibited a series of measurements made on October 2, 1931, between 11 a m. and 1 p.m. G.M.T. This was a day on which a magnetic storm was in progress. It will be seen that, even for frequencies up to $5 \cdot 9 \times 10^6$ cycles per second, reflection took place from the Kennelly-Heaviside layer. On this day therefore we were unable to measure the critical frequency at noon and can only give its inferior limit. As will be shown later the maximum ionisation in the lower region increases with increase of critical penetration frequency and, as we have very often found magnetic activity associated with a high value of critical frequency, we may conclude that the effect of a magnetic storm is very frequently to increase very markedly the maximum ionisation in the Kennelly-Heaviside layer.

4. *The Relation between Maximum Ionisation and Critical Penetration Frequency.*

It has been stated above that total reflection of waves incident normally on the ionised layer may be supposed to take place at a place where the index

* 'Proc. Phys. Soc.,' vol. 42, p. 321 (1930).

† 'Proc. Roy. Soc.,' A, vol. 131, p. 428 (1931).

of refraction μ of the medium is reduced to zero by the presence of ions or electrons. (We here use the term "refractive index" in the sense used by Lorentz,[*] limiting it to the real part of the complex refractive index used by other writers.) According to the simple theory of dispersion, however, the refractive index is never diminished quite to zero, even for very intense ionisation, if the motion of the electric charges in the medium is subjected to frictional forces, and such forces must always be regarded as present at the range of
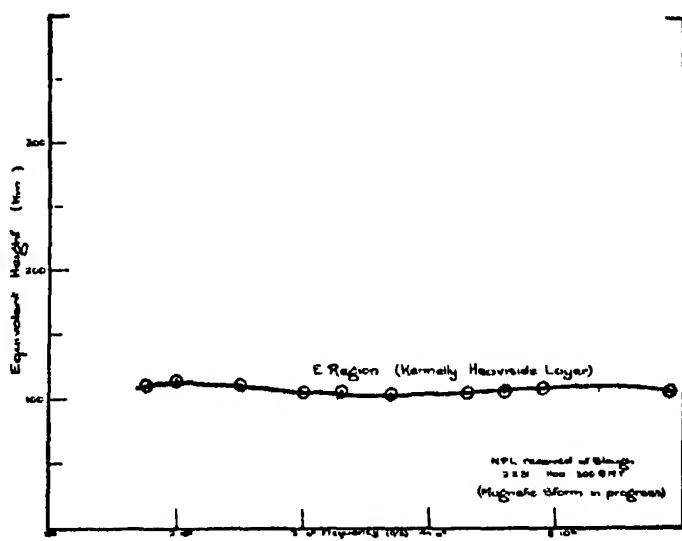
FIG. 2.

atmospheric heights we are considering here. But it should be noted that it is just for the conditions in which μ is very small compared with unity that the simple treatment of wireless wave propagation in terms of rays breaks down, since it is not then possible to consider the properties of the medium as "varying slowly" within a wave-length.[†] For such conditions the ray treatment must be replaced by the wave-treatment of these problems previously given by Hartree.[‡] Further need for such a change is to be found in the experimental fact that, as the frequency of the waves is increased, the change

---

[*] Lorentz, "Theory of Electrons," p. 153.

[†] The wave-length in the medium is here indicated. The value of this quantity approaches infinity as μ tends to zero.

[‡] 'Proc. Camb. Phil. Soc.,' vol. 25, p. 97 (1929) and 'Proc. Roy. Soc.,' A, vol. 131, p. 428 (1931).

over from reflection at Region E to reflection at Region F, although rapid, is not exactly discontinuous, there being a small transitional range of frequencies in which the simultaneous reflection from both regions is observed. Such an effect clearly cannot be explained in terms of a ray treatment according to which reflection is complete or non-existent.

Without a knowledge of the nature of the relative distribution of ionisation with height (as distinct from the actual values of ionisation content at different heights) we are unable at present to make use of Hartree's treatment. It can, however, be regarded as certain that marked reflection can only take place from regions where μ does not differ substantially from zero, and we feel justified in taking as a first approximation the condition $\mu = 0$ as expressing the properties of the medium in which the waves are reflected. Such a procedure may also be justified by regarding the problem in another way. If we imagine the process of deviation as approximating to reflection from a stratum of sufficient thickness with a relatively sharp boundary (the wave-length being large as μ tends to zero) the reflection coefficient ρ (defined as the ratio of the reflected and incident amplitudes) is given by

$$\rho = \frac{\left(\mu - \dfrac{i\kappa c}{p}\right) - 1}{\left(\mu - \dfrac{i\kappa c}{p}\right) + 1},$$

where κ is the absorption coefficient, c the velocity of light *in vacuo*, and p the angular frequency of the waves. When absorption is very small, as is the case in the problems we are considering, reflection becomes marked when the value of μ approaches zero.

At present we are unable to state with certainty whether the effective electrical carriers in the Kennelly-Heaviside layer are of electronic or ionic mass although it is fairly clear, from experiments carried out between East London College and King's College, London, by Mr. G Builder and one of the writers, that electrons alone are of importance in causing reflection from the upper ionised region. Now the general expression for the refractive index of an ionised medium for waves propagated in any direction relative to the earth's magnetic field is

$$\left(\mu - \frac{i\kappa c}{p}\right)^2 = 1 + \frac{2}{2(\alpha + i\beta) - \dfrac{\gamma_T^2}{1 + \alpha + i\beta} \pm \sqrt{\dfrac{\gamma_T^4}{(1 + \alpha + i\beta)^2} + 4\gamma_L^2}}, \quad (1)$$

where κ, c and p have the significance stated above and the quantities α, β and γ are similar to those used by Lorentz in his theory of dispersion, namely

$$\left.\begin{aligned}
\alpha &= \frac{-mp^2}{4\pi Ne^2} - \tfrac{1}{3} \\[2mm]
\beta &= \frac{pm}{4\pi\tau Ne^2} \\[2mm]
\gamma_T &= \frac{pH_T}{4\pi cNe} \\[2mm]
\gamma_L &= \frac{pH_L}{4\pi cNe}
\end{aligned}\right\} \tag{2}$$

Here N is the number of electric charges (of mass m and charge e) per cubic centimetre, τ is the time between two successive encounters of a charge with gas molecules, and H_L and H_T are respectively the components of the earth's magnetic field along and at right angles to the wave normal.

If friction is neglected we can put β and κ equal to zero in (1), which then becomes[*]

$$\mu^2 = 1 + \frac{2}{2\alpha - \dfrac{\gamma_T^2}{1+\alpha} \pm \sqrt{\dfrac{\gamma_T^4}{(1+\alpha)^2} + 4\gamma_L^2}}, \tag{3}$$

from which we deduce that $\mu^2 = 0$ when

$$\left.\begin{aligned}
1 + \alpha &= 0 && \text{(lower sign)} \\
\text{and}\quad 1 + \alpha &= \pm\sqrt{\gamma_L^2 + \gamma_T^2} = \pm|\gamma| && \text{(upper sign)}
\end{aligned}\right\}, \tag{4}$$

or when

$$N = \tfrac{3}{7}\frac{\pi m}{e^2}\cdot f^2 \qquad \text{(lower sign)} \tag{5}$$

and

$$N = \tfrac{1}{7}\frac{\pi m}{e^2}(f^2 \pm f f_H), \qquad \text{(upper sign)} \tag{6}$$

f being the frequency of the waves and f_H equal to

$$\frac{e\sqrt{H_T^2 + H_L^2}}{mc}$$

or He/mc.

[*] It is important to note here that, if β is made equal to zero, the right-hand side of (1) is equal to μ^2 only so long as it is zero or positive. If it is negative it is equal to $-\kappa^2 c^2/p^2$ and μ^2 is then equal to zero.

It should here be noted that the relations (3), (4), (5) and (6) hold only for frictionless conditions which, as stated above, do not actually exist. Since, however, we know that absorption is small, we assume that the condition $\mu = 0$ for zero friction gives us the condition when μ is approximately equal to zero for small friction.

If, in (5) and (6), f is what we have called the critical penetration frequency, N clearly represents the maximum value of the ionisation content in the Kennelly-Heaviside layer. The question therefore arises as to which of the three expressions in (5) and (6) we should take to calculate N_{max} when f is known. If the electrical carriers are of molecular mass (e.g., negatively charged oxygen atoms) the value of f_H is so very small that (5) and (6) are practically equivalent. For electrons, however, the influence of the earth's magnetic field cannot be neglected and we are faced with the difficulty that μ is equal to zero for three values of N. Until the somewhat complex magneto-ionic theory is further unravelled we are unable to state how much reflection takes place at the three heights at which these three values of N are successively attained. This uncertainty would therefore, on general grounds, lead us to take the intermediate value indicated by (5) as an average, though it also happens that there is a certain amount of justification derived from experiments made on the polarisation of downcoming wireless waves for doing this. If we imagine a plane-polarised wave passing vertically into the upper atmosphere theory indicates that, in general, it is split up into two elliptically polarised waves of opposite rotational sense and different absorption coefficients. Although for directions of propagation along and at right angles to the field such components (which in these special cases are circularly and linearly polarised respectively) travel in regions of increasing N without change of polarisation, the same cannot be said for other directions inclined to the magnetic field. Here the characteristic polarisations change as increasing values of N are reached. If the increase of N takes place slowly with increase of height we should therefore expect the components to be continually splitting and re-splitting as they progress further into the layer, so that signal impulses might be increased in duration. This process does appear to take place in the case of reflection from the upper ionised region, especially at night. On the other hand, if the maximum value of N were reached for a small depth of penetration, as appears to be the case for the lower region we are considering, the changes of polarisation (apart from those due to the difference in the two absorption coefficients) may not be so marked. Now it is known from the magneto-ionic theory that the right-handed component for propagation

vertically upwards (and the left-handed component for propagation vertically downwards) has the lower absorption coefficient and this agrees with the experimental fact that downcoming waves, on their arrival at the ground, are found to possess a predominant left-handed polarisation. Since components of lower absorption coefficient are associated with the value of μ from which (5) is derived, (6) referring, in similar manner, to the component of greater absorption, we find support in the polarisation results for using (5) in the present instance. However, although in the later discussion of results we actually choose to do this, it should be noted that the results for (5) in the case of electrons would not be very markedly different if we were to choose (6) with the upper or lower sign.
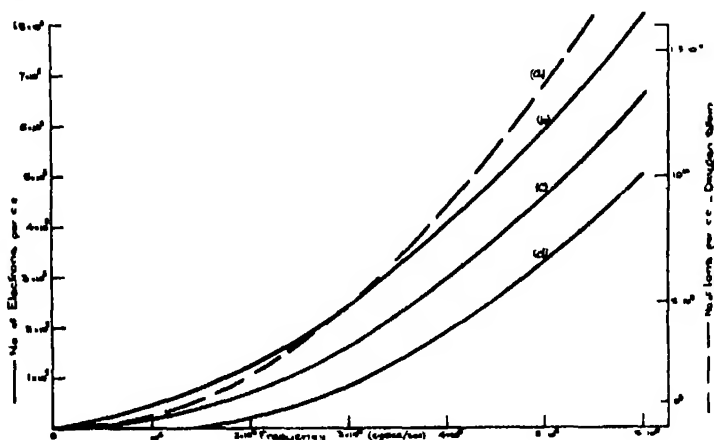
Fig. 3.

In fig. 3 are plotted the relations (5) and (6) for the different cases. The curve (*a*) represents the relation between N_{max} and f for ions of molecular mass (*e g.*, 0 atoms) the scale of ordinates being on the right. The curves (*b*), (*c*) and (*d*) represent the relations between N_{max} and f for electrons, (*c*) illustrating (5), and (*b*) and (*d*) illustrating (6) for the upper and lower signs respectively. The ordinate scale for curves (*b*), (*c*) and (*d*) is on the left-hand side. In accordance with the discussion above we therefore translate the experimental values of f into values of N_{max} (ions) using curve (*a*), and into N_{max} (electrons) using curve (*c*).

5. *The Diurnal Variation of Critical Frequency.*

In order to investigate the diurnal variation of critical frequency, isolated measurements were first made at different times of the day to find approxi-

mately the nature of the variation. This enabled us to develop a system of measurement which permitted hourly determinations of the critical frequency throughout the whole day. Such 24-hour runs were carried out in winter, spring and summer. The procedure adopted was to make enough determinations of the equivalent height at different frequencies to enable us to draw a curve such as is shown in fig. 1, from which can be deduced the limits within which the critical frequency must lie. The mean of such limits was taken as the critical value. Since, with our present experimental technique, about 10 minutes is required both to change from one frequency to the next and to make a satisfactory determination of equivalent height, only six measurements of equivalent height could be made within an hour. It was therefore necessary to ensure that the critical frequency should lie within the frequency range used. This was possible from the results of the general surveys previously made.

The results of the three 24-hour runs are shown in figs. 4, 5 and 6, which may be taken as illustrating the diurnal variation in winter, spring and summer respectively. The data for these curves were obtained using the National Physical Laboratory as the emitting station, the requisite equivalent height determination being made, using the frequency-change method, at Radio
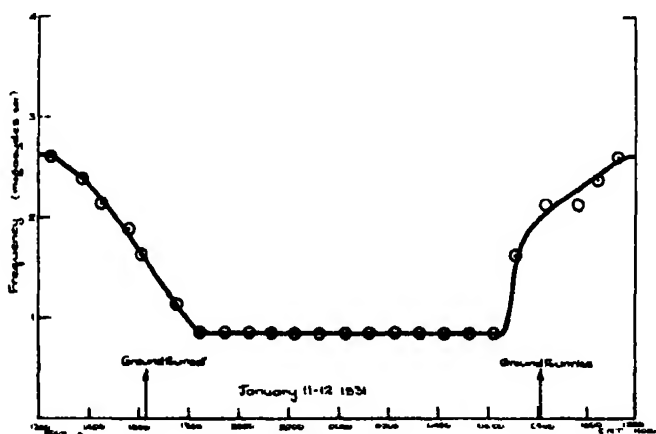
Fig. 4.

Research Station, Slough, and at King's College, London. A certain number of simultaneous observations were also made at the Cambridge University Officers Training Corps Rifle Range at Cambridge. Good agreement was obtained between the values of the critical frequency deduced from the observations at the different stations.

6. *Discussion of Results.*

With the aid of the curves in fig. 3, the data of the diurnal variation curves of figs. 4, 5 and 6 can be translated into graphs showing the variation of N_{max}.
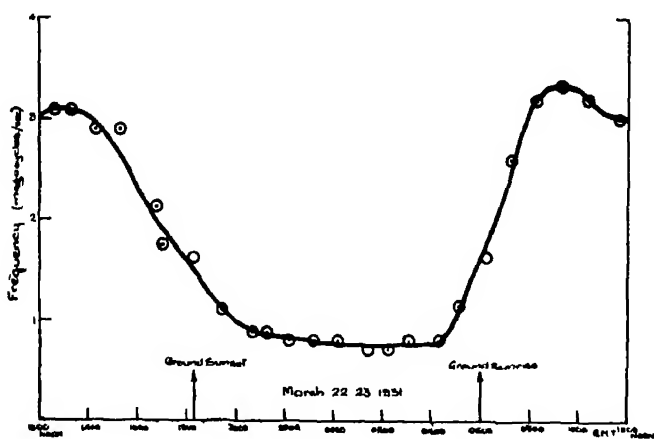
Fig. 5.
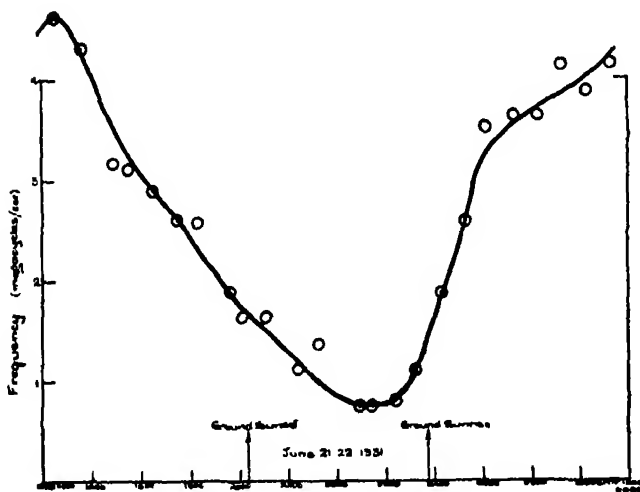
Fig. 6.

throughout the day. Taking the spring day as typical the results of this translation for March 22/23 is shown in fig. 7, the left-hand scale of ordinates referring to electrons, and the right-hand scale referring to ions. The corresponding curves for winter and summer have the same general characteristics.

It is seen that, in all cases, the ionisation is a maximum about noon* and falls off steadily as sunset approaches. The ionisation continues to fall rapidly
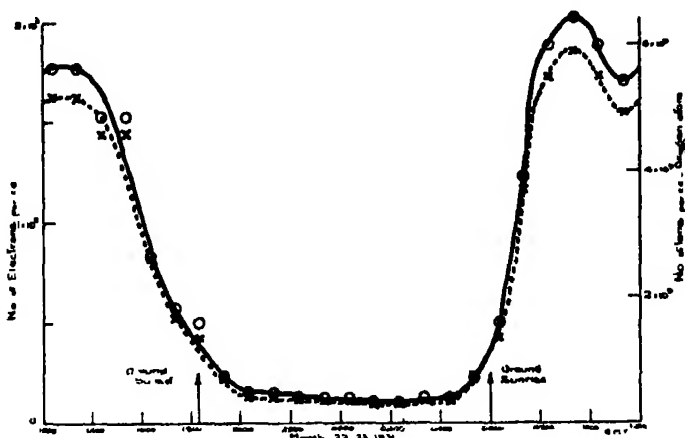
FIG. 7.—× Ions. ⊙ Electrons.

after sunset until an almost stationary night value is reached. Before ground sunrise the ionisation is replenished due to solar influence, the value of N_{max} increasing rapidly. Such an increase of ionisation before ground sunrise is readily understood when it is realised that we are dealing with events at a height of 80 to 100 km. above the earth's surface. It is clearly evident from the spring and summer curves that the minimum of ionisation occurs just before dawn. (The constant value of critical frequency for the winter night, illustrated in fig. 4, is due to the rather wide spacing of the frequencies used in finding the limits of the critical value on this, our first, 24-hour run. All the available wireless evidence suggests that the ionisation, in general, falls slowly to a minimum just before dawn during winter, as well as during summer nights.)

The results obtained enable us to make a comparison of the maximum noon ionisation on summer and winter days. The data for such a comparison are tabulated in Table I.

It will be seen that, if we assume that the effective electrical carriers are of electronic mass, the ratio of summer to winter ionisation is 3·1 to 1, whereas if we assume that the carriers are ions the corresponding ratio is 2·7 to 1.

A figure of about the same value is obtained whatever curve in fig. 3 we choose as illustrating the relation between N_{max} and f. There can be little

* The pre-noon maximum in the spring curve is probably an accidental characteristic of this particular day, but further observations on this point are being made.

Table I.

Season.	Noon critical frequency (cycles per sec.).	N_{max} electrons per cubic centimetre.	N_{max} ions per cubic centimetre
Winter	$2 \cdot 6 \times 10^6$	$1 \cdot 2 \times 10^5$	$3 \cdot 7 \times 10^9$
Spring	$3 \cdot 2 \times 10^6$	$1 \cdot 9 \times 10^5$	$5 \cdot 5 \times 10^9$
Summer	$4 \cdot 5 \times 10^6$	$3 \cdot 75 \times 10^5$	$10 \cdot 1 \times 10^9$

doubt, therefore, that the ratio of summer noon ionisation to winter noon ionisation is represented by a figure of 2 to 3. In this connection it is interesting to compare these results with those obtained by S. Chapman* in his theoretical investigation of the absorption and dissociative ionising effect of monochromatic radiation in an atmosphere on a rotating earth. In this investigation it is found that for the latitude of London ($51 \cdot 5°$ N) the summer to winter ratio of the maximum rate of absorption of the radiation at noon is $3 \cdot 4$. Now if we assume that the process responsible for the decay of ionisation is that of ordinary recombination, the equation relating the ionisation N to time t is

$$\frac{dN}{dt} = q - \alpha N^2, \qquad (7)$$

where q is the number of charges produced by the ionising agency per second and α is the coefficient of recombination. Now at noon dN/dt is zero so that

$$q = \alpha N^2. \qquad (8)$$

Now, according to Chapman, the ratio of the summer and winter values of q is $3 \cdot 4$ so that the ratio of the summer and winter values of N (electrons or ions) is $\sqrt{3 \cdot 4}$ or $1 \cdot 84$.

There is, however, another possible dissipative process to be considered if the effective ionisation consists of carriers of electronic mass. It is most likely that the oxygen molecules in the upper atmosphere are photo-electrically dissociated into oxygen atoms so that there is the possibility that electrons may become attached to such atoms and thus relatively cease to be effective in influencing radio propagation. We should, therefore, in such a case, replace (7) by an equation of the form

$$\frac{dN}{dt} = q - \beta N, \qquad (9)$$

* 'Proc. Phys. Soc.,' vol. 43, p. 26 (1931) and vol. 43, p. 483 (1931).

where β is the attachment coefficient, since we may expect the number of attachments per second to be proportional to the total number of electron collisions with oxygen atoms. As dN/dt is zero at noon we now have

$$q = \beta N, \tag{10}$$

in which case we should expect the ratio of summer to winter values of N to be 3·4. We therefore see that a consideration of the two processes of ionic or electronic dissipation lead us to expect a ratio of summer to winter noon ionisation of the order 1·8 to 3·4. The experimental values of 2·7 and 3·1 lie within this range and perhaps suggest that, while both the processes of recombination and attachment are present, the latter is the more important dissipative influence

The general trend of the diurnal variation curves and their marked correlation with sunset and sunrise leave little doubt that the chief agency responsible for the ionisation is of solar origin and travels through the earth's atmosphere in straight lines. It must therefore consist of either aetherial radiation (ultra-violet light) or uncharged material particles   In this connection S. Chapman* has recently given reasons, derived from the evidence of the daily variations of terrestrial magnetism, for believing that the ionising agent for the lower ionised region consists of neutral atoms shot out by the sun and travelling with a velocity of the order of $1 \cdot 6 \times 10^8$ cm. per second. Such corpuscles would be unaffected by the earth's magnetic field and travel in straight lines through the upper atmosphere, ionising the air molecules by collision   There is, however, a difficulty in accepting this agency as that responsible for the ordinary diurnal variation we have described above. We refer to the results of the wireless experiments† made in England during the solar eclipse of 1927 in which it was found that the effect of the eclipse was to cause a partial return to night-time conditions. Now a striking feature of these results was that there was practically no lag between the changes in the Kennelly-Heaviside layer and the deprivation and restoration of the solar radiation from and to the earth by the moon. The equivalent height and the reflection coefficient of the ionised layer reached their maximum values just about totality. Now Chapman assumes that the same type of solar emission causes both the ordinary diurnal variation of ionisation and the marked increase of this quantity which

* 'Proc. Roy Soc.,' A, vol. 132, p. 353 (1931).

† Appleton, 'J. Inst. Elec. Eng.,' vol. 66, p. 872 (1930); see also 'Radio Research Special Report No. 7 of the D S.I.R.'

is associated with magnetic storms. The stream of particles from the sun is considered as electrically neutral and as consisting of positive and negative charges as well as a certain number of neutral atoms. The electrified particles are deflected by the earth's magnetic field towards the polar regions where they give rise to the aurora while the neutral particles travel in straight lines and cause the ionisation in the lower region.

A magnetic storm is therefore to be regarded as resulting from an increase in the intensity of this solar stream. the nature of the constituents remaining the same as on an undisturbed day. We can therefore reasonably assume that the velocity of the particles in question can be estimated from data acquired in the study of magnetic storms Now Greaves,* from an examination of Greenwich solar and magnetic data has derived evidence consistent with the " solar stream " theory of the origin of magnetic storms which suggests an interval of $1\frac{1}{2}$ days for the time taken by the stream to travel from the sun to the earth.

A simple calculation shows that such a solar stream would take $4\frac{1}{2}$ minutes to travel the moon's distance from the earth, as compared with an interval of just over 1 second for ultra-violet light. At first we were inclined to interpret the 1927 eclipse results as deciding in favour of an ultra-violet light theory as against a particle theory, in view of the fact that the maximum wireless effect occurred more nearly to 1 second than to $4\frac{1}{2}$ minutes after totality. But, on informing Professor Chapman of our views as to the possibility of using eclipses for deciding between these theories and of our deductions from the data already available, he very kindly investigated the matter further, and found that the time of travel of the supposed particles was not the main factor determining the time-relations between what may be called the " particle eclipse " and the " optical eclipse." In a paper shortly to be communicated to the Royal Astronomical Society he has shown that, in 1927, the " particle eclipse " would have been expected to occur about $1\frac{3}{4}$ hours before optical totality. In the 1927 eclipse no special search was made for wireless effects at a period $1\frac{3}{4}$ hours before the eclipse, nor would any observations at that time have had much value since the ordinary night-time variations would still have been present. In the forthcoming total eclipse in Canada on August 31, 1932, however, totality occurs after noon so that it will be possible to make observations over the whole period in which particle and ultra-violet light eclipses are to be expected, and we wish to draw attention to the importance

* " Third Report of the Commission on Solar and Terrestrial Relationships (Int. Res. Council)," p. 69 (1931).

E 2

of this opportunity of deciding between the rival theories.* Meanwhile we are inclined to interpret the 1927 eclipse results obtained by one of us as demonstrating that ultra-violet light is an ionising agent of the lower region and look to the eclipse of this year as showing whether or not a neutral stream of particles is also present.

During the greater part of the year 1931 we have made weekly determinations of the critical frequency for Region E. These show that although the seasonal variation described above takes place, there are many days on which the ionisation is above the normal value. Divergences from the ordinary appropriate seasonal value of ionisation are always increases and not decreases. Such departures from what may, in the wireless sense, be called undisturbed seasonal values may be ascribed to the influence of particles constituting the solar stream. Summarising the above arguments, therefore, our experiments lead us to accept ultra-violet radiation as one of the causes, if not the chief cause, of the ordinary diurnal replenishment of the ionisation in Region E and to regard the "solar stream" of neutral particles as causing the extraordinary effects on abnormal days.

We now turn to consider certain other experimental facts derived from our experiments. Although the data in figs. 4, 5 and 6 indicate that, for the nights in question, the ionisation in Region E steadily decreased as the night advanced we have noted, on quite a number of nights, that the ionisation in Region E can actually increase at a period during the night when any solar radiation propagated rectilinearly could not possibly be reaching it. It therefore appears as if there is some other agency which produces nocturnal ionisation beyond the ordinary amount constituting the residue from the day-time and it is therefore possible that part of the ordinary night-time value of 10^4 electrons, or 3×10^8 ions, indicated in fig. 7 can also be ascribed to this unknown influence.

The present series of observations does not give us any clue as to whether the electrical carriers are of electronic or atomic or molecular mass. The reason for this is that the essential quantity measured in these experiments is N/m, N being the number of charges (each of mass m) per cubic centimetre. We have accordingly expressed the results for N in two ways, namely (a) for ions, and (b) for electrons. But other wireless evidence may be expected to shed light

---

* It will be seen from the results described in this paper that possibly the most suitable wave-length for use in these experiments would be one which was just greater than the critical value, so that a small reduction of ionisation would permit penetration of Region E.

on this question in the following way. If the charges in question are of electronic mass we may expect that in the process of deviation the two magneto-ionic components resulting from a very short signal pulse will be separated in time because of the difference in group velocities.* Also we should expect that, in experiments with a sustained signal, the waves, deviated by the upper atmosphere would, on their arrival at the ground, exhibit some characteristic polarisation due to the differential absorption experienced by the two components. Now, as mentioned above, Mr. Builder and one of the writers† have observed the doubling of signal pulses in the case of signals returned from the upper ionised region. Characteristic polarisations are also noted for waves reflected by the same region. There is therefore no doubt that, for the upper region, the electrical carriers are of electronic mass. In the case of the lower region the evidence is not so complete, but it is known that a characteristic polarisation is produced indicating the existence of electrons in sufficient numbers to produce absorption. Observations on the doubling of signal impulses, although actually observed in the case of Region E, cannot be ascribed to magnetic influence with the same certainty as in the case of Region F. The results therefore so far lead us to conclude that while electrons must constitute a proportion of the ionisation in Region E, it cannot yet be said that ions exert a negligible influence on wireless propagation as can be said in the case of Region F.

Although this paper is concerned primarily with the ionisation in the lower of the two atmospheric ionised regions it is of interest to compare the results described above with the corresponding values for the upper region obtained by Mr. G. Builder and one of the writers in experiments carried out between East London College and King's College, London. (In these experiments the ionisation in Region F was found by determining the frequency of the waves which just penetrated both regions at normal incidence.) The results of this comparison may be summarised as follows :—

(1) The day-time ionisation in Region F is about four or five times as intense as that in Region E.

(2) The ionisation in Region F reaches a maximum 2 or 3 hours after mid-day, whereas the ionisation in Region E is a maximum at noon. This difference is readily attributable to the difference in the recombination

---

* The condition most favourable for such a separation would be for the ionisation content to be sensibly constant over a considerable range of the atmospheric path so that the two components would be propagated independently.

† Appleton and Builder, ' Proc. Phys. Soc ,' vol 44, p. 82 (1932)

coefficients in the two regions, recombination being more rapid in the lower than in the upper region.

(3) The ratio of summer to winter day-time ionisation is about 1·8 to 1 for Region F, whereas it is about 2·5 to 1 for Region E.

Summary.

Experimental work on the reflection of wireless waves by the upper atmosphere has shown that if the frequency of waves, projected vertically upwards, is steadily increased, the Kennelly-Heaviside layer (Region E) is ultimately penetrated and reflection takes place at the upper region (Region F) The critical penetration frequency, for which reflection at Region E ceases and reflection at Region F begins, is found to vary diurnally and seasonally. From measurements of the critical penetration frequency made in South-east England the variation in the maximum ionisation content of the Kennelly-Heaviside layer has been studied. The value of this ionisation is found to be at a maximum about noon and at a minimum just before dawn The diurnal variation curves are found to correspond very closely to the theoretical curves obtained by S. Chapman in his study of the atmospheric ionisation produced by a solar stream of monochromatic radiation. Summer noon ionisation is found to be about $2\frac{1}{2}$ times as intense as winter noon ionisation.

On a Large Scale Crystalline Structure in Certain Glasses of Exceptional Composition.

By Lord Rayleigh, For Sec. R.S.

[Plates 1–3]

Some years ago I described a doubly refracting structure in silica glass.[*] This was detected by examining the glass between crossed nicols, using the necessary precautions to get a really dark field, so that very weak double refractions are brought into evidence.

The character of this double refraction was such that it could not be attributed to mechanical stress, and had rather to be assimilated to the "liquid crystals" observed by Lehmann in some melted organic substances.

For example, a disc of fused silica might indeed show the usual dark cross indicating mechanical stress, but superposed on this was a much smaller granular structure of crystalline or quasi crystalline origin   This latter was still so large that it could be well examined without magnification, the size of the granules being about 0·5 mm. On melting and drawing out this material, the granules were elongated into crystalline strings or fibres, and commercial silica rod and tubing was found to contain numerous strings or fibres of this kind, restoring light with crossed nicols at 45°, but giving extinction at 0° or 90°. These fibres are immersed in amorphous material. It might be supposed possible to prepare silica glass entirely amorphous, but I have not met with such. The double refraction of the crystalline parts is very weak, and was estimated at 0·05 that of rock crystal.

In that paper it was stated that similar effects had not been met with in any of the ordinary complex glasses—flint glass, crown glass, bottle glass. This remains true. Nevertheless, it will be shown that the case of silica glass is not unique.

My attention was recalled to this subject by casually examining a plate of "corex" glass, of high ultra-violet transparency, made by the Corning Company, U.S.A. This consists in the main of calcium phosphate, and shows between crossed nicols a structure very similar to that formerly found in silica

[*] 'Proc. Roy. Soc.,' A, vol. 98, p. 284 (1920). See also 'Proc. Optical Convention,' Pt. I, p. 41 (1926).

glass. A preliminary notice was sent to 'Nature,'* and the intention was expressed of examining other glasses of exceptional composition.

In doing this, the nicols were used as before without lenses or glass caps between them, since these are unfavourable for getting the darkest possible field. The specimens when procured from outside sources were in many cases polished, but glasses which are highly unstable in moist air cannot well be polished. In such cases, and in home preparations generally, the surfaces were ground flat, to the desired thickness (2 to 3 mm.) and cover slips as used in microscopic work were cemented with Canada balsam on either side of the specimen. These thin covers do not seriously spoil the dark field.

Since field lenses are not admissible, the size of the specimen that can be photographed at one exposure is limited by the cross section of the nicol prism available. A long camera was used to take the photographs of twice the actual size They could then be printed by contact, without the trouble of secondary enlargement. A pointolite lamp was used with a condensing lens which passed a slightly converging beam through the large polarising nicol and then through the specimen. The radiant came to a focus on the small analysing nicol in front of the photographic lens. In spite of the convergency, the beam emerging from the polarising nicol was large enough to cover the majority of the specimens

The left-hand photographs on the plates, marked $+$ are taken with the planes of vibration vertical and horizontal. The right-hand ones marked $\times$ are taken with the position of the specimen unaltered, but the crossed nicols rotated to the 45° position. The reproductions are 1·3 times actual scale.

Some of the specimens examined were sent me by Professor W. E S. Turner, of the Department of Glass Technology, Sheffield University, who had seen my letter in 'Nature' and most kindly responded to a request for any specimens of exceptional glasses which he might have available. Others were of commercial origin, and others were prepared in my own laboratory with the simple appliances which were to hand. I had no means of measuring the temperatures of fusion, or of making more than small pieces. The annealing was carried out in a small resistance oven with a mercury thermometer reading to 500° C. to control the temperature

I have found that some to whom I have shown the photographs have been inclined at first sight to attribute the structure to mechanical stress, and have a difficulty in understanding how this view could be excluded. It may be

remarked in the first place that patchy or string-like structures of this kind are almost always conspicuously shown in silica glass, and are never seen at all in ordinary flint or crown glass. Silica glass is much less expansible by heat, and therefore much less liable to stress due to bad annealing; so that it is not very plausible on the face of it to resort to this explanation.

There is, of course, nothing to prevent the materials here treated from showing patterns due to mechanical stress, if in fact they are badly annealed. The question is how these patterns are to be distinguished from the others, and it admits of a simple answer. Let us take the case of a circular disc. If this is badly annealed, then, as all opticians know, it shows a dark cross the arms of which are the traces of the vibration planes of the crossed nicols. In extreme cases there may be coloured rings in addition. The arms of the cross are diametrical to the disc, and thus bear a simple relation to its geometry as a whole. In the case of a rectangular or oval specimen we shall also get a dark cross, if the planes of vibration of the crossed nicols are set along the principal axes of the specimen; and even an irregular piece, if suitably oriented shows something similar.*

Some specimens similar to those shown have been watched in the process of annealing. A specimen of borax like that shown in 7+ and 7× when poured out on a stone slab and allowed to cool in the open is very apt to fly to pieces, especially if it is more than 2 cm in diameter. If by good luck it does not do so, then it shows in the polariscope a thin dark cross, fig. 1, A, with coloured
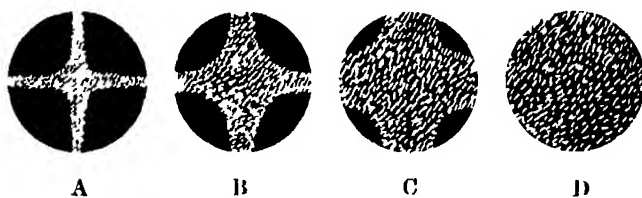
A   B   C   D
Fig. 1.

rings near the margin. The general glare is so great as completely to flood out the phenomenon under investigation with false light. On placing the specimen in an oven and raising the temperature to 400° C. (which is about the minimum for effective annealing of this material) the stress pattern fades away in the course of a few hours. At 450° C. the action is very much more

---

* See photograph No. 8+, in which case the specimen was by inadvertence not sufficiently annealed to get rid of the stress structure altogether, and the dark cross remains visible.

rapid. The process can be interrupted and the specimen allowed to cool for interim examination. The colours disappear, the arms of the cross become thicker, fig. 1, B, and the central dark region expands. In the penultimate stage, fig. 1, C, only narrow marginal patches in each of the four quadrants remain bright, and finally the central dark region has expanded to cover the whole specimen, fig. 1, D. Towards the later stages, as the false light due to stress diminishes the much fainter crystalline structure pattern comes into view. In practice the distinction between the two is obvious at a glance. Once the stress pattern has been got rid of, further changes due to a modification of the crystal-structure, so far as they occur at all, are extremely slow. Not much has been done in the way of looking for such changes. In describing the actual observations it will be convenient to begin with glasses of high silica content, which link up most naturally with the pure silica glass formerly investigated.

No. 1 is a glass received from Professor Turner (his label P.128) who gives the composition as $91 \cdot 6$ per cent. SiO_2 and $8 \cdot 4$ per cent. Na_2O. It was made from pure materials, and melted in platinum at $1700°C$, crushed and remelted. It was stirred with a platinum rod, poured and carefully annealed.

No. 2 is also from Professor Turner (his label P.124) and the composition is given as $4SiO_2$ $1Na_2O$, $79 \cdot 5$ per cent. SiO_2 and $20 \cdot 5$ per cent. Na_2O. This was melted at $1400°C$. In other respects the treatment was as in the previous case.

No. 3.—This is commercial pyrex glass, from the Wear Glass Works, Sunderland. It was taken from the bottom of a dish made for domestic use. In many cases pyrex shows no conspicuous structure, remaining dark between crossed nicols. In others, there are occasional isolated curved doubly refracting filaments, with the direction of extinction at any point along the tangent and normal to the filament. In others again there is faint patchy structure. The specimen here shown was much the most striking out of eight or ten vessels that were examined.

Pyrex, containing about 80 per cent. of SiO_2, seems to be near the minimum silica content for showing this structure in the class of silica glasses. Even in pyrex, as we have just seen, the structure is often absent or inconspicuous. In ordinary window glass which contains 72 per cent. of silica, I have never been able to detect any trace of crystalline structure. It is also entirely absent from flint glass (50 per cent. SiO_2) and from baryta crown glass.

Coming next to glasses in which silica is not the important constituent, we have in 4 the " corex " glass already mentioned, which was the origin of the
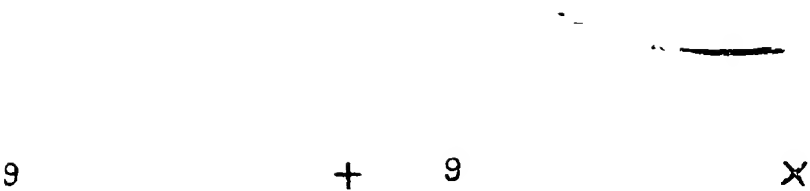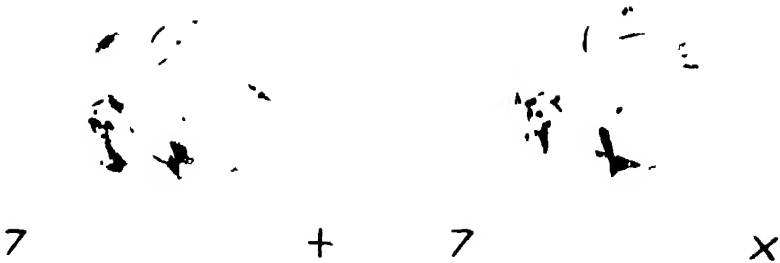
present work. This is the variety most transparent to ultra-violet light. Its composition is probably about the same as the following analysis* :—

P_2O_5 66·45 per cent., CaO 25·16 per cent., B_2O_3 4·63 per cent., SiO_2 2·12 per cent., Al_2O_3 0·37 per cent., Fe_2O 0·03 per cent., MgO 0·60 per cent., Na_2O 0·56 per cent.

It will be noticed that a large part of the specimen remains dark in both positions + and × of the nicols, and may be regarded as isotropic. Coloured corex glasses (green, " red purple " and " blue purple ") are also made by the Corning Company. These show the same kind of structure as the white corex.

Corex is one example of a phosphate glass. Another was prepared in the laboratory by fusing microcosmic salt. Small specimens made in this way up to 2 cm. diameter were often isotropic all over. In other cases they showed a doubly refracting structure over part of the area.

No. 5 is a pure boric oxide glass prepared under Professor Turner's direction, by fusing in platinum at 1400° C. It was received in the form of a roughly shaped rod of rectangular section. Two parallel faces were ground flat, scraped, and immediately protected with cover glasses before they could become cloudy. The material is very clear and free from bubbles. It was first of all examined visually, then carefully re-annealed, but the general appearances were not modified by this treatment. The photographs were taken after re-annealing.

No. 6 is a specimen of the same prepared in my own laboratory by fusion at a much lower temperature. The results are generally similar to the preceding.

The remaining photographs are of fused borax glass.

No. 7 is a specimen prepared in the laboratory by melting and pouring out. It is for the most part isotropic, with a few crystalline patches.

No. 8 is a slice prepared by grinding down a lump of commercial fused borax. The left-hand photograph (+ position of nicol) as already mentioned, suffers from imperfect annealing, and would probably be dark all over if better annealed. The right-hand photograph (× position of nicols) brings the structure into view. The indications suggest that a large mass of the fused material has been broken up after cooling. The " planes of bedding " shown in section in 8 are probably nearly parallel to the free surface of the initially fused mass and represent crystalline laminæ, each lamina having its principal directions of vibration in, and at right angles to, its own plane.

Reference has already been made to the elongated crystals found in drawn-

* D. Starkie and W. E. S. Turner, 'Trans. Soc. Glass Technology,' vol. **12**, p. 308 (1928).

out silica rod. It was of interest to see whether the same effect could be got in borax glass. Some borax was melted and poured out on a stone slab. Chisel-shaped pieces of iron were pressed down as quickly as possible and pulled apart so as to elongate the piece while still soft. It was then annealed and examined in the polariscope. No. 9 shows the result of an experiment of this kind. In the + position of the nicols there is nothing to be seen, but in the × position two crystalline ribbons or fibres make their appearance, which show straight extinction, i.e., the principal directions are along and perpendicular to the length, as in the case of silica glass. In attempting to estimate the strength of the double refraction, we meet the difficulty that the doubly refracting parts are immersed in a matrix of a different character. For this reason only rough estimates have been made.

In no case has the double refraction been strong enough to give perceptible colour. In order to use the interferential tint as a criterion of the amount of double refractive, it is necessary to superpose a crystal plate of known retardation, and to observe the addition or subtraction effect.

Thus, superposing a quarter wave plate on the pyrex No 3, we find in one position darkness, and in the other a straw yellow along an exceptionally conspicuous filament, about 2 mm. wide. The retardation in the filament is then about quarter wave, and if we assume the thickness to be about the same as the breadth, this indicates that about 8 mm. would be required to give one wave retardation   About 0·05 mm. of crystalline quartz is required to give the same (one wave) retardation.   Thus the double refraction of quartz is about 160 times greater by this rough test.

Outstanding Questions.

The present work by no means exhausts the questions opened up by the observations. It would be important to determine carefully the effect, if any, of prolonged heating at carefully controlled temperature, on the crystalline structure, and the relation of their effect to ordinary devitrification. In one case, I was able to observe the development of the structure in a glass prepared by fusion of microcosmic salt, which was initially isotropic, by prolonged heating below the softening point. Other experiments of the same kind caused rapid devitrification, resulting in opacity. I am under the impression that to get satisfactory and reproducible results in this direction, great care would be necessary to avoid contamination with particles of impurity, and to maintain constant temperatures.

It would be important, too. to study what are the conditions for getting these glasses completely isotropic. It would not seem that this is likely to be a very tractable problem, for the occurrence of the crystalline structure is sporadic even in large scale commercial products like pyrex and corex glasses, which, one would suppose, must be made under uniform and well-controlled conditions.

An urgent problem is to determine the relation, if any, between the large scale crystalline structure here investigated, and the minute structure revealed in glasses in general by means of X-rays.* It should not be specially difficult to isolate or " dig out " pieces of silica glass or pyrex having an exceptionally strong double refraction and to examine these under X-rays, in comparison with the parts apparently isotropic. 1 have not been able to go into this, owing to lack of facilities, and preoccupation with quite other problems.

I wish to express my thanks to Lady Rücker for the loan of the large nicol prisms used, and to my assistant, Mr. R. Thompson, for efficient help in carrying out the experiments.

Summary.

The weak doubly refracting structure of a quasi-crystalline nature formerly found in pure silica glass occurs also in highly siliceous glasses down to 80 per cent. silica content. It occurs likewise in phosphatic glasses such as " corex " and in boracic glasses such as fused borax and fused boric oxide.

* Randall, Rooksby and Cooper, ' Z Kristallog.' vol 75, p 198 (1930), also ' Trans Soc Glass Technology,' vol. 14, p. 219 (1930),

On Protein Monolayers.

By A H. Hughes and E. K. Rideal, F.R.S.

(Received March 17, 1932)

[Plate 4.]

Part I.

General Characteristics and the Behaviour of Gliadin.

In recent years examination by means of the X-rays, expecially in the hands of Meyer and Mark,* and of Astbury.† and Bernal,‡ has gone far to elucidate the structure of natural proteins existing in the filamentous form. Other important natural proteins occur as membranes, which, in many cases at least, are apparently so thin that one is led to suspect that they might be true films or monolayers. It appeared desirable to attempt an examination of the properties of very thin artificially prepared protein films.

Before any attempt can be made to elucidate the structure of such layers and to compute the thickness of a film from experimental data on the weight per square centimetre and the bulk density, it is necessary to ensure both the uniformity and continuity of the film under observation. One might suppose that a true uniform protein monolayer would exist with a thickness as low as 4 A , which is the lesser dimension as determined by means of the X-rays of the cross section of a simple polypeptide chain. Further, in the compression of films of long chain hydrocarbon molecules with polar heads, transitions of state in the two dimensions are observable : vaporous, liquid and solid films being readily identified. It is improbable that such will be obtained with protein films, for with the extremely long polypeptide chain extended on the surface a vapour liquid transition would be difficult to detect. Moreover, the solid form, if such is formed, on account of the hydrophilic character of the chain, would be expected to possess properties entirely different from the solid form of the non-polar hydrocarbon chain containing molecules where we may consider that a two-dimensional microcrystalline structure results. Two methods of quantitative examination present themselves : the force area

---

* " Der Aufbau der Hochpolymeren Organischen Naturstoffe " (1930).

† ' Nature,' vol. 126, p. 913 (1930) , vol. 127, p. 663 (1930).

‡ ' Z Krystallog.,' vol. 78, p. 363 (1931).

method devised by Langmuir and applied extensively by N. K. Adam,* and the method of surface potentials developed by Schulman and Rideal.† Information on the nature and change in the packing or configuration of the surface layer is obtainable by the former, and the uniformity of the film as well as the change in configuration, involving an alteration in the magnitude of the vertical component of the electric moment of the polar groups can be investigated by the latter method

The earliest method for forming thin protein films was to allow the protein to arrive at the surface from the bulk of the liquid. Du Nouy‡ and Hercik§ have attempted to obtain quantitative estimation of the thickness of the adsorbed layer from surface tension measurements. The magnitude of the values obtained, 30-40 Å, casts some doubt on the assumptions made as to the complete removal of the protein from the bulk phase, as well as the extent of adsorption on the walls of the vessel

Wu and Ling,‖ from an examination of the rate of coagulation at the surface of solutions of proteins by shaking, concluded that the thickness of an albumen film was 34 Å. This coagulation of proteins at the interface, or the separation in a solid, insoluble or "denatured" form has been observed by numerous investigators, notably by Ramsden¶ and by Robertson,** and there can be little doubt that membranes of considerable thickness may be formed in this manner. The second method of obtaining films of the proteins consists in dispersing the protein in water or dilute alkali and dropping a small quantity on the surface of the liquid, a method employed by Devaux,†† Metcalf,‡‡ and by Keenan §§ Devaux obtained from the maximum spreading areas computed thicknesses for albumen, peptone and casein of from 30–80 Å. Metcalf obtained 30 Å as the minimum thickness of a solid film of peptone whilst Keenan obtained for gelatine on mercury at p_H 4·8 a thickness of only 7·5 Å.

Gorter and Grendel‖‖ replaced the method of computing the film thickness from the maximum spreading area by examination of the force area character-

* "The Physics and Chemistry of Surfaces" (1930)
† 'Proc. Roy. Soc.,' A, vol 130, p. 259 (1931)
‡ "Surface Equilibria of Biological and Organic Colloids" (1929).
§ 'Kolloidzschr,' vol. 56, p. 2 (1931).
‖ 'Chinese J. Physiol,' vol 1, p 407 (1927)
¶ 'Proc. Roy. Soc.,' A, vol 72, p. 156 (1903)
** "Physical Chemistry of the Proteins" (1918).
†† 'J. Physique,' vol 3 p. 450 (1904)
‡‡ 'Z. phys. Chem.,' vol. 52, p. 1 (1905)
§§ 'J. phys. Chem,' vol. 33, p 371 (1929).
‖‖ 'Proc. Acad Sci. Amst,' vol. 29, p 371 (1926), 'Biochem. Z,' vol 201 p 391 (1928).

istics of films spread in this manner on water and buffer solutions, in a Langmuir trough.   Their values for thicknesses of various proteins extrapolated to zero compression vary from 10 Å. to 300 Å., whilst gelatine appears to give still thicker films.

Their values for the limiting molecular areas for the fatty acids spread in a similar manner from dilute solutions of caustic soda are much lower than the generally accepted minimum of 20·5 Å.[2] on the same substrates (in some cases as low as 4 Å [2]).   It is reasonable to assume, as indeed was observed by these investigators, that the material initially in the form of colloidal micelles may take a long time to become homogeneous, and at the same time with some proteins, solution may take place.   The film under examination is, therefore, composite and far from homogeneous.

Zocher and Stiebel[*] have applied their technique of dark field ultra-microscopy to examine various protein films.   Serum proteins spread by Gorter and Grendel's method revealed the presence of solid films which showed inhomogeneity, whilst Spierer[†] has examined by a similar method naked films of albumen sol containing 2·5 per cent. glycerine.   Definite signs of stratification were observed, which he interprets as due to elementary lamellæ of protein micelles with a thickness of 20–30 Å.

Experimental.

Apart from objections already mentioned to the use of solutions of proteins in water or dilute caustic soda for spreading films, the possibility of actual hydrolysis of the protein renders this method unsuitable for obtaining films, and attempts were made to form them by the direct spreading of the protein. It was noticed that when a particle of solid precipitated egg albumen was placed on the surface of an aqueous solution, it spread to a thin film with great rapidity.   Examination of various proteins by this method revealed that whilst some, like keratin, would not spread at all, and others, like gelatine, spread but formed readily soluble films, a number spread uniformly to form films which were quite stable.   To examine the resultant film quantitatively, it was necessary to devise a means of weighing the minute protein particle.   This was achieved by a simple modified form of Nernst microbalance, fig. 1.

The microbalance consisted of a thin fused quartz fibre AB, about 25 cm. long, sealed with hard picene wax into a protecting glass tube.   The free end is

* ' Z. phys. Chem.,' vol. 147, p. 401 (1930).
† ' Kolloidzschr.,' vol. 55, p. 36 (1931).

Fig 6 —Egg Albumen   Collapsed film   N,100 HCl, 15° C, < 30

Fig 7 —Palmitic Acid   Collapsed film   N 100 HCl, 15° C,   30

bent at right angles and protrudes a short distance through a hole in the tube. The tube is clamped horizontally and the end of the horizontal portion of the fibre is observed against a vertical scale in the eye-piece of a microscope of magnification 10.

Two instruments were constructed with sensitivities respectively at $6 \cdot 6 \cdot 10^{-6}$ and $3 \cdot 4 \cdot 10^{-6}$ gm. per eye-piece division, legible to $0 \cdot 2$ division.

The instrument was calibrated with reference to myristic acid which spreads spontaneously to a unimolecular film. A small crystal of the acid is melted on to the tip of the quartz fibre and the scale reading of the fibre is taken. The
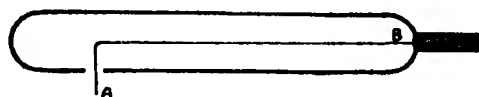
Fig. 1.

tip is then held in the surface of N/100 HCl contained in a Langmuir trough when the film is allowed to spread to a surface pressure of about $0 \cdot 5$ dyne per centimetre. The film is now compressed and both the force area curve as well as the surface potential area curve determined. Comparison with the values established on this substrate by the two methods by Adam and by Schulman and Rideal respectively, gives directly the weight of myristic acid on the surface, and this is compared with the change in deflection observed on the microscope scale.

These two independent methods of calibration gave close agreement, as is observable in the following experimental data.

Table.

Tempera-ture.	Balance, divs. x.	Film area a. sq. cm.	Surface pressure or potential.	Area/mol. A sq Å.	a/Ax.	Gm./division (a/Ax) 3 76 . 10⁻⁶
°C.						
13·0	5 6	473	0·2 dyne	48 5	1·74	6 5 . 10⁻⁶
15·5	4·8	320	250 mv.	38·0	1 75	6·6 . 10⁻⁶

In spreading the protein the tip of the fibre is first coated with paraffin wax (m.p. *ca.* 25° C.), then dipped into the protein ; surplus protein blown away and the deflection recorded. It was found advisable to use small quantities of protein, for with large amounts on the fibre, results were sometimes obtained showing deviations which could only be interpreted as due to minute particles

of protein which had spread too rapidly, becoming embedded in the remainder of the film and failing to reach equilibrium in the duration of the experiment.

The surface pressures of the films so obtained were measured with a Langmuir trough of Adam's type having a single torsion wire and reading to 0·2 dyne per centimetre, whilst the surface potentials were measured with an apparatus of the type described by Schulman and Rideal, modified in respect to the polonium coated wire which serves as an air electrode. Originally this electrode was fixed over the surface of the liquid; but in the apparatus used in these experiments it was attached to an arm which moved over a plate parallel to the surface of the liquid By this means the surface potential over the whole area of the liquid can be explored, and the homogeneity of the film tested.

Preliminary experiments revealed the fact that the proteins gliadin, glutenin and egg albumen spread spontaneously on N/100 HCl at 20° C., glutenin more slowly than the other two. The film at first was perfectly fluid, but as more protein is added the rate of spreading decreases and equilibrium is finally reached with a definitely solid film. These solid films are quite different in character from those of the long chain aliphatic substances such as palmitic acid. They exhibit a peculiar gelatinous appearance and are remarkable both for their compressibility and elasticity. These gelatinous films appear, in respect to their mechanical properties at least, to be the two-dimensional analogue of the three-dimensional rigid elastic systems usually termed gels as formed by gelatine and water, and provisionally we may refer to this type of film as a gel. There is no sharp boundary between the liquid and gelatinous film. Some observations made on the two-dimensional sol-gel transformation as effected by pressure will be given later.

Some points of interest are presented by a study of the collapse of these films under high compression, by means of the dark-field ultramicroscope of Zocher and Stiebel.* These workers have described the various characteristic phenomena of collapse in films of various types, including those of long chain aliphatic compounds and those of serum albumen and globulin, casein and hæmoglobin. These proteins were spread by the method of Gorter and Grendel, and while the latter two on N/10 HCl gave completely homogeneous films, for the serum proteins it was difficult to decide whether the films were truly homogeneous.

The protein films here examined (gliadin, egg albumen and glutenin), spread directly from the solid, appeared clear under the microscope, apart from the

---

* ' Z. phys. Chem.,' A, vol. 147, p. 401 (1930).

usual dust specks which it seems impossible to eliminate. This, however, is not in itself evidence of homogeneity. A "point structure" of colloidal particles such as is seen clearly on compression of a film of, say, myristic acid, might well exist in the case of the protein and yet remain invisible on account of the small difference in refractive index between a highly solvated protein particle and the substrate.

The accompanying microphotographs illustrate the difference in structure of a film of a typical long chain aliphatic compound (palmitic acid) and of a protein film (egg albumen), as shown by the collapse under high compression

The photographs, figs. 6 and 7, Plate 4, are of a film which has been compressed until definite strain lines appeared under the microscope and then slightly expanded. The very long folds visible in the case of egg albumen are typical of the protein films examined, and retain their longitudinal continuity on expansion, being only partially reversible   The lines appearing in the case of palmitic acid (in both cases the lines are perpendicular to the direction of compression) are formed by the aggregation of a "point structure" and on expansion break up, fig. 7, Plate 4, revealing their microcrystalline character.

The Behaviour of Gliadin.

Gliadin was chosen as the first protein for investigation, for not only does it spread readily and smoothly, but it yields relatively simple products on hydrolysis, revealing as much as 44 per cent. of glutamic acid and some 13 per cent. of proline, a fact of great assistance in the analysis of the results.

We are indebted to Dr. Fisher, of the Flour Millers' Research Association, for a sample of gliadin, the method of extraction performed by Dr. Halton being as follows.

Flour gluten was extracted several times with 70 per cent. alcohol so as to remove the larger part of the gliadin.   It was then stirred into $0 \cdot 2$ per cent. potassium hydroxide solution and the protein precipitated from the solution by neutralisation with caustic potash.   The precipitated protein was then extracted with 70 per cent. alcohol and the process repeated on the gluten several times.   The gliadin obtained in this way was unaffected by contact with the alkali, for samples obtained by simple extraction and by this method possessed the same optical rotation.

The alcoholic solution of gliadin was evaporated under reduced pressure to remove the alcohol and the concentrated solution was poured into distilled water containing 10 gm. per litre of sodium chloride.   The separated gliadin

was washed with distilled water and dissolved in 70 per cent. alcohol. The alcoholic solution was filtered, concentrated by evaporation under reduced pressure and again poured into 1 per cent. sodium chloride solution. The gliadin was redissolved in 70 per cent. alcohol, the solution concentrated and poured into absolute alcohol. The separated gliadin was dissolved in 70 per cent. alcohol, the solution concentrated and the gliadin precipitated by pouring into a mixture of alcohol and ether. The gliadin was finally washed with absolute alcohol and then ether. The isoelectric point of gliadin is given by Tague as p_H 6·5,[*] and more recently by Kondo and Hayashi,[†] to be between p_H 6·41–6·59 and the molecular weight from analysis and from its combining capacity is given by Cohn[‡] to be 20,700; presumably it is to be classified with Svedberg's first group of true proteins (MW 34,500) The moisture content was determined by the method recommended by Astbury and by Denham, namely, drying in dry air at 110° C. until of constant weight. The analytical data are given below : —

Weight taken . .	0·2505 gm.
Final loss of weight	0·0265 gm.
Per cent. moisture	10·6

The protein was spread on three substrates N/100 HCl, N/100 NaOH and a phosphate buffer of p_H 5·9, prepared according to the directions of Clark[§] with an M/15 mixture of KH_2PO_4 and Na_2HPO_4

The rate of spreading on the buffer solution was found to be slower than on either of the two former solutions.

The compressibility curves on these substrates are shown in fig. 2, where F, the force in dynes per centimetre, is plotted against γ, the weight of dry protein in grams per cm.² This procedure avoids any questionable assumptions as to either the molecular weight or density of the protein in the surface film.

Compressibility Curves.

For comparison, curves are included derived from the experimental data of Gorter and Grendel for gliadin on N/100 and N/10 HCl, obtained by the spreading from an aqueous dispersion of the protein. The probable lack of homogeneity in films of this character has already been mentioned. The

* ' J. Amer. Chem. Soc.,' vol. 47, p. 418 (1925).

† ' Mem. Coll. Agric. Kyoto Imp. Univ.,' vol. 11, p. 1 (1931).

‡ ' Phys. Rev.,' vol. 5, p. 377 (1925).

§ " The Determination of Hydrogen Ions," p. 203, 3rd Edn.

presence of protein in the system in any other form than that of the monolayer (either in bulk solution or as unspread colloidal micelle), will cause the observed values of the surface pressure to be proportionately smaller for a given estimated weight per square centimetre of protein. This is the probable explanation of the deviations observed along the curves shown.

The results here obtained show that a surface pressure ($0 \cdot 2$ dyne/cm.) is first noticed with $\gamma = 0 \cdot 36 . 10^{-7}$ gm./sq. cm., while the slope of the curve increases to a maximum at $0 \cdot 7 \quad 10^{-7}$ gm./sq. cm. under a pressure of 2 dynes/cm. This slope is maintained up to about 13 dynes/cm. and $\gamma = 1 \cdot 6 . 10^{-7}$ gm./ sq. cm. By rapid compression the linear increase continued to still higher pressures, up to 22 dynes/cm and $\gamma = 2 \cdot 4 . 10^{-7}$ gm./sq. cm.; but over this latter range the film is definitely metastable and the pressures show a slow decrease to a more stable value. The film becomes gelatinous from about $\gamma = 1 \cdot 6 - 1 \cdot 8 . 10^{-7}$ gm./sq. cm. under a pressure of about 15 dynes/cm. The final equilibrium pressure is reached at about 22 dynes/cm. The equilibrium pressure, obtained by placing excess of protein on the surface, is, however, only about 16 dynes/cm , so that the surface spreading pressure of the substance is sufficient for it just to reach the gelatinous form but not enough to cause any compression of the gel It is doubtful whether the equilibrium spreading pressure of 16 dynes/cm. is strictly comparable to the values obtained for the crystal equilibrium pressures of, say, the fatty acids, for in the case of the protein the small particles not only undergo surface solution but also imbibe water after equilibrium is attained with the film. A comparison must be sought with a swelling or imbition pressure rather than with a surface solubility. This process of imbition can be followed in the dark field ultramicroscope, as the change in the refractive index of the particle during the process is quite marked

On the dilute caustic soda solution, a similar curve is obtained, but the change to a gel occurs at a lower pressure range than on the acid substrate, namely from 13–15 dynes whilst the linear relation holds over a longer range of pressure, up to about 30 dynes/cm. in the metastable film, falling to a limit pressure of about 27 dynes/cm. on waiting

On the phosphate buffer solution, the rate of spreading of the protein is slower. No sensible pressure is reached until γ reaches about $0 \cdot 6 . 10^{-7}$ gm./sq. cm. and the initial portion of smaller slope has nearly vanished. From $0 \cdot 7 . 10^{-7}$ to $3 \cdot 0 . 10^{-7}$ gm./cm.^{2} a straight line is obtained with the same slope as for the curve on caustic soda, but less than the slope on the acid substrate. Gelation takes place at a noticeably lower pressure, 12–14 dynes from

$\gamma = 1 \cdot 4 - 1 \cdot 8 \cdot 10^{-7}$ gm./cm.^{2}. The pressure in the metastable region of the film may rise to 35 dynes or more by rapid compression but the final equilibrium pressure is about 26 dynes.

The values obtained for the change in surface potential (ΔV) caused by the presence of films of the protein on the various substrates are also shown in the curves, fig. 2. As abscissæ the values of γ in gm./cm.^{2} are given as in the compressibility curves, together with the approximate mean thickness of the film based upon a density of $1 \cdot 33$ for the protein.
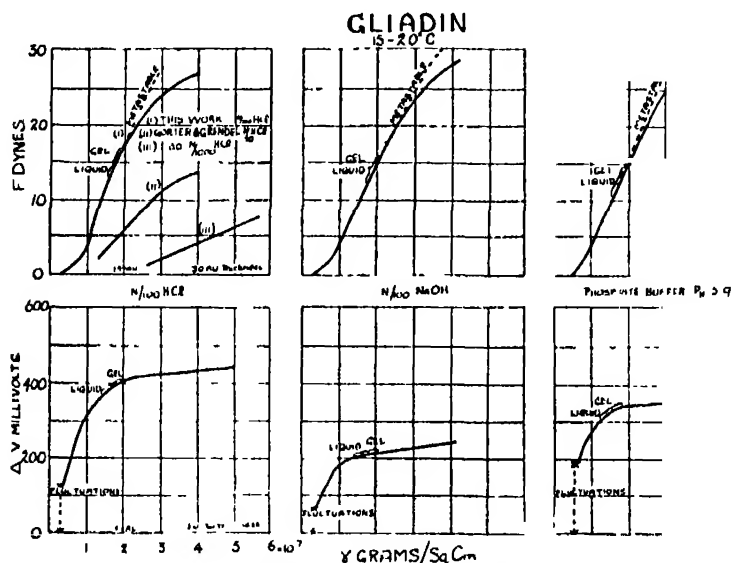
FIG. 2.—Potential γ curves.

On the acid substrate, fluctuating values for the surface potential are obtained, indicative of a non-uniform film until γ reaches $0 \cdot 36 \cdot 10^{-7}$ gm./sq. cm. with a surface potential change of $\Delta V = 130$ mv. Further compression gives a linear increase of potential up to about 250 mv. and $0 \cdot 7 \cdot 10^{-7}$ gm./sq. cm., the film still being perfectly fluid.

The slope of the curve then gradually decreases and gelation sets in, the potential tending slowly to a maximum value of some 450 mv. with γ rising to over $5 \cdot 10^{-7}$ gm./sq. cm.

The linear portion of the curve is reversible on expansion, but above this region expansion produces a fall of potential below the compression curve. On waiting the potential rises more or less to its original value according to the extent of the compression of the film into the gelatinous region and the time

that it has been left in that region—the higher the pressure and the larger the interval before expansion the less the recovery of the potential.

On the alkaline substrate the values of the surface potentials and also the slope of the curve are considerably smaller than on the acid. Fluctuating potentials are obtained up to 75 mv., again ceasing at about $0.36 . 10^{-7}$ gm./cm.^{2}. On compression a steady reversible linear graph is obtained up to 160 mv. and $\gamma = 0.7 . 10^{-7}$ gm./cm^2. The curve then bends away as before to a limit value of some 240 mv. at 4.0–$5.0 . 10^{-7}$ gm./sq. cm. Gelation sets in from $\gamma = 1.6$–$2.0 . 10^{-7}$ gm /sq. cm.

On the phosphate buffer, as usual at low values for γ, fluctuating potentials are obtained but they extend to a larger weight per square centimetre— $0.6 . 10^{-7}$ gm./sq. cm at 190 mv.—than in either of the previous cases, the uniform film obtained on the other substrates from $\gamma = 0.36 . 10^{-7}$ being absent up to $\gamma = 0.60 . 10^{-7}$ gm./sq. cm.

On compression, the value of ΔV rapidly attains a maximum. The film gelatinises, at a lower surface pressure than on the other substrates, over the range $\gamma = 1.5$–$1.7 . 10^{-7}$ at about 320 mv and reaches a final limit value of 360 mv. With the buffer not only is the rate of surface solution slow, but there is definite indication that there is less tendency to expansion of the film. The mutual cohesion of the polypeptide chains has in this case, near the isoelectric point, a greater influence on the character of the film than the adhesion to the surface, which has been reduced to a minimum.

Discussion of the Results

Both on N/100 HCl and on N/100 NaOH definitely homogeneous films of gliadin can be obtained with a surface concentration as low as $0.36 . 10^{-7}$ gm./sq. cm. of surface or about 3 Å. in thickness. In this state it gives rise to an increase of the air/liquid surface potential of some 130 mv. on N/100 HCl and 70 mv. on N/100 NaOH, the value altering with the nature of the substrate. At approximately the same surface concentration as that at which we obtain a uniform protein film over the whole surface, we obtain, as would be expected by the closing up of the film, the first noticeable film pressure— a pressure of more than 0.2 dyne/cm., the limit of sensitivity of the apparatus.

If a truly molecularly dispersed " vapour " film exists at all, its vapour pressure must be extremely small.

In the range 0.36–$0.7 . 10^{-7}$ gm./sq. cm. on the acid and on the alkaline substrate we observe a sharp linear increase in potential, but the concomitant

pressures are small. The film is readily compressible up to $2 \cdot 0$ dynes/cm. on the acid and to $1 \cdot 5$ dynes/cm. on the alkali, as shown by the initial portion of lesser slope. The electric moment per gram as measured by $d\Delta V/d\gamma$ is approximately constant. Beyond this range we are dealing with a somewhat different type of film in which a change is occurring in the polar groups, for $d\Delta V/d\gamma$ begins to decrease steadily, indicating a fall in the vertical component of the electric moment. At the same time the pressure increases sharply in a linear manner up to the point where the interesting phenomenon of gelation sets in, about $\gamma = 1 \cdot 5 \,.\, 10^{-7}$ gm./sq. cm. (approximate film thickness 11–12 A.U.). Above this region the rise of pressure becomes dependent on the rate of compression of the film. Rapid compression gives a continuation of the linear pressure increase, but the pressure will fall away slightly to a stable value which is obtainable on slower compression of the film.

If we assume for gliadin the general type of chain suggested by Fischer, we may suppose the probable fundamental structure of the protein to be constituted of a reduplicated basic unit :—

$$\begin{array}{ccc} & \text{H} & \\ & \text{--N--} & \text{H} \\ \diagdown\text{C} & & {\diagup}\atop{\text{C}} \\ \| & & \text{R} \\ \text{O} & & \end{array}$$
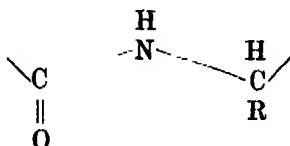
where the side chain R differs along the primary chain and gives rise on hydrolysis of the protein to different amino-acids. We have seen that gliadin yields on hydrolysis about 44 per cent. glutamic acid, 13 per cent. proline and about 10 per cent amino acids where R is definitely non-polar. Whether the pyrrolidine nucleus exists as such in the protein, or is formed by subsequent condensation on hydrolysis is uncertain. We may provisionally regard the side chains of gliadin as consisting largely of the glutamyl residue $-CH_2 -CH_2$ $-COOH$ with its free carboxyl group, alternating now and then with the non-polar group $-CH_2 -CH_2 -CH_3$. There are smaller quantities of side chains such as lysyl and arginyl, containing the $-NH_2$ group. A review of the hydrolysis products shows moreover that the mean length of side chain is three carbon atoms, with free acid groups preponderating over the combined non-polar and basic groups.

It is reasonable to suppose that in a film the position of minimum potential energy will be found when the whole structure is lying flat on the surface, the main anchorage being provided by the strongly polar free $-COOH$ and $-NH_2$ groups, and to a lesser extent by the $-CO -NH-$ peptide unions. The

relatively non-polar side chains will also lie flat on the surface if given oppor-
tunity.

We thus obtain as our first picture fig. 3, that of the fully " expanded "
protein.

It is at this point that a surface pressure will first be obtained due to the
contact of the side chains of neighbouring primary chains. From the mass of
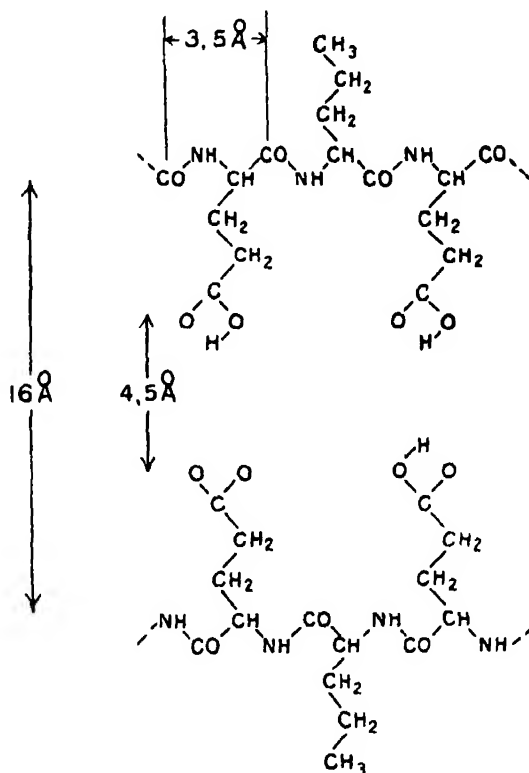
FIG. 3.—Gliadin, State I, Expanded Film

the basic unit —CO —NH —CHR— and its known dimensions, we can calcu-
late to what value of γ such a structure corresponds.

Thus, if we consider the maximum and minimum mass corresponding to a
side chain of three carbon atoms, we have

$$\text{(i) } R = -CH_2 -CH_2 -COOH, \quad CO . NH . CHR = 129$$
$$\text{(ii) } R = -CH_2 -CH_2 -CH_3, \quad CO . NH . CHR = 99$$

Referring to fig. 3, the area per unit $CO . NH . CHR$ is 16×3.5 sq. A. These

values are obtained from the X-ray data of Meyer and Mark (*loc. cit.*), who give $3 \cdot 5$ A. for the spacing

$$\text{CO}\diagdown_{\text{NH}}\diagup^{\text{CHR}}\diagdown_{\text{CO}}$$

$$3 \cdot 5$$
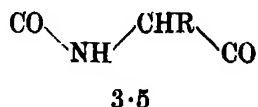
along a polypeptide chain, together with the value $2 \cdot 54$ A. for a hydrocarbon zig-zag. The minimum closeness of approach of the side chains in this state is taken as $4 \cdot 5$ A. provisionally, being based upon an extrapolation from the X-ray data on the crystalline fatty acids

Calculating γ in gm./sq. cm. for this packing, we have

$$\gamma = \frac{129}{6 \cdot 06 \quad 10^{23} \times 16 \times 3 \cdot 5 \times 10^{-16}} = \underline{0 \cdot 38 \cdot 10^{-7}} \text{ gm./sq. cm.} \quad R = 129,$$

or

$$\frac{99}{6 \cdot 06 \cdot 10^{23} \times 16 \times 3 \cdot 5 \times 10^{-16}} = \underline{0 \cdot 29 \cdot 10^{-7}} \text{ gm./sq. cm} \quad R = 99.$$

These extreme values dependent on the nature of the side chain are in agreement with the observed point at which we first obtain a homogeneous film on acid and on alkali, namely, $0 \cdot 36 \cdot 10^{-7}$ gm./cm.^{2}.

The surface potential can be expressed in the form

$$\Delta V = 4\pi n\mu + \Delta V_u,$$

where n is the number of dipoles per square centimetre of vertical component μ, and ΔV_u is the change of potential in the surface of the substrate due to the presence of the film.

The chief sources of potential in the film itself are the dipoles of the free —COOH and —NH$_2$ groups, and presumably of the peptide linkages —CO —NH—, but it is clearly impossible as yet to assign definite respective values to these groups. The sign of ΔV for the proteins is, however, the same as for a film of a fatty acid or an amine. The values of $d\Delta V/d\gamma$ which are proportional to the electric moment per gram of gliadin in the film can be expressed in terms of the moment per —CO . NH . CHR protein unit. The values of this moment, together with the values of ΔV_u are given in the following table, and refer to the liquid " expanded " film, where the moment remains constant. The mean value is taken of the two cases where R is —CH$_2$CH$_2$COOH or CH$_2$CH$_2$CH$_3$.

The order of magnitude of the derived moment per unit is that of the —COOH group in the liquid condensed films of myristic or palmitic acids $(1 \cdot 6 \cdot 10^{-19}$

Substrate	$\dfrac{d\varDelta V}{d\gamma}$	Dipole moment per CO . NH . CHR e.s.u. $\times 10^{18}$.	$\varDelta V$, in milliv
N/100 HCl	320	1·6	15
N/100 NaOH	230	1·2	—20
Phosphate buffer p_H 5 9	280	1 4	— 5

e.s.u.). It is of interest that an acidic group is giving a marked contribution to the resulting moment of the protein in view of the reduction of the moment on the alkaline substrate.

On compression of the " expanded " protein film, fig. 3, we might anticipate that the primary chains would close in laterally as far as possible, giving a

FIG. 4.—Gliadin, State II, Condensed Film.

close packed film in state II, fig. 4, with the side chains still lying flat on the surface.

The value of γ corresponding to this packing may be calculated as before and gives $\gamma = 0·74 . 10^{-7}$ and $0·56 . 10^{-7}$ gm./cm.^{2} for the probable side chains considered in the previous case. These values agree very well with the observed point about $0·7 . 10^{-7}$ gm./cm.^{2} where the slope on the F/γ curves reaches a maximum, and the linear portion on the $\varDelta V$, γ curves of constant moment ($\mu =$ constant) ceases.

Compression beyond this point must mean some drastic alteration in the film structure, since it is now a close packed monolayer. We find indeed that compression gives us a noteworthy change in the $\Delta V/\gamma$ graph, while it is in the same region that we observe gelation of the film, hitherto perfectly mobile. On the hypothesis outlined above, the most likely occurrence will be the tilting of the side chains out of the surface. Whether they tilt above into the air or below into the liquid will be decided by the stereochemical considerations as well as by the nature of the side chain, those terminating in polar heads tilting downwards and non-polar chains upwards. We have indeed found that the air exposed surfaces of gels formed in this manner possess hydrophobic characteristics, an account of which will be given later. In no case is an impossible expenditure of work called for in view of the very rapid rise in the surface pressure at this juncture.

Thus we finally reach the third type of film.
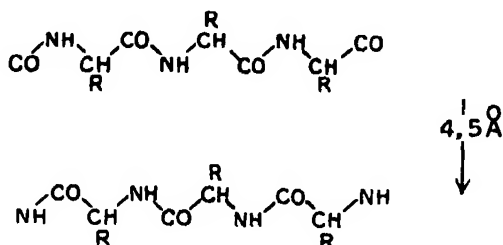
Fig 5.—Gliadin, State III, Gel Film.

This is still a monolayer with respect to the primary peptide chains, but with a much larger mean thickness than the first two states, namely, about 12 A.

We might anticipate that such a film would exhibit rigidity due not only to the mutual attraction of the primary peptide chains which are in close proximity, but also from the adhesion of the now vertically close-packed carbon side chains.

If we suppose that the interval between adjacent polypeptide chains in the surface is of the order of $4 \cdot 5$ A in this third type of film, a reasonable supposition on the basis of the X-ray data, then the corresponding value of γ calculated as before lies between $1 \cdot 35$ and $1 \cdot 03 \times 10^{-7}$ gm /cm.^{2} according to the nature of the side chain. The formation of the gelatinous film as observed by the motion of talc on the surface sets in at about $1 \cdot 5 \times 10^{-7}$ gm./cm.^{2}.

How far it is possible for the primary peptide chains to approach closer than about $4 \cdot 5$ A., still retaining the monolayer, it is difficult to say. Further compression of the solid film may cause rupture, in the form of long folds as observed in the dark field ultramicroscope. It is, however, conceivable that

we may be causing further interaction between adjacent peptide groups with the formation even of chemical linkage by secondary valencies.

Thus we observe that once this compact film has been formed and maintained under compression for a time, the film becomes definitely irreversible on expansion with respect both to surface potential and to pressure. This phenomenon may be akin to the phenomenon of denaturation, but there is no reason to suppose, as do some writers, that all protein films are *ipso facto* " denatured," although we see here that some definite process of association occurs on maintaining the film under compression.

Summary.

(1) A general review is given of methods hitherto employed in the production and examination of thin films of proteins at liquid surfaces

(2) It is shown that films obtained by these methods are probably inhomogeneous

(3) A new method is described in which the film is spread directly from the solid protein on to the surface. The weight of protein in the film thus produced is measured on a simple micro-balance (with an error of $1 \cdot 5$ per cent. on 10^{-4} gm.).

(4) These films have been examined quantitatively by the methods of surface pressures and of surface potentials, and qualitatively by means of the dark field ultramicroscope.

(5) It is shown that for gliadin, the first protein studied in detail, homogeneous films can be obtained with a thickness as low as 3 A. Compression of the film is accompanied by a change from a liquid film to a gelatinous film, and this transition is reflected in the electrical as well as the mechanical properties of the film. The films have been examined on N/100 HCl, N/100 NaOH and on a phosphate buffer, p_H $5 \cdot 9$.

(6) In the light of recent X-ray data on proteins and allied compounds it is possible to assign a general structure to the protein film in its various stages of compression, on the supposition that the basic polypeptide chains of the protein are stretched out flat on the surface of the liquid in the most expanded state of the film. On compression, the side-chains to the main polypeptide chain are forced out of the surface, this change being associated with the gelation of the film The observed values of the weight of protein per square centimetre of surface agree well with those calculated from the known dimensions of a —CO—NH—CHR— polypeptide unit.

An Alternative to the Rejection of Observations.

By HAROLD JEFFREYS, M.A., D.Sc., F.R.S., Reader in Geophysics, University of Cambridge.

1. It is widely felt that any method of rejecting observations with large deviations from the mean is open to some suspicion. Suppose that by some criterion, such as Peirce's and Chauvenet's,[*] we decide to reject observations with deviations greater than $4\,\sigma$, where σ is the standard error, computed from the standard deviation by the usual rule, then we reject an observation deviating by $4\cdot5\,\sigma$, and thereby alter the mean by about $4\cdot5\,\sigma/n$, where n is the number of observations, and at the same time we reduce the computed standard error. This may lead to the rejection of another observation deviating from the original mean by less than $4\,\sigma$, and if the process is repeated the mean may be shifted so much as to lead to doubt as to whether it is really sufficiently representative of the observations

In many cases, where we suspect that some abnormal cause has affected a fraction of the observations, there is a legitimate doubt as to whether it has affected a particular observation. Suppose that we have 50 observations. Then there is an even chance, according to the normal law, of a deviation exceeding $2\cdot33\,\sigma$. But a deviation of $3\,\sigma$ or more is not impossible, and if we make a mistake in rejecting it the mean of the remainder is not the most probable value. On the other hand, an observation deviating by only $2\,\sigma$ may be affected by an abnormal cause of error, and then we should err in retaining it, even though no existing rule will instruct us to reject such an observation. It seems clear that the probability that a given observation has been affected by an abnormal cause of error is a continuous function of the deviation; it is never certain or impossible that it has been so affected, and a process that completely rejects certain observations, while retaining with full weight others with comparable deviations, possibly in the opposite direction, is unsatisfactory in principle.

2. The question has arisen in the treatment of seismological observations,[†] though it is obviously of much wider application. The time of arrival of a given wave may normally have a standard error of order 7 seconds, arising

---

[*] Chauvenet, " Spherical and Practical Astronomy," vol. 2, pp. 558–566 (1863).

[†] Jeffreys, ' Mon. Not. R. Astr. Soc.,' Geophys. Suppl. 2, p. 329 (1931).

from the combination of several known causes, but about a fifth of the observations are affected by an uncertainty of the order of 20 seconds, arising in most cases from the difficulty of identifying the exact beginning of a phase when microseisms are present.

The distribution of the probability of error is therefore taken to be

$$f(x_r) = (1 - m) \frac{h}{\sqrt{\pi}} e^{-h^2 (x_r - x)^2} + m \frac{k}{\sqrt{\pi}} e^{-k^2 (x_r - x - y)^2}. \tag{1}$$

This expresses the conditions (1) that if x is the true value the probability, given x, that an observation will lie between x_r and $x_r + dx_r$ is $f(x_r) dx_r$; (2) the probability that an observation will be affected by the abnormal error is m, (3) the normal observations follow a normal law with modulus of precision h; (4) the abnormal ones follow another normal law with modulus k, but are subject also to an unknown systematic error y. Our problem is to find the most probable value of x, and incidentally y, from a given set of observed values $x_1, x_2, \ldots, x_n$.

2.1. Suppose first that h, k and m are already known from previous work on data of the same type. Then the probability, for given x and y, of obtaining the observed values is proportional to

$$\prod_{r=1}^{n} f(x_r) = f(x_1) f(x_2) \ldots f(x_n), \tag{2}$$

and, by the principle of inverse probability, the probability that x, y lie in ranges of lengths dx, dy is proportional to

$$P(x, y) \prod f(x_r) \, dx \, dy, \tag{3}$$

where $P(x, y) \, dx \, dy$ is the prior probability that x and y are in these ranges. In most practical cases this prior probability is uniformly distributed, and therefore $P(x, y)$ can be treated as constant. The most probable values of x and y are therefore given by the two equations

$$\Sigma \frac{\partial f(x_r)/\partial x}{f(x_r)} = 0; \quad \Sigma \frac{\partial f(x_r)/\partial y}{f(x_r)} = 0. \tag{4}$$

Carrying out the differentiations and simplifying, we obtain

$$\Sigma v_r (x_r - x) = 0; \quad \Sigma w_r (x_r - x - y) = 0, \tag{5}$$

where

$$v_r^{-1} = 1 + \{mk/(1 - m) h\} \exp \{h^2 (x_r - x)^2 - k^2 (x_r - x - y)^2\}, \tag{6}$$

$$w_r^{-1} = 1 + \{(1 - m) h/mk\} \exp \{k^2 (x_r - x - y)^2 - h^2 (x_r - x)^2\}, \tag{7}$$

$$v_r + w_r = 1. \tag{8}$$

Evidently (5) reduce x and $x + y$ to weighted means of the observed values, the weights being continuous functions, as we expected. If either m or k is zero, the most probable value of x is the arithmetic mean, while y is indeterminate. This was to be expected, since m zero means that the abnormal source of error is known to be absent; while k zero, with m finite, means that the abnormal errors are expected to be indefinitely widely distributed, so that the number of them within any finite range is negligible. Again, for $x_r - x$ small, the second term in v_r^{-1} is a small fraction, and the weight v_r is nearly 1; but when $x_r - x$ is large this term is exponentially large, and the weight is insignificant. Hence the large deviations have small weight in the determination of x. On the other hand, it is the small deviations that have small weight in the determination of $x + y$.

The actual solution of (5) will be carried out by successive approximation. The maximum frequency of the observed values, or a rough mean of the central values, may be taken as a trial value of x, and y in the first instance neglected in the exponents. Thus we get preliminary weights v_r and w_r, and can derive weighted means for x and $x + y$. Substituting these in the exponents, we obtain a revised set of weights and new means; we then repeat the process until the numerical values repeat themselves.

2.11. Given (3), the probability that x lies in a given short range is proportional to

$$F(x) = \int_{-\infty}^{\infty} \Pi f(x_r) \, dy. \tag{9}$$

This could be evaluated in finite terms, the integrand being a linear combination of exponentials, but the number of terms would be large. But we can obtain a compact approximation, when n is large, by putting

$$\log f(x_r) = g(x_r). \tag{10}$$

We denote the values of x and y obtained as the most probable by x_0 and y_0. Then provided $x - x_0$ and $y - y_0$ are not too great, we can write

$$\log \Pi f(x_r) = \Sigma g_0(x_0) + \Sigma \left\{ (x - x_0) \frac{\partial g(x_r)}{\partial x} + (y - y_0) \frac{\partial g(x_r)}{\partial y} \right\}$$
$$- \{A (x - x_0)^2 + 2B (x - x_0)(y - y_0) + C(y - y_0)^2\}. \tag{11}$$

The first term does not involve x and y and is therefore irrelevant, since we need consider only ratios of probabilities of different values. The second vanishes by (4) since the partial derivatives are evaluated at x_0, y_0; while

A, B, C are half the second derivatives of $\Sigma g\,(x_r)$ with their signs changed. Then F (x) is proportional to

$$\int_{-\infty}^{\infty} \exp\left[-\left\{A\,(x-x_0)^2 + 2B\,(x-x_0)\,(y-y_0) + C\,(y-y_0)^2\right\}\right] dy$$
$$= \sqrt{\left(\frac{\pi}{C}\right)} \exp\left\{-\left(A - \frac{B^2}{C}\right)(x-x_0)^2\right\}, \quad (12)$$

and the probability of the true values of x is distributed about x_0 with a modulus of precision $(A - B^2/C)^{\frac{1}{2}}$.

Now we see that

$$-\tfrac{1}{2}\Sigma\,\frac{\partial g\,(x_r)}{\partial x} = h^2\Sigma v_r\,(x_r - x) + k^2\Sigma w_r\,(x_r - x - y) \quad (13)$$

$$-\tfrac{1}{2}\Sigma\,\frac{\partial g\,(x_r)}{\partial y} = k^2\Sigma w_r\,(x_r - x - y), \quad (14)$$

and the second term in (13) makes a contribution to A equal to B. Again, the observations that make important contributions to (14) have w_r nearly 1, and hence nearly

$$B = C = k^2\Sigma w_r\,; \quad A = h^2\Sigma v_r + B, \quad (15)$$

$$A - B^2/C = h^2\Sigma v_r \quad (16)$$

Thus the modulus of precision for x is nearly $h\,(\Sigma v_r)^{\frac{1}{2}}$, which is less in the ratio $(\Sigma v_r/n)^{\frac{1}{2}}$ than for the mean of n observations derived from a pure normal law. This estimate is, of course, an approximation, but it serves to show that in ordinary cases the values obtained are not much less precise than the arithmetic mean is when the normal law holds.

2.12. As a specimen of the method, let us consider the residuals of the times of arrival of the P wave at distances near $67\cdot5°$. They are given to the nearest number of seconds of the form $5s + 2$, where s is an integer, positive or negative. We take $h = 0\cdot10$, corresponding to a standard deviation of $7\cdot1$ seconds; $k = 0\cdot02$, $m/(1-m) = 0\cdot1$. Our first trial values are $x = +2$ seconds, $y = 0$ The resulting values of v_r and w_r are computed and given in the third and fourth columns. The resulting weighted means are $x = +2\cdot94$, $x + y = +5\cdot7$. A new set of weights was then computed with $x = +3$, $x + y = 6$; they are given in the fifth and sixth columns. The resulting means are $x = +3\cdot03$, $x + y = +4\cdot8$. It is evident that further approximation will not change x appreciably. The value obtained in an earlier paper was $x = +3\cdot2$, on the hypothesis that abnormal observations were equally probable in all groups, so that $k = 0$, $m = \infty$, but mk was finite.

Residual.	Number of observations.	First solution.		Second solution.	
		v_r	w_r	v_{r}	w_{r}
−38	2	0 00	1 00	0 00	1·00
−33	0	0 00	1 00	0 00	1·00
−28	1	0 01	0 99	0 01	0·99
- 23	1	0·11	0 89	0 07	0·93
−18	1	0·52	0 48	0 43	0 57
−13	2	0 85	0·15	0·82	0·18
− 8	10	0 95	0 05	0 94	0 06
− 3	32	0 97	0 03	0 97	0 03
+ 2	68	0 98	0 02	0 98	0 02
+ 7	37	0 97	0 03	0 98	0 02
+12	14	0 95	0 05	0 95	0 05
+17	6	0·85	0 15	0 88	0 12
+22	5	0 52	0 48	0 58	0 42
+27	1	0 11	0 89	0 14	0 86
+32	3	0 01	0 99	0 01	0 99
+37	1	0 00	1 00	0 00	1 00

3. The foregoing method is correct when h, k and m are known already, as from an analysis of a larger number of observations of the same type. If these quantities also are to be found from the observations under discussion, (3) must be replaced by the statement that the probability, given the observed values, that x, y, h, k, m lie in given ranges of extent dx, dy, dh, dk, dm is proportional to

$$P(x, y, h, k, m)\, dx\, dy\, dh\, dk\, dm\; \Pi f(x_r), \tag{17}$$

where P expresses the prior probability that x, y, h, k, m lie in these ranges. As a rule the prior probability is uniformly distributed with regard to x and y; but h and k are restricted to be positive, and m to lie between 0 and 1. There is reason for saying that in these circumstances* P is proportional to $1/h$ and $1/k$. The variation of P with m rests on the same kind of conditions as for the prior probabilities of different compositions of a complete class in the theory of sampling; if we follow Laplace we should take it independent of m, but in any case its form makes little difference to the final result if the number of observations is large, and we are satisfied that m is not exactly 0 or 1.† Hence we take P proportional to $1/hk$. As before, we replace $\log f(x_r)$ by $g(x_r)$ and say that the most probable values of the five unknowns are obtained by making $\Sigma g(x_r) - \log(hk)$ stationary. Then we have again

$$\Sigma v_r (x_r - x) = 0 \tag{18}$$

$$\Sigma w_r (x_r - x - y) = 0, \tag{19}$$

* Jeffreys, "Scientific Inference," p. 67 (1931).

† Jeffreys, *loc. cit.*, pp. 33, 191; J. B. S. Haldane, 'Proc. Camb. Phil. Soc.,' vol. 28, p. 55 (1932).

and also

$$\Sigma v_r \{1 - 2h^2 (x_r - x)^2\} - 1 = 0 \qquad (20)$$

$$\Sigma w_r \{1 - 2k^2 (x_r - x - y)^2\} - 1 = 0, \qquad (21)$$

while the equation for m is

$$\Sigma \frac{h \exp\{-h^2 (x_r - x)^2\} - k \exp\{-k^2 (x_r - x - y)^2\}}{(1 - m) h \exp\{-h^2 (x_r - x)^2\} + mk \exp\{-k^2 (x_r - x - y)^2\}} = 0 \qquad (22)$$

which can be written in the forms

$$\frac{m}{1 - m} = \frac{\Sigma w_r}{\Sigma v_r}; \qquad m = \frac{\Sigma w_r}{n}. \qquad (23)$$

To apply this method we first choose a value of h that will represent the central groups approximately. With $x = +2$, $h = 0 \cdot 15$, it is found that we obtain a fair representation of the groups from -13 to $+17$. In the 9 groups outside this range there are 15 observations. There are 16 groups in all, which may therefore be estimated to contain at least 27 abnormal observations. The total number of observations is 184, and we therefore estimate $m = 0 \cdot 15$. We now consider the observations outside the range -13 to $+17$, determine the sum of their squares and divide by 27 to obtain a rough standard deviation for the abnormal observations; this proves to be 21 seconds, implying $k = 0 \cdot 034$. This is probably an underestimate. Then $mk/(1 - m) h = 0 \cdot 04$. We denote this function by μ.

The left sides of the equations (18) to (21) and (23) were computed first with the set of values $h = 0 \cdot 15$, $k = 0 \cdot 034$, $\mu = 0 \cdot 04$, $x = +2$, $y = 0$. Then in turn h was taken equal to $0 \cdot 14$, k to $0 \cdot 040$, and $\mu = 0 \cdot 05$. The weights are not very sensitive to small changes in x and y. The resulting changes in (20), (21) and (23) were found, and led to three simultaneous equations for the increments in h, k, μ needed to satisfy these three equations. The results were

$$h = 0 \cdot 133; \quad \mu = 0 \cdot 10; \quad k = 0 \cdot 041, \quad m = 0 \cdot 24$$

The change in μ is unexpectedly large; h, m and k have all varied so as to increase it. It appears also that x is about $+2 \cdot 5$, $x + y = +6 \cdot 6$.

These results were next made the basis of a further approximation, but it was soon found that h had been lowered too much, and accordingly the standard values for the next approximation were

$$h = 0 \cdot 145; \quad k = 0 \cdot 040; \quad \mu = 0 \cdot 10, \quad x = +2 \cdot 0; \quad x + y = +7 \cdot 0.$$

The functions on the left of (20) and (21), and $m - \Sigma w_r/n$, were computed

with these values, and again with, respectively, $h = 0 \cdot 133$, $k = 0 \cdot 050$, and $\mu = 0 \cdot 009$. These led to the further set of equations

$$5 \cdot 1 - 10 \cdot 0\, h' - 3 \cdot 0\, k' + 2 \cdot 0\, \mu' = 0$$

$$1 \cdot 99 + 1 \cdot 99\, h' - 25 \cdot 14\, k' + 1 \cdot 64\, \mu' = 0$$

$$0 \cdot 0090 - 0 \cdot 0020\, h' - 0 \cdot 0354\, k' + 0 \cdot 0090\, \mu' = 0,$$

where $h' = \delta h/0 \cdot 012$, $k' = \delta k/0 \cdot 01$; $\mu' = \delta\mu/0 \cdot 01$, and hence to the further approximation

$$h = 0 \cdot 152, \quad k = 0 \cdot 0417; \quad \mu = 0 \cdot 107; \quad m = 0 \cdot 281.$$

Finally the results were recomputed with these values; then it was found that

$$\Sigma v_r \{1 - 2h^2 (x_r - x)^2\} - 1 = 133 \cdot 5 - 131 \cdot 4 - 1 = + 1 \cdot 1$$

$$\Sigma w_r \{1 - 2k^2 (x_r - x - y)^2\} - 1 = 50 \cdot 5 - 49 \cdot 2 - 1 = + 0 \cdot 3$$

$$m - \Sigma w_r/n = 0 \cdot 281 - 0 \cdot 275 = 0 \cdot 006.$$

The solution is therefore sufficiently close. Further, the values found for $\Sigma v_r (x_r - x)$ and $\Sigma w_r (x_r - x - y)$ always indicated that x was within a fraction of $+ 2$, and $x + y$ close to $+ 7$. But v_r and w_r are very insensitive to small changes in x and y, since they involve only their squares. Hence we can estimate x and $x + y$ by ignoring the changes in the weights when we give them their most probable values instead of the approximate ones we have used. Then we have

$$x = 2 + \frac{\Sigma v_r (x_r - 2)}{\Sigma v_r} = + 2 \cdot 23$$

$$x + y = 7 + \frac{\Sigma w_r (x_r - 7)}{\Sigma w_r} = + 5 \cdot 73.$$

The final weights are of some intrinsic interest. If n_r denotes the number of observations in each group, we have

Observed value	−38	−33	−28	−23	−18	−13	−8	−3
n_r	2	0	1	1	1	2	10	32
$n_r v_r$	0	0	0	0	0	0·29	6·37	27·97
$n_r w_r$	2	0	1	1	1	1·71	3·63	4·03

Observed value	+2	+7	+12	+17	+22	+27	+32	+37
n_r	68	37	14	6	5	1	3	1
$n_r v_r$	62·02	31·63	7·84	0·57	0	0	0	0
$n_r w_r$	5·98	5·37	6·16	5·43	5	1	3	1

The values of $n_r w_r$ represent roughly the number of abnormal observations in each group, and follow roughly a normal law with a larger scatter than that of the normal ones. We notice that v_r is negligible in the groups at $+17$ and $+22$; all the observations in this group are practically treated as abnormal, as a natural result of the work. It appears that previously insufficient allowance was made for abnormal observations, and too many were retained in these two groups, so that x was overestimated by nearly a second. Professor H. H. Turner, in a previous paper on a similar set of data, determined x by fitting a normal distribution to the four central groups; the results were not very different.

4. While this method is correct in principle, the labour is excessive; each approximation took about 6 hours' work, using a Marchant calculating machine and the tables of Milne-Thomson and Comrie. It should, however, be possible to devise a shorter method that would give almost as accurate results. We may note that the final value of h corresponds to a standard error of $4 \cdot 65$ seconds, and a standard error of the mean of $0 \cdot 34$ second Accordingly, the difference of x from $+2 \cdot 00$ seconds is barely significant. Thus approximate values of h, k and m should be enough to determine x; and k and m practically influence x only through the quantity μ. If then we can estimate h and μ from an inspection of the data we can compute v_r as if k was zero, and thereby obtain x as a weighted mean, which should be close enough for all ordinary purposes.

The observations discussed so far were such as to raise the problem of the treatment of abnormal observations in an unusually acute form; for while it was clear that the smaller errors followed the normal law, there were so many abnormal ones that the computation of a standard deviation and even a mean would have been practically meaningless if some method of rejection had not been adopted. The method actually chosen was to reduce all the values of n_r by the same amount, this being so chosen as to leave the central groups isolated by zeros. If the reduction is s, this is equivalent to treating each observation as having weight $1 - s/n_r$ when $n_r > s$, and weight zero if $n_r < s$. Actually the contribution to n_r from the observations satisfying the normal law is statistically $n_0 \exp \{ -h^2 (r - x_0)^2 \}$; and if there are s abnormal ones in each central group

$$n_r = n_0 \exp \{ -h^2 (x - x_0)^2 \} + s$$

$$1 - \frac{s}{n_r} = \left[1 + \frac{s}{n_0} \exp \{ -h^2 (x - x_0)^2 \} \right]^{-1},$$

which is precisely our form of v_r for the case $k = 0$, with μ replaced by s/n_0. There is therefore no difference between this method and the one just suggested; any difference in the results arose from an underestimate of μ.

5. When the number of abnormal observations is smaller, such methods may still be helpful. If only one observation deviates by more than, say, three times the standard deviation, we obviously cannot determine k; for even if we were sure that the observation is abnormal, a single observation fixes only a most probable value of $x + y$ and gives no information about the precision, k. Without such information we cannot infer how many observations within the region of considerable frequency may actually be affected by abnormal errors, and no progress is possible. In such circumstances, if we have no previous knowledge of the probability of abnormal observations, there may be no better course than rejection or retention according to the probability of a deviation of the observed magnitude, given the total number of observations and an approximate determination of h from the majority of the observations. This is essentially Chauvenet's criterion. If, however, there are three dubious observations we have the means for a rough determination of k, m, and $x + y$, and the method of the present paper can be applied. If only two observations are in doubt, we cannot infer all of $x + y$, k, and m, but we may be able to estimate μ and then proceed as for $k = 0$, but mk finite. In any case where the rejection of a single observation by some recognised criterion leads on re-application to the rejection of a further observation, we should suspect the presence of a number of abnormal observations with small deviations, and allow for them by a system of weighting. It should be noticed that with a small number of observations, whether normal or abnormal, the distribution of the prior probability of the precision constant has some influence. The assumption in this paper that $P(h, k)$ was proportional to $1/hk$ was responsible for the unit terms in (20) and (21); that in (20) turned out to be practically unimportant, but that in (21) had an appreciable effect.

The present method has some affinity with Peirce's criterion, a full account of which is given by Chauvenet. This criterion considers the possibility of a certain number of observations being abnormal; P, the probability of obtaining the whole set of observations from the normal law, is compared with P_1, that of obtaining a given number of abnormal ones and at the same time the remainder from the normal law. If $P < P_1$, the observations with the largest deviations are rejected. The probability of an abnormal observation occurring is m (y in Chauvenet's notation) which is adjusted to make P_1 as large as possible. This may be the best procedure where only one observation is doubtful and we

have no better way of estimating m; but a method of continuous weighting is needed in other cases.

Summary.

A method is given for dealing with sets of observations, appreciable fractions of which are affected by abnormal errors. The probability of an error is taken to be given jointly by two normal laws, one for the normal and the other for the abnormal errors, and a method of solution for the five unknowns is provided. An approximate solution may also be obtained by a method of weighting, the weight of an observation being a continuous function of its deviation.

The Oxidation of Carbon Monoxide.

By G. HADMAN, H. W. THOMPSON and C. N HINSHELWOOD, F.R.S.

(Received April 1, 1932.)

Introduction.

Although the reaction between carbon monoxide and oxygen has long been the subject of experimental study, the mechanism of the process is far from being completely understood. Most of the earlier investigations of Dixon and others were concerned with the initiation and propagation of flame or detonation waves in mixtures of the two gases, and showed especially the important part which water plays in the reaction.* More recently experiments have been made in different laboratories† on the kinetics of the slow reaction occurring below the ignition temperature. From the results of these it should be easier to draw conclusions about the mechanism of the change than it is from experiments on the explosive combination, but on account of the differences in the conditions under which the various investigations have been made, and, to some extent, of the divergences in the results themselves, it is still difficult to correlate all the available information and form a coherent theory of the oxidation. The lack of uniformity in some of the previous work may be attributed partly to variation in water content of the gases used, for, as the

---

* Bone, 'J. Chem. Soc,' p. 345 (1931).
† Topley, 'Nature,' vol. 125, p. 560 (1930); Cosslett and Garner, 'Trans. Faraday Soc.,' vol. 27, p. 176 (1931).

experiments of Bone and Weston* have shown, the catalytic oxidation in presence of water and the direct combination are probably distinct and independent processes.

It seemed of interest therefore to examine the problem further, investigating under more strictly comparable conditions the influence on the rate of the slow reaction of various factors such as vessel size, and concentrations, in particular that of water. With this knowledge about the kinetics of the " wet " reaction it was proposed to proceed to the study of the reaction which can be made to take place at higher temperatures between the carefully dried gases. If the " dry " reaction is determined, as some have thought, by the residual traces of moisture, the kinetics must remain essentially the same as in the " wet " reaction. They appear in fact to be entirely different. This shows once more that the direct oxidation of dry carbon monoxide is possible.

The primary process in the interaction of the wet gases appears to be a reaction between carbon monoxide and water on the wall of the vessel; the hydrogen produced sets up reaction chains which pass through the bulk of the gas and are finally broken by oxygen adsorbed on the surface. An estimate of the chain length can be made and gives a result of the order of a million

The work of Semenov,† Topley (*loc. cit.*) and Garner (*loc. cit.*) has shown that in a region of relatively low pressure the reaction abruptly becomes explosive. What occurs is not the normal thermal explosion, which must supervene when the velocity of an exothermic reaction becomes too great for the conditions to remain isothermal, but is something analogous to the low pressure explosion of hydrogen and oxygen, carbon bisulphide and oxygen and other gas mixtures. Whether the underlying mechanism is really the same is not yet known. This phenomenon, which was found by Semenov with carbon monoxide and oxygen saturated with water vapour, we have found still to occur with the carefully dried gases, though the part which residual traces of water may be playing in it is not yet clear.

Experimental Method.

Since the reaction is accompanied by a change in pressure it was convenient to follow it statically. The experimental method was that described in detail in previous papers. The reaction vessel, usually of quartz, was heated in an electric furnace kept at a temperature constant to within a degree. It was connected by means of capillary tubes to gas holders and to a high vacuum

---

* ' Proc. Roy. Soc.,' A, vol. 109, pp. 176, 523 (1925).

† Kopp, Kovalsky, Sagulin and Semenov, ' Z phys. Chem.,' B, vol. 6, p. 307 (1930).

pump. Changes in pressure were recorded by means of a mercury manometer. The temperature was measured by a thermocouple. Condensation of water was prevented by winding the capillaries with electrically heated resistance wire.

Carbon monoxide was prepared by the dehydration of formic acid with concentrated sulphuric acid, carbon dioxide being removed by strong caustic potash solution. The gas was generated in an evacuated apparatus and was thus free from air. It was dried by passage over phosphorus pentoxide. Cylinder oxygen was used after it had been found to behave in all respects like the pure gas obtained by heating potassium permanganate. Water vapour was introduced into the reaction vessel from a small bulb of liquid water. The iodine vapour used in the later experiments was produced in the reaction vessel by decomposing isopropyl iodide.

Of the reaction vessels used four were cylindrical quartz bulbs of different diameter, two were similar bulbs filled with small quartz spheres and another was a cylindrical quartz vessel packed with lengths of quartz tubing. A porcelain vessel was also used.

The " Wet " Reaction

The curves in fig. 1 show the course of the reaction between carbon monoxide, oxygen and steam at 560° C. Curves of this kind were plotted for all the experiments made, and tangents drawn at the origin. In this way the influence of the various concentrations on the initial rate of reaction was found.
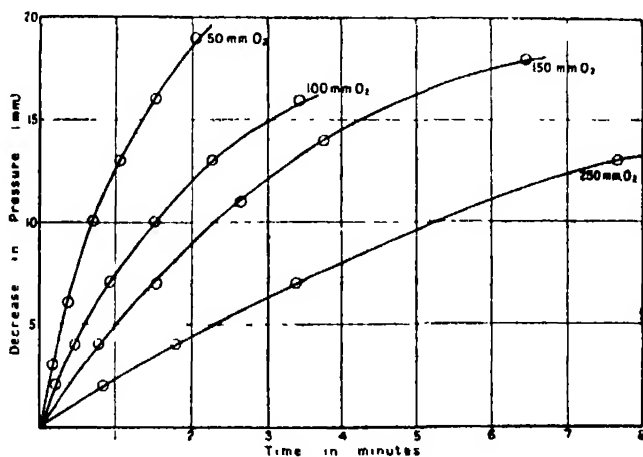
Fig. 1.—Course of reaction with different initial oxygen concentrations. CO = 50 mm. $H_2O = 10$ mm.

The results can be summarised approximately by saying that the rate of reaction is proportional to the concentrations of water and of carbon monoxide and inversely to the concentration of oxygen.

Direct proportionality to the concentration of water vapour holds over the whole of the range investigated in the unpacked bulbs, namely, between 540° and 620° C. and from 5 to 50 mm. Fig. 2 shows the results obtained with the largest of the unpacked bulbs, at 560° C.

Temperature 560° C.   CO = 50 mm. O_2 = 250 mm.

Pressure of steam (mm.).	Initial rate (mm. per minute).
10	2 1
15	3 2
20	3 9
25	5 2
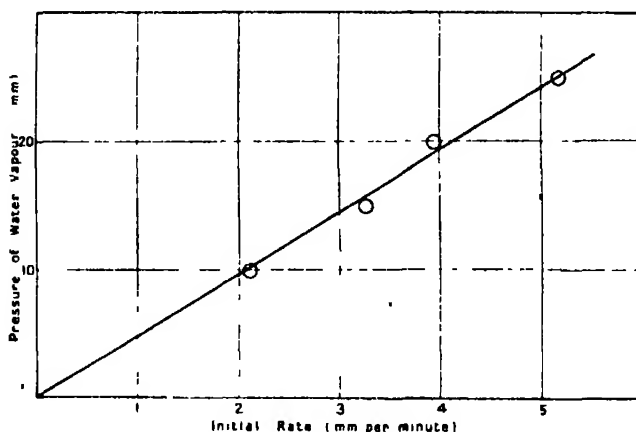
Fig. 2.—Influence of water concentration.   CO = 50 mm. O_2 = 250 mm.

In some of the bulbs the rate, while increasing linearly with the steam pressure, appeared not to approach zero for zero water concentration. This was specially marked in the sphere-packed vessel, and appears to be due to the fact that a direct oxidation proceeds concurrently with the water-catalysed reaction. That it is most in evidence in the sphere-packed vessel suggests that it takes place on the surface. In the second part of this paper it will be discussed in greater detail.

Fig. 3 shows the linear relation between rate and concentration of carbon monoxide: the experiments were made in the largest of the unpacked bulbs and at 560° C.
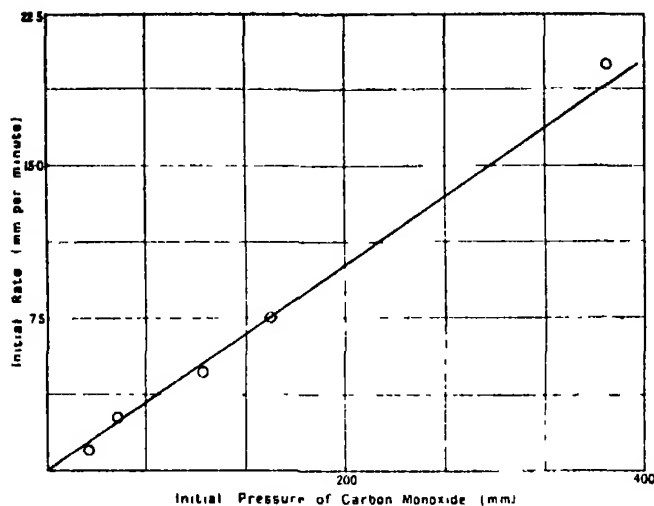
FIG. 3.—Influence of carbon monoxide concentration. $O_2 = 250$ mm. $H_2O = 10$ mm.

Similar results were found at other temperatures and in other vessels.   The following numbers were obtained with the second largest bulb at 600° C.

Water = 10 mm. $O_2 = 350$ mm.

Pressure of carbon monoxide.	Initial rate.
mm.	mm per minute.
50	9
115	19
150	25
220	57

In the tube-packed vessel, however, the rate of reaction passes through a flat maximum as the pressure of carbon monoxide is increased, and then falls off again as shown in the following table.

Temperature 620° C.   Pressure of water = 10 mm.   Oxygen = 250 mm.

Pressure of carbon monoxide.	Initial rate
mm	mm. per minute
50	31 3
100	37 5
150	61
210	70
270	75
345	50

Fig. 4 shows the diminution in velocity of reaction caused by increase in the partial pressure of oxygen. Fig. 1 shows the same effect, which was found at all temperatures and in all the vessels used. The experiments from the results of which fig. 4 is plotted were made at 600° in one of the smaller unpacked bulbs. The following figures were found at 560° in the largest of the bulbs.
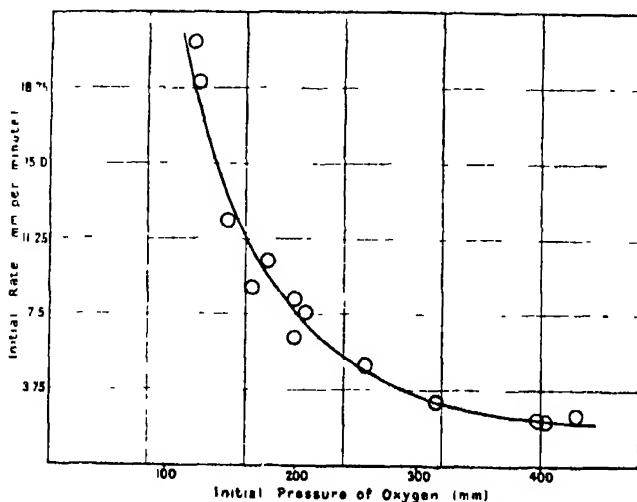
Fig. 4 —Influence of oxygen concentration. $H_2O - 10$ mm. $CO = 50$ mm.

Water = 10 mm.   Carbon monoxide = 50 mm.

Pressure of oxygen	Initial rate.
mm.	mm. per minute
350	1 0
250	2·3
150	5·4
100	8 0
50	16·0
40	(explosion)

The rate of reaction is very much decreased by a reduction in the dimensions of the vessel. For a series of four similar cylindrical silica bulbs at 600° C. the rates of reaction found are shown in the table on p. 93. (The value 45 for the greatest rate was not observed directly, but was extrapolated from a series of results for higher oxygen concentrations.) In the sphere-packed vessels the rate was still smaller.

Diameter.	Initial rate of reaction for 200 mm. O_2, 50 mm CO and 10 mm. H_2O.
cm	mm per minute
7 5	45
4 9	15
3 2	7 5
1 8	1 5

These results can only be explained by assuming the presence of reaction chains which are broken at the wall of the vessel.

Since the rate of reaction is directly proportional to the concentration of water and of carbon monoxide, a natural hypothesis is that the chains start with the process $CO + H_2O = CO_2 + H_2$ and that the inhibiting influence of oxygen is due to its power of breaking them. Since the influence of vessel diameter shows the chains to be broken at the wall, it is here that the action of the oxygen must be exerted, presumably in oxidising and destroying some substance which would otherwise have continued the chain (*e.g.*, H-atoms). But there is another way in which oxygen might act. If the primary process takes place at the surface—and there is reason to believe that the water gas reaction at these temperatures is heterogeneous—then high concentrations of oxygen might " poison " it. The experiments described in the next section show that this alternative is improbable, and that the oxygen acts by breaking the chains at the surface rather than by " poisoning " the primary reaction.

The Influence of Iodine.

The simplest explanation of all the experiments is that the first stage in the oxidation is the interaction of carbon monoxide and water at the surface with liberation of hydrogen, which then brings about the propagation of chains. This idea is supported by the fact that in the region of temperature with which we are concerned, hydrogen combines with oxygen by a chain reaction.[*] The mechanism of this chain can easily be modified to include carbon monoxide. It might, for example, be supposed that hydroxyl radicles, formed by the union of hydrogen and oxygen, initiate the following series of changes :—

$$H_2 + O_2 = 2OH$$
$$OH + CO = CO_2 + H$$
$$H + O_2 + CO = CO_2 + OH$$
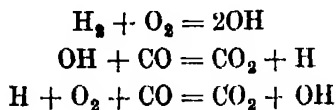
* ' Proc. Roy. Soc.,' A, vol 118, p. 170 (1928); vol. 119, p. 591 (1928): vol. 122, p. 610 (1929).

This scheme was suggested for the reaction occurring in flames by Farkas, Haber and Harteck on the basis of the ideas which Bonhoeffer and Haber* developed from considerations quite different in nature from those of the present paper. It must be remembered that other mechanisms have been suggested for the interaction of hydrogen and oxygen, and that these can be equally well modified to include carbon monoxide as a link in the chain. We have here adopted the Haber mechanism for purposes of illustration since it has the advantage of being the simplest to express in symbols.

The combination of hydrogen and oxygen is very much slowed down by iodine, which apparently breaks the chains in the gas phase. Without knowing the exact cycle of changes occurring in the carbon monoxide oxidation, we may anticipate that, if it involves the same intermediate products as the hydrogen-oxygen reaction, it will also be inhibited by iodine. This antici-pation is confirmed by experiment. At $580°$ C., the highest temperature at which the rate could be measured conveniently in the largest bulb, the reaction in presence of small amounts of iodine was too slow to observe accurately, and the temperature had to be raised $100°$ to obtain a suitable speed. For a given temperature the ratio of the speeds in the presence and in the absence of 1 mm. iodine is of the order 1 to 100. Furthermore, the influence of vessel diameter on the rate largely disappears in presence of iodine : at $680°$ C. for example, the ratio of the speeds in the largest and smallest bulbs is about 3 to 1, compared with 30 to 1 in the absence of iodine at $600°$. Thus there is clear evidence that wall deactivation is relatively unimportant compared with deactivation in the gas.

This provides a means of distinguishing between the two possible modes of action of oxygen in inhibiting the reaction. If normally the retarda-tion by oxygen is due to a poisoning of the primary process, then it should persist even in presence of iodine ; if, on the other hand, it is due to the breaking of chains at the wall, then it should almost disappear when iodine is present to prevent most of the chains from reaching the wall at all.

In the large unpacked vessel, with iodine, oxygen is found no longer to retard but actually to favour the reaction, as shown in the table below.

| Temperature. | Pressure in millimetres mercury. | | | | Initial rate. |
	Iodine.	Water.	Carbon monoxide	Oxygen.	
° C.					mm per minute.
650	0 4	15	100	50	1 0
	0 4	15	100	100	1 3
	0·4	15	100	200	1 8
680	1 7	22	55	50	2 0
	1 7	22	55	150	3 0
	1·7	22	55	200	4 5
	1 7	22	55	400	6 8
680	1 7	42	65	50	2 5
	1 7	42	65	100	3 8
	1 7	42	65	200	5 5

In the smallest of the unpacked bulbs the inhibiting influence of oxygen is still observable at higher pressures, as shown below. This is understandable if we assume that a few of the chains now reach the vessel wall.

Temperature 680° C.   Iodine 1·7 mm.   Carbon monoxide 100 mm.

Pressure of oxygen	Initial rate
mm	mm per minute
50	1 0
150	2 5
200	2 5
250	2 4
300	1 8
350	1 2

That there should be an actual accelerating effect of oxygen in the larger bulb needs further explanation   The oxygen evidently favours the propagation of the chains in the gas, in competition with the iodine which breaks them.   The dual rôle of oxygen in favouring the propagation of chains in the gas and breaking them at the surface explains why the rates recorded in the above table pass through a maximum ; increase in concentration beyond a certain limit no longer helps the chains, and then the surface retardation begins to predominate.   There are analogous examples of chain reactions where the reaction velocity increases with the concentration of one of the gases at lower pressures and then becomes independent of it, for example, the photochemical combination of hydrogen and chlorine, where the rate, after increasing

with the hydrogen concentration, eventually becomes independent of it. In the absence of iodine, when nearly all the chains reach the wall, the surface deactivation by oxygen controls the situation.

Estimation of the Chain Length.

If we accept the hypothesis that the chains are started by the interaction of carbon monoxide and water, then an estimate of the chain length can be made by comparing the rate of this primary process, measured in the absence of oxygen, with the total rate of oxidation.

For this purpose the rate of the " water gas reaction " was measured, by allowing mixtures of steam and carbon monoxide to react for known times, withdrawing samples and analysing in a Bone and Wheeler apparatus. The reaction proved to have all the characteristics of a surface process ; it is rather erratic, and the surface of the vessel becomes progressively more active as it is used. The rate is only measurable some 200° above the temperature of the experiments on the " wet oxidation." The reaction takes place on a silica surface in the same region of temperature as the reverse reaction on the surface of heated platinum and tungsten wires. It is unlikely to give rise to chains since it is only feebly exothermic. It is impossible to make a detailed study of the kinetics since the results were variable and the method of experiment very tedious, there being no volume change and every determination requiring a complete analysis. The following results, therefore, are only to be regarded as giving the order of magnitude. This, however, is all that is required for an estimate of the chain length of the principal reaction.

" Water-gas Reaction " in Large Unpacked Bulb.

Temperature.	Initial pressures		Time.	CO_2 found.	CO_2 corrected.
	CO.	H_2O			
°C			mins.		
800	285	70	20	11·4	12
	334	77	20	16	13·1
	275	75	40	17·2	17·5
700	267	71	71	1	1·1
	298	79	100	1	0·9
	319	77	240	5·3	4·5

The last column gives the carbon dioxide formed corrected to initial pressures of 70 mm. water and 300 mm. carbon monoxide, making the rough assumption

that the amount of change is linearly proportional to the initial pressures. With this same assumption, and extrapolating to 600° C., the rate for 10 mm. water and 50 mm. carbon monoxide is found to be of the order 10^{-5} mm. per minute. This figure is admittedly very rough ; it may be in error by a factor of 3 or 4, but the nearest power of 10 is enough for our purpose. Under the same conditions, but with 100 mm. oxygen present, the rate of oxidation would be 19 mm. per minute. Thus the length of the chains appears to be of the order $19/10^{-5}$, or rather more than 10^6.

Since the chains appear to traverse the vessel from one side to the other, this is not an improbable result. The efficiency of collisions in propagating the chains can now be calculated as follows. From the Einstein formula for the mean displacement, x, of a molecule in time t, $x^2 = 2Dt$, taking 5 as a mean value for the diffusion coefficient, D, at the temperature and pressure under consideration, the mean time required for a chain to traverse the free space is found to be about 1 second. The number of collisions which a molecule experiences during this time at 600° C. and a total pressure of 160 mm. is found from the formula

$$Z = N\sigma_{12}^2 \left\{ 8\pi RT \left(\frac{1}{M_1} + \frac{1}{M_2} \right) \right\}^{\frac{1}{2}},$$

to be $5 \cdot 6 \times 10^8$, taking σ_{12} to be about 3×10^{-8} cm, and M_1 and M_2 to be 30. Thus there occur $5 \cdot 6 \times 10^8 / 1 \cdot 9 \times 10^6 = 3 \times 10^2$ collisions for each fresh link in the reaction chain. In other words, the efficiency of collisions for the propagation of the chains is of the order of 1 in a 100, which, compared with the normal efficiency in chemical reactions, is very high, and corresponds to hardly any activation.*

The Interaction of the Dried Gases.

In the absence of water the kinetics of the reaction are fundamentally different.

For the investigation of the " dry " reaction the apparatus was modified ; the water bulb was removed and the gas holders were replaced by large globes

---

* An arbitrary value of oxygen concentration has been used in this calculation. It would perhaps be more correct to use a value corresponding to the maximum influence which oxygen can exert, since otherwise there is the likelihood that chains are ' reflected ' backwards and forwards several times There are indications of such a maximum oxygen influence even in fig. 4. Allowing for this, the efficiency of collisions is found to be about ten times smaller.

containing a supply of pure phosphorus pentoxide. All the taps were lubricated with " Apiezon " grease. A globe in which carbon dioxide was stored to dry was also sealed to the apparatus ; its purpose will be explained later.

The first experiments were made after the gases had been drying for 3 weeks, and the reaction vessel had been baked out at about 800° C. But it is to be noted that the criterion of dryness in this investigation is not the prescription of the method of drying, the adequacy of which is always contestable, but the behaviour of the gases after the treatment.

Measurable reaction now began only at temperatures 100° higher than with the wet gases. The vastly slower oxidation is not determined by such residual traces of moisture as there are, for, under the new conditions, oxygen no longer retards the reaction.

Temperature 691° C.

Initial pressures.		Initial rate.
Carbon monoxide	Oxygen.	
		mm. per minu
320	200	0·36
300	100	0 25
320	200	0 37
150	200	0 21

The reaction rate is proportional to a power of each of the concentrations less than the first.

In the following table the rates in an unpacked and a sphere-packed vessel having an area/volume ratio about 15 times as great are compared.

Sphere-packed Bulb.   Temperature 685° C.

Initial pressures.			Initial rate
Carbon monoxide.	Carbon dioxide.	Oxygen.	
			mm. per minute
100	80	50	3·1
100	80	100	3 0
100	80	200	2 9
100	80	300	3 1
100	80	400	2·7

Unpacked Bulb.   Temperature 685° C.

Initial pressures.			Initial rate.
Carbon monoxide.	Carbon dioxide.	Oxygen.	
			mm. per minute.
100	80	200	0·179
100	80	400	0·256

(In these experiments carbon dioxide was added initially to raise the total pressure above that of the " explosion limit," as will be explained below.) It will be seen from these results that the reaction velocity is increased in the sphere-packed bulb in proportion to the increase in the surface/volume ratio. This indicates that the process occurring is to a large extent a heterogeneous reaction.   In the packed vessel the rate of oxidation is independent of the oxygen concentration, while in the unpacked vessel the rate increases with concentration.   This might be taken to indicate that a certain proportion of the reaction in the unpacked vessel is really homogeneous.   Attempts were made to measure this gaseous reaction by suitably increasing the pressure and temperature so as to make it predominate over the wall reaction.   This attempt was frustrated in two ways.   In the first place only moderate pressures of the gases were available ; this made it necessary to attempt to work at higher temperatures.   But here there exists a region of explosion at lower pressures similar to that observed in the hydrogen-oxygen combination and other reactions.   The limiting pressure, above which the mixture must be for slow reaction, is displaced upwards as the temperature becomes greater.   At the higher temperatures mixing of the gases in the reaction vessel inevitably led to explosion, while at lower ones the rate of combination at pressures above the critical limit was still so small that the homogeneous reaction had no chance to predominate.   The explosion area was mapped out by Semenov using moist gases.   In the present series of experiments with the dry gases, though it could only be determined somewhat roughly, it was found to be situated in the same region of pressure and temperature as described by Semenov, so that the same phenomenon is evidently occurring.   The limits were discovered by experiments in which mixtures prepared at a lower temperature were slowly heated up to the point of ignition, the amount of reaction preceding the entry into the explosion area* usually being small.   It is remarkable that,

* The boundaries of this area are such that at 650° C. approx. explosion occurs if the pressure lies between 20 mm. and 160 mm. for $O_2 : CO = 1 : 2$.

although the gases were dried to the extent that the slow reaction was retarded something like a hundredfold, the low pressure explosion was relatively little affected. This, at first sight, suggests that the explosion is a phenomenon independent of water, but, in the absence of more precise knowledge of its mechanism, this conclusion is a doubtful one. It is possible that without any trace of water to set up chains the " low pressure explosion " might be inhibited.

This explosion is quite different in nature from the thermal explosion which Dixon and others have studied, and which is largely dependent on the concentration of water vapour. In the experiments with the wet gases in the larger unpacked bulbs it was possible to increase the concentration of water or carbon monoxide, or to reduce the concentration of oxygen, to a point where the velocity of combination became so great as to pass into an explosion. But with the dry gases increase in the concentration of carbon monoxide, although increasing the reaction velocity, tended to stop the low pressure explosion, *i.e.*, raised the ignition temperature.

Experiments are being carried out with the object of finding out more about the conditions governing the explosion of the dry gases in this low pressure area.

Summary.

(1) In the presence of water the oxidation of carbon monoxide takes place at a rate which is approximately proportional to the concentrations of water and carbon monoxide and inversely proportional to that of oxygen. The rate in a series of cylindrical bulbs is roughly proportional to the square of the diameter.

(2) These facts are explained by the assumption that the primary process is the interaction of carbon monoxide and steam giving hydrogen, which then sets up reaction chains analogous to those occurring in the simple combination of hydrogen and oxygen.

(3) The retarding action of oxygen is explained by the breaking of the chains by an oxidation process at the wall of the vessel (*e.g.*, removal of hydrogen atoms), not by a " poisoning " of the primary process. This is shown by the fact that in the presence of iodine, which prevents nearly all the chains from reaching the wall, the inhibiting action of oxygen disappears.

(4) By comparing the rate of the primary interaction of carbon monoxide and steam in the absence of oxygen with the total rate of oxidation, the chain length is found to be of the order 10^6 in a $7 \cdot 5$ cm. diameter silica vessel at $600°$ C. The efficiency of collisions in propagating the chain is as high as 1 in 100.

(5) The kinetics of the interaction of dried carbon monoxide and oxygen are fundamentally different, confirming the view that direct oxidation takes place independently of residual traces of moisture. The direct oxidation is predominantly a heterogeneous reaction under the conditions of the experiments.

(6) At lower pressures with the dried gases there exists a region of explosion, bounded by limits outside which the reaction is very slow. This region corresponds approximately to that found by Semenov for the moist gases.

Fluorescent Excitation of Mercury by the Resonance Frequency and by Lower Frequencies.—IV.*

By Lord RAYLEIGH, For. Sec. R S

[PLATES 5 AND 6.]

The present paper deals entirely with " core " excitation of mercury vapour, that is to say, fluorescent excitation by the atomic resonance line λ 2537, the primary action of which is, without doubt, to produce $2\,{}^3P_1$ excited atoms in the vapour.

§ 1. *Experimental Arrangements.*

The source was a small commercial mercury lamp in silica, of the standard pattern made by the Thermal Syndicate of Wallsend. It was immersed in a tank of water, kept cool by a constant flow through. A magnetic field from a bar electromagnet kept the discharge pressed forward. The magnet was placed vertically above the lamp, and the iron core alone dipped a short distance into the water. The beam made parallel by a quartz condenser was filtered through 5 cm. of saturated bromine vapour and 15 cm. of chlorine gas at atmospheric

* I, ' Proc. Roy. Soc.,' A vol. 125, p. 1 (1929) ; II, ' Proc. Roy. Soc.,' A, vol. 132, p. 650 (1931) ; III, ' Proc. Roy. Soc.,' A, vol. 135, p. 617 (1932).

pressure. This combination of filters approximately isolated the resonance line. It is true that the group of lines near λ 2652 was largely transmitted, but the other strong mercury lines between this and the green line were completely suppressed. Reproduction No. I is a direct spectrogram of the source thus filtered. The exposure has been pushed as far as possible, short of fogging the plate by the diffuse light of the instrument, and it is seen that even so no trace of the strong mercury lines is obtained. The importance of this will appear later.

The fluorescence vessel was the same as that described in III, p. 619. The drawing is substantially reproduced here in fig. 1 for convenience of reference.
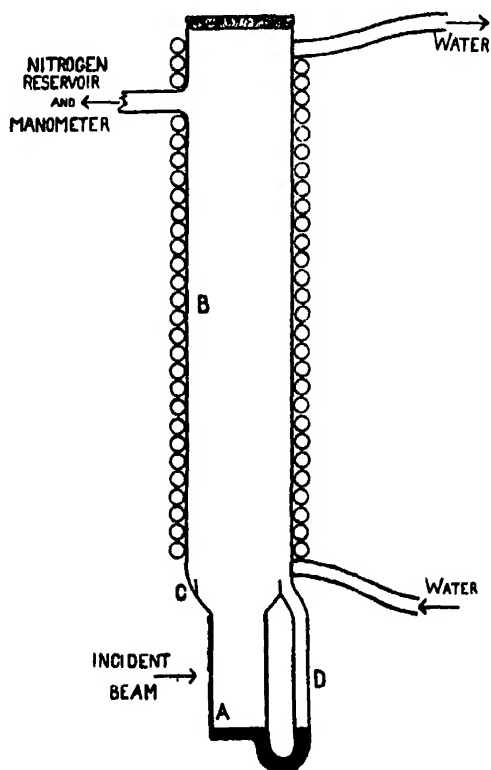
FIG. 1.—⅓ actual size.

A is a vessel 2 cm. square, built up from sheets of fused silica, ground and polished. It is prolonged above into a wide silica tube B serving as condenser. B is cooled by a coil of compo pipe of small diameter wound over it. It is advantageous to lag the outside of this with asbestos cloth, to prevent condensation of the water of combustion from the burner, which may otherwise

accumulate and ultimately run down, with objectionable results. Mercury boils in A over a burner, condenses in B and returns by the annular gutter C and the side tube D. The boiling takes place under an atmosphere of nitrogen of any desired pressure admitted to B. No nitrogen penetrates into A, which is full of mercury vapour. The issuing vapour keeps the nitrogen away from A as in a condensation pump.

The exciting beam enters on the left, half way up the square part of the vessel. A metal diaphragm covers the left-hand outer wall, and a hole about 3 mm. square admits the beam. The latter is parallel when it traverses the filtering tubes of about 7 cm. clear aperture, and is finally converged on to the small window by a quartz lens of 8 cm. diameter and 11 cm. focus, sometimes supplemented by a smaller one of 2·5 cm diameter and 5 cm focus A final convergence of 70° or more produced by using this small lens is advantageous in many experiments ; but where it is important to avoid stray light diffused by the square vessel, a smaller angle is preferable, so that the divergent beam can ultimately escape through the right-hand wall, without directly illuminating the front and back walls.

§ 2. *Direct Photographs of the Luminous Vapour Stream through Selective Filters.*

Using these arrangements, a series of photographs of the fluorescent light have been made with a quartz-fluorite achromat, through filters which selectively pass—

(a) The resonance line 2537 (40 cm. chlorine and 5 cm. bromine vapour combined).

(b) The band 3300 (5 cm. bromine vapour, 1 mm. blue uviol glass).

(c) The visual band 4850 (aesculene in gelatine filter, Wratten No. 2).

These photographs are reproduced in order to show how the fluorescent light distributes itself in the vessel, and how far this distribution is influenced by the motion of the stream of vapour, under various conditions of ebullition.

The exciting light is introduced locally into the middle of the vertical height. Owing to intense absorption due to the atomic absorption line it is unable to penetrate directly any distance into the vessel, and we may consider that the primary effect of the light is to generate locally in the mercury stream a concentrated supply of $2\,^3P_1$ atoms.

Photographs taken under nearly similar conditions have already been published in I, Plate 2 (upper row) and Plate 3. They brought out the important point that while the visual green fluorescence moves with the stream of

vapour when ebullition takes place under a pressure of 5 mm. or even more, the resonance radiation does not do so, until the atmosphere above the boiling mercury is reduced to a fraction of a millimetre. The two could therefore be *separated in space.* The phenomenon of conspicuously moving with the stream away from the place of excitation is referred to as " persistence."

The problem of explaining persistence seems simplest in the case of resonance radiation, owing to the smaller number of possibilities. The present photographs were taken under better conditions than the earlier ones, and are much more instructive. Nos. IV, *a*, V, *a*, and VI, Plate 6, are all taken in the light of the resonance line, with successively diminishing pressures. It will be noticed how conspicuously the luminosity spreads away laterally from the place of excitation, contrasting sharply in this respect with the visual fluorescence (compare IV, *b*) which latter moves up in a compact stream on one side of the vessel. As in the earlier work, the resonance luminosity is not affected by the vapour stream at pressures of 2 mm. An effect first begins to show at 1 mm. (V, *a*) and becomes more conspicuous when the nitrogen atmosphere over the mercury is pumped away altogether (VI).

These pictures will at first sight seem very different from those previously published, on account of the great lateral extension of the (photographic) luminosity. This is merely a matter of exposure. In fact, on reducing the exposure sufficiently, results similar to the old ones were obtained, the luminosity being limited to within 1 to 2 mm. from the place of entrance, when the pressure was 2 mm. of mercury. It will be evident that whatever the mechanism by which the luminosity spreads, it must be rapidly diluted by expanding in all directions as in reproduction IV, *a*. It clearly does expand in all directions, for the divergent cone of incident radiation which spreads out from the small window is only of 60° angle,* while the secondary luminosity spreads over the entire hemisphere, right up to the entrance wall of the vessel. So far from being carried *with* the vapour stream, it is clear that diffusion of the resonance luminosity at these higher pressures is able to take place sensibly as well *against* the stream. As the pressure is lowered and the stream becomes more rapid, this ceases to be the case, and the luminosity is carried up as in reproduction VI, Plate 6.

These photographs decidedly suggest that the diffusion of luminosity is by repeated handing on of a quantum of radiation from an atom to its neighbours, with ultimate escape ; indeed, it is difficult to imagine any other process by which this luminosity could be propagated not only with but also against the

---

* Or possibly much less ; unfortunately no record was made.

general motion of the vapour. The velocity of propagation by this process should increase with diminishing pressure. The velocity of the vapour stream does the same, and the evidence of the photographs indicates that this latter increase is the more rapid so that at low pressures the process of radiation transfer is not able to make headway against it, and the luminosity is carried up. The whole matter requires much closer scrutiny than it is possible to give in pioneering work like the present.

Other photographs have been taken with the light of the continuous maxima λ 3300 and λ 4850. These differ in a very striking way from the former. See reproductions IV, *a*, IV, *b*, IV, *c*, Plate 6, which show the vessel under unchanged conditions, photographed with the same lens, the only difference being in the filters which are arranged to admit either

$$\lambda\, 2537\ (IV,\, a)\quad \text{or}\quad \lambda\, 3300\ (IV,\, b)\quad \text{or}\quad \lambda\, 4850\ (IV,\, c)$$

There is no important difference between IV, *b* and IV, *c*, beyond what may be attributed to variations of photographic intensity These are at 2 mm. pressure.

Reproductions V, *a* and V, *b*, from a group at 1 mm. pressure, the former in the light of λ 2537, the latter in the light of λ 3300 and 4850 combined, as it was considered unnecessary to take separate photographs.

Comparing the other cases with the resonance radiation it is clear that we have to do with a separate phenomenon. There is nothing to suggest that the visual luminosity (4850) or the luminosity of λ 3300 have appreciable power of propagating themselves against the stream ; and this is quite in harmony with the view that has been taken. The process of " imprisonment of radiation " could have no place here, because these emission maxima *are not found in absorption.* The appearances are, on the other hand, quite suggestive of the view that the luminous centres, or the centres that are destined to become luminous, move along the stream lines of the vapour generally, in a way analogous to the threads of coloured liquid used in Osborne Reynolds' method of examining the flow of liquids ; making some allowance for the facility of gaseous diffusion which naturally leads to the luminous vapour column broadening out in a way that the liquid thread does not. Some apparent tendency to work from the walls to the centre would be expected. Near the walls, where the luminosity starts into being, the motion is slow, and the luminosity does not rise far before fading out. It is, however, carried out towards the centre of the vessel by lateral diffusion. Here the vertical motion is more rapid, and the luminosity does not fade out in so short a distance.

All this confirms the view usually taken that we have here to do with long-lived excited atoms or molecules. This subject has often been discussed, but for the most part only from a speculative point of view. Direct experimental evidence will here be presented that the visibly luminous vapour, as shown in reproduction IV, c, contains both kinds of metastable mercury atoms ; and that these have the same general space distribution as the fluorescent light : on the other hand their distribution is entirely different from that of the excited atoms (not metastable) which give rise to resonance radiation as in reproduction IV, a.

§ 3   *Detection of Metastable Atoms.*[*]

Metastable atoms are brought into evidence directly by the "forbidden lines" and, as we have seen,[†] the more excited kind $2\ ^3P_2$ are shown to be present in the fluorescent vapour by the forbidden line 2270, $1\ ^1S_0 - 2\ ^3P_2$. It is probable that the other forbidden line is present as well, but adequate investigation has not yet been made   This method is, however, too insensitive to be satisfactory for determining generally the presence and distribution of metastable atoms in the glowing mercury.   A much better test for them can be made by applying further excitation and observing the result.   The lower kind of metastable atom requires the higher frequency (violet) to bring it to $2\ ^3S_1$.   The higher kind is brought to the same level by green radiation.   The achievement of the $2\ ^3S_1$ level is brought into evidence by the complete visual triplet being emitted, and we can look for whichever component of the triplet is most convenient.   When using violet supplementary excitation, it is convenient to look for the green component, and when using green, the blue and violet are looked for.   These cases are illustrated in figs. 2 and 3.   The radiation
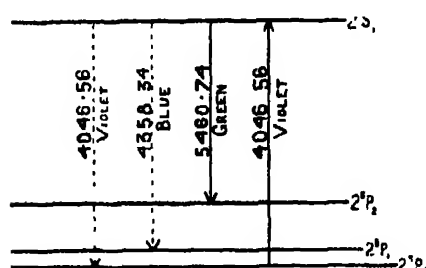
FIG. 2.   FIG. 3.
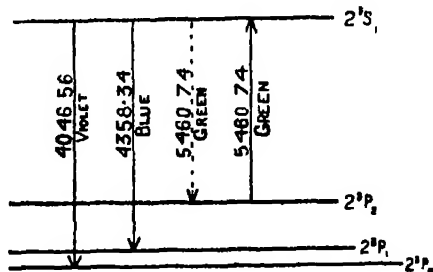
looked for are in each case shown by a full line arrow. The transitions marked by dotted line arrows doubtless occur, but are not convenient to observe.

The beam of violet light comes from a supplementary mercury arc in quartz.* It is easy to remove green light by any kind of blue or violet filter, but in addition we require the means of removing at pleasure either the blue line or the violet line, so as to estimate the comparative importance of $2\,^3P_0$ and $2\,^3P_1$ in any phenomenon under investigation. This may be done either by colour filters or by prismatic separation

As to colour filters, in many of the experiments 1 cm. thickness of Schott's blue uviol glass (BG3 in his catalogue) was used for passing the violet line and stopping the blue ; but later 4 mm of Schott's violet glass (UG3) was adopted as superior As in all such cases the thickness used is a compromise. Perfect separation means undue loss of light.

For transmitting the blue line and suppressing the violet, a solution of aesculene is effective, and was used at first. Later for the convenience of avoiding a liquid, 2 mm. thickness of Schott's pale yellow glass GG3 was substituted.

According to the data given by the makers, the transmission of the various glass filters is as follows :—

	10 mm. BG3	4 mm UG3	2 mm. GG3.
Violet line	0·312	0·52	0·017
Blue line ...	0·021	0·04	0·60

When prismatic separation was used the beam came out horizontally from the supplementary mercury lamp, limited by a 2 mm. horizontal slit. The "collimator" was 7 cm. diameter and 15 cm. focus. A large 60° carbon disulphide prism was used, with refracting edge horizontal and downwards. This refracted the beam obliquely upwards, and the horizontal direction was restored by a silver-on-glass reflector. The final convergence was by a lens of about 4 cm. diameter, which had a vertical movement in its own plane as well as the focussing adjustment. Various lenses were used from 12 cm. focus downwards. I have spoken of a "collimator," but actually the condensing lens was used to render the beam somewhat convergent, so that a smaller lens could be used to give the final convergence. The green ray was thrown far enough off to escape the comparatively small focussing lens entirely, so

---

* The best form of mercury arc has not been particularly studied. There might be advantage in using a water-cooled arc to get narrow lines free from self-reversal. It was suspected that the lamp worked less well for this purpose when hot.

that no filter was needed to suppress the glare due to it.   The blue and violet
rays were well separated, and the effect due to each could be seen separately
and compared directly.   This is the chief advantage which the prismatic
arrangement has over the filter, which is in other respects more convenient.

When it was desired to excite with the green ray, Wratten filter No. 9 was
used to cut out the blue and violet.   This is simple and efficient, involving
little loss of light.   There is no advantage in the prismatic monochromator for
this case.

The vessel used for this test is the same as in fig. 1.   Fig. 4 will help to
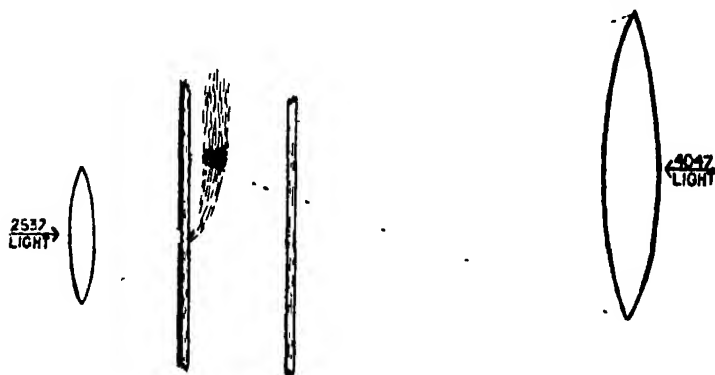
FIG. 4.—¾ actual size.

explain the method of applying it.   The exciting resonance radiation comes
in from the left through a small aperture in a metal diaphragm.   The green
fluorescence is seen to spring from the place where it enters the vapour as
indicated (see also reproduction IV, c).   This fluorescence by no means dis-
tributes itself over the whole cross section 2 cm. square, but remains isolated
with comparatively slight lateral spreading.   At a distance of, say, 1 cm. up,
it meets with the converging beam of violet light λ 4046 coming through the
right-hand wall of the vessel, and where the violet beam traverses it a marked
increase of luminosity is observed.

Viewing the rising stream of luminosity through a powerful direct vision
prism, it is seen that the locally enhanced luminosity is monochromatic, con-
sisting of the green atomic mercury line (the accompanying blue and violet
are visually too faint to be noticed).   It is only where the local enhancement
occurs that this line can be seen.*

---

* The green line is doubtless faintly present from the first, forming part of the complete
spectrum as in reproduction II, see below, § 4.   But it is not strong enough to be observed
visually under the conditions when the supplementary light is not acting.

The way in which the initial luminosity is locally enhanced should be evident from reproduction No. VIII of a photograph taken on an orthochromatic plate with a yellow screen. The lower arrow on the left indicates the direction of the original illumination, and the upper one on the right the auxiliary illumination. This photograph represents with the visual appearance without dispersion. If the prism is used, the initial continuous luminosity is dispersed away and diluted, while the monochromatic enhancement appears isolated. The photograph VIII, Plate 6, was taken with the blue and violet radiation mixed in the auxiliary light. IX, a, is with the violet alone, IX, b, with the blue alone. The technical difficulties are greater in this case, and the result not quite so good. But it will be evident enough that it is the violet and not the blue component which produces the local enhancement.

The beam of violet light can be swept up and down by making use of the vertical movement of the converging lens. The local development of the green mercury line can then be seen to follow the contour of the initial green fluorescence which has a continuous spectrum.

In this way it is clearly proved that metastable $2\,^3P_0$ atoms are present, and that they are distributed in the tube in the same manner as the green fluorescence, rising upwards along with it, and spreading laterally to the same moderate extent.

The same is true of $2\,^3P_2$ atoms, though these, as might be expected, are fewer in number, and produce less conspicuous effects. Using the green mercury line for supplementary excitation in the same way as the violet line was used before, we again get a local development of the visual triplet, which enhances the brightness of the initial rising fluorescence. In this case the observation cannot well be made visually, on account of the great brightness of the auxiliary green illumination. As already pointed out (see fig 3), the blue and violet components are the best to look for, and these lend themselves to photographic detection. At the same time the additional photographic brightness is not great. Wratten's filter No. 76 (deep blue monochromat) was used over the camera lens to favour the blue mercury line as much as possible. Reproduction No. X shows the result.

Spectrographic observations were made so as to establish the nature of the locally increased illumination, the rising column of vapour being focussed on the slit. It was found as expected that the blue and violet mercury lines came out locally at the level of the green supplementary illumination, which latter, it will be remembered, was filtered free of these components.

These experiments prove very clearly the presence of the two kinds of

metastable atoms in the rising green luminosity. As already stated, the test by illuminating with the blue line under similar conditions does not show the presence of $2\,^3P_1$ atoms to a comparable extent (reproduction IX, b). It will, however, doubtless occur to the reader that $2\,^3P_1$ atoms are the inevitable product of absorption of the resonance line, which is the primary process concerned. This is, of course, true, and in fact at 2 mm. pressure we can detect the $2\,^3P_1$ atoms by the test of auxiliary illumination, but only in the immediate neighbourhood of the point of excitation. They do not stream up to any important extent with the rising vapour, when the test is made at 2 or 1 mm. pressure.

The distribution of $2\,^3P_1$ atoms is, however, much more easily determined by the resonance radiation (reproductions IV, a, V, a, VI) which is a more sensitive indicator than the method of auxiliary blue illumination. The latter method gives the same result as a *short* photographic exposure to the resonance radiation, and at pressures of 1 mm. or more is only adequate to detect $2\,^3P_1$ atoms close to the point of excitation, where they are most numerous. At lower pressures they can be detected over a considerable volume in accordance with the distribution shown in reproduction VI. Making allowance for difference in sensitiveness, the results of the two methods are in agreement.

To sum up, the distribution of the two kinds of metastable atoms follows the visual green luminosity. The $2\,^3P_1$ atoms follow the luminosity in resonance radiation.

§ 4. *Line Spectrum in Fluorescence.*

The experiments of Fuchtbauer[*] and of R. W. Wood[†] have shown very clearly the mechanism of one type of process by which the mercury line spectrum may occur in fluorescence. What has been described above as the test for metastable atoms is in fact an example of this. It consists in the initial excitation of the mercury atom to the $2\,^3P_1$ level, and further excitation by the absorption of other frequencies. There may then be a descent to the metastable levels, and up again to levels not otherwise accessible.

I have had occasion to observe this type of process in the present work under a form which, if not essentially new, is nevertheless an interesting variant of some of Wood's experiments, and which may conveniently be described here for comparison with that which will follow.

In the work described so far, the chlorine and bromine filters substantially

isolated the resonance line (reproduction I). If these filters are removed, then a tongue of green light showing the monochromatic radiation 5461 projects into the fluorescence vessel. Fig. 5 represents the appearance at 1 mm. pressure showing how the green fluorescence of continuous spectrum passes up, while the tongue of monochromatic green light does not do so. Interposing the blue corex filter, which cuts out any possibility of false light from
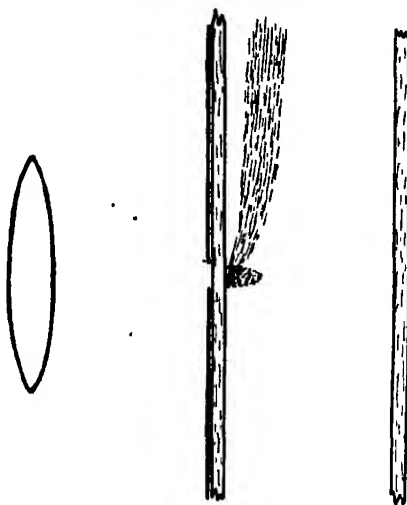
FIG. 5.—1·2 times actual size.

the source, these effects are unaltered, except for inevitable loss of intensity. In this case we have in the main the further excitation of $2\ ^3P_1$ atoms to $2\ ^3S_1$ by absorption of the blue line 4358 from the original source. The point to be emphasised is that the monochromatic green radiation produced in this way does not show the slightest sign of passing upwards in the mercury stream.

If the blue line 4358 is suppressed from the source, the green light in the luminous tongue disappears, but a yellow component, previously masked by the much greater brightness of the green, comes into view. This yellow component is produced by secondary absorption of the ultra-violet lines 3132 and 3126 (see fig. 6) and can be suppressed by interposing the chlorine cell which cuts out these lines from the source.

The colour contrast between the green fluorescence which moves up with the stream, and the yellow tongue which sticks out rigidly in a horizontal direction makes the experiment a striking one. At low pressures, 0·5 mm. for instance, the green fades away, leaving the yellow tongue. It is seen in reproduction VII which was taken through a yellow screen on a panchromatic plate.

The immobility of the tongue of monochromatic green or yellow radiation agrees, of course, entirely with the accepted view that emission of the green or yellow atomic line takes place in a time of the order of 10^{-8} seconds after excitation The gas stream cannot carry the excited atoms any sensible distance in so short an interval.
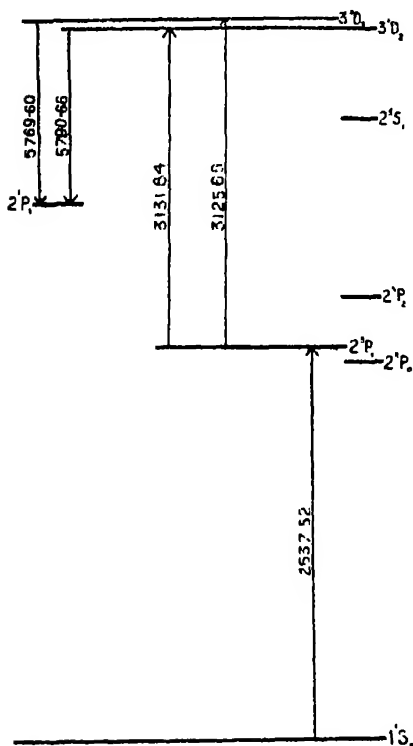
In the cases described so far, line spectrum fluorescence essentially depends on the presence of radiations other than λ 2537 in the source.

I have now to describe a different phenomenon which we get when λ 2537 is isolated by the selective filters, the spectrum of the source being as in reproduction 1. It is found that when the green fluorescence, seen rising as in reproduction IV, c, is examined spectrographically, the complete line spectrum is obtained,[*] superposed on the band spectrum.

A wire was stretched across the wall of the silica vessel, fig. 1, so as to indicate the level of the exciting beam, and the rising luminosity was focussed on the slit of the spectrograph by means of a quartz-fluorite achromat, the obscuring wire being depicted about the middle of the slit. The spectrum (12 hours exposure) is shown in reproduction No. II. 1 cm. of vertical distance on the column of vapour is represented by a slightly longer distance on the reproduction, see scale to the right It is clear that the atomic mercury lines are carried up above the level of the exciting beam in just the same way as the continuous maxima of the band spectrum. I have not so far succeeded in getting satisfactory monochromatic pictures of the rising fluorescence in the light of the various lines, but the evidence of spectrogram III makes it nearly certain that a distribution similar to IV, c, would be shown. The spectrogram shows in addition that the resonance radiation is distributed quite differently

Fig. 6.

* A preliminary account of this result was given in ' Nature,' vol. 128, p. 905 (1931).
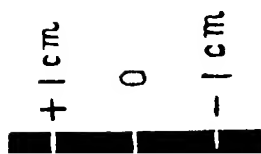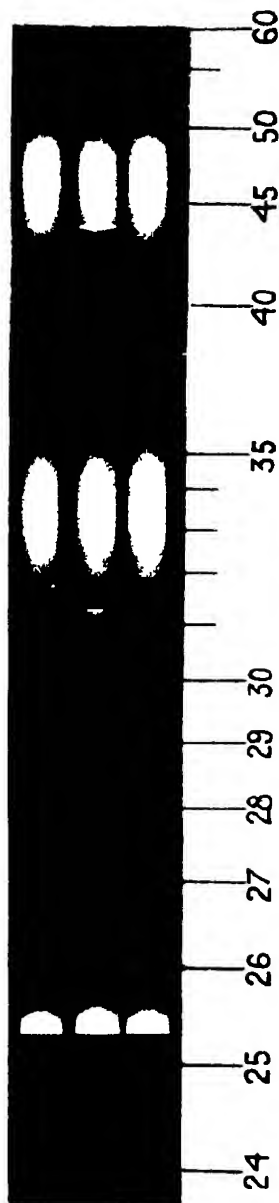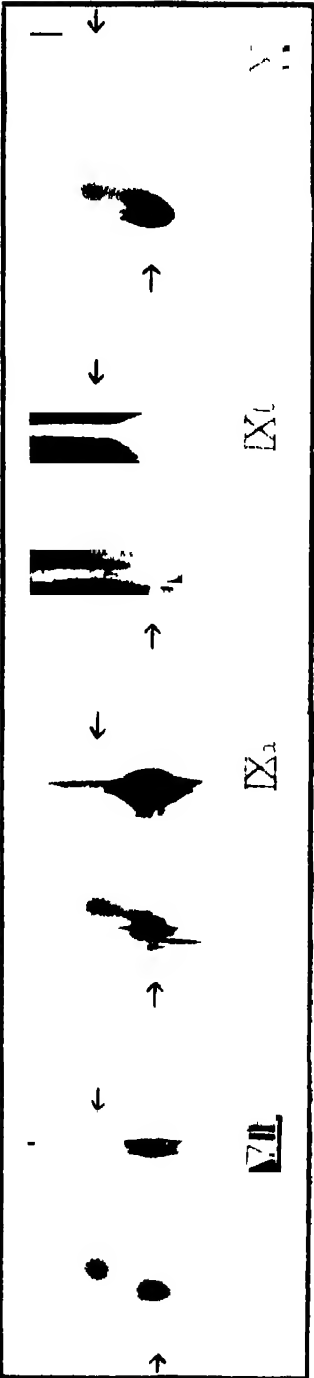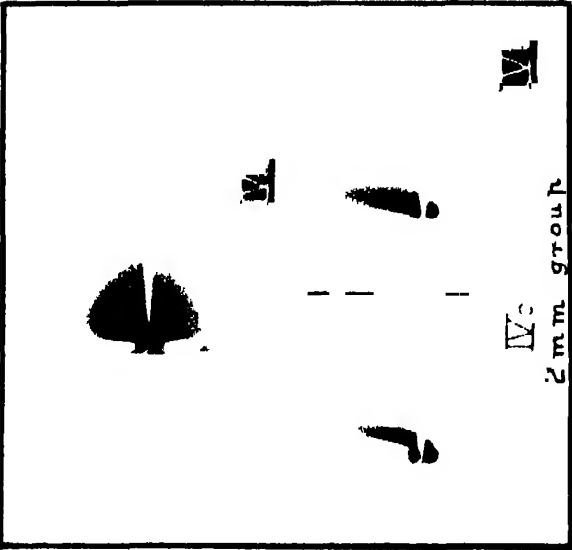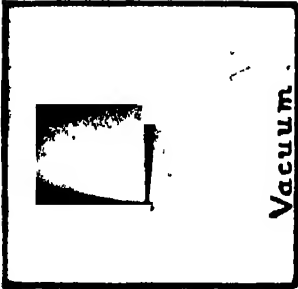
from the other features, being almost as conspicuous below the level of the exciting beam as above it. This is another illustration of what has already been insisted on in connection with the reproduction IV, *a, b, c*. It is necessary to emphasise once more that these atomic lines are effectively filtered out from the source, and cannot be detected by any exposure direct on the filtered source, even to the point of fogging out everything with the light of the resonance line. They originate *de novo* in the fluorescence vessel. Further, they differ from the atomic lines produced by stepwise excitation, in that they are carried along with the mercury stream, or show *persistence.*

The origin of these lines presents one more difficulty in the already involved problem of mercury fluorescence. Since they require higher excitation than the resonance line, the question arises whether we have here a case of multiple excitation. It is known that the band spectrum intensity, including even Wood's bands which are of considerably higher frequency than the exciting resonance line, varies as the first power of the exciting intensity.[*] This was ascertained by Wood's test with perforated zinc, the intensity being found the same whether the latter is placed over the primary source or over the secondary fluorescent source. The perforated zinc used cut down the aperture sixfold.

Using the same perforated zinc in the present case, it is found that the line intensity is much greater when the zinc is over the secondary source, see reproduction No. III. The middle strip represents this case, the outer strips being taken with the perforated zinc over the primary source. This is merely a sample of many such tests. Usually a considerable number of alternate exposures were made on the same plate. The result was always as above.

It appears then that the intensity of the line spectrum increases much more rapidly than the first power of the exciting intensity, probably as the square. This is also the case with the ionisation known to be produced by the resonance line[†] and I fully expected to find that these phenomena were closely connected. So far, however, the experiments made to establish such a connection have not given any positive result. Assuming the line spectrum to be emitted during the recombination process, we should expect that the application of an e.m.f. would make dark a space round the negative electrode, as is found to be the case for the luminous vapour rising from the mercury arc.[‡]

[*] See III, pp. 624–625.

[†] Rouse and Giddings, ' Proc. Nat. Acad. Sci.,' vol. 11, p. 514 (1926) and vol. 12, p. 447 (1926); also Houtermans, ' Z. Physik,' vol. 41, p. 619 (1927).

[‡] See for example ' Proc. Roy. Soc.,' A, vol. 91, p. 92 (1914).

To test this point, two wire electrodes 1 mm diameter and 2 mm. clear distance apart were arranged so as to be bathed in the fluorescent light, fig. 7, using the same filtered source as before. The space between the electrodes was focussed on the spectrograph slit, so that the spectrum should be taken from the region where the electric field was strongest, and that no light should be taken from any other region. 140 volts was applied between the electrodes, and a number of comparable photographs were taken on the same plate with
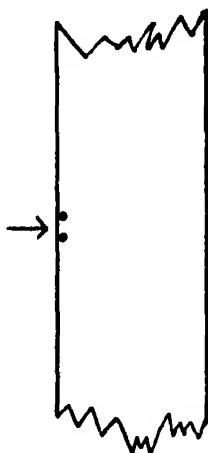
Fig. 7.—Actual size.

the field on and off alternately. This was tried at pressures of 3, 2 and 1 mm , the exposure time being usually 10 minutes. The current passing between the electrodes was of the order of 10^{-7} ampere, but I had no test to determine how much of it was due to a photo-electric discharge from the negative electrode, and how much to direct ionisation of the vapour. No definite difference could be detected in the intensity of the lines, either near the negative electrode or elsewhere, according to whether the field was on or off

It was desired to check this result by visual observation, but the spectrum was not bright enough for the purpose. No change could be seen in the unanalysed visual intensity when the field was applied, but this test is a poor one, owing to predominance of band spectrum.

Removing the chlorine and bromine filter, a strong stepwise excitation of the green mercury line was obtained as before. As might be expected, this luminosity was quite unaffected by the field.

§ 5. *Summary.*

The paper deals with the " core effect," that is to say, fluorescent excitation by the atomic resonance line.

It is shown, more clearly than in previous work, that in a moving current of vapour the resonance luminosity behaves differently from the other components of the fluorescence. It can diffuse itself independently of, and against the vapour stream under conditions when the visual fluorescence is dominated by the vapour stream, and completely carried along with it. It is only at lower pressures that the resonance luminosity is affected by the stream, presumably owing to the greater velocity of the latter.

It is proved by direct experiments that the visual luminosity contains meta-

stable atoms of both kinds—2 $^3P_0$ and 2 $^3P_2$. These are provisionally regarded as supplying the energy from which the persistent luminosity is derived.

The resonance luminosity, on the other hand, contains only 2 $^3P_1$ atoms, and the persistent luminosity in this case is attributed to "imprisonment of radiation."

It is found that the complete line spectrum of mercury is present when excitation is by the resonance line *only*, other wave-lengths being absent from the source. The spectrum thus excited is dominated, like the band spectrum, by the motion of the vapour stream. In this it differs altogether from the line spectrum excited by successive absorptions, as investigated by R. W. Wood.

This new development of the line spectrum is found to increase much more rapidly than the exciting intensity—probably as the square. It appears to be indifferent to an electric field, and for this reason it is difficult to connect it with the ionisation known to be produced by the same kind of excitation.

I have pleasure in thanking my assistant, Mr. R. Thompson, for efficient help in this work.

DESCRIPTION OF PLATES.

PLATE 5.

I —Spectrum of exciting light used. Cooled mercury lamp Resonance line 2537 approximately isolated.

II —Spectrum of fluorescent stream of mercury. 2 mm. pressure Exciting light introduced at the level 0 (zero), marked by an obscuring wire. Vertical distances shown by scale on the right. Note maxima at 2650, 3300, 4850, also line spectrum not present in the source. These are all carried along stream. The resonance line and the band near it are as conspicuous down stream as up stream, compare No. IV, *a*.

III.—Spectrum of fluorescence at 5 mm. pressure. Middle strip, fluorescence cut down sixfold by perforated zinc. Top and bottom strips, perforated zinc removed to source. Band spectrum intensity unaltered. Line spectrum much reduced.

PLATE 6.

The reproductions on this plate are 0·85 actual size.

IV.—Fluorescence, direct photographs at 2 mm. pressure. Level of exciting beam marked by a dark obscuring line.

    a. In light of the resonance line.

    b. In light of the continuous maximum 3300.

    c. In light of the continuous maximum λ 4850 (visual).

V.—Fluorescence, direct photographs at 1 mm. pressure. *a.* in light of the resonance line. *b.* in light of the continuous maxima 3300 and 4850 not separated.

VI.—Fluorescence, direct photograph, in light of resonance line λ 2537. Vacuum, *i.e.*, no gas atmosphere over boiling mercury.

VII.—Yellow fluorescence obtained by simultaneous excitation with 2537 and the pair 3132–3126. Note that it does not rise with the mercury stream. 1 mm. pressure Through yellow filter.

VIII.—Test for 2 $^3P_0$ metastable atoms in the rising green fluorescence. Local brightening due to supplementary excitation by the violet line, the blue not being separated. Arrow on left, original excitation. Higher arrow on right, supplementary excitation 1 mm. pressure.

IX, *a*.—The same, with violet line only (blue suppressed). Local brightening seen.

IX, *b*.—The same, blue line only (violet suppressed). No local brightening seen.

X.—Test for 2 $^3P_2$ metastable atoms. Supplementary excitation by the green line. Shows local brightening of the fluorescence, as photographed in blue light.

A Method of Measuring the Effective Resistance of a Condenser at Radio Frequencies, and of Measuring the Resistance of Long Straight Wires.

By E. B Moullin.

1. *Introduction.*

When the effective resistance of a high frequency circuit is measured by a resonance method, it is usual to find that the resistance exceeds the calculated resistance of the coil. Some of the discrepancy may be due to energy loss in the condenser, and it is desirable to have some means of measuring this loss. The energy loss in high power condensers is now measured regularly by thermal methods and may be as small as $0 \cdot 025$ per cent. of the volt ampere product. But a thermal method is impracticable for the small condensers used in a laboratory because the power absorbed would be less than $0 \cdot 1$ W.

Most of the energy loss in an air condenser is presumably due to the dielectric supporting the plates and to poor contacts between the plates. Dye* has developed a very elegant method for measuring the energy loss in a condenser, which presumes that all the loss occurs in the solid dielectric. In his method there is a special condenser which consists of two capacities in parallel, and

* 'Proc. Phys. Soc.,' vol. 40, p. 285 (1928).

screened from one another.   One portion of this compound condenser contains the insulating supports for the second portion.   Accordingly the second portion contains no solid dielectric and is a pure air condenser and is presumed to have no loss.   This condenser consists of a single circular disc, which may have one of three sizes, contained within a cylindrical box ; the plate hangs from a metal stem which is supported on quartz blocks contained in a chamber above the cylindrical box.   The total capacity may be considered to be in two parts. One between the metal stem and the case and having a dielectric which is partly quartz and therefore imperfect, the other between the circular disc and the case and having no dielectric except air and therefore being perfect. The condenser to be tested can be connected in parallel with the special condenser and its capacity is adjusted to be equal to that between the circular disc and the case.   The disc can be detached from the stem and so leave only the imperfect portion of the special condenser.   The condenser under test is then placed in parallel with the imperfect portion, resulting in a total capacity unchanged by the substitution process.   But the substitution has replaced a capacity without loss for an equal capacity with loss.   The total circuit resistance is measured by a resonance method before and after the substitution and the difference of value is ascribed to the loss in the condenser under test. Since the special condenser is provided with three different discs the resistance of the condenser under test could be measured at three different settings.

By this method Dye found that the effective resistance of the condenser he tested could be expressed as a constant series resistance together with a constant power factor in the insulation and a constant shunt resistance.

A convenient instrumental arrangement has been described by Wilmotte* for making the necessary substitution of the condenser under test for a condenser which has already been calibrated, say, by Dye's method.   Wilmotte finds that the resistance of an ordinary condenser for use in a laboratory can be represented by a constant series resistance together with a constant power factor in the insulation.

An elegant thermal method has been described by Wilmotte,† in which the coil of a resonant circuit consists of a mercury spiral inside a glass tube and the thermal expansion of the mercury allowed the coil to act as its own thermometer.   The total resistance of the circuit was measured by a resonance method using a measured high frequency current and the reading of the "coil thermometer" was noted.   The steady current required to produce the same

* ' J. Sci. Instr.,' vol. 5, p. 369 (1928).
† ' Proc. Roy. Soc.,' A, vol. 109, p. 508 (1925).

thermometer reading was then measured and therefrom the effective resistance of the mercury coil was deduced. The measured and deduced values of circuit resistance were then compared and any discrepancy was attributed to the effective resistance of the condenser. Wilmotte found that the effective resistance of his condenser was too small to be appreciable compared with that of his coil, which was about 1 ohm.

Dye's special condenser and Wilmotte's thermometer coil are devices for separating the resistance of the condenser from the total resistance of the circuit.

Callis* has described a method of measuring the resistance of a condenser by the use of two identical coils. The total circuit resistance is measured first when using the one coil and then when using the second coil. It is again measured when using both coils in series but placed relatively to one another so that the total circuit inductance is the same as if only one coil was in use. It is assumed that the total coil resistance in the third measurement is equal to the sum of the coil resistances in the first two measurements and hence the resistance of the condenser can be deduced. The method is not quite sound, because it ignores the mutual resistance of the two coils and the change of self capacity.

The method of measurement now to be described separates automatically the total circuit resistance into two components, one depending on the coil and one depending on the condenser. In this respect it is equivalent to the method of Dye's condenser or of Wilmotte's coil, but it requires no special apparatus except similar coils wound with wire of different materials. The simplicity of the necessary apparatus makes the method available for any laboratory or works test room.

The particular application of the method described here gives also a check of the skin effect formula for the high frequency resistance of straight wires.

2. *Principle of the New Method.*

The method of measuring the effective resistance of a condenser now to be described, depends on providing an oscillatory circuit with a series of inductance coils which are identical in form but are wound with wires of different specific resistance. The total resistance of a resonant circuit is measured when the inductance is a coil of copper wire and again when this inductance has been replaced by an identical coil of brass or German silver wire. In substituting

* 'Phil. Mag.,' vol. 1, p. 428 (1926).

one coil for another, the only change in the circuit is the specific resistance of the conductors, and therefore any losses which are not located in the wire will remain unchanged by the substitution. At a given frequency the total resistance of the circuit may be expected to consist of a constant component due to losses in the condenser and the supports of the coil and a second component which is a function of ρ, the specific resistance of the wire.

If R_n is the calculated resistance of the coil at a given frequency then R, the total resistance of the circuit, may be expected to be of the form

$$R = \alpha + \beta R_n,$$

where the constant α represents the effective resistance of the condenser and other dielectric losses, and β is a factor which will depend on the self-capacity of the coil ; when the self-capacity effect is small, β will tend to the value unity. Since the relation between R and R_n should be a straight line, α will be determined by the intercept on the resistance axis and its value determines the resistance the circuit would have if the coil could be made of a material having infinite conductivity.

By varying the form, area and construction of the coil without changing the inductance, it is possible to find what fraction of α is due to the condenser and what fraction is due to dielectric loss in the supports of the coil. The slope β of the line is a measure of the amount for which the effective resistance of the conductors differs from that calculated by Butterworth's formulæ,[*] which are derived on the supposition that self-capacity effects are negligible. By relating the change of β with the form of the coil, it should be possible to separate the effect of self-capacity

Hence this method of procedure leads to a means of finding the effective resistance of a condenser at a given frequency and also the effective resistance of the conductors of the coil ; ultimately this leads to a means of checking the formulæ for the high frequency resistance of coils.

By using sets of coils having different inductances, it is possible to relate α with the capacity value at a given frequency and so to find the different factors on which α depends.

The experimental work described here has been mainly directed to establishing the relation $R = \alpha + \beta R_n$. The use of the method to split α into its various components has not been the main purpose of this investigation and such use as is described in this paper should be considered subservient to the general scheme. Probably the subdivision of α can be performed more

* ' Phil. Trans.,' vol. 222, p. 57 (1921).

conveniently by Wilmotte's method, but his method requires the effective resistance of the standard condenser to be known; this can be found very simply by the method here described.

3. *Characteristics of the Coils used in the Measurements.*

The principle of this method is applicable to coils of any shape and form. But since it was desired to establish rigorously the validity of the method, it seemed desirable to choose a form of coil for which the resistance could be calculated with great certainty. For this reason the coils must have a form for which the effect of distributed capacity can be calculated approximately and shown to be negligible in amount. Also the resistance of the coil must not be sensitive to small deformations of shape, for otherwise it would be difficult to trace the effect of a small imperfection of manufacture.

The coils consisted of single turn narrow rectangles, 60 cm. and 89 cm. long, in which the spacing between the wires was twenty times their diameter; the ratio of length to breadth of rectangle ranged between 20 : 1 and 3 : 1 according to the diameter of the wire, but in most of the experiments it was 15 : 1.

This form of coil is an approach to a long uniform two-core cable, in which the longitudinal distribution of current is known to be sinusoidal, and in which the velocity of propagation is sensibly equal to that of free electromagnetic waves *in vacuo*. Hence if J is the current at the far end of the rectangle of length l, the entering current is $I = J \cos 2\pi l/\lambda$, where λ is the wave-length in free space. Assuming that the resistance per unit length is constant and equal to R, we have for the resistance loss

$$W = \int_0^l i^2 R \, . \, dx$$

$$= \frac{I^2 R}{2 \cos^2 2\pi l/\lambda} \int_0^l \left(1 + \cos \frac{4\pi x}{\lambda}\right) dx$$

$$\doteqdot I^2 R \left(1 + \tfrac{4}{3} \cdot \frac{\pi^2 l^2}{\lambda^2} - \tfrac{64}{15} \cdot \frac{\pi^4 l^4}{\lambda^4}\right). \tag{1}$$

This formula should give a very close approximation to the apparent input resistance so long as l is less than, say, $\lambda/10$; but it presumes the current is the same at corresponding points in each leg of the rectangle, and this would be true only if the circuit were isolated in space. One terminal of the tuning condenser is connected to the screen case and thus the corresponding terminal of the rectangle is at earth potential; hence it may be a closer approximation

to reckon l as the perimeter of the rectangle. Most of the rectangles in my experiments were 60 cm. long, and hence the self-capacity correction should be between 1 per cent. and 4 per cent. when the wave-length is 30 m. Though it may not be possible to calculate the self-capacity correction exactly, it is possible to assign superior and inferior limits. Since the current distribution will not depend appreciably on the material of the conductor, the self-capacity correction at a given frequency will not be changed if a copper rectangle is replaced by a similar one of another material and hence the expected linear relationship between R and R_n should not be disturbed by self-capacity effect.

It can be shown that the loss per unit length of two long conductors each of diameter d, spaced apart a distance D, is greater than the loss per unit length of one isolated conductor in a ratio which is less than $D/(\sqrt{D^2 - d^2})$. In the rectangles used in these measurements $D/d = 20$, and so the resistance per unit length was increased by the return conductor by less than $0 \cdot 125$ per cent. This increment is so small that the resistance per unit length of a finite narrow rectangle must be very nearly constant and the end effect will be negligible. Moreover, since the resistance will not be sensitive to small deformations of the rectangle, precision of construction is unnecessary.

The proximity effect will be ignored and the resistance per unit length calculated from the formula for the skin effect of an isolated wire; this is

$$R_n/R_0 = \frac{\sqrt{2Z + 1}}{4},\tag{2}$$

where

$$Z^2 = \frac{\pi p d^2}{\rho},$$

where R_n is the resistance at frequency $n = p/2\pi$, and R_0 is the resistance for steady currents. The meaning of this well-known formula may be exhibited more instructively by writing it in the form

$$R_n = \frac{\sqrt{\rho n}}{r} + \frac{R_0}{4}$$

$$= \frac{\sqrt{\rho n}}{r}\left(1 + \frac{1}{4\pi r}\sqrt{\frac{\rho}{n}}\right).\tag{3}$$

All measurements were made at frequencies greater than 3×10^6 cycles per second on wires not smaller than 1 mm. radius and the greatest value of ρ was 2×10^4, so in the worst case the term within the bracket is only 5 per cent.

greater than unity. To simplify the plotting of the measurements the term within the brackets has usually been ignored and accordingly a linear relation should obtain between R_n and $\sqrt{\rho n}/r$. For the purposes of these measurements the resistance can be written conveniently in the form

$$R_n = \sqrt{\pi R_0 l n} + R_0/4, \qquad (4)$$

where R_0 is the steady current resistance of the whole rectangle of perimeter l; here again the term $R_0/4$ is usually negligible and it is sufficiently accurate to plot R against $\sqrt{R_0 n}$. The radiation resistance of the largest rectangle is $0 \cdot 004 \ \Omega$ at a wave-length of 30 m.; the component due to radiation resistance is negligible in all the experiments.

4. *Method of Measuring the Resistance.*

It was impracticable to measure the total resistance of the tuned circuit by adding known increments of resistance, because these would have made an appreciable change in the circuit inductance; hence it was essential to deduce the resistance of the circuit from the shape of the resonance curve. It is well known that if an oscillatory circuit consists of a capacity C and an inductance L of resistance R, then the ratio R/pL can be deduced from the fractional width of the resonance curve at a known fraction of its maximum height. The distuning can be produced by a continuous change either of circuit capacity or of impressed frequency; both methods have been used in the measurements described here.

Since the inductance of the loops was of the order of one microhenry only, and since the internal inductance of the tuning condenser was known to be of the order of $0 \cdot 2 \ \mu$H, it seemed possible that the system would not behave as a simple inductance in series with a concentrated capacity. But when the square of the wave-length was plotted against the corresponding resonance values of capacity, the result was an accurate straight line between $25 \cdot 6$ m. and 90 m., thus showing that the apparent inductance was constant over this range of frequency and hence the geometry of the simple resonance curve is applicable to the circuit. When the inductance was a rectangle 60 cm. × 4 cm., the slope of the line showed that the effective circuit inductance was $1 \cdot 0 \ \mu$H and the residual capacity was 7 $\mu\mu$F, of which 5 were due to the thermionic voltmeter connected across the condenser and used as the indicator. When two similar loops were connected in series, the apparent total inductance was $1 \cdot 88 \ \mu$H, from which it follows that the residual inductance of the condenser was $0 \cdot 12 \ \mu$H and the inductance of the rectangle was $0 \cdot 88 \ \mu$H. The calculated

inductance of the rectangle was 0·93 μH for steady currents, tending to the limiting value of 0·86 μH for very high frequencies and hence the measured value of inductance agrees closely with the calculated value.

Since most of the circuits had a very sharp resonance curve, distuning by capacity must be performed by a vernier condenser in parallel with the main tuning capacity. It was found that this usual procedure led to erroneous measurements, and great labour was expended in locating the cause of the error. One cause is the internal inductance of the main condenser ; the effect of this is to make the apparent capacity between the condenser terminals greater than the nominal capacity value. Consequently the fractional width of the resonance curve obtained by varying the vernier condenser is credited with a larger value than it should have ; this effect would become inappreciable only if the circuit inductance exceeded about 20 μH.

A second cause of error is due to mutual inductance between the coil and the leads connecting the vernier to the main capacity. This mutual inductance induces a voltage in the leads of the vernier which is cophased or antiphased with the voltage across the main condenser ; the effect of this is to increase or decrease the apparent capacity of the vernier in a constant ratio, and so makes the apparent width of the resonance curve fictitious. This important source of error appears to have escaped notice previously, and is so difficult to eliminate that the use of a vernier is practically inadmissable, unless it is contained in the same screen case as the main condenser.

The use of a vernier capacity had to be abandoned, and capacity distuning could be used only when the resonant capacity and the resistance were such that the resonance curve could be plotted by varying the capacity of the main condenser. The necessary distuning was produced by changing the impressed frequency by means of a vernier condenser attached to the generator, and the fractional change of frequency thereby produced was measured by well-known methods. Table I shows a comparison between the width of the resonance curve measured by frequency change and the width measured by capacity

Table I.

Material.	Diameter of wire	λ_m.	ΔC.	Equivalent ΔC.
	mm.			
German silver	2	80	78	78·6
Brass	2	80	47	48 6
German silver	2	59	33	32 4
Eureka	2 63	79	89	89 4

change, for four circuits which had a large enough resistance to allow the distuning to be measured on the main condenser.

To allow direct comparison between the last two columns of this table, the fractional change of frequency is expressed as an equivalent change of tuning capacity. The two largest values of ΔC are necessarily the most reliable, and here the agreement is closer than $0 \cdot 75$ per cent.; for the other two the agreement is within 3 per cent. The comparison has been made many times and the agreement has always been within 3 per cent. This shows that the same resonance curve is obtained whether the alteration is made in the receiver or the generator, and so presumably the circuit has the supposed characteristics and the method of measuring the ratio R/pL is valid and reliable.

The ratio R/pL for a simple circuit can be deduced from the fractional width of the resonance curve at any given fraction of its maximum height and, for example, it is equal to the fractional width at $1/\sqrt{2}$ of the height. Since all the different rectangles of each series had the same inductance the resistance of any one is proportional to the fractional width of the corresponding resonance curve, and it is more convenient to plot this fraction against R_n than to deduce the value of the resistance. The ratio $R/pL = f$ is called the power factor of the circuit: since R is composed of two portions, one due to conductor-resistance and one due to the effective resistance of the condenser, the power factor may be considered to consist of a portion f' due to the conductors and a portion f'' due to the condenser. The portion f'' is given by the intercept on the axis of f and this intercept will be termed the residue power factor; it is the power factor of the condenser whose effective resistance r'' may be found from the relation $f'' = r''pC$.

5. *Some Experimental Results.*

Several series of similar rectangles were made of copper, aluminium, brass, German silver and eureka wire, and for these materials ρ had the relative values of $1 \cdot 0$, $1 \cdot 3$, $2 \cdot 05$, $3 \cdot 5$ and $5 \cdot 35$ respectively. Curves of f and $\sqrt{R_0}l$ were plotted at many frequencies between 10^7 and $3 \cdot 5 \times 10^6$ cycles per second and the result was always a straight line not passing through the origin. Each rectangle of a series had the same diameter of wire; the diameter of the wire was $2 \cdot 2$, $2 \cdot 63$, $6 \cdot 42$ or $9 \cdot 6$ mm. and for each of these D/d was made equal to 20; there were thus four series of rectangles of a given perimeter, each of the same inductance, but having circuit areas ranging from 240 to 1200 sq. cm.

It was found that the intercept and slope of the line relating f and $\sqrt{\rho}$ was

independent of the diameter of the wire, thus showing that the residue power factor is not a function of the area of the circuit. When this had been established it was more convenient to plot f against $\sqrt{\rho/r}$ (see formula (3)) or f against $\sqrt{R_0 l}$ (see formula (4)) because this procedure gave more points from which to determine the line. If a line is plotted for rectangles of wire of the same diameter, it must be determined from only five points, but plotting f against $\sqrt{R_0 l}$ made ten rectangles available and then, if desired, ten points could be used to determine the line.

The observation points in each of figs. 1 and 2 refer to rectangles of the same perimeter and inductance but not necessarily having the same diameter of wire. Fig. 1 shows f plotted against $\sqrt{R_0 l}$ for rectangles with a perimeter of 120 cm.
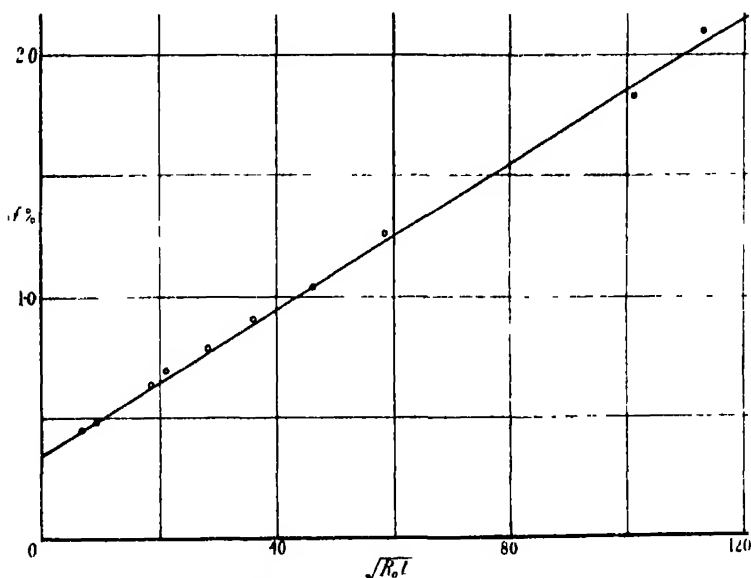
FIG. 1.—Rectangles 120 cm. perimeter at 75 m. $C_0 = 1550\ \mu\mu F.$

at a frequency of 4×10^6 cycles per second ($\lambda = 75$ m.); the ten observation points lie close to the straight line which cuts the axis where $f = 0.35$ per cent. At this frequency the residue power factor is accordingly 0.35 per cent. and presumably this is the power factor of this condenser at this frequency when the capacity is 1500 $\mu\mu F.*$

Corresponding lines for frequencies of 3.34, 3.75, 5.0 and 8.7 k.c./s. are plotted in fig. 2. The residue power factor at $\lambda = 80$ m. is much greater than

* In figs. 1 and 2, R_0 is measured in $m\Omega$ and l in centimetres.

that for the three other lines, because part of the tuning capacity had a dielectric of mica ; this effect is discussed below.
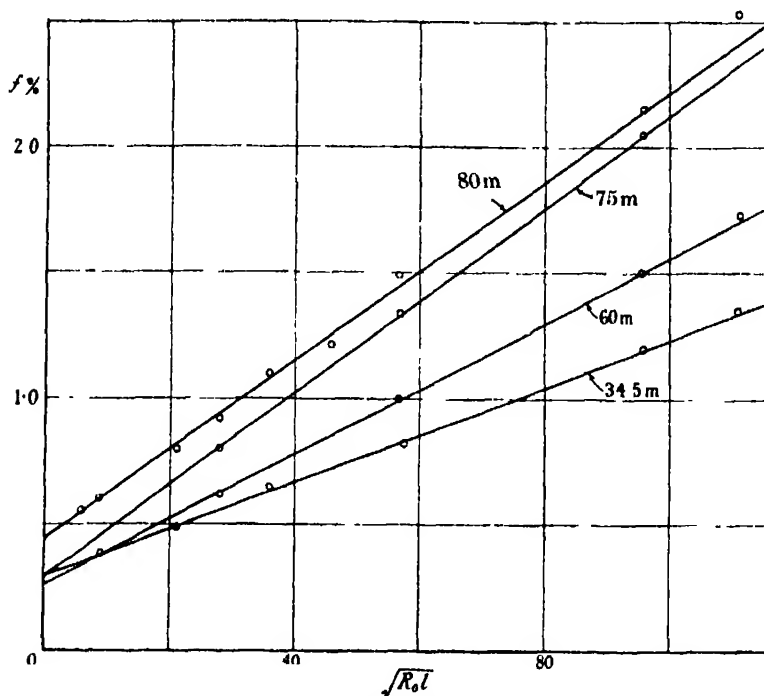
FIG. 2.—Rectangles 120 cm. perimeter.

Fig. 3 shows corresponding lines for copper, brass and German silver rectangles 183 cm. perimeter at frequencies of $8 \cdot 75$ and $6 \cdot 1$ k.c./s.
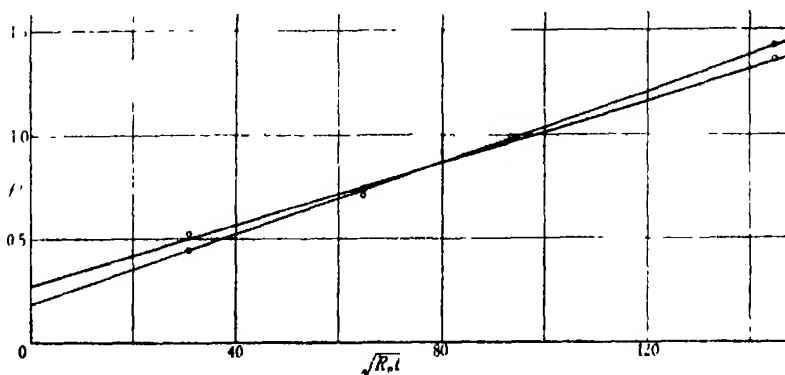
FIG. 3.—Rectangles 183 cm. perimeter at $\lambda = 49$ m. and $34 \cdot 5$ m.

Fig. 4 is derived from figs. 2 and 3, and shows the total resistance of the circuit plotted against $\sqrt{\rho/r}$ at a frequency of $8 \cdot 75$ k.c./s. for rectangles of

120 cm. perimeter and for rectangles of 183 cm. perimeter.   If the coil resistance
is proportional to the length of the wire, then the slopes of these two lines should
be in the ratio $183/120 = 1\cdot52$, whereas in fact they are in the ratio $1\cdot51$.
The self-capacity correction for the longer loop is more important than for the
shorter, using formula (1) and reckoning l as the perimeter, this correction
should be $7\cdot4$ per cent. and $3\cdot2$ per cent respectively   Accordingly the slopes
should be in the ratio $1\cdot52 \times 1\cdot042 = 1\cdot58$, and clearly they are not in this
ratio.   If l is taken equal to half the perimeter, the slope should be in the ratio
$1\cdot52 \times 1\cdot01 = 1\cdot53$, and this agrees with experiment within the limits of
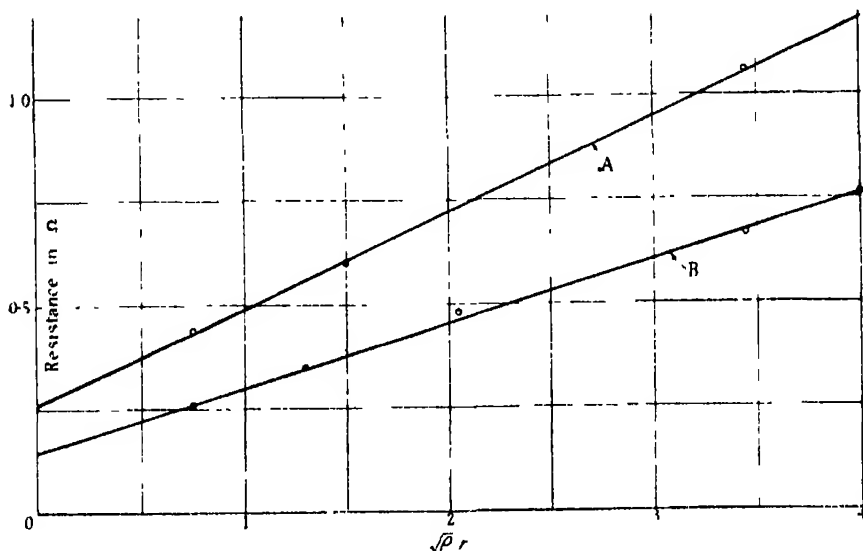
Fig. 4.—A, 183 cm. rectangle ; B, 120 cm. rectangle λ = 34 5 m C_0 = 220 $\mu\mu$F
or $C_0 = 330\ \mu\mu$F.

experimental error.   Thus it seems that the upper limit for the self-capacity
correction is considerably too large.   Figs. 1, 2 and 3 establish the fact that at
a given frequency the total resistance of a circuit consists of a portion which is
independent of the coil and a portion which depends on the specific resistance
of the wire.   Fig. 4 establishes the fact that the apparent resistance of these
rectangular coils is proportional to the length of wire.

6. *Comparison between the Calculated and Measured Resistance of the Conductors.*

Having thoroughly established the linear relationship between R and R_n
and disposed of the self-capacity correction, we are now in a position to make a

E. B. Moullin.

further check of the method by proving that the constant β in the relation

$$R = \alpha + \beta R_n$$

is unity; if β turns out to be unity we have also made an experimental check of the skin effect formula, which is quoted in equations (2), (3) and (4).

Fig. 5 shows the measured resistance of the circuit plotted against the calculated resistance for four different frequencies; the result should be straight lines of unit slope not passing through the origin.
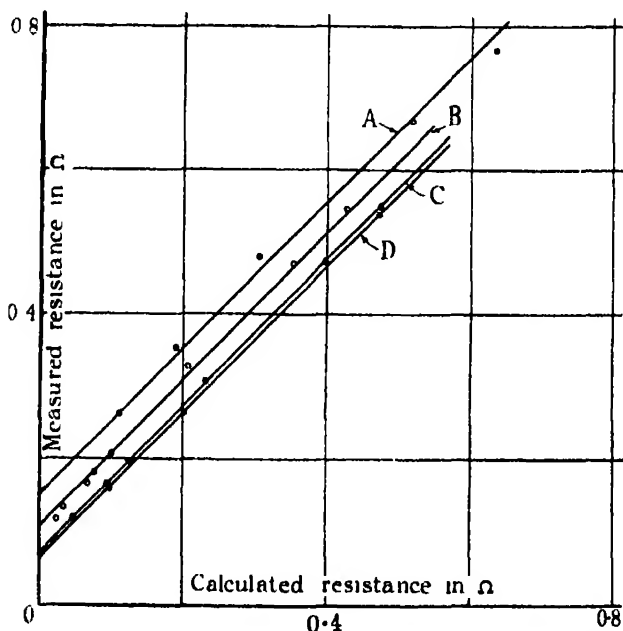
Fig. 5.—A, B and C, 120 cm. rectangles at λ 34·5, 75 and 60 m. respectively; D, 183 cm. rectangle at $\lambda = 104·5$ m.

The lines in fig. 5 are drawn with unit slope and are not drawn through the observation points; but it will be seen that the observation points do lie very close to the straight line of unit slope. This is particularly well exemplified for wave-lengths of 60 m. and 104·5 m. In general there is a strong tendency for the best line through the points to have a slope of about 1·05, but since there are examples where the slope is unity, it would seem that such discrepancies must be attributed to some small error in the system of measurement which sometimes is present and sometimes is not present. The extreme difficulty of measurements of this precision will be well understood by those accustomed to make measurements at frequencies higher than 4 M.c./s. There is some

cause, not yet fully understood by the writer, which gives a tendency for the line to be too steep without producing a tendency for the points to depart from the line.

The magnetic permeability of all the materials has been assumed to be unity in this discussion, but if magnetic impurities made the permeability $1 \cdot 1$, the high frequency resistance would be increased by 5 per cent. The susceptibility of all the 2 mm. wires was measured and the German silver had the greatest value, which was $8 \cdot 7 \times 10^{-6}$; hence there is nothing to suggest that the high frequency resistance should have a value higher than that calculated from formula (4) The discrepancy between the measured and calculated slope of the line connecting f and $\sqrt{R_0 l}$ was for a long time so universal that it seemed as if the effect might well be real, and might possibly be due to the surface skin of the material having less conductivity than the core. At high frequencies the depth of penetration is very small and it may be calculated that 87 per cent of the loss in copper at a frequency of 4 M c /s. occurs in a surface skin of thickness $0 \cdot 025$ mm. , therefore the material just near the surface is all important to the high frequency resistance It was thought that the process of drawing the wire might possibly produce a hard skin which had less conductivity than the core, and that this might be removed by careful annealing. Accordingly a Eureka rectangle was thoroughly annealed by bringing it to a dull red heat by means of an electric current But the circuit power factor after annealing was within 1 per cent of that before annealing.

Although many of the experiments suggest that the conductivity of wires is slightly less for high frequency currents than for steady currents, yet there is also considerable evidence to show that there is no difference. Having regard to the improbability of any appreciable difference, and also to the extreme difficulty of the measurements, it seems right to give more weight to those experiments which agree with calculation than to the larger number of experiments in which there is a small discrepancy between the measured and calculated values.

7. *The Residue Power Factor.*

The residue power factor was determined at several frequencies from the intercept of lines such as those shown in figs. 1-4 It was also determined by measuring the total power factor of the circuit consisting of the condenser and the rectangle of copper rod $9 \cdot 6$ mm. diameter and subtracting from this the calculated power factor due to the conductor resistance. With this rectangle the calculated power factor due to the conductor resistance was always

only about 20 per cent. of the total, so the difference should not be very sensitive to small errors of measurement.

The tuning condenser had a range of 60–1100 μμF and within the screen case there was a fixed mica condenser of 1000 μμF capacity which could be connected in parallel with the variable portion. So it was possible to measure the residue when the capacity was 1100 μμF of air condenser and also when it was 1000 μμF of mica dielectric together with 100 μμF of air. With the rectangles of 120 cm. perimeter, this occurred at a wave-length of 62 m.; for all longer wave-lengths the dielectric was partly air and partly mica.

A line similar to those shown in the figures was obtained at 62 m. wave-length by using the four rectangles of wire 2 mm. diameter; when all the dielectric was air the residue power factor was 0·33 per cent., but when 91 per cent. of the capacity had a mica dielectric the residue was 0·63 per cent. The increment of 0·3 per cent. must be due to the mica condenser. The same difference of residue was obtained when the rectangle of 9·6 mm. rod was used as the coil.

Fig. 2 shows that the residue power factor for these circuits is substantially independent of frequency, but it may still be asked why this residue should be attributed to the condenser.

It has been seen that the residue can be increased by 0·3 per cent. by substituting a mica condenser for an equal capacity of air dielectric, a change which was performed by closing a light switch and revolving the spindle of the air condenser; therefore the change was definitely due to something within the screen case of the condenser. A thermionic voltmeter was connected across the condenser, but the addition of a second one in parallel showed no appreciable increase of residue power factor; the residue therefore cannot be attributed to the voltmeter. Also a variable condenser was connected in parallel with the voltmeter, and close to its terminals; when this capacity was at least five times that of the voltmeter the residue was the same as when the voltmeter alone was present. Evidently then the indicating instrument is not the cause of the residue, which accordingly must be attributed to the condenser. If the loss in the condenser is due to the insulating bushings, this loss should become relatively more important as the air capacity is reduced.

We will now consider the probable structure of the residue power factor and residue resistance. Both Dye and Wilmotte have shown that the effective series resistance of a condenser tends to have a constant portion r which is due to imperfect contact between neighbouring plates. The capacity of a variable condenser may be considered to consist of a fixed capacity C' which has

dielectric loss from the supporting insulators, in parallel with a variable portion which has no dielectric loss   If the power factor of the insulation is ϕ', then R_s, the effective series resistance when the capacity is C and the frequency is $n = p/2\pi$, is given by

$$R_s = r + \phi'C'/pC^2.$$

It is common experience that ϕ' is roughly independent of frequency and we shall expect to find a linear relationship between R_s and $1/pC^2$.

Fig. 6 shows the observed values of R_s plotted against $10^6/nC^2$, where n is the frequency in M.c./s. and C is the capacity in $\mu\mu F$ The five points lie close to the straight line whose equation is

$$R_s = 0 \cdot 05 + 10^6/11C^2n.$$

Assuming that C' is of the order of 20 $\mu\mu F$, then ϕ', the power factor of the ebonite insulation, is about $2 \cdot 6$ per cent   Fig 6 covers a range of wave-
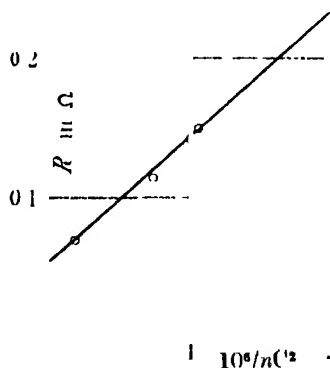
Fig 6.

length from 34 to 60 m. and a range of capacity from 220 to 1000 $\mu\mu F$.   The constant series resistance is of the same order as that found by Wilmotte, but the power factor of the ebonite considerably exceeds his values.

When the fixed mica condenser of capacity 1000 $\mu\mu F$ is in parallel with the air variable condenser, the relation of apparent series resistance to total capacity and frequency is shown in Table II.

There seems to be no simple function relating these quantities.   But since at $4 \cdot 75$ M c./s. the total power factor of the circuit was $0 \cdot 33$ per cent. without

Table II.

n in M c /s.	Total capacity.	R_v in Ω.
2 86	2030	0 065
3 75	1880	0 088
4 0	1550	0 11
4 75	1100	0·18

the mica condenser and 0·63 per cent. with the mica condenser, it is clear that the construction of this condenser must have been quite unsuited to these frequencies. It is absurd to attribute so large a power factor to dielectric loss in the mica and it is scarcely worth while to analyse a loss which must have been due to unsuitable construction. The process of measurement shows at once that this mica condenser is quite unsuited to high radio frequencies , as the condenser was contained in a sealed case, the method of connection to the mica condenser was not investigated.

Figs. 1 and 2 show that at frequencies of the order of 5 M c./s., the power factor of an ordinary high-grade condenser is more than half the total power factor of a copper circuit. Consequently the design of the coil is not of as much practical importance as the design of the condenser. However, it is easy to obtain a circuit power factor of 0·5 per cent. at a frequency of 5 M c./s., whereas considerable skill is required to obtain this power factor as a frequency of, say, 500 k c /s.

In fig. 7 is plotted the residue power factor of a circuit in which the coil was a rectangle of 120 cm. perimeter ; the figure covers a range of wave-length from
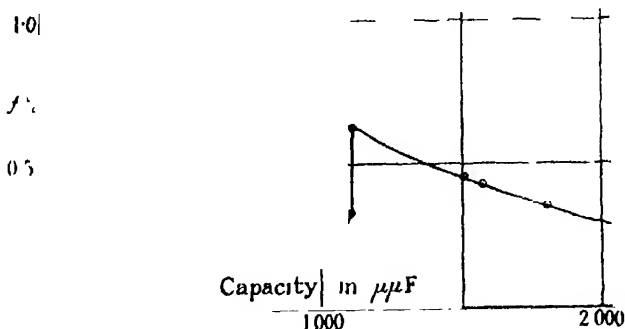
Fig. 7.

30 to 80 m. The sudden discontinuity when $C = 1100$ $\mu\mu$F is due to sub- stituting 1000 $\mu\mu$F of mica condenser for the same capacity of air condenser.

Between 200 and 1100 μμF the residue power factor is sensibly constant. According to the expression derived for R_s, the equation connecting f and C should be

$$f = \frac{1}{2 \times 10^4} \sqrt{\frac{\overline{C}}{L}} + \frac{0 \cdot 57}{C},$$

where C is in μμF and L in μH. For this circuit L = 1 μH, and substitution will show that f should remain sensibly constant for values of C between 200 and 1100, with an ill-defined minimum when C = 700.

Summary

The resistance of a high frequency circuit usually exceeds the calculated resistance of the inductance coil and the discrepancy is often attributed to the condenser. This paper describes an experimental method of separating the total resistance into a component due to the resistance of the conductors of the coil and a component which is independent of the coil. The method consists in using similar coils wound with wires of different specific resistance and in plotting the measured resistance of the circuit against the calculated resistance of the coil. The result is found to be a straight line not passing through the origin, thus showing there is a component of resistance which does not depend on the conductivity of the wire in the coil; the intercept on the resistance axis shows the resistance of the condenser at the frequency in use. The slope of the line gives a measure of the amount by which the true resistance of the coil exceeds the calculated resistance and this can be used to examine the self-capacity correction.

The manner in which the resistance of a condenser depends on frequency and capacity can be studied from the intercepts given by a family of such lines. An example of such an analysis is given, and it is found that the condenser tested has a constant series resistance and a constant power factor in the insulation.

The coils used for the experiments were long, narrow rectangles, and for such the skin effect formula for a long straight wire is applicable without modification. For frequencies between 3 and 10 million cycles per second the measured resistance of a wire agrees with the calculated value.

Electrolytic Valve Action and Electrolytic Rectifiers.

By EDGAR NEWBERY, D.Sc., F.I.C., University of Cape Town.

[PLATES 7-9]

Introductory.

The theories of electrolytic valve action and electrolytic rectification of alternating currents are at present in a somewhat unsatisfactory state, several conflicting theories having been put forward recently.

Schulze* suggested that valve action is caused by an insulating skin of ultra-molecular thickness with a thin layer of gas within it. This theory is now generally discredited.

Muller and Konopicky† suggest that in the case of aluminium, a layer of negatively charged hydroxide gel is formed, and this is pressed against the metal, squeezing out the electrolyte when the aluminium is the anode, the process being reversed when the aluminium is the cathode. It appears impossible to imagine this process occurring with sufficient rapidity to rectify an alternating current with a frequency of 50 or more per second. The heat developed at the electrode surface would be far greater than is ever found in practice, and the work to be described in this paper shows this theory to be untenable.

Pietenpol and Freisen‡ suggest a double layer of aluminium oxide and hydroxide, the hydroxide acting as a semi-permeable membrane to certain ions. The accumulation of negative ions in the double layer is supposed to account for the high resistance and for the counter e.m.f. observed. This appears to be a much more possible explanation of the observed phenomena. The idea of the formation of a semi-permeable membrane was put forward independently by the present author in the same year in a communication to the Royal Society of South Africa and later published in a paper on the theory of electrodes § It is doubtful, however, if the formation of hydroxide plays an essential part in the process, or whether the presence of such a double layer is

---

* 'Trans. Faraday Soc.,' vol. 9, p. 266 (1913).
† 'Z. Phys. Chem.,' vol. 141, p. 343 (1929).
‡ 'Phys. Rev.,' vol. 33, p. 277 (1929).
§ 'J. Amer. Electrochem. Soc.,' vol. 58, p. 187 (1930).

not to be looked upon as a secondary effect to be avoided as much as possible. This point was investigated in the course of the present work.

Lilienfelt, Appleton and Smith* treated the formed aluminium anodes as condensers and investigated the change in rate of leak under various conditions. They concluded that the observed deterioration of the condenser during idleness was not due to loss of oxygen or oxide from the anodic layer but to a re-arrangement of the molecules previously oriented in this layer by the electric field They also concluded that conduction through the layer occurred by the passage of electrons from molecule to molecule. This ascription of metallic conductivity to aluminium oxide or hydroxide appears improbable.

In the course of a discussion on the above paper, Coulter stated that the hardness of the anodic film on aluminium in immediate contact with the metal is 50 times that of the outer surface layer and 70 times that of the metal itself.

In view of the differences of opinion shown by these workers, it was decided to attempt the application of the cathode ray oscillograph to the solution of the problem, since this apparatus has proved itself of great value in the study of other forms of electrode phenomena.†

Experimental.

The essential parts of the apparatus used are shown in fig 1. Owing to the complicated nature of the complete apparatus certain parts (*e g* , the filament, high tension battery, motor, etc.) have been omitted in order to simplify the diagram, but a complete diagram of the oscillograph connections has been shown in a previous communication (*loc. cit*). The present apparatus differs from that previously used for over-voltage work in several important respects :—

(1) The double commutator C is arranged to reverse the current through the experimental cell E, giving the effect of a rectilinear alternating current when the cell is replaced by a metallic resistance.

(2) No standard electrode is used in the cell E, and no standard cells are used for marking potential points on the photographs

(3) By means of the mercury cups *a*, *b*, .. *h*, the current could be passed either directly through the cell E whilst the electrodes were connected

---

* ' Trans. Amer. Electrochem. Soc.,' vol. 58, p. 285 (1930).

† ' Proc. Roy. Soc.,' A, vol. 107, p. 486 (1925); vol. 111, p. 182 (1926); vol. 114, p. 103 (1927); and vol. 119, p. 680 (1928).

to the deflecting plates of the oscillograph, thus giving records of the voltage changes at the electrodes, or through the deflecting coils DD
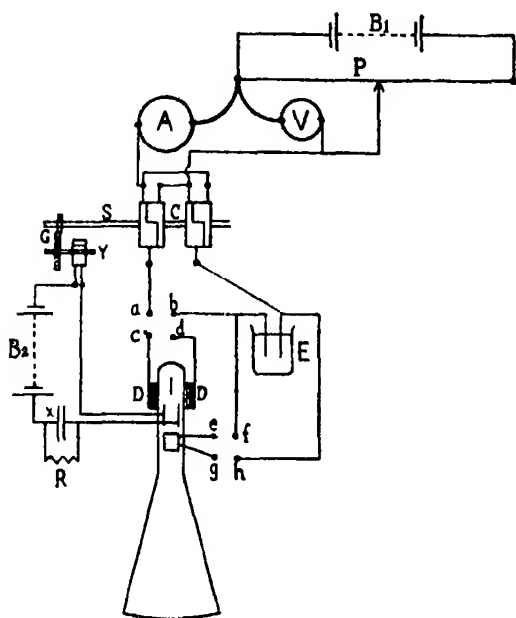
Fig. 1

and then through the cell E, thus giving records of the current changes through the cell.

(4) Since voltages up to 24 volts were used, and the currents through the coils DD were from 25 to 1000 milliamperes, the deflections of the cathode ray were so great that a thermionic valve was not needed. Two pairs of coils, 240 and 30 turns respectively, were employed, the latter for studying the effects of very high current densities, but all the photographs here shown were obtained with the use of the larger coils

(5) The previous arrangement for the horizontal deflection of the cathode ray, although very suitable for commutator speeds of the order of 200 per minute, was not suited for the speeds of the order of 1200 per minute used in the present work.

Two different devices were utilised for this purpose. The first consisted of a discarded motor car magneto which was rewound with 32 gauge wire and fitted with a two-part commutator with adjustable brushes. The small gear wheel of the magneto (40 teeth) was fitted to the spindle S of the commutator C, and the large gear wheel (80 teeth), was fitted to the spindle of the magneto.

When the brushes were adjusted in a position at right angles to that usual for continuous current, and connected to the vertical deflecting plates of the oscillograph, the spot was drawn horizontally across the screen with a fly-back motion, once for every revolution of the commutator. The motion near the centre was fairly uniform and the length of the line thus drawn could be adjusted by means of a variable shunt connected across the brushes. The first six photographs, figs. *a* to *f*, Plate 7, were obtained with this apparatus. The disadvantage of this method lies in the fact that although it gives excellent representation of the behaviour of the electrodes when the current is reversed in one direction, it does not show the behaviour on reversal in the other direction, unless the current through the whole apparatus is reversed and a separate photograph taken.

In order to remedy this defect and obtain both effects on one photograph, a smaller gear wheel (20 teeth) was fitted to the spindle S, but this proved unsatisfactory as the speed of the magneto was now too low to produce a suitable horizontal deflection The device shown in fig. 1 was therefore constructed (1 represents a pair of gear wheels, 2 to 1 ratio, with an ebonite cylinder Y fitted on the same spindle as the larger gear wheel In the circumference of this cylinder, a narrow brass bar was embedded and two platinum tipped brushes, pressing against the cylinder, were electrically connected by the brass bar, once in each revolution. By this means, the condenser X (3 micro-farads) was charged from battery B_2 (36 volts) and allowed to leak through the resistance R (20,000 ohms) once for every *two* revolutions of the commutator, thus drawing the cathode ray across the screen at half the speed obtained with the magneto device The remaining photographs, *g* to *p*, were obtained in this way.

The rest of the apparatus needs little comment. The main battery B_1 was 24 volts, the potentiometer P, 90 ohms, the ammeter A, a three-scale instrument reading from 0·1 milliampere to 1·2 ampere, and the voltmeter V, a high resistance (150,000 ohms) instrument reading from 0·3 to 36 volts.

For the estimation of rectification efficiency, a second ammeter was introduced between the points *a* and *b*, and its reading compared with that of A. Both ammeters were for direct current only.

Results

The nature of the current supply to the cell may be seen from fig. 2, Plate 9, which was obtained by replacing the cell E with a metallic resistance adjusted

to give the same current at the same voltage that was applied to the cell with platinum electrodes, the curve of which is shown in fig. *o*, Plate 9.

The following table gives the data relative to the curves shown in Plates 7 to 9. In the last column, the letter C denotes that the coils DD were connected with the cell, thus giving a record of the current changes in the cycle, and the letter V denotes that the deflecting plates of the oscillograph were connected with the cell, giving a record of voltage changes.

Plate.	Electrodes	Electrolyte	Current in milliamperes.	Voltage	
I, *a*	Al-Pb	$(NH_4)_2HPO_4$	25	10	C
b	"	"	100	13 5	C
c	Ta-Pt	H_2SO_4 N/1	25	10	C
d	"	"	100	15 6	C
e	"	"	25	10	V
f	"	"	100	15 6	V
g	Bi-Ni	NaOH N/1	100	2 1	C
h	"	"	100	2 1	V
II, *i*	Al-Pb	$(NH_4)_2HPO_4$	25	10	C
j	"	"	100	13 5	C
k	"	"	25	10	V
l	"	"	100	13 5	V
m	Sb-Pb	"	100	2 1	C
n	Bi-Pb	"	100	2 4	C
o	Pt Pt	H_2SO_4 N/1	100	1 2	C
p	"	"	100	1 2	V

The lower portion of each curve shows the path of the cathode ray when the *first* named metal is the anode.

The spot was in all cases drawn from left to right of the photograph.

The zero line is marked on the voltage curves, except fig. *p* The lower portions of curves *a* to *d* and *i* to *j*, lie on the zero line. In figs *g*, *m*, *n* and *o*, the position of the zero line is indicated by a series of dots produced by the small insulating gaps in the commutator.

It was found that the general character of the curves was unaltered by variations of the commutator speed between 600 and 1800 per minute. The commutator was therefore rotated at a uniform speed of 1200 per minute for all the photographs shown. All the electrodes were flat plates having an exposed area of 1 sq. cm. and were fixed about 1 cm. apart. The surfaces were bright and polished to begin with. Iridescent films were formed on the Ta, Sb and Bi electrodes, but all retained the polished appearance. The backs of the electrodes and the leads were coated with paraffin wax. The temperature was $18° \pm 1°$.

Discussion of Results.

The above photographs have been chosen out of a large number in order to illustrate the following conditions :—

Valve action.	Rectifying action	Chemical action	Fig.
None	None	None	2
None	None	Strong	*o, p*
Strong	Small	Strong	*g, h, m, n*
Strong	Perfect	None	*a* to *f, i* to *l*

Fig. *o* shows very clearly the effect of the chemical action of the deposited gases on platinum electrodes in increasing the current at the moment of reversal. The extremities of the four parts of the curve are slightly outside the print.

In figs. *m* and *n*, the behaviour of Sb and Bi electrodes in ammonium phosphate electrolyte is illustrated   These electrodes show very pronounced valve action inasmuch as an applied potential of 24 volts will only produce a steady current of about 2 milliamperes when they are anodes, whereas the resistance of the cell is 10,000 times less when the current is reversed. Nevertheless the curves indicate that little or no rectification of a rapidly alternating current occurs, and this was confirmed by including a D C. ammeter in the cell circuit, the current registered being less than 0 1 milliampere   It is therefore necessary to distinguish between valve action and rectifying action as two partially independent phenomena   From the shape of the curves it is evident that chemical action at the electrodes is pronounced

Fig. *g*, obtained with bismuth and nickel electrodes in sodium hydroxide electrolyte, shows a further stage in which indications of rectification are more definite. The upper portions of the curve are now nearly horizontal, the slight downward bend being due to the slow reduction of bismuth oxide.

The lower portions of the curve are remarkable, their length being approximately twice that included in the photograph, the extremities falling outside the oscillograph screen. This indicates a very rapid and violent oxidation of the previously reduced bismuth oxide with formation of a film which very quickly reduces the current to a small value. In spite of this sudden rush of current, the total quantity of current passed is less than that obtained in the rest of the cycle and partial rectification of the alternating current occurs, but only to the extent of about 5 per cent. of the total current under these conditions. It is evident from this curve that the rectification efficiency will

be higher if the commutator speed is reduced. This was confirmed by direct observation.

The fact that anodic oxidation of Bi takes place more rapidly and completely than cathodic reduction of the oxide is further shown by the formation of an oxide coating on the Bi electrode when alternating current is passed.

As a consequence of this, a clean Bi electrode will at first allow a larger current to pass when this electrode is positive than when it is negative. As the insulating film increases in thickness, the rectified current falls to zero and then again increases in the reverse direction

The original inverse rectification is more easily observed in ammonium phosphate electrolyte than in alkali.

A zinc electrode in ammonium phosphate electrolyte gives oscillograph curves very similar to those obtained with Bi in NaOH.

In figs. *a* to *d*, *i* and *j*, the whole character of the curves is completely changed. The lower portions of the curves are now horizontal straight lines lying on the zero line, indicating the absence of all current and all chemical action. The upper portions are now sharply rising to a constant value instead of falling as in the previous cases. It is therefore very improbable that any chemical action is occurring at these points since such chemical action would tend to assist the current, specially at the instant of reversal, and would therefore bend the curves in the opposite direction. This absence of any assisting chemical action is partly responsible for the greatly increased resistance of the cell when true rectification occurs, but the source of the greater part of this increase must be located on the surfaces of the Al or Ta electrodes. This subject will be discussed later. Substituting Pt for Pb in the ammonium phosphate electrolyte, or for Ni in NaOH, or replacing Pt by Pb in the H_2SO_4 electrolyte had no effect upon any of the curves here shown. Also the curves obtained with Al–Pb or Al–Pt in a saturated borax-boric acid electrolyte were identical with those shown for the ammonium phosphate electrolyte.

A " dry " rectifier composed of a copper plate covered with powdered native bornite in contact with a plate of surface-oxidised magnesium was also tried and gave curves similar to figs. *i*, *j*, but the current was very irregular, apparently due to sparking at the numerous contacts. This subject will be studied further.

Theory of Electrolytic Rectification.

It is evident from the work described that whereas a rectifying electrode must of necessity show valve action, it by no means follows that a valve

electrode need show any appreciable rectifying action. The stoppage of the current by a valve electrode when it is anode is undoubtedly due to the formation of an insulating compound of the metal of the anode with the anion or some part of the anion, this compound being insoluble in the electrolyte. When the current is reversed, cations (usually H) must be deposited on the metal of the electrode before they can be discharged and thus allow current to flow, but before they can reach the metal they must first pass through the anodic film already formed. This film must therefore act as a semipermeable membrane, permeable to hydrogen ions but not to the larger anions present.

Now if this anodic compound (usually the oxide) is reducible by the discharged H ions, chemical action will occur, gaseous hydrogen being prevented from forming in quantity sufficient either to produce transfer resistance or to set up any appreciable back e m f When the current is reversed, chemical action will again occur, namely the re-oxidation of the metal surface, allowing a considerable quantity of current to pass before the insulating film has become thick enough to stop it Under such conditions, little or no rectification of an alternating current occurs unless the frequency is very low. At the same time, the effective electrical resistance of the cell will be low   Antimony, bismuth and zinc electrodes in suitable electrolytes, behave in this way. If the anodic compound is not reducible by the discharged H ions, no chemical action can occur after the continuous semi-insulating film has formed. Hydrogen gas can now accumulate on the valve electrode and oxygen gas on the other, and these gases cannot be removed electrolytically from either, owing to the blocking of the current in the necessary direction by the inability of the large anions to penetrate the film on the valve electrode. Transfer resistance will therefore be in evidence at both electrodes, over-voltage phenomena will appear, and the back e.m.f. due to the gases on the electrodes will also oppose the flow of current. There is, however, another factor which may have as great an effect in raising the total effective resistance of the cell as all three of these factors. When the large anions strike the membrane and are unable to penetrate it, there must be a powerful hammering action tending to close up the pores of the membranes so much that the number sufficiently large to admit a H ion will be considerably diminished. When the current is reversed, some of these pores, the walls of which have been in a state of strain, will open out ; others will be opened further by the stream of H ions entering and by the discharged gas escaping. The former process will occur very rapidly, the latter more slowly, but both will increase the available area for the deposition of H ions and lower the total resistance of the cell. The effect of the former process

which is really due to the natural elasticity of the film, is well shown by the sharply rising portions of the curves in figs. *a* to *d*. The effect of the latter process is not evident from these figures as the time interval is too short, but is readily observed if the commutator is stopped in the valve electrode-cathode position. This was done after taking photograph *b*, and the voltage needed to maintain a current of 100 milliamperes fell from 13·5 to 5·0 in the course of 30 seconds.

It is obvious from this theory and from the appearance of the curves that an increase in the frequency of the alternating current should increase the apparent resistance of an electrolytic rectifier. This was tested with an Al-Pb pair in ammonium phosphate electrolyte, and it was found that change of commutator speed from 900 to 1800 revolutions per minute increased the apparent resistance by 7 per cent.

Composition of the Rectifying Film.

Most of the theories quoted in the introduction to this paper assume the presence of aluminium hydroxide in the rectifying film on an Al electrode. In order to test this, a polished Al electrode was heated to dull redness and then cooled in a desiccator to ensure a coating of oxide only on the surface. This was then fitted up in the apparatus in such a way that the last electrical connection was made by the immersion of the aluminium in the ammonium phosphate electrolyte. Rectification was instantaneous and perfect.

Other electrodes were cut from a polished aluminium sheet and treated in the same way, with and without the preliminary heating, and the results obtained were identical in every case, the electrodes remaining bright and quite unchanged in appearance after use   We are therefore bound to conclude that it is an oxide and not a hydroxide film which is responsible for electrolytic rectification, and further that this film is already present on a bright aluminium sheet which has been exposed to the atmosphere. Also there appears to be no orientation of the molecules of the film by the electric field as postulated by Lilienfeld, Appleton and Smith. The so-called "formation" of an aluminium electrode for rectifying purposes is therefore quite unnecessary if bright Al is used, at least for the comparatively low voltages (24 volts) used in this work. For higher voltages, some thickening of the film may be necessary.

In order to examine the formation of the electrode as usually carried out, the surface of a used electrode was roughened and the original film destroyed by rubbing with fine emery cloth. On connecting up with the apparatus, the

series of changes roughly illustrated in fig. 3 was observed. As the whole series only took about 30 seconds to complete, it was not possible to obtain suitable photographs, but the sketches will give some impression of the gradual diminution of chemical action and stoppage of the current when the Al is the anode, due to the re-formation of the oxide film.

1   2

Fig 3

It is probable therefore that the deterioration of an aluminium electrolytic condenser studied by Lilienfeld, Appleton and Smith (*loc. cit.*) is due to the slow hydration of this oxide film expanding it, rendering it less adherent and more porous, and thus exposing the underlying metal to further chemical action. The greater hardness of the layer next to the metal observed by Coulter (*loc. cit.*) is due to this layer being composed entirely of oxide whereas the outer layers are more or less hydrated. The presence of hydroxide is therefore a marked disadvantage, as it increases the resistance of the cell and reduces the condenser capacity without contributing to the rectifying action. An electrolyte which would prevent or hinder this hydration would therefore improve the life and action of an aluminium rectifying cell or electrolytic condenser. Possibly the addition of a very soluble and hygroscopic solute or the use of a non-aqueous electrolyte might effect this.

The Tantalum Rectifier.

This needs but little comment. Its action appears to be exactly similar to that of aluminium, its rectifying action being nearly perfect. Rotating the commutator by hand shows that even after long cathodic treatment, when the current is reversed, it drops to zero in about 0·01 second. After anodic

treatment, the cathodic current requires about 20 to 30 seconds to rise to its maximum value for a given voltage, this value being about double that obtainable with rapid alternations at the same voltage.

Determining Factors for Electrolytic Valve Action and Rectifying Action.

For an electrode to show valve action, the following conditions must be fulfilled :—

(1) The compound formed by the anodic action must be a good insulator.
(2) This compound must adhere closely to the electrode.
(3) The compound must be insoluble in the electrolyte present.
(4) The film thus formed must be permeable to hydrogen ions but not to the anions present.

If the electrode is to show rectifying action, it must have all the above properties and in addition-

(5) The anodic compound must be irreducible by electrolytic hydrogen, and not further oxidisable by discharged anions

Only a few electrodes can be found to fulfil the first set of conditions and fewer still to fulfil the last. With regard to condition (1), so many of the anodic oxides are electronic conductors that passivity is much more common than valve action, and it is even possible to convert a rectifying electrode into a passive electrode by anodic oxidation. A magnesium electrode which has been heated in the air until it is well covered with a hard film of oxide, when placed in a NaOH electrolyte with a subsidiary nickel electrode gives very good rectification of an alternating current for a few seconds only, the oscillograph record resembling fig. *j*. In a short time, however, a series of changes similar to those shown in fig. 3 proceeds backwards, and the curve finally resembles fig. *o*. On stopping the commutator with the Mg as anode, oxygen is freely evolved from the now passive Mg electrode. The insulating MgO has apparently been oxidised to some higher oxide which has electronic conductivity.

Condition (2) is more often fulfilled than (1). Silver, mercury, and tin anodes in a sodium hydroxide electrolyte afford examples of loosely adherent anodic deposits, but most anodic oxides adhere to the electrode very strongly.

Condition (3) with suitable choice of electrolyte, can be fulfilled with nearly all the metals except those of the alkalies.

a

$\bar{b}$

c

d

e

f

g

h

k

l

Newbery.

Proc. Roy. Soc. A. col 137 Pl 9

m

n

o

p
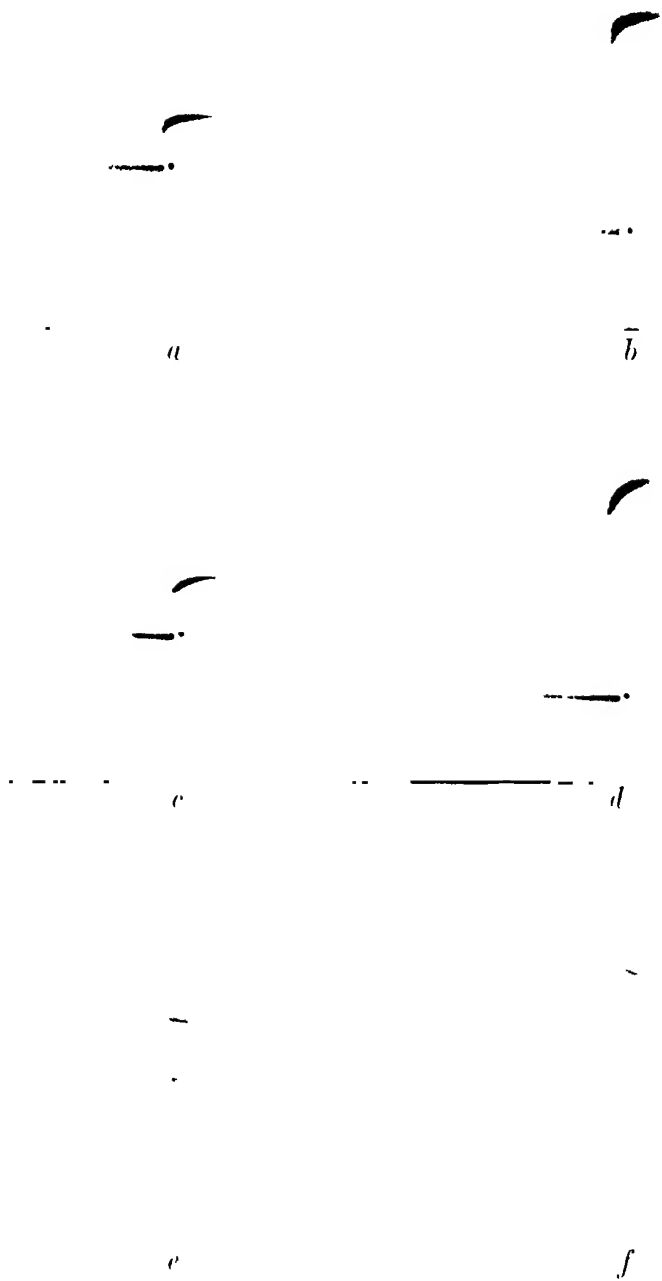
Fig 2

Condition (4) is fulfilled by all the insulating anodic films so far investigated if they adhere to the electrode.

Condition (5) is fulfilled by the films on aluminium, tantalum, and possibly certain other metals not yet investigated.

Summary.

The behaviour of various valve electrodes and rectifying electrodes has been investigated with the aid of the cathode ray oscillograph.

Valve action is due to the formation of an adherent insulating anodic film which is permeable to H ions but not to the anions present.

Rectifying action occurs when such a film is not reducible by the electrolytic hydrogen produced on it, and is also unchanged by further anodic action.

The film responsible for the rectifying action of an aluminium electrode is the oxide only. Hydration of this oxide destroys its rectifying efficiency.

Some Tests on the Stability of Thin Strip Material under Shearing Forces in the Plane of the Strip.

By H. J. Gough, D.Sc., M.B.E., and H. L. Cox, B.A.

Introduction.

1. The introduction of metal construction for aeroplanes, more particularly in relation to the wing spars, has resulted in a need for some simple test on thin sheet metal which will serve to discriminate between desirable and undesirable properties. Hitherto it has been customary to demand some minimum value of the " 0·1 per cent. proof load," defined as the tensile stress that produces 0·1 per cent. permanent extension. This procedure is, however, difficult to justify on rational grounds, because the failure of a metal wing spar normally occurs by local buckling in some region where compression stresses are operative, and hence it may reasonably be anticipated that the *stress-strain properties in compression* are criteria of the suitability of a material, as they are known to be in the case of straight struts.* There is no reason to

---

* R. V. Southwell, 'Engineering,' August 23, 1912 ; A. Robertson, " Selected Engineering Report No. 28 of the Inst. C.E." (1925).

believe that such properties are revealed by the proof stress in *tension*, and although it is possible that experience may indicate some degree of correlation over a restricted range, some test of more direct application is desirable.

When this problem was under discussion by the Aeronautical Research Committee, it was suggested by Professor Southwell that a suitable test of flat sheet material might be made by determining the intensity of shearing stress required to make a long strip of the material buckle by reason of instability into a waved form   The stability of a flat strip clamped at each edge and subjected to shearing forces had been discussed by him in a paper written in collaboration with Miss S. W. Skan,* so that some notion could be formed of the results which might be expected.   It was decided that experimental work should be initiated with two objectives :—

(1) To check the conclusions of this theoretical treatment , and
(2) To investigate the possibility of standardising some test of this nature as an " acceptance test."

2 For the attainment of this second aim, it was required that the buckling produced should be of inelastic type, since, if the wave form were developed elastically, the critical stress would depend primarily on the elastic constants and not on any limiting strength property of the material.   It may be said at once that the second objective was not attained, mainly because (apart from other objections) the technique of the test proved to be too complicated for ordinary specification purposes.   The work done under this heading is to be described elsewhere, and practical aspects, that is, the application of the experiments to testing, will not receive further notice in this paper

3. There remains the question of a comparison of the experimental results with the theory of Southwell and Skan (*loc. cit*).   The present paper discusses from this aspect such tests in the series as were made on strips of sufficient width for their critical loads (according to theory) to be within the limit of elastic proportionality of the material.

In the first series of tests, the buckling load was determined by purely visual examination, as the load at which waves were first detected by the distortion of images reflected in the surface of the strip.   The results of this series of tests suggested the existence of a serious discrepancy between theory and experiment, in that the " collapsing loads " (defined as above), were found to be represented by an expression differing in form, as well as in absolute magnitude, from the theoretical formula for the " critical load."   Reconsideration of the problem in analogy with other types of test on stability, for

* ' Proc. Roy. Soc.,' A, vol. 105, p. 582 (1924).

example, strut testing, showed, however, that the expectation of sudden buckling at the critical load was not likely to be fulfilled. The lateral deflection of an initially bent strut subjected to compressive end load increases progressively as the end load is increased, and an exactly similar phenomenon is to be expected in the buckling of a nominally flat sheet, if initial irregularities from the plane of the sheet exist. Such initial irregularities certainly existed in the strips tested, and therefore additional tests were made in which the growth of the amplitude of waving was *measured* during the test and plotted against the increasing loads. It then appeared that the loads which had previously been termed " collapsing loads " had no relation with instability—the curves relating load and amplitude showing no appreciable discontinuity at such points. Within a restricted range, the form of the curve relating wave-depth and applied load was hyperbolic, as theory would suggest ; but in tests on the narrower strips, deviation from this theoretical form occurred before any upper asymptote, corresponding with the theoretical " critical load," had been clearly indicated. By analysis of the theoretical wave form determined by Southwell and Skan, it was found that the deviation from the true hyperbolic form coincided with the attainment by the tensile stresses, due to bending at the crests of the waves, of a value agreeing closely with the elastic limit of the material.

4. More recently an attempt has been made to analyse the observations of load and deflection, that is, the amplitude of waving, on the lines of a method suggested by Southwell in his note " On the Analysis of Observations in Problems of Elastic Stability."[*] According to this method, if S be the intensity of applied shear stress, and w is the maximum depth of the wave, then within a range of small, but not extremely small, deflections it may be expected that values of w/S, when plotted against w, will fall on a straight line, and the slope of this line will represent a stress which should be comparable with the critical shear stress of theory. Unfortunately, in our problem, the range of readings over which the hyperbolic relation can be expected to apply is seriously restricted by the fact that at small loads the true wave formed is not properly developed and the readings obtained are somewhat irregular (Southwell, *loc. cit*). For fairly wide strips, a range of readings sufficiently wide to determine the hyperbola with fair accuracy is usually available, but for very narrow strips the range of readings available may be too short for any estimate of the best fitting hyperbola to be made. There is, in addition, some difficulty in the actual analysis of the readings obtained ; attention is drawn to this in the Appendix. Nevertheless, it may be claimed that the analysis of the tests here described

[*] ' Proc. Roy. Soc.,' A, vol. 135, p. 601 (1932).

does indicate upper asymptotes of the (wave-depth) — (shear load) curves in fairly close agreement with the values of the " critical load " which are predicted by the analysis of Southwell and Skan. Although the tests which have been analysed in this way are not numerous, it is thought that the results may be of interest, as indicating in what direction an explanation may be sought for apparent discrepancies between Southwell and Skan's theory and experiments which have been conducted abroad. Since the appearance of their paper a considerable amount of work has been done in this field, notably by F. Bollenrath,* but notwithstanding the care with which experiments have been conducted, discrepancies between theory and experiment are reported without any attempt to explain them In this paper we have tried to show that our sheared strips, although imperfectly flat, did behave as theory would predict, until an amplitude of waving was attained which can be seen to entail failure of their elasticity.

5 *Description of Mode of Test.*—The mode of test adopted in the experiments consists in the application to the edges of a long strip of the material of shearing forces in the plane of the strip. The apparatus used is shown in figs. 1 and 1(a). The strip is rigidly clamped between three parallel pairs of bars, two of the pairs being fastened to the edges of the strip and the third being arranged midway between them. The central bar is attached to the upper head of the testing machine, whilst the edge bars are connected through links to a plate attached to the lower head of the testing machine. In this way equal loads are applied simultaneously to two identical specimens, one on each side of the central member; the edges of the strip are constrained only to remain in the original plane of the strip.

In all the tests in which measurements of wave-depth were made, the ratio of the length of the specimen to the free width was 20 : 1 ; and the regularity of the resulting wave systems showed that this ratio gave a close representation of the case of an infinitely long strip—the theoretical case which it was required to reproduce. The boundary conditions at the short edges of the strip are of no importance if the strip is long enough to be considered infinite. In some of the tests these edges were left free ; but in some of the later tests they were clamped between hard-wood blocks, in order to avoid the production of localised waves at the ends before general waving occurred. With the same object, in some of the later tests, the links connecting the edge bars to the lower head of the testing machine were spread-eagled, fig. 1, so that their lines of

* F. Bollenrath, ' Luftfahrtfors.,' vol. 6, p. 1 (1929) ; S. Bergmann and Reissner, ' Z. Metallk.,' vol. 20, p. 475 (1929) ; Seydel, ' Luftfahrtfors.,' vol. 8, p. 71 (1930).

action passed approximately through the tops of the inner edges of the strips under test. This was done with the object of minimising the small bending moments imposed on the strips when the loads were applied parallel to the edge bars—bending moments which, by setting up transverse compressive
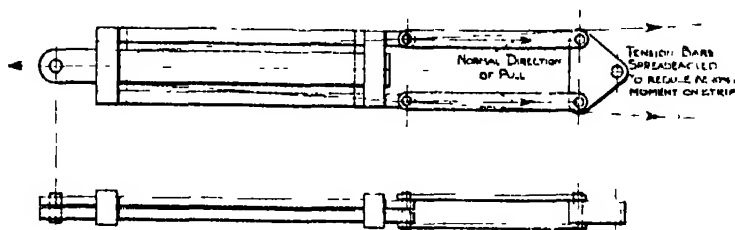
FIG. 1.—Diagram of Apparatus.

stresses in the lower ends of the strips, tended to cause the specimens to collapse from the bottom upwards

6. *Theoretical Investigations.*—A complete analysis of the stability of an infinite thin strip subjected to shearing forces along its edges has been given by Southwell and Skan (*loc cit.*). They showed that the load (S) per unit length of the strip, which will just cause buckling, should be given by the formula

$$S = A\tfrac{2}{3} \frac{Eh^3}{1 - \sigma^2} 1/b^2, \qquad (1)$$

where

E = Young's modulus of material
σ = Poisson's ratio of material
$2h$ = Thickness of material
$2b$ = Width of strip

in any consistent system of units,

and where $A = 22 \cdot 18$ if the edges of the strip are clamped or $13 \cdot 21$ if these edges are simply supported.

Since an infinite length of strip was considered, the wave forms corresponding to these buckling loads were necessarily periodic in the direction of the length of the strip and the ratio of the wave-length to the width of the strip was found to be $1 \cdot 6$ in the case of clamped edges or $2 \cdot 67$ when the edges were simply supported. If initial irregularities are present in the plane of the sheet, there will in general be a component of the wave form corresponding to the first buckling load defined by equation (1) above. If the initial amplitude of this component be w_0, it may easily be shown that the effect of a shear load S is to multiply this amplitude in the ratio $S/(S_0 - S)$, S_0 being the buckling

load. Thus, if simultaneous values of S and w be recorded, they should satisfy a relation $w = Sw_0/(S_0 - S)$ and from the experimental points, the values of S_0 and w_0 may be determined (Southwell, *loc. cit.*).

7. *Measurement of Wave-depth.*—The results of the tests in which measurements of wave-depth were made indicated that a process of gradual waving, culminating in elastic failure in bending at the crests of the waves, was a feature of all the tests. Accordingly, the only process available for the determination of the true buckling load is that based upon the presumed hyperbolic relation between the wave-depth and the load, and described by Southwell (*loc. cit.*), therefore only those tests in which measurements of wave-depth were made could be utilised

The measurements of wave-depth were obtained in the following way. The pointed ends of two rods, rigidly connected by two cross members, were held in contact with the surface of the strip, in such a manner that the line joining the points was parallel to and midway between the long edges of the strip. The distance between the points was adjusted to one-half the expected wavelength and a measure of the wave-depth was obtained by recording the tilt of a mirror attached to the frame connecting the two pointed rods. Correction for tilt of the whole apparatus was obtained from the readings of a second mirror attached to the frame of the testing apparatus as close to the tilting frame as possible.

The tests were carried out on a series of strips all $0 \cdot 0126$ inch in thickness and $\frac{1}{2}$, $\frac{3}{4}$, 1, $1\frac{1}{4}$ and $1\frac{1}{2}$ inches in width; the length of the specimen tested was in every case twenty times the width. The readings obtained from the deflection meter actually represent values of the expression $12,000\ w/b$. The value of the deflection meter reading at each value of applied shear load for each strip is given in Table I, and in figs. 2 and 3 also, the actual deflection meter readings have been used. The actual wave-depth can in any case be determined by multiplying the deflection meter reading by $b/12,000$.

8. *Analysis of Experimental Results.*—In fig. 2, the values of w/S derived from these data have been plotted against w for each strip and the value of S_0 has been determined by the best fitting line through the plotted points. Two difficulties arise in this analysis; one of them is of general application and is discussed by Southwell; the other is associated with determining the best fitting line. In justification of the results obtained a short note on the nature of the difficulties is given in the Appendix, together with a description of the approximate method of least squares which has been used in the determination of the best fitting line. This method has been used, not

in the hope of obtaining more accurate results, but with the object of eliminating the personal error in judging the best straight line through the experimental points.
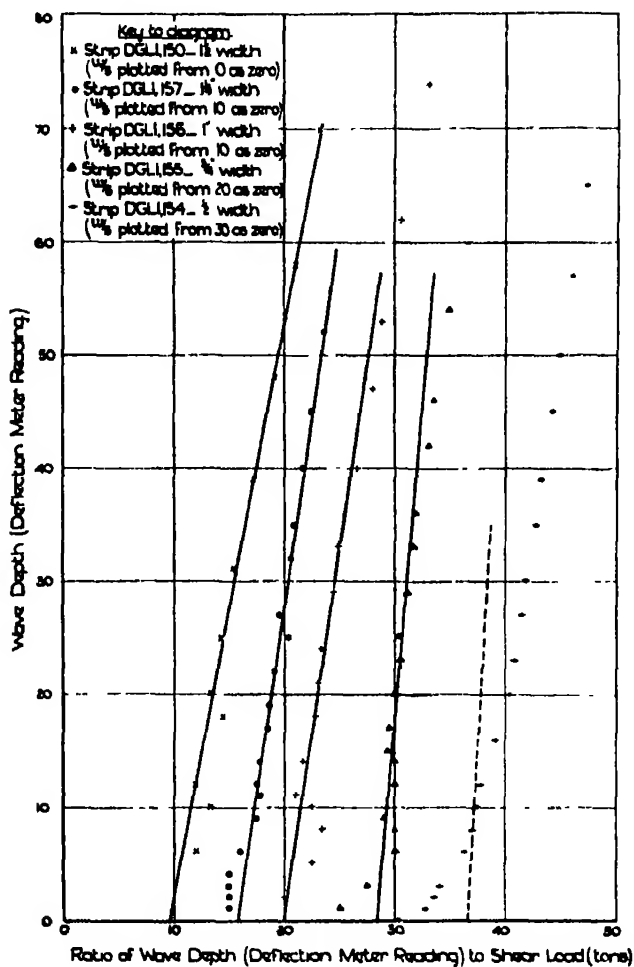
Fig. 2.—Determinations of buckling load from measurements of wave-depth.

× Strip DGLI, 150—1½ inch width (w/S plotted from 0 as zero).
⊙ Strip DGLI, 157—1¼ inch width (w/S plotted from 10 as zero).
+ Strip DGLI, 156—1 inch width (w/S plotted from 10 as zero).
△ Strip DGLI, 155—¾ inch width (w/S plotted from 20 as zero).
← Strip DGLI, 154—½ inch width (w/S plotted from 30 as zero).

In Table I, the theoretical values of the buckling loads are given, together with the values deduced from the wave-depth measurements. The ranges of the deflection meter readings that have been used for the determination of

Table I.—Details of Strips Tested and Measured Values of Wave-depth.

Reference mark of strip.	DGLI, 154.	DGLI, 155.	DGLI, 156.	DGLI, 157.	DGLI, 150.
Width (inches)	½	¾	1	1¼	1½
Length (inches)	10	15	20	25	30
Thickness (inches)	0 0126	0 0126	0 0126	0 0126	0 0126
Theoretical buckling load (tons)	16 3	10 9	8 2	6 5	5·4
Buckling load estimated from wave depth readings (tons)	—	11 4	6 65	6 86	5 29

Shear load (tons)					Shear load (tons).	Wave-depth.*
0 2	0	0	0	0	0 25	0
0 4	0	6	2	1	0 50	1
0 6	1	7	5	2	0 75	6
0 8	2	9	8	3	1 00	10
1 0	3	12	10	4	1 25	12
1 2	6	14	11	6	1 50	18
1 4	8	15	14	9	1 75	20
1·6	10	18	18	11	2 00	25
1·8	12	20	21	12	2 25	31
2 0	16	21	24	14	2 50	39
2 2	20	23	29	17	2 75	48
2·4	23	26	33	19	3 00	58
2·6	27	29	40	22	3 25	70
2 8	30	31	47	25	3 50	90
3 0	35	35	53	27	3 75	115
3 2	39	39	62	32	4 00	150
3 4	45	42	74	35	4 25	195
3 6	50	48	89	40	4·50	252
3 8	57	52	104	45	4 75	323
4 0	65	60	127	52	5·00	401

* The values of deflection reading used for determining the critical loads are those included between the horizontal lines marked in the table.

the critical loads are indicated in Table I; in every case the readings corresponding to very small wave-depths have been neglected (*loc. cit.*, § 10).

9. Fig. 2 and Table I show that, when analysed in this way, the results of tests on fairly wide strips do indicate a definite and close agreement with theory; the values of the critical loads thus determined from the experimental results of the tests on the strips DGLI, 150, and DGLI, 157, agree closely with the theoretical values and are, moreover, very little affected by shift of origin, etc. (see Appendix). In the tests on the narrower strips, the range of points available for analysis is so seriously restricted between the initial irregularities and the point of departure from linearity due to the commencement of elastic failure, that the value of the critical load is not clearly defined; in the case of the strip DGLI, 156, this restriction was rendered still more severe by the relatively great depth of the initial irregularities. Nevertheless, it may be claimed that the results obtained do indicate buckling loads in close agreement with the theoretical values; although they must also be regarded as emphasising the necessity, in practical design, of combining with a consideration of actual stability a consideration of elastic failure consequent upon the initiation of buckling.

10. *Effect of the Elastic Limit and of Permanent Waves on the Process of Gradual Waving.*—In this connection attention may be drawn to a conclusion which constitutes perhaps the most definite result of the present tests. By calculations based upon the theoretical wave form determined by Southwell and Skan, it was found that the tensile stress (p) due to bending at the points of maximum curvature of the strip was given by the formula $p = 8\cdot18\ \mathrm{E}h/b^2\,w$, where w is the wave-depth and where E, h and b are as defined in § 6. For the particular strip material tested, this formula indicates that the stress p will exceed the elastic limit of the material, if w is greater than $1\cdot05\ b^2/h \times 10^{-4}$. The deflection meter readings used for the wave-depth measurements throughout the present paper actually represent values of w/b, the unit of the scale corresponding to a wave-depth of $b/12{,}000$ inches. Thus the actual deflection meter reading at the elastic limit should be equal *numerically* to 200b.

Three difficulties arise in applying this result to the experimental tests. Firstly, since the development of waves was not in general uniform over the whole length of the strip, permanent waves would be produced locally before the *average* wave-depth exceeded the critical value. Secondly, the deflection meter was not always placed exactly over a crest and hollow of a wave, so that the wave-depths recorded did not always represent the full wave-depth even of the one wave. Thirdly, the maximum tensile stress due to bending alone is

not the true maximum tensile stress in the strip, since, in addition to the bending stresses due to waving, there is a uniform shear stress in the sheet. In order to eliminate the error due to this last cause, it would have been necessary to consider wave-depth and shear stress simultaneously, and since this could only be done by reference to the experimental results, the process would have been somewhat complicated. On the other hand, due to the other two causes, permanent waves were formed when the measured wave-depths were well below the limiting values theoretically determined; accordingly it was decided to consider all three sources of error as acting together to reduce the value of the measured wave-depth at which permanent waves were first observed.

In some of the tests the load was applied in several stages, and between each stage the load was removed and then again applied in small increments up to the maximum load previously attained. In this way a series of curves was obtained connecting wave-depth with shear load, in addition to actual measurements of the depth of the permanent waves produced. Now, if the shear load S is connected with the wave-depth w by a relation $w = Sw_0/(S_0 - S)$, where w_0 is the initial (average) wave-depth and where S_0 is the theoretical buckling load, then the initial slopes of the $S - w$ curves will represent the ratio w_0/S_0; thus, if the value of S_0 be assumed, the values of w_0 can be calculated from these initial slopes. The values of w_0 thus determined should be equal to the value obtained in the first test (when the elastic limit had not been exceeded), plus the depths of the permanent waves produced; hence, if these values of w_0 be plotted against the readings of permanent wave-depth, the result should be a straight line, the slope of which should represent the ratio of the measured wave-depth to the true average wave.

This analysis was carried out in the case of one strip (DGLI, 156) and the results are shown in figs. 3 and 3A. It will be seen that a good straight line was obtained, and that this line indicated a ratio of measured wave-depth to average wave-depth of approximately 1 : 2·62. Now permanent set in the average wave should (according to calculation) have commenced when the average wave-depth was about 100 (width of strip = 1 inch), when the measured wave-depth would be 100/2·62 = 38. Reference to fig. 2 will show that when the *recorded* wave-depth was 38, departure from the hyperbolic form was just commencing.

Summary.

The paper describes the results of tests on the buckling of long strips of material under the action of shearing forces applied along the edges of the strip.

The test was designed in the first place as an acceptance test for thin strip material ; but in the present paper attention is paid only to the theoretical aspects of the tests. The buckling load of an infinitely long strip has been
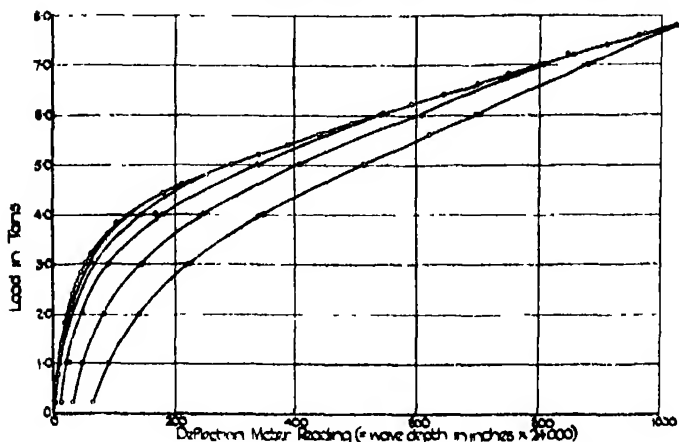
Fig 3.—Load deflection curves for the strip DGLI, 156.

determined theoretically by Southwell and Skan, and in the present paper it is shown that, if the effect of initial departures from planity of the strip be taken into account, the buckling loads determined by experiment are in good
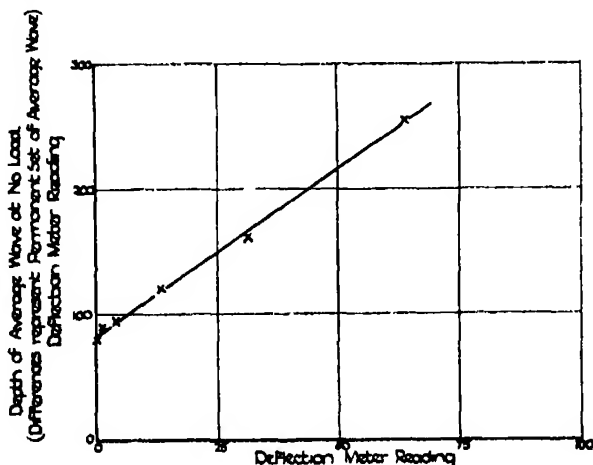
Fig. 3A.—Determination of ratio of measured wave to average wave by measurement of permanent set. (Specimen DGLI, 156.)

agreement with the theoretical values. This agreement has been demon-strated by plotting the depth of the waves produced against the shear load and by determining the buckling load on the assumption, which is justified by the

experimental results, that these quantities fulfil the hyperbolic relation predicted by theory.

APPENDIX.

Notes on the Analysis of Observations believed to obey a Hyperbolic Law.

If a series of simultaneous values of two variables S and w are believed to obey a law of the form $Sw + aS + bw + c = 0$, the most probable values of a, b and c can be determined by estimating their values by any method and then by obtaining corrections to these estimated values by the ordinary method of least squares. Unless the curvature of the hyperbola is very well defined, however, this method is scarcely feasible owing to the extraordinary accuracy necessary in the arithmetical working. This difficulty can be avoided if, by choosing a suitable origin, the constant c is eliminated, when the method of analysis described by Southwell (*loc. cit.*) becomes available ; Southwell has pointed out (*loc. cit.*, § 10) that by plotting from several different origins, the value of c can be determined by choosing that origin which yields the best straight line.

A second difficulty arises if the method of reciprocal plotting, described by Southwell, does not indicate any definite straight line ; for the method of least squares cannot be applied directly to the derived quantities (*e.g.*, w/S in the present paper). The results obtained in the tests on strip in shear are such that some systematic method of determining the best-fitting straight line is definitely required. Accordingly, the following method has been developed.

Since the values of the shear load S can be assumed to be without error, it is required to choose the constants S_0 and w_0 so that the sum $\Sigma (w - w')^2$ is a minimum, w' and w being the values of the wave-depth as actually recorded and as given by the formula $w = Sw_0/S_0 - S$ respectively. Owing to the occurrence of $(S_0 - S)$ in the denominator of the expression for $(w - w')$, the

equations which express the conditions for a minimum value of $\Sigma \left[(w - w')^2 \right]$ do not yield simple expressions for w_0, S_0. But this difficulty disappears if, instead of $\Sigma \left[(w' - w)^2 \right]$, the sum $\Sigma \left[(w' - w) \, w'/w \right]^2$ is made a minimum, since

$$(w' - w)\frac{w'}{w} = w' \left\{ w' \frac{(S_0 - S)}{Sw_0} - 1 \right\},$$

and therefore the conditions for a minimum value of $\Sigma \left[(w' - w) \, w'/w \right]^2$ reduce to

$$\left. \begin{aligned} \Sigma \left| \frac{w'^3}{s} \left\{ \frac{w'(S_0 - S)}{S_0} - w_0 \right\} \right| &= 0 \\ \Sigma \left[w'^3 \left\{ w' \frac{S_0 - S}{S} - w_0 \right\} \right] &= 0 \end{aligned} \right\}.$$

The justification for this procedure consists in the fact that, for all but the smallest values of w' the values of w'/w are all nearly unity ; hence the adjustment merely results in weighting the lower values of w' somewhat erratically. These lower values of w' have very little effect on the final result, but, if for other reasons, these values are neglected, even this source of error is eliminated.

On the basis of the criterion $\Sigma \left\{ (w' - w) \, w'/w \right\}^2$ to be a minimum, the best value of S_0 is given by the formula

$$S_0 = \frac{4/1 \cdot 3/0 - 4/0 \cdot 3/1}{4/2 \cdot 3/0 - 4/1 \cdot 3/1},$$

and of w_0 by the formula

$$w_0 = \frac{(4/1)^2 - 4/0 \cdot 4/2}{4/2 \cdot 3/0 - 4/1 \cdot 3/1},$$

where m/n stands for $\Sigma \, w'^m/S^n$.

The values of the critical load determined from the experimental results and tabulated in Table I have been obtained by means of the formula above.

Long Wave Transmission, treated by Phase Integral Methods.

By T. L. ECKERSLEY.

The effect of a sharply defined upper conducting layer in guiding long wireless waves round the earth has been considered by G. N. Watson,[*] who gives a very comprehensive mathematical analysis of this case.

Recent investigations of the upper Kennelly Heaviside layer by many investigators in England, America, Germany, etc , leave no doubt that the ionised conducting layer in the upper atmosphere is not sharply defined and the transition region from zero to maximum electronic density and conductivity may comprise many wave-lengths of the wave considered.

For example, in the lower ionised layer (E layer) at a height of approximately 100 km. the electronic density begins to be appreciable at about 80 km. and reaches a maximum at some 100 to 110 km.

The transition distance is of the order of 20 to 30 km. and the layer cannot be considered as sharply defined for any wave-length in the radio range, say, up to 25 km.

Watson's analysis is not adequate to describe the nature of radio transmission. It requires extending to cases of ill-defined layers. The short wave range 10 to 100 m. can be adequately treated by means of a geometrical ray theory. For such wave-lengths and in regions above 80 or 90 km. the ionised layer acts as one of variable but real refractive index less than unity, and the effective electronic density gradient is so small compared with the wavelengths that geometrical ray methods can be used.

The refractive index μ is real and less than unity because with such waves, the electrons move relatively freely in the field of the wave, that is to say, they can execute vibrations to and fro in the average time τ between collisions, i.e , ($\tau \gtrsim 10^{-6}$ seconds).

With longer waves the conditions are quite different.

In the first place, although the layer is graded, the change of effective refractive index in a wave-index may be quite rapid enough to invalidate the use of ray methods. Also for such wave-lengths the refractive index is no

[*] 'Proc. Roy. Soc.,' A, vol. 95, p. 546 (1919).

longer real. The electrons may make many collisions with molecules during a time period of the waves and the convection current is in phase with the electric force and 90° out of phase with the displacement current. In such a case $\mu^2 - 1$ is practically purely imaginary. The constant phase surfaces, the normals to which determine rays in the usual sense, and the constant amplitude surfaces, which determine the direction of energy flow, are not the same, and ray methods are not adequate. A complete analysis on the lines carried out by Macdonald, Love, Nicholson, and Watson is required.

The simplicity of geometrical optics is lost in a maze of symbols complex even in the case of the simplest distribution of electronic concentration.

The phase integral method, previously described by the writer,* is particularly appropriate for treating such problems as these, and can be used to extend Watson's analysis to cases where the reflecting layer is not well defined.

The full wave analysis of the transmission between spherical conducting shells leads to an expression for the field intensity as the sum of terms of the form

$$\frac{A_s}{(\sin\theta)^{\frac{1}{2}}} \cdot \cos(n_s\theta - \pi/4). \tag{1.1}$$

The main part of the analysis consists in determining the values of n_s finite in number, which fix the transmission characteristics of the waves.

These proper values, as they may be called, on account of their formal relation to the proper or Eigen values of quantum analysis, can be simply determined by phase integral methods, when the reflection coefficient of the upper conducting shell or Heaviside layer is known

Thus it is shown that if the reflection coefficient ρ is $\rho = e^{-\delta\phi}$ where the imaginary part of $\delta\phi$ represents the phase change and the real part the amplitude alteration at reflection, then the phase integral rule gives the following :

$$2 \cdot \frac{2\pi i}{\lambda} \int_{r_0}^{r_0+H} \left\{ 1 - \frac{n(n+1)\lambda^2}{(2\pi r)^2} \right\}^{\frac{1}{2}} dr + \delta\phi = 2\pi i S, \tag{1.2}$$

where S is an integer, λ = wave-length, r = distance from earth's centre, and the values of n_s which satisfy this condition are the proper values of the direction cosines of the waves, complex when attenuation ensues.

n_s can be determined from the above equation, the imaginary part of it giving the attenuation coefficient.

Thus if $\delta\phi$ is given, the attenuation of each proper value, corresponding to each integral value of S, is given.

The problem therefore resolves itself into the determination of $e^{-\delta\phi}$, the reflection coefficient, of the assumed layer (graded vertically) as a function of the angle of incidence of the wave normal and the constants of the layer.

In general, where the height of the layer is small compared with the radius of the earth and where $\sin\theta$ is not too small, θ being $90 - \phi_1$, where ϕ_1 is the angle of incidence of the wave on the layer, the phase integral

$$2 \cdot \frac{2\pi i}{\lambda} \int_{r_\bullet}^{r_\bullet + \mathrm{H}} \left\{ 1 - \frac{n(n+1)\lambda^2}{(2\pi r)^2} \right\}^{\frac{1}{2}} dr \tag{1.3}$$

can be replaced by the equivalent integral for the case of two planes, i.e.,

$$\frac{2\pi i}{\lambda} \cdot 2n_1 \int_{r_\bullet}^{r_\bullet + \mathrm{H}} dr = \frac{2\pi i}{\lambda} 2n_1 \mathrm{H}. \tag{1.3}$$

$$n_1 = \sin\theta.$$

In all the cases considered, however, where the upper layer is graded the reflection is greatest and the attenuation least for nearly grazing angle incidence, and thus it is only the waves of grazing incidence that are of practical importance.

It is the wave that is practically tangent at the earth's surface which has the largest angle of incidence at the layer, and hence it is such a wave that we are most concerned with. In this case

$$\frac{n(n+1)\lambda^2}{(2\pi r_0)^2} = 1 \text{ very nearly,} \tag{1.4}$$

for

$$n\theta \simeq \frac{2\pi r_0 \theta}{\lambda}$$

and

$$\exp i(n\theta - pt) = \exp i\left(\frac{2\pi r_0 \theta}{\lambda} - pt\right),$$

which represents a wave travelling parallel to the earth's surface. We have to investigate the value of the phase integral in such a case.

Suppose

$$1 - \frac{n(n+1)\lambda^2}{(2\pi r_0)^2} = 1 - m_0^2 = n_0^2, \tag{1.5}$$

where n_0 is very small. Then since r is nearly equal to r_0 in the whole range of integration, we may put, as a close approximation

$$\int_{r_\bullet}^{r_\bullet + \mathrm{H}} \left\{ 1 - \frac{n(n+1)\lambda^2}{(2\pi r)^2} \right\}^{\frac{1}{2}} dr = \int_0^{\mathrm{H}} \left\{ \left(n_0^2 + \frac{2m_0^2}{r_0} \zeta \right) \right\}^{\frac{1}{2}} d\zeta, \tag{1.6}$$

where

$$\zeta = r - r_0,$$

which is

$$\tfrac{2}{3} \frac{r_0}{2m_0{}^2} \left\{ \left(n_0{}^2 + \frac{2m_0{}^2}{r_0} H \right)^{3/2} - n_0{}^3 \right\}. \qquad (1.7)$$

For the tangent ray n_0 can be neglected and $m_0 = 1$ and thus becomes

$$\tfrac{2}{3}H \sqrt{\frac{2H}{r_0}}. \qquad (1\,8)$$

Now $\sqrt{\dfrac{2H}{r_0}} = \sin \theta_0$ where θ_0 is complement of the angle of incidence at the layer of the wave tangent at the earth's surface.

Comparing this with the plane layer case we see that it is of the same form as $H \sin \theta_0$, but the equivalent value of $\sin \theta_0$ is $2/3 \sin \theta_0$. We shall use this value throughout in the following investigations.

§ 2 The general differential equation must take into account the direction of polarisation of the electric force

It follows from Maxwell's equations that for transmission in a region of variable electronic concentration these equations are, when X, Y, Z have the factor $e^{2\pi i \nu t}$,

$$\nabla^2 X + \left(\frac{2\pi}{\lambda} \right)^2 \left(1 - \frac{\nu_0{}^2}{\nu^2} \right) X - \frac{\partial}{\partial x} \frac{1}{1 - \nu_0{}^2/\nu^2} E\nabla . \frac{\nu_0{}^2}{\nu^2} = 0$$

$$\nabla^2 Y + \left(\frac{2\pi}{\lambda} \right)^2 \left(1 - \frac{\nu_0{}^2}{\nu^2} \right) Y - \frac{\partial}{\partial y} \frac{1}{1 - \nu_0{}^2/\nu^2} E\nabla . \frac{\nu_0{}^2}{\nu^2} = 0 \qquad \Bigg\}, \quad (2\,1)$$

$$\nabla^2 Z + \left(\frac{2\pi}{\lambda} \right)^2 \left(1 - \frac{\nu_0{}^2}{\nu^2} \right) Z - \frac{\partial}{\partial z} \frac{1}{1 - \nu_0{}^2/\nu^2} E\nabla . \frac{\nu_0{}^2}{\nu^2} = 0$$

where X, Y, Z are the components of E, the electric force,

$\nu =$ frequency,

$\lambda =$ wave-length,

$\nu_0{}^2 = \dfrac{Ne^2c^2}{\pi m(1 + i\alpha)}$, which in respect of N is a function of x, y, z,

$\alpha = \dfrac{T}{k\pi\tau} = \dfrac{\nu_c}{k\pi\nu}$,

$T =$ time period of waves,

$\tau =$ mean time between collisions $= 1/\nu_c$.

We have to deal, almost entirely, with the case where the gradient of N, the electronic density, is almost wholly vertical, in which case (z being vertical)

$$\frac{d^2Z}{dz^2} + \left(\frac{2\pi}{\lambda}\right)^2 \left(\sin^2\theta - \frac{v_0^2}{v^2}\right)Z - \frac{d}{dz}\frac{1}{1 - v_0^2/v^2} Z\frac{d}{dz}\left(\frac{v_0^2}{v^2}\right) = 0, \qquad (2.2)$$

and

$$\frac{d^2Y}{dz^2} + \left(\frac{2\pi}{\lambda}\right)^2 \left(\sin^2\theta - \frac{v_0^2}{v^2}\right)Y - \frac{d}{dy}\frac{1}{1 - v_0^2/v^2} Z\frac{d}{dz}\left(\frac{v_0^2}{v^2}\right) = 0. \qquad (2.3)$$

Y being normal to Z and the ray direction.

Where the electric force is polarised wholly horizontally, $Z = 0$, and remains everywhere zero, and

$$\frac{d^2Y}{dz^2} + \left(\frac{2\pi}{\lambda}\right)^2 \left(\sin^2\theta - \frac{v_0^2}{v^2}\right)Y = 0, \qquad (2.4)$$

the normal ray differential equation.

When $Z \neq 0$ the differential equation is

$$\frac{d^2Z}{dz^2} + \left(\frac{2\pi}{\lambda}\right)^2 \left(\sin^2\theta - \frac{v_0^2}{v^2}\right)Z - \frac{d}{dz}\frac{1}{(1 - v_0^2/v^2)} Z\frac{d}{dz}\left(\frac{v_0^2}{v^2}\right) = 0, \qquad (2.5)$$

which is of the form

$$\frac{d^2Z}{dz^2} + P\frac{dZ}{dz} + Q = 0, \qquad (2.6)$$

where

$$P = -\left(\frac{d\xi^2}{dz}\right)\Big/(1 - \xi^2), \qquad (2.7)$$

and $\xi = v_0/v$

$$Q = \left(\frac{2\pi}{\lambda}\right)^2 \left\{(\sin^2\theta - \xi^2) + \left(\frac{\lambda}{2\pi}\right)^2\frac{dP}{dz}\right\} Z. \qquad (2.8)$$

If we substitute $Z = Z_1/\sqrt{1 - \xi^2}$, then the differential equation for Z_1 is

$$\frac{d^2Z_1}{dz^2} + \left\{\left(\frac{2\pi}{\lambda}\right)^2(\sin^2\theta - \xi^2) + \tfrac{1}{2}\left(\frac{dP}{dz} - \tfrac{1}{2}P^2\right)\right\} Z_1 = 0, \qquad (2.9)$$

in which the correction to the normal differential equation is

$$\tfrac{1}{2}\left(\frac{dP}{dz} - \frac{P^2}{2}\right)\left(\frac{\lambda}{2\pi}\right)^2.$$

This quantity, according to (2.7) above, is sufficiently small if the gradient $d\xi^2/dz$ is sufficiently small.

Thus for small gradients the normal differential equation, independent of the direction of polarisation, suffices.

For example, a uniform gradient $\xi^2 = z/z_0$, where z_0 is the height at which total reflection occurs, then

$$\frac{d^2 Z_1}{dz^2} + \left(\frac{2\pi}{\lambda}\right)^2 \left\{\sin^2 \theta - \frac{z}{z_0} - \tfrac{3}{4}\left(\frac{\lambda}{2\pi z_0}\right)^2 \frac{1}{(1 - z/z_0)^2}\right\} Z_1 = 0, \qquad (2.10)$$

i.e., the correction term has the factor $(\lambda/2\pi z_0)^2$ and is proportional to the gradient of N, and is only significant in the total reflecting region ($z \doteq z_0$).

§ 3. *Examples.*

Some simple examples of reflection coefficients have been worked out to illustrate the behaviour of long waves in various circumstances.

The simplest case of all is that of a sharply defined layer, for which the analysis is given in order to contrast the transmission characteristics of horizontally and vertically polarised waves.

Vertically Polarised Wave.—If σ is the conductivity EM units, λ the wavelength and c the velocity of light, then the reflection coefficient of a sharply defined layer of these constants is approximately $e^{-\delta\phi}$, where

$$\delta\phi = \frac{2}{nx^{\frac{1}{2}}} e^{-i\pi/4}, \qquad (3.1)$$

$x = 2\sigma\lambda c$, and n is the direction cosine of the normal to the wave front on the vertical z axis.

Employing the phase integral relation, we find that so long as $x \gg 1$ and $S = 0$, the attenuation coefficient is

$$\frac{1}{2H} \bigg/ (4\sigma\lambda c)^{\frac{1}{2}}$$

i.e., $\qquad\qquad\qquad\qquad\qquad\qquad\qquad\qquad (3.2)$

$$\frac{1}{2H}\left(\frac{\rho p}{8\pi c^2}\right)^{\frac{1}{2}}$$

$$\rho = \text{resistivity} - 1/\sigma,$$

$$p = 2\pi\nu,$$

which agrees with the value obtained in the pure wave theory for transmission between layers. Also, if S is a positive integer, the attenuation coefficient is

$$\frac{1}{H}\left(\frac{\rho p}{8\pi c^2}\right)^{\frac{1}{2}}, \qquad (3.3)$$

double the previous value.

Horizontally Polarised Wave.—In this case the reflection coefficient is $e^{-\delta\phi}$ where

$$\delta\phi = \frac{2n}{\sqrt{x}}\, e^{-i\pi/4} + i\pi, \tag{3.4}$$

where n and x have the same significance as before.

The phase integral method then gives

$$\text{attenuation coefficient} = \frac{1}{H}\frac{1}{(4\sigma\lambda c)^{\frac{1}{4}}}\,\sin^2\theta \;\text{ nearly, } (\theta \text{ small}),$$

or

$$\frac{1}{H}\left(\frac{pp}{8\pi c^2}\right)^{\frac{1}{4}}\sin^2\theta$$

$$= (\alpha_r)\sin^2\theta, \tag{3.5}$$

where (α_r) is the attenuation of the vertically polarised wave of any but the zero order.

For small angles, this is very much less than the attenuation of the vertically polarised wave   This is, of course, connected with the fact that the reflection coefficient for horizontally polarised waves is very much greater than for vertically polarised rays, especially for large angles of incidence (n small). For vertically polarised rays, there is a critical angle given by $n = 1/2x^{\frac{1}{2}}$ for which the reflection is a minimum (*i.e.*, Brewster's polarising angle).

The results for metallic reflection are shown in fig 1
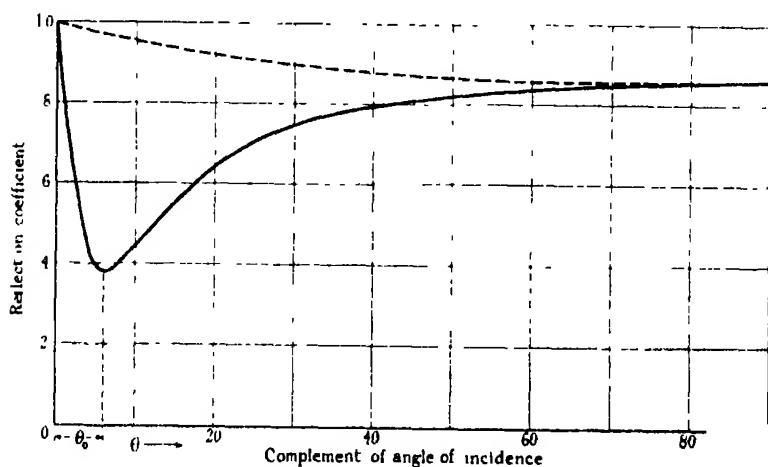
Fig. 1.—Ground Reflection. $\lambda = 30$, $K = 5$, $\sigma = 1/(2 \times 10^{12})$.
—— Vertically polarised ray.
...... Horizontally polarised ray.

It will be seen that the reflection for the vertically polarised ray is always less than that for the horizontally polarised ray.

This form of the functional dependence of the reflection coefficient on n results in the two forms of attenuation coefficient for the vertically and horizontally polarised waves shown above.

For the vertically polarised waves $\theta > \theta_0$, the reflection improves as θ increases. Therefore waves of high angles are better reflected, *i e*, lose less on reflection, but in order to travel over a given distance they have to make more reflections; the two effects, therefore, compensate, and the attenuation of the various order rays is the same

On the other hand, the horizontally polarised waves are worse reflected the higher the angle; they also make more reflections over a given distance with the result that the attenuation rapidly increases with the angle of elevation as in formula (3 5).

Case where $N \propto z^2$.—The next is an example where the electronic concentration varies as the square of the height.

This case is of importance because actual measurements show that the electronic density in the E region of the Kennelly Heaviside layer varies approximately in this manner.

We assume that

$$\nu_n^2 \qquad \frac{z^2}{z_0^2 (1 + i\alpha)} - \frac{Ne^2c^2}{\pi m \nu^2 (1 + i\alpha)} \qquad (3\ 6)$$

$\alpha = \nu_0/k\pi\nu$, where ν_0 is the collision frequency. According to Dr Burnett,[*] the numerical constant $k = 3/2$, where $\nu_0 = 2N_1 i^2 \sqrt{\pi/hm}$ in his notation is the collision frequency and α is small. Where α is large $k - 16/3\pi$. From (3.6) z_0, the depth of penetration is in this case proportional to ν. Put $z_0' = z_0(1 + i\alpha)$.

We use an extension of the result of Hartree,[†] who shows that when $2\pi z_0' \sin^2 \theta/\lambda$ is large

$$\delta\phi = \frac{i \pi z_0'}{\lambda} \sin^2 \theta - \tfrac{1}{2}\pi i. \qquad (3.7)$$

Using the phase integral method for a plane layer the attenuation coefficient becomes (when α is small)

$$\frac{3}{2} \frac{\pi^2 z_0 \alpha^i \sin^3 \theta}{\lambda H\, 2^{3/2} \cos \theta} = \frac{3}{2} \frac{\pi^{3/2} (z_0)_{\lambda_1} \cdot \lambda_1 \nu_0^i}{(2\lambda)^{3/2} C^i H \cos \theta k^i} \sin^3 \theta, \qquad (3.8)$$

[*] 'Proc. Camb. Phil. Soc.,' vol. 27, p. 581 (1931).

[†] 'Proc. Roy. Soc.,' A, vol. 131, p. 428 (1931).

where $(z_0)_\lambda \cdot \lambda_1$ is the penetration distance at a wave-length λ_1 and is a constant.

When, however, $2\pi z_0' \sin^2 \theta/\lambda$ is not large we have to distinguish between two cases (a) where the wave is polarised with the electric force horizontal, (b) electric force vertical.

It follows from (2 5) that the normal differential equation (2.4) is only appropriate to the case (a) horizontally polarised wave ; the reflection of the vertically polarised waves depends on the solution of the more complex differential equation (2.5).

Considering then (a) only we find that the phase change on reflection is given by

$$\tan \frac{i\delta\phi}{2} = \frac{2}{(\xi)^i} \cdot \frac{\Gamma_4^1 (\xi + 3)}{\Gamma_4^1 (\xi + 1)} \tan \pi/4 \, (\xi - 1). \tag{3.9}$$

where

$$\xi = \frac{2\pi z_0'}{\lambda} \sin^2 \theta \tag{3 10}$$

when ξ is small compared with 1,

$$\Gamma_4^1 (\xi + 3)/\Gamma_4^1 (\xi + 1)$$

is approximately $1/3$, actually

$$1/2 \cdot 97 = 1/\beta, \text{ say}, \tag{3.11}$$

and

$$\tan \frac{i\nu\gamma}{2} = -\frac{2}{\xi^i} \frac{1}{\beta}$$

if ξ is small, $\tan i \, \delta\phi/2$ is large, and

$$i \frac{\delta\phi}{2} \to -\frac{\pi}{2} \text{ nearly}. \tag{3.12}$$

Let $i \, \delta\phi/2 = \chi - \pi/2$, χ small, then

$$\tan \frac{\chi}{2} = \frac{(\xi)^i \beta}{4}$$

approximately, and $i\delta\phi$ the change of phase at reflection is

$$\beta\xi^i - \pi. \tag{3.13}$$

The phase integral relation for this case gives

$$\frac{2\pi i}{\lambda} 2 \cdot \frac{2}{3} \sin \theta \cdot H + i\beta\xi^i - i\pi = 2\pi i S. \tag{3.14}$$

Now ξ in this case, where α is large, is $(2\pi/\lambda)\, z_0 \sqrt{i\alpha}\, \sin^2 \theta$, and we get, if we put $n = n_0 + i\delta n_0$, where n_0 is the eigen value,

$$\delta n_0 = \frac{\gamma n_0 \sin \pi/8,}{2\mathrm{H} \cdot 2/3 + \gamma \cos \pi/8} \qquad (3\ 15)$$

where

$$\gamma = \left(\frac{\lambda z_0}{2\pi} \sqrt{\alpha}\right) \frac{\beta}{2} \qquad (3\ 16)$$

and the attenuation constant is

$$\frac{2\pi}{\lambda} \frac{\sin\,0}{\cos\,0}\, \delta n_0 = \frac{2\pi}{\lambda} \frac{\sin^2\, 0\, \gamma \sin \pi/8.}{(2\mathrm{H} \cdot 2/3 + \gamma \cos \pi/8)} \qquad (3.17)$$

$4/3$ H is in general $\geqslant \gamma \cos \pi/8$, and the attenuation constant varies inversely as λ^2 and directly as $(z_0)_{\lambda_1}{}^{\frac{1}{2}}\, \lambda_1{}^{\frac{1}{2}}$.

The transmission characteristics of this graded layer in which $N \propto z^2$, as well as others in which $N \propto z$ and $N \propto e^{-z/z_0}$, the discussion of which is omitted here for want of space, can be summarised as follows.

The attenuation constants $\bar{\alpha}$ for all types of graded layers have certain features in common . —

(1) $\bar{\alpha}$ is some inverse function of the gradient of the electronic concentration so that the less the gradient the greater the attenuation.

(2) $\bar{\alpha}$ is in every case inversely proportional to the height of the layer above the earth.

This is a general characteristic of transmission between layers, and may be explained physically on the following grounds.

The bounding walls take a certain toll of energy, depending only on E, the electric force, and the constitution of the layers. The store of energy to be drawn from is, however, proportional to the distance apart of the layers, therefore the percentage of energy lost per unit distance is less the greater H, i e , the attenuation constant varies inversely as H.

(3) The attenuation in every case varies inversely as some power of λ, *i.e.*, is less the greater the wave-length.

This is because the specific resistance of the layers, considered as guiding conductors, decreases with increasing wave-length.

(4) High angle transmissions are normally much more attenuated than gliding angle waves.

This is, of course, associated with the fact that in all cases of a not

too sharply defined layer, reflection is best for glancing incidence and rapidly decreases for higher angles.

(5) The attenuation decreases with increasing ionic concentration, other quantities remaining fixed; this decreases the resistance of the guiding walls and so decreases the loss.

(6) The attenuation increases with increasing collision frequency, for, other quantities remaining constant, this increases the resistance of the guiding walls.

§ 4 *Experimental Evidence.*

The experimental evidence obtained from a number of sources* is best exhibited in the form of a curve, fig. 2.

The transmission formula $\dfrac{A}{(R \sin \theta)^{\frac{1}{2}}} e^{-\bar{a}d}$ has an exponential factor $e^{-\bar{a}d}$ which represents the attenuation of the waves.

If d is taken as 1000 km. the factor $\exp(-\bar{a}\,1000)$ expressed in decibels will give the attenuation characteristics of the transmission. The actual values of this quantity plotted as a function of the wave-length are given in fig. 2.
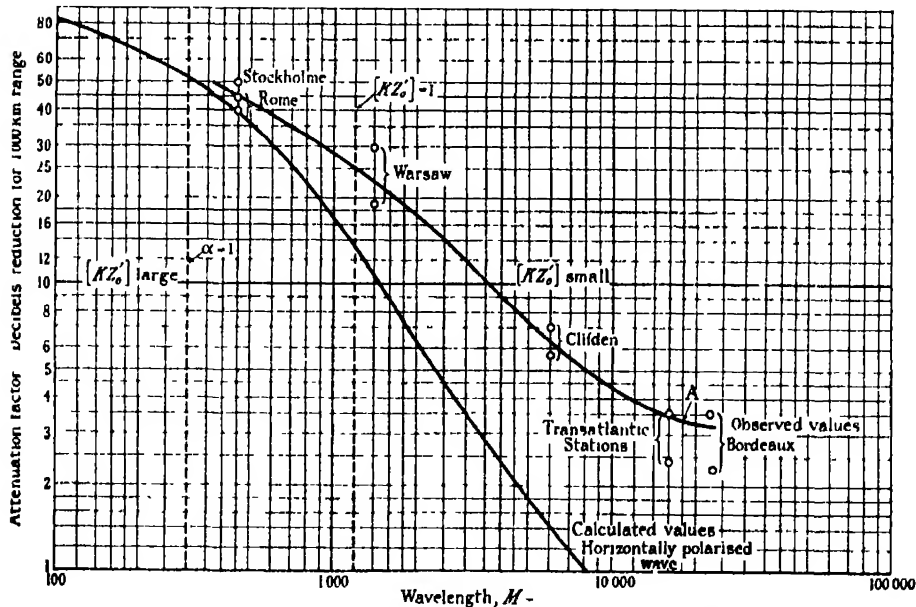
FIG. 2.—Characteristics of long-wave daylight transmission.

* 'J. Inst. Elec. Eng. Lond.,' vol. 63, p. 933 (1925), Espenschied Anderson and Bailey, 'Bell System Tech. J.,' vol. 4, p. 459 (1925); and 'Proc. Inst. Rad. Eng.,' vol. 14, p. 7 (1926).

The quantity even for daylight transmission is not constant but varies with the latitude, season, epoch in the eleven-year sunspot period, and also to a certain extent throughout the day. The upper and lower points for given wavelength give the extreme limits observed.

The curve A then gives the average attenuation observed on wave-lengths between 400 m. and 23,000 m.

The observed attenuation increases rapidly as the frequency is increased.

The theory given in the previous section may be used to explain the results. For a numerical comparison we require to make a definite choice of a model to represent the conditions in the Kennelly Heaviside layer.

Experimental evidence of the distribution of electronic concentration in this layer has been obtained by Appleton.[*] The curve given on p. 336 represents observations of the measured equivalent path as a function of the frequency. The relation is nearly linear, which implies that N, the electronic density, varies in proportion to the square of the height above 82 km.

We may put $N = N_0(z/z_0)^2$ where N_0 is the value of N when $z = z_0$; $N_0 = 10^5$ approximately when $z = z_0 = 30$ km.

For a complete numerical determination of the attenuation coefficient by formulæ (3.8) and (3.17) we require the value of α, i.e., $\nu_c/\pi\nu k$, where ν_o is the mean collision frequency of electrons and molecules. This, unfortunately, is not constant throughout the layer.

Values of ν_c are given by S. Chapman for the region occupied by the E layer. They are shown in the following table :—

H	70	80	90	100	110	120
ν_o	10^7	$3 \cdot 3 \times 10^6$	$1 \cdot 1 \times 10^6$	$3 \cdot 5 \times 10^5$	$1 \cdot 2 \times 10^5$	$3 \cdot 8 \times 10^4$

Since the depth of penetration of the waves at glancing incidence is small we have taken as a first approximation the value of α corresponding to the value of ν_o at the base of the layer, i.e., 82 km.; ν_o is then $2 \cdot 5 \times 10^6$.

With this data it is possible to compute the values in the formulæ (3 8) and (3.17) and to draw the theoretical attenuation curve.

The nature of the formulæ depend on (1) whether α is large or small, (2) whether ξ is large or small. As a preliminary, therefore, we can calculate the values of λ at which $\alpha = 1$ and $\xi = 1$ respectively. With the above value for ν_o, α is unity for a wave-length of approximately 300 m.

The value of ξ is

$$\frac{2\pi}{\lambda} z_0 \sqrt{1 + \iota\alpha} \times \sin^2 \theta, \qquad (4.1)$$

so that

$$|\xi| = \left|\frac{2\pi z_0}{\lambda} \sqrt{\alpha} \sin^2 \theta\right| \qquad (4.2$$

when α is large. With $\sin \theta = 0 \cdot 178$ (tangent wave) and $z_0 = 3 \times \lambda$ km., this becomes unity at $\lambda = 1 \cdot 20$ km.

With this data the theoretical curve (2) has been constructed.

For a wave-length about 400 m. the observed and theoretical curves agree ; with longer waves the two diverge, the computed values being too small.

It must, however, be remembered that with the longer waves, greater than about 1 km., the computed values only refer to horizontally polarised waves while the observed values refer to vertically polarised waves. The transmission characteristics of horizontally and vertically polarised waves are only the same when ξ is large, i.e., for wave-lengths below 1000 m.

The theoretical curves begin to diverge at this point. The correct attenuation values for the longer wave vertically polarised waves depend upon the reflection coefficients computed by the more complicated differential equation (2.9).

If we can be guided by the case of sharply defined layers to which limit conditions tend as $\xi \to 0$ we can infer that, as in the cases considered in § 2, the vertically polarised waves are much more attenuated than the horizontally polarised. This would appear to account for the fact that the computed values $\bar{\alpha}$ fall below the observed values when ξ is small. The high attenuation and small reflection coefficient on the broadcast band is adequately accounted for on this theory, and it is unnecessary to involve magneto ionic effects as a cause.

Magneto ionic effects have been neglected, and it is believed rightly so, since in day-time the reflection occurs in regions where the collision frequencies are large enough to swamp the natural rotation period of the electrons in the earth's magnetic field H_0, i.e., $eH_0/2\pi m$.

At night-time the layer rises to regions where the collision frequencies are some 10 times smaller than in the day-time.

For such regions magneto ionic effects will have to be taken account of.

Fig. 3 exhibits very clearly the physical significance of the type of attenuation curve observed.

It represents the depth of penetration of the electromagnetic waves into the
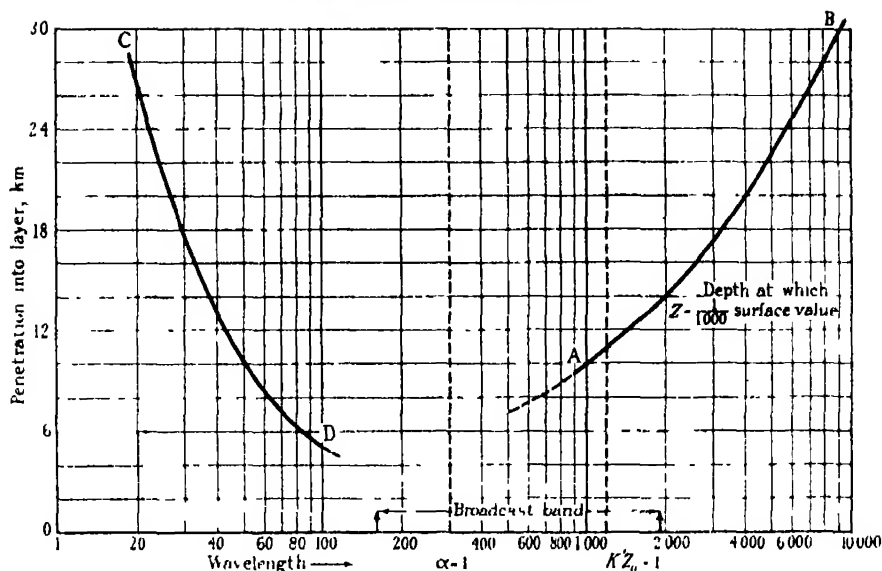
FIG. 3.—Depth of penetration (E layer). Tangent wave.

layer. In the region where ξ is small the intensity in the layer may be represented at considerable depth in the layer by the asymptotic formula for $D_n(z')$

$$D_n(z') = e^{-\frac{1}{2}z'^2} . z'^n \left\{ 1 - \frac{n(n-1)}{2z'^2} \right\} + \text{etc.,} \tag{4.2}$$

which is the solution of the differential equation (2 4) when $\nu_0^2/\nu^2 = z^2/z_0'^2$ appropriate to the case where E vanishes at $z = \infty$.

z' here is the quantity

$$\frac{z}{\left(\frac{z_0' \lambda}{2\pi} \right)^{\frac{1}{3}}} \tag{4.3}$$

and

$$n = \left(\frac{2\pi}{\lambda} z_0 \sqrt{\iota\alpha} . \sin^2 \theta - 1 \right) \bigg/ 2, \tag{4.4}$$

where n is nearly $-\frac{1}{2}$ for small values of ξ.

With known values of z_0, the contour at which E is reduced to a certain fraction of its surface level can easily be calculated. The portion of the curve AB shown in the figure is such a contour for which E is $1/1000$ of its surface value. Where α is small and ξ large the ordinary ray theory holds and the depth of penetration, *i.e.*, the apex of the ray of incidence $90° - \theta$, is $z_0 \sin \theta$, and the portion of the curve (1) represents the penetration in this region.

The transition region where ξ is neither large nor small is more difficult to calculate, but it is clear from physical considerations and questions of continuity that the penetration decreases to a minimum in the region between 100 m. where α is small and 1000 m. where ξ is unity. The penetration is equivalent to the skin effect in an ordinary conductor. So long as $\alpha > 1$ the layer acts as a metallic conductor for which the depth of penetration decreases as the frequency increases. The earth and the outer conducting shell, the Kennelly Heaviside layer, act, apart from geometrical factors depending on the spherical shape, as a transmission line, the two bounding shells representing the conductors. The attenuation of such a generalised transmission line is proportional to the effective resistances per unit length of the two guiding surfaces As the frequency increases the penetration decreases, and the resistivity of the upper layer increases, and hence the attenuation is greatest for the highest frequencies within the range for which the layer acts as a metallic conductor, $i\,e$, within the range for which $\alpha > 1$.

We may say approximately that the large upper layer attenuation is associated with the small penetration of the waves into the upper layer in these regions. This effect is accentuated by a factor which has been neglected in this analysis, $i\,e$, the decrease of the collision frequency with the height above the surface of the layer. This in general causes an accentuation of the attenuation as the penetration decreases, for where the penetration is small the energy is confined to regions near the base of the layer where the collision frequency and therefore the specific attenuation is greatest

Summary.

The phase integral method[*] is shown to lead to appropriate solutions of the problem of the transmission of long wireless waves guided round the earth's surface by the upper conducting Kennelly Heaviside layer.

The problem of a sharply defined upper conducting layer has been considered by G. N. Watson. In this paper the extension to the case where the layer is stratified in a vertical direction is considered. The phase integral method can be used when the reflection coefficient of the layer as a function of the angle of incidence is known

It is shown that the transmission characteristics of horizontally and vertically polarised waves are different when the electronic gradient is great enough. The example of a layer in which the electronic density N is proportional to the

---

square of the height is discussed, and used to give a theoretical interpretation of the observed results in long-wave transmission. Fair agreement is obtained for wave-lengths between 400 and 1000 m   On longer waves the theoretical and observed attenuation curves diverge, the former only applying to horizontally polarised waves and the latter to vertically polarised waves   The physical significance of the wave-length attenuation relation is considered to be associated with the penetration of the waves into the layer, the attenuation being greatest where the penetration is least.

In conclusion, I should like to express my thanks to the Marconi's Wireless Telegraph Company for allowing me to publish these results.

The Excitation Function of Helium.

By J. H. LEES (H. H. Wills Physical Laboratory, University of Bristol)

[PLATE 10.]

1. *Introduction.*

There are two methods of investigating inelastic collisions between atoms and electrons.   By measuring the energies of the scattered electrons we obtain at once the probabilities of excitation to the various levels.   Small energy differences, however, cannot be resolved electrically and so only the probabilities of excitation to the lower, widely separated levels can be obtained in this way.

In the method described in this paper the intensities of the spectral lines emitted by the atoms after collision are measured.   It is possible by this means to estimate the absolute probability of excitation to a given state by collision with an electron of known velocity.   The probability of excitation to a given state plotted as a function of the velocity of the exciting electrons is known as the excitation function of that excited state.

Although much work has recently been done on this subject, every determination of the excitation function so far made has been open to criticism. In every case an electron beam of known velocity is passed through helium, and the spectrum of some point in the beam is photographed at various electron

velocities. Clearly it is most important to know the electron current density at the point photographed, and not merely the total current in the electron beam. This has not been done in any previous work, which is therefore liable to very considerable errors due to changes in the shape of the beam.

In the work to be described this source of error is eliminated by photographing a complete cross-section of the beam; this allows not only the integration of the total intensity in the beam, but also makes it possible to detect and, if necessary, to allow for any background of diffuse light due to scattered electrons or any other cause. The results show only a general agreement with those previously obtained.

2. *Apparatus.*

The apparatus is shown in fig. 1. The electrodes are partly of molybdenum and partly of staybrite steel, and are enclosed in a glass tube 5 cm. diameter
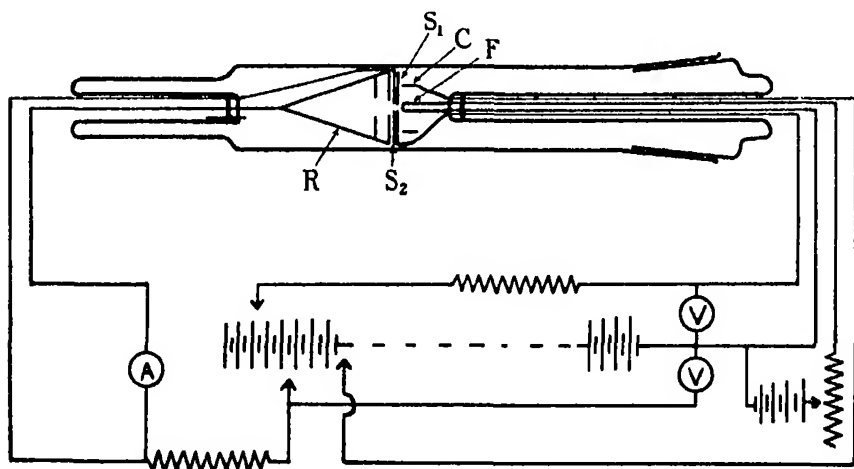
FIG. 1.

and 30 cm. long. The filament (F) is an oxide-coated platinum strip suspended for convenience in renewing, from a ground glass joint at one end of the tube. In front of the filament is a plate (S_1) with a slit 5 mm. by 1 mm. which is used for accelerating the electrons away from the filament, and beyond this slit is the field free box. This consists of a second slit (S_2) of the same dimensions as the first, with behind it a cone (R) which collects the electrons. The cone has two discs across its mouth, each pierced with a large slit intended to prevent the escape of scattered electrons; it is between these discs that the light is photographed. This arrangement for measuring the light at the point where

the electrons enter the measuring collector makes the actual current and the measured current identical at all values of the mean free path, so that variations due to change in electron voltage or in helium pressure do not affect the accuracy of the current measurement. No special window is necessary as the tube itself is sufficiently transparent, and a slight distortion of the image of the electron beam does not matter. A light trap, however, is essential to avoid reflected light being photographed, and this takes the form of a bent glass cone attached to the tube opposite the spectrograph.

The apparatus is connected through a charcoal tube in liquid air to the pumps and to the helium supply; there is also a second charcoal tube directly attached to it. The electrodes were out-gassed by means of an induction furnace, and the whole tube with the exception of the ground joint at the extreme end was baked out at 300° C. The ground joint was sealed with wax on the outside, and owing to the very large pumping resistance offered by the ground joint the charcoal could easily deal with any impurity due to this. On no occasion was there any sign of lines due to impurity even in the spectra photographed with exposures of over 24 hours.

The electrical arrangements are shown in fig. 1. The voltage drop along the effective part of the filament is 0·3 volts and the homogeneity of the beam was tested by applying stopping potentials between the collector cone and the other electrodes. A typical curve is shown in fig. 2, the current being plotted against the stopping potential for 60-volt electrons, (A), and the differentiated curve, (B), is also shown. This curve only gives an outside limit to the inhomogeneity of the beam, owing to such factors as the divergence of the beam, but even so it shows that 90 per cent. of the electrons lie within a $3\frac{1}{2}$-volt range. A further test was made by applying a magnetic field which bent the beam as a whole with no appreciable loss in sharpness, showing that the beam is approximately homogeneous.
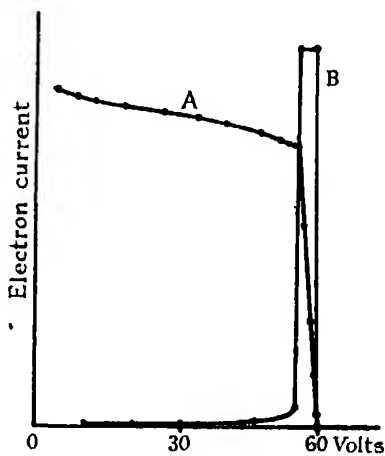
Fig. 2.

During a series of exposures the electron current is measured by a micro-ammeter, and is maintained constant by adjusting the filament heating current. The first slit (S_1) is provided in order to obtain the maximum possible electron

current.   Owing to negative space charges, saturation of the emission is only reached for fairly high values of the field, which could not always be obtained if the slit were omitted.   The electrons are strongly accelerated to the first slit, resulting in the formation of many positive ions, and they are then retarded to the speed required by entering the second slit.   The ions, owing to their low mobility, diffuse away slowly, and consequently they largely neutralise the negative space charge.   This arrangement gives a copious supply of quite slow electrons.   It is also desirable to keep the first slit at a potential positive relative to the field free box in order that any secondary electrons emitted from it will be unable to enter the observation chamber.   The only exception to this is made when working at voltages over 1000, when the slit is made 20 volts negative to the filament in order to keep the electron current down to the required value, as it is found that if the reduction is made entirely by reducing the filament temperature the electron current becomes extremely unstable. At the lower voltages, however, the slit may be used at any potential positive relative to the field free box, most suitable to bring the electron current to the required value or to focus the beam.   The focus may also be altered by choosing a suitable potential for the cylinder (C) round the filament.

As the electron emission is very sensitive to change of filament temperature, the heating current is provided by accumulators, and all the potentials are maintained by batteries of accumulators in order to obtain the utmost steadiness.

3. *Optical Arrangement.*

A photographic method of measuring the intensity is used, as the light source is weak.   A Hilger E_1 quartz spectrograph is used and its dispersion of about 13 A. per millimetre allows the use of a very wide slit (0·3 mm.) whose image on the photographic plate is magnified by tilt to 0·8 mm.   This makes for great accuracy in photometry.   An image of the electron beam is thrown on to the spectrograph slit perpendicular to it, so that a cross-section of the beam is photographed.

Ilford Iso-Zenith plates were chosen, as these give the best compromise between high speed, small grain size and low background density, while the density-log intensity curve is of a suitable form to give reasonable accuracy in photometry over a large range of intensities.   The plates were developed under standard conditions, using amidol in a special tank arranged to give extremely powerful and regular stirring.

A typical photograph, fig. 3, Plate 10, consists of a spectrum where the centre of each line is very intense, corresponding to the centre of the electron

4026   2 ³P   5 ³D

3965   2 ³S   3 ³P

3889   2 ³S — 3 ³P

3820   2 ³P — 6 ³D
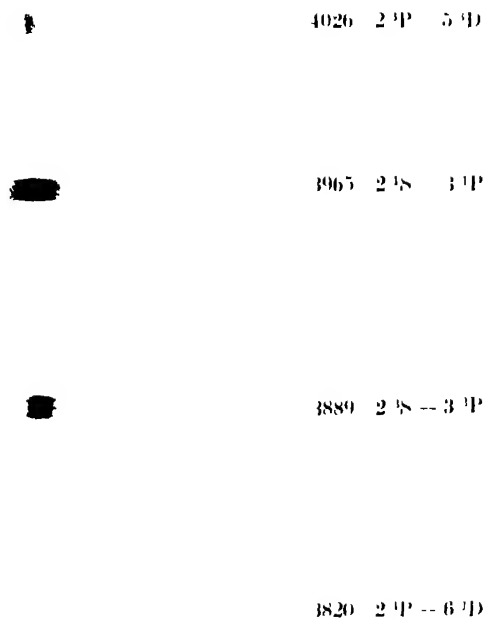
Fig. 3

beam, and fading away on each side. The line is photometered by a self-recording microphotometer described elsewhere* and the resulting curve indicates the degree of blackening. As the photometer deflection is not proportional to the original light photographed, a calibration is necessary, and this is done by means of a neutral wedge placed over the spectrograph slit and illuminated by a uniform patch of helium light from a low pressure arc. As the density gradient of the wedge is known for all wave-lengths, this gives the calibration directly. A blank photograph taken under similar conditions, but without the wedge, serves to correct for any slight irregularities in the illumination of the spectrograph slit.

By means of this calibration the curve recorded by the photometer is converted to true intensity, and the area beneath the true intensity curve is measured to give the integrated intensity of the whole beam.

The relative intensities of the different lines were determined by the use of a calibrated lamp. A photograph of the lamp was taken and developed under standard conditions, and the photometric determination of the intensity at different wave-lengths was correlated with the energy distribution given by a previous calibration made at the National Physical Laboratory. In order to determine the efficiency of excitation, an approximate estimate of the actual number of quanta photographed was also made.

4. *Results.*

The dependence of the light intensity on the electron current was first investigated. It was found that within experimental error all the lines measured showed a linear relationship, fig. 4. This shows that a single electron only is involved in the collision process and it also serves as a check on the accuracy of the photometry.

Next, the relation between light intensity and helium pressure was measured, and the results of this are shown in fig. 5. It will be seen that while the intensity of the lines 4438 ($2\,^1P-5\,^1S$) and 4922 ($2\,^1P-4\,^1D$) show a linear relationship with the pressure, this is not exactly so in the case of the lines 5016 ($2\,^1S-3\,^1P$), 3965 ($2\,^1S-4\,^1P$) and 4472 ($2\,^3P-4\,^3D$). It is clear that if simple collision excitation takes place the light intensity will depend on the number of collisions, *i.e.*, on the gas pressure, so that in the case of 4438 and 4922 the linearity observed indicates that only simple excitation takes place. In the case of the lines which deviate from simple proportionality a further peculiarity is to be

---

* J. H. Lees, 'J. Sci. Instruments,' vol. 8, p. 273 (1931).

observed. The light of these lines does not all come from the electron beam, but a large proportion comes from points as much as 1 cm. from the beam. Apparently this spreading has not been observed hitherto owing to the method generally used of photographing a spot in the electron beam instead of a whole
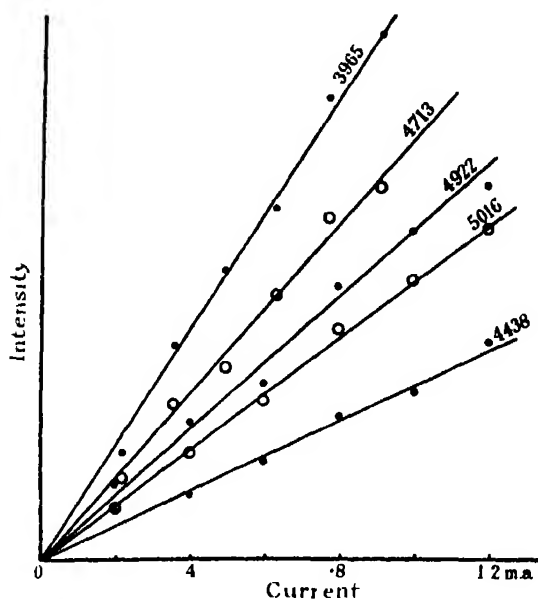
Fig 4.
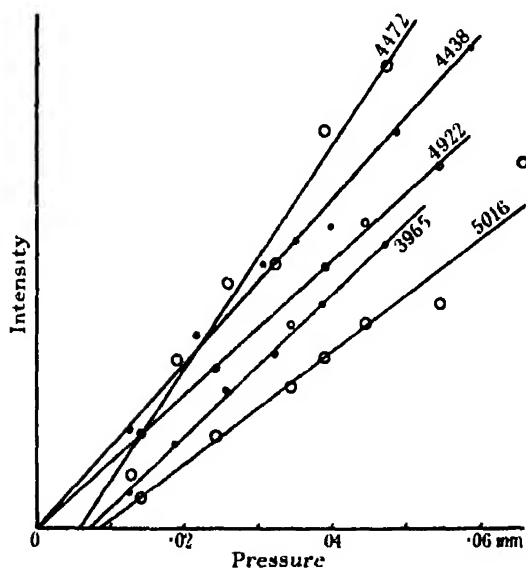
Fig. 5.

cross-section. It is found that all the lines showing spread deviate from a simple proportionality between intensity and pressure. The discussion of these effects will be given in a second paper.

The results of the intensity-electron voltage measurements are shown in figs. 6–11. The ordinates, when multiplied by the appropriate factor shown on the figures, give the atomic cross-section of helium for collisions resulting in the emission of one quantum of the radiation in question. The abscissæ show the electron voltages plotted on a logarithmic scale. A helium pressure of 0·044 mm. was used and an electron current of 0·8 milliamperes.

Fig. 6 shows the curves of the singlet sharp series 4438 ($2\,^1P-5\,^1S$) and 4169 ($2\,^1P-6\,^1S$). In each case there is a steady rise to a maximum at about 37 volts, and a gradual decline as the electron voltage increases further.

LINE	FACTOR
4438	$\times 7\cdot5\times10^{-21}\,cm^2$
4169	$\times 3\times10^{-21}\,cm^2$
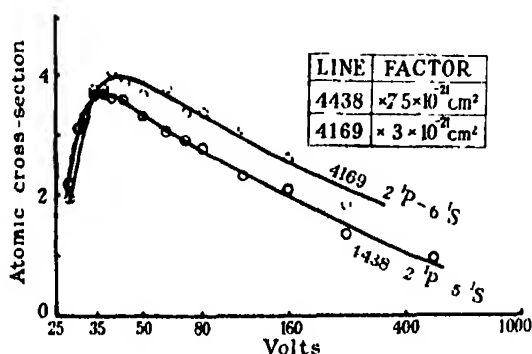
FIG. 6.

In fig. 7 are given the singlet principal series 5016 ($2\,^1S-3\,^1P$), 3965 ($2\,^1S-4\,^1P$) and 3614 ($2\,^1S-5\,^1P$). These curves are all very similar, each

LINE	FACTOR
5016	$\times 1\cdot5\times10^{-19}\,cm^2$
3965	$\times 6\times10^{-20}\,cm^2$
3614	$\times 1\cdot5\times10^{-20}\,cm^2$
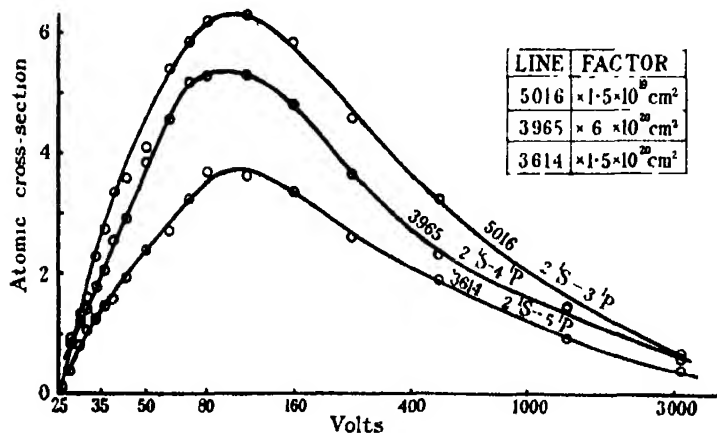
FIG. 7.

showing a very slow rise to a maximum at 100 volts, and a very slow fall
beyond.

The singlet diffuse series, 4922 ($2\,^1P-4\,^1D$) and 4387 ($2\,^1P-5\,^1D$) is shown
in fig. 8, and here the maximum lies at about 80 volts.
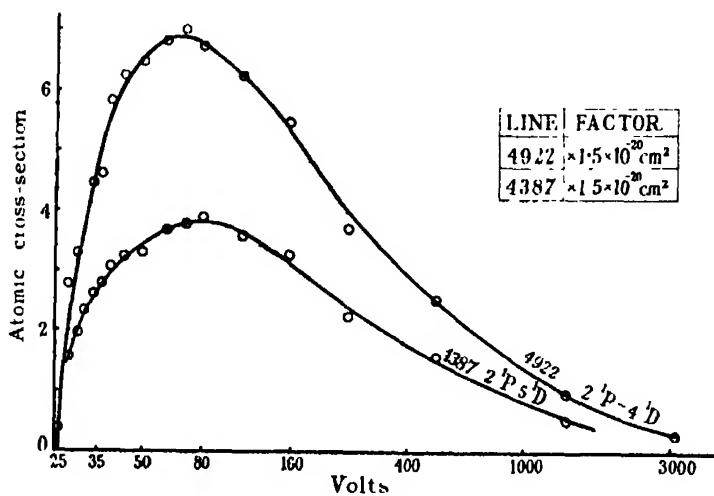
Fig. 8.

In the case of the triplets the sharp series 4713 ($2\,^3P-4\,^3S$) and 4121
($2\,^3P-5\,^3S$) is shown in fig. 9. These curves have an extremely rapid rise to
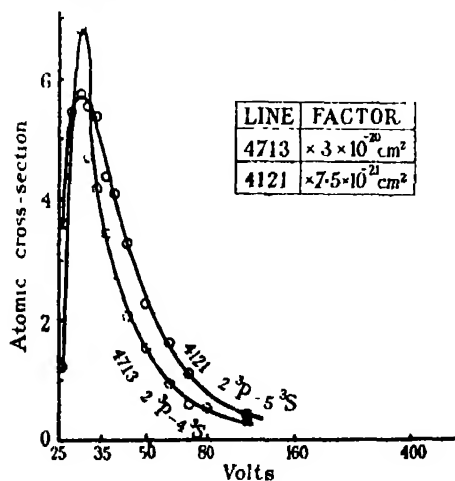
Fig. 9.

a maximum at about 30 volts, and beyond this an almost equally rapid fall,
the intensity beyond 100 volts becoming too small to be measured.

Fig. 10 shows the triplet principal series of which only one line, 3889 (2 ^{3}S—3 ^{3}P) lies in the range of wave-lengths investigated. This curve rises to a rather blunter maximum at 32 volts, after which it falls steeply.
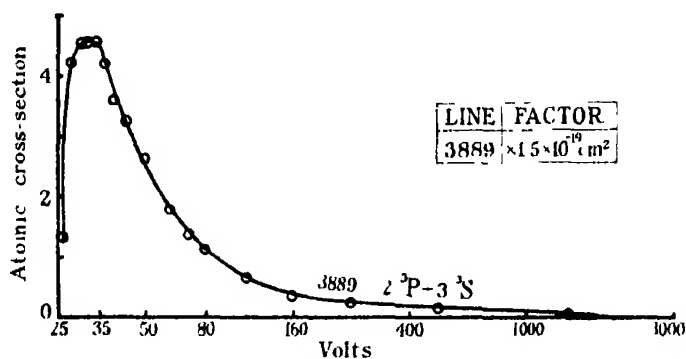
FIG. 10.

The triplet diffuse series is shown in fig. 11. Three lines were measured, 4472 (2 ^{3}P—4 ^{3}D), 3820 (2 ^{3}P—6 ^{3}D) and 3705 (2 ^{3}P—7 ^{3}D). 4026 (2 ^{3}P—5 ^{3}D) could not be resolved from 4021 (2 ^{1}P—7 ^{1}S) and was not measured. The
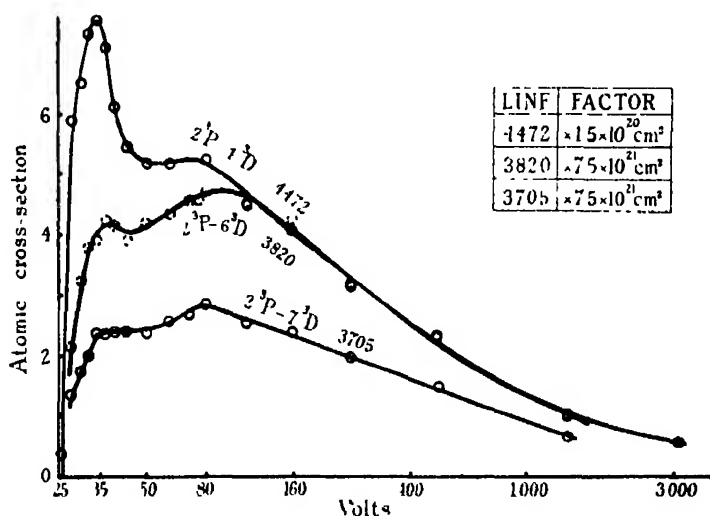
FIG. 11.

members of this series show a progressive change in the shape of the curve. The lowest member (2 ^{3}P—4 ^{3}D) shows a marked maximum at 34 volts, while between 48 volts and 78 volts there is scarcely any drop in intensity, and beyond 80 volts the curve drops slowly. The next line measured (2 ^{3}P—6 ^{3}D)

shows a peak, although much smaller, at 34 volts, and it also shows a second maximum at 85 volts. The last line ($2\,^3P-7\,^3D$) shows only a trace of the 34 volt peak, while the second peak at 85 volts is very pronounced.

4. *Discussion.*

These results agree only approximately with those of previous authors. Hughes and Lowe* were unable to work at voltages lower than 34 volts and their curves are therefore incomplete. Their photometric methods were, moreover, incapable of great accuracy and the lack of linearity between intensity and current, and intensity and pressure shows that their conditions were unsatisfactory. Their results, however, do not show any very striking differences with those given above. On the other hand, Peteri and Elenbaas† obtained extremely different curves, and, as was pointed out in a preliminary account of the present work,‡ this was probably due to incorrect current measurements. Hanle§ has obtained results agreeing fairly well with those given here except in the case of the $2\,^3P-m\,^3D$ series, and this difference is probably due to insufficient observations at low voltages. Elenbaas∥ however, found that all the lines without exception show a slight maximum at about 60 volts. This is probably due to a change in the shape of the electron beam, giving an increase in the current density at the spot photographed at about 60 volts. Like Hanle, he was unable to obtain accurate proportionality between intensity and electron current or helium pressure, showing that the photometry or experimental conditions were not satisfactory. Michels¶ obtained this proportionality approximately, but, like Hanle and Elenbaas, he did not integrate the total intensity of the beam, and the second maxima he obtained at about 80 volts for all lines are probably due, therefore, to changes in the width of the electron beam. Michels, moreover, used a non-homogeneous beam of electrons, 90 per cent. only lying within a 10-volt range, and so a very large correction had to be applied to the excitation curves obtained. While this correction is unimportant at high electron velocities, it is impossible to obtain accuracy near the excitation potential on account of the very rapid changes in the excitation probabilities in this region.

* 'Proc. Roy. Soc.,' A, vol. 104, p. 480 (1923).

† 'Z. Physik,' vol. 54, p. 92 (1929).

‡ Lees and Skinner, 'Nature,' vol. 123, p. 826 (1929).

§ 'Z. Physik,' vol. 56, p. 94 (1929).

∥ 'Z. Physik,' vol. 59, p. 289 (1930).

¶ 'Phys. Rev,' vol. 36, p. 1363 (1930).

The estimates made by some of the above authors of the relative intensities of the lines should be accurate except in the case of the lines which spread. For these lines, however, the intensities must be wrong owing to the large proportion of light which comes from outside the electron beam and so is not measured. It seems, therefore, that the results given here must be more accurate than those of previous workers owing to the improved methods used.

6. *Excitation Probabilities.*

We must now consider what knowledge the intensity-voltage curves obtained give us of the probabilities of excitation to a certain state for various electron voltages. The intensity measured is proportional to the number of atoms in a certain excited state whether excited directly or indirectly. Thus the intensity of the line (2 ^{3}S—3 ^{3}P) gives the number of excited atoms in the 3 ^{3}P state, and these may have been excited by electron impact giving a (1 ^{1}S—3 ^{3}P) transition, or by cascade from a higher ^{3}S or ^{3}D level, or by the recombination of an ion with an electron. The proportion of excited atoms due to cascade cannot be measured, but we know that for large quantum numbers the classical rule is approximately correct that the intensity in quanta per second due to any transition from a given state depends on ν^3. As cascade involves low frequency, high quantum number, transitions the intensity due to this is probably small. The possibility of recombination was tested by means of a special apparatus arranged with a powerful electrostatic field at right angles to the electron stream. The field strength was sufficient to sweep all helium ions to the electrodes in 2×10^{-8} seconds after formation and slow electrons in 10^{-10} seconds. It was found, however, that apart from a displacement of the whole electron beam the electrostatic field had no effect at all, proving that ionisation and recombination plays no part in the emission of light in the region investigated. This experiment served also to show that slow electrons played no part in the excitation process. Thus it is probable that the indirect excitation is quite small. There is, however, one exception to this in the case of the spreading lines. The mechanism of spreading will be dealt with fully in the following paper, and it will be shown that while the intensity curves of the (2 ^{1}S—n ^{1}P) lines represent the excitation function of n ^{1}P levels, the curves for the (2 ^{3}P—n ^{3}D) lines are composed partly of the excitation function of n ^{1}P levels and partly of n ^{3}D levels. The true n ^{3}D excitation curve gives the low voltage peak shown by the (2 ^{3}P—n ^{3}D) lines and the spurious n ^{1}P excitation gives the high voltage peak. With this single exception, however, the intensity curves may be regarded as approximately true excitation curves.

In one special case the absolute probability of excitation may be accurately found. The line 3889 (2 ³S—3 ³P) is the only line which can possibly be radiated by atoms in an excited 3 ³P state and in this case the absolute probability is equal to the number of quanta shown as ordinate in fig 10. In the case of all the other lines measured, however, the selection rules permit several transitions from the excited state. Thus the 3705 radiation (2 ³P—6 ³D) is radiated by atoms in a 6 ³D state which may drop to any of two ³F states or four ³P states. If the relative probabilities of these allowed transitions were known, then the total number of atoms in the excited state could be deduced by measuring the intensity of any one of the lines emitted. These probabilities have not been worked out for helium, and although the classical rule mentioned above is true for large quantum numbers it is not correct for small quantum numbers But in each case the line measured is that of the shortest wavelength and is therefore the most probable transition ; thus the number of excited atoms will be roughly equal to the number of quanta of the observed radiation. The (2 ¹S—n ¹P) series is the only exception to this because the (1 ¹S—n ¹P) radiation is much more probable than the observed radiation.

A comparison of the excitation curves with those obtained theoretically by Massey and Mohr* shows some agreement. Thus they obtain the steep rise and fall for the triplet series, and the gradual rise and fall of the singlet series which are found experimentally. In detail, however, there are serious differences. All the theoretical curves show maximum excitation probabilities at much lower voltages than are found experimentally, and this discrepancy cannot be due to the inhomogeneity of the electron beams used. There is a definite disagreement in the case of the (2 ³P—n ³S) series, which theoretically is predicted to have a blunter excitation curve than the (2 ³S—n ³P) or the (2 ³P—n ³D) series. Experimentally, however, the (2 ³P—n ³S) series shows the sharpest peak, and it is quite impossible to see in the experimental work any explanation for this difference.

Since the publication of the paper referred to above, Massey has found a numerical error in the calculations for the (1 ¹S—n ¹P) lines, and the revised curves show a gradual rise to a late maximum just as is found experimentally.

The values predicted for the atomic cross-sections can only be compared with the values estimated experimentally in the cases of the 3 ¹P and 3 ³P states, as these are the only cross-sections which have been estimated both theoretically and experimentally. The theoretical cross-sections for these states for electrons of 200 volts, are $1 \cdot 3 \times 10^{-19}$ cm.² and 9×10^{-25} cm.²

* 'Proc. Roy. Soc.,' A, vol 132, p. 605 (1931).

respectively. *Fig.* 7 shows that at this voltage the cross-section for a quantum of $2\,^1S—3\,^1P$ radiation is 8×10^{-20} cm^2. The cross-section for excitation to a $3\,^1P$ state must be slightly greater than this, which agrees with the calculated value. Fig. 10, however, shows that the cross-section for a quantum of $2\,^3S—3\,^3P$ radiation, which, if the contribution to the $3\,^3P$ state by cascade can be neglected, is equal to the cross-section for excitation to a $3\,^3P$ state, is 4×10^{-20} cm.^{2}. This is enormously greater than the theoretical value and, although part of the light measured will be due to excitation by electrons which have already made one or even more inelastic collisions, this additional excitation cannot account for such a very large discrepancy.

We may summarise the results of the excitation curves as follows :—

(1) The excitation curve for each state shows a single maximum at the electron voltage V_m giving the maximum probability of excitation.

(2) The excitation curves of states in the same series, *e g.*, $n\,^1P$, are similar in shape

(3) The sharpness of the maximum of an excitation curve is related to the value of V_m. A low value of V_m goes with a sharp maximum, and a high value with a blunt maximum.

(4) Comparison of the excitation curves shows that for a triplet state the value of V_m is considerably smaller than for the corresponding singlet state.

(5) Among the singlet or triplet states themselves, the value of V_m tends to increase as we pass from the S to the P and D terms. Table I gives the values.

Table I.

Wave-length.	Level.	Maximum atomic cross-section.	V_m.
Å 4438 4169	$2\,^1P—5\,^1S$ $2\,^1P—6\,^1S$	28×10^{-21} 12×10^{-21}	volts 36
5016 3965 3614	$2\,^1S—3\,^1P$ $2\,^1S—4\,^1P$ $2\,^1S—5\,^1P$	1000×10^{-21} 340×10^{-21} 57×10^{-21}	100
4922 4388	$2\,^1P—4\,^1D$ $2\,^1P—5\,^1D$	110×10^{-21} 60×10^{-21}	74
4713 4121	$2\,^3P—4\,^3S$ $2\,^3P—5\,^3S$	210×10^{-21} 45×10^{-21}	30
3889	$2\,^3S—3\,^3P$	720×10^{-21}	32
4472 3820* 3705*	$2\,^3P—4\,^3D$ $2\,^3P—6\,^3D$ $2\,^3P—7\,^3D$	120×10^{-21} 9×10^{-21} 5×10^{-21}	34

*The values for the lines 3820 and 3705 are taken from the part of the curve giving the low voltage peak only.

Summary.

An accurate method of measuring the excitation functions of helium is described, and the results obtained are given.

The variation of light intensity with electron current and with helium pressure is measured. Certain of the spectrum lines are found to be emitted not only from the electron beam but also from points some distance from the beam. These spreading lines show anomalous intensity-pressure curves.

The relation is discussed between the intensity-voltage curves found experimentally, and the curves showing the actual probability of electrons of given velocity exciting an atom to any given state. An estimate is made of the absolute probability of excitation to certain states.

The author wishes to thank Dr. H. W. B. Skinner for suggesting the work.

Notes on the Excitation Processes in Helium.

By J. H. LEES and H. W. B SKINNER, Wills Physical Laboratory, Bristol.

1. *Introduction.*

In the preceding paper* an account has been given of experimental work on the excitation function of helium. Here we propose to enter into a fuller discussion of some of the problems involved. We shall give a detailed examination of the phenomenon of spreading, reported in the previous work, and also we shall put forward a rough but simple conception of the excitation process which allows an understanding in terms of elementary ideas of the main characteristics of the excitation process.

2. *Spreading.*

When a well-defined electron beam passes through a gas at low pressure, the light emitted from the majority of the spectrum lines comes almost entirely from those points of the gas which are traversed by the electrons. But for some classes of lines, there is a considerable amount of light emitted by those parts of the gas which lie outside the electron beam. This is the phenomenon

---

* p. 173 ; to be quoted as Paper I.

which we describe as spreading. We may define the spread of a line as the ratio of the light emitted from outside the electron beam to that emitted from within it. The lines which show this effect most clearly in helium are the lines for which the upper state of the atom is an $n\,^1P$ state and these all spread, to about the same extent, independent of the voltage of the exciting electron beam. Second in order of spreading are the lines for which the excited atom is in an $n\,^3D$ state, and in this case it is observed that the degree of spreading increases with n. For the other helium lines the spreading is very slight, though it almost certainly exists for all. In mercury, a casual observation has shown that the resonance line $(1\,^1S-2\,^3P)$ spreads extremely strongly, and a number of the other lines spread to a less extent.

A photograph, taken with the spectrograph slit perpendicular to the electron beam is given for helium in Paper I (fig 3), and shows the spreading lines very clearly ; and a photometer curve, fig. 1, showing a spreading and a non-spreading line photographed using the same electron beam shows the magnitude of the effect. The line $\lambda\,5016$ represents the transition $(2\,^1S-3\,^1P)$, and the line $\lambda\,4713$ $(2\,^3P-4\,^3S)$. The distance between the two vertical lines corresponds to 1 mm in the apparatus. The pressure was $0 \cdot 044$ mm. and the voltage of the electron beam 36 volts
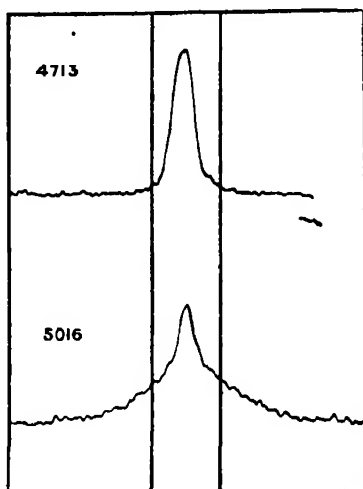
Fig. 1.

The spreading, however, is found to be rather insensitive to both these quantities.

The spreading is associated, in the case of the helium lines $(2\,^1S-n\,^1P)$ with a non-proportionality of the curves of light intensity plotted against the gas pressure. In fact, as fig. 5 of Paper I shows, the experimental results can roughly be fitted to a straight line, which, however, does not pass through the origin of the co-ordinates. The line $(2\,^3P-4\,^3D)$ shows a similar characteristic. The curves of light intensity plotted against current, on the other hand, show proportionality. In this way it is made evident that no double electron impact processes are concerned in the spreading. In particular, any effect from metastable atoms is ruled out as an explanation of the spreading of the ^1P and ^3D lines, though it may possibly be involved in the slight spreading which most of the other lines show.

This conclusion was further verified directly by an apparatus providing two beams of electrons parallel but 5 mm. apart, one of 60 volts and the other of 22 volts. The 22-volt beam alone produced no light, but when the 60-volt beam was started the slow beam showed a trace of 3889 (2 ^{3}S—3 ^{3}P). This shows that the (2 ^{3}S—3 ^{3}P) radiation was slightly absorbed in the 2 ^{3}S metastable atoms produced by the slow beam, and was then again radiated. There was, however, still no trace of (2 ^{1}S—3 ^{1}P) radiation from the 22-volt beam but, as this might be due to the low efficiency of 22-volt electrons for producing 2 ^{1}S metastables compared with 2 ^{3}S states, a further test was carried out by illuminating the electron beam by an intense helium arc. No effect on the spread was observed, showing that absorption and re-emission of those helium lines transmitted by the glass window of the arc is very small.

A further possibility is the formation of helium ions which, owing to their long life, can diffuse out of the electron beam with eventual recombination and radiation The apparatus described in the previous paper proved, however, that spread due to this must be negligible.

In the case of Hg, we have at present no corresponding data and it is quite possible that metastable atoms are involved for some of the lines. We shall therefore consider only the He lines, for which we have sufficient data to put forward a theory of the effect. But the case of the Hg line 2537 (1 ^{1}S—2 ^{3}P) is very suggestive because this is an absorption line of Hg. It is known that the absorption coefficient of Hg vapour, even at a very low pressure, is extremely high for this line when it is produced under conditions which preclude any considerable broadening of the line. Now in the electron tube used, working with a pressure of 1/1000th of a millimetre in the case of Hg, for the study of the excitation potentials, this condition is very well fulfilled. It is therefore certain that the spreading of the line 2537 is due to the absorption of the radiation initially excited by electron impact, by those parts of the Hg vapour which lie outside the electron beam. The absorbing atoms will subsequently re-emit radiation of the same wave-length. The effect therefore is that, viewed by the light of λ 2537, the whole gas will be seen to glow.

This gives a useful clue to the spreading effects in He For a somewhat similar mechanism will account for the spreading of the (2 ^{1}S—n ^{1}P) lines of helium. Here the n ^{1}P levels are excited by direct electron impact and radiate partly the line (2 ^{1}S—n ^{1}P) and partly (1 ^{1}S—n ^{1}P). The latter radiation is absorbed by atoms at a distance from the beam, raising them to the n ^{1}P state and these atoms again radiate the (2 ^{1}S—n ^{1}P) and (1 ^{1}S—n ^{1}P) light. As the (1 ^{1}S—n ^{1}P) radiations lie too far in the ultra-violet to be photographed,

their spread cannot be observed, and it is the $(2\,^1S - n\,^1P)$ lines which show the observed spreading.

In this way a simple explanation of the spreading of the $(2\,^1S - n\,^1P)$ lines is obtained. This explanation is the basis of the statement made in Paper I that the excitation functions of the ^1P states are not affected by the existence of the spreading effect; for each quantum of light emitted may be traced back to the excitation of an atom into ^1P state in the beam. We shall now proceed to a detailed examination of the various effects associated with the spreading of the $(2\,^1S - n\,^1P)$ lines in terms of the absorption theory.

If we compare at very low voltages the intensities in quanta of the $(2\,^3P - 5\,^3S)$ and $(2\,^1P - 5\,^1S)$ lines we find that the probability of exciting the $5\,^3S$ state is approximately twice that of exciting the $5\,^1S$ state. The same ratio between the probabilities of triplet and singlet excitation is obtained from the observed intensities of the $(2\,^3P - 4\,^3D)$ and $(2\,^1P - 4\,^1D)$ lines. We might therefore expect that, at low voltages, there would be about twice as many atoms excited to the $n\,^3P$ state as to the $n\,^1P$ state. If so, the intensity of the $(2\,^1S - 3\,^1P)$ radiation should be about 24 times less than the $(2\,^3S - 3\,^3P)$, because of the preferred transition $(1\,^1S - 3\,^1P)$. Actually a triplet singlet ratio of only $5:1$ is found, and this unexpectedly small value is explained on the absorption theory. It was stated above that excited $n\,^1P$ atoms radiate partly the $(1\,^1S - n\,^1P)$ line and partly the $(2\,^1S - n\,^1P)$ line, and that the former is absorbed by atoms in the ground state which later re-emit. The absorption will not, however, be complete, and the proportion absorbed within a radius r is given by $(1 - e^{-n\tau_a})$ where τ_a is the atomic absorption coefficient for $(1\,^1S - 3\,^1P)$ radiation, and n the number of atoms per cubic centimetre. If f is the total probability of an excited $n\,^1P$ atom falling to the $2\,^1S$ level, and $(1 - f)$ the probability of falling to the $1\,^1S$ level, then the total number (Q) of quanta of $(2\,^1S - 3\,^1P)$ radiation emitted is roughly given by the infinite series

$$Q = N\left\{ f + (1-f)(1 - e^{-n\tau_a})f + (1-f)^2(1 - e^{-n\tau_a})^2 f + \ldots \right\}$$

$$= \frac{Nf}{1 - (1-f)(1 - e^{-n\tau_a})},$$

where N is the number of excited $3\,^1P$ atoms in the electron beam. We have assumed here that after absorption at any point in the gas, the radiation is always re-emitted from the centre. This will certainly not be accurate, but an exact calculation is very difficult.

Thus we obtain a large increase in the observed intensity of $(2\,^1S - 3\,^1P)$

line owing to the absorption of $(1\,^1S—3\,^1P)$ radiation and the emission of $(2\,^1S—3\,^1P)$ radiation by atoms outside the beam

It is now possible to explain the form of the intensity pressure curves obtained for the lines which show spreading. Since N is proportional to the gas pressure (p), we have

$$Q = \frac{cpf}{1 - (1 - f)(1 - e^{-np\tau_a})} .$$

The coefficient f is given by

$$f = \frac{A_{32}}{A_{31} + A_{32}} ,$$

where A_{32}, A_{31} are the Einstein Transition probabilities for the $3 \to 2$, $3 \to 1$ switches

The probabilities may be approximately calculated by taking the He atom as hydrogen-like and using the formulæ of Gordon.* Suitable screening constants are used for the upper and lower states and a correction amounting to multiplication by a factor of 2 is applied in the case of A_{31} on account of the equivalence of the two electrons in the ground state. We obtain the value $0 \cdot 08$ for f.†

Using this value, a curve agreeing very well with the observed intensity-
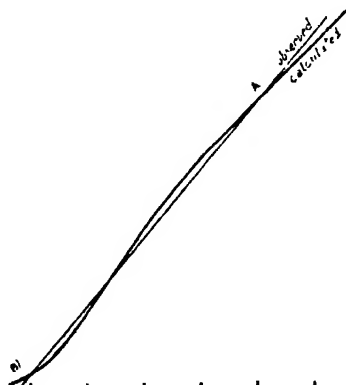
Fig 2

pressure curve is obtained, fig. 2, if we assume an atomic absorption coefficient τ_a for the $(3 \to 1)$ resonance radiation of $2 \cdot 3 \times 10^{-15}$. The asymptotic portion

* 'Ann. Physik,' vol 2, p. 1031 (1930).

† The constants C of Gordon, corrected both for screening and equivalence, are for helium $0 \cdot 34$ and $3 \cdot 0$ The corresponding values for hydrogen are $0 \cdot 52$ and $3 \cdot 07$.

(A) of this curve corresponds to strong absorption due to the high pressure, when every atom excited to a $3\,^1P$ state leads eventually to a quantum of $(2\,^1S - 3\,^1P)$ radiation. The portion (B) near the origin corresponds to negligible absorption.

This absorption coefficient is of the right order of magnitude to explain the observed fall off in intensity in the spreading curve, fig. 1. Though the actual absorption coefficients at the pressures used are quite appreciable, their effect on spreading is rather small compared with the $1/r$ fall off due to the geometry of the apparatus on account of the smallness of f. Thus no great change will be found in the spreading curves taken at different pressures. It was observed experimentally that the spreading curve does not depend much on the pressure

We may go a step further and compare the observed absorption coefficient with a calculated value. It may be shown that the value of τ_a, the atomic absorption coefficient for the resonance line, is given by

$$\tau_a = \frac{\lambda^2}{8\sqrt{2\pi}} \frac{A_{n1}}{\Delta v} \frac{g_n}{g_1}, \tag{1}$$

g_n and g_1 are the weights of the upper and lower states ; in our case, g_n/g_1 is 3. A_{n1} is the Einstein coefficient for the transition $n \to 1$, and Δv is the actual breadth of the line. For this, the natural breadth $\Delta v_0 = \sum_m A_{nm}$ may be inserted or any other breadth, such as the Doppler breadth, to suit the problem. The formula applies only when the emitting atoms are subjected to the same broadening influences as the absorbing atoms, as in the case under consideration. It must also be borne in mind that it gives only the initial absorption coefficient, since the centre of the line is most heavily absorbed, and so the shape of the line does not remain constant. The absorption coefficient therefore diminishes as the radiation passes through the gas. The formula (1) is derived from the obvious expression for τ_a, namely,

$$\tau_a = \frac{h v}{c} B_{1n},$$

where $B_{1n}\,\rho_{n1}$ is the probability of an absorption transition $1 \to n$ in a field of radiation of total density ρ_{n1} corresponding to the frequency of the $n \to 1$ transition. The quantities A_{n1}, B_{1n} may be expressed as integrals over the line breadth in terms of partial coefficients $a_{n1}(v)$, $b_{1n}(v)$, which give the transition probabilities for defined frequencies. Using Einstein relations between

a_{n1}, b_{n1} and b_{1n}, and also assuming a Gaussian form* for the shape of the line, we come to the above result.

Calculating in this way and substituting for the Doppler breadth we reach a value for τ_a which is some 40 times greater than the value obtained from the experimental results. We have seen that the calculated value represents only an initial absorption coefficient; at the actual pressure in the apparatus the effect of the self-reversal must certainly be considerable. It seems unlikely that any collision process or perturbation can, under the experimental conditions, reduce the absorption coefficient by giving the line an extra broadening comparable with the Doppler broadening. And, therefore, though the effect of the self-reversal is hard to estimate, we think it may be assumed to account for the discrepancy.

We may thus claim to have formed a fairly complete theory of the spreading of the $(1\,^1S - n\,^1P)$ lines of helium. We must now go on to the case of the $(2\,^3P - n\,^3D)$ lines, which spread appreciably, though to only about half the extent of the $n\,^1P$ lines. It is clear at the outset that the explanation for these lines must be quite different from that for the $n\,^1P$ lines, because the $n\,^3D$ lines cannot possibly be associated with any absorption effects of the normal helium atom. Further we have seen that any effects concerned with metastable atoms or ions are ruled out on experimental grounds.

It is therefore obvious that this spreading must be the result of some rather unexpected process. The following process seems to us after a careful examination of every alternative, to provide the only way of explaining the facts. It is based on the approximate equality of the energy values of the $n\,^3D$ terms with the corresponding $n\,^1P$ terms. The energy difference between the $4\,^1P$ and $4\,^3D$ levels is 6 millivolts, while between the $7\,^1P$ and $7\,^3D$ levels it is only $1\cdot4$ millivolts. This energy difference is much less than the energy of thermal agitation. We have stated that the degree of spreading for the $n\,^3D$ lines also increases with n. It is therefore tempting to suppose that the process

$$\text{He } (1\,^1S) + \text{He } (n\,^1P) \rightarrow \text{He } (n\,^3D) + \text{He } (1\,^1S)$$
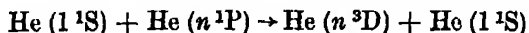
(and, of course, the reverse process) can occur in a collision between a normal

---

* It has been pointed out to us by Professor R. H. Fowler, F.R.S., to whom we are indebted for much discussion of the formula (1) that the adoption of the Gaussian form for the natural breadth is not correct. We ought to use the form of the radiation emitted by a damped classical oscillator (see Weisskopf and Wigner, ' Z. Physik,' vol. 62, p. 54 (1930)). The effect on (1) is, however, only a small alteration of the numerical constant, and as the Gaussian form must be adopted for the Doppler breadth, we have retained it throughout. The formula (1) is therefore only an approximation.

and an excited helium atom, the extra energy being taken from the kinetic energies. If this process is possible, since we have a supply of $n\,^1P$ atoms distributed everywhere in the gas, the spreading of the $n\,^3D$ lines would follow. Since the mean life of an atom in the $n\,^1P$ state is only about 10^{-8} seconds, we have to suppose that the effective diameter for the collision process $(n\,^1P \rightarrow n\,^3D)$ must be fairly large.

Assuming that an atom in a ^1P state has during its life-time a chance of 1/10th of making a collision which gives rise to a ^3D atom, we obtain for the collision radius of the process the value $1 \cdot 2 \cdot 10^{-7}$ cm. From the observed intensities the value 1/10th must be of the right order of magnitude and the result can hardly lie outside the range from 1 to $2 \cdot 10^{-7}$ cm. This collision radius is about the same as the radius of the atom in its 5th or 6th excited state.

We proceed to an examination of the way in which it may account for the observed facts. In the first place, lines of the series $(2\,^3P\!-\!n\,^3D)$ show similar intensity-pressure curves to those for the series $(2\,^1S\!-\!n\,^1P)$ which are illustrated in fig. 2. Further, as may be seen from fig. 11, Paper I, the observed intensity-voltage curves for the $(2\,^3P\!-\!n\,^3D)$ lines show a type of double maximum. The observed curves seem to be compounded of two, one with an early maximum like a triplet excitation curve, and one with a late maximum like a singlet excitation curve. On the theory put forward, the first type of curve represents the true excitation function into the ^3D state ; the second would represent a spurious excitation into a ^1P state. The fact that the predominance of the second kind of curve, as well as the spreading itself, increases with n may be taken as a strong confirmation of our point of view.

The question arises whether any evidence of similar collision processes in helium can be found. Since all the states $n\,^1P$, $n\,^1D$ and $n\,^3D$ are in close resonance for large values of n, the processes to be considered are $(n\,^1P \rightarrow n\,^3D)$, $(n\,^1P \rightarrow n\,^1D)$, $(n\,^1D \rightarrow n\,^3D)$, and the reverse processes. The first is that already dealt with and, as we have seen, shows itself most clearly in two ways, (a) in the spreading effect, and (b) in the double peak of the ^3D excitation curves. For a process $(A \rightarrow B)$ to show itself in either of these ways, a considerable excess of atoms in the A state over those in the B state is required at the relevant voltages. Thus the excess of $n\,^1P$ atoms over $n\,^3D$ atoms at 100 volts is about tenfold and both effects are clear. For the reverse processes $(n\,^3D \rightarrow n\,^1P)$ and $(n\,^1D \rightarrow n\,^1P)$ and also for the processes $(n\,^1D \rightleftarrows n\,^3D)$, this excess does not exist at any voltage, and so no traces of these processes could be seen. An excess exists in the case $(n\,^1P \rightarrow n\,^1D)$, but here the excitation

curves are too similar for any effect on them to be seen. On the other hand, a spreading of the lines $(2\,^1P—n\,^1D)$ is actually observed, although it is smaller than the spreading of the lines $(2\,^3P—n\,^3D)$. The process $(n\,^1P \to n\,^1D)$ may thus occur with a rather smaller frequency than that suggested for $(n\,^1P \to n\,^3D)$, but the evidence is not conclusive.

Finally, it is of interest to compare our process $(n\,^1P \to n\,^3D)$ with similar processes reported by other observers. In our case, only identical atoms are involved and this appears to be a novel characteristic. Connected with this is the extreme closeness of the resonance which, as far as we know, has not been approached in any other case.

Resonance collision processes are generally observed when normal atoms strike metastable atoms, and can mostly be interpreted as involving a simple electron exchange. The fact that in our case the metastable atom is replaced by an unstable excited atom makes the type of process unusual ; and, further the process cannot be regarded as due to exchange.

The process most similar to ours is, as far as we know, one found by Beutler and Eisenschimmel[*] in a mixture of mercury and krypton. The process is

$$\text{Hg}\,(1\,^1S_0) + \text{Kr}\,(2\,^3P_1) \to \text{Hg}\,(6\,^1D_2) + \text{Kr}\,(1\,^1S_0),$$
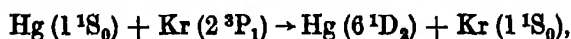
and occurs with a resonance defect of 19 m.v. This process also involves an unstable atom $\text{Kr}(2\,^3P_1)$; and a further similarity is to be observed, namely, that here also the total spin of the colliding atoms is not conserved. Wigner[†] originally proposed the rule that in collision processes the total spin (defined as a possible vectorial sum of the spins of the two atoms) must be conserved, if one neglects the coupling between orbital and spin momentum. Beutler and Eisenschimmel were able to show in the case of mercury-krypton mixtures that this rule is more strictly obeyed when the colliding krypton atom is metastable than when it is unstable, and they suggest that the breach of the rule is in some way connected with the dipole moment of the unstable atom. But the case of mercury and krypton is not a very good one from the point of view of the theory since intercombination lines are strong, and therefore the basis of Wigner's rule is not satisfied.

In our case, however, Wigner's rule is also violated ; and in helium the spin-orbital coupling is negligible and so the basis for the rule would seem to be firmly established. Indeed, in spite of the fact that the resonance is much better than is usual in collision processes, it is hard to visualise what forces

---

[*] 'Z. phys. Chem.,' vol. 10, p. 89 (1930).

[†] 'Nachr. Ges Wiss. Göttingen,' p. 375 (1927).

can be responsible for turning round the spin of the electron. The process proposed seems therefore to be fundamentally distinct from any hitherto observed collision process. Yet, as far as we can see, there exists no alternative supposition which is capable of explaining the facts.

It might be thought at first sight that a similar process could be involved in the spreading of the $(2\,{}^1S - n\,{}^1P)$ lines, which has been explained by absorption. That is to say, that the excitation might be handed out from atom to atom by collisions without the emission of radiation. It is easily seen, however, that such a process would have no such effect on the spreading, because the probability of the emission of a quantum is an exponential function of the time ; and after the collision the decay curve will continue unchanged. Thus, apart from effects due to scattering which tend to keep the light confined to the beam, the collision process cannot affect the spreading. We may thus conclude that spreading is primarily due entirely to light absorption.

3. *The Process of Excitation.*

In Paper I, a comparison has already been given between observed excitation of helium and the results of the calculation of Massey and Mohr,[*] and it was seen that though there is some general agreement between the observed and calculated effects, any detailed agreement is lacking. In the paper quoted they have used the method of Dirac, which admittedly is not strictly applicable to the case of low electron velocities, which is required for the present purpose. Recently, however, we are informed by these authors that they have tried the application of the methods of Holtsmark and Faxen without any better success.

While it is perhaps open to doubt whether any of the existing mathematical methods are capable of dealing with the problem, the following discussion[†] based on general idea, though crude and qualitative, may perhaps be not altogether superfluous. At any rate it has the advantages of giving an easily visualised picture of some aspects of the excitation process, and of providing an accurate account of some features of the excitation.

The view we shall put forward is based on an admittedly rather arbitrary division of the excitation process. We shall regard it as divided into two parts (1) an energy transfer from the exciting electron to the atom and (2) an angular

---

[*] 'Proc. Roy. Soc.,' A, vol. 132, p. 605 (1931).

[†] This is a development of a tentative suggestion put forward by the authors in 'Nature,' vol. 123, p. 826 (1929).

momentum transfer. We shall fix attention mainly on the latter. This may again be split up into two parts : (a) transfer of orbital angular momentum, and (b) transfer of spin angular momentum. We may justifiably regard these two parts as *separately* conserved, since the coupling of the two is very weak in helium. By making these assumptions a qualitative theory of some aspects of the polarisation of mercury lines, excited by directed electron impact, was found possible.*

Let us first attempt a comparison between excitation to an $n\,^3S$ and an $n\,^1S$ level. In each case a certain energy transfer is necessary If $n > 1$, the energy transfer is nearly the same in the two cases. No transfer of orbital angular momentum is required in either case. For excitation to the ^3S level, however, the antisymmetrical electron spin arrangement of the $1\,^1S$ ground state must be changed to a symmetrical arrangement ; this may be regarded as an exchange between an atomic electron and the exciting electron. The probability of such an exchange will depend on the closeness of approach of the electron to the atom, and on the duration of the collision. Thus, if the electron has an energy only slightly in excess of the excitation energy, the duration of the collision will be long, and the probability of exchange high. When the electron has a higher energy the collision time will be shorter and exchange will not be so probable. Thus we may expect that at low voltages, the probability of excitation into $n\,^1S$ and $n\,^3S$ states will be roughly equal ; but when the voltage is increased, we may expect the excitation probability into the ^3S state to fall off more rapidly. In this simple way we can explain the characteristic difference between the observed excitation curves for singlets and triplets.

We shall next take the case when no transfer of spin momentum is required and compare the excitations into $n\,^1S$, $n\,^1P$ and $n\,^1D$ levels. If V_1, V_2 are the incident and emergent electron velocities and p_1, p_2 the corresponding striking radii, then in excitation we must have

$$p_1V_1 - p_2V_2 = \frac{h}{2\pi}\,\Delta l,$$

where Δl is the change in the quantum number l in excitation, and so equal to 0 for ^1S excitation, to 1 for ^1P, and to 2 for ^1D.

An exact solution of this equation is impossible without a more detailed consideration of the process. But it may be seen that while for the ^1S excitation, no limitation on the closeness of approach in the excitation collision is

* Skinner and Appleyard, 'Proc. Roy. Soc.,' A, vol. 117, p. 224 (1927).

imposed, in the case of the ^{1}P and ^{1}D levels a definite limitation is imposed. We shall assume that excitation is most probable when the distance of approach (p) is least. This condition is best satisfied when

$$p\mathrm{V} \sim \frac{h}{2\pi} \Delta l,$$

where p and V represent values of p_1, p_2 and $\mathrm{V_1}$, $\mathrm{V_2}$. This relation will only apply for small velocities; when the velocity is high, and the value of p becomes small compared with the atomic diameter it will certainly break down. For example, with V corresponding to 50 volts and $\Delta l = 1$, we obtain $p = 2 \cdot 7 \cdot 10^{-9}$ cm., which is still of the order of the atomic size.

The application of the above relationship thus sets a limit on the closeness of approach for excitation to ^{1}P and ^{1}D levels, and thus we might expect a slower rise of the excitation probabilities with increasing voltage for these levels than for ^{1}S levels. This is actually observed. In the case of ^{1}P levels, however, there is another factor to be considered which lies outside the scope of the present picture. This consists of the fact that transitions to the ^{1}P levels are optically allowed. In fact it has been shown by Bethe[*] that for very high exciting velocities, the excitation should be only into ^{1}P states. A direct experimental confirmation of this point is difficult because with very high voltages the light excited by the primary processes is weak and that due to secondary slow electrons correspondingly strong. However, some confirmation may be seen in the fact that while for excitation to ^{1}S states, the maximum probability occurs at a relatively low voltage (37 volts) the maximum probability for ^{1}P and ^{1}D excitation occurs at voltages of 100 and 74 respectively.

We finally come to the case where both spin and orbital angular momentum transfer is required. We shall consider excitation into $n\,^3$S, $n\,^3$P and $n\,^3$D levels. Comparing each with the corresponding singlet state, we shall expect that owing to the necessity of exchange phenomena, the maximum probability of excitation will occur at a lower voltage for the triplets. This is in fact observed. Comparing the triplets amongst themselves, we shall expect, as with the singlets, a progressively slower rise of the excitation curves for $n\,^3$S, $n\,^3$P and $n\,^3$D states. Here, however, we have no added complication from any of the transitions being optically allowed, and it is actually found that the maximum of the excitation curves fall at progressively higher voltages (30, 32 and 34 volts). We may point out that this progression is opposite to that predicted by Massey and Mohr (*loc. cit.*).

[*] 'Ann. Physik,' vol. 5, p. 325 (1930).

In conclusion, we must again emphasise the limitations and dangers of this type of reasoning. The only value of our considerations is that they are able to predict the general shape of the curves obtained from an easily visualised picture of the process.

Summary.

(1) When a defined beam of electrons is passed through helium at a low pressure, it is found that the light emitted in the lines $(2\,^1S-n\,^1P)$ and $(2\,^3P-n\,^3D)$ is considerably spread outside the electron beam. An interpretation of this effect is given. The spreading of the $(2\,^1S-n\,^1P)$ lines is ascribed to absorption of the corresponding resonance lines $(1\,^1S-n\,^1P)$ by the gas, while the spreading of the $(2\,^3P-n\,^3D)$ lines is ascribed to a collision process

$$\text{He}\,(n\,^1P) + \text{He}\,(1\,^1S) = \text{He}\,(1\,^1S) + \text{He}\,(n\,^3D)$$
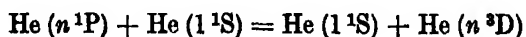
which involves only a small energy transfer. Corresponding anomalies in the intensity-pressure curves and excitation curves for these lines are also interpreted in this way.

(2) A rough qualitative picture of the excitation process in helium is given.

X-Ray Absorption Coefficients in the Range 0·3 to 2·0 Å.

By L. H. MARTIN, Ph.D., Senior Lecturer, and K. C. LANG, M.Sc., Dixon Scholar, University of Melbourne.

An account is given of two methods which have been devised in an attempt to eliminate some of the experimental difficulties associated with the measurement of X-ray absorption coefficients. Although the accuracy claimed for these measurements does not represent an improvement on that claimed by previous workers, it is hoped that the methods possess some features of interest, and it is believed that the data obtained, even where they refer to materials previously investigated, are of value in a field of measurement remarkable for the lack of agreement between different workers.

In the first method ionisation chambers are used for the measurement of intensity, the wave-lengths investigated lying within the range 0·3 Å. to 0·6 Å. In the second method the photographic effect is used for the comparison of X-ray intensities, and the wave-length range is extended to 2·0 Å.

When the X-ray source is a tube excited by a transformer connected directly to a commercial A.C. supply, it is difficult to maintain steady conditions while the ratio of the incident and emergent intensities is determined. This is especially so when a demountable type of tube is employed. The effect of variations in the intensity of the source has been overcome to some extent by the use of balance methods,* but these usually suffer from a lack of sensitivity, which could only be improved by increasing the widths of the spectrometer slits, and so sacrificing homogeneity in the X-ray beam diffracted by the crystal. If two similar beams are employed the procedure of balancing can be very tedious, since a slight wandering of the focal spot on the target of the X-ray tube produces a continual shift of the electrometer zero. Further, it is essential that the wave-length of both beams shall always be the same, a requirement which is not easily fulfilled in the short wave-length range where the angles of incidence are small.

PART I.—IONISATION BALANCE METHOD.

The first part of this paper describes measurements made by an ionisation balance method in which one beam of X-rays only is utilised.

* Siegbahn and Wingårdh, ‘Phys. Z.,’ vol. 21, p. 83 (1920); Wingårdh, ‘Z. Physik,’ vol. 8, p. 363 (1922); Stoner and Martin, ‘Proc. Roy. Soc.,’ A, vol. 107, p. 312 (1925).

A beam of X-rays of small wave-length range selected by diffraction in a calcite crystal, passed through two ionisation chambers placed one behind the other. The chambers were rigidly mounted, beams of different wave-length being obtained by moving the tube. Between the chambers a rotating sector of variable aperture was mounted together with a frame for holding the metal foils.

Balance was first obtained with the absorbing foil in position, the gases in the chambers being mixed with air in the right porportion to give approximately the maximum transmission of the sector (0·497). The foil was then withdrawn and the sector again adjusted to produce a balance. If T_1 and T_2 are the transmissions of the sector with the absorber in and out of position then

$$(\mu/\rho) \cdot m = 2\cdot303 \log T_1/T_2,$$

where m is the mass per unit area of the metal foil.

Experimental Details

The arrangement of the apparatus is shown in fig 1.
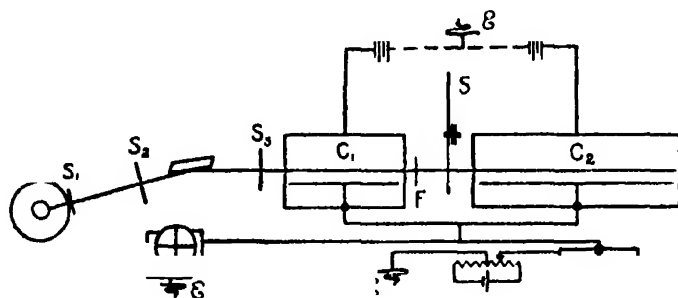
Fig. 1.

The ionisation chambers were constructed of glass tubing 6 cm. in diameter with windows of cellophane, all joints being made air-tight with rubber gaskets so that the chambers could be exhausted. The first, C_1, was 15 cm. long and contained either sulphur dioxide or ethyl bromide, while the second, C_2, was 25 cm. long and contained methyl iodide. Ionisation currents of opposite sign were obtained from the chambers, and were led to a common pair of quadrants of a Compton electrometer working at a sensitivity 10,000 mm. per volt. Small insulation leaks were balanced out with the aid of an artificial leak produced by a uranium oxide resistance. The X-ray source was a broad focus Mueller tube which, after being adapted for continuous water cooling, could dissipate continuously nearly 1 kilowatt.

With a tube slit 0·10 mm. wide, 1° of the sector was equivalent to an ionisation current producing a deflection of two divisions per minute. This seriously limited the accuracy, and an enquiry as to the effect of increasing the slit width was made both experimentally and by calculation.

The effect of increasing the slit width S_1 is to increase the range of wavelengths in the beam incident on the absorber. If the width of the tube slit S_1 is $2t$, whilst the limiting slit of the ionisation chambers is $2a$ ($a = 0·10$ cm.) distant D (20 cm.) from the tube slit, it was found that the ratio of the energy incident on the absorber to the energy entering C_2 should be independent of t for slit widths less than 0·5 mm. This limit was determined by the angular width of the focal spot.

The extent to which this conclusion is justified experimentally is shown in Table I, which gives the mass absorption coefficients for $\lambda_0 = 0·448$ Å.

Table I.—Absorption Coefficients as a Function of t.

Slit (t).	Fe.	Ni.	Cu.	Mo.	Pd.	Ag.
mm.						
0·50	10 1	13 2	14 1	34 7	42·5	47 9
0 25	10 0	13 0	13 8	35 1	43·7	49·6
0 10	10 1	13 4	13 8	35 4	44·3	51·2

It has been assumed in the above calculation that the ratio of the ionisation to the intensity of radiation is independent of the wave-length; this is legitimate if the tube is operated at such a voltage that the maximum of the general radiation coincides with the nominal wave-length λ_0. Ulrey,[*] and Wagner and Kulenkampff[†] have shown that the wave-length λ_m of the maximum intensity is given approximately by $\lambda_m = \frac{3}{2}\lambda_0$, where λ_0 is the short wave-length limit of the continuous spectrum. The tube was operated therefore at a voltage V KV given by

$$V = \tfrac{1}{2}\frac{12·3}{\lambda_0}.$$

This value of the voltage is compatible with the requirement that there shall be no second order radiation diffracted into the chambers. Care was also taken to adjust the position of the tube so that the beam entering the chambers was symmetrical about the angular position.

[*] 'Phys. Rev.,' vol. 11, p. 401 (1918).
[†] 'Phys. Z.,' vol. 23, p. 503 (1922).

The values of the coefficients shown in Table I are for the wave-length nearest the K absorption edges of palladium ($\lambda_K = 0 \cdot 506$ A.) and silver ($\lambda_K = 0 \cdot 485$ A.). If the range of wave-lengths reflected is determined by the geometry of the apparatus, the longest wave-length reflected is $0 \cdot 486$ A., for the widest slit, so that in every case with the exception of silver, wave-lengths longer than the critical wave-length should be excluded. The low values for the wider slits in the case of palladium and silver indicate that some of these wave-lengths are entering the chamber C_2 after traversing the absorber. Assuming a K absorption jump* of 7 for silver, the amount of radiation of wave-length longer than λ_K necessary to account for the difference of the values for slit widths $0 \cdot 25$ mm. and $0 \cdot 10$ mm. is some 2 per cent. of the total beam. It seems probable that this amount could be scattered from the inner surfaces of the slit jaws. The amount scattered which ultimately falls on the crystal surface would decrease as the slit was narrowed.

Since the value of μ/ρ measured is independent of slit width provided the precautions mentioned above are observed, preliminary settings were always made with the widest slits, and the balance points checked with the narrowest slit $0 \cdot 10$ mm.

A battery-driven generator set was available for short intervals on a couple of occasions, and it was possible to determine the coefficients by the direct method for the $0 \cdot 1$ mm. slit, and check the results obtained by the balance method.

The final values of μ/ρ obtained for the different absorbing materials used are shown in Table II.

Table II.—Values of μ/ρ for slit width $0 \cdot 1$ mm.

Wave-length.	Fe.	Ni.	Cu.	Mo.	Pd.	Ag.
Å.						
0·320	3·85	4·90	5·20	14 0	17·7	20·4
0·387	6·90	8 65	9·25	23 0	29·6	34·2
0 448	10 1	13 2	13·9	35·4	44·3	51·2
0·506	15 0	18·7	19·6	49 4	—	—
0·556	19·8	24·3	25·8	64·8	12·5	14 2
0·595	23·5	29·3	31·1	—	14·5	17·0

While the method above possesses advantages, it still suffers from a weakness inherent in all balance methods. The balance is determined by measuring the ionisation currents when the balance is disturbed first in one direction and

* "Handbuch der Experimentalphysik," vol. 24, part 1, p. 257.

then in the other so that the necessity for maintaining the source constant is not wholly eliminated. In the second series of measurements the apparatus was essentially the same as that used by Stoner and Martin (*loc. cit.*), with the exception that the ionisation chambers are replaced by a photographic film. This integrates the energy falling on it, and so can be used in such a manner that the effects of source variations are eliminated.

PART 2.—PHOTOGRAPHIC BALANCE METHOD.

Two beams of X-rays are limited by slits S_1 and S_2, giving two short spectrum lines L_1 and L_2 of the same wave-length one above the other, as shown in fig. 2. A foil, mass per unit area m_s, is interposed in the path of one beam, and an
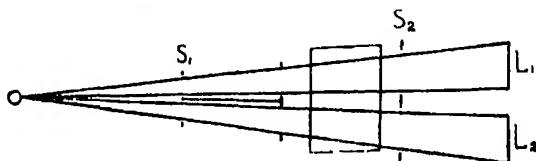
FIG. 2.

aluminium foil, mass per unit area m_a, in the path of the other. If I^0 is the incident intensity in each case, and I_s and I_a are the emergent intensities respectively, then

$$(\mu/\rho)_s = \frac{m_a}{m_s}(\mu/\rho)_a - \frac{1}{m_s}\log_e \frac{I_s}{I_a}.$$

Actually no attempt was made to ensure that the incident intensity was accurately the same for each beam. A picture of the emission line was taken with the absorbing screens withdrawn and the intensities of L_1 and L_2 measured. If I_a^0 and I_a^0 are the intensities, the final expression for $(\mu/\rho)_s$ is

$$(\mu/\rho)_s = \frac{m_a}{m_s}(\mu/\rho)_a - \frac{1}{m_s}\log_e \frac{I_s I_a^0}{I_a^0 I_a}.$$

The value for $(\mu/\rho)_a$ was taken from measurements made by a number of workers.* The best representation of the values available in the wave-length range 0·4 A. to 1·9 A. was found to be

$$\mu/\rho = 14\cdot3\ \lambda^{2\cdot88}.$$

This is almost identical with the expression $\mu/\rho = 14\cdot0\ \lambda^{2\cdot92}$ given by Allen†

---

* " Handbuch der Experimentalphysik," *loc. cit.*, p. 231.
† ' Phys. Rev.,' vol. 28, p. 907 (1926).

for a range of wave-lengths extending from 0·08 A. to 3·93 A , and the expression $\mu/\rho = 14\cdot3\,\lambda^{2\cdot 91}$ found recently by Backhurst* for the wave-length range 0·6 A. to 2·0 A.

Experimental Details.

A demountable type of X-ray tube† was used, the target of which could be readily changed to give suitable characteristic radiations. These were analysed with a calcite crystal and registered on the photographic film as the corresponding line spectrum. The wave-lengths of the principal lines have been measured accurately in special precision spectrographic work,‡ so there can be no doubt of the wave-lengths used.

Soon after these measurements were started, the authors were made aware of an extensive series of measurements carried out by Jonsson§ in which a photographic method had been used. He arranged a rotating disc to cut out different fractions of the reflected beam, and matched the density of the line transmitted through the absorber. This method has the advantage of measuring absolute coefficients, but the procedure is rendered somewhat lengthy by the number of photometer records which have to be made. The use of a rotating disc also limits the measurements to one line per exposure. The method described here has the advantage that several lines can be recorded on one film simultaneously.

Some X-ray intensity measurements‖ carried out in this laboratory in connection with chemical analysis, indicated that greater accuracy than that obtained by Jonsson—probably in many cases less than 3 per cent.—should be possible, and it was decided to continue this work and investigate the possible accuracy using a photographic method.

Photographic Measurement of Intensity.

The film used was Agfa double coated X-ray film developed in a metol-hydroquinone developer recommended by the makers, care being taken to carry out the development always at 18° C., and to agitate the film during development. Slight variations in the film have little effect as a result of the procedure adopted. The intensity of a beam of X-rays, I, is related in a

---

* ' Phil. Mag.,' vol. 7, p. 353 (1929).

† Martin, ' Proc. Camb. Phil. Soc.,' vol. 23, p. 783 (1927).

‡ Siegbahn, " X-ray Spectroscopy " (1925).

§ " Dissertation," Uppsala (1928).

‖ Eddy and Laby, ' Proc. Roy. Soc.,' A, vol. 127, p. 20 (1930).

definite manner with the density D produced by it on a photographic film. Density is defined as $\log_{10} I_0/I_t$, where I_0 is the intensity of a beam of light after it has passed through the film exposed to general radiation on either side of the line and I_t is the intensity of this beam after it has passed through the line. A Moll microphotometer was used for the measurement of the densities.

The following procedure was adopted in determining the relation between I and D. The double slits were replaced by a triple slit system. Aluminium sheets of known thickness were interposed in the path of two of the three beams, thus cutting down the intensity of these by known amounts. An exposure was made, then the film holder was moved slightly, and a second similar exposure made, with new thicknesses of aluminium. Usually three such exposures were made on each piece of film, the tube emission being held as constant as possible during the exposures. Variations of emission which did occur were slight, and could be allowed for from the measured density of the unabsorbed beam for each exposure.

The film was calibrated for three wave-lengths namely, 1·537 Å. (Cu K_{a_1}), 0·558 Å. (Ag K_{a_1}), and at the bromine K absorption edge 0·918 Å. For this last the L_{γ_1} (0·924 Å.) and L_{γ_2} (0·901 Å.) lines of gold were used, the bromine edge lying between the two. The points obtained with each radiation, when D is plotted against log I, fall on a smooth curve over the range of densities measured, that is, from 0·1 to 1·2, and, within the limits of experimental error, the curves for the three wave-lengths are identical. In fig. 3 it will be seen that the density is proportional to the intensity for densities lower than 0·8.

The linear relation between D and I for densities less than 0·8 has been observed previously by Friedrich and Koch* and by Glocker and Traub,† both of whom used approximately homogeneous radiation. More recently Busse‡ has obtained the same result using crystal analysed radiation. The independence of the Hurter and Driffield curves of wave-length has been established by Glocker and Traub over a range of wave-lengths 0·4 Å. to 1·1 Å. They used the K series fluorescent radiations of different elements. Bouwers§ has extended the range, using filtered radiations of mean wave-lengths 0·18 Å., 0·71 Å. and 1·54 Å. Similar results have also recently

* 'Ann. Physik,' vol. 45, p. 399 (1914).

† 'Phys. Z.,' vol. 22, p. 345 (1921).

‡ 'Z. Physik,' vol. 34, p. 11 (1925).

§ 'Z. Physik,' vol. 14, p. 374 (1923).

been obtained by Rogers* for γ rays which were filtered by different thicknesses of lead.

Since the H and D curves for the Agfa film used at the two extremes of the wave-length range were identical with that at the bromine K edge, where any

A   D - 120 l
B   D - 120 l
C   D - 119 l

A Bromine K Edge
B Ag Kα₁
C Cu Kα₁

A   B   C
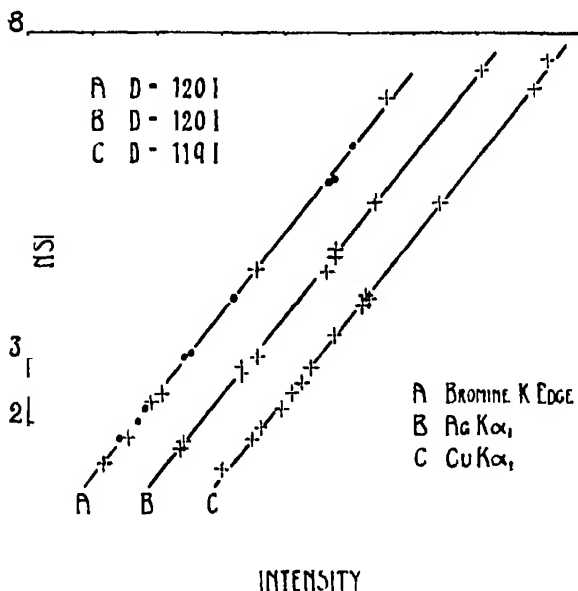
INTENSITY
Fɪɢ. 3.

change of behaviour might reasonably be expected to be most pronounced, it was deemed unnecessary to calibrate the film for each separate wave-length used in the absorption measurements.

During the experiments a curious photographic inversion effect was observed. The L series lines of gold were registered on a film, but, owing to a breakdown of the window of the tube, the bare film was accidentally light fogged by the filament of the tube. On development the lines appeared as white lines on the dark ground of the light fog. It was found, however, that with the same relative densities the effect is not produced when the film is light fogged before the X-ray lines are registered on it.

Fig. 4 shows the photometer curves for the case of the iron K$_{a_{1}}$ lines. One half of the film was protected, while the other was exposed to a very weak source of light after the X-ray lines were registered. These curves emphasise the importance of a safe dark room as the slightest light fog would diminish

the densities of different lines by amounts depending on the relative densities of the lines and the fog.

Absorption Experiments.

The following procedure was adopted for the measurement of absorption coefficients. The crystal was rocked by means of a heart-shaped cam, and the spectrum of the target registered first without the absorbing foils in position. The film holder was then displaced slightly and the lines registered after passing through the foils. In order to eliminate as far as possible errors introduced
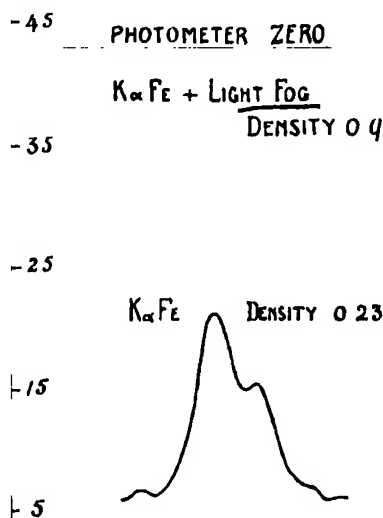
Fig. 4.

by lack of uniformity in the metal foils, these were mounted just behind the crystal where the reflected beam covers the greatest area. The exposures were chosen so that as far as possible the densities were less than $0 \cdot 8$ when the densities could be taken directly as measures of the intensities. For densities greater than this the intensities were calculated from the H and D curves.

A typical set of results is given in Table III for nickel.

The ratio m_a/m_s was adjusted to keep the difference term as small as possible, usually a few per cent. of $(\mu/\rho)_a$.

The collected results for this experiment are given in Table IV. Log μ/ρ is shown plotted against log λ in figs. 5 and 6, for two typical cases, silver and copper respectively.

Table III.

$$m_s = 0\cdot0859 \text{ gm. cm.}^{-2}; \quad m_a = 0\cdot830 \text{ gm. cm.}^{-2}; \quad \lambda = 0\cdot558 \text{ Å.}$$

Film.	Density.		Log intensity		$\frac{m_a}{m_s} (\mu/\rho)_a.$	$\frac{2\cdot303}{m_s}\log\cdot\frac{I_s{}^0I_a}{I_sI_a{}^0}$	$(\mu/\rho)_s.$
	$I_s, I_a.$	$I_s{}^0, I_a{}^0.$					
1	0·536	0·810	0 646	0 842	25·3	−1·3	24 0
	0·583	0·950	0 684	0 930			
	0·564	0 859	0 066	0·874	—	−0 9	24·4
	0 591	0·954	0 688	0 931			
2	—	—			25·3	−1 2	24·1
						−0 5	24 8
3	—	—			25 3	0	25 3
						−0·2	25·1
						Mean .	24 6 ± 0 4

Table IV.—Values of μ/ρ from Photographic Measurements.

Line.	A.U.	Fe.	Ni.	Cu.	Zn.	Ag.	Sn.
Fe $K\alpha_1$	1·93	71	93	98	106	—	—
Ni $K\alpha_1$	1·66	427	62	65	77	—	—
Cu $K\alpha_1$	1·54	327	47·3	49·4	58·3	—	—
W $L\alpha_2$	1 49	—	—	46·4	54·5	—	—
W $L\alpha_1$	1·47	286	332	46·4	54·1	—	247
Zn $K\alpha_1$	1 43	270	322	42·1	50 2	193	233
Au $L\alpha_2$	1·29	—	—	261	36·9*	144	174
W $L\beta_1$	1 28	—	—	—	264*	—	—
Au $L\alpha_1$	1 27	194	230	254	—	136	166
W $L\beta_2$	1·24	184	—	231	265	126	153
W $L\gamma_1$	1 10	—	—	—	186	—	—
Au $L\beta_1$	1 08	129	146	166	177	89	108
Au $L\beta_2$	1 07	120	139	157	166	83	105
Au $L\gamma_1$	0·92	80 3	97	110	120	57·0	66·5
Mo $K\alpha_1$	0·71	37·6	49	51·2	58·2	28·4	32 6
Mo $K\beta_1$	0·63	28 5	34·2	38 1	—	20·6	23·5
Ag $K\alpha_1$	0·56	20 3	24·6	26 8	29·6	14·4	17·5
Ag $K\beta_1$	0·50	14·6	17 8	19 0	21·4	10 0	11·9
Sn $K\alpha_1$	0 49	13·9	16·1	18·5	20·5	—	10 2
Sn $K\beta_1$	0·43	9·7	12·2	12 9	14·5	45 6	8·7

* Siegbahn in his " Spectroscopy of X-rays," p 136, quotes for the wave-length of the K absorption edge of zinc, 1 296 Å. (measured by Duane, Blake, Hu, Stenstrom, Fricke, Shimidzu), and 1·280 Å. (measured by Walter). The value obtained from the microphotometer records of these lines agrees exactly with that of Walter.
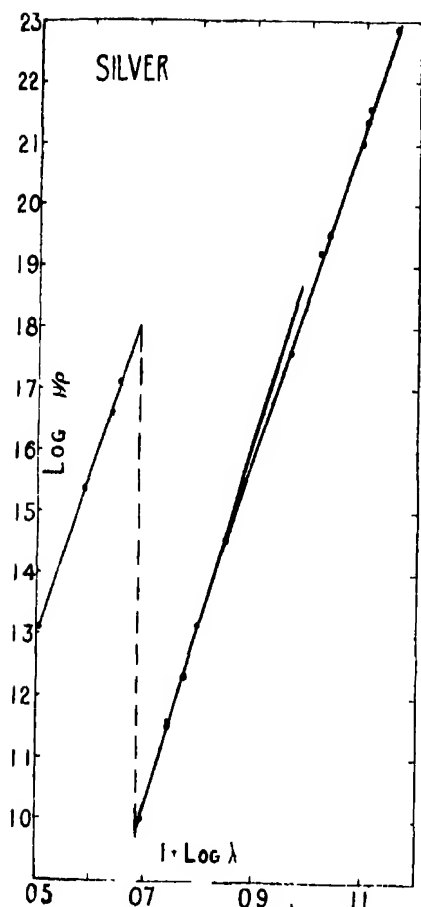
Fig. 5.
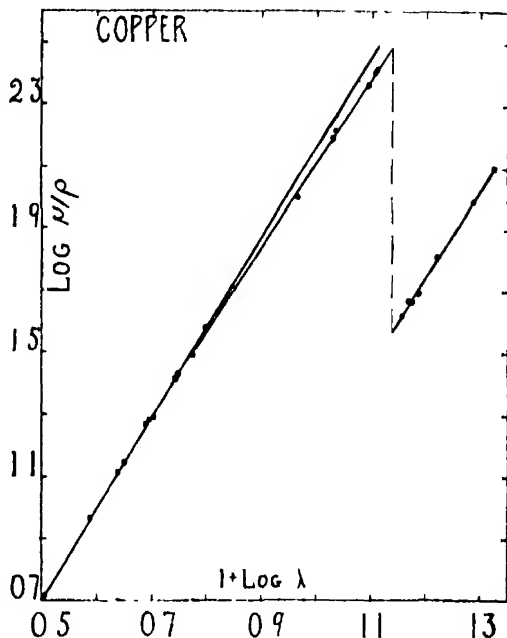
Fig. 6.

Comparison of Results.

The coefficients for metals common to both experiments agree in general within the limits of experimental error in the overlapping range of wavelengths. The coefficients can be represented by relations of the form $\mu/\rho = a\lambda^n + b$, where a, n and b have the values as shown in Table V.

The accuracy of these experiments is not sufficiently great to justify an evaluation of the residual b in most cases. This quantity, usually identified with the scattering coefficient, is only of importance, in so far as it affects the exponent of λ, for the shortest wave-lengths.

In the case of the four lighter elements, Fe, Ni, Cu and Zn, the results on the short wave-length side of the K edge resolve themselves into two parts.

Table V.—Values of a, n and b.

Element.	Wave-length range.	n.	a	b.
Fe	0 3 Å. to 0 6 Å	3 0	111	0 2
	0 6 Å to λ Fe$_k$	2 74	100	—
Ni	0 3 Å. to 0 6 Å.	2 97	138	0 2
	0 6 Å. to λ Ni$_K$	2 68	120	—
	λ Ni$_K$ to 1 9 Å	2 97	13 4	—
Cu	0 3 Å to 0 6 Å.	2 95	145	0 2
	0 6 Å to λ Cu$_k$	2 74	130	—
	λ Cu$_k$ to 1 9 Å	2 81	15 2	—
Zn	0·4 Å. to 0 7 Å	2 91	162	0 2
	0 7 Å to λ Zn$_K$	2 61	145	—
	λ Zn$_k$ to 1 9 Å	2 87	17 6	—
Mo	0 3 Å. to 0 6 Å	2 75	322	—
Pd	0 3 Å to 0 5 Å	2 75	406	—
Ag	0 3 Å to λ Ag$_K$	2 75	470	—
	λ Ag$_k$ to 0 7 Å	2 94	78	—
	0 7 Å to 1 4 Å.	2 74	72	—
Sn	λ Sn$_K$ to 0 9 Å.	2 92	88 5	0 5
	0 9 Å to 1 5 Å	2 72	86	—

Near the K edges the exponents of λ have values between 2·6 and 2·7, but become greater than 2·9 for the shortest wave-lengths When log μ/ρ is plotted against log λ, see fig. 5, the change in slope is quite distinct, but the number of points on the curve is not great enough to decide whether the change is an abrupt one. Unfortunately, there are few emission lines which can be conveniently excited in this critical range of wave-lengths This change of exponent near the K absorption edges in the case of these elements was first observed by Allen,* and the values of a, n and b given in Table V are in fair agreement with those given by him Particularly good agreement is found in the case of copper with results given by Backhurst,† who finds $\mu/\rho = 131 \, \lambda^{2\,72}$ for the range 0·6 Å. to λ_K, indeed, for this element the values of μ/ρ found by Allen, Backhurst, Jonsson, and ourselves agree to within 3 per cent in the ranges of overlapping wave-lengths.

In the case of Mo, Pd and Ag, the wave-length range is not great, but the exponent of λ appears to be very close to 2·75. For Mo and Ag, Richtmeyer and Bishop‡ find $\mu/\rho = 375 \, \lambda^3 + 1$ and $\mu/\rho = 545 \, \lambda^3 + 1$ respectively, while

* ' Phys. Rev.,' vol. 28, p. 907 (1926).

† ' Phil. Mag,' vol. 7, p. 353 (1929).

‡ ' Phys. Rev.,' vol. 27, p. 294 (1926).

for Ag, Allen* gives $\tau/\rho = (540 \rightarrow 580) \lambda^{2\cdot 92}$. On the other hand, Bragg and Peirce† in some early measurements found that the total absorption coefficient was proportional to $\lambda^{5/2}$ Stoner and Martin for silver and palladium also give 2·5 for the exponent, although as they were forced to use fairly wide slits (up to 0·3 mm.) it is probable that this value is slightly low, on account of the effect, associated with the use of wide slits near an absorption edge, discussed in the first part of this paper It will be noticed that the value given to the residual b by Richtmeyer is probably much greater than the scattering coefficient. Since the total absorption coefficient itself is not very great, this would have the effect of giving a high value of the exponent. While it may be contended that faulty spectrometer arrangements have been responsible for low values of n near the K absorption edges of heavy elements, this objection cannot hold in the case of iron, nickel, copper and zinc, since the measurements were made with spectrum lines, and there can be no question of the homogeneity or the wave-length of these.

On the long wave-length side of the K edges the exponent is at first approximately 2·9, but for wave-lengths on that side, far removed from the edge, n falls to a lower value, of the order 2·7 This change is well shown in fig. 6 for silver, and is in good accord with the results of Allen for silver and tin. Backhurst, on the other hand, finds that a straight line is obtained when log μ/ρ is plotted against log λ for silver The slope of this line is 2·79. In view of this lack of agreement it is interesting to notice the effect which an error in μ/ρ produces in the exponent of λ Suppose an error Δ produces a change δ in n, i.e.,

$$(\mu/\rho) + \Delta = a\lambda^{n+\delta} + b.$$

Then

$$\delta = \log \{1 + \Delta/(\mu/\rho)\}/\log \lambda$$

Since log λ occurs in the denominator it follows that a systematic error in μ/ρ produces values of δ of opposite sign on each side of $\lambda = 1$. The numerical value becomes large at this point, decreasing rapidly on either side. Assuming a 2 per cent error in μ/ρ, δ has the following values :—

λ (Å.)	0·5	0·9	1·1	1·5
δ	—0·03	—0·2	+0·2	+0·03

It will be seen from this table that there is a maximum uncertainty in the

slope at $1\cdot0$ Å. This region is a critical one, since it effectively determines the change in the slope of the log μ/ρ — log λ curves.

The photographic measurements suffer from the disadvantage that they yield relative values only. The percentage error in μ/ρ is proportional to the sum of the errors in m_a, m_x, and $(\mu/\rho)_{al}$. We estimate that the values of $(\mu/\rho)_{al}$ used by us have a possible uncertainty of 1 per cent. The error in m_a is always negligible compared with that in m_x. We believe that our ultimate accuracy was almost wholly determined by that of m_x. It was impossible to make measurements for Ag and Sn for wave-lengths greater than $1\cdot473$ Å., since it was found that lack of uniformity in the metal foils available produced large variations in density along the spectrum lines.

A comparison method possesses one valuable feature. It shows directly whether the absorber is following the same law of absorption as the standard substance. In the present case

$$\frac{(\mu/\rho)_x}{(\mu/\rho)_{al}} = \frac{m_a}{m_x} + \frac{2\cdot303}{m_x\,(\mu/\rho)_{al}}\log\frac{I_a}{I_x}.$$

If the exponent of λ is the same for both elements, and the scattering coefficient may be neglected, $\log\dfrac{I_a}{I_x}\Big/(\mu/\rho)_{al}$ should be a constant. For example, in the case of Zn we had

A U			$\dfrac{2\ 303}{m_x\,(\mu/\rho)_{al}}\cdot\log\dfrac{I_a}{I_x}$
$1\cdot655$		1 257	0 007
1 485		1 257	0 014
1 473		1 257	0 010
1 432		1 257	0 011

Some measurements were made to give absolute coefficients using the photographic film, but it was found difficult to reproduce results to better than 5 per cent. In the balance method the effects of variations in photographic film and development are reduced to a minimum, coefficients being reproducible to at least 2 per cent. The main advantage of the photographic method lies in the fact that it deals with a homogeneous beam This is particularly important near absorption discontinuities. The photographic effect is a cumulative one, making possible the use of faint lines and comparatively thick absorbing screens. With care the films form a permanent record. It must be

admitted, however, that owing to the time taken in the photometry of the film, the method is slow.

Discussion of Results.

A number of expressions, theoretical and practical, have been put forward in an attempt to represent the absorption coefficients as a function of the atomic number Z of the absorber, and wave-length λ of the absorbed radiation

The simplest of these is that derived empirically by Hull and Rice,[*] Richtmeyer and Warburton,[†] and Richtmeyer,[‡] who find for the short wave-lengths (0·1 Å to 0·4 Å) :

$$\mu/\rho = a\lambda^3 + b \tag{1}$$

Walter[§] has extended the use of this formula to represent the available data in a range of wave-lengths 0·1 Å to 1·0 Å. He states that the following values of a represent the available data with an accuracy of the order of 5 to 7 per cent. For

$$\left.\begin{array}{ll} \lambda < \lambda_K & a = 1·6 \times 10^{-2} Z^{3·94}/A \\ \lambda > \lambda_K & a = 5·29 \times 10^{-4} Z^{4·30}/A \end{array}\right\}$$

Here A is the atomic weight, and λ is measured in Ångstrom units. The well-known theoretical expressions of L de Broglie[||] and Kramers[¶] are of this type.

There can be no doubt, however, that the departure from the λ^3 law, at least in the case of Fe, Ni, Cu and Zn, is a real one. For example, in the case of Fe, extrapolation from a wave-length 0·3 Å to λ_K with a λ^3 law gives a value of μ/ρ, which is nearly 20 per cent. greater than the value observed. The present experiments show that in the case of the heavy elements also, the exponent is less than 3 near their K absorption edges. This has led J. A. Gray[**] to modify equation (1) in the following manner

For 0·1 Å. $< \lambda < \lambda_K$ he gives

$$\left.\begin{array}{l} \dfrac{\tau}{\rho} \cdot \dfrac{A}{L} = 1·92 \times 10^{-26} (1 + 0·008 \, Z) \left(1 - \dfrac{\lambda}{4 \, \lambda_K} - \dfrac{\lambda}{50 \, \lambda_K^2}\right) Z^4 \lambda^3 \\[2mm] \text{for } \lambda_K < \lambda < \lambda_{L} \\[2mm] \dfrac{\tau}{\rho} \cdot \dfrac{A}{L} = 0·255 \times 10^{-26} Z^4 \lambda^2 \end{array}\right\} \tag{3}$$

* 'Phys. Rev.,' vol. 8, p. 326 (1916).
† 'Phys. Rev.,' vol. 22, p. 539 (1923).
‡ 'Phys. Rev.,' vol. 27, p. 1 (1926).
§ 'Fortschr. Rontgenstr,' vol 35 (1927).
|| 'J. Physique,' vol 6, p. 33 (1922).
¶ 'Phil. Mag,' vol. 44, p. 836 (1923).
** 'Proc. Roy. Soc. Canada,' vol. 21, p. 179 (1927).

But both of these general empirical relations fail to give a good representation of the ratio, the K + L + etc., to the L + M + etc. absorption, over a range of atomic numbers. It has already been pointed out by Richtmeyer, and by Stoner and Martin, that the expressions of both de Broglie and Kramers fail to account for the observed values of the K jump. According to Kramers the K jump should be approximately 5·5 for all elements, while the values given by de Broglie are much too great, although they vary with atomic number in the right direction

Richtmeyer* and Jonsson (*loc. cit.*) have both pointed out the striking fact, that the K jump is approximately equal to E_K/E_{L_1}, the ratio of the energy levels of the K and L_1 electrons respectively. Table VI shows that the present results are in excellent accord with this principle

<p align="center">Table VI.—Values of the K Jump</p>

Element.	$\dfrac{E_K}{E_{L_1}}$.	Authors.	Allen.	Jonsson	Richt-meyer	Stoner and Martin.	Back-hurst.	Walter.	Gray.
Fe	8·46	8 8	9 2	—	—	—	—	9 4	8 0
Ni	8 32	8 0	8 2	8 3	—	—	—	9 1	7 7
Cu	8 23	8·3	8 5	8 2	—	—	8 15	9 0	7 6
Zn	8 16	7 7	7 5	—	—	—	—	8 9	7·4
Pd	6 77	6 6	—	—	—	6 8	—	7 6	5 7
Ag	6 72	6 7	7 3	—	7 3, 7·8	6 7	—	7 6	5·5

Jonsson, making use of this principle, has found that absorption coefficients can be satisfactorily correlated in a manner quite different from any hitherto suggested. He calculates an electron absorption coefficient $(\mu_e)_K$ by dividing the atomic absorption coefficient $\dfrac{\tau}{\rho} \cdot \dfrac{A}{L}$ for the K + L + M, etc., electrons by Z. If $\lambda > \lambda_K$ so that the L + M + etc. electrons only are concerned, (μ_e) is multiplied by the K jump (given by E_K/E_{L_1}), or if the M + N, etc., electrons only are concerned, by $\dfrac{E_K}{E_{L_1}} \cdot \dfrac{E_{L_1}}{E_{M_1}}$.

Jonsson finds that log $(\mu_e)_K$ plotted against log $(Z \cdot \lambda)$ gives a smooth curve the equation of which is

$$(\mu_e)_K = C \cdot (Z \cdot \lambda)^{f(Z \cdot \lambda)}, \tag{4}$$

where, according to Jonsson, $f(Z \cdot \lambda)$ changes continuously from 3 to 2·3 as $(Z \cdot \lambda)$ changes from 8 to 800. With this curve Jonsson is able to represent the data of different observers with an accuracy of the order of ± 5 per cent.

In adjusting the relative importance of the different electron shells in the absorption process, constant values of the different jumps have been used, but the relations in Table VI show clearly that the K jumps, at least, vary with the wave-length. In some new experiments we have recently obtained evidence of a similar variation in the case of the L jumps of tungsten. The relative absorptions due to the L shells were deduced from measurements of the intensities of chosen lines in the L series, when these were excited by X-rays of different wave-length. For a change of wave-length in the exciting radiation $1 \cdot 0$ A. to $0 \cdot 45$ A. the absorption of the L_I shell relative to the L_{II} shell increases approximately 17 per cent, while the relative absorptions of the L_{II} and L_{III} shells remain unchanged. At present, however, it is impossible to reduce the absorptions of the different shells to a common basis, but in view of Jonsson's result it seems possible that if this could be carried out a simple relation might be found to exist between the absorption produced by electrons in a condition common to all, and the two parameters, Z and λ.

Wentzel* has attacked the problem of absorption using the methods of wave-mechanics. He considers the case of a hydrogen-like atom and obtains for the K absorption coefficient

$$\left(\frac{\tau}{\rho}\right) \cdot A - 1 \cdot 82 \times 10^{12} \left(\frac{\lambda}{\lambda_K}\right)^{5/2} [3\,(\overline{A})\,\lambda^{1/2} + (\overline{B})\,\lambda_K^{1/2}],$$

where $\overline{A}$ and $\overline{B}$ cannot be theoretically evaluated.

Replacing λ_K by a constant multiple of Z^{-2}

$$\left(\frac{\tau}{\rho}\right) \cdot A = aZ^5\lambda^{7/2} + bZ^4\lambda^3 + cZ^3\lambda^{5/2}.$$

As might be expected, this expression can be made to fit the experimental results fairly well. At present the accuracy of the large body of experimental results is not sufficient uniquely to determine the constants a, b and c, so that it is impossible to decide whether they are themselves independent of Z and λ. The following values: $a = 5 \cdot 0 \times 10^{-5}$, $b = 3 \cdot 0 \times 10^{-3}$, and $c = 1 \cdot 70 \times 10^{-1}$ have been found to represent the K absorption to better than 5 per cent.

Summary.

Two balance methods for the measurement of X-ray absorption coefficients are described, one an ionisation, the other a photographic method.

* ' Z. Physik,' vol. 40. p. 575 (1926).

In connection with the latter, a detailed account is given of the comparison of X-ray intensities by photographic means.

Absorption coefficients have been measured for Fe, Ni, Cu and Zn over a range of wave-lengths 0 3 Å. to 2·0 Å., while those of Mo, Pd, Ag and Sn have also been measured, but over shorter ranges.

The values of μ/ρ are compared with those of other observers and the value of the exponent of λ in the law of absorption shown to be a function of λ.

It is shown that for Fe, Ni, Cu, Zn, Pd, Ag, the K jump equals E_K/E_{L_1} in agreement with the observations of Richtmeyer and Jonsson.

The values of $\left(\dfrac{\tau}{\rho}\right)_K$, for the K absorption of the above elements, can be represented by the following expression

$$\left(\frac{\tau}{\rho}\right)_K . A = 5\cdot0 \times 10^{-5} Z^5\lambda^{7\cdot2} + 3\cdot0 \times 10^{-3} Z^4\lambda^3 + 1\cdot70 \times 10^{-1} Z^3\lambda^{5/2}.$$

In conclusion, we wish to thank Professor T. H. Laby, F.R.S., for his helpful criticism in this work.

On the Hyperfine Structure of Certain Hg I Lines in the Electrodeless Discharge.

By T. S SUBBARAYA and T G. SRINIVASA IYENGAR

[PLATE 11]

Introduction

The hyperfine structure of a large number of mercury lines has been investigated by several observers and their results often show considerable variations, which have often been ascribed to the different modes of excitation. The line 4916 Å is one which exhibits such differences. Janicki[*] and other early observers have described this line as single, while Hansen[†] was the first to resolve it into five components, the satellites being quite close to the main

---

[*] 'Ann. Physik,' vol 29, p 833 (1909).

[†] 'Nature,' vol. 119, p. 237 (1927).

line. Venkatesachar.* using a long column of low density arc discharge, photographed a pattern which showed six or seven components. Subsequently the wave-lengths of these lines were fixed by Venkatesachar and Sibaiya† from fresh photographs taken with a number of Lummer plates, using the axial radiation from an arc discharge about a metre long. Later Tolansky,‡ using a high frequency electrodeless discharge, reported that he failed to observe the structure recorded by Venkatesachar and Sibaiya.

Experimental

It was thought desirable to analyse the line 4916 A. and other mercury lines with a view to tracing the source of this difference, and particularly to see if the structure changed with the mode of excitation A diagram of the apparatus is shown in fig. 1.
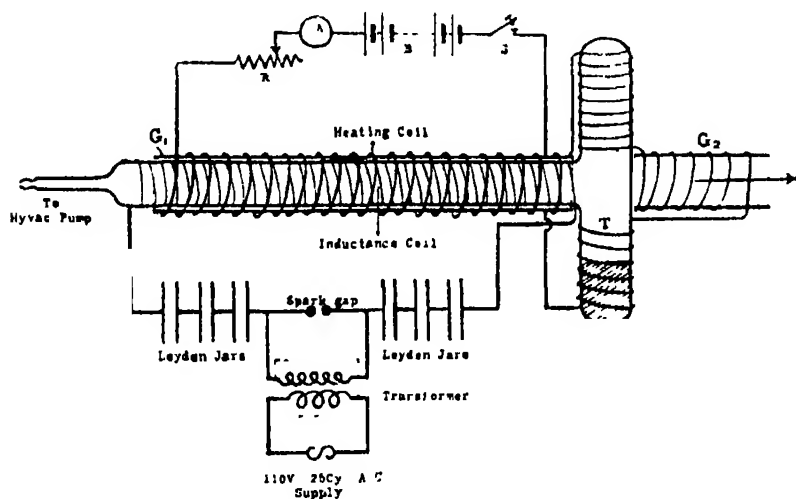
Fig. 1.

The mercury, purified and distilled, was placed in the side limb T, attached to the main tube over which a large number of turns of enamelled copper wire were closely wound. The ends of this coil were joined in series with a number of Leyden jars and a spark gap connected to the terminals of the secondary of a 10,000-volt wireless transformer. The apparatus was evacuated by a Cenco Hyvac pump, which was kept running throughout an exposure An air jet

---

* " Presidential Address, Mathematics and Physics Section, Indian Science Congress " (1930).

† ' J. Mysore Univ.,' vol. 4, p. 145 (1931).

‡ ' Proc. Roy. Soc.,' A, vol. 130, p. 558 (1931).

was directed against the spark gap to prevent arcing. The discharge was found to be very bright when the tube was heated to about 100° C. by a heating coil wound over a glass tube G_1 and slipped over it. The observation window was also kept free from the troublesome deposit of mercury by keeping the heated glass tube G_2 in front of it. The oscillations were found to correspond to a wave-length of 103 metres as measured by a precision wavemeter. The energising coils were closely wound because we found that this brightened the discharge. This probably speaks for the electromagnetic origin of this kind of damped oscillatory discharge.*

The axial radiation from the tube described above was analysed by means of two Lummer plates made by Hilger, one of glass of 4·7 mm. thickness, and the other of quartz 7·44 mm. thick, placed after the collimator of a Hilger constant deviation spectrograph. The light was polarised by a Nicol when the quartz plate was used. The plates were measured on a Hilger's photo-measuring micrometer and also on a Gaertner measuring microscope. The wave-lengths were determined in the manner detailed by Schramment† and also according to the method proposed by P. Kunze.‡ The results from the different plates agree to within 0·005 A.; we could not push the accuracy much farther since a large number of plates could not be measured. The observed wave-length-separations of the satellites are given below.

Results.

4916.			6123.	6234.	6072
$\delta\lambda$	Int	$\delta\nu$			
+0·145 (2)	−599		+0 248 (6)	+0 074 (5)	+0 036 (7)
+0 040 (?)	−165		+0 168 (7)	0 (10)	0 (10)
+0 028 (2)	−116		+0 086 (9)	−0 055 (3)	−0 044 (8)
0 (10)	0		0 (10)	---	−0 156 (6)
−0 026 (3)	+107		−0 082 (?)	---	---
−0 052 (1)	+215		–	---	---
−0 150 (3)	+620		---	---	---

The line +0 088 observed by Venkatesachar and Sibaiya falls on −0 150 in the glass Lummer plate and on −0 052 in the quartz plate.

---

* This aspect of the question has been much discussed; see J. J Thomson, 'Phil. Mag.,' vol. 4, p. 1128 (1927); Townsend and Donalson, 'Phil. Mag.,' vol. 5, p. 178 (1928); Nethercot, 'Phil. Mag.,' vol. 7, p. 600 (1929); McKinnon, 'Phil. Mag.,' vol. 8, p. 605 (1929), Stuhlman. jr, and Whitaker, 'Rev Sci Inst.,' vol. 1, p. 772 (1930), Brasefield, 'Phys. Rev.,' vol. 35, p. 1073 (1930), vol 37, p. 82 (1931), Smith. Lynch and Hilberry, 'Phys Rev.' vol. 37, p. 1091 (1931).

† 'Ann. Physik,' vol. 83, p 1161 (1927).

‡ 'Ann. Physik,' vol. 79, p. 531 (1926).

Theoretical.

Commenting on the structures obtained by them, Venkatesachar and Sibaiya* suggested the possibility of interpreting the complicated hyperfine structure of Hg I lines if two different nuclear moments of $\frac{1}{2}$ and $1\frac{1}{2}$ were assigned to two different isotopes of mercury. Recently, in a very interesting paper, Schüler and Keyston† have shown that the structures can be quantitatively explained if to the isotope 199 is assigned a nuclear moment $\frac{1}{2}$, while to the isotope 201 is ascribed the moment $1\frac{1}{2}$, and Murakawa‡ has come to the same conclusion. Now, the structure given by these authors for 4916 Å does not agree completely with that given here. Hence an attempt was made to see whether the present results agreed with theoretical expectations. The guiding principle here is that the same common differences should occur in the same order in all the lines 4916, 5791 and 5770 which have the $6\,^1P_1$ level in common. On the basis of the common differences 243, 360 and 600 occurring in all three, the structure of the $6\,^1P_1$ level was fixed; with the help of this and the known structure of 5791 the separations of the $6\,^1D_2$ level were obtained. Taking the structure of the $6\,^3P_2$ level as given by Murakawa and that of the $6\,^1D_2$ level obtained above, the structure of the line 3663·28 ($6\,^3P_2 - 6\,^1D_2$) was deduced. This theoretical structure is in agreement with that obtained experimentally. Similarly, from a knowledge of the $6\,^3P_2$ level and the structure of the line 3654·83 ($6\,^3P_2 - 6\,^3D_2$) the intervals of the level $6\,^3D_2$ were fixed; combining this with the structure of the $6\,^1P_1$ level, the structure of the line 5770 ($6\,^1P_1 - 6\,^3D_2$) was obtained and found to be in agreement with the experimental structure. The values here assumed for 4916 are the weighted averages of Venkatesachar and Sibaiya's and our own measurements, while the structures of the other lines are taken from Nagaoka § Level schemes and the structures of the lines are given below, and notes on individual lines have been added. In the diagrams of the structures the heights of the lines indicate the observed intensities, while the theoretical intensities calculated as a percentage of the total intensity of the line are marked at the top of each line. Theoretically predicted but unobserved components are distinguished by placing a small cross below. Some components which have been observed, but which do not find a place in the scheme, are left without their theoretical intensities being marked. Lines due to even isotopes are marked with broken lines. The

observed wave-number separations in thousandths of a cm.$^{-1}$ are given below each component, and also on the line indicating that transition in the level scheme. The Roman numerals I, II, III and IV stand for the even isotopes 198, 200, 202 and 204 respectively

4916.—This line shows more components than theory can account for. The very close satellites that have been observed by Hansen and others do not fit into the scheme of levels of the odd isotopes as given here. The structure of the $6\,^1P_1$ level now proposed appears to be the correct one as it has been tested in the lines 5791 and 5770. The magnitudes of the separations of the close components are very small and are nearly of the same order as those of the components of the main line of 5461 Since the latter can be explained by ascribing a nuclear moment to one of the even isotopes * we make the

λ4916 (6'P₁−8'S₀)
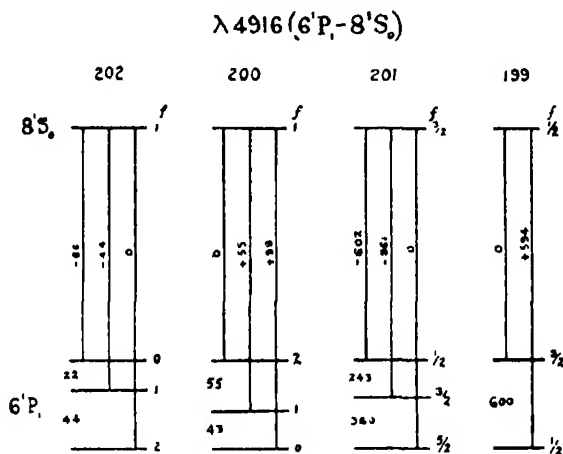
Fig 2

Note —The satellites | 0 055 and − 0·066 have been given by Hansen and Tolansky ; 0 044 is a satellite predicted by the theory here proposed, but too close to − 0 066 to be resolved.

* H. Schuler, ' Naturwiss ,' vol. 19, p 950 (1931).

suggestion that these close satellites are to be ascribed to the isotopes 200 and 202 with a nuclear moment 1. But the suggestion has to remain tentative till other independent evidence is adduced in its favour. Even after this extension of the theory there is one satellite at $+ 0\cdot306$ which does not figure in the scheme, though it is indubitably exhibited in the microphotometer curve (marked C in fig. 3) of a pattern of 4916 taken from one of Venkatesachar and Sibaiya's plates by Messrs Carl Zeiss and reproduced in fig 3. A theoretical
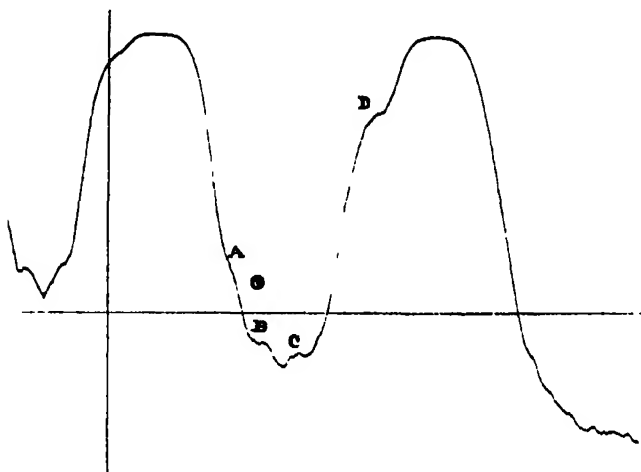
FIG 3 —Microphotogram of a pattern of 4916 Å taken with a quartz Lummer plate 7 44 mm. thick. (Reproduced with kind permission of B. Venkatesachar and L. Sibaiya)

curve based upon the calculated intensities and on considerations of the resolving power of the quartz Lummer plate used is given in fig. 4 for comparison. The component $+ 0$ 306 has been marked here by a curve with broken lines since it is not obtained theoretically, and it is easy to see that the small hump at C in fig 4 is due to this satellite The existence of such satellites is not peculiar to this line, for even in the case of 5461 a satellite occurs at $\delta\lambda = - 0\cdot154$, which does not come into Schuler and Keyston's scheme Considering the uncertainties introduced by the photographic plate, the agreement may be considered satisfactory The structure now given removes the anomaly noted by Schuler and Keyston in the isotope displacements of the $^1P_1$ levels The lines 3655 ($6\,^3P_2 - 6\,^3D_2$) and 3126 ($6\,^3P_1 - 6\,^3D_2$) show a displacement of about 400 (in thousandths of a cm.$^{-1}$) in the positions of the even isotopes, which must be ascribed to the $6\,^3D_2$ level since both the $6\,^3P_2$ and $6\,^3P_1$ levels show no such displacement. Now 5770 ($6\,^1P_1 - 6\,^3D_2$) shows

a displacement of about 150, so that the displacement of the $6\,^1P_1$ level is about 250 The line 4916 shows a somewhat smaller displacement, while 5791 shows a displacement of about 300 Considering the approximate nature of the magnitudes of these displacements, we may conclude that the
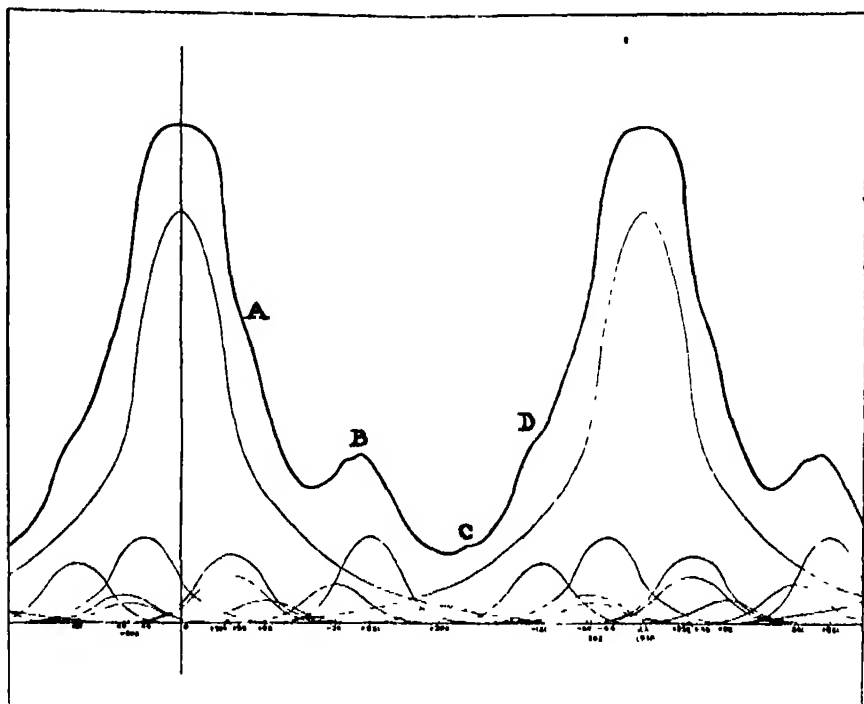
Fig 4.—Theoretical intensity distribution in 4916 Å. for comparison with fig. 3.

displacement of the $6\,^1P_1$ level is about 250 and that the $6\,^1D_2$ level has no displacement. The fact that the line 3663 ($6\,^3P_2$—$6\,^1D_2$) shows no displacement will then be explained. The anomaly in the magnitudes of the fine separations of the $^1P_1$ levels is also partly removed.

5791.—The component at $+ 0\cdot753$ has been observed by Janicki, though Nagaoka omits it. The assignment of $+ 0\cdot361$, $0\cdot000$ and $- 0\cdot391$ to the even isotopes is borne out by the fact that according to Lunelund their Zeeman patterns are all similar.

3663.—The structure of this line has been calculated from the previously known $6\,^3P_2$ and $6\,^1D_2$ levels, and is seen to agree well with the observed pattern. The two components $+ 0\cdot678$ and $+ 0\cdot104$ are given by Ruark,[*]

* 'Phil. Mag,' vol. 1, p. 977 (1926).

but Nagaoka does not get them. They, as well as the faint satellite at − 0·245 do not appear in our scheme. Of the predicted satellites that are not observed, all, except − 0·412, are very weak and some are too far off while others fall very near strong components
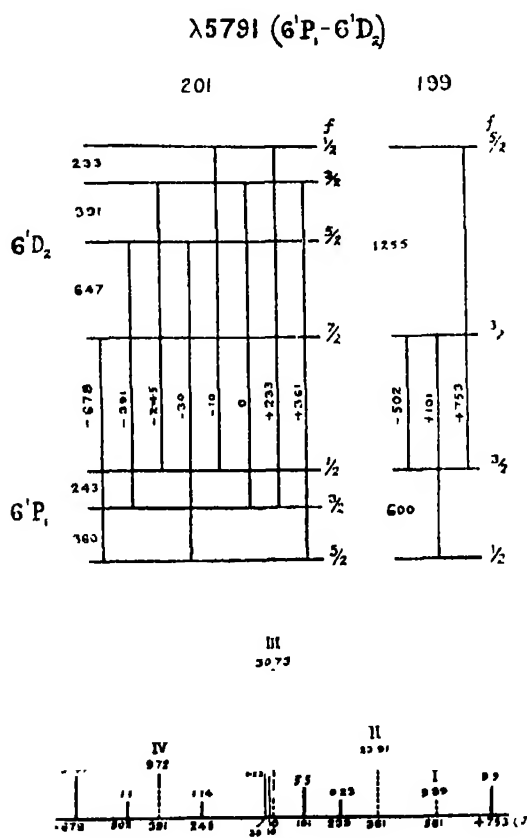
Fig 5

3655 —This line has led to the recognition of the $6\,^3D_2$ level separations. One faint component at + 0·160 does not enter into the scheme The faint component at + 0·223 must be identical with the + 0·242 that appears in the scheme of levels. The component —0·145 has been calculated from the separation 366 between the $^3P_2$ ($f = 5/2$) and $^3P_2$ ($f = 7/2$) levels, as has been given by Murakawa. Schüler and Keyston give 400 as the separation of these levels and, if this is correct, this component becomes −0·111 and may be expected to fuse with −0·071. The other predicted components that are not observed are too faint and too close to other satellites.

λ 3663 (6³P₁ – 6³D₂)
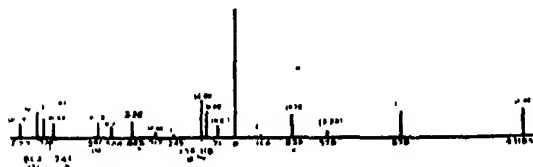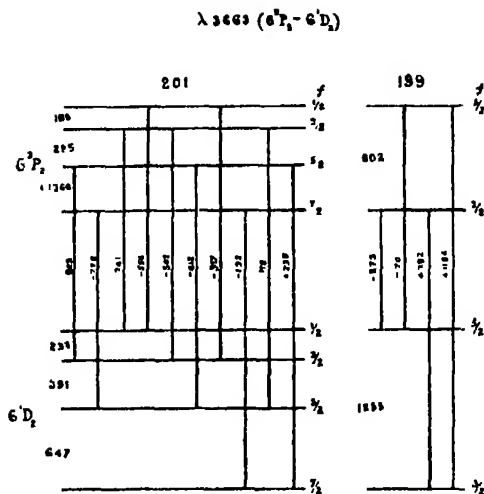
Fig 6.

5770—The structure of this line has been calculated from the structure of the 6 ¹P₁ and 6 ³D₂ levels found above. The agreement is good. One component at − 0·445 which may be expected to appear has not been observed. The one at + 0·724 has been observed by Sibaiya,* but given by him as a doublet, + 0 619 and + 0·771. Here also the similarity of the Zeeman patterns of the main line and the satellites + 0·150 and − 0·132 noted by Lunelund finds an explanation.

3126.—The structure of this line also has been calculated from that of the 6 ³P₁ level given by Schuler and that of the 6 ³D₂ level found above. There is a discrepancy of about 40 between the separations given by Schüler and Keyston and by Murawaka. The observed components at −0·723, +2·105, + 1·032, + 0·362 and + 0·085 do not come into the scheme and may not be real. The component at −0·157 must be due to a poor measurement

* ' Proc. Ind. Sci. Congress Abs.' (1932).

Fig 10

$$\lambda\,3655\,(6\,^2P_2 - 6\,^2D_2)$$
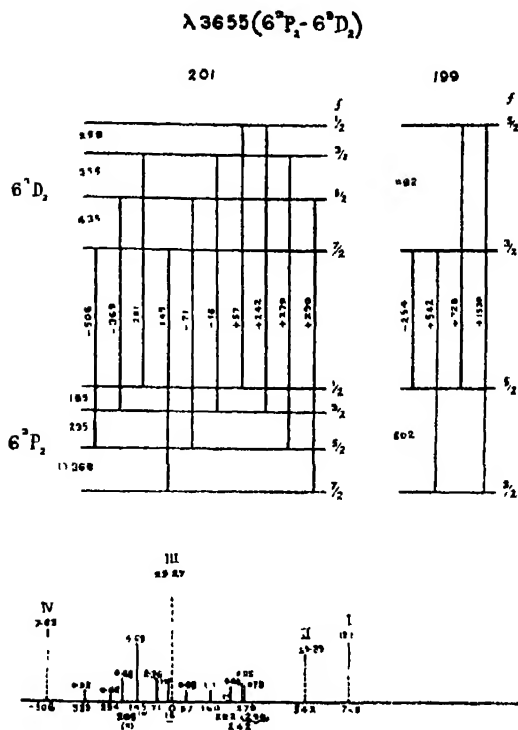
Fig. 7.

caused by the overlapping of three satellites at this place. The predicted components at $+0\cdot406$ and $+0\cdot613$ are too faint to be observed, while $+0\cdot531$ is too near to $+0\cdot495$.

Discussion

A consideration of the above results shows that there is good agreement between theory and experiment and that the structure here given for the $6\,^1P_1$ level is the correct one. The structures of the lines also exhibit the regularities found by Schüler and Keyston regarding the equality of the total separations for the isotopes 199 and 201 and the relatively inverted positions of their fine levels.

Though the observed components are nearly all explained, there remain a few which are often real and yet are not accounted for by the theory. Regarding intensities also the theory generally gives correct results, but some intensity anomalies cannot easily be explained. It was noticed some considerable time

ago that hyperfine structures differed when different sources were employed, but it has only recently been demonstrated by Schüler and Keyston* that slight variations in the conditions of excitation in the same source can introduce
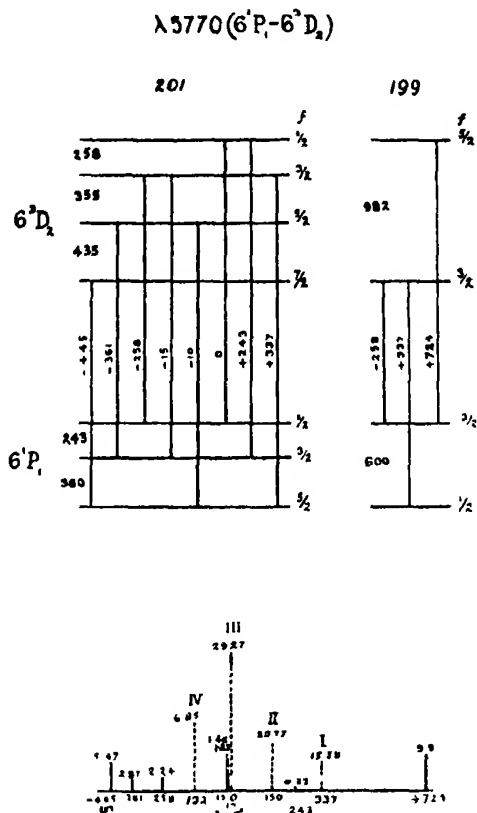
FIG. 8.

large intensity anomalies. This is also shown in the two photographs of the line 5461 taken by the authors and reproduced in Plate 11   These were taken under nearly identical conditions except that the current in the heating coil used in our experiment was 2 amps. in the case of A and 2·5 amps. in that of B   That such small external changes can influence the interaction between the nucleus and the outer electron shell is rather astonishing   Yet there seems to be some regularity even in these anomalies.   Thus the component due to the even isotope 204, when not complicated by the overlapping of lines due to other isotopes, is found to be consistently brighter in ordinary sources than is pre-

* 'Z. Physik,' vol. 71, p. 413 (1931).

dicted by theory and observed in sources of small absorption. Similarly, the component due to the isotope 198 when not disturbed by other lines seems to be weakened. This is well shown in the table on p. 228.
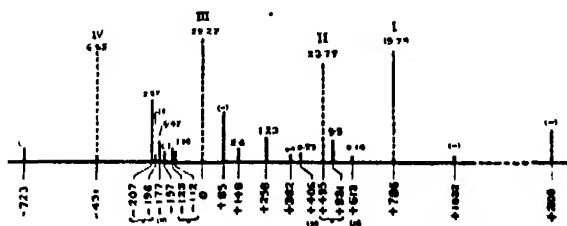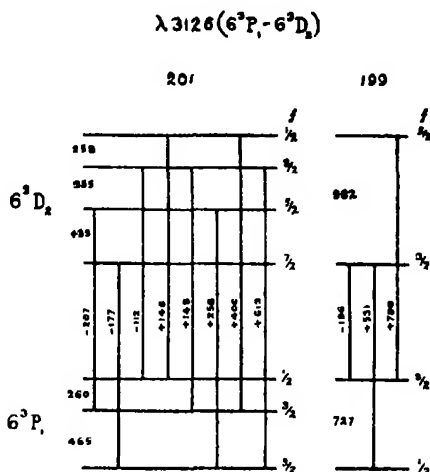
Fig. 9.

Summary.

The structure of the line 4916 Å. of Hg I has been examined, using as the source a high frequency electrodeless discharge. The structure found coincides with that previously given by Venkatesachar and Sibaiya. On the basis of this structure the splitting of the $6\,^1P_1$ level has been determined and the structures of the lines $5790 \cdot 66$, $5769 \cdot 60$, $3663 \cdot 28$, $3654 \cdot 83$ and $3125 \cdot 66$ have been explained. The structures of the lines 6123, 6234 and 6072, experimentally obtained, have also been given. The present analysis of the levels exhibits the regularities found by Schüler and Keyston such as the approximate

Table.

	Line.	Component due to isotope 204.	A.	B.	Component due to isotope 198	A.	B.
Analysed in the present work.	4916	−0·121	5 in 10 (Hansen)	2 in 30 (Tolansky)	0·221	1 in 10 (B.V. & L.S.)	2 in 10 (Theoretical)
	5791	−0·391	8 in 10 (Long Column)	10 in 30 (Theoretical)	0·561	1 in 10 (Gale & Lemon)	10 in 30 (Theoretical)
	5770	−0·132	5 in 10 (Gale & Lemon)	7 in 30 (Theoretical)	0·345	1 in 10 (Nagaoka)	15 in 30 (Theoretical)
	3655	−0·506	6 in 10 (Nagaoka)	7 in 30 (Theoretical)	0·728	5 in 10 (Nagaoka)	19 in 30 (Theoretical)
	3126	−0·431	9 in 10 (Nagaoka)	7 in 30 (Theoretical)	0·786	9 in 10 (?) (Nagaoka)	20 in 30 (Theoretical)
Analysed by Schuler and Keyston.	6072	0·118	7 in 10 (B.V. & L.S)	7 in 30 (Schüler & Keyston)	−0·241	1 in 10 (B.V. & L S)	10 in 30 (Schüler & Keyston)
	6716	0·122	2 in 10 (B.V. & L.S.)	3 in 30 (Tolansky)	−0·233	5 in 10 (B.V. & L.S. fusion of −0·274 and −0·233)	20 in 30 (Schüler & Keyston sum of −0·274 and −0·233)

equality of the total separations and the relatively inverted positions of the levels due to the two isotopes 199 and 201. The structure now proposed shows that the anomaly noted by Schüler and Keyston regarding the magnitudes of the isotope displacements and the fine intervals does not exist in the $6\,^1P_1$ level.

In conclusion, we should like to record our deepest thanks to Professor Venkatesachar for his guidance and encouragement throughout this work. One of us is indebted to the University of Mysore for the award of a scholarship.

Experiments with High Velocity Positive Ions. II.—The Disintegration of Elements by High Velocity Protons.

By J. D. Cockcroft, Ph D., Fellow of St. John's College, Cambridge, and E T. S. Walton, Ph.D.

[Plate 12.]

1. *Introduction.*

In a previous paper* we have described a method of producing high velocity positive ions having energies up to 700,000 electron volts. We first used this method to determine the range of high-speed protons in air and hydrogen and the results obtained will be described in a subsequent paper. In the present communication we describe experiments which show that protons having energies above 150,000 volts are capable of disintegrating a considerable number of elements.

Experiments in artificial disintegration have in the past been carried out with streams of α-particles as the bombarding particles ; the resulting trans-mutations have in general been accompanied by the emission of a proton and in some cases γ-radiation.† The present experiments show that under the bombardment of protons, α-particles are emitted from many elements ; the disintegration process is thus in a sense the reverse process to the α-particle transformation.

---

* ' Proc. Roy. Soc.,' A, vol. 136, p. 619 (1932) denoted as (I) hereafter.

† Rutherford, Chadwick and Ellis, " Radioactive Substances."

2. *The Experimental Method.*

Positive ions of hydrogen obtained from a hydrogen canal ray tube are accelerated by voltages up to 600 kilovolts in the experimental tube described in (I) and emerge through a 3-inch diameter brass tube into a chamber well shielded by lead and screened from electrostatic fields. To this brass tube is attached by a flat joint and plasticene seal the apparatus shown in fig. 1. A target, A, of the metal to be investigated is placed at an angle of 45 degrees to the direction of the proton stream. Opposite the centre of the target is a side tube across which is sealed at B either a zinc sulphide screen or a mica window.
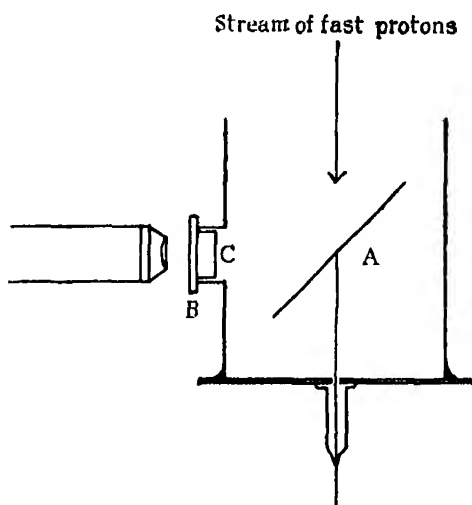
Fig. 1.

In our first experiments we used a round target of lithium 5 cm. in diameter and sealed the side tube with a zinc sulphide screen, the sensitive surface being towards the target. The distance from the centre of the target to the screen was 5 cm. A sheet of mica, C, of stopping power 1·4 cm. was placed between the screen and target and was more than adequate to prevent any scattered protons reaching the screen, since our range determinations[*] and the experiments of Blackett[†] have shown that the maximum range of protons accelerated by 600 kilovolts is of the order of 10 mm. in air. The screen is observed with a microscope having a numerical aperture of 0·6, the area of screen covered being 12 sq. mm. This arrangement with the fluorescent surface inside the vacuum is generally used in the preliminary investigations

---

[*] In course of publication.

[†] ' Proc. Roy. Soc.' A, vol. 134, p. 658 (1931).

of elements and when it is necessary to detect the presence of particles of short range.

The current to the target is measured by a galvanometer and controlled by varying the speed of the motor used for driving the alternator exciting the discharge tube (see Paper I). Currents of up to 5 microamperes can be obtained. Since metals bombarded by high-speed positive ions emit large numbers of secondary electrons for each incident ion, it is necessary to prevent the emission of these electrons if an accurate determination of the number of incident ions is required. This has been effected by applying a magnetic field of the order of 700 gauss to the target. Since it is well known that the majority of the secondary electrons have energies below 20 volts, such a field should be adequate to prevent secondary electron emission being a serious source of error.

An accurate determination of the exact composition of the beam of ions has not yet been made, but deflection experiments with a magnetic field in a subsidiary apparatus have shown that approximately half the current is carried by protons and half by H_2^+ ions. The number of neutral atoms appears to be small.

The accelerating voltage used in the experiments is controlled by varying the field of the alternator exciting the main high tension transformer. The secondary voltage of this transformer is measured by the method described in an earlier paper,* which rectifies the current passing through a condenser. A microammeter on the control table allows a continuous reading of this voltage to be obtained. The value of the steady potential produced by the rectifier system varies between 3 and 3·5 times the maximum of the transformer voltage according to the brightness of the rectifier filaments. The actual value of the voltage is determined by using a sphere gap consisting of two 75-cm. diameter aluminium spheres, one of which is earthed. In each experiment the multiplication factor of the rectifier system is determined for several voltages and intermediate points obtained by interpolation. The accuracy of the determination of the voltage by the sphere gaps has been checked by measuring the deflection of the protons in a magnetic field. It has been found that corrections of the order of 15 per cent. may be required as a result of the proximity of neighbouring objects or unfavourable arrangements of the connecting leads. The voltages given in this paper have all been corrected by reference to the magnetic deflection experiments.

* ‘Proc. Roy. Soc.’ A, vol 129, p. 477 (1930).

3. *The Disintegration of Lithium.*

When the current passing to the target was of the order of 1 microampere and the accelerating potential was increased to 125 kilovolts, a number of bright scintillations were observed on the screen, the numbers being proportional to the current collected and of the order of 5 per minute per microampere at 125 kilovolts.

No scintillations were observed when the proton current was cut off by shutting off the discharge tube excitation or by interposing a brass flap between the beam and the target. Since the scintillations were very similar in appearance and brightness to α-particle scintillations, the apparatus was now changed to allow a determination of their range to be made For this purpose a mica window having a stopping power of 2 cm. was sealed to the side tube in place of the fluorescent screen, which was now placed outside the window. It was then possible to insert mica screens of known stopping power between the window and the screen. In this way it became apparent that the scintillations were produced by particles having a well-defined range of about 8 cm. Variations of voltage between 250 and 500 kilovolts did not appear to alter the range appreciably.

In order to check this conclusion, the particles were now passed into a Shimizu expansion chamber, through a mica window in the side of the chamber having a stopping power of 3·6 cm. When the accelerating voltage was applied to the tube a number of discrete tracks were at once observed in the chamber whose lengths agreed closely with the first range determinations. From the appearance of the tracks and the brightness of the scintillations it seemed now fairly clear that we were observing α-particles ejected from the lithium nuclei under the proton bombardment, and that the lithium isotope of mass 7 was breaking up into two α-particles.

In order to obtain a further proof of the nature of the particles the experiments were repeated with an ionisation chamber, amplifier and oscillograph of the type described by Wynn Williams and Ward.* The mica window on the side tube was reduced to a thickness corresponding to a stopping power of 1·2 mm. with an area of about 1 sq cm., the mica being supported on a grid structure. The lithium target was at the same time reduced in size to a circle of 1 cm. diameter in order to reduce the angular spread of the particles entering the counter. The ionisation chamber was of the parallel plane type having a total depth of 3 mm. and was sealed by an aluminium window having a stopping

---

* 'Proc. Roy. Soc.,' A, vol. 132, p. 391 (1931).

power of 5 mm. The degree of resolution of the amplifier and oscillograph was such that it was possible to record accurately up to 2000 particles per minute. With the full potential applied to the apparatus but with no proton current, the number of spurious deflections in the oscillograph was of the order of 2 per minute, whilst with an accelerating potential of 500 kilovolts and a current of 0·3 microamperes the number of particles entering the ionisation chamber per minute was of the order of 700.

In figs. 8, 9, 10 and 11, Plate 12, are shown the oscillograph records obtained as additional mica absorbers are inserted. It will be seen that the size of the deflections increases as additional mica is inserted, whilst the numbers fall off rapidly when the total absorber thickness is increased beyond 7 cm In fig 2 is plotted the number of particles entering the chamber per minute per micro-ampere for increasing absorber thickness and for accelerating potentials of 270 kilovolts and 450 kilovolts The stopping power of the mica screens of windows has been checked and the final range determination made by a comparison with the α-particles from thorium C We find that the range is 8·4 cm. Preliminary observations showed that between the lowest and highest voltages used, the range remained approximately constant. It is, however, of great interest to test whether the whole of the energy of the proton is communicated to the α-particles, and it is intended at a later date to examine this point more carefully. The general shape of the range curve, together with the evidence from the size of the oscillograph deflections, suggests that the great majority of the particles have initially a uniform velocity, but further investigation will be required with lower total absorption to exclude the possibility of the existence of particles of short range

As is well known, the size of the oscillograph kicks are a measure of the ionisation produced by the particles. At the beginning of the range the size of the kicks observed was very uniform, whilst the average size varied with the range of the particle corresponding to the ionisation given by the Bragg curve. Fig. 3 shows the variation of the ionisation of the most numerous particles with range.

The sizes of the deflections were now compared with the deflections produced in the same ionisation chamber by α-particles from a polonium source, these deflections being recorded in fig. 12, Plate 12, for comparison. It has been shown in this way that the maximum deflection for the two types of particle is the same. This result, together with the uniformity of the ionisation produced by the particles, is sufficient to exclude the possibility of some of the particles being protons, since the maximum ionisation produced by a
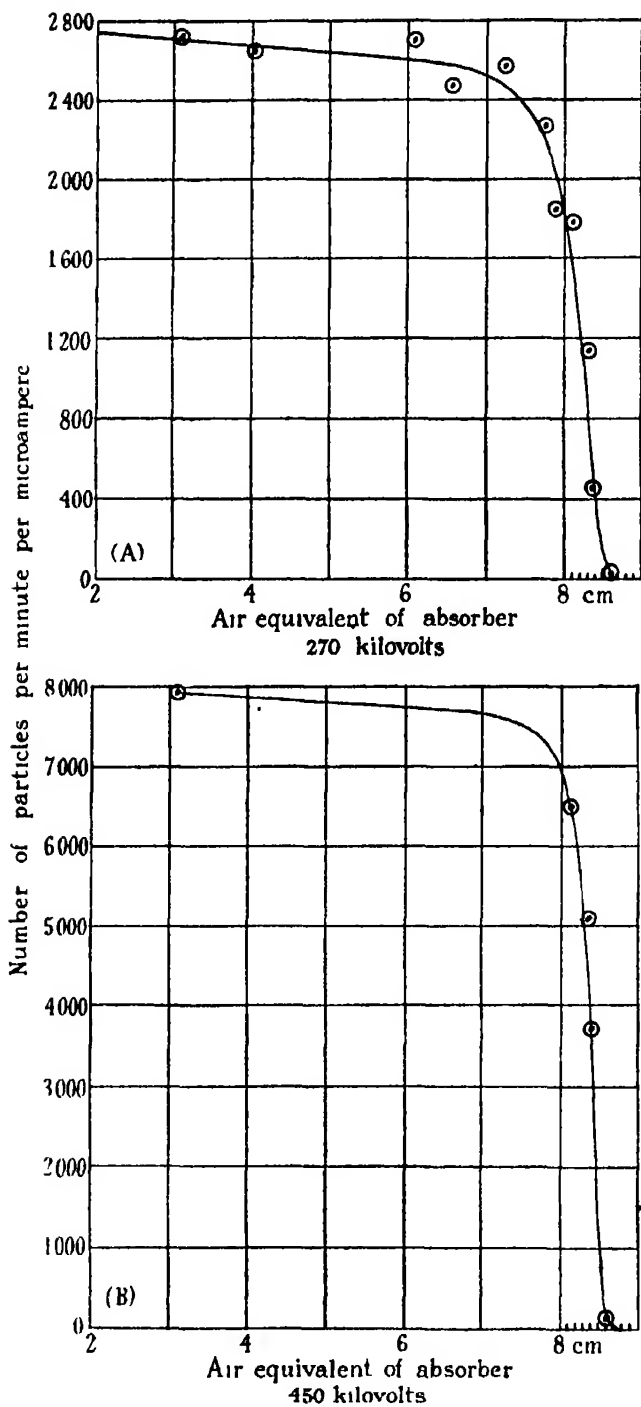
Fig. 2.

proton is less than 40 per cent. of the maximum ionisation produced by an α-particle.
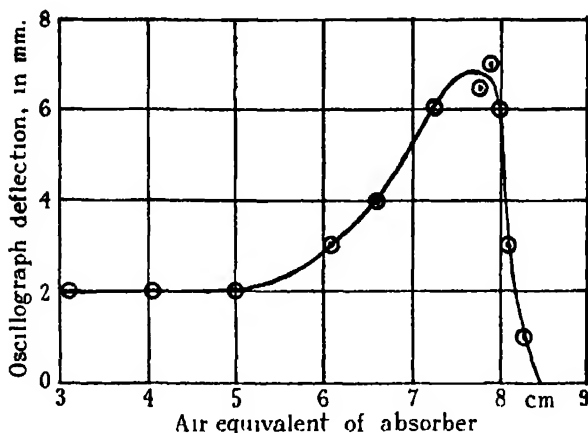
Fɪɢ. 3.

The variation of the numbers of particles with accelerating voltage was determined from the oscillograph records between 200 kilovolts and 500 kilovolts, the change in numbers being clear from the records, figs. 13, 14, 15, Plate 12. For voltages between 70 kilovolts and 250 kilovolts, the numbers of particles entering the ionisation chamber were counted by a single stage thyratron counter of the type described by Wynn Williams and Ward.* The results are plotted in fig. 4. The numbers increase roughly exponentially with the voltage at the lower voltages and linearly with voltage above 300 kilovolts.†

It is of great interest to estimate the number of particles produced by the bombardment of a thick layer of lithium by a fixed number of protons. In making this estimate we have assumed that the particles are emitted uniformly in all directions and that the molecular ions produce no effect. With these assumptions the number of disintegrations for a voltage of 250 kilovolts is 1 per 10^9 protons, and for a voltage of 500 kilovolts is 10 per 10^9 protons.

In considering the variation in numbers of particles with voltage it has, of course, to be borne in mind that with a thick target the effects are due to

---

* 'Proc. Roy. Soc ,' A, vol. 131, p. 191 (1931).

† All the measurements in a single run, in which more than 2000 particles were counted are included in the figure. The spread of the points in the centre part of the curve is probably due to variations in the vacuum and therefore in the voltage applied during the experiment. In other runs no evidence was obtained for such a variation.

protons of all energies from the maximum to zero energy. It will be very important to determine the probability of disintegration for protons of one definite energy, and for this purpose it will be necessary to use thin targets. Preliminary experiments using evaporated films of lithium show that the probability or " excitation " function does not increase so rapidly with voltage as for the thick target, but owing to the small numbers of particles obtainable these experiments have not yet been completed.
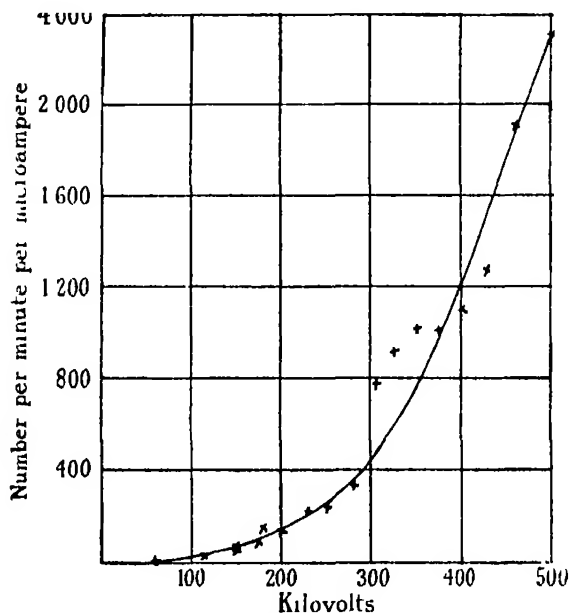
Fig 4.

4. *The Interpretation of Results.*

We have already stated that the obvious interpretation of our results is to assume that the lithium isotope of mass 7 captures a proton and that the resulting nucleus of mass 8 breaks up into two α-particles. If momentum is conserved in the process, then each of the α-particles must take up equal amounts of energy, and from the observed range of the α-particles we conclude that an energy of 17·2 million volts would be liberated in this disintegration process. The mass of the Li_7 nucleus from Costa's determination is 7·0104 with a probable error of 0·003. The decrease of mass in the disintegration process is therefore $7·0104 + 1·0072 - 8·0022 = 0·0154 \pm 0·003$. This is equivalent to an energy liberation of $(14·3 \pm 2·7) \times 10^6$ volts. We conclude, therefore, that the observed energies of the α-particles are consistent with our

hypothesis. An additional test can, however, be applied. If momentum is conserved in the disintegration, the two α-particles must be ejected in practically opposite directions and, therefore, if we arrange two zinc sulphide screens opposite to a small target of lithium as shown in the arrangement of fig. 5, we should observe a large proportion of coincidences in the time of appearance of the scintillations on the two screens. The lithium used in the experiments was evaporated on to a thin film of mica having an area of 1 sq. mm. and a stopping power of 1·1 cm., so that α-particles ejected from the lithium would pass easily through the mica and reach the screen on the opposite side of the lithium layer.

The two screens were observed through microscopes each covering an area of 7 sq. mm. and a tape recording machine was used to record the scintillations,
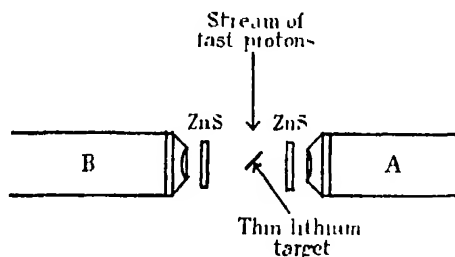
Fig 5

a buzzer being installed in the observation chamber to prevent the noise of the recording keys being audible to the observers. Five hundred and sixty-five scintillations were observed in microscope A and 288 scintillations in microscope B, the former being nearer the target. Analysis of the records showed that the results are consistent with the assumption that about 25 per cent. of the scintillations recorded in B have a corresponding scintillation in A. If we calculate the chance of a scintillation being recorded by B within x seconds of the record of a scintillation in A, assuming a perfectly random distribution of scintillations, and compare this with the observed record, the curve shown in fig. 6 is obtained. It will be seen that as the interval x is made less, the ratio of the observed to the random coincidences increases. We also plot for comparison the theoretical curve (shown by broken line) which would be obtained if there were 25 per cent. of coincidences. It will be seen that the two curves are in good accord. The number of coincidences observed is about that to be expected on our theory of the disintegration process, when we take into account the geometry of the experimental arrangement and the efficiency of the zinc

sulphide screens.   It is clear that there is strong evidence supporting the hypothesis that the α-particles are emitted in pairs.   A more complete investigation will be made later, using larger areas for the counting device, when it is to be expected that the fraction of coincidences should increase.
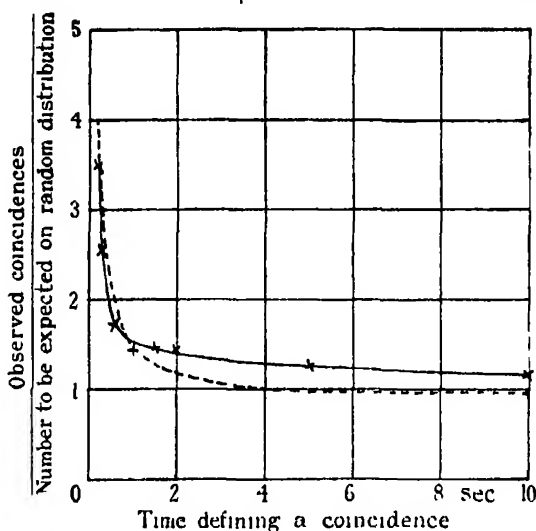
Fig. 6.

5. *Comparison with the Gamow Theory.*

In a paper which was largely responsible for stimulating the present investigation, Gamow[†] has calculated the probability W_1^* of a particle of charge Ze, mass m and energy E, entering a nucleus of charge $Z'e$.   Gamow's formula is

$$W_1^* = e^{\frac{-4\pi \sqrt{(2m)}}{h} \frac{ZZ'e^2}{\sqrt{(E)}}} J_k,$$

where J_k is a function varying slowly with E and Z.   Using this formula, we have calculated W_1^*, the probability of a proton entering a lithium nucleus, for 600, 300 and 100 kilovolts, and find the values $0 \cdot 187$, $2 \cdot 75 \times 10^{-2}$ and $1 \cdot 78 \times 10^{-4}$.   Using these figures, our observed variation of proton range with velocity for a thick target, and assuming a target area of 10^{-25} cm.^{2}, the number of protons N required to produce one disintegration may be calculated. For 600 kilovolts we find N to be of the order of 10^6, and for 300 kilovolts of the order of 2×10^7.

The order of magnitude of the numbers observed is thus smaller than the

number predicted by the Gamow theory, but a closer comparison must be deferred until the results for a thin target are available.

6. *The Disintegration of other Elements.*

Preliminary investigations have been made to determine whether any evidence of disintegration under proton bombardment could be obtained for the following elements : Be, B, C, O, F, Na, Al, K, Ca, Fe, Co, Ni, Cu, Ag, Pb, U. Using the fluorescent screen as a detector we have observed some bright scintillations from all these elements, the numbers varying markedly from element to element, the relative orders of magnitude being indicated by fig. 7 for 300 kilovolts The results of the scintillation method have been confirmed by the electrical counter for Ca, K, Ni, Fe and Co, and the size of the oscillograph kicks suggests that the majority of the particles ejected are α-particles.
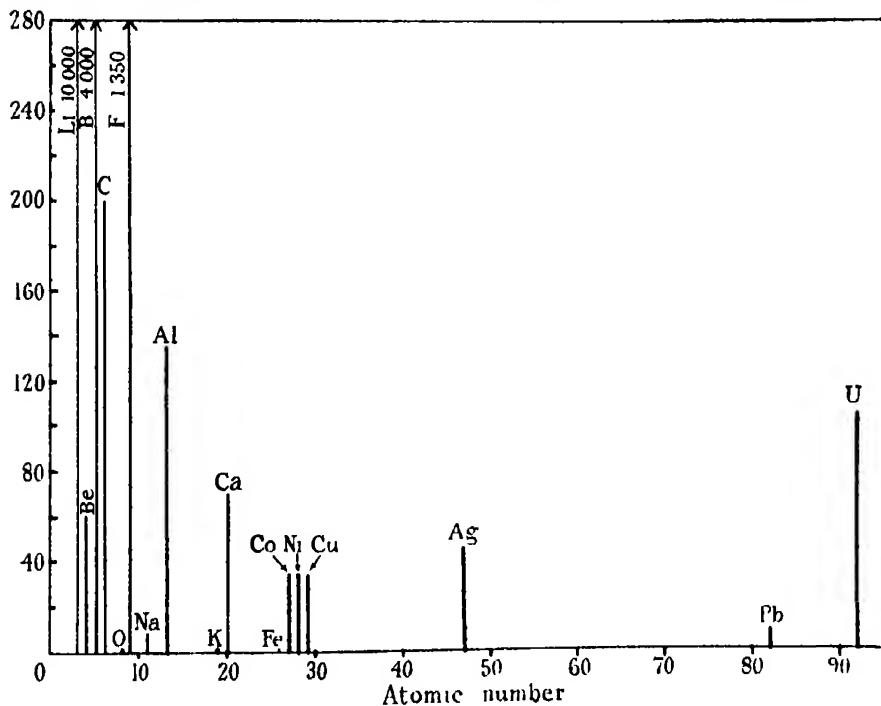
Fig. 7.

The numbers of particles counted have up to the present not been sufficient to enable these figures to be taken as anything other than an order of magnitude. In particular, the possibility must be borne in mind that some of the particles observed may be due to impurities. It may, however, be of some interest to

describe briefly the general character of the effects observed in some of the more interesting cases.

Beryllium.—Two types of scintillation were observed with beryllium, a few bright scintillations having the appearance of α-particle scintillations together with a much greater number of faint scintillations appearing at about 500 kilovolts, the numbers increasing rapidly with voltage. We were not able to observe the faint scintillations outside the vacuum chamber, so that they are presumably due to particles of short range.

Boron.—Next to lithium, boron gave the greatest number of scintillations, most of the particles having a range of about 3·5 cm. Scintillations were first observed at voltages of the order of 115 kilovolts, the numbers increasing by more than 100 between this voltage and 375 kilovolts. The interesting problem as to whether the boron splits up into three α-particles or into Be_8 plus an α-particle must await an answer until more detailed investigation is made.

Fluorine.—Fluorine was investigated in the form of a layer of powdered calcium fluoride. A few scintillations were first observed at a voltage of 200 kilovolts, the numbers increasing by a factor of about 100 between this and 450 kilovolts. The range of the particles was found to be about 2·8 cm. On the assumption that they are α-particles, the energy would be $4 \cdot 15 \times 10^6$ electron volts. If now we assume that the reaction is

$$F_{19} + H_1 = O_{16} + He_4$$
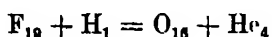
it is of particular interest to compare the observed energy with the energy to be expected from the mass changes, since all the masses involved are known, from the work of Aston, with fairly good precision.

Using Aston's data, the energy liberated should be $5 \cdot 2 \times 10^6$ electron volts. Allowing for the energy taken by the recoil of the oxygen nucleus and the energy of the bombarding proton, the energy of the α-particle should be about 4·3 million volts, giving a range of 2·95 cm. in air, in good accord with the observed ranges.

Sodium.—A small number of bright scintillations were observed beginning at 300 kilovolts, the particles having ranges between 2 and 3·5 cm. In addition to the bright scintillations, a number of faint scintillations were observed similar to those seen in the case of beryllium. The faint scintillations are again presumably due to particles of short range since they could not be observed outside the tube. The probable α-particle transition would be

$$Na_{23} + H_1 = Ne_{20} + He_4.$$
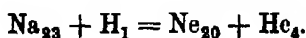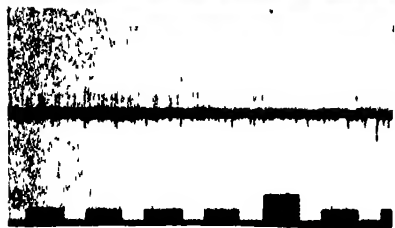
Fig. 8   270 Kv 4 0 cm absorber

Fig. 9 —270 Kv 5·0 cm absorber

Fig. 10 —270 Kv 6·6 cm absorber

Fig. 11 - 270 Kv 7·9 cm absorber
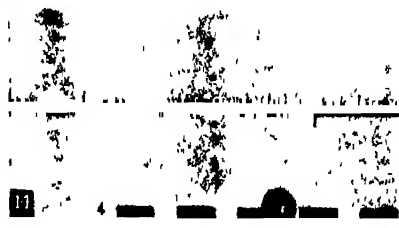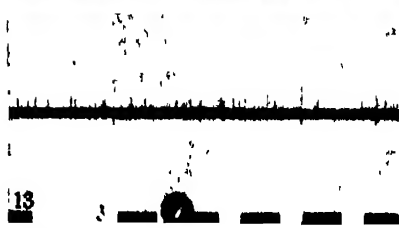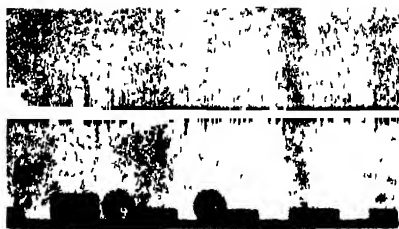
Fig 12   Polonium α-particles 2 cm
    absorber

Fig 13 -250 Kv 3 1 cm absorber

Fig 14 —210 Kv 3 1 cm absorber

Fig 15   175 Kv 3 1 cm absorber

Potassium.—Potassium is of special interest on account of its radioactivity. The very small effects observed may easily be due to an impurity. The most likely reaction to occur

$$K_{39} + H_1 = A_{36} + He_4,$$
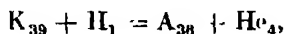
would probably have a negative energy balance.

Iron, Nickel, Cobalt, Copper.—These elements follow each other in the periodic table, so that the small result obtained for iron compared with that for the following three elements is of special interest. The effect for iron is of the same order as that for potassium, and again may be due to impurity. For these elements most of the particles had a range of about 2·5 cm., but a few particles were present having a slightly longer range.

Uranium—Using potentials of up to 600 kilovolts and strong proton currents, the number of scintillations observed was about four times the natural radio-active effect, and the artificially produced particles appeared to have a longer range than the natural ones. The numbers obtained did not appear to vary markedly with voltage.

We hope in the near future to investigate the above and other elements in much greater detail and in particular to determine whether any of the effects described are due to impurities. There seems to be little doubt, however, that most of the effects are due to transformations giving rise to an α-particle emission. In view of the very small probability of a proton of 500 kilovolts energy penetrating the potential barrier of the heavier nuclei by any process other than a resonance process, it would appear most likely that such processes are responsible for the effects observed with the heavier elements.

We have seen that the three elements, lithium, boron and fluorine give the largest emission of particles, the emission varying similarly with rise of voltage. These elements are all of the $4n + 3$ type, and presumably the nuclei are made up of α-particles with the addition of three protons and two electrons. It is natural to suppose that the addition of a captured proton leads to the formation of a new α-particle inside the nucleus. In the case of lithium, it seems probable that the capture of the proton, the formation of the α-particle and the dis-integration of the resulting nucleus into two α-particles must at this stage be regarded as a single process, the excess energy appearing in the form of kinetic energy of the expelled α particles.* Until further and more accurate data are available it is not desirable to discuss at this stage the possible bearing of

---

* Such a view does not preclude the possibility that sometimes part of the energy may appear in another form, for example, as γ-radiation.

these new observations on the problems of astrophysics and on the question of the abundance of the elements.

THE BAKERIAN LECTURE.—*The Combustion of Hydrocarbons.*

By WILLIAM A. BONE, D Sc , F R.S., Professor of Chemical Technology at the Imperial College of Science and Technology, London

(Received May 11, 1932 —Read June 9, 1932.)

INTRODUCTION.

The question of how a hydrocarbon is attacked by oxygen in combustion has always been of great interest to chemists ; and now that the motive power for aircraft and road vehicles is derived from hydrocarbon-air explosions it is being studied also by engineers the world over   The occasion is therefore opportune for its discussion, and as present-day investigators seem none too familiar with the work of former times, in what follows I will endeavour to review the principal discoveries, to illustrate some of them experimentally, and to consider certain theories concerning them   And I would stress the importance of viewing the subject widely, because what is most needed to-day is a balanced judgment embracing the whole range of conditions from those of slow combustion right up through flames and explosions under high pressures to detonation.

I.—NINETEENTH CENTURY DISCOVERIES.

My story begins with the discoveries of John Dalton (1803–4) about the partial combustion of " marsh gas " (methane) and " olefiant gas " (ethylene) which, being the only two hydrocarbons then recognised, were distinguished as the " light and heavy carburetted hydrogens " respectively.   In his " New System of Chemical Philosophy " (1807) Dalton used the results of his eudiometric analysis of them to illustrate his " law of multiple proportions," and he also described two very remarkable experiments upon the explosion of each with its own volume of oxygen   Of these, the one with ethylene is so important that it is best recounted in his own words —

" If 100 measures of oxygen be put to 100 of olefiant gas and electrified, an explosion ensues, not very violent, but instead of a diminution, as usual, there is a great increase of gas (instead of 200 measures there will be found about 360) , some traces of carbonic acid are commonly observed, which disappear on passing two or three times through lime water ; there will remain perhaps 350 measures of permanent gas, which is all combustible, yielding by an additional dose of oxygen

carbonic acid and water, the same as if entirely burnt in the first instance. What, therefore, is this new gas in the intermediate state? It is carbonic oxide and hydrogen mixed together, an equal number of atoms of each. One-third of the oxygen requisite for the complete combustion suffices to convert the carbon into carbonic oxide, and the hydrogen at the instant is liberated; hence the other two-thirds are employed, the one to convert the carbonic oxide into acid, the other the hydrogen into water."[*]

Thus did Dalton disclose the bed-rock fact that the explosive combustion of ethylene involves the intermediate production of carbonic oxide and hydrogen without any separation of carbon or appreciable steam formation, as follows :—

$$C_2H_4 + O_2 = 2CO + 2H_2.$$
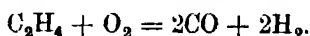
He also found that methane may similarly be exploded with its own volume of oxygen ' without any material change in volume," and that after removal of small amounts of carbonic anhydride " the residue is found to possess all the characteristics of a mixture of equal volumes of carbonic oxide and hydrogen."

It seems strange that such decisive results were seemingly ignored by Dalton's contemporaries and successors for nearly 85 years, and that throughout the greater part of last century the notion of a preferential burning of hydrogen in hydrocarbon combustion should have universally prevailed. Such, however, was the case, a striking example of how, even in science, a doctrine utterly opposed to facts may long be exalted into an article of faith and accepted without question.

It arose during the lifetime of Sir Humphry Davy, and has sometimes, though I think unjustifiably, been attributed to him, apparently through a misunderstanding of an ambiguous passage in one of his papers about the separation of carbon in hydrocarbon flames being due to " *the decomposition of a part of the gas towards the interior of the flame when the air was in smallest quantity.*" It was certainly endorsed by Faraday in his lectures on the " Chemistry of a Candle " (1848–49 and 1860–61) at the Royal Institution. And as late as 1884, in his Cantor Lectures on " The Uses of Coal Gas " at the Royal Society of Arts, H. B. Dixon, speaking of the combustion of ethylene as bearing on the

---

[*] " New System of Chemical Philosophy " (1807), Part II, p. 442. It is obvious from the experimental results that Dalton's " olefiant gas " was not all ethylene, because had it been so, the final volume of gas after the explosion would have been about 395 instead of the 360 actually observed; it probably contained air and possibly some methane also.

luminosity of hydrocarbon flames, said : " *This ethylene, when it is raised to a high temperature in contact with air is decomposed, the hydrogen burning first and the carbon afterwards.*"

The whirligig of time, however, brought its revenges when, seven years later in Dixon's own laboratory in Manchester, not only was the true result of exploding ethylene with its own volume of oxygen (as shown by Dalton) re-discovered, but it was also found that acetylene behaves similarly, in accordance with the equation

$$C_2H_2 + O_2 = 2CO + H_2.$$
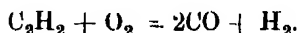
Experiment.—In the ethylene experiment, which will now be repeated, a mixture containing $C_2H_4 = 49·4$, $O_2 = 17·7$, and $N_2 = 2·9$ per cent., was fired in a leaden coil at an initial pressure (p_i) of 756 mm., the resulting explosion was violent and, to our great surprise at the time, the cold products were found to be under a pressure (p_2) of 1503 mm or practically double that of the original mixture $(p_2/p_1 = 1·988)$.* They burned with a bluish flame, and on subsequent analysis were found to be composed of substantially equal volumes of carbonic oxide and hydrogen, their exact composition being as follows : $CO_2 = 0·35$, $CO = 49·1$, $C_2H_4 = $ nil, $CH_4 = 1·0$, and $H_2 = 48·8$ per cent.†

It may be recalled how Dixon directed attention to these results in the Bakerian Lecture of 1893,‡ when from the rates of explosion of hydrocarbon-oxygen mixtures he also inferred that in the wave itself the carbon burns to the monoxide, its further oxidation being an after occurrence. Indeed, of all methane-oxygen or acetylene-oxygen mixtures, the equimolecular had been found to have the fastest rate of explosion, thus :—

$CH_4 + O_2$	$CH_4 + 1\frac{1}{2}O_2$	$CH_4 + 2O_2$
2528	2470	2322 metres per second.

$C_2H_2 + O_2$	$C_2H_2 + 1\frac{1}{2}O_2$	$C_2H_2 + 2\frac{1}{2}O_2$
2961	2716	2391 metres per second.

It was during 1891–92 that I first began assisting Dixon in such experiments, and subsequently at his suggestion, and in conjunction first with B. Lean and afterwards with the late J. C. Cain, I studied the behaviour of both ethylene

---

* Bone and Lean, ' J. Chem. Soc.,' vol 61, p. 873 (1892).

† In this and all similar connections throughout this memoir p_1 indicates the initial firing pressure in an explosion and p_2 the pressure of the cold gaseous products. Also, in all subsequent cases, the pressure and analytical data refer to the nitrogen-free gases.

‡ ' Phil. Trans.,' A, vol. 184, p. 161 (1893)

and acetylene on explosion with less than an equimolecular proportion of oxygen, with results which were published in 1892 and 1897.[*]

About this time also, Smithells and Ingle discovered large quantities of hydrogen and carbonic oxide in the interconal gases of aërated hydrocarbon flames, and concluded that "when the hydrocarbon first burns in the inner cone, there is a distribution of the limited supply of oxygen between the carbon and hydrogen, such, that either carbon monoxide and water or carbon monoxide, water and hydrogen are first formed,"[†] this being followed by the reversible water gas reaction $CO + OH_2 \rightleftharpoons CO_2 + H_2$ as the medium cooled down ; so that in the case of methane, for example, the probable sequence of changes might be considered as

$$\text{(i)} \quad CH_4 + O_2 = CO + H_2O + H_2 ; \quad \text{and}$$

$$\text{(ii)} \quad CO + OH_2 \rightleftharpoons CO_2 + H_2,$$
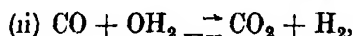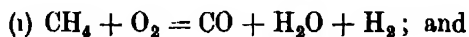
thus recalling the results previously obtained by Dalton.

As the outcome of all these experiments, the dogma of the preferential combustion of hydrogen, which had so long blocked progress, was finally overthrown , and in its place was revived the opposite idea, originally put forward by Kersten in 1861, that in hydrocarbon flames generally "*before any part of the hydrogen is burnt all the carbon is burnt to carbonic oxide*"[‡]

While doubtless, in the light of the then known facts, this may have seemed a satisfactory viewpoint, it was vigorously opposed by H E Armstrong, who considered it "unwise at present to infer that the oxidation of the hydrocarbon or the separation of carbon and also of hydrogen from them takes place in any one way " and eventually it has had to be abandoned.

The position at the end of last century was that, while the old idea of the preferential combustion of hydrogen had collapsed under the weight of contrary evidence, no other met with general acceptance. Albeit, as far back as 1874, H. E. Armstrong[§] had suggested another alternative—namely, that the successive stages in the burning of hydrocarbons involve the transient formation of unstable hydroxylated molecules which, according to circumstances, would decompose more or less rapidly under the influence of heat giving rise to simple intermediate products so that the process might be visualised as essentially

---

[*] ' J. Chem. Soc.,' vol. 61, p. 873 (1892) and vol. 71, p. 26 (1893).

[†] ' J. Chem Soc ,' vol. 61, p. 214 (1892)

[‡] ' J. Prakt. Chem.,' vol. 84, p. 290 (1861).

[§] " Manual of Organic Chemistry," pp. 216, 241 and 275, 1st ed. (1874).

one of " hydroxylation " ; but no attempt had been made to explore it experimentally, though, as will presently be seen, it ultimately turned out to be a potent key to the problem.

II.—DEVELOPMENT OF THE HYDROXYLATION THEORY, 1900–15

During 1898–1912, in conjunction with various collaborators,[*] at both Manchester and Leeds Universities, I was enabled to carry out a systematic investigation of the subject embracing both slow and explosive combustion right up to detonation, the results of which established the hydroxylation theory as a working hypothesis, and I will now summarise the new evidence which thus became available.

(A) *Evidence from Slow Combustion.*

Hitherto, save in one or two isolated instances, all the evidence had reference to explosive combustion, and practically nothing was known about the slow combustion of hydrocarbons ; yet obviously, if unstable oxygenated molecules of any kind are initially formed, the chances of detecting and isolating them would be far greater in slow combustion than at the high temperature and rapid changes in flames.

(1) *Experimental Methods* —Therefore, in this new attack upon the problem, it was decided to concentrate first of all upon the slow combustion of methane, ethane, ethylene and acetylene which, being the simplest cases, were most likely to yield results amenable to definite interpretation. Fortunately, also, a few preliminary experiments sufficed to dispel all *a priori* fears that the course of their oxidations might or would be masked or interfered with by secondary interactions between the primary products. For it was found that suitably proportioned hydrocarbon-oxygen mixtures will react with measurable velocities at temperatures much below those required for any appreciable reaction in

$$2H_2 + O_2, \quad 2CO + O_2 \text{ (moist)}, \quad CO + OH_2 \rightleftharpoons CO_2 + H_2,$$
$$CH_4 + OH_2, \text{ etc., media.}$$
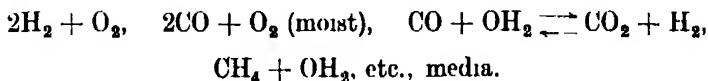
The two experimental methods adopted and which proved most effective

for the purpose in view, consisted in (i) sealing up hydrocarbon-oxygen mixtures, of suitably graded compositions in each case, at atmospheric temperature and pressure in cylindrical bulbs of borosilicate glass (usually *circa* 60 to 70 c.c. but sometimes about 500 c c. capacity) which were afterwards kept in an enclosure at some suitable constant temperature (usually between 300° and 350°) for various time periods, after which they were withdrawn and their contents completely analysed, and (ii) continually circulating selected hydrocarbon-oxygen (or air) mixtures at a constant rate in a closed system comprising (*a*) as " reaction-zone " a combustion tube packed with fragments of porous porcelain and kept uniformly at some pre-determined constant temperature between 400° and 500°, such as would ensure the gases reacting at a convenient speed, (*b*) suitable cooling and condensing arrangements to ensure rapid removal of soluble and condensable products, and (*c*) a manometer whereby pressure-time records could be obtained. It should be noticed that whereas in (i) reaction would usually occur at pressures somewhere between 2 and 2·2 atmospheres, according to the temperature, in (ii) it would usually start at a pressure somewhere between 400 and 600 mm , but steadily falling as time went on to somewhere between 50 and 80 per cent. of its original value, according to circumstances.*

(2) *General Features* —By such means, not only were new intermediate products detected and isolated, but also several other significant points were established.

Thus, for example, it was found (*inter alia*) that (i) all the four hydrocarbons examined undergo quiet flameless combustion producing oxides of carbon, steam, aldehydes and acids, *without any appearance whatever of carbon or hydrogen*, in circumstances precluding any appreciable oxidation of either hydrogen or carbonic oxide, (ii) methane is less readily so oxidised than the other three, (iii) while equimolecular hydrocarbon-oxygen mixtures were seemingly the most reactive, and the 2 : 1 (*i e.,* 2C_2H_6 + O_2) very nearly so,† an excess of oxygen beyond the equimolecular proportion always greatly retarded the reaction— this being a most remarkable feature of the results, to which special attention was directed—and (iv) in *all* cases aldehydic formation is prominent at an early stage in the oxidation, definite evidence being obtained

---

* This circulation method, so introduced, has since been widely adopted in principle, though with minor alterations, by subsequent investigators.

† Although at the time this seemed to be the case, there was little to choose between them, and the comparison was only a rough one ; recent more refined comparisons made both in my laboratories and others have shown the 2 : 1 hydrocarbon-oxygen mixture to be the most reactive.

in the case of ethylene of its preceding any formation of either steam or oxides of carbon, while with acetylene there was indication of the initial transient formation of an oxygenated molecule $C_2H_2O_2$ which immediately gave rise to carbonic oxide and formaldehyde before any steam appeared Another outstanding feature of all the oxidations was the persistent formation of carbon dioxide in circumstances which, while precluding its arising by the secondary oxidation of the monoxide, favoured its doing so by the oxidation of formic acid which was always present among the products.

(3) *Intermediate Aldehyde, etc , Products.*—The intermediate formation of the following aldehydes and acids was proved :—

(i) *Methane*—Formaldehyde and formic acid.

(ii) *Ethane*—Acet- and form-aldehydes and formic acid.

(iii) *Ethylene* -- Acet- and form-aldehydes and formic acid.

(iv) *Acetylene*—$C_2H_2O_2$ and its polymeride polyglycolide $(C_2H_2O_2)_x$, formaldehyde and formic acid.

All the foregoing features pointed unmistakably to an initial association of the hydrocarbon and oxygen producing in each case an oxygenated molecule which subsequently either decomposes or is further oxidised, according to circumstances ; indeed, in this respect the evidence was quite conclusive.

(4) *The Initial Product.*—A prime consideration was the nature of the initial oxygenated molecule , but here at first matters were so uncertain that for some time I halted between two opinions.   For while most of the facts accorded with H. E. Armstrong's view of the successive stages of hydroxylation, proof of an initial formation of either methyl alcohol in the case of methane, or of ethyl alcohol in that of ethane, although diligently sought for, was wanting.   This deficiency was mitigated, however, on our finding that (i) under our experimental conditions the alcohols in question were oxidised much faster than the corresponding hydrocarbons, and (ii) on oxidation with ozone at 100°, ethane yields successively ethyl alcohol, acetaldehyde and acetic acid,* thus :—

$$
\begin{array}{c}
\underset{\underset{CH_3}{|}}{CH_3} \longrightarrow \underset{\underset{CH_2OH}{|}}{CH_3} \longrightarrow \underset{\underset{H_2O + CH_3.CHO}{\overbrace{\qquad\qquad}}}{\overset{CH_3}{\underset{|}{CH(OH)_2}}} \longrightarrow CH_3.C\!\!\begin{array}{c}\nearrow OH\\ \searrow O\end{array}
\end{array}
$$
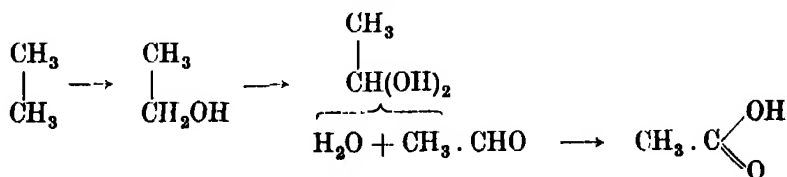
Finally the void has been filled by the decisive proof recently obtained by

* J. Drugman, ' J. Chem. Soc ,' vol. 89, p. 939 (1906).

Drs. D. M. Newitt and A. E. Haffner of the primary and plentiful formation of methyl alcohol in the direct pressure-oxidation of methane.*

In the case of ethylene, also, where the early appearance of acetaldehyde pointed to an initial formation of its very unstable isomeride vinyl alcohol, $H_2C : CH(OH)$, the evidence of hydroxylation was fairly clear; but in the case of acetylene, the simultaneous formation of carbonic oxide and formaldehyde, following the appearance of a polymeride of glyoxal, pointed to an initial formation of $C_2H_2O_2$, which the recent work of Kistiakowsky and Lenher in America† leaves no room for doubt was indeed glyoxal $H . C : O.$
$$H . C : O.$$
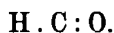
Viewing the evidence broadly and as a whole from the standpoint of organic chemistry, it seems difficult to explain the outstanding fact that in *all* the cases under consideration the hydrocarbon was oxidised to oxides of carbon, steam and aldehydes, *without any liberation of either carbon or hydrogen*, except on the supposition of such products having arisen by the thermal decomposition of some intermediate hydroxylated molecule or molecules, and to my mind this is a ruling consideration, irrespective of other and more direct evidence of "hydroxylation" which has recently come to light. For to me it seems almost inconceivable that the foregoing products could arise, *without any liberation of carbon or hydrogen* from the thermal decompositions of unhydroxylated molecules of (say) a "peroxide" type.

(5) *General Course of Oxidation* —We were thus led to visualise the slow oxidation of these hydrocarbons—subject to the aforementioned *proviso* about the initial stage in the case of acetylene—as essentially *involving* throughout a series of successive hydroxylation and thermal decompositions, mainly as follows :—

(a) $CH_4 \rightarrow CH_3OH$ · $CH_2(OH)_2$ $\qquad$ OH $\qquad$ OH

$\qquad$ $\overbrace{H_2O + H_2 : C : O}$ $\rightarrow$ $H . \overset{.}{C} : O$ $\rightarrow$ $HO . \overset{.}{C} : O$

$\qquad\qquad\qquad$ $\overbrace{H_2O + CO}$ $\quad$ $\overbrace{H_2O + CO_2}$

(b) $H_3C . CH_3 \rightarrow H_3C . CH_2OH$ · $H_3C . CH(OH)_2$ $\qquad$ OH $\quad$ OH

$\qquad$ $\overbrace{H_2O + H_3C . CHO}$ $\rightarrow$ $H_2C . \overset{.}{C} : O$

$\qquad\qquad\qquad$ $\overbrace{H_2O + CO + H_2 . C . O}$

$\qquad\qquad\qquad\qquad\qquad\qquad$ etc.
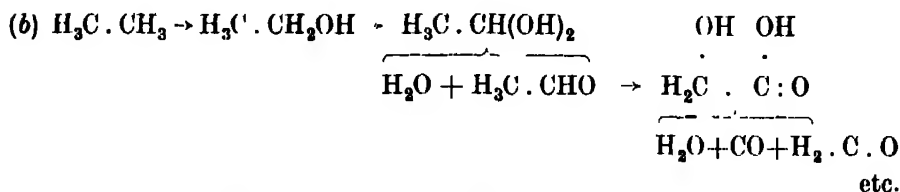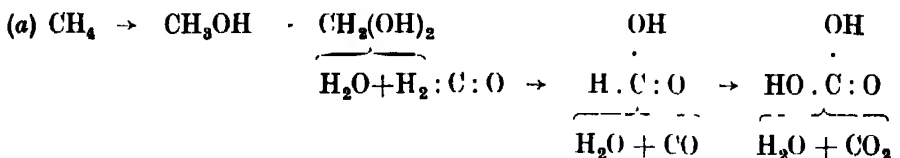
* 'Proc. Roy. Soc.,' A, vol. 134, p 591 (1932).
† 'J. Amer. Chem. Soc.,' vol. 52, p. 3785 (1930).

(c) $H_3C : CH_3 \rightarrow H_2C : CH(OH) \rightarrow (HO)CH : CH(OH)$

$$\underbrace{H_3C \quad CHO} \qquad \underbrace{2H_2 . C . O} \rightarrow \overset{OH}{\overset{\textstyle\cdot}{H . C . O}} \rightarrow \overset{OH}{\overset{\textstyle\cdot}{HO . C : O}}$$

$$\underbrace{H_2O + CO} \quad \underbrace{H_2O + CO_2}$$

(d) $HC . CH \rightarrow \underbrace{C_2H_2O_2}$

$$\underbrace{CO + H_2 : C \ O} \rightarrow \overset{OH}{\overset{\textstyle\cdot}{H \ C : O}} \rightarrow \overset{OH}{\overset{\textstyle\cdot}{HO \ C \ O}}$$

$$\underbrace{H_2O + CO} \qquad \underbrace{H_2O + CO_2}$$
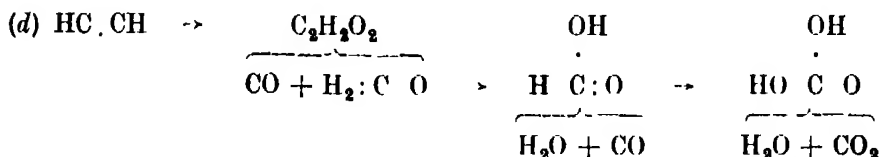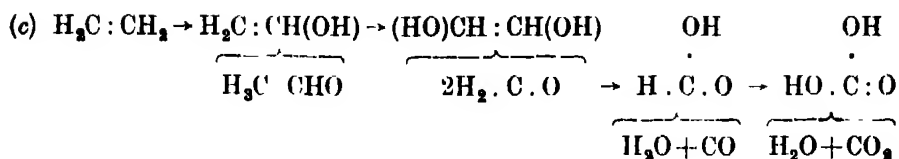
The requirements of the scheme were also satisfied by the results of " circulation " experiments upon the oxidations of ethyl alcohol, acetaldehyde and formaldehyde vapours, respectively, so that the cumulative effect of the evidence as a whole seemed irresistible. It also satisfactorily solved the enigma of the production of carbonic anhydride in circumstances precluding its having arisen through carbonic oxide

(B) *Extension of the Theory to Explosive Combustion*

(1) *General Considerations* —Although the conditions prevailing in hydrocarbon flames and explosions are obviously much more complex than those of slow combustion, it soon became evident that the main course of the chemical changes concerned therein may be satisfactorily interpreted on the supposition that the result of the initial encounters between hydrocarbon and oxygen is the same in both, namely, the formation of an " oxygenated " (and usually a " hydroxylated ") molecule Undoubtedly at the higher temperatures of flames, secondary thermal decompositions come into play at an earlier stage, and play a more conspicuous rôle, than in slow combustion, but there are the strongest reasons for believing that they do not precede the onslaught of the oxygen upon the hydrocarbon, but arise in consequence thereof Moreover, on both thermo-chemical and kinetic grounds, it seems probable that in explosive combustion, whenever the oxygen supply suffices, there will be a " non-stop " run through the *mon-hydroxy* to the *di-hydroxy* stage before thermal decomposition occurs , albeit, in default of such oxygen sufficiency some decomposition at the mon-hydroxy stage would probably occur.

In view of the complexities of flames and of the great difficulties in tracking by chemical analysis the course of events therein, the utmost that can be reasonably required of any acceptable theory about them is that it shall be consistent with facts, provide a rational view thereof, and in a general way

enable the main happenings in a particular case to be predicted. It can scarcely be expected that in *all* circumstances *all* the combustible molecules will be attacked by the oxygen in precisely the same way, for no such uniformity seems possible, and in any given circumstances a small percentage of abnormalities may arise.

What we are now concerned with, however, are the normal occurrences, and I will endeavour to demonstrate some of the more outstanding features of the explosive combustion of hydrocarbons and how they fall into line with, and can be explained by, the theory as already outlined.

(2) *Thermal Decompositions of Alcohols and Aldehydes.*—Before doing so, however, something must be said about how the various oxygenated molecules intermedially formed during slow combustion would or might be thermally decomposed in flames. Fortunately, information is available concerning the effects of heat upon some of them, though in places it is incomplete. Moreover, with one or two exceptions, their mode of decomposition varies with temperature, and therefore it is well to remember that there are wide differences in the mean temperatures of flames, especially according as the composition of the explosive medium concerned is near one or other of the limits of inflammability or far removed from both of them.

Alcohols.—At fairly low temperatures the vapours of primary alcohols decompose primarily into steam and an unsaturated hydrocarbon molecule or residue, but at higher temperatures into hydrogen and the corresponding aldehydes. In intermediate ranges both changes may occur simultaneously, and in flames they are always followed by secondary decompositions and/or hydrogenations, according to circumstances. Thus, for example, we might have :—

CH_3OH primarily resolved into (i) $H_2 : C + H_2O$ and/or (ii) $H_2 : C : O + H_2$ (— 9·3 K.C.Us.), followed by secondary resolutions of the $H_2 : C :$ residues ultimately into $C + H_2$ and of the $H_2 . C : O$ into $H_2 + CO$ (*vide* formaldehyde), and (in favourable circumstances) by hydrogenations of $H_2 . C .$ residues to CH_4.

C_2H_5OH primarily resolved into (i) $C_2H_4 + H_2O$ (+ 7 K.C.Us.) and/or (ii) $H_2 + CH_3 . CHO$ (— 10 K C.Us), followed by secondary resolutions of C_2H_4 into $C_2H_2 + H_2$ and/or $2C + 2H_2$, and of $CH_3 . CHO$ into $CH_4 + CO$ and/or $C + 2H_2 + CO$ (*vide* acetaldehyde).

Aldehydes -- At temperatures between about 400° and 600° (or thereabouts)

aldehyde vapours containing one — CHO group and one or more other carbon atoms are primarily resolved into CO and a saturated hydrocarbon; thus with *acetaldehyde* :—

$$\text{(i)} \quad CH_3 . CHO = CH_4 + CO \qquad + 2 \text{ K.C.Us}$$
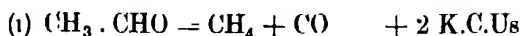
With further rising temperature, the breakdown becomes progressively more complete, tending at very high temperatures to some such final stage as —

$$\text{(ii)} \quad CH_3 CHO = C + 2H_2 + CO^* \qquad - 19 \ 8 \ K \ C \ Us$$
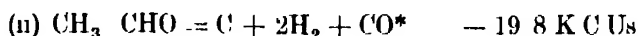
Formaldehyde.—It is important to note (i) that of all the oxygenated molecules known to be formed in slow combustion, the vapour of formaldehyde is pre-eminently that which at *all* temperatures in flames decomposes primarily into carbonic oxide and hydrogen (*plus* maybe, some trace of methane) without any separation of carbon whatever, thus .—

$$H_2 : C . O = H_2 + CO \ . \ -13 \cdot 5 \text{ K.C Us.}$$
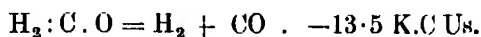
and (ii) that, since $H_2 C O$ is inherently a much stabler configuration than $H . C OH$, it would readily be formed therefrom, an important consideration in connection with the partial combustion of olefines

Glyoxal vapour probably would be resolved at *all* temperatures primarily into $CO + H_2 \cdot C : O$ and secondarily into $2CO + H_2$, also without any carbon deposition, but precise knowledge is wanting.

Consequently, whenever the explosion of a hydrocarbon-oxygen medium results in substantially nothing but carbonic oxide and hydrogen, without any carbon deposition, an intermediate formation of formaldehyde, or possibly glyoxal (or both), may reasonably be inferred.

Seeing that my own experiments have been mainly concerned with the explosive combustion of gaseous hydrocarbons whose molecules contain not more than four C-atoms, in what follows under this section I shall not go beyond them. Indeed, beyond the C_2-members conditions rapidly get so complex and incalculable that the difficulties of chemical interpretation soon

---

* The whole sequence may perhaps be pictured as follows :—

$$CH_3 . CHO \rightarrow CH_4 + CO \ \rightarrow \ CH_3 + H + CO \rightarrow$$

$$\rightarrow \ CH_2 + \begin{Bmatrix} 2H \\ H_2 \end{Bmatrix} + CO \rightarrow \ CH + \begin{Bmatrix} 3H \\ H_2 + H \end{Bmatrix} + CO \rightarrow : C \cdot + \begin{Bmatrix} 4H \\ 2H_2 \end{Bmatrix} + CO,$$
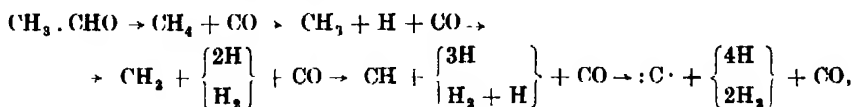
which would account for the spectrographic evidence of the presence of $.CH_3$, CH_2, CH and $:C:$ in such hydrocarbon flames; and so with other similar decompositions.

become insuperable, owing to the rapidly increasing number of possible secondary reactions masking the primary changes. Also, from a chemical point of view, most is to be learnt from explosions of media containing no more oxygen than the $C_nH_m + \frac{n}{2} O_2$ proportion; indeed between about the $C_nH_m + \frac{n+m}{2} O_2$ proportion and that required for complete combustion all that can be revealed by chemical analysis is the operation of the "water-gas reaction" $CO + OH_2 \rightleftharpoons CO_2 + H_2$ during the cooling period.

(3) *The Relative Combustibilities of Hydrocarbons and Hydrogen or Carbonic Oxide.*—The first general fact to lay hold of is that, as will be shown presently, the affinities of hydrocarbons so greatly exceed that of either hydrogen or carbonic oxide for oxygen that in explosions of hydrocarbon-hydrogen (or carbonic oxide)-oxygen media where oxygen is very deficient the hydrocarbon is burnt, as it were, preferentially. Moreover, the mutual affinity between oxygen and a hydrocarbon so overpowers any tendency for the latter to decompose thermally in flames that, whenever there is free oxygen at hand in the medium, a hydrocarbon molecule will always combine with it rather than decompose. Hence the old notion, which still haunts chemical literature, of a hydrocarbon molecule normally undergoing thermal decomposition before oxidation in homogeneous explosions must be abandoned. For such decomposition will only occur in regions where no oxygen is at hand for the hydrocarbon to lay hold of. This being so, it is wrong to speak of the preferential combustion of either hydrogen or carbon in hydrocarbon flames; on the contrary, the hydrocarbon molecule, though it may have been "activated," is still intact when it seizes and incorporates the oxygen, whether atomic or molecular.

Experiments.—(a) To illustrate these points, I cannot do better than repeat a very striking experiment, first made in my laboratory in 1905, in which a mixture of acetylene and electrolytic gas of the composition $C_2H_2 + O_2 + 2H_2$ was exploded in a sealed glass bulb at an initial pressure, p_1, of 534 mm. The oxygen has here the opportunity of dividing itself between the hydrocarbon and the hydrogen, according to its relative affinities for them; and anyone, not knowing beforehand what actually happens, would probably predict some, and possibly a large, formation of steam as well as a resolution of part of the acetylene into its elements. Yet on firing the mixture, as you will see, a sharp bluish flame fills the vessel, but neither carbon separates nor does any steam condense on cooling. In the experiment made in my laboratory, the

pressure of the products in the bulb after the explosion, p_2, was 653 mm., the ratio p_2/p_1 being 1·22, and their percentage composition was —

$$CO_2 = 0·2, \ CO = 39·8, \ CH_4 = 0·2, \ \text{and} \ H_2 = 59·8 \ \text{per cent} *$$

showing that the whole of the original acetylene had been burnt to carbonic oxide and hydrogen, leaving the original hydrogen quite intact, in accordance with the equation :—

$$C_2H_2 + O_2 + 2H_2 = 2CO + 3H_2.$$

Our recent photographic investigation of this explosion has shewn its flame to be a very compact layer of incandescent gas, about 1 cm. in thickness, with sharply defined front and no " after-burning," in which the duration of luminosity is 1·6 millisecs only. Indeed we have found this to be the most *intensively* burning of all mixtures of acetylene and electrolytic gas, in the sense of both time and space concentration of the chemical change

(b) To prove that such result is not due to any peculiarity of acetylene, I will next similarly explode a mixture of ethylene, hydrogen and oxygen of the composition $C_2H_4 + O_2 + H_2$ at an initial pressure, p_1, of 600 mm , when it will again be seen that neither carbon separates nor does any steam condense on cooling The pressure of the explosion products, p_2, will be *circa* 900 mm. $(p_2/p_1 = 1·49)$ and their composition —

$$CO_2 = 0·35, \ CO = 39·6, \ C_2H_2 = 1\ 25, \ CH_4 = 3·65, \ \text{and} \ H_2 = 55·15,*$$

showing that substantially the whole of the ethylene has been burnt to carbonic oxide and hydrogen, leaving the original hydrogen intact, as follows ·—

$$C_2H_4 + O_2 + H_2 = 2CO + 2H_2.$$
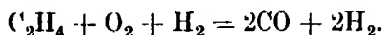
(c) Much the same result is obtained, as will now be shewn, by similarly exploding a mixture of propylene, hydrogen and oxygen corresponding with the formula $C_3H_6 + 1\frac{1}{2}O_2 + H_2$. When the experiment was made in my laboratory at an initial pressure of $p_1 = 497$ mm , the whole of the carbon was accounted for in the gaseous products and only 10 per cent of the original oxygen appeared as water, the details of experiment being as follows :—

$$p_1 = 497 \ \text{mm} , \ p_2 = 847·8 \ \text{mm.}, \ p_2/p_1 = 1·705.$$

Gaseous Products —$CO_2 - 1·10, \ CO = 43·5, \ C_nH_m = 0·8, \ CH_4 = 2·4$ and $H_2 = 52·2$ per cent.

---

* It may be pointed out that the very small percentages of carbon dioxide in these products is in itself a proof of practically no steam having been formed during the explosions.

Such data nearly correspond with the equation :—

$$C_3H_6 + 1{\cdot}5O_2 + H_2 = 3CO + 4H_2$$

I would commend these experiments to my fellow-workers in the field as being of the highest significance in connection with the theory of explosive combustion generally And I would also direct their attention to the photographic studies of " Explosions of Mixtures of Acetylene and Electrolytic Gas " recently published from my laboratories in which the subject is dealt with more fully than is possible here.*

(4) *Evidence from Explosions of Methane, Ethane, Ethylene and Acetylene with its own volume of Oxygen. Methane.*—It has already been mentioned that on explosion with its own volume of oxygen—or just half that required for complete combustion—methane yields principally carbonic oxide, hydrogen and steam, in conformity with the equation :—

$$CH_4 + O_2 = CO + H_2 + H_2O,$$

although a relatively small amount of carbon dioxide is produced owing to the " water-gas reaction " $CO + OH_2 \rightleftharpoons CO_2 + H_2$ coming into play during the cooling period.

Experiment —This will be demonstrated by firing the mixture in a sealed glass bulb at an initial pressure of 730 mm. There is a sharp bluish flame without any separation of carbon, but steam is seen to condense on cooling. If time permitted an examination of the cold gaseous products, their pressure would be found to be about 750 mm. $(p_2/p_1 = 1{\cdot}027)$ and their composition as follows :—

$$CO_2 = 6{\cdot}5, \ CO = 42{\cdot}0, \ H_2 = 50{\cdot}5, \text{ and } CH_4 = 1{\cdot}2 \text{ per cent}$$

Such result is just what might be predicted from the " hydroxylation " theory, supposing a " non-stop " run through the *mon-hydroxy* to the *di-hydroxy*-stage followed immediately by a complete breakdown of formaldehyde into carbonic oxide and hydrogen and subsequent " water gas reaction " during the cooling thus :—

$$CH_4 \longrightarrow CH_3OH \longrightarrow \underbrace{CH_2(OH)_2}_{\displaystyle H_2O + \underbrace{H_2:C.O}_{\displaystyle H_2 + CO}}$$

and $CO + H_2O \rightleftharpoons CO + H_2.$
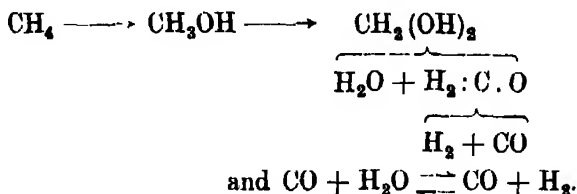
* W. A. Bone, R. P. Fraser and F. Lake, ' Proc. Roy. Soc.,' A, vol. 131, p. 1 (1931).

Although at atmospheric pressure, methane-oxygen mixtures containing less than 40 per cent. of oxygen are non-explosive, yet by sufficiently raising the pressure they become so down to the 70 CH_4/30 O_2 limit or thereabouts. My colleague, Dr. D. T. A. Townend, who recently investigated the matter very thoroughly, found the results of their explosions to agree well with the theory, breakdowns occurring at both the mono- and dihydroxy-stages.[*] When, for instance, a $1CH_4 + 3O_2$ mixture was exploded in a bomb at initial pressures of 6 and 10 atmospheres respectively, neither was any carbon deposited nor did more than about 2 per cent. of the original methane survive in the products, proving that the original oxygen had been initially distributed over much more than its own volume of the hydrocarbon, a conclusion which was also confirmed by his other experiments. Another point of importance was that the proportion of oxygen surviving as steam in the final products at corresponding pressures was greatest in the $5CH_4 + 2O_2$ and least with the $3CH_4 + 2O_2$ explosions, which latter seemed to mark a definite turning point. It may be pointed out, in passing, that such facts, while quite consistent with the hydroxylation point of view, are opposed to recent suppositions about an initial " peroxidation "

Ethane.—(a) " *Inflammation*." The explosion of an equimolecular mixture of ethane and oxygen was immediately seen to be crucial as between the former idea of a preferential burning of the carbon and the " hydroxylation " theory. For, whereas, according to the former, only carbonic oxide and hydrogen should result, thus :

$$C_2H_6 + O_2 = 2CO + 3H_2, \text{ with } p_2/p_1 = 2\cdot5,$$
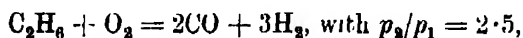
the " hydroxylation " theory would require the formation of methane, carbon, hydrogen, carbonic oxide and steam, with some carbon deposition and a p_2/p_1 ratio $< 2\cdot5$ as follows :—

$$C_2H_6 \longrightarrow C_2H_5OH \dashrightarrow CH_3 . CH(OH)_2$$
$$\overbrace{H_2O + CH_3 . CHO}$$
$$\begin{cases} CH_4 + CO \\ \quad\downarrow \\ C + 2H_2 + CO \end{cases}$$
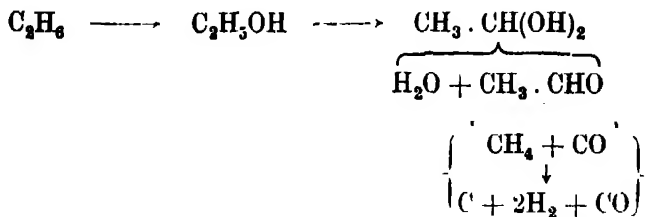
Experiment.—The experiment will now be repeated of firing a $C_2H_6 + O_2$ mixture in a sealed bulb at an initial pressure (p_1) of 730 mm. It will be observed

that a lurid yellowish-red flame fills the vessel, accompanied by a black cloud of carbon particles ; and a close inspection will reveal a considerable condensation of water also   If the bulb were opened, rinsed out with water, the presence of aldehydic products could be demonstrated by means of Schiff's reagent.   A detailed examination of the cold gaseous products would show their pressure to be some 50 per cent greater than that of the original mixtures ($p_2/p_1 = 1\cdot5$), and their composition as follows :—

$CO_2 = 4\cdot2$, $CO = 33\cdot5$, $C_nH_m = 2\cdot7$, $CH_4 = 11\cdot0$, and $H_2 = 48\cdot6$ per cent.,

about one-sixth of the original carbon having been deposited as such.   All this is in conformity with the hydroxylation theory.

It should be noted that in such an explosion the proportions of carbon separating during the reactions and of steam surviving in the products therein vary with the flame temperature and rate of cooling, both of which are influenced by the surface/volume ratio of the containing vessel   The smaller this ratio the hotter the flame and the slower the cooling, and, while the former favours carbon deposition, the latter allows of more unburning of the steam by carbon $C + OH_2 = CO + H_2$.   Indeed both the separation of carbon and the formation of steam and oxides of carbon in hydrocarbon explosions are secondary effects in the sense that all result from the thermal decomposition of the primary oxidation products.

Experiments showing Effects of Firing a $C_2H_6 + O_2$ Mixture in (a) a Long Tube, and (b) Globe of Equal Capacity

This point may be illustrated by firing the equimolecular $C_2H_6 + O_2$ mixture in two glass vessels having approximately the same volume but widely different surface areas.   For this purpose (a) a closed tube about 100 cm long and 2·5 cm internal diameter, and (b) a globe of 9·5 cm internal diameter have been selected   Both these vessels have the same volume (*circa* 500 c.c.), but the surface area of the tube is about 2·75 times greater than that of the globe. They have both been previously filled with the same $C_2H_6 + O_2$ mixture at a pressure of about 700 mm.   On now comparing the results of the two explosions, it is at once evident that more water and less carbon have survived in the tube than in the globe experiment   Indeed the p_2/p_1 ratio is about 1·45 only in the former as compared with about 1·75 in the latter, and an examination of the products would show that the difference is accounted for by a much greater survival of steam, aldehydes, acetylene and ethylene in

the tube experiment. Thus, in similar experiments (Table I) in my laboratories we found :—

Table I.—Inflammation of an Equimolecular Mixture of Ethane and Oxygen.

		(a) In long tube	(b) In large globe
p_1		701 mm.	685 mm
p_2		1018 ,,	1187 ,,
p_2/p_1		1 45	1 73

		(a) In long tube	(b) In large globe
	CO_2	4 20	3 40
Percentage	CO	31 80	36 10
composition	C_2H_2	5 00 ⎫	0 15
of gaseous	C_2H_4	2 65 ⎬ 7 65	
products	CH_4	8 85 ⎭	7 25
	H_2	44 50	53 05

	C	H_2	O_2	C	H_2	O_2
Original mixture	691	1041	354	678	1017	346
Gaseous products	643	738	220	558	805	255
Difference	51	303	134	120	212	91
Percentage difference as free carbon, H_2O and aldehyde	7 6	29	37 8	18	20	27 5

(b) *"Detonation."* It was the result of such an experiment as the foregoing which finally convinced the late H. B Dixon, who was following the investigation very closely, of the validity of the " hydroxylation " theory as applied to ordinary explosion flames and made him curious to know whether it could be extended to " detonation " also Accordingly, this being a crucial case, in 1905-06 both he and I quite independently succeeded in " detonating " an equimolecular mixture of ethane and oxygen in a leaden coil at initial pressures (p_1) between 1·5 and 1·75 atmospheres. In each case a little carbon was deposited, and steam condensed on cooling, while the ratio of the pressure of the cold gaseous products (p_2), which contained about 8 per cent. of methane, to that of the original mixture was from 1·9 to 2 0, and the rate of detonation was 2180 metres per second.

Unfortunately, it is not possible to repeat the experiment on a lecture table, so I must be content with reproducing the following particulars of our 1905-06 results which satisfied us both that, even under the extreme conditions of detonation, the main reactions had been as predicted by the theory, though

naturally there has been greater " shattering " of the $CH_3 . CHO$ molecules and subsequent unburning of steam by the separated carbon than in the milder initial phase of the explosion combustion.

Detonation of a $C_2H_6 + O_2$ Mixture.

	p_1.	p_2	p_2/p_1	Percentage composition of gaseous products				
				CO_2.	CO.	C_nH_m.	CH_4.	H_2
H. B D	mm 1363	mm 2725	2 00	0 75	38 55	1 10	8 15	51 10*
W A. B.	1180	2240	1 90	1·80	39 10	1 40	7 70	50 00

* Commenting upon this result in a private communication to me, dated March 8, 1927, Dixon said . " I think the main reaction taking place in the explosion wave is the one I understand you adopt --

$$C_2H_6 + O_2 = CH_3 CHO + H_2O$$
$$CH_3 . CHO = CH_4 + CO$$
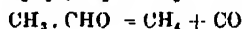
But I would not conclude the other reaction [he was referring to $C_2H_6 + O_2 = 2CO + 3H_2$] as impossible because this is the main one. I imagine the oxygen molecules running into the ethane molecules at all sorts of angles, with regard to the ' axis of orientation ' of the ethane and therefore possibly uniting with the two carbons straight You, I take it, consider the ethane to swallow the oxygen whole and then split up as in the above equation."

These results were also borne out by those, which I communicated to the Society in 1915,* of a series of $C_2H_6 + O_2$ explosions in bombs at various initial pressures between 10 and 40 atmospheres.

Ethylene and Acetylene.—The preferential burning of carbon which *apparently* occurs when either ethylene or acetylene is exploded with its own volume of oxygen, is just what would be predicted from the theory outlined herein as follows :—

$$\text{(i) } H_2C . CH_2 \longrightarrow [H_2C : CHOH] \longrightarrow \overset{H}{HO} . \overset{H}{C} . \overset{}{C} OH$$

$$2H_2 : C . O$$

$$2H_2 + 2CO$$

$$\text{(ii) } HC : CH \longrightarrow \overset{O}{HC} . \overset{O}{CH}$$

$$CO + H_2 : C : O$$

$$H_2 + CO$$
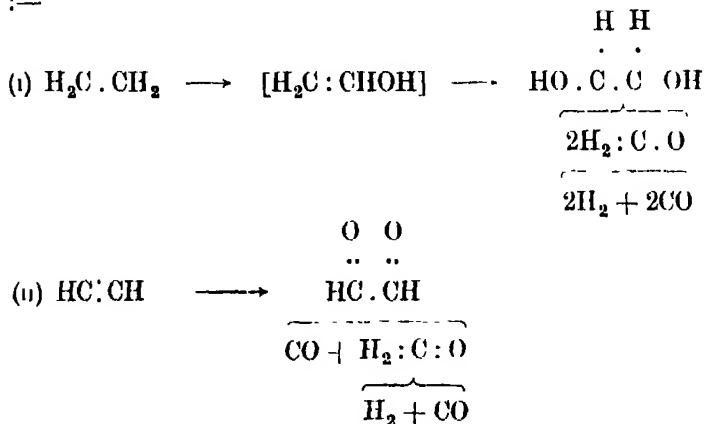
Experiments.—Each of these equimolecular (a) $C_2H_4 + O_2$ and (b) $C_2H_2 + O_2$ mixtures will now be fired in sealed bulbs at an initial pressure (p_1) of about 500 mm. It will be seen that in neither case is there even the slightest separation of carbon on condensation of steam on cooling, which is in striking contrast with what happened in the corresponding $C_2H_6 + O_2$ explosion. An investigation of the cold products would reveal in each case a large increase in the pressure—namely, (a) almost a doubling in the ethylene-, and (b) by nearly 50 per cent. in the acetylene-explosion—and their composition would be :—

- (a) $CO_2 = 0.5$, $CO = 50.0$, $H_2 = 47.5$, and $CH_4 = 2.0$ per cent. with $p_2/p_1 = 1.95$ *
- (b) $CO_2 = 0.75$, $CO = 67.0$, $H_2 = 30.75$, and $CH_4 = 1.5$ per cent. with $p_2/p_1 = 1.47$.*

(5) *Contrast between the Behaviours of Paraffins and the corresponding Olefines in Explosions of $C_nH_{2n+2} + \frac{n}{2}O_2$ and $C_nH_{2n} + \frac{n}{2}O_2$ Mixtures.*

I now come to a most arresting and significant feature of the experimental evidence to which I would invite the closest attention. It is that whereas all the gaseous hydrocarbons of the C_nH_{2n} series (i.e., ethylene, propylene, trimethylene and butylene) on explosion with a proportion of oxygen $C_nH_{2n} + \frac{n}{2}O_2$ always yield substantially carbonic oxide and hydrogen only without any separation of carbon or material steam formation—*as though* there had been a preferential burning of their carbon in accordance with the equation

$$C_nH_{2n} + \frac{n}{2}O_2 = nCO + H_2 —$$
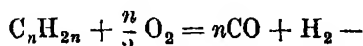
explosions of the corresponding members of the C_nH_{2n+2} or paraffin series (i.e., ethane, propane, and butane) with oxygen in the $C_nH_{2n+2} + \frac{n}{2}O_2$ proportion, all result in dense clouds of carbon, steam, methane and oxides of carbon, just as has already been seen in the case of the $C_2H_6 + O_2$ mixture.

Experiments.—In order further to demonstrate and drive home this crucial point, two series of sealed bulbs, (a) the one filled at 500 mm. with olefine $C_nH_{2n} + \frac{n}{2}O_2$ mixtures and (b) the other at 730 mm. with the corresponding

---

* Here again, it may be pointed out, the very small percentages of carbon dioxide in the products prove the practical non-formation of steam during the explosions.

paraffin $C_nH_{2n+2} + \frac{n}{2} O_2$ mixtures will now be exploded, the results being supplemented in Table II by full particulars of similar experiments carried out in my laboratories.

It is difficult to explain the very significant behaviours of such olefine $C_nH_{2n} + \frac{n}{2} O_2$ mixtures except by supposing that their explosions involve the successive eliminations of some oxygenated group or substance, such as formaldehyde, capable of rapidly decomposing in the flame into equal volumes of carbonic oxide and hydrogen without carbon separation or material steam-formation. In the case of propylene, for example, the process might perhaps be rather crudely pictured, somewhat as follows :—

$$CH_3 . CH \cdot CH_2 \;\rightarrow\; CH_3 . CH : CHOH \;\rightarrow\; \underset{\displaystyle \nearrow}{CH_2 . CH_2} + \underset{\overbrace{}}{H_2 \cdot C : O}$$

$$CO + H_2$$

$$CH_2 : CHOH \;\rightarrow\; CHOH \; CHOH$$

$$\underset{\overbrace{}}{2H_2 \cdot C : O}$$

$$2CO + 2H_2$$
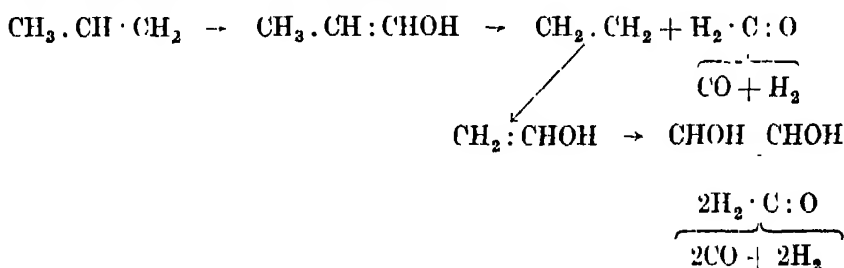
On the other hand, it is much harder to conceive of such result as following upon (say) an initial "peroxidation" of the propylene to $CH_3 . CH \; CH_2$ in the
$$\quad\quad\quad\quad\quad\quad\quad\quad\quad\quad | \;\;\; |$$
$$\quad\quad\quad\quad\quad\quad\quad\quad\quad\quad O - O$$
flame because of the probability of the latter decomposing immediately into

$$\underset{\overbrace{}}{CH_3 . CHO} \quad + \quad \underset{\overbrace{}}{H_2 : C : O}$$

$$\left\{ \begin{array}{c} CH_4 + CO \\ C + 2H_2 + CO \end{array} \right\} \quad\quad CO + H_2$$
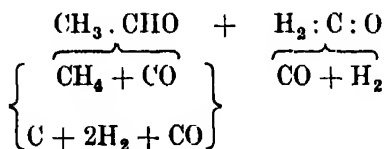
Indeed, the non-production of carbon, together with the negligibly small appearance of methane, in such explosions seems to me decisive as between the "hydroxylation" and "peroxidation" theories.

(6) *Explosions of Olefine-Oxygen Mixtures containing less Oxygen than*
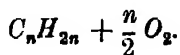
$$C_nH_{2n} + \frac{n}{2} O_2.$$

Another very remarkable feature of the explosion of olefine-oxygen mixtures is that whereas little or no steam is produced when the oxygen

Combustion of Hydrocarbons.

Table II.—Results of Comparative Explosions of $C_nH_{2n+2} + \frac{n}{2}O_2$ and $C_nH_{2n} + \frac{n}{2}O_2$ Mixtures.

Original mixture.	C$_2$H$_6$ + O$_2$			C$_3$H$_8$ + 1½O$_2$			C$_4$H$_{10}$ + 2O$_2$			C$_2$H$_4$ + O$_2$			C$_3$H$_6$ + 1½O$_2$			C$_4$H$_8$ + 2O$_2$ n-Butylene			Iso-butylene		
p_1 (mm)	698			592			617			545 3			563			479			438		
p_2 (mm)	1048			1028			1221			1053 5			1244			1169			982 5		
p_2/p_1	1 50			1 737			1 978			1 93			2 20			2 43			2 20		
Percentage composition CO$_2$	4 30			4 1			3 7			0 3			0 1			0 90			1 40		
CO	34 75			38 0			41 7			50 0			50 9			50 50			50·20		
C$_n$H$_m$	3 90			3 8			3 4			Nil			1 0			0 65			1 90		
CH$_4$	9 20			8 0			8 5			1 7			1 5			1 60			3 00		
H$_2$	47 85			46 1			42 7			48 0			46 5			46 35			43 5		
Units in—	C.	H$_2$.	O$_2$	C	H$_2$	O$_2$	C	H$_2$	O$_2$	C	H$_2$	O$_2$	C'	H$_2$	O$_2$	C	H$_2$	O$_2$	C'	H$_2$	O$_2$
Original mixture	698	1047	349	708	945	355	823	1028	411	545	545	272	675	675	338	630	630	322	384	384	292
Gaseous products	587	756	227	593	700	237	741	790	299	547	541	267	677	634	318	634	590	305	574	515	260
Differences	111	291	122	115	245	118	82	238	112	—	—	—	—	41	20	—	40	17	10	69	32
General features	Lurid yellow-red flame—copious carbon deposit and considerable steam formation. Aldehyde reaction of condensates									Sharp bluish flames No separation of carbon whatever (or barely visible) condensation of steam The products of the iso-butylene experiment contained formaldehyde											

present corresponds with the $C_nH_{2n} + \frac{n}{2}O_2$ proportion, more and more of it will appear in the cooled products if and as the oxygen-ratio is progressively diminished therefrom, even though progressively more carbon is simultaneously deposited.

Experiment —To illustrate this point, mixtures $3C_2H_4 + 2O_2$, $C_3H_6 + 1\frac{1}{4}O_2$ and $C_4H_8 + 1\frac{1}{2}O_2$ respectively, will now be exploded in sealed bulbs at initial pressures of *circa* 600 mm. It will be seen that in each case the flame is accompanied by a copious separation of carbon, and an inspection of the cooled products will enable the condensation of steam to be verified.

Particulars of similar experiments previously carried out in my laboratories are shown in Table III as follows.

Table III.—Results of Olefine-Oxygen Explosions.

Original mixture		$3C_2H_4 + 2O_2$			$C_3H_6 + 1\frac{1}{4}O_2$			$C_4H_8 + 1\frac{1}{2}O_2$		
p_1 (mm.)		562 3			682 0			574 0		
p_2 (mm.)		816 4			1213 0			1094 0		
p_2/p_1		1 45			1 78			1·90		
Percentage composition of gaseous products	CO_2	2 50			3 20			3 50		
	CO	37 20			43 05			41 40		
	C_nH_m	6 40			4 90			4 75		
	CH_4	6 50			6 90			7 55		
	H_2	47·40			41 95			42 80		
		C.	H_2.	O_2.	C.	H_2.	O_2.	C.	H_2.	O_2.
Units in original mixture		670	670	227	918	918	376	899	899	347
,, gaseous products		482	572	172	763	766	300	678	713	265
Differences		188	98	55	155	152	76	221	186	82
Percentage of original O_2 in condensed products as H_2O and aldehyde		24 4			20			23 6		

General features —Carbon deposited and steam condensed on cooling. Products gave distinct aldehydic reactions.

Again, such results are what might be anticipated from the hydroxylation theory; because, whenever the oxygen originally present in the medium is *less* than that which is requisite for the successive elimination as $H_2 : C : O$ of *all* the postulated · CH_2 units, there must finally be some breakdown of a CH : CHOH complex with production of both carbon and steam. And further experiment showing that in such circumstances the proportion of the

original oxygen surviving as steam in the cold products increases always with a growing oxygen-defect in the original medium strongly supported " hydroxylation."

In addition to these experiments which have been specifically referred to, during years 1900-15 we made a great many others, embracing every possible condition between slow combustion and detonation, and at initial pressures ranging from as low as one-third of an atmosphere up to as high as about 50 atmospheres, and the cumulative effect of all the evidence so obtained was so overwhelmingly in favour of the " hydroxylation " theory that the latter was left firmly established as a working theory in terms of which all the then known facts could be correlated and expressed   And, I still regard it as affording the best general view of the normal course of hydrocarbon combustion.

III.—Recent Developments—Hydroxylation *v* Peroxidation.

In recent years the number of workers in the field has so multiplied the world over that the task of reviewing the results of all their activities is impossible of accomplishment within the limits at my disposal, the utmost I can attempt is to deal with matters of outstanding interest only in so far as they bear upon the mechanism of hydrocarbon-combustion.

Most of the new evidence has been derived from experiments upon slow combustion, much of it relates to that of the hydrocarbons found in petrol, and, owing to their much greater inherent complexities, it is far less amenable to interpretation than that derived from the simpler gaseous hydrocarbons which have so far been considered

Another difficulty is that rarely have recent authors published sufficiently detailed analytical results for any sure conclusion being drawn concerning the interpretation of their work ; for it cannot be too strongly insisted that inferences drawn merely from observed pressure-time records and the like, without complete quantitative analytical data enabling " carbon-hydrogen-oxygen " balances to be made at a sufficient number of selected points so as to manifest what is actually going on in the medium, may be quite unreliable and misleading.   Also, conclusions which may be rightly drawn from a study of one particular case under narrowly restricted conditions must be carefully weighed and compared with well-authenticated facts previously observed in other cases of hydrocarbon combustion before being accepted as generally applicable to the problem as a whole.   Moreover, care needs to be

taken to discriminate between the *usual* and *unusual* courses of events observable in any particular circumstances so as to avoid mistaking the abnormal for the normal, or the secondary for the primary, happening. For, especially in regard to explosive combustion, it is always the balance of evidence that is of most importance

(i) *Formation of Aldehydes. Alcohols, etc* —In regard to recent experimental work on slow combustion, the intermediary formation of aldehydes has been so abundantly confirmed by numerous investigators that it is now part of the generally accepted facts which any valid theory must account for. Also, several observers have proved the intermediate formation of alcohols. Indeed, the tendency has been to increase rather than diminish the number of such recognisable intermediate products, with the result that some of the more recently devised " oxidation " schemes purporting to account for them appear fantastically complex.

(ii) *Induction and Reaction Periods in Slow Combustion.*—Another fact which has been commonly observed in cases of slow combustion at low temperatures is the occurrence of a well-defined " induction period," before any discernible reaction sets in, when a homogeneous hydrocarbon-oxygen mixture is introduced into an enclosure maintained at a constant temperature conducive to a measurable non-explosive oxidation without the medium being thereby self-heated.

The duration of such " induction period," which is marked by the absence of any perceptible pressure-change in the medium, depends in any particular case upon such factors as temperature, pressure and the proportion of hydrocarbon to oxygen in the medium ; but at the end of it the pressure begins to rise fairly rapidly, continuing to do so during the subsequent " reaction period," and finally becoming constant again at some higher level when oxidation has ceased. The duration of the " reaction-period " is similarly dependent upon the same factors as control the induction-period, and both are considerably shortened by the presence of quite small amounts of moisture, alcohols aldehydes, etc., in the system *

(iii) *Durations of Induction and Reaction Periods dependent upon Hydrocarbon Concentration.*—Several investigators have confirmed, what had first been observed more than 25 years ago, that the rate of reaction in such homo-

---

* Experimental proof of the statements contained in this paragraph was given in two recent papers from my laboratories relating to the slow combustion of ethane and methane, respectively, ' Proc. Roy. Soc ,' A, vol. 129, p. 434 (1930) and vol. 134, p. 578, to which readers are referred.

geneous slow combustion is mainly dependent upon the hydrocarbon (and not the oxygen) concentration. Thus, for example, H. W. Thompson and C. N. Hinshelwood have observed that with both methane and ethylene, as well as with benzene, the rate of reaction increases very rapidly with increasing hydrocarbon concentration, but is relatively little influenced by oxygen[*]; and in the case of acetylene, G. B. Kistiakowsky and S. Lenher found the rate of reaction proportional to the square of the hydrocarbon concentration but independent of that of the oxygen.[†] More recently still it has been proved in my laboratories, that with each of the first three members of the paraffin series (*i.e.*, methane, ethane and propane) both the shortest induction period and the fastest subsequent rate of oxidation are obtained with a 2 : 1 hydrocarbon ratio in the medium, as the following comparative data show :—

Table III.- Durations of (i) Induction, and (ii) Reaction Periods, respectively, in the Slow Combustion of Hydrocarbon-Oxygen Mixtures.

Hydrocarbon.	Methane				Ethane.				Propane			Ethylene.		
Temperature, °C	447°				316°				267°			300°		
Hydrocarbon-oxygen ratio	3 1	2.1	1·1	1 2	2 1	1 1	1.2		2·1	1.1	1.2	2 1	1:1	
Duration of— (i) Induction-period (mins) (ii) Reaction period (mins)	10 150	3 5 35	10 400	18 *	3 13	30 35	60 225		110 14	170 21	700 32	16 11	47 33	

* Too long to be measured

Note.—The methane oxygen and ethylene-oxygen mixtures used were *all* saturated with moisture at room temperature, but *all* the others (ethane and propane) were P_2O_5-dried

Also, with propane and ethylene, we have recently found small amounts of aldehydes, *but without any "peroxide,"* to be formed towards the end of the "induction period"

(iv) *The Initial Reaction—"Peroxidation"* or *"Hydroxylation"* ?—While none of the foregoing facts disagree with the "hydroxylation" theory—and there is now considerable consensus of opinion that, as was said 25 years ago, most probably the solution of the problem lies " in the assumption of an initial *association* of the hydrocarbon and oxygen forming an unstable ' oxygenated ' molecule,"—some investigators prefer to regard the *initial* association of the

[*] ' Proc. Roy. Soc.,' A, vol. 125, p. 277 (1929).

[†] ' J. Amer. Chem. Soc ,' vol. 52, p. 3785 (1930)

hydrocarbon and oxygen as resulting in a " peroxide " rather than a hydroxy-lated molecule, and we may now profitably consider this suggestion.

Alkyl peroxides (e.g , $CH_3 . O \ O . H$, and $CH_3 . O . O . CH_3$) which were first described by Baeyer and Villiger* in 1900–01 and have recently (1928–29) been re-investigated by Rieche and his collaborators,† are prepared by acting upon a di-alkyl sulphate with hydrogen peroxide in alkaline solution. At room temperature all but the di-methyl-peroxide are unstable endothermic liquids which readily explode upon being suddenly heated or subjected to " shock "; their explosive decomposition is very complex, producing mainly aldehydes and hydrogen together with hydrocarbons, alcohols, acids and steam. According to Reiche. an alkaline solution of methyl-hydrogen-peroxide decomposes in a complex manner with the principal formation of a formate and hydrogen.

The suggestion of an initial peroxidation of a hydrocarbon in combustion seems to have sprung from certain observations purporting to show the formation of substances of such a " peroxide " character when air is drawn through liquid hydrocarbons at fairly low temperatures ; and unstable " alkyl per-oxides " formed in such circumstances have been reported.

In 1927 experiments made at the Imperial College, under the direction of the late Professor H. L. Callendar, upon the slow combustion of hexane, and which resulted in the formation of valeraldehyde, acetaldehyde and formaldehyde in great profusion without any detectable initial hexyl alcohol $C_6H_{13} . OH$, led him to consider that the initial oxidation of a hydrocarbon in air more probably involves the formation of an alkyl peroxide " by the direct incorporation of the oxygen molecule in the hydrocarbon molecule and after direct collision," which subsequently decomposes giving rise to aldehydes and water thus :—

$$
\begin{array}{ccc}
\overset{H}{\overset{\cdot}{R} . C} \ \overset{H}{\overset{\cdot}{C} . R} + O . O = R \ \overset{H}{\overset{\cdot}{C}} \ \overset{H}{\overset{\cdot}{C}} . R & \text{or} & \overset{H}{\overset{\cdot}{R} . C} . O . O . \overset{H}{\overset{\cdot}{C}} . R, & \text{etc.}‡ \\
\underset{H}{\underset{\cdot}{} } \ \underset{H}{} & & \underset{H}{} \ \underset{H}{}
\end{array}
$$
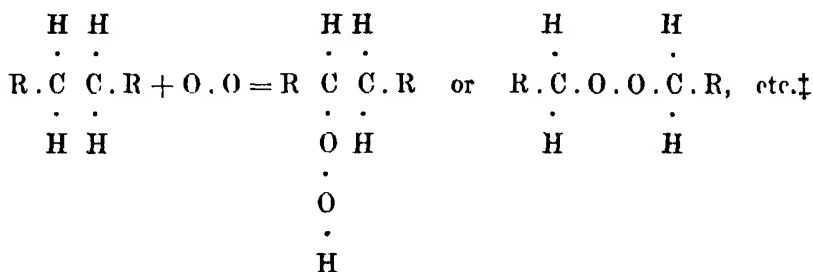
* ' Ber. deuts. chem. Ges.,' vol. 33, p. 3387 (1900), and vol. 34, p. 738 (1901).

† ' Ber. deuts. ohem. Ges.,' vol. 61, p. 951 (1928), vol. 62, p. 218 (1929), and vol. 62 , p. 2438 (1929).

‡ ' Engineering,' vol. 123, pp. 147, 182 and 210 (1927).

In a paper entitled " Kinetics of the Oxidation of Ethylene " communicated to the Society in 1930, H. W. Thompson and C. N Hinshelwood* steered a *via media* between the two views by suggesting that while " the first stage of the reaction is the formation of an unstable peroxide " . . . " there is no doubt that Bone's interpretation of the complete course of oxidation as a process of successive hydroxylation is essentially correct " and that " the two views are not incompatible, and a combination of them suggests an explanation of the facts " For (they continued) if the initial unstable $C_2H_4 : O_2$ " collides with another ethylene molecule the oxygen is shared and two hydroxylated molecules, *e.g.*, CHOH, are produced, which continue the chain. If,

$$\overset{..}{\underset{CH_2}{C}}\overset{\bullet}{H}$$

however, the peroxide collides with oxygen it may either be decomposed or oxidised completely to stable products which do not happen to be effective in continuing the chain."

Perhaps the latter view might be paraphrased thus. Although the *initial* collision between ethylene and oxygen molecules results in the unstable $C_2H_4 . O_2$, the easiest next step is the formation of two CHOH molecules by its

$$\overset{..}{CH_2}$$

collision with a second ethylene molecule, in which case the further oxidation proceeds by successive " hydroxylation ", and since collision with oxygen would result in stable products which would be ineffective in continuing the chain, the main course of oxidation *after* the first collision will be by successive hydroxylations.

Thus regarded, the two views would seem to be so nearly alike that, for most practical purposes, the difference between them is of no great moment ; nor need they be mutually exclusive, and might perhaps even be supplementary. Only a very rash or inexperienced person would nowadays assert that *every* fruitful collision between hydrocarbon and oxygen molecules (or oxygen-atoms) must always have precisely the same result as regards the particular " oxygenated " molecule initially produced And in any given circumstances there is always the *possibility* of the oxidation proceeding by *both* of two likely routes, albeit for the most part by one of them.

I shall endeavour to keep an open mind on the subject ; but, having during more than 30 years of continuous experimenting received so many satisfying proofs of an initial " hydroxylation," I should want some much more cogent

* 'Proc. Roy. Soc.,' A, vol. 125, p. 277 (1929).

and verifiable evidence of an *initial* " peroxidation " than has yet been forth-coming before I could accept it even in a supplementary sense.

In examining the kind of experimental evidence of it so far adduced, I am impressed mostly by its inadequacy and incompleteness. It is not enough to show, as some have done, that during the slow oxidation of a hydrocarbon products are formed capable of liberating iodine from a solution of potassium iodide, because, at least in presence of oxygen, aldehydes will do so. Nor would it suffice to prove the formation of some unidentified " peroxide " during the combustion process without also proving it to be the *initial* product and not merely a peroxide incidentally formed during the further oxidation of acetaldehyde or the like ; but so far such direct evidence has been wanting. From what I have read about their work, neither the late Professor Callendar in his experiments upon the slow combustion of hexane, nor yet Thompson and Hinshelwood in theirs upon ethylene, adduced any experimental proof of the actual presence of the " peroxide " whose *initial* formation they postulated. And although for some time past my collaborators and self have diligently sought for some such proof, up to now our search has been in vain, although in certain cases we have found some evidence of peroxidation supervening upon the first appearance of acetaldehyde, etc.

Perhaps the nearest approach to anything like direct evidence so far made is in some experiments by MM. P. Dumanois, P. Mordain-Monval and B. Quanquin* in which on passing mixtures of air with excess of the vapours of octane, heptane, hexane or pentane respectively through a tube maintained at 270°, a pale bluish flame accompanied by white acrid fumes was observed ; and on condensing the latter, two liquid layers separated, the lighter of which contained hydrocarbons, alcohols and aldehydes, while the heavier one contained an explosive oil with the properties of an alkyl peroxide which was not, however, identified.

(v) *Further Evidence from the Slow Combustion of Methane, Ethane, Propane and Ethylene* —(a) *Methane.*   If an initial " peroxidation " is general in hydro-carbon combustion, it must happen with methane, the simplest one of all. Accordingly, some time ago I decided to have its slow combustion thoroughly re-investigated in my laboratory, both at ordinary and under high pressures, with results which have been communicated to the Society† so recently that it

---

* ' C. R. Acad. Sci. Paris,' vol. 191, p. 299 (1930) , ' Chim et Ind.,' vol 27, p. 771 (1932).

† W. A. Bone and R. E. Allum, ' Proc Roy. Soc ,' A, vol. 134, p. 578 (1932), and D M. Newitt and A. E. Haffner, *ibid* p. 591.

scarcely seems necessary to recall them now. Suffice it to say that, while no sign whatever of " peroxidation " could be detected at any stage of the process, substantial quantities of methyl alcohol and formaldehyde were isolated in the pressure-oxidation, and the most reactive methane-oxygen mixture was found to be that having the alcohol-forming $2CH_4 + O_2$ composition I can scarcely conceive of any stronger evidence of " hydroxylation," or that can be less gainsaid.

(*b*) *Ethane* —With reference to ethane, the next higher paraffin, I need only recall how we had previously shown in similar experiments that at 316° and atmospheric pressure the alcohol-forming $2C_2H_6 + O_2$ mixture is much more reactive than the equimolecular one ; and although inconsiderable amounts of some " peroxide " were undoubtedly formed as a concomitant of acetaldehyde, no evidence was forthcoming of any earlier " peroxide " occurrence. Indeed the experiments made me wonder whether other workers may not have confused peroxidation of intermedially formed aldehydes with that of the original hydrocarbon. In this connection it may not be out of place to quote Messrs A C Egerton and S. F Gates, who, in discussing the action of " anti-knocks " in petrol-air explosions, said . " If the hydrocarbon by encounter with oxygen may form peroxides, it would seem that they should be formed still more favourably by aldehydes, and this might be a reason for the ease with which aldehydes can be ignited, and for the great effect of anti-knocks upon them."

My colleague, Dr D M Newitt, is now completing a most enlightening study of the direct pressure-oxidation of ethane during which he has isolated large quantities of ethyl and methyl alcohols, acet- and form-aldehydes without finding any trace of peroxide Thus in one experiment at 275° and 100 atmospheres, with a mixture initially containing 90 ethane and 10 oxygen, no less than 36·5 per cent. of the carbon of the ethane burnt has been isolated as ethyl alcohol, another 30 per cent. of it as methyl alcohol, 7·5 per cent. more as acetaldehyde and 0·5 per cent more as formaldehyde—or altogether nearly 75 per cent of it as such intermediate products—without any sign whatever of any " peroxide " accompanying them A very remarkable feature was the isolation of so much methyl alcohol, whose formation seems probably due to the thermal decomposition $CH_2(OH)$ $CHO = CO + CH_3OH$ And, indeed, so far from supporting " peroxidation," the experiment has proved almost *quantitatively* the following complete hydroxylation scheme :—

$$
\begin{array}{cc}
CH_3 & CH_3 \\
| \rightarrow | \\
CH_3 & CH_2OH
\end{array}
\qquad
\begin{array}{c}
CH_3 \\
\rightarrow | \\
CH(OH)_2
\end{array}
\qquad OH \quad H
$$

$$
H_2O + CO + CH_3CHO \rightarrow H_2 \cdot C \ . \ C : O \rightarrow
$$

$$
CO + CH_3OH
$$

$$
\left\{
\begin{array}{c}
OH \ . \ OH \\
\cdot \quad \cdot \\
H_2 : C \ . \ C \cdot O \\
CO + H_2O + H_2 : C . O \rightarrow
\end{array}
\right.
\quad
\begin{array}{c}
HO \\
{\Large >}C : O \rightarrow \\
H
\end{array}
\quad
\begin{array}{c}
HO \\
{\Large >}C \quad O \\
HO
\end{array}
$$

$$
H_2O + CO \qquad H_2O + CO_2
$$
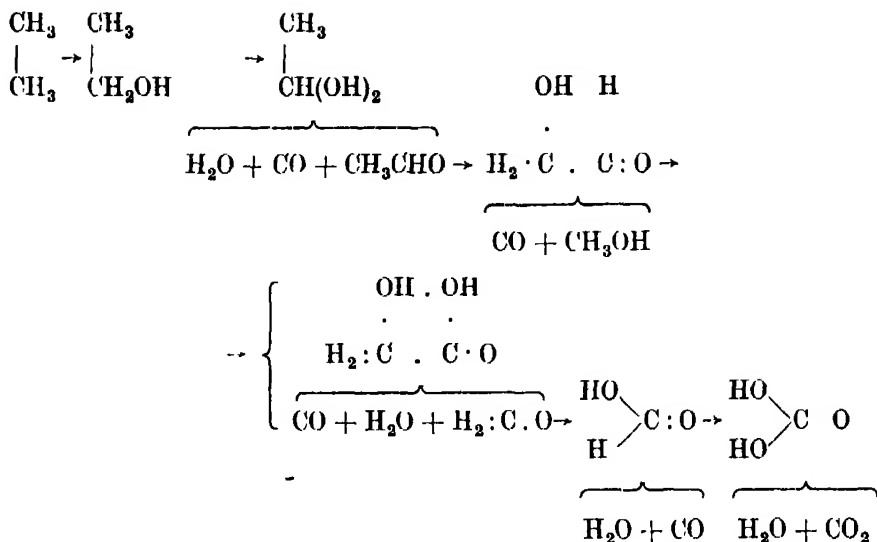
Surely no more conclusive experimental proof of "hydroxylation" could be desired

(c) *Propane* —In the course of experiments now proceeding on the slow oxidation of propane at 267°, the alcohol-forming $(2C_3H_8 + O_2)$ has again proved itself more reactive than the equimolecular $(C_3H_8 + O_2)$ mixture; moreover, definite proof has been forthcoming that, although three-quarters way through the "induction period" small amounts of aldehydes are present, no trace of "peroxide" can be simultaneously detected in the medium, notwithstanding that the test for "peroxide" is (if anything) rather more sensitive than that for aldehyde. This proves that the formation of aldehydes *precedes* that of any peroxide.

(d) *Ethylene* —In similar experiments which we are making upon the slow oxidation of ethylene at 300° it has been proved that a $2C_2H_4 + O_2$ is much more reactive than a $C_2H_4 + O_2$ and that the formation of aldehydes, which can be observed towards the end of the induction period, precedes that of peroxides

Hitherto my experiments have been confined to gaseous hydrocarbons, that is, up to and including butane and butylenes, because I have always felt that the increasing complexities met with in ascending the series further would impose well-nigh insuperable difficulties in interpreting the results; and I am still of the opinion that, from a chemical point of view, at present there is little or no advantage in going higher.

IV.—SUMMARY AND CONCLUSIONS.

Having thus set forth the principal experimental facts and theories of hydro-carbon-combustion, so far as I am able to judge the present position of matters seems to be as follows :—

(i) While there is general agreement that, both in slow and explosive com-bustion, there is an initial association of the hydrocarbon and oxygen forming an oxygenated molecule, opinions have recently differed as to whether it is " hydroxylation " or " peroxidation."

(ii) The " hydroxylation " theory is supported by such a cumulative weight of evidence, both qualitative and quantitative, and is capable of explaining and correlating so vast a majority of the known facts, as regards both slow and explosive combustion, that it may be regarded as having thereby proved its credentials as a working theory of the normal course of hydrocarbon com-bustion. In certain typical cases of slow combustion, not only have all its postulated intermediate hydroxylated molecules (or their known thermal decomponents) been actually isolated, many of them in considerable amounts, but in one case (ethane) the proof has been quantitative, including no less than a 36 per cent. yield of the initial product ethyl-alcohol, without any trace of " peroxide." With methane, also, hydroxylated products, including methyl alcohol, have been isolated and estimated without any sign whatever of " peroxidation ", and even in cases where traces of peroxide have been observed they have resulted not from the *initial* but from *later* happenings, namely, only *after* (and not *before*) the appearance of aldehydes. From the kinetic point of view, also, the evidence is all in favour of an *initial* mon-hydroxylation. Finally, some of the characteristic phenomena of explosive combustion, which I have recalled and demonstrated, can best be explained by " hydroxylation " and seem incompatible with " peroxidation."

(iii) On the other hand, when closely examined, the credentials of " per-oxidation " appear doubtful. For, so far as I know, in no case of slow com-bustion has the postulated initial " peroxidation " yet been proved by the actual isolation of the particular peroxide involved. And, even in cases where the presence of small (usually inconsiderable) quantities of peroxides has been proved, no conclusive evidence of identification has been forthcoming. Also, sufficient care has not always been taken to avoid confusing an incidental " peroxidation " of intermedially formed aldehydes with an *initial* " peroxida-tion " of the original hydrocarbons ; for in certain cases recently examined, *e.g.,* ethylene, ethane and propane, the formation of aldehydes definitely precedes

that of any peroxide. Finally, the idea of an initial " peroxidation " seems countered by certain facts relating to explosive combustion, and notably by the results of exploding $C_nH_{2n} + \frac{n}{2}O_2$ mixtures at ordinary pressure, and of methane-oxygen mixtures intermediate between $5CH_4 + 2O_2$ and $CH_4 + O_2$ at high pressures Therefore, while admitting the likelihood of incidental " peroxidation " of intermedially formed aldehydes and the possibility of an initial " peroxidation " of a small minority of hydrocarbon molecules concomitantly with the " hydroxylation " of the remainder, as yet the preamble of the case should be regarded as experimentally " not proven "

(iv) In any case, even if eventually proved valid in particular cases or circumstances, " peroxidation " can scarcely be regarded as being more than supplementary to " hydroxylation," nor " peroxide " as more than a side-product. In other words, it might possibly afford an explanation of " knock " as an abnormal feature of hydrocarbon-air explosions but scarcely of the normal course of oxidation therein

In closing this review, two further points should be stressed One is the need of further investigation of the " induction period " in hydrocarbon-combustion which, though most easily observed in slow combustion, can also be detected in explosive combustion when the igniting source (*e g*, spark) is below a certain intensity Next to nothing is known for certain about its meaning, and so obvious a void in our knowledge needs filling up. The other is the danger of concentrating attention too much upon slow combustion to the comparative exclusion of explosive combustion and detonation. For it is only by taking all conditions into account comprehensively that a true view of the subject can be gained.

Velocity of Propagation of Light in Vacuo in a Transverse Magnetic Field.

By C. Coleridge Farr, F.R.S , and C. J. Banwell, B.Sc.

[Plate 13.]

This investigation was undertaken to find, within the limits of sensitivity of the apparatus used, the effect of a transverse magnetic field on the velocity of propagation of light *in vacuo*. An interference method was used, one of the two rays from the first mirror of a Jamin refractometer being passed through a strong magnetic field, while the other ray passed through a weaker field. The two rays were recombined at the second mirror, and the resulting interference bands viewed with a microscope lens combination. Any relative change in the velocities of the two rays would be observed as a movement of the bands.

As far as the limited facilities of this part of the world have enabled the authors to ascertain there has not been a very great deal of experimental work done on this aspect of the relations between optical and magnetic phenomena.

Theoretical investigations have been carried out by Nordstrom and Weyl to relate gravitational and other fields of force, by Larmor who discusses the alterations necessary in the velocity of light to bring gravitation or any other field of force into the electrodynamic scheme, and by Whittaker who ascribes magnetic properties to the photon and has treated the subject from a different aspect.* Watson has endeavoured to determine experimentally the effect (if any) of a transverse magnetic field on the velocity. In the present work, which was in progress at the time when Watson's paper was published, a different experimental method is adopted and the apparatus developed carries the same conclusion as he obtained, but to twenty times the sensitiveness which he ascribed to his results.

Description of Apparatus.

Optical System.—Fig. 1 is a general plan of the apparatus, being a horizontal section through the gaps of the magnets C, D and E. Light from the source L falls on the hemi-cylindrical lens *p*, and then on to the first mirror A of the refractometer. Here, by reflection at the back and front surfaces of A the

---

* 'Proc. Roy. Soc.' A., vol. 125, p. 345 (1929).

light is divided into two rays 1 and 2, shown by the dotted lines. Of these rays 1 passes through the strong field in the gaps, while the other ray 2 passes in front of the gaps in the weaker leakage field. The two rays then fall on the second mirror B where they are recombined by reflection at the back and front surfaces. Mirror B is capable of fine adjustment about vertical and horizontal axes, and when B is accurately parallel with A interference bands appear, and the image of these bands formed by the lens q is viewed with the microscope M, which has a scale in its eyepiece. M had a nominal magnification of some
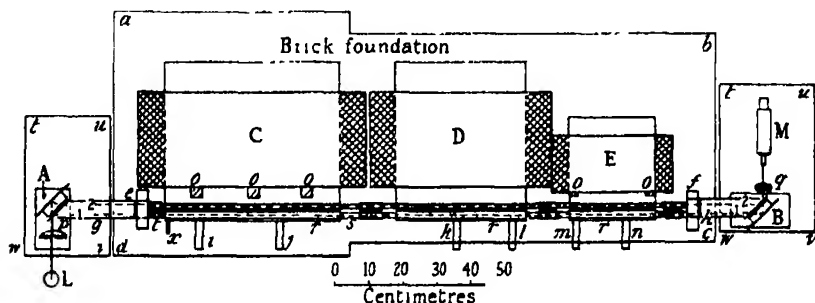
FIG. 1.

sixty times, giving a distance of five scale divisions between adjacent black bands.

On account of the fact that the ray which does not actually pass through the gap in the magnet poles still passes through the leakage fringing field, the arrangement was not ideal, but had points of convenience which outweighed for the time being its disadvantages.

The mirrors were supported on marble slabs t, u, v, w, which were attached to wooden supports bolted to the heavy brick foundation a, b, c, d.

The source of light L was either a mercury vapour lamp or a frosted incandescent lamp. The incandescent lamp was generally used for the actual observation as it gave somewhat clearer bands. The band system consists, in the case of the mercury vapour light, of many black bands, and with white light, of two black bands with 5 to 6 coloured bands of increasingly poor visibility on each side of these black bands. As the black bands are more distinct and stand out well against the general bright background, one of them is chosen for observation.

Along the length of the three magnets, the paths of both rays were enclosed in an air-tight casing r, fig. 1. This air-tight system was closed at each end by optically plane parallel faced glass plates (the compensating glasses from

an ordinary Jamin interferometer) mounted in heavy lead blocks *e* and *f*, fig. 1. These blocks were connected to the remainder of the vacuum system on the magnets by means of short flexible rubber tubes, in order to avoid all possibility of movements of the magnets or pole pieces distorting the glass plates, and thus causing spurious band movements. In order to prevent air currents in the remaining unenclosed parts of the ray paths from causing stray movements of the bands, these parts were enclosed in sheet brass boxes *g* and *h*, which were supported on the blocks *e* and *f*, and reached to within approximately 2 mm. of the faces of the mirrors.

In order to prevent reflection of light at oblique incidence from the faces of the gaps as far as possible, these surfaces were lampblacked, as were other internal surfaces.

By tests with a Nicol prism the light was found to be very largely polarised in a vertical plane, although with the Nicol set for minimum brightness, the bands were still faintly visible.

Sensitivity.—The band movement caused by a relative change in velocity of the two rays 1 and 2 is given by

$$\frac{v_1 - v_2}{v_1} = \frac{n\lambda}{l},$$

where

v_1 is the velocity in one path,

v_2 is the velocity in the other,

λ is the wave-length of the light used,

l is the length of one path,

n is the number of bands which pass a point in the field of view.

For the purposes of the present calculation, l is taken as the total length of the magnetic field, which is 112·5 cm.

Owing to the lack of sharpness of the bands the smallest value of n which can be observed with certainty is about 0·1.

Taking λ as $5460\cdot742 \times 10^{-8}$ cm. we find from the above values,

this being the smallest relative change in velocity which will give an observable shift of the bands, and corresponding to a change in velocity of 14 metres per second.

Magnets.—The field is produced by three electro-magnets C, D and E,

through the gaps of which ray 2 passes. Figs. 2 and 3 give respectively front and end elevations of magnet C, which may be taken as typical.
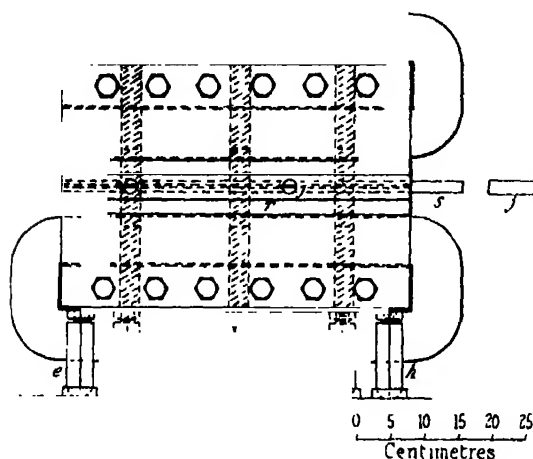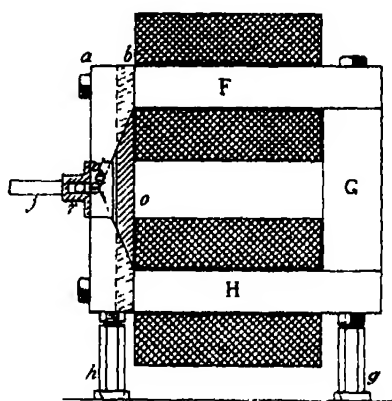
Fig. 2.   Fig. 3.

The magnetic circuit consists of three mild-steel slabs, F, G and H, bolted together as shown, fig. 3, the wrought iron pole pieces, one of which is lettered a, b, c, d, and the air-gap which is $\frac{1}{8}$-inch wide. The windings are shown cross-hatched in figs. 1 and 3 and at K and L in fig. 2. In order to prevent the attractive forces across the gap from causing movements of the poles, brass bars o, figs. 1 and 3, which are shown diagonally hatched, were let into the pole pieces, and screwed to them. The pole pieces of D were braced in a slightly different manner. This bracing reduced the movements of the poles to less than 0·001 mm

Measurement of Field.—In order to provide access to the gap for the insertion of a fluxmeter search-coil, to obtain field measurements after the apparatus had been set up, tubes i, j, k, l, m, n, fig. 1, were soldered into the brass casting r. The field in, and just outside the gap in the path of ray 1, was measured at each tube, and the mean effective field calculated as follows. The values of the field in and outside the gap at each point assumed to remain constant throughout half the length of that magnet, and the difference between the fields at each point was assumed to be the effective field. Calling H_1 and H_2 the fields in and outside the gap at each point, and l the length of gap over which the field is assumed to be uniform, then H the mean effective field is given by

$$\bar{H} = \frac{\Sigma (H_1 - H_2) l}{\Sigma l},$$

$l =$ total length of all the magnets.

The value of $\overline{\text{H}}$ thus obtained, at the same current through the windings as was used in the actual experiment was 17,992 gauss. The leakage field was of the order of 3000 gauss.

Current Supply.—Current was taken from the 230-volt D.C. main, applied directly to the magnet windings, all in series, without any additional resistance. The current thus obtained varied from 65 to 70 amperes, but as the iron of the magnets was not far from saturation with this current, the variation in current did not cause a very large variation in the field. In order to prevent sparking at the switch due to the inductance of the windings, two large electrolytic rectifiers in series were connected across the ends of the magnet windings and also the switch used had both carbon and metallic contacts, so arranged that the arc formed took place between the carbon contacts.

The sense of the windings was so arranged that there was only one polarity at the top and likewise at the bottom.

Although as far as the field was concerned a narrower gap would have been desirable, it was found that a gap much below 3 mm. caused a serious blurring of the bands, which increased the minimum shift which could be observed. The 3 mm. gap had scarcely any effect on the appearance of the bands.

Vacuum.—Each gap was enclosed behind and in front, along its entire length with an airtight brass casing screwed and soldered to the pole pieces. The front casing was a brass casting *r*, figs. 1, 2 and 3, projecting sufficiently from the front of the pole pieces to accommodate the ray 1 within the enclosure. The ends of each casing were closed with brass plates into which were soldered brass tubes, shown by the two circles in fig. 3, the axis of one tube being along the centre-line of the gaps, and that of the other along the axis of ray 1. Such tubes can be seen at *s* and *t* in figs. 1 and 2. The tubes of adjacent magnets and corresponding tubes on the blocks *e* and *t* were joined with rubber tubing, thus making the whole enclosure a continuous system.

The apparatus was evacuated by means of charcoal in liquid air, and a mercury condensation pump backed by a Hyvac pump. The charcoal tubes were connected to the apparatus by glass tubes through rubber corks in the tubes *j*, *k* and *n*. The condensation pump was connected by means of a wide bore rubber tube to the tube *x* at the left-hand end of the casing on magnet C. In order to follow the progress of the evacuation a discharge tube was attached to the front casing of magnet E, between *m* and *n*. The procedure during exhaustion was to bake out the three charcoal tubes in electric furnaces at about 400° C. with the Hyvac pump running, and after the tubes had cooled sufficiently they were immersed in liquid air. After some 20 minutes the

pressure was down to a point where a bright green coloured shimmer appeared on the walls of the discharge tube, and little or no glow inside (*i.e.*, about soft X-ray condition). Subsequent calibration with a MacLeod gauge showed this appearance to correspond to a pressure of approximately 0·005 mm., although the pressure from experiment to experiment varied a little.

Foundation and Supports.—All the apparatus with the exception of the source of light was mounted on the brick and concrete foundation shown in fig. 1, and in Plate 13. This foundation was 102·5 cm. high, and its other dimensions as in fig. 1. The magnets were supported on adjustable brass legs, *e, f, g, h*, fig. 2, which rested in brass cups. The height and level of each magnet could thus be varied to bring the gaps into line.

The tables supporting the mirrors and microscope were supported on wooden frameworks bolted to the ends of the brick foundation.

In order to prevent lateral movements of the magnets as far as possible, iron straps were bolted across between adjacent pole pieces at top and bottom, as in the photograph, Plate 13.

The source of light L was supported on a separate stand, which did not touch the table supporting A at any point.

The entire apparatus excepting the switch and rectifiers was enclosed in a wooden framework over which was stretched black cloth, the enclosure being large enough to accommodate an observer who could thus take readings of the bands in comparative darkness, without being dazzled by the arc formed on opening the switch.

The photograph corresponds almost to an elevation view of fig. 1. The mercury vapour lamp is on its stand at the left, and the three liquid air containers are in place enclosing the charcoal tubes. The mercury condensation pump and backing pump can be seen on the floor at the base of the brickwork. One of the cloth sides of the enclosure has been removed in order to obtain the photograph. The T-shaped discharge tube can be seen standing up from the casing of E immediately above the third liquid air container from the left.

Spurious Effects.—A very small movement of the tables supporting the mirrors was sufficient to cause an appreciable movement of the bands, and it was necessary to ensure that no mechanical effect due to the field caused such a movement. These effects may be divided into :—

(*a*) movements of the magnets and windings due to stray fields ; and

(*b*) forces acting on iron parts of the mirror supports and tables due to the stray field.

Effects due to (*a*) were avoided as far as possible by taking care that no direct mechanical connection existed between parts of the magnet system and the tables supporting the mirrors. Some vibration of the magnets took place on breaking the circuit, and this was transmitted via the foundation to the mirrors causing the bands to dither slightly and become blurred, and as this could not readily be prevented, its effect on the observations was eliminated by either entirely ignoring movements at the opening of the circuit, or by noting whether the bands settled in a new position after the disturbance had died away.

Effects due to (*b*) were avoided by using only brass and lead for the metal parts associated with the tables, and replacing all steel parts in the mirror mountings by brass.

There is a possibility that magneto-strictive effects in the small quantity of residual oxygen in the apparatus may cause a sufficient difference of pressure of this gas between the paths of the two rays to shift the bands, but calculation shows that even with oxygen at atmospheric pressure, the effect would be less than one-fifth of the smallest observable band movement.

Methods of Observation.—When the highest possible vacuum had been reached, the edge of one black band was lined up with a graduation in the eyepiece scale of the microscope, and the observer signalled to an assistant at the switch. The switch was kept closed for about 5 seconds, this being sufficient time for the current to approach its final value. With observations lasting as long as this it was possible to take ten to twelve readings before the windings became very warm.

As it was evident from preliminary experiments that the effect would be very small, it was felt desirable to secure a number of independent readings by separate trained observers. Several others in addition to three observers who had done special work with the bands, were given two to three readings each, and these results were later tabulated. Owing to the blurred nature of the bands and the extreme smallness of the movement, previous knowledge of the direction of movement to be expected might influence the decision of an observer, and for this reason none of the observers was told the decisions of the others until the experiment was finished.

Nine observers took independent readings, in three separate experiments, attention being directed to the behaviour of the bands on closing the circuit: altogether 19 observations were obtained in this way. Of the 19 readings 8 implied an increase in velocity of the ray through the gaps with the field on,

5 a decrease, 4 no effect, and 2 were doubtful.   All agreed that the movement, if any, was very small.

The effect is evidently smaller than the minimum observable accurately with the present apparatus, and the conclusion that can be drawn is that whilst there is a possibility of an increase in velocity such apparent increase may be spurious.

Subsequent readings taken with a Nicol prism between p and A, set for either maximum or minimum brightness, showed no alteration either in the brightness or position of the bands, when the current was switched on.   Thus whether the direction of vibration of the light is in or at right angles to the direction of the field, makes no difference to the effect.

Conclusion.

The result of the investigation is then that in a transverse magnetic field of effective value 17,992 gauss, the change in velocity of light *in vacuo* is less than one part in 2×10^7, or about 14 metres per second.

Summary.

An experimental attempt to find an alteration in velocity of light in a transverse magnetic field is described.   The sensitivity of the apparatus is considerably greater than that reached by previous experimenters, whose work has been available to the Authors, but a null result is found.   An interference method was used, one of the two rays from the first mirror of a Jamin refractometer being passed through a strong magnetic field in the gaps of three electromagnets, while the other ray passed through a weaker field.   The two rays were recombined at a second mirror and the resulting bands viewed with a microscope lens combination.   Any relative change in the velocities of the two rays would be observed as a movement of the bands.   The path along which the rays travelled was exhausted by means of coconut charcoal and liquid air to a pressure of ·005 mm. of mercury during the experiment.   The average field strength difference between the two-ray paths was 17·992 Gauss, while the optical system was capable of detecting a relative change in velocity of 1 part in 2×10^7.

The Growth of Waves on Water due to the Action of the Wind.

By the late Sir Thomas Stanton, F.R.S., and Dorothy Marshall and R. Houghton.*

[Plates 14 and 15.]

The behaviour of the surface of water over which a wind is blowing was considered mathematically by Kelvin.† Assuming the air and the water to be perfect liquids moving irrotationally, he found that the motion is governed by the following relation between U′ the velocity of the wind relative to the water, λ the wave-length and c the wave-velocity.

$$c^2 = \frac{g\lambda}{2\pi} \frac{\rho - \rho'}{\rho + \rho'} + \frac{2\pi T}{(\rho + \rho')\lambda} - \frac{\rho\rho'}{(\rho + \rho')^2} U'^2, \tag{1}$$

where ρ, ρ' are the densities of the water and air respectively and T is the surface tension of the water-air boundary. In any actual case the air will not be moving irrotationally; also, it is difficult to specify what is to be considered as the velocity of the air, owing to the considerable velocity gradient which exists near any fixed boundary, so that the equation (1) cannot be confirmed experimentally

The behaviour of the surface of water to which any given pressure distribution is applied can be calculated, but it is not at present possible to calculate the pressures which will be exerted on the water by a turbulent air stream; without this step it is not possible to discuss completely the growth of waves formed by a wind. The work described in the present paper is an attempt to provide some of the experimental data required for the consideration of this problem.

The work may conveniently be divided into two parts :—

(1) An examination of the behaviour of a water surface over which a wind is blowing.

(2) The measurement of the distribution of normal pressure on the surface of a wooden model of a train of waves over which a wind is blowing

* The investigation described in the present paper was initiated by, and carried out under the supervision of, the late Sir Thomas Stanton, at the time of whose death the experimental work was practically completed. The paper has been prepared by the other authors.

† " Baltimore Lectures," p. 590 ; ' Phil. Mag.,' vol. 42, p. 368 (1871).

PART 1.

These experiments were carried out in a horizontal tunnel about 50 feet long and 12 inches by 12 inches cross section.   The tunnel was filled with water to a depth of 5 inches, the water being retained by sloping beaches at the ends of the tunnel.   The inlet and outlet of the tunnel are so shaped that the air stream enters and leaves the tunnel in a direction parallel to the water surface. Two sets of glass windows are fitted in the walls of the tunnel at distances of about 15 feet and 41 feet from the inlet end ; through these the behaviour of the water surface can be observed.

The velocity of the air stream was measured by means of a pitot-static tube placed at the centre of the 7 inches by 12 inches space above the water.   The length and frequency of the waves were estimated by several methods

It was found that, when a beam of light was passed through the surface of the water from below, a pattern, of which photographs could be taken, was formed on a translucent screen placed above the tunnel , from these photographs, two of which are shown in figs 1 and 2, Plate 14, it is possible to estimate the length of the waves.   The length of those waves which were too long to be included in the field of the camera was estimated by adjusting the distance between two small cork floats until the rod joining them rose and fell without pitching ; the distance between the floats is then approximately equal to the wave-length.   The results obtained by this method are in fair agreement with those obtained photographically.

The frequency of the waves was measured by observing the wave profile through a stroboscope.   Although successive waves differed from one another, it was possible to obtain an approximately stationary image, and from this an approximate estimate of the wave-length could be made.

It was subsequently decided to record the wave-length and wave-velocity simultaneously by taking a cinematographic record of the pattern on the translucent screen.   Short lengths of two of the records are shown in figs. 3 and 4, Plate 15.

Through each set of windows observations were made at various wind speeds, the results obtained by the several methods are recorded in Tables I and II and figs. 5 and 6.   Although some individual values are rather widely scattered, it is possible to deduce relations between the wind speed and the wave-length or the wave-frequency, from which a relation between wave-length and wave-velocity can be calculated.   This relation is shown in fig. 7 ; in this figure the relation found by Kelvin is also shown.

One set of observations was made to determine the ratio height/wave-length, but owing to the large differences between successive waves no great accuracy was expected. It was found that the ratio lay between 0·12 and 0·2. Only a small range of wave-lengths (15–35 cm.) was examined; within this range, there was a tendency for the longer waves to have greater values of the ratio.

Table I.—Observations taken 15 feet from inlet.

Wind speed (cm./sec.).	Wave-length (cm.).	Wave-frequency (per sec.).	Wave-velocity (cm./sec.).	Method of observation.
445	5 6			Plate camera.
600	8 6	—	—	
730	10 9	—	—	
850	14 6	—	—	
410	5	6 9	—	
423	5	6 6	—	
445	5	6 1	—	
483	6	6·2	—	
520	6	5 9	—	
543	7	5 6	—	
603	8	4 8	—	
638	9	4 7	—	Stroboscope.
645	9	4 6	—	
692	9	4 2	—	
720	10	4 0	—	
755	10	4 3	—	
790	13	3 6	—	
802	12	3 8	—	
855	13	3 5	—	
625	10	·	—	
715	11	—	—	Floats.
835	14	—	—	
476	7·0		32	
575	8 3		40	
610	9·0	—	39	Cinematograph camera
615	10 2	—	46	
865	13 0	—	45	

The minimum velocity of the wind required to cause the formation of waves has been observed, although, as has been pointed out, the value obtained will depend to a great extent on the conditions of the experiment. At a wind speed of about 200 cm./sec. the surface of the water was covered with ripples, about 3 cm. long, which did not grow very noticeably as they travelled down-wind; from their size it can be deduced that they are governed chiefly by capillarity. True gravity waves were first formed when the wind speed, measured at the centre of the space above the water about 41 feet from the inlet, reached about 250 cm./sec. These waves had, at the observation window 41 feet from the inlet, a length of about 6 cm.

Table II.—Observations taken 41 feet from inlet.

Wind speed (cm./sec.).	Wave-length (cm.).	Wave-frequency (per sec.).	Wave-velocity (cm./sec.).	Method of observation.
226	5·2	—	—	Plate camera.
243	7 0	—	—	
265	9·0	—	—	
306	11·0	—	—	
324	13 0	—	—	
333	13 0	—	—	
305	9	4·6	—	Stroboscope.
382	14	3·5	—	
387	11·₈	3·7	—	
415	13	3·3	—	
436	13	3·1	—	
447	17	3 1	—	
466	18	3·0	—	
514	23	2 8	—	
515	20	2 6	—	
575	25	2·3	—	
623	—	2 4	—	
675	35	2 1	—	
740	—	2 1	—	
767	—	2·0	—	
505	25	—	—	Floats.
525	26	—	—	
570	28	—	—	
590	29	—	—	
635	30	—	—	
665	33	—	—	
715	35	—	—	
300	7·9	—	39	Cinematograph camera.
332	9·6	—	43	
400	16·9	—	54	
452	19·9	—	61	
528	22·6	—	63	
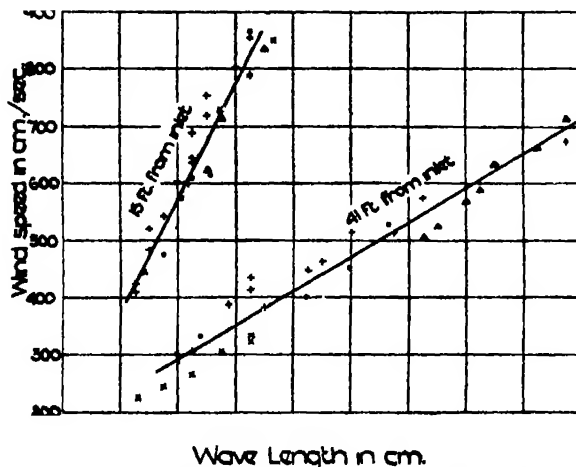
Fig. 5.—Observed variation of wave-length with wind speed.

Fig 1

(167) U_1 145 cm /sec λ 6 cm

Fig 2.

(138) $U_1 - 730$ cm /sec $\lambda - 11$ cm

Fig. 3.
$U_1 = 332$ cm/sec
41 feet from inlet

Fig. 4.
$U_1 = 400$ cm/sec
41 feet from inlet.
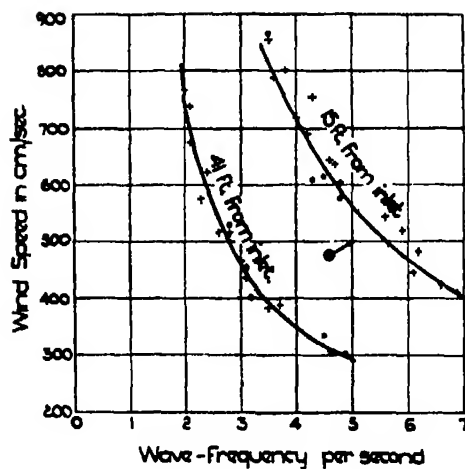
FIG. 6.—Observed variation of wave-frequency with wind speed.
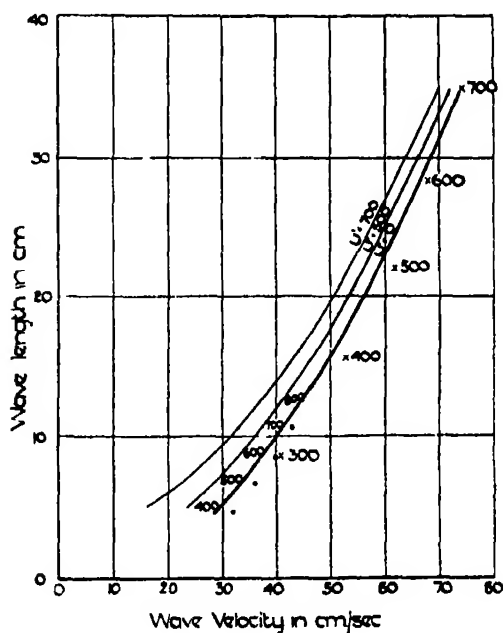
FIG. 7.—The figure against each observed point is the wind speed in centimetres per second on the axis of the air space; that is, 9 cm. above the mean water level.

— Calculated from Kelvin's theory.

• Mean of observations 15 feet from inlet.

× Mean of observations 41 feet from inlet.

PART 2.

For the measurement of the pressure distribution on the surface of a train of waves, the water was removed from the tunnel and a wooden model substituted for it. The model was placed so that its mean depth was the same as that of the water in Part 1. The profile of the working length of the model was a series of 27 simple harmonic waves, the height of which increased uniformly down-wind. The ratio height/wave-length was $0 \cdot 20_6$ for all the waves ; the length of the first (that at the up-wind end) was $5 \cdot 1$ cm. and of the 27th was $21 \cdot 6$ cm. The normal pressure was measured at two sets of points, on the surface of the 10th and 27th waves. It is convenient to express the results of the pressure measurements by means of the non-dimensional quantity $p/\rho U^2$, where p is the difference between the normal pressure at a point on the surface of the model and the static pressure in the air stream and $\frac{1}{2}\rho U^2$ is the velocity head of the air stream at the centre of the space above the model ; U is thus the maximum velocity of the air. The results of these measurements in the 12-inch tunnel are given in Table III and fig. 8.

Table III.—Values of $p/\rho U^2$ on the surface of model waves.   The wave profile is given by $\zeta = a \cos 2\pi x/\lambda$.

|	10th wave.		27th wave	
a in cm. λ in cm.	$1 \cdot 1_1$ $10 \cdot 8$		$2 \cdot 2_8$ $21 \cdot 6$	
ρU^2 in dynes/cm.^{3} U in cm./sec.	128 325	273 470	135 330	408 580
$2\pi x/\lambda$ in degrees				
324	$+0 \cdot 014$	$+0 \cdot 006$	$-0 \cdot 076$	$-0 \cdot 078$
0 crest	$-0 \cdot 030$	$-0 \cdot 032$	$-0 \cdot 119$	$-0 \cdot 230$
36	$-0 \cdot 010$	$-0 \cdot 013$	$-0 \cdot 065$	$-0 \cdot 125$
72	$-0 \cdot 005$	$-0 \cdot 004$	$-0 \cdot 018$	$-0 \cdot 022$
108	$-0 \cdot 005$	—	$-0 \cdot 012$	$-0 \cdot 005$
144	$-0 \cdot 004$	$-0 \cdot 001$	$-0 \cdot 006$	$+0 \cdot 005$
180 trough	$0 \cdot 000$	—	$+0 \cdot 004$	$+0 \cdot 029$
216	$+0 \cdot 007$	$+0 \cdot 016$	$+0 \cdot 035$	$+0 \cdot 067$
252	$+0 \cdot 027$	$+0 \cdot 042$	$+0 \cdot 082$	$+0 \cdot 137$
288	$+0 \cdot 060$	$+0 \cdot 076$	$+0 \cdot 077$	$+0 \cdot 101$
324	$+0 \cdot 007$	$+0 \cdot 024$	$-0 \cdot 025$	$-0 \cdot 078$
0 crest	$-0 \cdot 036$	$-0 \cdot 040$	$-0 \cdot 141$	$-0 \cdot 267$
36	$-0 \cdot 014$	$-0 \cdot 012$	$-0 \cdot 065$	$-0 \cdot 113$

These values have been corrected for the pressure gradient in the tunnel.

Since the height of these waves was not very small compared with that of the air stream above them, it was decided to construct models by which this condition would be satisfied. Two models were fitted in a wind tunnel of 3 feet square cross section. Each of these was of the form of a series of simple
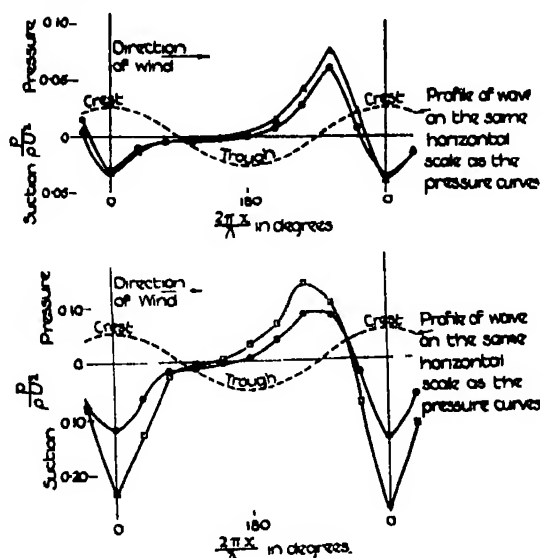
Fig. 8.—Distribution of normal pressure on the surface of model waves The wave profile is given by $\zeta = a \cos 2\pi x/\lambda$.

A (above). 10th wave $a = 1 \cdot 1_1$ cm.,
$\qquad \lambda = 10 \cdot 8$ cm.
$\qquad \odot$ U — 325 cm./sec.
$\qquad \triangle$ U — 470 cm./sec.

B (below). 27th wave $a = 2 \cdot 2_2$ cm.,
$\qquad \lambda = 21\ 6$ cm.
$\qquad \bullet$ U $= 330$ cm./sec.
$\qquad \square$ U   580 cm./sec.

harmonic waves of uniform height, the ratio height/wave-length was $0 \cdot 4$, the wave-lengths being $7 \cdot 6_2$ cm. and $2 \cdot 6$ cm.

The $7 \cdot 6_2$ model extended the whole length of the tunnel; the inlet flare was modified so that there was no sudden contraction of the air stream due to the presence of the model, the mean height of which was 1 inch. At one wind speed, two sets of pressure measurements were made, at 40 and 80 wave-lengths from the commencement of the uniform series; since these two sets were in good agreement with one another, the pressure distribution at other speeds and on the $2 \cdot 6$ cm. model was examined at one place only. In order to investigate the effect of very small irregularities in the surface, such as tool marks the portion of the model containing the observation holes was reversed and the observations repeated; it was found that the effect of this reversal on the pressure distribution was small.

The 2·6 cm. model extended down-wind from the mouth of the tunnel and the pressure measurements on it were made at 122 wave-lengths from the beginning of the uniform series. In order to investigate the effect of small changes in the ratio height/wave-length, a set of six waves was removed from the model and a set of the same wave-length but having a ratio of 0·44 was inserted in their place ; the pressure distribution on the surface of these waves was examined.

The results of the measurements in the 3-foot tunnel are given in Tables IV and V , those on the 7·6₂ cm. model are also shown graphically in fig. 9.

Table IV —Values of $p/\rho U^2$ on the surface of a corrugated sheet.   The profile of the corrugations is given by $\zeta = a \cos 2\pi x/\lambda$. $a = 1\cdot 5_2$ cm. $\lambda = 7\cdot 6_2$ cm.

ρU^2 in dynes/cm²	2425	2500	2350	266
U in cm./sec	1410	1425	1390	465
Distance from inlet	40 λ	80 λ	80 λ	80 λ
$2\pi x/\lambda$ in degrees				
270	+0 004	+0 006	—	+0 007
285	+0 010₅	+0 013	—	+0 015
300	+0 022	+0 024₅	—	·—
315	+0 025	+0 027	—	+0 028₅
330	+0 012₅	+0 013	+0 013	··
345	—0 010	—0 008₅	0 009₅	—
360 crest	·0·018	—0 017	—0 019₅	—0 012
15	—0 013	—0 013	—0 012₅	—0 006
30	—0 010	—0 009	—0 011	—
(45)	—	—	—0·009	—
60	—0 007	—0 006₅	—0 008	—0 003₅
(75)	—	—	—0 009	—
90	—0 010	—0 009₅	—0·011	—
120	—0 010₅	—0 011₅	—0 012₅	—0·004₅
150	—0 002₅	—0 002	0 004	+0 001
180 trough	0 000	0 000	0·000	0·000
210	—0 004₅	—0·005	—0 005	—0·003
240	—0 010	—0 009₅	—0 011₅	—0·011
270	+0 004₅	+0 002	—0 001₅	+0·002₅
285	+0 016₅	+0 014	—	—
300	+0 026	+0 026	+0 025	—
315	+0 026	+0 026	—	+0·027
330	+0 008	+0 009	+0 012₅	—
345	·0 011₅	—0 011₅	—0 015	—
360 crest	—0 020	—0 020	—0 023	—0 012
15	—0·013₅	—0 013₅	—0 015	—
30	—0 010₅	·0 011	—0 013₅	—
(45)	··	—	—0·011₅	—
(60)	—	·	—0 011	—
(75)	—	—	·0 012₅	—
(90)	··	··	—0 013	—

These values have not been corrected for the pressure gradient in the tunnel, which was about 0·001 ρU^2 per wave-length.

Table V.—Values of $p/\rho U^2$ on the surface of a corrugated sheet. The profile of the corrugations is given by $\zeta = a \cos 2\pi x/\lambda$. $\lambda = 2\cdot6$ cm. Distance from inlet $= 122\ \lambda$.

	0 51	0 56
a cm.	0 51	0 56
ρU^2 in dynes/cm ^{2}	2370	2400
U in cm /sec	1390	1400
$2\pi x/\lambda$ in degrees		
270	$+0\ 010$	$+0\ 007$
315	$+0\ 024$	$+0\ 028_5$
360 crest	$-0\ 002$	$-0\ 002_5$
45	$+0\ 005$	$+0\ 002$
90	$+0\ 002$	$+0\ 001$
135	$+0\ 003$	$+0\ 004$
180 trough	$+0\ 003_5$	$+0\ 004$
225	$+0\ 003_5$	$+0\ 001_5$
270	$+0\ 009_5$	$+0\ 004$
315	$+0\ 027$	$+0\ 024$
360 crest	$-0\ 003_5$	$-0\ 002_5$
45	$+0\ 003$	$+0\ 001_5$
90	$0\ 000$	$0\ 000$

These values have not been corrected for the pressure gradient in the tunnel, which was less than $0\ 000_5\ \rho U^2$ per wave-length
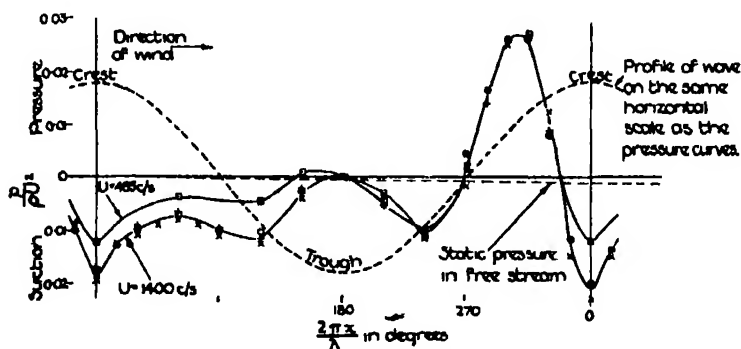
Fig. 9.—Distribution of normal pressure on the surface of model waves. The wave profile is given by $\zeta = a \cos 2\pi x/\lambda$ $a - 1\cdot5_2$ cm., $\lambda = 7\cdot6_2$ cm.

⊙ Readings taken at 40 λ from inlet
+ ,, ,, 80 λ ,,
× ,, ,, 80 λ ,, with model reversed
▣ ,, ,, 80 λ ,, U — 465 cm./sec.

U = 1400 cm./sec.

Since it is approximately true that the growth of any wave is affected only by a pressure distribution of the same periodicity, it is interesting to resolve these observed pressure distributions into their harmonic components. Two of the sets of observations recorded in Table III have been analysed; the mean of the observations at about 1400 cm /sec. given in Table IV has also

been analysed. The results of these analyses are given in Table VI. The large second harmonics will cause the wave profile to depart from a simple harmonic curve.

Table VI.—Harmonic Analysis of Pressure Distribution. Wave profile given
by $\zeta = a \cos \theta$, that is $\theta = 2\pi x/\lambda$.

A.—Models in 12-inch tunnel —

Mean depth of air stream, 18 cm

1. $\lambda = 10 \cdot 8$ cm. $a = 1 \cdot 1_1$ cm. $U = 325$ cm/sec.

$p/\rho U^2 = + 0 \cdot 005 \quad - 0 \cdot 006 \cos \theta \quad - 0 \cdot 020 \cos 2\theta \quad - 0 \cdot 010 \cos 3\theta$
$\qquad\qquad\qquad - 0 \cdot 023 \sin \theta \quad - 0 \cdot 005 \sin 2\theta \quad + 0 \cdot 005 \sin 3\theta$

2. $\lambda = 10 \cdot 8$ cm $a = 1 \cdot 1_1$ cm $U = 470$ cm/sec

$p/\rho U^2 = + 0 \cdot 011 \quad - 0 \cdot 007 \cos \theta \quad - 0 \cdot 024 \cos 2\theta \quad - 0 \cdot 012 \cos 3\theta$
$\qquad\qquad\qquad - 0 \cdot 003 \cos 4\theta$
$\qquad\qquad\qquad - 0 \cdot 030 \sin \theta \quad - 0 \cdot 007 \sin 2\theta \quad + 0 \cdot 007 \sin 3\theta$
$\qquad\qquad\qquad + 0 \cdot 005 \sin 4\theta$

3. $\lambda = 21 \cdot 6$ cm $a = 2 \cdot 2_1$ cm $U = 330$ cm/sec

$p/\rho U^2 = - 0 \cdot 007 \quad - 0 \cdot 053 \cos \theta \quad - 0 \cdot 051 \cos 2\theta \quad - 0 \cdot 013 \cos 3\theta$
$\qquad\qquad\qquad - 0 \cdot 043 \sin \theta \quad + 0 \cdot 001 \sin 2\theta \quad + 0 \cdot 008 \sin 3\theta$

4. $\lambda = 21 \cdot 6$ cm. $a = 2 \cdot 2_1$ cm $U = 580$ cm/sec

$p/\rho U^2 = - 0 \cdot 012 \quad - 0 \cdot 102 \cos \theta \quad - 0 \cdot 085 \cos 2\theta \quad 0 \cdot 030 \cos 3\theta$
$\qquad\qquad\qquad - 0 \cdot 082 \sin \theta \quad + 0 \cdot 006 \sin 2\theta \quad + 0 \cdot 011 \sin 3\theta$

B.—Model in 3-foot tunnel —

Mean depth of air stream, 89 cm

5. $\lambda = 7 \cdot 6_1$ cm $a = 1 \cdot 5_1$ cm $U = 1400$ cm./sec
$p/\rho U^2 = - 0 \cdot 003 \quad + 0 \cdot 001 \cos \theta \quad - 0 \cdot 002_1 \cos 2\theta \quad - 0 \cdot 009 \cos 3\theta$
$\qquad\qquad\qquad - 0 \cdot 003 \cos 4\theta$
$\qquad\qquad\qquad - 0 \cdot 008 \sin \theta \quad - 0 \cdot 008 \sin 2\theta$

It appears from fig. 7 that the mathematical relation between wave-length and wave-velocity on the free surface of a perfect liquid is, to a first approximation, valid even in the presence of a wind. This is in agreement with the pressure observations, the observed pressures being much less than those required to cause the water to behave in accordance with equation (1). For example, supposing the behaviour of the liquids to be as postulated by Kelvin, the maximum pressure or suction on the surface of the water is given by $p/\rho U^2 = 2\pi a/\lambda$; for the wave considered in the last column of Table III we have $2\pi a/\lambda = 0 \cdot 65$, but the maximum observed value of $p/\rho U^2$ is $0 \cdot 27$.

The theory considers only the stability of the water surface and gives no account of the rate of growth of the waves; the present experiments confirm the result of common observation, that the size of the waves formed, by a wind of any given speed, is a function of the distance from the shore; this function

cannot, however, be determined from these experiments since observations were taken at two places only.

Summary.

It is possible to calculate the behaviour of the surface of a liquid to which a given pressure distribution is applied ; it is not, however, possible to calculate the pressure exerted by a natural wind on the surface of waves, except by making certain assumptions which are known to be invalid. The work described in the present paper furnishes some of the experimental data required for further investigation of the growth of waves due to the action of the wind.

The experiments have been devoted to :—

(1) An examination of the behaviour of a water surface over which a wind is blowing

(2) The measurement of the distribution of normal pressure exerted by the wind on the surface of models of the waves.

The experiments were carried out in a 12-inch wind tunnel filled with water to a depth of 12·7 cm (5 inches), the speed of the wind was between 300 and 800 cm /sec , the waves formed were, in some experiments, as long as 35 cm

It was found that the relation between wave-length and wave-velocity was approximately that found mathematically by supposing the water to be a perfect fluid moving irrotationally, the motion of the air being neglected. The pressure distribution on the surface of the model waves was remarkable for the large second harmonics ; these will cause the profile of waves formed on water to vary considerably from a simple harmonic curve.

Argon and Amorphous Carbon, 15° to 710° C.

By Morris W. Travers, F.R.S.

In a previous paper, Broom and the author* have shown that the process by which equilibrium is reached between the oxides of carbon, methane, and hydrogen, on the one hand, and amorphous carbon on the other, at temperatures above 700° C. is essentially chemical in character. In the case of methane, some experiments were carried out at lower temperatures, and these appeared to indicate that, while the gas was still absorbed rapidly, it could be recovered reversibly, suggesting that the mechanism of absorption was distinct from that by which the chemical equilibrium was finally established. This observation led to the following experiments on argon, which is not supposed to be taken up by carbon at moderately high temperatures.

As in the former experiments, the principle of allowing the gas to remain for several days in contact with the carbon was adhered to ; for though the rate of absorption was at first rapid at all temperatures, the time taken for equilibrium to be established increased as the temperature fell, and ultimately became so long that it was impossible to obtain results of any value in a reasonable time A good deal of the published work on adsorption of gases seems to be vitiated by the fact that the experiments have been too hurried.

Atmospheric argon was liquefied, and the first and last fractions were rejected. The middle fraction was mixed with oxygen, and *sparked*† over potash. The gas was transferred by means of a gas burette and the Topler pump to a clean tube. The oxygen was removed by means of phosphorus, the gas being again transferred to a clean tube by the same method The apparatus used in the experiments was that already described and illustrated (*loc. cit.*, p. 315).

The reaction bulb contained 19·8 grams of the coconut shell carbon used in the previous experiments, and in these experiments the material was not heated to above 750°. A measured quantity of argon was introduced into the apparatus, and the pressure was adjusted in the manner described elsewhere.

---

* ' Proc. Roy. Soc.,' A, vol. 135, p. 512 (1932).

† Lord Rayleigh's method is much more certain and satisfactory than any method involving the passing of the gas over heated reagents. It is most easily carried out by using an induction with the commutator out of action, and alternating current of 3 or 4 amperes at 220 volts from town's service through the primary circuit. An arc can be maintained between platinum points in the gas for many hours without attention.

When equilibrium was established, usually after 2 or 3 days, a sample of gas was taken from the apparatus, and, after measuring its volume, it was purified by sparking with oxygen and again measured, so as to obtain data for the calculation of the true partial pressure of the argon in contact with the carbon. The temperature of the apparatus was then raised to 750°, and exhaustion was continued overnight, the gas collected being purified by sparking, and afterwards measured The sum of the two quantities of argon collected, less the volume of gas in the bulb, calculated from the partial pressure of the argon, the volume and temperature of the bulb, and the volume and temperature of the stem and dead space, gave the volume absorbed by the charcoal. It was observed that there was always a small loss of argon, due to leakage through the silica.

As was not unexpected, since the same result was obtained by observers at other temperatures, it was found that the isotherms for argon on charcoal were linear.* This result was obtained from two separate groups of experiments which do not belong to the general series, as the charcoal was subjected to subsequent treatment which might have slightly altered its properties. In each separate experiment in these two groups the whole series of operations described above was gone through The details are given in Table I.

Table 1

Experiment	Temperature	Pressure	Gas on carbon. (10° C.)
	° C	mm	c c
A 1	458	171 7	1 38
A 2		343 0	2 46
A 3		704 0	5 21
B 1	361	278 0	2 52
B 2		548 0	5 20

The results of the series of experiments carried out to determine the variation of the amount of argon adsorbed with temperature are given in Table II.

The chief source of error, which affects all the results equally, lies in the difficulty in maintaining the temperature exactly constant over long periods. The results at the highest and lowest temperatures for the volumes of argon adsorbed are probably too low In the operation of sampling at the high

* Peters and Weil, ' Z. phys. Chem.,' A, vol. 148, p. 1 , Bawn. ' J. Amer. Chem. Soc.,' vol. 54, p. 72 (1932).

Table II.

Experiment.	Temperature.	Pressure.	Gas on carbon (10° C.)	Gas on carbon at 760 mm. (10° C)
	° C.	mm	c c	c c.
C	607	864 0	2·60	2·28
D	707	756 4	1 43	1 43
E	579	723	2 375	2·495
F	678	656 0	1 47	1 71
G	468	558 3	2 83	3·85
H	525	598 3	2 21	2·81
J	208	385 8	7 51	14·8
K	288	463 9	5 80	9·50
L	380	563 4	4 36	5 88

temperatures, while withdrawing the gas from the bulb, owing to the ease with which adsorption is reversed, argon may be removed from the carbon. The calculated value of the partial pressure of the argon, and consequently of the amount of argon in the gas phase is then too high, and the apparent quantity of gas on the carbon too low. At low temperatures it may be doubtful whether true equilibrium is really attained. In an experiment carried out at 15°, a volume of 32 c c. of gas was introduced into the apparatus. The pressure was observed daily for a period of 12 days, and the observations are recorded in Table III.

Table III.

Days	3	5	7	9	11	12
Pressure (mm.)	479	465	455	447	441	438

At the end of this period the charcoal had taken up 3·7 c c of argon, equivalent to 6·4 c.c. at 760 mm. This is very much less than the quantity taken up at 200°, but the experiment suggested that equilibrium would only be reached after a very long time, and that in the experiments of which the results are recorded in Table II, those at the lower temperatures may be slightly vitiated from a similar cause. The true form of the graph representing the relationship $d \log V_{760}/d\,(1/T)$ may therefore be taken as practically linear, and that of the isobar over the greater part of the range of temperature 300° to 700°, calculated from it, of the form shown in fig. 1 rather than of the more flattened form required to include the points representing the results at the highest and lowest temperatures

The slope of the linear graph representing the relationship $d \log V_{760}/d\,(1/T)$ is found to be $0·98 \times 10^3$, so that the energy change in the adsorption process between 300° and 700° is 4500 calories per gram molecule, which is not

far from the approximate value 2000 calories to be expected for purely physical, or " van der Waals," adsorption. That the isotherms are at least approximately linear suggests that no condition of the surface, such as the existence of " active points," has anything to do with the phenomenon.

It has been pointed out that though the initial rate of adsorption is rapid, the establishment of equilibrium is a relatively slow process. The same phenomenon was also observed in the cases of the absorption of *active* gases at higher temperatures. However, there is no indication in either case of more than one process being involved, much less do the experiments indicate that, at any temperature, the process is partly reversible and partly irreversible, as
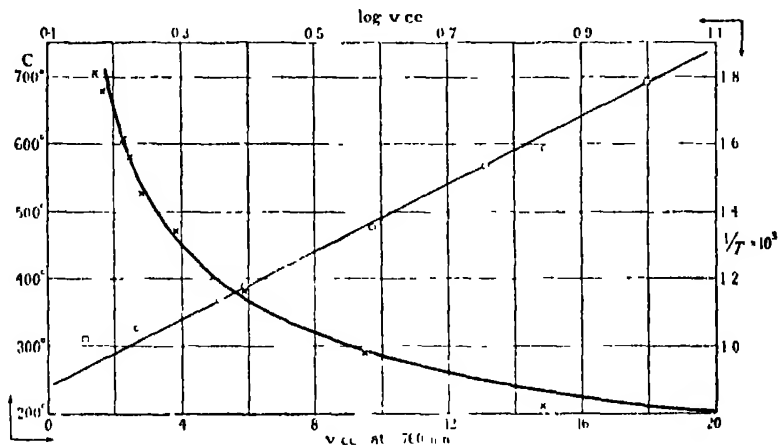
Fig. 1.

other authors have suggested   However, the results give rise to the question— In experimental work with gases at low temperatures, is a state of true equilibrium ever arrived at ?

Also, with reference to the work at high temperatures, it was observed that the temperature coefficient of the rate of absorption was generally very small (*loc cit.*). It was suggested that the phenomenon which was observed was a physical one, and that we were really measuring the rate of flow of the gas towards the surface. It is possible, however, that the process of absorption of such a compound as methane is similar to that of the absorption of argon ; but that equilibrium in the case of methane is due to chemical processes which take place on the surface.

In conclusion, I wish to convey my thanks to Imperial Chemical Industries Limited, and to the University of Bristol Colston Research Society for assistance in carrying on the work.

The Intensities of Certain Nebular Lines and the Mean Lives of Atoms emitting them.

By A. F. Stevenson, Department of Applied Mathematics, University of Toronto.

§ 1. *Introduction.*

There are certain prominent lines in the spectra of the galactic nebulæ—in particular the "nebulium" green lines, N_1 ($\lambda = 5007$) and N_2 ($\lambda = 4959$), which dominate most nebular spectra—whose identification remained till recently a mystery † In 1927, however, Bowen proposed his now well-known hypothesis that such lines are due to transitions from metastable states in certain ions ‡ The spectra involved are those of O III (which includes the lines N_1, N_2), N II, O II, S II, and O I §

To explain the fact that such lines occur, although they are "forbidden" transitions, Bowen postulated that there is a non-zero, though relatively small, probability of transition between the states in question. The strength of such lines is then accounted for if we suppose there is a large concentration of ions in the initial states in question due to transitions from higher levels, and that, due to the very low density in the nebulæ, such atoms remain undisturbed by collisions long enough for the radiation to become effective. The non-occurrence of such lines in the laboratory (except the O I lines observed by Hopfield, *loc. cit*) is thus explained by our inability to reproduce such conditions.

Although the agreement obtained between the calculated and observed wave-lengths is so close as to leave little room for doubt as to the substantial correctness of Bowen's hypothesis, it is evidently desirable to have additional information concerning the theoretical intensities of such lines, and the mean lives of the atoms when in the initial states in question, and to see whether any

---

† For a full account of nebular spectra in general, see Becker and Grotrian, 'Ergebn. exakt naturwiss,' vol. 7, p 8 (1928).

‡ Bowen, 'Nature,' vol. 120, p. 473 (1927) . 'Astrophys. J.,' vol. 67, p. 1 (1928) , 'Proc. Nat. Acad. Sci. Wash.,' vol. 14, p. 30 (1928) . 'Nature,' vol. 123, p. 450 (1929) , A. Fowler, 'Nature,' vol. 120, pp. 582, 617 (1927)

§ Paschen, 'Naturwiss,' vol 18, p. 752 (1930) ; Hopfield, 'Phys Rev,' vol. 37, p 160 (1931)

additional confirmation is thereby obtained. Preliminary calculations to this end have been made by Bartlett,[†] who, however, confined himself to calculating relative intensities only. His calculations, moreover, are incomplete, due to the approximations adopted, so that his results, though in the main confirmatory of Bowen's hypothesis, remain somewhat inconclusive.

In this paper we make calculations of the intensities and mean lives for O III and N II, which are the most important These calculations are complete if the contributions of double transitions to the intensity can be neglected, a neglect which cannot yet be tested It will be found that the relative intensities calculated here are in agreement with those observed in the nebulæ as far as comparison is possible, and the result for the mean lives--which, it is hoped, are fairly accurate—furnishes interesting information concerning the physical conditions in the nebulæ

The ordinary dipole term in the intensity vanishes of course for the lines in question, since they are " forbidden " transitions A possible explanation is that the transitions are due to the presence of ionic electric fields in the nebulæ , but this explanation must be rejected, since such fields must be very weak on account of the low density, and, moreover, if such were the case, a broadening of the nebular Balmer lines should result, which is not observed [‡] We shall follow Bartlett in ascribing the lines to quadripole radiation , taking into account the quadripole terms sufficient to ensure the non-vanishing of the intensities It may now be regarded as fairly definitely established that the occurrence of " forbidden " lines—unless due to disturbing external fields of some kind— can usually be ascribed to quadripole radiation (or possibly radiation of higher poles, though this does not yet seem to have arisen in practice). The hypothesis of quadripole radiation in relation to forbidden lines has been shown to be in satisfactory agreement with experiment in the case of the absorption spectra of the alkalis,[§] the Zeeman effect in potassium,[||] and the Zeeman effect in the auroral green line of O I.[¶]

In the case of O III and N II we have, effectively, a two-electron problem,

† Bartlett, ' Phys. Rev.,' vol. 34, p. 1247 (1929)

‡ Becker and Grotrian, *loc cit*, p 69 *Cf.* also Huff and Houston, ' Phys Rev ,' vol 36, p. 842 (1930).

§ Stevenson, ' Proc. Roy. Soc ,' A, vol 128, p 591 (1930) , Whitelaw and Stevenson, Nature,' vol 127, p 817 (1931).

|| Segrè, ' Z. Physik,' vol. 66, p. 827 (1930)

¶ Frenchs and Campbell, ' Phys Rev ,' vol. 36, p. 1460 (1931) For a summary of quadripole radiation in general, see Segrè, ' Nuovo Cimento,' Anno VIII, N. 2 (1931).

and our calculations are based on the work of Gaunt[†] on the triplets of helium, in which he also considered to some extent the present problem, and to which this paper is much indebted. Gaunt extended the Dirac wave-equation to the case of two electrons, but although his calculations gave a satisfactory account of the fine structure of He, it should be mentioned that subsequent work by Breit[‡] has shown fairly conclusively that the form of the spin interaction energy adopted by Gaunt is incorrect. Breit gives a closer approximation for it, and also works with more accurate wave-functions, and succeeds in obtaining a better agreement with experiment for He than does Gaunt. The correct form of the Dirac wave-equation for more than one electron is not yet known—and, indeed, it is not yet certain whether the equation for a single electron is entirely correct. In the present instance, however, we cannot hope for great accuracy in the calculations in any case, and it appears that Gaunt's methods, which entail less calculation than those of Breit, should be sufficient for our purpose.

After giving the requisite formula for the intensity in § 2, the method of calculating the wave-functions by a perturbation method is explained in § 3; the perturbation theory used is similar to that of Gaunt, but somewhat more straightforward. In §§ 4, 5 we give the calculations for the wave-functions and intensities, and in § 6 the numerical values are given and discussed with special reference to the nebulæ. We summarise briefly the conclusions in § 7.

§ 2. *Intensity of Quadripole Radiation.*

Following the method of Rubinowicz,[§] it was shown in a previous paper (*loc. cit*, equation (3)) that the intensity of quadripole radiation, per unit solid angle, in the z-direction, is

$$J = \frac{\pi^3 \nu^4}{c^5}\left[\left|\int z\,(S_x + \iota S_y)\,d\tau\right|^2 + \left|\int z\,(S_x - \iota S_y)\,d\tau\right|^2\right].$$

In this, the current density is taken as the real part of $Se^{2\pi\iota\nu t}$, where ν is the frequency of the radiation, and the integrals are taken throughout space.

Quantum-mechanically, in place of S we have, for a transition from state s to state t, a three-dimensional current density

$$S_{st}\,e^{2\pi\iota\nu_{st}t} + S^*_{st}\,e^{-2\pi\iota\nu_{st}t} = 2R\,(S_{st}\,e^{2\pi\iota\nu_{st}t}),$$

[†] 'Phil. Trans.,' A, vol. 228, p. 151 (1929), referred to hereafter as "G." Also 'Proc Roy. Soc.,' A, vol 122, p 513 (1929).

[‡] Breit, 'Phys. Rev,' vol. 34, p. 553 (1929); vol. 36, p. 385 (1930).

[§] 'Phys. Z,' vol. 29, p. 817 (1928); 'Z. Physik,' vol. 53, p. 267 (1929).

where ν_{st} is the frequency of the emitted radiation, and S_{st} is the (s, t) element in the matrix for S in a Heisenberg " co-ordinate system " (representation) ; so that the intensity, for a transition $s \rightarrow t$, becomes†

$$J_{s \rightarrow t} = \frac{4\pi^3 \nu_{st}{}^4}{c^5} \left[\left| \int z \left(S_x + iS_y \right) d\tau \right|^2 + \left| \int z \left(S_x - iS_y \right) d\tau \right|^2 \right]. \quad (2.1)$$

Now in a two-electron problem, the current density j is a six-dimensional vector, and

$$S_x = \left[\int j_{x_1} d\tau_1 \right]_{\binom{x_1 \, y_1 \, z_1}{= x, \, y, \, z}} + \left[\int j_{x_2} d\tau_2 \right]_{\binom{x_1 \, y_1 \, z_1}{= x, \, y, \, z}}$$

etc , where 1 and 2 refer to the configuration spaces of the two electrons, so that

$$\int z S_x \, d\tau = \int \left(z_1 j_{x_1} + z_2 j_{x_2} \right) d\tau_1 \, d\tau_2,$$

etc. Therefore (2.1) becomes, for a two-electron problem

$$J_{s \rightarrow t} = \frac{4\pi^3 \nu_{st}{}^4}{c^5} \left\{ \left| \int \left[z_1 \left(j_{x_1} + i j_{y_1} \right) + z_2 \left(j_{x_2} + i j_{y_2} \right) \right] d\tau_1 \, d\tau_2 \right. \right.$$
$$\left. \left. + \int \left[z_1 \left(j_{x_1} - i j_{y_1} \right) + z_2 \left(j_{x_2} - i j_{y_2} \right) \right] d\tau_1 \, d\tau_2 \right|^2 \right\} \quad (2.2)$$

On the Dirac theory, the components of j_{st} (in the one-electron case) are given by‡

$$(j_{st})_i = -\psi^*_s \alpha_i \psi_t, \qquad (i = 1, 2, 3), \quad (2.3)$$

where the α's are certain matrices. The generalisation of this to the two-electron case is obtained without difficulty , but with the wave-functions used by Gaunt, this would give zero for all components. Gaunt's approximations, however, amount essentially to using Schrodinger's wave-functions with spin factors attached, and it is evident that the same approximations will give the Schrodinger expressions for the current in place of (2.3). We therefore take§

$$j_{st} = \frac{eh}{4\pi i m_0} \left(\psi_s \, \nabla \psi^*_t - \psi^*_t \, \nabla \psi_s \right),$$

† In the previous paper, the factor 4 was omitted ; as, however, we were there concerned only with relative intensities, the results are unaffected.

‡ Dirac, " Principles of Quantum Mechanics," p. 246.

§ h (not $2h$!) denotes Planck's constant.

where a summation over the spin co-ordinates is now included. Since

$$\int z_1 \psi_s \frac{\partial \psi^*_t}{\partial x_1} d\tau_1 d\tau_2 = - \int z_1 \psi^*_t \frac{\partial \psi_s}{\partial x_1} d\tau_1 d\tau_2,$$

etc., we have finally, from (2 2), for the intensity

$$J_{s \to t} = \frac{\pi e^2 h^2}{m_0{}^2 c^5} \cdot \nu_{st}{}^4 \cdot I^{(st)}, \tag{2.4}$$

where

$$
\begin{aligned}
I^{(st)} = \quad & \left| \int (z_1 \psi_s \vartheta_1 \psi^*_t + z_2 \psi_s \vartheta_2 \psi^*_t) \, d\tau_1 d\tau_2 \right|^2 \\
+ \quad & \left| \int (z_1 \psi_s \vartheta^*_1 \psi^*_t + z_2 \psi_s \vartheta^*_2 \psi^*_t) \, d\tau_1 d\tau_2 \right|^2 \\
= \quad & |\, I_1^{(st)} \,|^2 + |\, I_2^{(st)} \,|^2, \quad \text{say,}
\end{aligned}
\tag{2.5}
$$

and

$$\vartheta_k = \frac{\partial}{\partial x_k} + \imath \frac{\partial}{\partial y_k} \; ; \quad \vartheta^*_k = \frac{\partial}{\partial x_k} - \imath \frac{\partial}{\partial y_k}, \quad (k = 1, 2). \tag{2.6}$$

The integrals in $I^{(st)}$ include summation over the spin-factors in the wave-functions. The problem now is to calculate the required approximations to the wave-functions.

In all this theory, however, the possible contributions of double transitions to the quadripole radiation have been neglected. We shall have to be content here to evaluate the one type of contribution only; even this is a lengthy matter. More accurate discussions, including the effects of double transitions, have never yet been given so far as we know Even Bartlett's work, in spite of its form, really proceeds from the fundamental equations of this section and discusses only the contributions of simple type.

§ 3. *Perturbation Theory*

In Gaunt's theory we have to deal with systems whose energy levels are nearly equal in pairs—"nearly degenerate systems" as Gaunt terms them—which necessitates a slight modification of the usual perturbation theory. We give a treatment which gives, of course, the same results as Gaunt's (G., § 3), but which seems rather more simple and straightforward.

Let the equation

$$L(\psi) = E\psi \tag{3.1}$$

have a number of eigenvalues E_m near some value E', say,

$$E_m = E' + \delta E_m \quad (m = 1, 2, ..., p)$$

with corresponding eigenfunctions ψ_m. We can allow for any of these states themselves being degenerate by supposing that some of the δE_m's are equal, while the corresponding ψ_m's are linearly independent.

Now consider a perturbed equation

$$(L + V) \psi = E\psi, \tag{3.2}$$

where V is small and of the same order of magnitude as the δE_m. We may now assume an expansion for the eigenfunctions of (3 2) of the form

$$\psi = \sum_{m=1}^{p} \alpha_m \psi_m + \chi, \tag{3.3}$$

where χ is a series in terms of other eigen-ψ's of (3.1) than those having eigenvalues near E'; on account of the δE_m's being small, we must consider the a_m's to be of the same order of magnitude. Further, let the eigenvalues of (3 2) near E' be

$$E = E' + \varepsilon.$$

Then the ordinary perturbation method gives the following set of equations for the coefficients a_m in (3 3)

$$\sum_{m=1}^{p} a_m [V_{mn} - \delta_{mn} C_m (\varepsilon - \delta E_m)] = 0, \quad (n = 1, \ldots, p), \tag{3 4}$$

where

$$V_{mn} = \int V \psi_m \psi^*_n d\tau, \qquad C_m = \int |\psi_m|^2 d\tau$$

and the integrals include a summation over the spin-factors where such are present. The zero-approximations to the wave-functions ψ are thus determined, and the corresponding values of ε are given as the roots of the determinantal equation

$$| V_{mn} - \delta_{mn} C_m (\varepsilon - \delta E_m) | = 0. \tag{3.5}$$

Suppose now that instead of using the ψ_m's for the unperturbed wavefunctions, we use a set of p independent orthogonal linear combinations of them, say,

$$\psi'_i = \sum_{j=1}^{p} b_{ij} \psi_j, \qquad (i = 1, \ldots, p). \tag{3.6}$$

Then the form of (3.4) and (3.5) will be altered owing to the presence of the δE_m's. If we neglect the δE_m's, it is known that (3.4) transform to others of the same form, say,

$$\sum_{i=1}^{p} a'_i [V'_{ij} - \delta_{ij} C'_j \varepsilon] = 0, \qquad (j = 1, \ldots, p), \tag{3.7}$$

where

$$V'_{ij} = \sum_{m,\,n} b_{im} b_{jn} V_{mn}. \tag{3.8}$$

In our case, however, we have, from (3.4), $V_{mn} + \delta_{mn} C_m \delta E_m$ in place of V_{mn}. Hence, from (3 8), we must add to the V'_{ij} in (3 7) the quantities

$$\sum_{m,\,n} b_{im} b_{jn} \delta_{mn} C_m \delta E_m = \sum_m b_{im} b_{jm} C_m \delta E_m$$

Thus (3.4) transform to

$$\sum_{i=1}^{p} a'_i [V'_{ij} + \sum_{m=1}^{p} b_{im} b_{jm} C_m \delta E_m - \delta_{ij} C'_j \varepsilon] = 0. \qquad (j = 1, \quad , p), \tag{3 9}$$

and (3 5) transform to

$$| V'_{ij} + \sum_{m=1}^{p} b_{im} b_{jm} C_m \delta E_m - \delta_{ij} C'_j \varepsilon | = 0. \tag{3.10}$$

This is the modification of the usual perturbation theory required ; it does not, unlike Gaunt's analysis, require the calculation of matrix elements of V other than the V'_{ij}.

We now consider briefly another point arising in the perturbation theory used in this paper. In Gaunt's work, the perturbation V consists of two parts

$$V = P + S,$$

where $P \succ S$ Now, in general, perturbative effects are " additive " *only* when the unperturbed system is non-degenerate , that is to say, if we first work out the first order change in the energy levels, and the zero-approximations to the wave-functions, taking $V = P$, and then do the same thing for the system so obtained taking $V = S$, we shall *not* get the same results as if we took $V = P + S$ and performed the calculations in one step, unless the original system is non-degenerate. This may be seen easily by considering the equations (3 9) and (3.10) (whether or not the δE_m's are included makes, of course, no difference). If, however, $P \succ S$, the perturbative effects *are* additive in the above sense, correct to $O(S/P)$. This can be proved formally from (3.9) and (3.10), but this is hardly necessary, since the statement is fairly obvious from physical considerations

In the present case, the zero-approximations to the wave-functions have already been calculated by Gaunt for the perturbation P alone, and partly also for S alone. The method adopted here is therefore to use as the initial

wave-functions (*i e.*, the ψ'_t of (3.6)) those which are correct zero-approxi-mations after perturbation by P alone *and* by S alone, and then to calculate the zero-approximations to the wave-functions to terms of order S/P by the method indicated above (it is necessary to include terms of order S/P in order to get non-vanishing intensities). This makes the calculation of the wave-functions very simple when the required matrix elements of S have been calculated ; some, but not all, of these have already been calculated by Gaunt. It may be mentioned that this method gives very simply the relative intensity of ortho-para to para-para transitions in He (G., p 177)

§ 4 *Calculation of the Wave-functions*

The states that are to be considered for the nebular lines are the lowest energy states of O^{14} and N^+, for which the electronic configuration is $(1s)^2$ $(2s)^2 (2p)^2$, giving rise to the terms (in ascending order of energy levels) $^3P_{0, 1, 2}$; $^1D_2$; $^1S_0$. No transition is possible between these states for dipole radiation by Laporte's rule,[†] and we therefore proceed on the assumption of quadrupole radiation.

We treat the problem as if the two $2p$ electrons were in a central field of force directed to the nucleus, and under the influence of their mutual inter-action We adhere to Gaunt's notation as far as possible to facilitate reference. Gaunt adopts the following form for the interaction energy V :

$$V = P + S,$$

where P, S are respectively the electrostatic and spin parts of the interaction ; also $P = e^2/r$, and (G. (2 6) and G (2 7))

$$S = T_1 + T_2 + U = -\frac{e^2 h}{4\pi^2 m_0^2 c^2} \left[-\left(\frac{r_0}{r^2} \times p_2\right) \cdot \sigma_1 + \left(\frac{r_0}{r^2} \times p_1\right) \cdot \sigma_2 \right.$$
$$\left. + \left(\frac{eh}{4\pi m_0 c}\right)^2 \cdot \frac{(\sigma_1 \cdot \sigma_2) - 3(\sigma_1 \cdot r_0)(\sigma_2 \cdot r_0)}{r^3}, \quad (4.0)\right.$$

where the suffixes 1 and 2 refer to the two electrons, p is the momentum, $rr_0 = r_1 - r_2$, r being the distance between the electrons, and the components of the σ's are Dirac matrices.

---

† This rule holds rigorously for dipole radiation to any order of the perturbation by P and S. Weyl, " Theory of Groups and Quantum Mechanics," pp. 201, 203 (English edition, 1931).

We take the following 15 independent wave-functions for the unperturbed $(2p)^2$ state (G., p 184) :—

$$\psi_\beta{}^2 = [\phi_1{}^0(1)\,\phi_1{}^1(2) - \phi_1{}^0(2)\,\phi_1{}^1(1)]\chi_a(1)\,\chi_a(2)$$

$$\psi_\epsilon{}^2 = \phi_1{}^1(1)\,\phi_1{}^1(2)\,[\chi_a(1)\,\chi_b(2) - \chi_b(1)\,\chi_a(2)]$$

$$\psi_\beta{}^1 = [\phi_1{}^{-1}(1)\,\phi_1{}^1(2) - \phi_1{}^{-1}(2)\,\phi_1{}^1(1)]\chi_a(1)\,\chi_a(2)$$

$$\psi_\gamma{}^1 = [\phi_1{}^0(1)\,\phi_1{}^1(2) - \phi_1{}^0(2)\,\phi_1{}^1(1)][\chi_a(1)\,\chi_b(2) + \chi_b(1)\,\chi_a(2)]$$

$$\psi_\delta{}^1 = [\phi_1{}^0(1)\,\phi_1{}^1(2) + \phi_1{}^0(2)\,\phi_1{}^1(1)][\chi_a(1)\,\chi_b(2) - \chi_b(1)\,\chi_a(2)]$$

$$\psi_a{}^0 = [\phi_1{}^0(1)\,\phi_1{}^1(2) - \phi_1{}^0(2)\,\phi_1{}^1(1)]\chi_b(1)\,\chi_b(2)$$

$$\psi_\beta{}^0 = [\phi_1{}^0(1)\,\phi_1{}^{-1}(2) - \phi_1{}^0(2)\,\phi_1{}^{-1}(1)]\chi_a(1)\,\chi_a(2)$$

$$\psi_\gamma{}^0 = [\phi_1{}^{-1}(1)\,\phi_1{}^1(2) - \phi_1{}^{-1}(2)\,\phi_1{}^1(1)][\chi_a(1)\,\chi_b(2) + \chi_b(1)\,\chi_a(2)] \qquad \left.\right\} \text{ (4 1)}$$

$$\psi_\delta{}^0 = [\phi_1{}^{-1}(1)\,\phi_1{}^1(2) + \phi_1{}^{-1}(2)\,\phi_1{}^1(1)][\chi_a(1)\,\chi_b(2) - \chi_b(1)\,\chi_a(2)]$$

$$\psi_\epsilon{}^0 = \phi_1{}^0(1)\,\phi_1{}^0(2)\,[\chi_a(1)\,\chi_b(2) - \chi_b(1)\,\chi_a(2)]$$

$$\psi_a{}^{-1} = [\phi_1{}^{-1}(1)\,\phi_1{}^1(2) - \phi_1{}^{-1}(2)\,\phi_1{}^1(1)]\chi_b(1)\,\chi_b(2)$$

$$\psi_\gamma{}^{-1} = [\phi_1{}^0(1)\,\phi_1{}^{-1}(2) - \phi_1{}^0(2)\,\phi_1{}^{-1}(1)][\chi_a(1)\,\chi_b(2) + \chi_b(1)\,\chi_a(2)]$$

$$\psi_\delta{}^{-1} = [\phi_1{}^0(1)\,\phi_1{}^{-1}(2) + \phi_1{}^0(2)\,\phi_1{}^{-1}(1)][\chi_a(1)\,\chi_b(2) - \chi_b(1)\,\chi_a(2)]$$

$$\psi_a{}^{-2} = [\phi_1{}^0(1)\,\phi_1{}^{-1}(2) - \phi_1{}^0(2)\,\phi_1{}^{-1}(1)]\chi_b(1)\,\chi_b(2)$$

$$\psi_\epsilon{}^{-2} = \phi_1{}^{-1}(1)\,\phi_1{}^{-1}(2)\,[\chi_a(1)\,\chi_b(2) - \chi_b(1)\,\chi_a(2)]$$

In these functions, the arguments 1 and 2 refer to the two electrons, and (G (4 03) and G. (4.04) ; we use R in place of g_{n1}),

$$\phi_1{}^u = 3P_1{}^u R, \qquad (|u| \leqslant 1), \tag{4.2}$$

where R is the radial part of the wave-function, and, following Darwin,

$$P_k{}^u = e^{iu\phi}(k - u)! \,(1 - \mu^2)^{u/2}\left(\frac{d}{d\mu}\right)^{k+u}\frac{(\mu^2 - 1)^k}{2^k k!}, \qquad (\mu = \cos\theta). \tag{4.3}$$

The χ's are spin-factors with components

$$\left.\begin{array}{l}\chi_a = 0,\, 0,\, 1,\, 0 \\ \chi_b = 0,\, 0,\, 0,\, 1\end{array}\right\}. \tag{4.4}$$

The wave-functions are not normalised ; we denote the normalisation factors by such symbols as $C_\beta{}^2$. They are divided into five groups, corresponding to the different values of the total angular momentum (orbit + spin), and indicated

by the superscripts, which we shall call m, of the ψ's. The functions with suffixes α, β, γ arise in the perturbation by S alone (*i.e.*, the ^{3}P states); those with suffixes δ, ε in the perturbation by P alone (^{1}S and ^{1}D). The five groups are "non-combining" for perturbations by both P and S, and can therefore be treated separately, but the sub-groups, symmetrical and anti-symmetrical in the position co-ordinates, combine when both P and S are taken into account.

As regards the perturbation by P alone, the above functions are all correct zero approximations as they stand, except ψ_δ^0 and ψ_ε^0. A perturbation calculation replaces these two by ψ_4^0, ψ_5^0, where (G. (9 22))

$$\left.\begin{aligned}\psi_4^0 &= \psi_\delta^0 + 4\psi_\varepsilon^0 \\ \psi_5^0 &= \psi_\delta^0 - 2\psi_\varepsilon^0\end{aligned}\right\}, \qquad (4\ 5)$$

with P perturbation energies given by (G. (9 19))

$$\left.\begin{aligned}\Delta E_4 &= \frac{D_0}{C} + \frac{1}{25}\frac{D_2}{C} \\ \Delta E_5 &= \frac{D_0}{C} + \frac{2}{5}\frac{D_2}{C}\end{aligned}\right\}, \qquad (4\ 6)$$

where (G. (9 17)),

$$C = 18\,(4\pi)^2 \left| \int_0^\infty R^2 r^2\,dr \right|, \qquad (4\ 7)$$

and (G. (9.15) and G. (9 01))

$$D_0 = 18\,(4\pi)^2 c^2 \iint_0^\infty \frac{1}{r_{\max}} R^2(1)\,R^2(2)\,r_1^2\,r_2^2\,dr_1\,dr_2,$$

$r_{\max}$ being the greater of r_1, r_2. By dividing the range of integration for r_2 into the two intervals $(0, r_1)$ and (r_1, ∞) and changing the order of integration in the second part, the integral for D_0 may be replaced by

$$D_0 = 36\,(4\pi)^2 c^2 \int_0^\infty dr_1 \int_0^{r_1} dr_2 \ \ r_1 r_2^2 R^2(1)\,R^2(2). \qquad (4\ 8)$$

Similarly, from G. (9 12)

$$D_2 = 36\,(4\pi)^2 c^2 \int_0^\infty dr_1 \int_0^{r_1} dr_2 \cdot \frac{r_2^4}{r_1} R^2(1)\,R^2(2). \qquad (4.9)$$

The wave-function ψ_5^0 then refers to the ^{1}S$_0$ term, with extra P energy ΔE_5, ψ_4^0 and the other functions symmetrical in the position co-ordinates refer to ^{1}D$_2$, with extra P energy ΔE_4, while the functions antisymmetrical in the positions refer to the ^{3}P term, with extra P energy (G. (9.25))

$$\Delta E_1 \,(= \Delta E_2 = \Delta E_3) = \frac{D_0}{C} - \frac{1}{5}\frac{D_2}{C}. \qquad (4.10)$$

The next step is to obtain zero-approximations to the wave-functions correct to order S/P, taking into account the total perturbation P + S, by the method of § 3. This is facilitated if we first find the correct wave-functions anti-symmetrical in the positions after perturbation by S alone.

We consider in detail first the group $m = 0$. For this group, the calculations have already been made by Gaunt (G. (9.63)). He finds for the wave-functions (since there is an arbitrary multiplying factor in each) :

$$\left.\begin{array}{l}\psi_1{}^0 = \psi_a{}^0 - \psi_\beta{}^0 - \psi_\gamma{}^0 \\[4pt] \psi_2{}^0 = \psi_a{}^0 + \psi_\beta{}^0 \\[4pt] \psi_3{}^0 = -2\psi_a{}^0 + 2\psi_\beta{}^0 - \psi_\gamma{}^0 \end{array}\right\}, \qquad (4.11)$$

and (G (9.61)) for the S perturbation energies (giving the fine structure of the triplet) :

$$\left.\begin{array}{l}\delta E_1 = \dfrac{5}{3}\eta_1 + \dfrac{1}{3}\eta_2 - \dfrac{11}{4}\dfrac{T}{C} \\[8pt] \delta E_2 = \eta_1 + \eta_2 + \dfrac{15}{4}\dfrac{T}{C} \\[8pt] \delta E_3 = \dfrac{2}{3}\eta_1 + \dfrac{4}{3}\eta_2 + \dfrac{5}{2}\dfrac{T}{C} \end{array}\right\}, \qquad (4.12)$$

where η_1, η_2 are the spin energies for a single $2p$ electron in a central field of force, and (G. (9 53))

$$T = \gamma^2 a^2 e^2 \cdot \frac{36}{5}(4\pi)^2 \cdot \int_0^\infty dr_1 \int_0^{r_1} dr_2 \cdot \frac{r_2{}^2}{r_1} R^2(1) R^2(2), \qquad (4 13)$$

where

$$\gamma = \frac{2\pi e^2}{hc}, \qquad a = \frac{h^2}{4\pi^2 m_0 e^2}.$$

The terms 1, 2, 3 are $^3P_2$, $^3P_1$, $^3P_0$ respectively.

We now take $\psi_1{}^0, \ldots, \psi_5{}^0$ for the independent orthogonal linear combinations ψ'_i of (3.6). The ψ_m of § 3 are the ψ_1, , ψ_5 of G. (9.31); the b_{ij} of § 3 can be read off from G. (9.62) (allowing for the factor by which $\psi_2{}^0$ has been multiplied in (4.11)); and the δE_m's are given in G. (9.37). The C_m of (3 10) are given by G. (9.36), and the C'_j, which we write $C_1{}^0, \ldots, C_5{}^0$ in the present notation, are given from (4.5), (4.11), and G. (9.34) as follows :—

$$C_1{}^0 = C_a{}^0 + C_\beta{}^0 + C_\gamma{}^0 = 12C,$$

and similarly

$$C_2{}^0 = 4C, \qquad C_3{}^0 = C_4{}^0 = 24C, \qquad C_5{}^0 = 12C.$$

There remains the calculation of the matrix elements $V_{ij}^0 = P_{ij}^0 + S_{ij}^0$, which are the V'_{ij} of (3.10) The P_{ii}^0 are, of course, the ΔE's introduced above, and $P_{ij}^0 = 0$ ($i \neq j$). The S_{ij}^0 can also all be calculated from the results of Gaunt. We have, in fact, from (4.0)

$$S_{aa}^0 = 2(T_1)_{aa}^0 + U_{aa}^0, \text{ etc.}$$

and $(T_1)_{aa}^0 \dots, U_{aa}^0$ are given from G. (9.52) and G. (9.54). S_{ij}^0 ($i, j = 1, \dots, 5$) are then given by (4.5) and (4.11). We thus find†

$$S_{11}^0 = S_{aa}^0 + S_{\beta\beta}^0 + S_{\gamma\gamma}^0 - 2S_{a\beta}^0 - 2S_{a\gamma}^0 + 2S_{\beta\gamma}^0 = -33T,$$

and similarly

$$S_{22}^0 = 15T, \quad S_{33}^0 = 60T, \quad S_{14}^0 = 30T, \quad S_{15}^0 = 6T, \quad S_{34}^0 = -12T,$$
$$S_{35}^0 = 36T, \quad S_{12}^0 = S_{13}^0 = S_{23}^0 = S_{24}^0 = S_{25}^0 = S_{44}^0 = S_{45}^0 = S_{55}^0 = 0.$$

The determinant of (3.10) now becomes :—

$33T + 4C(5\eta_1 + \eta_2)$ $+12C(\Delta E_1 - \epsilon)$	0	0	$30T + 8C(\eta_1 - \eta_2)$	$6T$
0	$15T + 4C(\eta_1 + \eta_2)$ $+4C(\Delta E_1 - \epsilon)$	0	0	0
0	0	$60T + 16C(\eta_1 + 2\eta_1)$ $+24C(\Delta E_1 - \epsilon)$	$-12T$	$36T + 16C(\eta_1 - \eta_2)$
$30T + 8C(\eta_1 - \eta_2)$	0	$-12T$	$16C(2\eta_1 + \eta_2)$ $+24C(\Delta E_4 - \epsilon)$	0
$6T$	0	$36T + 16C(\eta_1 - \eta_2)$	0	$8C(2\eta_1 + \eta_2)$ $+12C(\Delta E_5 - \epsilon)$

(4.14)

The third order sub-determinant at the beginning of the principal diagonal is that arising from the triplet, the fourth diagonal element that from the ${}^1D_2$ state, and the fifth diagonal element that from the ${}^1S_0$ state. From the manner in which it has been obtained, it is evident that to a sufficient approximation the roots, ϵ, of (4 14) equated to zero are obtained by equating to zero the elements of the principal diagonal, which gives, of course, just Gaunt's values for the energy levels (disregarding an unimportant spin correction to the singlet terms).

According to the method of § 3, the zero-approximations to the wave-functions are then given correct to order S/P by, say,

$$\Psi_i^0 = \sum_{j=1}^5 a_{ij}\psi_j^0 \qquad (i = 1, \dots, 5),$$

† Not all these matrix elements need be calculated for our immediate purpose, but the complete calculation affords a check on the work.

where $|a_{ij}|$ is the determinant (4.14). Retaining only terms of order S/P, this gives for the root

$\varepsilon = \Delta E_1 + \delta E_1 \, (^3P_2):$

$$a_{11}[30T + 8C(\eta_1 - \eta_2)] + a_{14} \cdot 24C(\Delta E_4 - \Delta E_1) = 0$$

$$a_{11} \cdot 6T + a_{15} \cdot 12C(\Delta E_5 - \Delta E_1) = 0$$

$$a_{12} = a_{13} = 0.$$

Hence, using (4.6) and (4.10)

$$\frac{a_{14}}{a_{11}} = -\frac{125}{24}\frac{T}{D_2} - \frac{25}{18}\frac{C}{D_2}(\eta_1 - \eta_2)$$

$$\frac{a_{15}}{a_{11}} = -\frac{5}{6}\frac{T}{D_2}$$

We may therefore take

$$\Psi_1^0 = \psi_1^0 - \left[\frac{125}{24}\frac{T}{D_2} + \frac{25}{18}\frac{C}{D_2}(\eta_1 - \eta_2)\right]\psi_4^0 - \frac{5}{6}\frac{T}{D_2}\psi_5^0.$$

Similarly

$\varepsilon = \Delta E_1 + \delta E_2 \, (^3P_1):$

$$\Psi_2^0 = \psi_2^0$$

$\varepsilon = \Delta E_1 + \delta E_3 \, (^3P_0):$

$$\Psi_3^0 = \psi_3^0 + \frac{25}{12}\frac{T}{D_2}\psi_4^0 - \left[5\frac{T}{D_2} + \frac{20}{9}\frac{C}{D_2}(\eta_1 - \eta_2)\right]\psi_5^0$$

$\varepsilon = \Delta E_4 \, (^1D_2):$

$$\Psi_4^0 = \psi_4^0 + \left[\frac{125}{12}\frac{T}{D_2} + \frac{25}{9}\frac{C}{D_2}(\eta_1 - \eta_2)\right]\psi_1^0 - \frac{25}{12}\frac{T}{D_2}\psi_3^0$$

$\varepsilon = \Delta E_5 \, (^1S_0):$

$$\Psi_5^0 = \psi_5^0 + \frac{5}{6}\frac{T}{D_2}\psi_1^0 + \left[\frac{5}{2}\frac{T}{D_2} + \frac{10}{9}\frac{C}{D_2}(\eta_1 - \eta_2)\right]\psi_3^0.$$

We now carry out an exactly similar process for the groups $m = \pm 1, \pm 2$ of (4.1). For these groups, the S matrix components have not been calculated by Gaunt, except $S_{\beta\beta}^2 = -\frac{1}{2}T$ (G. (9.77)). Many of the wave-functions in these groups, however, differ only from those with $m = 0$ in having different spin factors. This enables some of the matrix elements to be found in terms of those with $m = 0$, by utilising the formulæ for the effect of T_1 and U on

the spin factors given in G., § 5, and the results of G. (9.50), G (9.51), G. (9.52). For instance, we thus find

$$2\,(\mathrm{T}_1)_{\beta\beta}{}^2 = -\,2\,(\mathrm{T}_1)_{\alpha\alpha}{}^0 = -\,5\mathrm{T}$$

$$\mathrm{U}_{\beta\beta}{}^2 = \mathrm{U}_{\alpha\alpha}{}^0 = -\,\tfrac{1}{2}\mathrm{T}.$$

We obtain in this way the following matrix elements†

$$\left.\begin{array}{ll}
S_{\beta\beta}{}^2 = S_{\alpha\alpha}{}^{-2} = -\dfrac{11}{2}\;\mathrm{T}, & S_{\gamma\gamma}{}^1 = S_{\beta\beta}{}^1 = S_{\gamma\gamma}{}^{-1} = S_{\alpha\alpha}{}^{-1} = 2\mathrm{T}, \\[2mm]
S_{\beta\gamma}{}^1 = -\,S_{\alpha\gamma}{}^{-1} = 13\mathrm{T}, & S_{\epsilon\epsilon}{}^2 = S_{\epsilon\epsilon}{}^{-2} = S_{\delta\delta}{}^1 = S_{\delta\delta}{}^{-1} = 0
\end{array}\right\} \quad (4.15)$$

Moreover, the integrals for T_1, U are in all cases *real*, so that they may be equated to their conjugates. By considering the relations between the wave-functions for $m = \pm 1$, and for $m = \pm 2$, it may thus easily be shown that

$$S_{\beta\delta}{}^1 = S_{\alpha\delta}{}^{-1}, \qquad S_{\gamma\delta}{}^1 = -\,S_{\gamma\delta}{}^{-1}, \qquad S_{\beta\epsilon}{}^2 = -\,S_{\beta\epsilon}{}^{-2}. \qquad (4.16)$$

Thus the only integrals that need be calculated explicitly are $(\mathrm{T}_1)_{\beta\delta}{}^1$, $(\mathrm{T}_1)_{\gamma\delta}{}^1$, $(\mathrm{T}_1)_{\beta\epsilon}{}^2$ (the corresponding U's vanish).

The calculation of these integrals is laborious; the method has been suffi-ciently indicated by Gaunt, and we only quote the results ‡ :

$$S_{\beta\epsilon}{}^2 = S_{\beta\delta}{}^1 = -\,S_{\gamma\delta}{}^1 = 7\mathrm{T}. \qquad (4.17)$$

Since the P matrix elements have already been found in connection with the $m = 0$ group, we now have all the required matrix elements.

Consider now, for example, the $m = 1$ group of wave-functions. We must first find the zero approximations after perturbation by S alone for the functions anti-symmetrical in the positions. We find

$$C_{\beta}{}^1 = C_{\gamma}{}^1 = C_{o}{}^1 = 4C. \qquad (4.18)$$

Omitting the η factors, since we merely wish to find the wave-functions, the S perturbation applied to the functions $\psi_{\beta}{}^1$, $\psi_{\gamma}{}^1$ gives the secular equation

$$\left|\begin{array}{ll}
2\mathrm{T} - 4C\epsilon, & 13\mathrm{T} \\
13\mathrm{T}, & 2\mathrm{T} - 4C\epsilon
\end{array}\right| = 0$$

---

† The elements $(\mathrm{T}_1)_{\beta\beta}{}^1$ and $(\mathrm{T}_1)_{\alpha\alpha}{}^{-1}$ are not given directly in this way; it can be seen that they vanish on account of the integrations with respect to ϕ_1, ϕ_2.

‡ It may be mentioned that the coefficients in the expansion of inverse powers of r in a series of Legendre polynomials, required for the evaluation of the integrals, are given very simply by some formulæ given by Routh, 'Proc London Math. Soc.,' vol. 26, p. 481 (1895), and do not require the special artifices used by Gaunt for finding them.

with roots $\varepsilon = \dfrac{15}{4}\dfrac{T}{C}$, $-\dfrac{11}{4}\dfrac{T}{C}$, so that $\psi_\beta{}^1$, $\psi_\gamma{}^1$ are replaced by linear combinations

$$\left. \begin{array}{l} \psi_1{}^1 = \psi_\beta{}^1 + \psi_\gamma{}^1 \\ \psi_2{}^1 = \psi_\beta{}^1 - \psi_\gamma{}^1 \end{array} \right\} \tag{4.19}$$

These refer to $^3P_1$, $^3P_2$ respectively. From (4.18) and (4.19),

$$C_1{}^1 = C_2{}^1 = 8C,$$

and from (4.19), (4.15), and (4.17)

$$S_{11}{}^1 = 30T, \quad S_{22}{}^1 = -22T, \quad S_{25}{}^1 = 14T, \quad S_{12}{}^1 = S_{15}{}^1 = S_{55}{}^1 = 0.$$

We now take $\psi_1{}^1$, $\psi_2{}^1$, $\psi_5{}^1$ for the ψ'_i of § 3. We next require the b_{ij}, δE_m, and C_m of (3.10), that is, we must express our wave-functions in terms of the fundamental Dirac solutions for a single electron. Analogously to G. (9·30) we find

$$\left. \begin{array}{l} \psi_\beta{}^1 = \psi_8 + 2\psi_9 \\ \psi_\gamma{}^1 = -\psi_8 + \psi_9 + 3\psi_{10} \\ \psi_5{}^1 = \psi_8 - \psi_9 + 3\psi_{10} \end{array} \right\} \tag{4.20}$$

where

$$\left. \begin{array}{l} \psi_8 = \psi_{-2}{}^{-1}(1)\,\psi_{-2}{}^1(2) - \psi_{-2}{}^{-1}(2)\,\psi_{-2}{}^1(1) \\ \psi_9 = \psi_1{}^{-1}(1)\,\psi_{-2}{}^1(2) - \psi_1{}^{-1}(2)\,\psi_{-2}{}^1(1) \\ \psi_{10} = \psi_{-2}{}^0(1)\,\psi_1{}^0(2) - \psi_{-2}{}^0(2)\,\psi_1{}^0(1). \end{array} \right\} \tag{4.21}$$

In the right-hand side of (4.21), the notation is that of G. (4.00); the suffixes here refer to Dirac's j. From (4.21) we have

$$\delta E_8 = 2\eta_1, \qquad \delta E_9 = \delta E_{10} = \eta_1 + \eta_2. \tag{4.22}$$

Also from (4.19) and (4.20)

$$\left. \begin{array}{l} \psi_1{}^1 = 3\,(\psi_9 + \psi_{10}) \\ \psi_2{}^1 = 2\psi_8 + \psi_9 - 3\psi_{10} \end{array} \right\} \tag{4.23}$$

Solving (4.20) for ψ_8, ψ_9, ψ_{10}, and using (4.18), we find

$$C_8 = \frac{4}{3}C, \qquad C_9 = \frac{2}{3}C, \qquad C_{10} = \frac{2}{9}C. \tag{4.24}$$

The b_{ij} can now be read off from (4.20) and (4.23); the δE_m are given by (4.22), and the C_m by (4.24).

The determinant of (3.10) now becomes

$$
\begin{vmatrix}
\left\{ \begin{matrix} 30T + 8C(\eta_1 - \eta_2) \\ + 8C(\Delta E_1 - \varepsilon) \end{matrix} \right\}, & 0 & , & 0 \\[2em]
0 & , & \left\{ \begin{matrix} -22T + \dfrac{8}{3}C(5\eta_1 + \eta_2) \\ + 8C(\Delta E_1 - \varepsilon) \end{matrix} \right\}, \ 14T + \dfrac{8}{3}C(\eta_1 - \eta_2) \\[2em]
0 & , & 14T + \dfrac{8}{3}C(\eta_1 - \eta_2) \ , \ \left\{ \begin{matrix} \text{`` } \eta \text{ '' terms} \\ + 4C(\Delta E_4 - \varepsilon) \end{matrix} \right\}
\end{vmatrix}.
$$

By the method used for the case $m = 0$, we find for the wave-functions :

$$
^3P_1 : \ \Psi_1{}^1 - \psi_1{}^1 ,
$$

$$
^3P_2 . \ \Psi_2{}^1 = \psi_2{}^1 - \left\lfloor \frac{175}{12} \frac{T}{D_2} + \frac{25}{9} \frac{C}{D_2} (\eta_1 - \eta_2) \right\rfloor \psi_\delta{}^1 ,
$$

$$
^1D_2 . \ \Psi_\delta{}^1 = \psi_\delta{}^1 + \left\lfloor \frac{175}{24} \frac{T}{D_2} + \frac{25}{18} \frac{C}{D_2} (\eta_1 - \eta_2) \right\rfloor \psi_2{}^1 .
$$

In a similar way, the groups $m = -1, \pm 2$ are treated ; we shall only give the final results :—

$\underline{m = -1}$

$$
^3P_1 : \ \Psi_1{}^{-1} = \psi_1{}^{-1}
$$

$$
^3P_2 : \ \Psi_2{}^{-1} = \psi_2{}^{-1} - \left\lfloor \frac{175}{12} \frac{T}{D_2} + \frac{25}{9} \frac{C}{D_2} (\eta_1 - \eta_2) \right\rfloor \psi_\delta{}^{-1}
$$

$$
^1D_2 : \ \Psi_\delta{}^{-1} = \psi_\delta{}^{-1} + \left\lfloor \frac{175}{24} \frac{T}{D_2} + \frac{25}{18} \frac{C}{D_2} (\eta_1 - \eta_2) \right\rfloor \psi_2{}^{-1}
$$

where

$$
\psi_1{}^{-1} = \psi_\alpha{}^{-1} - \psi_\gamma{}^{-1} , \qquad \psi_2{}^{-1} = \psi_\alpha{}^{-1} + \psi_\gamma{}^{-1} . \tag{4.25}
$$

$\underline{m = 2.}$

$$
^3P_2 . \ \Psi_\beta{}^2 = \psi_\beta{}^2 - \left[\frac{175}{24} \frac{T}{D_2} + \frac{25}{18} \frac{C}{D_2} (\eta_1 - \eta_2) \right] \psi_\epsilon{}^2
$$

$$
^1D_2 : \ \Psi_\epsilon{}^2 = \psi_\epsilon{}^2 + \left[\frac{175}{12} \frac{T}{D_2} + \frac{25}{9} \frac{C}{D_2} (\eta_1 - \eta_2) \right] \psi_\beta{}^2 .
$$

$\underline{m = -2.}$

$$
^3P_2 : \ \Psi_\alpha{}^{-2} = \psi_\alpha{}^{-2} + \left[\frac{175}{24} \frac{T}{D_2} + \frac{25}{18} \frac{C}{D_2} (\eta_1 - \eta_2) \right] \psi_\epsilon{}^{-2} ,
$$

$$
^1D_2 : \ \Psi_\epsilon{}^{-2} = \psi_\epsilon{}^{-2} - \left[\frac{175}{12} \frac{T}{D_2} + \frac{25}{9} \frac{C}{D_2} (\eta_1 - \eta_2) \right] \psi_\alpha{}^{-2} .
$$

Collecting our results, and using (4.5), (4.11), (4.19), (4.25) to express the wave-functions in terms of the original functions (4.1), we now have the following complete list of zero-approximations for the different states, correct to terms of order S/P :—

$$
\begin{aligned}
&{}^3P_2: \quad \psi_a{}^0 - \psi_\beta{}^0 - \psi_\gamma{}^0 + c_1\psi_\delta{}^0 + c_2\psi_\epsilon{}^0 \quad (12C) \\
&\qquad \psi_\beta{}^1 - \psi_\gamma{}^1 - c_3\psi_\delta{}^1 \quad (8C) \\
&\qquad \psi_a{}^{-1} + \psi_\gamma{}^{-1} - c_3\psi_\delta{}^{-1} \quad (8C) \\
&\qquad \psi_\beta{}^2 - \tfrac{1}{2}c_3\psi_\epsilon{}^2 \quad (2C) \\
&\qquad \psi_a{}^{-2} + \tfrac{1}{2}c_3\psi_\epsilon{}^{-2} \quad (2C) \\[6pt]
&{}^3P_1 \quad \psi_a{}^0 + \psi_\beta{}^0 \quad (4C) \\
&\qquad \psi_\beta{}^1 + \psi_\gamma{}^1 \quad (8C) \\
&\qquad \psi_a{}^{-1} - \psi_\gamma{}^{-1} \quad (8C) \\[6pt]
&{}^3P_0 \cdot \quad -2\psi_a{}^0 + 2\psi_\beta{}^0 - \psi_\gamma{}^0 + c_4\psi_\delta{}^0 + c_5\psi_\epsilon{}^0 \quad (24C) \\[6pt]
&{}^1D_2: \quad \psi_\delta{}^0 + 4\psi_\epsilon{}^0 + c_3\psi_a{}^0 - c_3\psi_\beta{}^0 + c_6\psi_\gamma{}^0 \quad (24C) \\
&\qquad \psi_\delta{}^1 + \tfrac{1}{2}c_3(\psi_\beta{}^1 - \psi_\gamma{}^1) \quad (4C) \\
&\qquad \psi_\delta{}^{-1} + \tfrac{1}{2}c_3(\psi_a{}^{-1} + \psi_\gamma{}^{-1}) \quad (4C) \\
&\qquad \psi_\epsilon{}^2 + c_3\psi_\beta{}^2 \quad (4C) \\
&\qquad \psi_\epsilon{}^{-2} - c_3\psi_a{}^{-2} \quad (4C) \\[6pt]
&{}^1S_0: \quad \psi_\delta{}^0 - 2\psi_\epsilon{}^0 - c_7\psi_a{}^0 + c_7\psi_\beta{}^0 + \tfrac{2}{5}c_6\psi_\gamma{}^0 \quad (12C)
\end{aligned}
\right\} , \quad (4.26)
$$

where

$$
c_1 = -\frac{145}{24}\xi - \frac{25}{18}\eta, \quad c_2 = -\frac{115}{6}\xi - \frac{50}{9}\eta, \quad c_3 = \frac{175}{12}\xi + \frac{25}{9}\eta,
$$

$$
c_4 = -\frac{35}{12}\xi - \frac{20}{9}\eta, \quad c_5 = \frac{55}{3}\xi + \frac{40}{9}\eta, \quad c_6 = -\frac{25}{3}\xi - \frac{25}{9}\eta,
$$

$$
c_7 = \frac{25}{6}\xi + \frac{20}{9}\eta,
$$

and

$$
\xi = \frac{T}{D_2}, \quad \eta = \frac{C}{D_2}(\eta_1 - \eta_2). \qquad (4.27)
$$

The normalisation factors—disregarding terms in ξ, η—are given in brackets. These may be compared with the functions given by Bartlett (loc. cit.).

§ 5 *Intensities and Mean Lives.*

We now calculate the integrals I_1 and I_2 of (2.5) for the quadrupole intensities for transitions between the various states. For the ϑ's of (2.6), we have the formulæ due to Darwin (G. (5 20))

$$
\left.
\begin{aligned}
\vartheta\,(P_1{}^u R) &= \tfrac{1}{3}\left[\left(\frac{dR}{dr} - \frac{R}{r}\right)P_2{}^{u+1} + u\,(1-u)\left(\frac{dR}{dr} + 2\frac{R}{r}\right)P_0{}^{u+1}\right] \\
\vartheta^*\,(P_1{}^u R) &= \tfrac{1}{3}\left[-\left(\frac{dR}{dr} - \frac{R}{r}\right)P_2{}^{u-1} + u\,(1+u)\left(\frac{dR}{dr} + 2\frac{R}{r}\right)P_0{}^{u-1}\right]
\end{aligned}
\right\}. \quad (5.1)
$$

From a consideration of the integrations with respect to the azimuths ϕ_1, ϕ_2, it can be seen that the integral $I_1{}^{(st)}$ vanishes unless $m_t = m_s + 1$, where m_s, m_t denote the m's of the initial and final states; and that the integral $I_2{}^{(st)}$ vanishes unless $m_t = m_s - 1$. This simplifies the calculations considerably, since only one of the integrals I_1 or I_2 can contribute anything in the combinations between the various wave-functions of the different states. Moreover, functions symmetrical in the spins can combine only with functions also symmetrical in the spins, and likewise for functions anti-symmetrical in the spins. The best plan is to calculate first the values of I_1, I_2 for the only possible combinations of wave-functions ϕ from (4.1) that can occur. The integrals always reduce to the product of two simple integrals, of which one is of the form

$$
\int z\phi_1{}^p \vartheta\,(\phi_1{}^{p+1})^* \, d\tau, \qquad (p = -1, 0), \tag{5 2}
$$

or

$$
\int z\phi_1{}^p \vartheta^*\,(\phi_1{}^{p-1})^* \, d\tau, \qquad (p = 1, 0), \tag{5 3}
$$

and the other of the form

$$
\int |\phi_1{}^p|^2 \, d\tau \tag{5 4}
$$

Using (4.2), (5.1) and $(P_k{}^u)^* = (-1)^u P_k{}^{-u}$, (5 2) becomes

$$
(-1)^{p+1} . 3 . 2\pi . \int_0^\pi d\theta \int_0^\infty dr\,[\dot{P}_1{}^p P_2{}^{-p} \sin\theta \cos\theta\,(r^3 RR' - r^2 R^2)
$$
$$
- (p+1)(p+2)\,P_1{}^p \dot{P}_0{}^{-p} \sin\theta \cos\theta\,(r^3 RR' + 2r^2 R^2)], \tag{5 5}
$$

where $R^1 = dR/dr$, and $\dot{P}_1{}^p$ stands for $P_1{}^p$ as defined by (4.3) without the ϕ factor. By an integration by parts

$$
\int_0^\infty r^3 RR' \, dr = -\frac{3}{2}\int_0^\infty r^2 R^2 \, dr,
$$

and the integrations with respect to θ can be performed without difficulty.

We thus find for (5.5) the value

$$12\pi \int_0^\infty r^2 R^2 \, dr = A, \quad \text{say,} \quad (p = -1, 0),$$

where $A^2 = \frac{1}{2}C$ by (4.7). Similarly (5.3) has the value $-A$, $(p = 1, 0)$ We easily find that (5.4) has the value A for $p = 0$, and 2A for $p = \pm 1$.

We can now make a table of values of $I^{(st)}$ for the various possible pairs of the ψ's of (4.26), including the summation with respect to the spin factors. The total intensity of a transition such as $^1D_2 \to {}^3P_2$, for instance, is then obtained by summing the values of $I^{(st)}$ where s is any wave-function of the $^1D_2$ state and t any wave-function of the $^3P_2$ state, after inserting the normalisation factors for the wave-functions. We shall omit the details and give only the final results :—

$$\begin{aligned}
&{}^1D_2 \to {}^3P_2: \quad I = \frac{625}{3 \cdot 12^3}(2097\xi^2 + 768\xi\eta + 80\eta^2) \\[6pt]
&{}^1D_2 \to {}^3P_1: \quad I = \frac{625}{9 \cdot 12^3}(1989\xi^2 + 768\xi\eta + 80\eta^2) \\[6pt]
&{}^1D_2 \to {}^3P_0: \quad I = \frac{625}{48}\xi^2 \\[6pt]
&{}^1S_0 \to {}^3P_2: \quad I = \frac{25}{48}\xi^2 \\[6pt]
&{}^1S_0 \to {}^3P_1: \quad I = \frac{25}{12 \cdot 324}(39\xi + 16\eta)^2 \\[6pt]
&{}^1S_0 \to {}^3P_0: \quad I = 0 \\[6pt]
&{}^1S_0 \to {}^1D_2: \quad I = 0
\end{aligned} \right\} \quad (5\,6)$$

The value 0 for $^1S_0 \to {}^3P_0$ is a special case of the result that the transition $j = 0 \to j = 0$ is forbidden for any multipole radiation (Bartlett, *loc. cit.*). The value 0 for $^1S_0 \to {}^1D_2$, however, has only been obtained because the functions ψ_s^0, ψ_s^0 in $^1S_0$ and ψ_s^1, ψ_s^{-1} in $^1D_2$ (which are the only ones that arise) occur in certain combinations; it is thus, so to speak, accidental, and it is clear that by taking account of higher order terms in the wave-functions we should get a non-vanishing result. It is only the perturbation by P which comes in question, and this perturbation is large when both electrons are in $2p$ orbits; in fact, it will be shown in the next section that the separation ratio is not in agreement with experiment, so that the wave-functions with which we work cannot be very good approximations.

To take account completely of the second order perturbation by P would require a great deal of additional calculation. We therefore make use of a modification of the usual perturbation theory which has been given by Lennard-Jones.† Let V_{ki} be the elements of the perturbation matrix ; then the first-order correction to the wave function ψ_k, energy E_k, is ordinarily given by

$$\sum_{i \neq k} \frac{V_{ki}}{E_k - E_i} \psi_i.$$

Lennard-Jones points out that this may be replaced by

$$\frac{V - \varepsilon_k}{E_k} \psi_k + \sum_{i \neq k} \frac{E_i}{E_k (E_k - E_i)} V_{ki} \psi_i, \tag{5.7}$$

where ε_k is the first-order correction to the energy-level E_k. The principal part of the correction is thus expressed in terms of the unperturbed eigen-function ψ_k, and if $E_k \gg E_i$ the second part may be neglected. In the case of O^{++} and N^+, the condition $E_k \gg E_i$ is not fulfilled, the levels from the $2s(2p)^3$ configuration, in particular, lying fairly close to the $(2s)^2 (2p)^2$ levels. Nevertheless, we may expect that the contribution from the second term in (5.7) will be comparatively small, and that—at least as regards order of magnitude—a fair approximation will be obtained by retaining only the first term in (5.7).

In the present case, $V = P = e^2/r$, so that, from (5.7), a wave-function ψ_s is to be replaced by

$$1 - \frac{\Delta E_s}{E} + \frac{e^2}{Er} \Big) \psi_s = \Big(1 + \alpha_s + \frac{\beta}{r} \Big) \psi_s, \quad \text{say} \tag{5.8}$$

where ΔE_s is the P-perturbation of the state in question, and E the unperturbed energy level—say, the mean of the levels ^1S, ^1D, ^3P. From (5.8) and (2.5)

$$I_1^{(st)} = \int z_1 \Big(1 + \alpha_s + \frac{\beta}{r} \Big) \psi_s \vartheta_1 \Big(1 + \alpha_t + \frac{\beta}{r} \Big) \psi^*_t \, d\tau_1 \, d\tau_2$$

$$+ \int z_2 \Big(1 + \alpha_s + \frac{\beta}{r} \Big) \psi_s \vartheta_2 \Big(1 + \alpha_t + \frac{\beta}{r} \Big) \psi^*_t \, d\tau_1 \, d\tau_2 \Bigg\} \tag{5.9}$$

Retaining only first-order terms in α, β and neglecting the terms independent of α, β since we know that they contribute nothing to the final result, the first integral in (5.9) gives

$$(\alpha_s + \alpha_t) \int z_1 \psi_s \vartheta_1 \psi^*_t \, d\tau_1 \, d\tau_2 + \beta \int \frac{z_1}{r} \psi_s \vartheta_1 \psi^*_t \, d\tau_1 \, d\tau_2$$

$$+ \beta \int z_1 \psi_s \vartheta_1 \Big(\frac{\psi^*_t}{r} \Big) d\tau_1 \, d\tau_2. \tag{5.10}$$

† ' Proc. Roy. Soc ,' A, vol. 129, p. 598 (1930).

The last integral in (5.10), after an integration by parts, gives

$$- \beta \int \frac{z_1}{r} \, \psi^*_t \vartheta_1 \psi_s \, d\tau_1 \, d\tau_2.$$

The second integral in (5.9) is similarly treated, so that we may put

$$I_1^{(st)} = (\alpha_s + \alpha_t) \int (z_1 \psi_s \vartheta_1 \psi^*_t + z_2 \psi_s \vartheta_2 \psi^*_t) \, d\tau_1 \, d\tau_2$$

$$+ \beta \int \frac{z_1}{r} (\psi_s \vartheta_1 \psi^*_t - \psi^*_t \vartheta_1 \psi_s) \, d\tau_1 \, d\tau_2 \qquad (5.11)$$

$$+ \beta \int \frac{z_2}{r} (\psi_s \vartheta_2 \psi^*_t - \psi^*_t \vartheta_2 \psi_s) \, d\tau_1 \, d\tau_2$$

$I_2^{(st)}$ has the same value with ϑ^* in place of ϑ The first integral in (5.11) has already been calculated ; the only new ones that need be calculated are the second and third in (5 11) and the similar expression for $I_2^{(st)}$.

Since we may expand $1/r$ in the form (G. (9.01) and G. (5.22))

$$\frac{1}{r} = \Sigma_u f_u (r_1, r_2, \theta_1, \theta_2) \, e^{iu (\phi_1 - \phi_2)},$$

it can easily be seen that only those wave-functions contribute to $I^{(st)}$ which do so when the corrections in (5 8) are neglected, and, moreover, that if one of the integrals $I_1^{(st)}$, $I_2^{(st)}$ does not vanish, the other one certainly does.   Since we are considering only the $^1S_0 \rightarrow {}^1D_2$ transition, this means, from (4.26), that we need only retain the wave-functions

$$\left.\begin{array}{ll} \psi_s^0 - 2\psi_s^0, & \text{for} \quad {}^1S_0 \\ \psi_s^1, \ \psi_s^{-1}, & \text{for} \quad {}^1D_2 \end{array}\right\}. \qquad (5.12)$$

The second and third integrals in (5.11) are of a type met with before in the work   There are a number of new integrals to be found   The best way is to proceed systematically with the functions ϕ that occur in (5.12) in the same way as before.   The calculations may be considerably shortened by observing that some of the integrals can be deduced from others by interchanging the variables 1 and 2, or equating an integral to its conjugate (since it is real).   We further have in our case, from (5.8)

$$\alpha_s = - \frac{\Delta E_5}{E}, \qquad \alpha_t = - \frac{\Delta E_4}{E}, \qquad \beta = \frac{e^2}{E},$$

and (4.6) may be used to express ΔE_4, ΔE_5 in terms of the integrals D_0, D_2. We again omit the details, and give only the final result :

$$^1S_0 \rightarrow {}^1D_2 : \quad I = \frac{216}{625}\left(\frac{D_2}{CE}\right)^2. \tag{5.13}$$

This now replaces the last of (5.6)

The relative intensity of lines with the same initial level, $^1S_0$ or $^1D_2$, are given, from (2.4), by the ratios of the values of I given by (5.6) and (5.13) multiplied by ν^4, where ν is the frequency of the line.

For the mean lives of the $^1S_0$ and $^1D_2$ states, we require the *absolute* intensities. The result (2 4) is the intensity per unit solid angle in the z-direction. For an individual transition between two wave-functions the radiation is, of course, polarised,† but the total radiation for a transition between two states is evidently unpolarised and the same in all directions. The total intensity per atom is therefore obtained by multiplying (2.4) by 4π and dividing by the weight of the initial state (1 for $^1S_0$, 5 for $^1D_2$) The probability of transition, per unit time, is obtained by division by a further factor $h\nu_{st}$. The total probability of transition, per unit time, from $^1S_0$ or $^1D_2$ to a lower level, is obtained by summing the probabilities so found over all lower levels, and are thus, from (2.4), (5 6), and (5.13), given by

$$A\,(^1S_0) = \frac{4\pi^2 h e^2}{m_0{}^2 c^2}\cdot\left(\frac{\nu_1}{c}\right)^3 \frac{216}{625}\left(\frac{D_2}{CE}\right)^2$$

$$A\,(^1D_2) = \frac{4\pi^2 h e^2}{m_0{}^2 c^2}\left(\frac{\nu_2}{c}\right)^3 \cdot \frac{125}{9\cdot 12^3}\,(8604\xi^2 + 3072\xi\eta + 320\eta^2) \tag{5.14}$$

where ν_1, ν_2 are respectively the frequencies of $^1S_0 \rightarrow {}^1D_2$, $^1D_2 \rightarrow {}^3P$. We have neglected the contributions to $A\,(^1S_0)$ of the $^1S \rightarrow {}^3P$ transitions, since they are relatively very small.

The mean life, τ_s, of an atom in state s is defined by

$$\frac{1}{\tau_s} = \sum_r A_{s\rightarrow r} \,,$$

where $A_{s\rightarrow r}$ is the Einstein " A " coefficient, and the summation is taken over all states r of lower energy than s, so that if no influences other than spontaneous

---

† By considering the field given by the retarded potentials, it can be shown that the radiation is circularly polarised parallel to the (x, y) plane. *Cf.* Rubinowicz, ' Z. Physik,' vol. **61**, p. 338 (1930).

emission are at work to increase or decrease the number of atoms in state s, that number will be

$$N = N_0 e^{-t/\tau_s}$$

after time t, where N_0 is the number at time 0. The mean life of an atom in state $^1S_0$ or $^1D_2$ is therefore the reciprocal of the corresponding expression in (5.14).

§ 6. *Numerical Values.*

So far the calculations have, of course, been general and apply to any atom or ion which can be treated as composed of two electrons in equivalent p orbits. We now wish to apply these results to the special cases of O^{++} and N^+, with reference to the nebular lines. The combinations of integrals of radial wave-functions which remain in the results can all be calculated from the experimental data. For, from (4.6) and (4.10), the separations between the different multiplet terms are given by

$$\left. \begin{array}{l} ^1D - {}^1S = \Delta E_5 - \Delta E_4 = \dfrac{9}{25} \dfrac{D_2}{C} \\[3mm] ^3P - {}^1D = \Delta E_4 - \Delta E_1 = \dfrac{6}{25} \dfrac{D_2}{C} \end{array} \right\} \qquad (6.1)$$

while from (4.12) the triplet separations are

$$\left. \begin{array}{l} ^3P_1 - {}^3P_2 = \delta E_1 - \delta E_2 = -\dfrac{13}{2} \dfrac{T}{C} + \dfrac{2}{3}(\eta_1 - \eta_2) \\[3mm] ^3P_0 - {}^3P_1 = \delta E_2 - \delta E_3 = \dfrac{5}{4} \dfrac{T}{C} + \dfrac{1}{3}(\eta_1 - \eta_2) \end{array} \right\} \qquad (6.2)$$

so that from the experimental values for the separations, the quantities D_2/C, T/C, $\eta_1 - \eta_2$, and hence also ξ and η, can be calculated

It is of interest first, however, to see how the observed separations fit in with the calculated values where such can be found. A discrepancy arises at once, however, as pointed out by Bartlett, for the ratio of the inter-multiplet separations given by (6.1) is 3 : 2 independently of the value of D_2/C, whereas this is not so experimentally, the ratio being about 23 : 20 for O^{++} and 17 . 15 for N^+. It is evident that this arises from the large value of the perturbation by P when both electrons are in $2p$ orbits, and the fact that our wave-functions are not sufficiently accurate (*cf.* the results on the intensity of $^1S_0 \rightarrow {}^1D_2$ of the last section). The necessary wave-functions, derived by the method of Hartree's self-consistent field, are available in the case of O^{++}, having been calculated by Hartree and his collaborators. The method of the self-consistent field has been amply justified by comparison of results derived from this

method with experiment, and has recently been justified theoretically as being a good approximation in many-electron atoms.[†]

With these radial wave-functions the integrals for T, D_2, C were calculated by numerical integration[‡] ; $\eta_1 - \eta_2$ is the spin-doublet separation for a single electron in a p orbit in a central field of force, and is given by[§]

$$\eta_1 - \eta_2 = \tfrac{3}{4}\gamma^2 a^2 e^2 \, \overline{\frac{Z}{r^3}} = \tfrac{3}{4}\gamma^2 a^2 e^2 \cdot \frac{\displaystyle\int_0^\infty \frac{Z}{r} R^2 \, dr}{\displaystyle\int_0^\infty R^2 r^2 \, dr},$$

where Z is the effective nuclear charge at distance r, so that, since Z is also obtained with the self-consistent field method, $\eta_1 - \eta_2$ can also be calculated.

The values thus found for the separations for O III, computed from (6 1) and (6.2), together with the experimental values (taken from Becker and Grotrian, *loc. cit*), are given below in cm^{-1} :—

	Observed	Calculated.	Separation ratio Observed	Separation ratio Calculated.
$^1D - {}^1S$	22913	16600	1·14	1·5
$^3P - {}^1D$	20160	11100		
$^3P_1 - {}^3P_2$	193	224	1·66	1·8
$^3P_0 - {}^3P_1$	116	125		

The inter-multiplet separations do not agree well with the observed values, as might be expected in view of the above, but the triplet separations come out as well as can be expected On the whole, then, we may expect our theory to yield reasonably accurate results for the intensities and mean lives, in spite of the inaccuracy of the wave-functions used after perturbation by P alone. For the numerical calculations, we shall now use the experimental data as explained above, taking the mean of the two values for D_2/C obtained from (6 1). The use of the experimental values for the quantities involved in this way may reasonably be supposed to increase the accuracy of the calculations, though this cannot be said with certainty.

We give, in Table I, the results for the relative intensities of lines from the same initial level, and the mean lives, as calculated from the formulæ of § 5,

[†] Fock, ' Z. Physik,' vol. 61, p. 126 (1930), Dirac, ' Proc. Camb. Phil. Soc.,' vol. 26, p. 376 (1930).

[‡] The values of D_2, C were supplied by Dr. Hartree. For the other integrals, a straight-forward method of numerical integration was actually adopted, although in similar cases, owing to the inverse powers of r in the integrand, it may sometimes be better to use a more indirect method. I am indebted to Dr. Hartree for pointing this out to me.

[§] Dirac, ' Proc. Roy. Soc.,' A, vol. 117, p. 624 (1928).

for the spectra O III, N II, and the similar spectrum C I (added for comparison), and also the observed values for the intensities of the nebular lines. The observed values of the separations in O III and N II, and of the average nebular intensities, are taken from Becker and Grotrian (*loc. cit.*); the data for C I are taken from a paper by Fowler and Selwyn.[†]

Table I.—Relative intensities of lines, and mean lives of metastable states, arising from $(2p)^2$ configuration. The intensities are relative for lines in the first group and for lines in the second group, but not for two lines in different groups.

	O III			N II.			C I.		
	$\lambda.$	Relative intensity		λ	Relative intensity.		$\lambda.$	Relative intensity	
		Calc.	Obs		Calc.	Obs		Calc.	Obs.
$^1D_2-^1S_0$	4363 21	1	1	5754 8	1	1	8732 09	1	—
$^3P_2-^1S_0$	2332 08	2×10^{-6}	0	3071 63	$3 < 10^{-7}$	0	4735 96	$4 \quad 10^{-9}$	—
$^3P_1-^1S_0$	2321 64	4×10^{-2}	0	3063 72	$6 \quad 10^{-3}$	0	4729 69	$4 . \quad 10^{-4}$	—
$^3P_0-^1S_0$	2315 40	0	0	3059 03	0	0	4726 56	0	—
$^3P_2-^1D_2$	5006 84 (N$_1$)	3	2	6583 6	3	2	10348 7	3	—
$^3P_1-^1D_2$	4958 91 (N$_2$)	1	1	6548 1	1	1	10319 3	1	—
$^3P_0-^1D_2$	4931 93	$7 < 10^{-4}$	0	6528 2	7×10^{-4}	0	10303 6	1×10^{-4}	—
Mean life $^1S_0$ state	0 10 seconds			0 11 seconds			0 12 seconds		
Mean life $^1D_2$ state	26 seconds			3 1 minutes			58 minutes		

The results for the relative intensities of the nebular lines corresponding to $^3P_{2, 1, 0}-^1D_2$ are very satisfactory; in particular, the calculated value of $3 : 1$ for the relative intensity of the nebulium lines N_1, N_2 in O III agrees quite as well as could be expected with the average observed value of $2 : 1$ Indeed, this ratio, which differs somewhat in the different nebulæ, should be more nearly $10 : 3$ according to Campbell and Moore   Similar remarks apply to the red nebular lines, $\lambda = 6583 \cdot 6$ and $\lambda = 6548 \cdot 1$, of N II. The extreme weakness of the line $^3P_0-^1D_2$ in both O III and N II accounts for these lines not being observed in the nebulæ.   Bartlett's results (*loc. cit.*) for the relative intensity of $^3P_{2\ 1\ 0}-^1D_2$ are :—

$$\left. \begin{array}{c} 3 \cdot 9 \, . \, 1 \cdot 2 : 1 \cdot 9 \\ 39 \ : \ 25 \, . \ 0 \\ 11 \ : \ 7 : 8 \end{array} \right\} \text{for O III,} \qquad \left. \begin{array}{c} 1 \cdot 9 : 1 \cdot 2 : 1 \cdot 4 \\ 39 \ : \ 25 : 0 \\ 11 \ : \ 7 : 8 \end{array} \right\} \text{for N II,}$$

[†] 'Proc. Roy. Soc,' A, vol. 118, p. 34 (1928).

the three different results being obtained by assuming three different " intermediate states " in the calculation of matrix elements.

It will be seen from (6 2) and (4 27) that when the ^3P triplet is not far removed from a " normal " one (separation ratio $= 2 \cdot 1$)—as is the case in all the spectra here considered—the ratio ξ/η is small ($\xi = 0$ for normal triplet). From (5.6), we see that it is the small value of ξ/η which accounts for the relative weakness of $^3P_0 - ^1D_2$. As the triplet departs farther from normality the line $^3P_0 - ^1D_2$ becomes stronger, though, owing to the nature of the coefficients in (5.6), the ratio of $^3P_2 - ^1D_2$ to $^3P_1 - ^1D_2$ is always close to 3 : 1. The relative intensity of $^3P_{2, 1, 0} - ^1D_2$ for a normal triplet is exactly 3 1 : 0 according to the present theory. It will be observed that the summation rules are not obeyed in these intensities.

The weakness of the lines $^3P_{1 \; 2} - ^1S_0$ compared to $^1D_2 - ^1S_0$ would also account easily for their not being observed ; but we have in addition the fact that these lines lie in the ultra-violet and so would not be observed in any case in the nebulæ. The line $^3P_1 \; ^1S_0$ (which the calculations show is much the stronger of the two) has, however, been observed in the similar spectrum Pb I † It should be pointed out, incidentally, that the value for $^1D_2 - ^1S_0$ is somewhat unreliable owing to the way in which we dealt with the first-order approximations to the wave-functions for this transition in § 5.

What is perhaps the most interesting result of the calculations from an astrophysical point of view is that for the mean lives of the metastable states $^1S_0$ and $^1D_2$, especially the latter, in O^+ ' and N^+. The figures for the $^1S_0$ state are not very reliable for the reason mentioned above, but those for $^1D_2$ should be fairly accurate It is usually very reasonably assumed that the physical conditions in the nebulæ must be such that the mean time between collisions suffered by the gaseous ions must be at least as great as the mean lives of the ions in the initial metastable states ; for otherwise the ions would be knocked out of these states so quickly by collisions of the second kind that the radiation would not be effective ‡ It is also necessary to suppose that the radiation from the exciting star is so weak that the induced absorption does not seriously impede the emission §

† Sur, ' Phil. Mag.,' vol. 2, p. 640 (1926) ; Gieseler and Grotrian, ' Z. Physik,' vol. 34, p. 374 (1925).

‡ This should not, however, be assumed without question, since emission lines from metastable states, as, for instance, the auroral green line of O I, have been observed in the laboratory where this condition would not, presumably, be satisfied. Frerichs and Campbell, ' Phys. Rev.,' vol. 36, p. 1460 (1931), suggest that the occurrence of this line in the laboratory is due to the strong excitation in laboratory sources.

§ Eddington, ' Mon. Not. R. Astr. Soc ,' vol. 88, p. 134 (1927).

We may therefore (probably) assume that the mean time between collisions in the nebulæ is at least about 26 seconds in regions where the nebulium O III lines are emitted, and about 3 minutes in regions where the red lines, $\lambda = 6583 \cdot 6$ and $6548 \cdot 1$, are emitted   The greater time necessary for the latter is consistent with the fact that the N_1, N_2 lines occur strongly in almost all the nebulæ, whereas the red lines occur only in a few ; the nitrogen spectrum, however, occurs less frequently than the oxygen in the nebulæ, and this may not have any significance.   The mean time between collisions depends on the temperature, density, and effective collision area of the colliding particles in the nebulæ, and these are not at all accurately known   Very rough estimates give a mean time ranging from 10^4 to 10^6 seconds for the diffuse nebulæ, and from 7 to 700 seconds for the planetary nebulæ †

The nebulium lines N_1, N_2 occur also in the spectra of novæ a certain time after their appearance.   If we accept the theory that these lines are emitted by a gaseous shell which expands radially outwards from the nova, then, as pointed out by Elvey,‡ the density of the shell at the moment the nebular lines are emitted must have decreased to such a value that the mean time between collisions is *just* sufficient for the radiation to become effective --about 26 seconds according to the present theory.   If the density of a nova shell at the moment of emission of the nebular lines could be found accurately,§ this, then, should give fairly precise information concerning the temperature (or *vice versa*).

§ 7. *Conclusions*

We are justified in drawing the following conclusions from the present work ·

(1) The only point at which direct comparison of the calculations with experiment can be made is in the relative intensity of the lines $^3P_{2\ 1\ 0}-^1D_2$; the agreement is very satisfactory.

(2) Assuming the validity of our results and of the hypothesis that the mean time between collisions suffered by the emitting atoms in the nebulæ must be at least as long as the mean lives of the atoms in the initial states, the physical conditions in the nebulæ must be such that the mean time between collisions is at least about 26 seconds in regions where the nebulium N_1, N_2

† Becker and Grotrian, *loc. cit.*, p 74.

‡ Elvey, ' Nature,' vol. 121, p. 12 (1928) , Pike, ' Nature,' vol. 121, p. 136 (1928) ; Elvey, ' Nature,' vol. 121, p. 453 (1928) ; Gerasimovic, *ibid.*

§ Elvey's estimate is 10^{-17} gr. cm.$^{-3}$, about the same as the estimated density in the nebulæ, but the data on which it is based can hardly be considered reliable. See Menzel, ' Nature,' vol. 121, p. 618 (1928).

lines are emitted, and at least about 3 minutes in regions where the red lines, $\lambda = 6583 \cdot 6$ and $\lambda = 6548 \cdot 1$, are emitted

(3) In the case of novæ exhibiting the N_1, N_2 lines in their spectra, the mean time between collisions should be about 26 seconds in the region where these lines are emitted at the moment the lines first appear strongly marked.

(4) All in all, this paper, as far as it goes, confirms Bowen's hypothesis concerning the origin of certain of the nebular lines, and the further assumption that these lines are due to quadripole radiation The final step in the confirmation would be the production of these lines in the laboratory if it should become possible to reproduce in some degree the nebular conditions (as has already been done in the case of the O 1 nebular lines by Hopfield, *loc. cit.*).

In conclusion, I should like to express my warm thanks to Mr. Fowler for his interest in this work, and his helpful advice ; also to Professor Hartree for supplying me with the numerical data for the radial wave-functions for O^{++}.

The Diffraction of Elastic Waves at the Boundaries of a Solid Layer.

By J. H. Jones, Ph.D., Chief Geophysicist, Anglo-Persian Oil Co , Ltd.

[Plates 16 and 17]

1. Introduction.

When a disturbance occurs near the free surface of a solid medium or near the interface of two solid media, many remarkable effects arise from imperfect reflection and refraction due to the curvature of the elastic wave-fronts.   In the case of a solid with a free surface, Lord Rayleigh predicted the existence of surface waves travelling with a velocity lower than that of the distortional waves.   These waves are usually very pronounced on earthquake records.

It has been demonstrated by Nakano that a large percentage of the energy of an earthquake will appear in the Rayleigh waves if the focus is near the surface, and conversely, for a very deep focus there will be little or no energy in these waves.   Another kind of surface wave was discovered by Love.   This wave exists when a layer of finite thickness rests on a deep solid layer and when the velocity of the distortional wave in the upper layer is less than that in the lower layer.

An effect of a different kind was observed by A. Mohorovicic in the records of near earthquakes. He found two distinct compressional and distortional wave pulses in the records. Mohorovicic accounted for the four pulses by assuming that the focus was in an upper layer of the crust and that one pair of waves had travelled directly along this layer, and that the other pair had been refracted into a deeper layer, and after travelling a certain distance along this layer, had been refracted to the surface again.

Later, other waves were discovered which indicate a still deeper layer in the earth's crust. The depths of these layers have been estimated from the time of travel of the waves. The same principles have been applied with success to the smaller scale problem of determining the depths of sedimentary formations close to the earth's surface. For this purpose, the disturbance is set up artificially with an explosion of a charge of gelignite or dynamite buried in the ground, and the earth movements are recorded by special types of portable seismographs.

In the spring of 1930, the geophysical staff of the Anglo-Persian Oil Company carried out an experimental seismic survey of the Masjid-i-Sulaiman oilfield in South Persia, in order to test the seismic method for determining the depth of a hard limestone bed which forms the oil reservoir. It will be shown in this paper that several diffracted wave pulses are formed at the upper and lower boundaries of the layer, and that the depth and thickness of the layer can be estimated from the velocities and the times of travel of these pulses.

2. Diffraction Effects in a Solid Layer embedded in a Medium possessing Lower Elastic Wave Velocities.

Suppose that the solid layer, which has two parallel surfaces at a distance d apart, lies horizontally at a depth h in the other medium. Let V_1 and V_1' represent the velocities of the compressional and distortional waves in the surrounding medium, and V_2 and V_2', the corresponding velocities in the solid layer.

Referring to the diagram, fig. 1, aa', bb' are the two boundaries of the layer, and O represents the position of the explosion near the surface of the ground.

Upper Boundary Wave.

Consider the compressional wave pulse which leaves the explosion point O and falls on the surface of the solid layer at A, so that OA makes an angle $\theta_1 = \sin^{-1} V_1/V_2$ with the normal at A.

According to the laws of geometrical optics there would be no energy transported along the surface aa' when a plane wave falls on the surface at the critical angle θ_1; the bulk of the energy would be reflected back to the original medium along AO' But when the wave-length is comparable to the radius of curvature of the wave-front, as is the case in our problem, it appears that the energy actually travels along the boundary aa', and is scattered back to the original medium along the paths A'C', A''C''', etc , which make the same angle θ_1 with the normal to the surface of the solid layer A simplified form of the problem has been studied theoretically by Jeffreys * He has considered the case of two compressible but non-rigid media, the lower medium transmitting the compressional wave with the greater velocity.
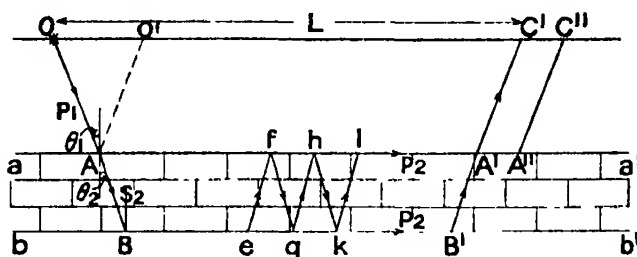
Fig 1.

The most important result from the practical point of view derived by Jeffreys in his paper, refers to the time of travel of the indirect wave in the lower layer. He has shown that the ordinary law of refraction gives the correct time of travel. In other words, the time of travel of the diffracted wave from O to C', fig. 1, is given by,

$$t_0 = \frac{OA}{V_1} + \frac{AA'}{V_2} + \frac{A'C'}{V_1}. \tag{1}$$

The time t_0 can be expressed in terms of the depth h of the upper surface of the layer and the distance OC'. The expression is

$$t_0 = \frac{L + 2h \cot \theta_1}{V_2}. \tag{2}$$

The depth h can be determined by means of this relation when the velocities V_1 and V_2 are known.

The usual method, however, of finding h is to find the distance L_1 on the time distance graph at which the time along the indirect path is the same as

* ' Proc. Camb. Phil. Soc.,' vol. 23, p. 472 (1927).

that along the direct path from O to C′. The time along the direct path is L_1/V_1 so that the condition for equality is

$$\frac{L_1}{V_1} = \frac{L_1}{V_2} + \frac{2h \cot \theta_1}{V_2},$$

which gives

$$h = \frac{L_1}{2}\left(\frac{1 - \sin \theta_1}{\cos \theta_1}\right). \tag{3}$$

Consider the two adjacent paths A′C′, A″C″, fig. 1. The difference in the times of arrival at C′ and C″ is merely due to the extra length A′A″ of the horizontal path in the solid layer. Thus the observed velocity of the indirect wave is

$$\frac{C'C''}{\Delta t} = \frac{A'A''}{\Delta t} = V_2$$

(Δt is the small difference in the times of arrival at C′ and C″). If the solid layer is inclined at an angle ϕ to the horizontal, it can be readily shown that the apparent velocity observed on the surface is given by

$$\frac{C''C''}{\Delta t} = \frac{V_2 \sin \theta_1}{\sin(\theta_1 \pm \phi)}.$$

The negative sign for ϕ refers to the wave travelling up the slope and *vice versa* Thus the apparent velocity of the indirect wave will be greater than the true speed of the compressional wave in the solid layer if the wave is travelling up the slope, and smaller than the true value if travelling down the slope of the upper surface.

Lower Boundary Wave.

When a compressional wave pulse falls on the surface aa' at the critical angle θ_1, it will give rise to a distortional pulse S_2 in the solid layer, which travels in the direction making an angle θ_2 with the normal. This angle θ_2 is given by $\sin \theta_2 = \sin \theta_1 V_2'/V_1$, where V_2' is the velocity of the distortional wave in the solid layer. But $\sin \theta_1 = V_1/V_2$, so that $\sin \theta_2 = V_2'/V_2$. Thus the distortional pulse falls on the lower boundary of the solid layer at the appropriate angle to form a reflected compressional pulse which travels along this boundary with the velocity of the compressional wave.

Owing to the curvature of the wave-front, it appears that a considerable proportion of the energy of the incident distortional pulse is transmitted along the lower boundary as a diffracted compressional wave pulse. Nakano[*]

---

[*] Nakano, 'Japanese J. Astr. & Geophs.,' vol. 2, p. 233 (1925).

has investigated theoretically the problem of the reflection of a distortional wave at a free surface, and he has shown that a compressional wave is formed at the free surface in addition to the Rayleigh wave. Nakano has also shown that the percentage of energy in these waves depends on the depth of the focus and the curvature of the wave-front of the primary distortional wave.

The diffracted compressional wave travelling along the lower boundary of the solid layer is similar in type to that discussed by Nakano It is also similar to the P*g* wave formed at the interface of the granitic and sedimentary layers and observed at stations near the epicentre of an earthquake.*

Each point on the lower boundary of the solid layer will become the source of small secondary distortional pulses, some of which leave the surface at the critical angle θ_2 and again strike the upper boundary and are transmitted into the upper medium and reach the surface.

For example, a small pulse leaves the lower boundary at B′, strikes the upper boundary at A′, and travels to the surface as a compressional pulse along the path A′C′. Part of the energy of the distortional pulse arriving at A′ will follow a distortional wave path in the upper medium, but this arrives later than the compressional pulse and need not be considered at present.

Referring to fig. 1, the time path of the lower boundary wave is OABB′A′C′, and the time from O to C′ is

$$t_2 = \frac{OA + A'C'}{V_1} + \frac{AB + B'A'}{V_2'} + \frac{BB'}{V_2} ,$$

which can be written in the form

$$t_2 = \frac{L}{V_2} + \frac{2h \cot \theta_1}{V_2} + \frac{2d \cot \theta_2}{V_2} . \tag{4}$$

The time of the upper boundary wave has been shown to be

$$t_0 = \frac{L}{V_2} + \frac{2h \cot \theta_1}$$

so that

$$t_2 - t_0 = \frac{2d \cot \theta_2}{V_2} . \tag{5}$$

This expression can be used to calculate the thickness of the solid layer.

Besides the pulse travelling along the path OABB′A′C′, there is an infinite number of other minute pulses which arrive simultaneously at the point C′. Thus consider the distortional pulse leaving the boundary at *e* and falling on

* H. Jeffreys, " The Earth," 2nd ed., p. 100.

the upper boundary at f, where it forms a compressional pulse travelling along the upper face to A' and finally along $A'C'$ to the surface. The complete time-path of this pulse is $OABefA'C'$, and the time of travel is given by (4) above. Again, consider the diffracted wave formed at the upper boundary. Each point on this surface is the origin of secondary distortional pulses travelling across the solid layer.

For example, a distortional pulse leaves the upper surface at f and falls on the lower boundary at g, travels along gB' as a compressional pulse, and along $B'A'$ as a distortional pulse. The complete path of this pulse is $OAfgB'A'C'$, and the time of travel is again given by (4).

It will be seen that all the pulses have crossed the solid layer twice with the velocity of the distortional wave, and have travelled partly along the lower and partly along the upper boundary of the layer with the velocity of the compressional wave.

It is clear that this secondary diffracted wave, being the resultant of an infinite number of minute pulses, will be stronger than the primary diffracted wave formed at the upper boundary. It will also maintain its energy better than the primary wave as the number of re-inforcements increases as the distance OC' increases.

Internal Reflections

The next pulse arriving at the surface will have suffered reflection either at the upper or lower face of the solid layer.

Referring to fig 1, the complete path of the constituents of this pulse will be similar to $OABefgB'A'C'$ and $OAfghkB'A'C'$. All these pulses have crossed the solid layer four times and they will arrive simultaneously at C'.

The time of travel is

$$t_4 = \frac{L}{V_2} + \frac{2h \cot \theta_1}{V_2} + \frac{4d \cot \theta_2}{V_2}. \tag{6}$$

so that

$$t_4 - t_2 = \frac{2d \cot \theta_2}{V_2}. \tag{5}$$

This pulse will be followed by one which has crossed the solid layer six times and the time of travel will be.

$$t_6 = \frac{L}{V_2} + \frac{2h \cot \theta_1}{V_2} + \frac{6d \cot \theta_2}{V_2}. \tag{6}$$

Thus the first part of the seismogram will consist of a comparatively **weak**

pulse formed at the upper boundary of the layer, and this will be followed by a strong second arrival at an interval of time,

$$t_2 - t_0 = \frac{2d \cot \theta_2}{V_2},$$

and by other pulses at the same interval. For convenience of reference to the various pulses, the upper boundary pulse will be called the α_0 pulse, the pulse which has travelled twice across the layer will be referred to as α_2, and the pulse which has crossed four times will be α_4, etc

Intermediate Pulses —There will be intermediate pulses formed by simple reflection at the lower boundary of the layer. The mode of formation of these pulses is illustrated in fig. 2
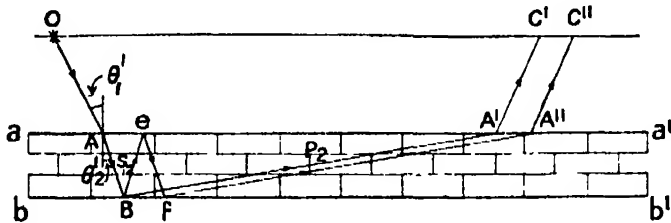
Fig. 2

A compressional wave pulse, leaving the focus at O, falls on the surface aa' at an angle θ_1', smaller than the critical angle θ_1 in fig 1, and the distortional pulse S_2 is formed by refraction. The incidence of this pulse on the lower boundary at an angle θ_2', smaller than the critical value θ_2 in fig. 1, produces a compressional pulse travelling along BA' and $A'C'$. The complete path of this pulse is $OABA'C'$.

When the distance OC' is large compared to d, the time t_1 along this path approximates to

$$t_1 = \frac{L}{V_2} + \frac{2h \cot \theta_1}{V_2} + \frac{d \cot \theta_2}{V_2} \tag{7}$$

The next pulse of this group will follow the path $OABefA''C''$, and the time of travel will approximate to

$$t_3 = \frac{L}{V_2} + \frac{2h \cot \theta_1}{V_2} + \frac{3d \cot \theta_2}{V_2}. \tag{8}$$

These pulses are referred to as α_1, α_3, etc.

Another complete series of pulses will be derived from the primary compressional pulse leaving the focus at O. These pulses will differ from the α pulses only in respect of the final part of the path across the overburden.

In this series, which may be referred to as the β series, the path A'C', figs. 1 and 2, will be distortional. There will be similar effects resulting from the primary distortional wave A diffracted distortional wave will be formed at the upper boundary of the solid layer, and there will be pulses corresponding to α_1, α_2, etc., with the path in the overburden entirely distortional.

3. Experimental Investigation into the Diffraction Effects at the Boundaries of a Solid Layer.

The limestone bed at Masjid-i-Sulaiman is several hundred feet thick and is covered by rocks composed of gypsum, salt, shales and sandstones. Below the limestone is a medium consisting chiefly of shales and marls. The elastic wave velocities in the limestone are appreciably higher than those in the media above and below, so that the physical conditions are similar to those discussed above. The underground conditions at this oilfield are known in great detail as the whole area has been carefully explored with the drill.

This knowledge was extremely useful in connection with the interpretation of the results

The Survey Instruments.

(a) *The Seismograph*—Early in 1929, the writer developed a portable seismograph for geophysical prospecting, a detailed account of which has recently been published.*

(b) *The Vibration Galvanometer.*—The time of explosion and other synchronising signals are recorded by a special type of vibration galvanometer in conjunction with transmitting and receiving wireless outfits.

The vibration galvanometer is similar in principle to the device for controlling the zero position of the seismograph It consists of a small cobalt steel magnet fitted with soft iron pole pieces about 3 mm. apart. Two magnetising coils are fitted on the pole pieces and connected together so that the magnetising actions are opposing each other. The effect of a small current flowing through the coils is to distort the magnetic lines of force outside the gap. A small soft iron element suspended in this field by a phosphor bronze strip will respond to the variations in the current flow through the coils.

(c) *The Recording Camera.*—The recording camera consists of a clockwork arrangement for driving the photographic paper at a uniform rate past a

---

* 'J. Sci. Instr.,' vol. 9, p. 8 (1932).

narrow slit. A small time-marking pendulum fixed inside the camera intercepts a narrow beam of light falling on the photographic paper so that an accurate time-scale is recorded on each seismogram.

The Method of Investigation.

The observation lines were arranged in most cases to run parallel to the long axis of the structure, and full use was made of the accurate underground contour map of the oilfield for this purpose. The seismograph stations were located at about 1000 feet intervals and on a line passing through the explosion point. The time of travel of the waves was measured to an accuracy of 0.005 second. At stations close to the explosion point the first pulse will have travelled directly through the upper medium, but at the more distant stations, the indirect wave will arrive earlier on account of the greater speed in the hard limestone layer.

There will be a discontinuity in the time curve at the point where the time along the indirect path is the same as that along the direct path in the upper medium. Thus in fig. 3, the line OAC is the graph of the times of arrival of the direct wave in the upper medium, and the slope of this line gives the velocity of the compressional wave in this medium.
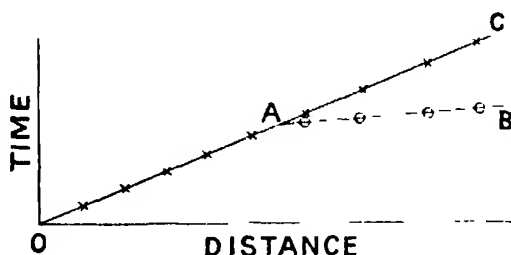

Fig 3.

At a certain distance from the explosion point, the indirect wave begins to appear before the direct wave. On the graph, the portion AB of the time-curve gives the apparent velocity in the second medium. This will be identical with the velocity of the compressional wave in the second medium if the interface is horizontal. In general, if the interface is not horizontal, it is necessary to observe the apparent speed of the wave travelling in the reverse direction to get the true speed of the compressional wave in the covered medium. The true speed of the indirect wave V_2, and the inclination ϕ of the layer,

can be calculated from the observed apparent velocities V_2' and V_2'' and the velocity V_1 in the upper medium, using the relations

$$V_2' = \frac{V_2 \sin \theta_1}{\sin (\theta_1 + \phi)} = \frac{V_1}{\sin (\theta_1 + \phi)} \qquad (8)$$

$$V_2'' = \frac{V_2 \sin \theta_1}{\sin (\theta_1 - \phi)} = \frac{V_1}{\sin (\theta_2 - \phi)}. \qquad (9)$$

The angles θ_1 and ϕ can be deduced from (8) and (9) and V_2 can then be determined from the relation, $V_2 = V_1/\sin \theta_1$.

So far the simple case of a single medium overlying the solid layer has been considered, but in practice the overburden may be composed of two, three or more layers with different elastic wave velocities.

Consider the general case of several parallel strata overlying the limestone layer, fig 4. All the layers are inclined at a small angle ϕ to the horizontal, and the elastic wave velocities are V_1, V_2, V_3, V_4 and V_L represents the velocity
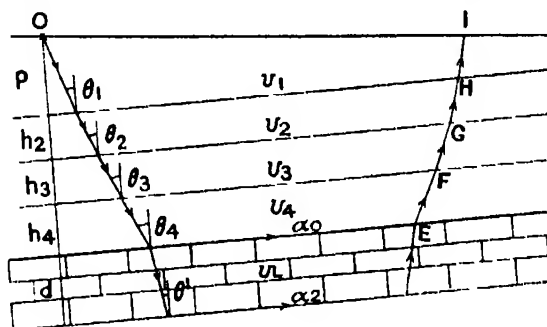

Fig. 4.

in the limestone layer. The thicknesses of the various beds are h_2, h_3, h_4, and p denotes the thickness of the upper medium at the explosion point

The minimum time paths of the α_0 and α_2 pulses are shown in the diagram; the angles θ_1, θ_2, etc., are given by $\sin \theta_1 = V_1/V_L$, $\sin \theta_2 = V_2/V_L$, etc. The time t_0 from O to I can be written in the form

$$t_0 = \frac{2p \cot \theta_1}{V_L} + \frac{1}{V_L} \Sigma 2h \cot \theta_1 + \frac{L}{V_{L_a}}, \qquad (10)$$

where V_{L_a} is the apparent velocity of the α_0 pulse. Similarly the time t_2 of the α_2 pulse will be given by

$$t_2 = \frac{2p \cot \theta_1}{V_L} + \frac{2}{V_L} \Sigma 2h \cot \theta_1 + \frac{L}{V_{L_a}} + \frac{2d \cot \theta'}{V}$$

where θ' is given by $\sin \theta' = V_L'/V_L$.

The Experimental Results.

In the following pages, attention will be confined chiefly to the important α pulses, as these appear first on the seismograms, and their identification is comparatively easy.

For the study of the diffraction effects, the traverse lines were arranged with the aid of the underground contour map to avoid large curvatures and inclinations of the surface of the limestone.

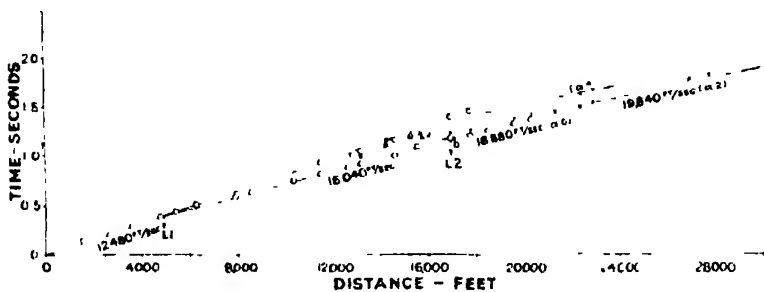Observations were made on several traverse lines but in this paper only

Fig. 5

three of these are considered. The time-distance graph for one of these traverses is shown in fig 5.

It will be seen from the time-curve that the overburden is composed of two media with elastic wave velocities of 12,480 feet per second and 16,040 feet per second respectively.

The limestone pulses begin to appear clearly on the seismograms at about 17,000 feet from the explosion point. The upper boundary pulse (α_0) appears as a first arrival at this distance but disappears again beyond 20,400 feet. The speed of this pulse is 16,880 feet per second. The average depth of the surface of the limestone has been calculated from the position of the two discontinuities at L_1 and L_2, and the values of the velocities through the overburden and along the upper surface of the limestone layer. This calculation is given in detail below.

Both the α_2 and α_4 pulses are very pronounced on the seismograms obtained on this traverse line. It will be seen that the velocity of these pulses is considerably higher than that of the α_0 pulse.

The higher velocity of the lower boundary pulses is shown in a striking manner on the actual seismograms reproduced in fig. 6, Plate 16. The distance of the

position of observation is indicated on each record and the three important pulses α_0, α_2 and α_4 are marked.

The seismograms show the α_2 pulse gradually overtaking the α_0 pulse, on account of the greater velocity of the former, and at a distance of 21,400 feet, the α_2 is the first arrival on the record   This difference in the speeds along the upper and lower boundaries of the limestone layer has been observed on most of the traverses at the Masjid-i-Sulaiman oilfield, although the difference is much more pronounced in some parts of the field than in others.   The lower velocity along the upper boundary is undoubtedly closely connected with the porosity and fissuring of the upper part of the limestone layer.   It has been found that the variation in the velocity of the α_0 pulse is intimately connected with the oil productivity in different parts of the field ; the velocity is lowest in the area of greatest productivity.   On the other hand the velocity of the lower boundary pulses is remarkably constant over the whole oilfield, thus indicating uniform conditions at the base of the limestone layer.   The velocity of the compressional wave pulses along the lower boundary is close on 20,000 feet per second, whereas the velocity of the upper boundary pulse varies from 19,200 feet per second to 15,800 feet per second.

A difference in the velocity along the upper and lower boundary will have considerable effect on the strength of some of the α pulses.

For example, the α_2 pulse which is compounded of minute pulses which have travelled partly along the lower and partly along the upper boundary, will not maintain its strength at the distant stations if there is a difference in the velocities along the two boundaries.   On the other hand, the α_4 pulse will not be affected by the velocity difference as most of the pulses of which this is composed will arrive simultaneously at the surface.   Consequently when there is a difference in the velocities of the elastic waves along the upper and lower boundaries of the limestone layer, the α_4 pulse would be expected to be stronger than α_2 at long distances from the explosion point.   This has been found to be the case on several traverses surveyed over the great producing areas at Masjid-i-Sulaiman.

The varying velocity in the limestone layer will introduce slight modifications in the expression for the time of the α pulses.   The time t_0 of the α_0 pulse will now be given by

$$t_0 = \frac{L}{V_{u_a}} + \frac{2}{V_u} \Sigma 2h \cot \theta + \frac{2p \cot \theta_1}{V_u},$$

where V_u is the true speed of the compressional wave along the upper boundary

and V_{u_a} is the apparent velocity observed on the surface. Similarly the time t_2 of the α_2 pulse will be given by

$$t_2 \quad \frac{L}{V_{L_a}} + \frac{2p \cot \theta_1}{V_L} + \frac{2}{V_L} \Sigma \, 2h \cot \theta + \frac{2}{V_L} \int_0^a \cot \theta \, dh.$$

The integral term represents the time of travel of the distortional pulse across the limestone layer and it replaces the term $2d \cot \theta / V_L$, which holds when the speed is constant throughout the limestone bed. The integral can be evaluated when the law of variation of velocity in the limestone layer is known Actually, only the velocities along the upper and lower boundaries can be determined experimentally, and it is necessary to make some assumption regarding the variation of the velocity across the layer The velocity at a depth h in the layer is assumed to be given by

$$V_h = V_u e^{ah},$$

also by the law of refraction,

$$V_h = V_L \sin \theta$$

Thus the integral

$$\frac{2}{V_L} \int_0^a \cot \theta \, dh = \frac{2}{aV_L} \int_{\theta_s}^{\theta_s} \cot^2 \theta \, d\theta = \frac{2d \, (\cot \theta_2 - \cot \theta_3)}{V_L \log V_L / V_u} - \frac{2d \, (\theta_3 - \theta_2)}{V_L \log V_L / V_u}$$

The angles θ_2 and θ_3 can be determined when the velocities are known, and the integral term can be evaluated in terms of d

The average depth of the upper surface of the layer can be calculated from the time-curve, fig. 5. The thickness of the upper layer in the overburden can be obtained from the position of the discontinuity L_1 at 4880 feet. This thickness is given by

$$p = \frac{L_1}{2} \frac{(1 \quad - \sin \theta_1)}{\cos \theta_1} .$$

Substituting $L_1 = 4880$ feet, $\sin \theta_1 = V_1/V_2 = 0\,78$, we get $p = 850$ feet.

The average depth of the upper face of the limestone layer can be deduced from the position of the second discontinuity at 17,000 feet.

The general relation is

$$p + h_2 \frac{\cot \theta_3}{\cot \theta_1} = \frac{L_2}{2} \frac{1 - \sin (\theta_1 \pm \phi)}{\cos \theta_1} - \frac{\Delta L_2}{2 \cos \theta_1} \,^{*}.$$

In the calculation we shall neglect the small angle ϕ. The angle θ_1 is given by $\sin \theta_1 = V_1/V_u = 0 \cdot 74$, so that $\cot \theta_1 = 0 \cdot 907$. Also $\sin \theta_2 = V_2/V_u = 0 \cdot 95$,

---

* This relation can be deduced by equating the time t_0 given by equation (10) above to $L_2 - \Delta L_2/V_1$, where $\Delta L_2 = ab$ in fig. 5.

and $\cot \theta_2 = 0 \cdot 327$. Substituting the value of L_2 and ΔL_2, we get $h_2 = 1250$ feet. Thus the average depth of the upper face of the layer is $p + h_2 = 2100$ feet.

Calculation of the Thickness of the Layer.

There are several methods of obtaining the thickness of the limestone layer. The most direct method is to calculate the thickness from the time interval $(t_4 - t_2)$, using the relation

$$t_4 - t_2 = \frac{2}{V_L} \int_0^a \cot \theta \, dh$$

$$= \frac{2d (\cot \theta_2 - \cot \theta_3)}{V_L \log V_L / V_u} - \frac{2d (\theta_3 - \theta_2)}{V_L \log V_L / V_u}.$$

Substituting $V_u = 16,880$ feet per second, $V_L = 20,000$ feet per second and the values of θ_2, θ_3, etc., the value of d is given by

$$1 \cdot 605 \cdot 10^{-4} d = 0 \cdot 130$$

or

$$d = 810 \text{ feet.}$$

Another value of the thickness can de deduced from the time of the α_2 pulse, assuming the depth of the layer calculated from the α_0 pulse.

The time t_2 is given by

$$t_2 = \frac{L}{V_{L_a}} + \frac{1}{V_L} \Sigma \, 2h \cot \theta + \frac{2}{V_L} \int_0^a \cot \theta \, dh.$$

At $L = 24,000$ feet, $t_2 = 1 \cdot 580$ seconds

$$\frac{L}{V_{L_a}} = 1 \cdot 210 \text{ seconds}, \quad \frac{1}{V_L} \Sigma \, 2h \cot \theta = 0 \cdot 199.$$

Thus

$$\frac{2}{V_L} \int_0^a \cot \theta \, dh = 0 \cdot 171,$$

which gives $d = 1060$ feet. The difference in the two values for the thickness of the layer is not surprising in view of the assumption made regarding the variation of the velocity within the layer. Further, some error will be introduced by neglecting the small angle of inclination of the layer. The average thickness of the limestone layer determined by the drill is about 900 feet, so that the above determinations are in fair agreement with this figure.
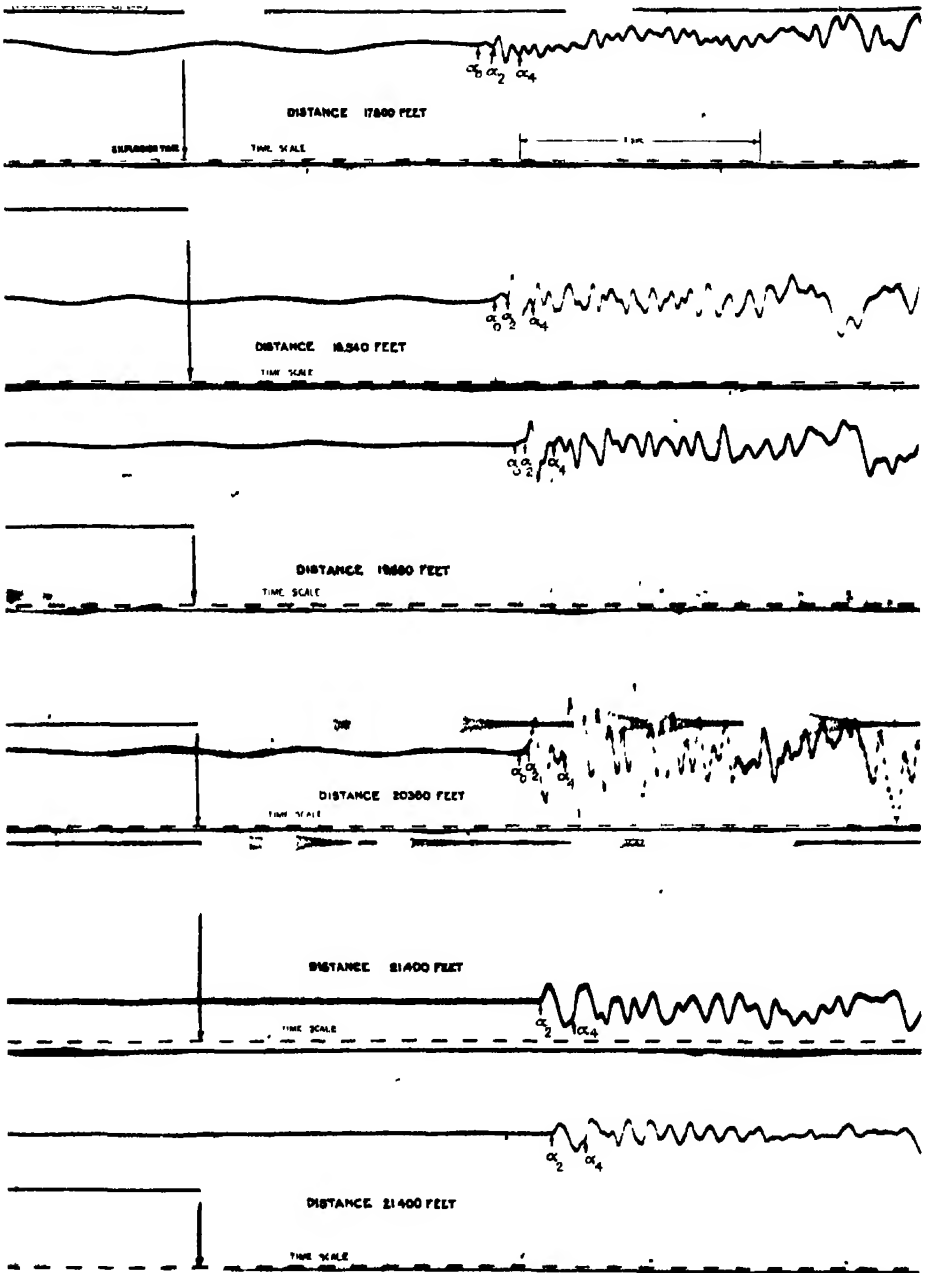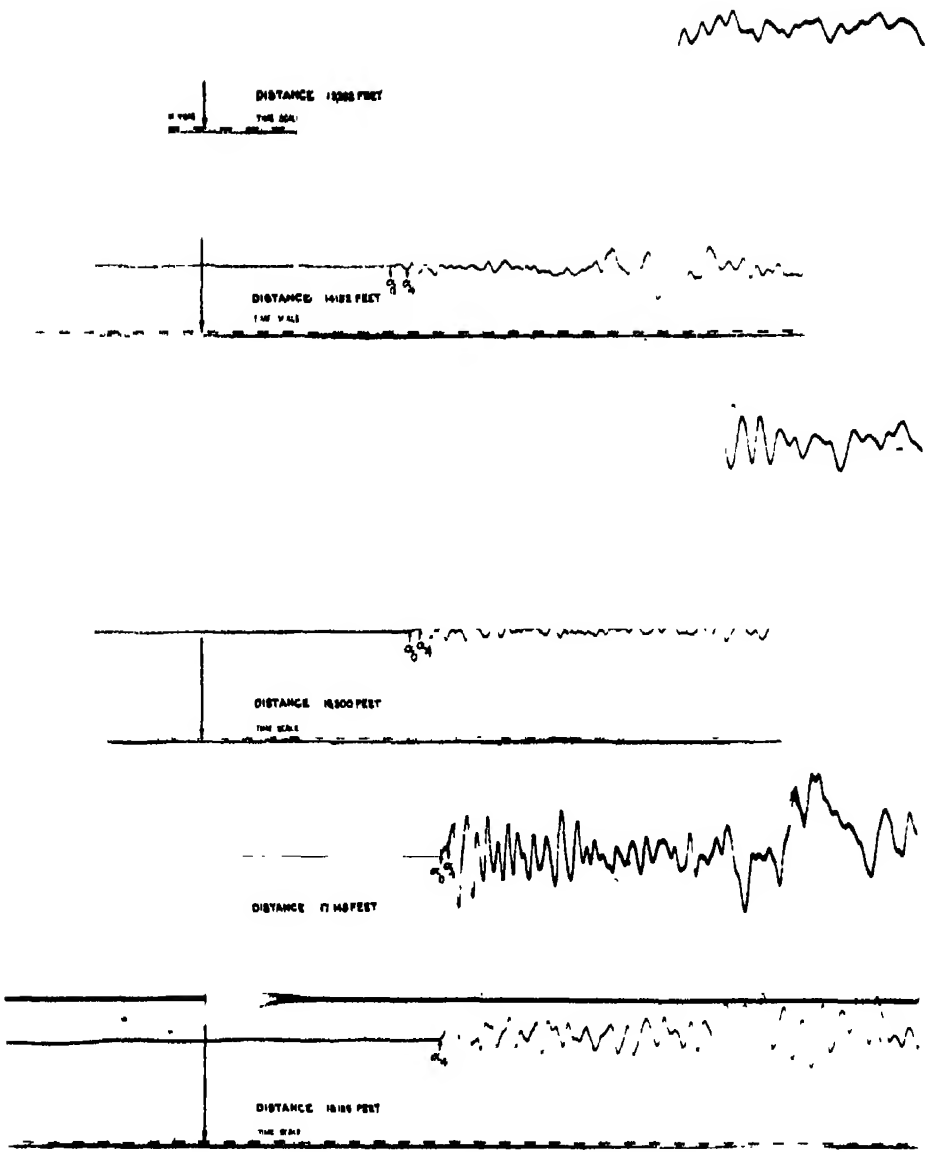
Fig 6.

FIG. 8.

Another time-distance graph is shown in fig. 7.

This traverse was located close to one of the greatest producing regions of the oilfields.

The α_0 pulse appears as a first arrival on the seismograms at about 10,000 feet from the explosion point and its velocity is about 15,840 feet per second.
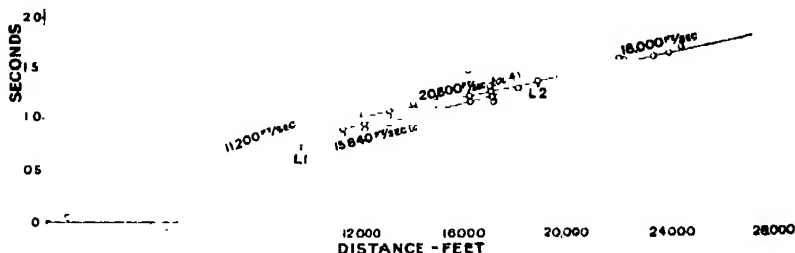

FIG. 7.

The pulse disappears at 17,000 feet. The low velocity of this pulse is quite consistent with the considerable degree of porosity and fissuring that must exist in this area of prolific oil production. The lower boundary pulse has a velocity of 20,600 feet per second. This is probably slightly higher than the true speed on account of a gradual rise in the layer along this traverse line. The highest point of the layer is reached at about 19,000 feet from the explosion point, and beyond this point the surface of the layer gradually falls again. This fall in the surface is the cause of the apparent low velocity of 18,000 feet per second at the end of the line. Some of the seismograms obtained on this traverse are shown in fig. 8, Plate 17. They show very clearly the higher speed and the greater strength of the lower boundary pulses. It will be observed that the high speed pulse has been marked α_4 on the graph. This is indicated by the calculation of the thickness of the limestone layer which is given below. It is possible that the α_3 pulse is too weak to show on the records on account of the large difference in the velocities along the upper and lower boundaries.

Calculation of the Depth and Thickness of the Layer.

Assuming $V_1 = 13,480$ feet per second, $V_2 = 15,840$ feet per second and $L_1 = 9700$ feet, the average depth of the upper boundary of the layer reduces to 1380 feet. This is in good agreement with the average known depth in the area. We have again neglected the small inclination of the surface. The

thickness of the layer can be deduced from the time of arrival of the α_4 pulse, assuming the depth given above.

$$t_4 = \frac{L}{V_{L_a}} + \frac{1}{V_L} \Sigma \, 2h \cot \theta + \frac{4}{V_L} \int_0^a \cot \theta \, dh.$$

At $L = 16,000$ feet, $t_4 = 1 \cdot 188$ seconds

$$\frac{L}{V_{L_a}} = 0 \cdot 776, \quad \frac{1}{V_L} \Sigma \, 2h \cot 0 = 0 \cdot 122,$$

so that

$$\frac{4}{V_L} \int_0^a \cot \theta \, dh = 0 \cdot 290,$$

which gives

$$d = 860 \text{ feet.}$$

The value of V_L has been taken to be 20,000 feet per second which is the mean of all determinations at the oilfield.

About 30 miles south-east of the oilfield, the limestone layer outcrops at the surface and forms the cover of an enormous mountain, reaching a height of 4700 feet above sea level.

A line was surveyed at the foot of this mountain for the purpose of checking the elastic wave velocities observed at the oilfield. All the observation stations and the explosion point were located on the surface of the limestone layer.

The time-distance graph is shown in fig. 9, and it will be observed that there are two different pulses plotted on the first part of the graph.
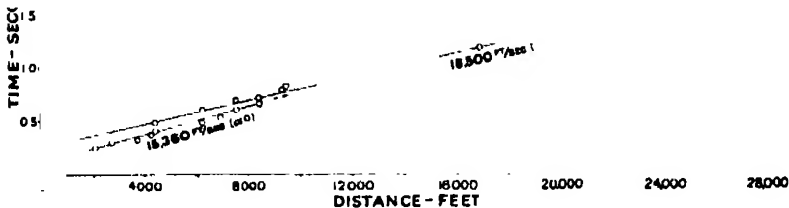

Fig. 9.

The first pulse with the velocity of about 15,360 feet per second has travelled along the surface of the limestone layer, and corresponds to the α_0 pulse detected at the Masjid-i-Sulaiman oilfield. The velocity is slightly less than the lowest value observed at the oilfield. This pulse was not detected beyond 8400 feet from the explosion point. The graph of this pulse does not pass through the

origin. This effect which is sometimes referred to as the " delay in starting " is probably caused by a very loose layer lying over the solid limestone and which transmits the disturbance with a very low velocity.

The second pulse plotted on the graph, becomes a first arrival at 8400 feet. and has a velocity of 18,500 feet per second. This corresponds to one of the lower boundary pulses detected at Masjid-i-Sulaiman. Owing to weathering and other actions, a considerable thickness of the limestone layer has been eroded from the base of the mountain and the actual thickness of the layer under the traverse line was between 400 and 500 feet. This thickness can be estimated from the times of arrival of the two pulses.
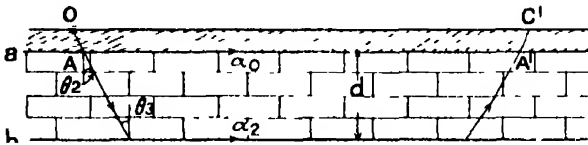

FIG. 10.

In the diagram, fig. 10, aa', bb', represent the upper and lower boundaries of the layer with a very loose layer above.

The path of the α_0 pulse is OAA'C'.

Let $OC' = AA'$ (approx) $= L$, so that

$$t_0 = \frac{L}{V_u} + \Delta,$$

where Δ is the time along the paths OA and A'C' in the thin cover. Again

$$t_2 = \frac{L}{V_L} + \frac{2}{V_L} \int_0^a \cot 0 \, dh + \Delta.$$

Thus

$$t_2 - t_0 = \frac{L}{V_L} - \frac{L}{V_u} + \frac{2}{V_L} \int_0^a \cot \theta \, dh.$$

Expressing the integral in terms of d we get,

$$1 \cdot 806 \; 10^{-4} d = (t_2 - t_0) + 0 \cdot 110 \, L \, 10^4.$$

At $L = 6000$ feet, $t_2 - t_0 = 0 \cdot 085$ second, so that

$$d = 840 \text{ feet.}$$

This is approximately twice the known thickness of the layer, so that the high speed pulse must be assumed to be α_4, and the thickness now reduces to 420

feet. This result is quite consistent with the facts established at the oilfield, where it was found that the first strong high speed pulse was nearly always α_4 in those areas where the upper part of the layer would be expected to be considerably fractured. We can also deduce the thickness directly from the time of arrival of the α_4 pulse.

$$t_4 - \Delta = \frac{L}{V_L} + \frac{4}{V_L} \int_0^a \cot \theta \, dh,$$

which reduces to

$$3 \cdot 612 \cdot 10^{-4} d = (t_4 - \Delta) - \frac{L}{V_L}.$$

At $L = 22,000$ feet,

$$t_4 - \Delta = 1 \cdot 342, \qquad \frac{L}{V_L} = 1 \cdot 189,$$

so that $d = 425$ feet, which is an excellent agreement with the previous determination.

Summary and Conclusions.

An account has been given of an experimental investigation into the diffraction of elastic waves at the boundaries of a limestone layer, embedded in a medium possessing lower elastic wave velocities.

Several diffraction pulses have been observed at the surface. The first of these pulses has travelled along the upper boundary of the layer with the speed of the compressional wave. This pulse is invariably weak and cannot be detected at the distant stations. Further, the speed of this pulse varies over a wide limit at the oilfield, and there appears to be an intimate connection between this speed and the degree of fissuring in the upper part of the limestone layer.

Several other pulses have been discovered which have a higher and more constant velocity, and possess greater energy at the distant stations.

The writer has advanced the view that these are formed by the critical reflection of distortional pulses at the lower boundary. The distortional pulses are transformed at reflection to compressional pulses travelling along the lower boundary. Some of the distortional pulses will be internally reflected within the limestone layer before being transformed at the lower boundary, and will arrive later at the surface. The time interval between the arrival of the successive pulses depends on the thickness of the layer and on the velocity of the distortional pulses across the layer. It is assumed that the higher speed of these pulses is the result of greater compactness at the base of the limestone layer. In this connection it is interesting to record that in one area of the

Masjıd-ı-Sulaıman oilfield, where the upper part of the lımestone layer ıs known from drilling records to be very compact, the velocıty of the upper boundary wave was observed to be close to that travellıng along the lower boundary.

The greatest dıfference in the velocıty was observed ın the great producing regıons.

In conclusıon the writer takes thıs opportunity to express his appreciatıon of the ınterest taken ın this work by Sır John Cadman, G.C.M.G., D Sc., and Mr. J. Jameson, C.B.E.   He also wishes to acknowledge his ındebtedness to his colleagues on the geophysıcal staff of the Anglo-Persıan Oıl Company for their valuable assistance, and to Professor A O. Rankıne, O.B E., D Sc., and Dr. Harold Jeffreys, F R S , for the benefit of theır vıews on thıs subject.

The Velocity of Corrosion from the Electrochemical Standpoint. Part II.

By U. R Evans and T P. Hoar.

In Part I of thıs serıes of papers,[*] an electrochemıcal survey was made of those types of corrosion, where large dıstınct anodıc and cathodıc areas are met wıth   Measurements showed that the corrosıon produced was equıvalent to the electrıc current flowing, whilst potentıal movements suggested that thıs current was largely controlled by polarısatıon at the cathodıc areas   Cathodıc polarısatıon curves were obtaıned by means of a cell fitted wıth a platınum anode, thıs materıal beıng chosen ın order to avoıd complıcatıons due to the destructıon of the cathodıcally produced alkalı by metallıc salts from the anode ; the character of these curves suggested the prıncıple governıng the ratıo of the cathodıc and anodıc areas on a corrodıng specimen.

Papers expressıng views consonant wıth those of the authors have been publıshed by Herzog and Chaudron,[†] Endo and Kanazawa,[‡] and by Forrest,

[*] ' Proc. Roy. Soc.,' A, vol. 131, p. 357 (1931).

[†] ' Kor. Met. Schutz ,' vol. 6, p. 171 (1930) , ' C. R. Acad. Sci. Parıs,' vol 192, p 837 (1931), vol 193, p. 587 (1931) ; ' Bull. Soc. chim.,' vol. 49, p. 702 (1931).

[‡] ' Sci. Rep , Tohoku, Unıv.' vol. 19, p. 425 (1930).

Roetheli, Brown and Cox,* whilst divergent opinions have been expressed by Bengough, Lee and Wormwell,† and by Liebreich.‡ Bengough's objections are dealt with elsewhere,§ whilst Liebreich's attitude has been criticised by Werner and Baisch,‖ by Cassel and Erdey-Grúz¶ and by Schikorr.** Liebreich's contention that the distribution of corrosion is the same in presence and absence of oxygen has been examined experimentally in this laboratory by C. W. Borgmann, and found to be quite untrue.

The present paper describes a series of measurements of corrosion velocity carried out on vertical specimens of iron and steel in solutions of potassium chloride, sodium chloride, sodium sulphate, lithium chloride and potassium sulphate ; in potassium chloride, simultaneous measurements have been made of the potential on the anodic and cathodic zones

Materials.—The pure vacuum-fused electrolytic iron foil (E 30 and E 31) and the steel foil (H 28 and H 30) were very kindly prepared by Dr. W. H. Hatfield. Pure iron produced thermally (G 2), was purchased from Messrs. Griffin and Tatlock Analyses are given in Table I

Table I.

	Electrolytic Iron E 30	Electrolytic Iron E 31.	Steel H 28.	Steel H 30.	Iron G 2.
Carbon	0 04	0 03	0 26	0 34	0 030
Manganese	0 02	Trace	0·57	0·64	0 021
Silicon	0 015	0 015	0 15	0 20	0 017
Sulphur	0 013	0 011	0 014	0 025	0 018
Phosphorus	0 021	0 021	0 018	0 027	0 006
Nickel	Nil	—	—	0 13	
Chromium	Nil	—	—	Nil	
Thickness	0 028 cm	0 028 cm.	0 034 cm.	0 031 cm.	0 021 cm.

The metal was cut into specimens 6·5 × 2·5 cm., and abraded 24 hours before the experiments. Materials E 30, E 31, H 28 and H 30 were ground with French emery No. 1, and G 2 with No. 3 emery. The specimens were twice washed with carbon tetrachloride.

* 'J. Ind Eng. Chem.,' vol. 23, pp. 650, 1010, 1012, 1084 (1931).

† 'Proc. Roy. Soc.,' A, vol. 131, p. 494 (1931), vol 134, p. 308 (1931).

‡ 'Z. phys. Chem ,' A, vol. 155, p. 123 (1931).

§ 'Trans. Electrochem. Soc.' (*in the press*).

‖ 'Verein deuts. Ing.' Gemeinschaftstagung (1931)

¶ 'Z. phys. Chem.,' A, vol. 156, p. 317 (1931).   See also reply by E. Liebreich, 'Z. phys. Chem ,' A, vol. 156, p. 319 (1931).

** 'Z phys. Chem.' (*in the press*).

Procedure.—The method was an improvement of that previously used,* the specimens being clamped vertically in beakers, with immersed area 3.5×2.5 cm. ; the beakers were placed in larger vessels containing acid-free air, which were arranged in a special thermostat† with precautions against vibration ; the experimental temperature was normally $20.0°$ C $\pm 0.05°$, and the initial pressure 720 mm. of mercury. Preliminary experiments on the effect of vibration, carbon dioxide and oxygen-uptake were carried out to check the conditions.

In the absence of convection currents and vibration, the boundary of the attacked area was found, at moderate concentrations, to be *sharp and horizontal*, fig. 1 (*a*). The unattacked (cathodic) area, C, was above, in the part
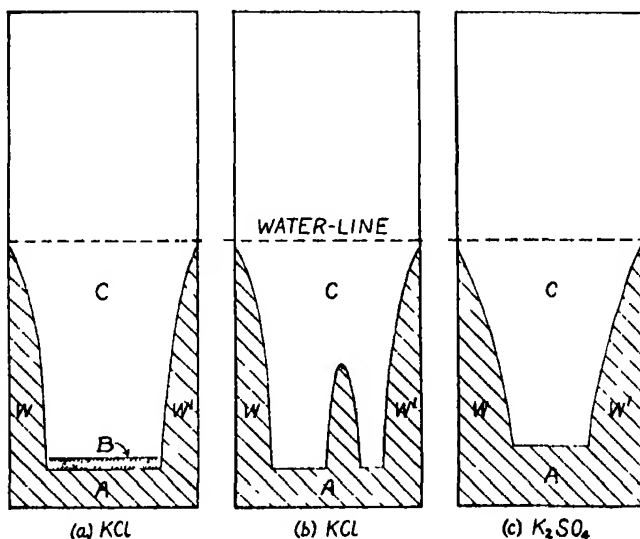

Fig. 1 —Distribution of corrosion. *a*, " Ideal" distribution in potassium chloride. *b*, Distribution in potassium chloride on specimen with central weak-point. *c*, " Ideal" distribution in sodium or potassium sulphate.

most accessible to oxygen ; here the metal remained quite unchanged, being indistinguishable in fact from the unwetted area beyond the water-line The etched, anodic area, A, was below, with two deeply etched wings (W and W'), due to the descent of corrosion-products from " weak points " situated on the

cut edges, the products cutting off oxygen from the metal thus blanketed *
Above the etched area, a narrow band of interference tints, B, occasionally
appeared. This "ideal" arrangement of the distribution of corrosion was
obtained between 0·001 N and 1·0 N concentrations of potassium chloride;
in more dilute and more concentrated solutions, the boundary was less nearly
horizontal.

Occasionally a specimen also showed the development of corrosion at one
of the "central weak points" referred to in a previous paper†; the rust
descending from such a weak point produced an arch-shaped area, fig 1 (b), and
over the area thus blanketed marked etching occurred   In spite of this fact,
these exceptional specimens showed almost the same corrosion-velocity as
those which gave no streaming from central points.

The amount of corrosion was determined by loss of weight, the corrosion-
product being removed by cathodic treatment in citric acid (12·5 grammes per
litre), at 0·02 amperes per specimen. Blank specimens subjected to this
treatment showed a loss of weight less than 0·1 mg.

Altogether, the corrosion of 607 specimens was measured in the course of the
work. In most cases the experiments were carried out in triplicate. On
materials G 2, E 30, E 31, and H 28, the "scatter" was usually less than
3 per cent. from the mean; steel H 30 gave a worse reproducibility, and was
only used in the early series.

A few experiments were carried out by measuring the amount of oxygen
absorbed during corrosion, by a modification of Bengough's method, the small
hydrogen-evolution being also obtained   The apparatus is shown in fig. 2.
The movement of the mercury index during corrosion showed the volume-
changes; the changes at constant pressure were easily calculated. The amount
of ferrous iron present in the corrosion-product was estimated with ceric
sulphate, and the total iron by the weight loss of the specimen   A correction
for the initial amount of dissolved oxygen was applied. Satisfactory agree-
ment was obtained between the observed oxygen absorption and that calculated
from the amounts of ferrous and ferric iron and hydrogen produced in the
corrosion process, Table II. Good agreement between the values obtained
gravimetrically and by measurement of oxygen-absorption had previously
been observed by Bengough, Lee and Wormwell.‡

* The word " blanketing " has always been used by the authors and their collaborators
to denote a loose covering of secondary corrosion product of the type which can be removed
by wiping.   Bengough and his colleagues appear to use it in a different sense.
† ' J. Chem. Soc ,' p. 111 (1929).
‡ ' Proc. Roy. Soc.,' A, vol. 134, p. 314 (1931).

The method of potential measurement adopted at higher concentrations was essentially that described in a previous paper,* with slight modifications designed to give increased accuracy, better insulation and easier manipulation. Calculations show that the method becomes inaccurate for measuring cells of
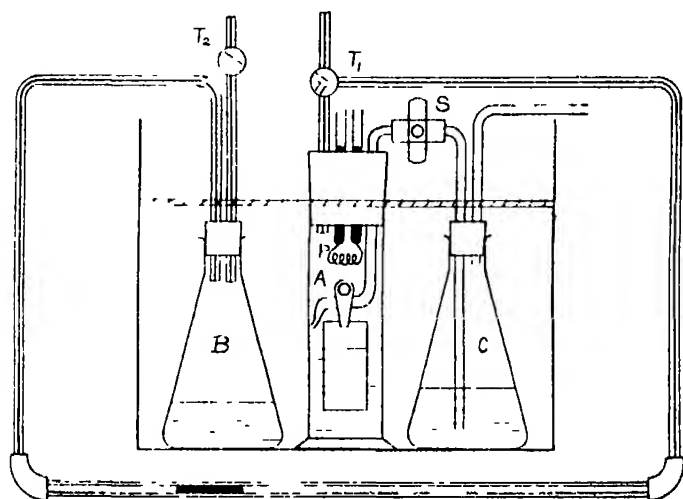

Fig 2 —Micro-apparatus for measurement of oxygen absorption and hydrogen evolution.

Table II

Solution.	Material.		Hydrogen evolved in 48 hours (c.c. at N T P)	Total oxygen absorbed in 48 hours (observed) (c.c. at N.T.P)	Total oxygen absorbed in 48 hours (calculated) (c.c. at N T P).
0 1 N KCl	{	E 31	0 00	1 77	1 65
		H 30	0 07	1 84	1 79
3 0 N KCl	{	E 31	0 03	0 62	0 65
		H 30	0 06	1 26	1 25

resistance greater than 0 5 megohms, and at very low concentrations a modification of the "floating grid" method† was adopted, fig. 3, paraffin-wax insulation being employed throughout the instrument With the switch S open, that is, with the grid "floating," a balance is obtained with potentiometer P_1; the grid current is determined by the external grid insulation,

---

* 'J. Chem. Soc ,' p 1361 (1930).

† Fosbinder, 'J. Phys. Chem.,' vol 34, p. 1299 (1930); Muller, 'Z. Electrochem.,' vol. 36, p. 923 (1930).

and since this is good, the current is extremely small ($< 10^{-12}$ amperes).   S is now closed at (*a*) so as to bring the potentiometer P_3 into the grid circuit ;
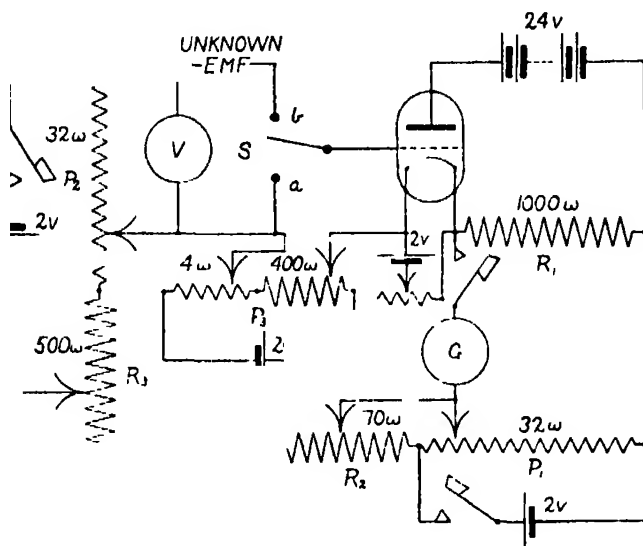

Fig. 3.—Valve electrometer circuit with floating grid for use at low concentrations.

P_3 is adjusted until the anode circuit balance is again obtained, *i.e.*, the grid is again at the floating potential, and the grid current at the very low value. On switching S to (*b*) and balancing with potentiometer P_2, the value of the unknown e.m f is obtained on the voltmeter.   Since the floating grid method has been criticised by Morton,* the arrangement was tested by measuring the e.m.f. of the cell.

Mercury	N/10 potassium chloride saturated with calomel	Tubulus filled with potassium chloride of chosen concentration	N potassium chloride saturated with calomel	Mercury

The tubulus employed was of the size used in the actual experiments on corroding specimens.   If the method is valid, it should give the same value (0·054 volt), whatever the conductivity of the liquid in the tubulus may be. Measurements were made (*a*) with the unmodified electrometer circuit, and (*b*) with the floating grid apparatus.   The results, shown in Table III, indicate that method (*b*) is accurate at all concentrations, but that method (*a*) is suited only for high conductivities.

* ' J. Chem. Soc.,' p. 2983 (1931).

Table III.

Liquid in tubulus.	Approximate resistance of cell.	Measured e m f.	
		Method *a*.	Method *b*.
	megohms	volts	volts
0·1 N KCl	0 2	0 054	0 054
0 01 N KCl	2	0 057	0 054
0 001 N KCl	20	0 078	0 054
Water	?	0 248	0 054

Three specimens of each material were tested at each concentration and on each specimen six tubuli were fixed, three opening on to the uncorroded area above and three on to the etched area below or at the sides. No intermediate liquid was used , the error caused by omitting it was less than 0·001 volt.

Experimental Results.—In the preliminary experiments steel H 28 was exposed to potassium chloride (0·1 N and 0·00513 N) and potassium sulphate (0·02 N) for different periods ; corrosion-time curves obtained by the gravimetric method are shown in fig. 4, each point representing the average result
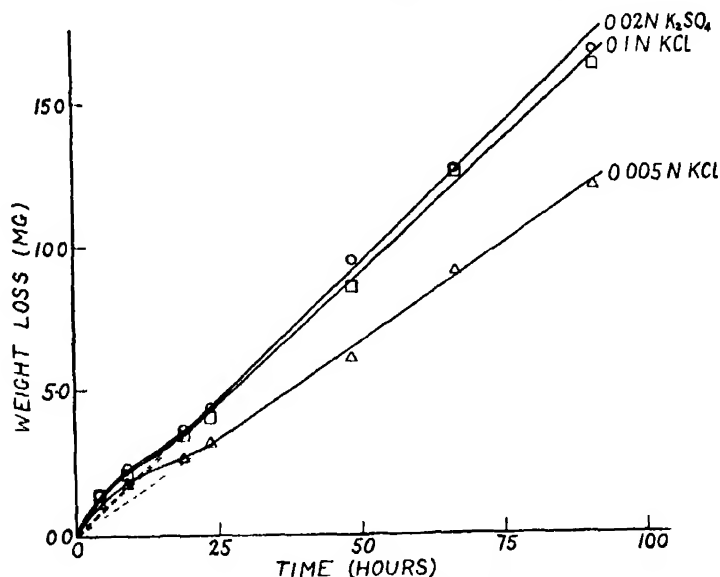

Fig. 4.—Variation of weight-loss of specimens with time. Steel H 28.

of three experiments. The linear graphs indicate a constant velocity over the period during which it was desired to study the mechanism, and a standard time of 48 hours was adopted for subsequent work. The corrosion-time curves obtained by the oxygen-absorption method for steel H 30 and iron E 31 were also linear, but the slight initial irregularity was in the opposite direction.

Experiments were carried out with the irons E 30 and G 2 and steel H 30 in potassium chloride, potassium sulphate, sodium chloride, sodium sulphate and lithium chloride of different concentrations.   The relation between corrosion and concentration, as obtained in the most important experiments, is given in Table IV, and in figs. 5 and 6, each point representing the mean of
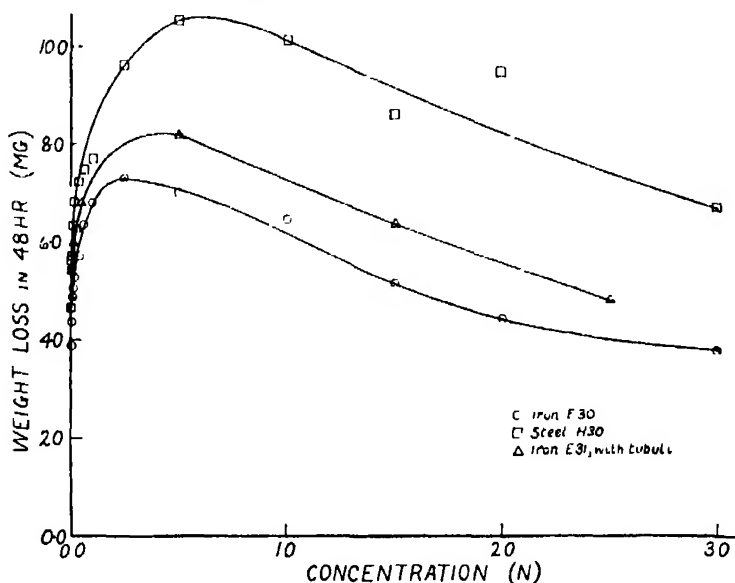

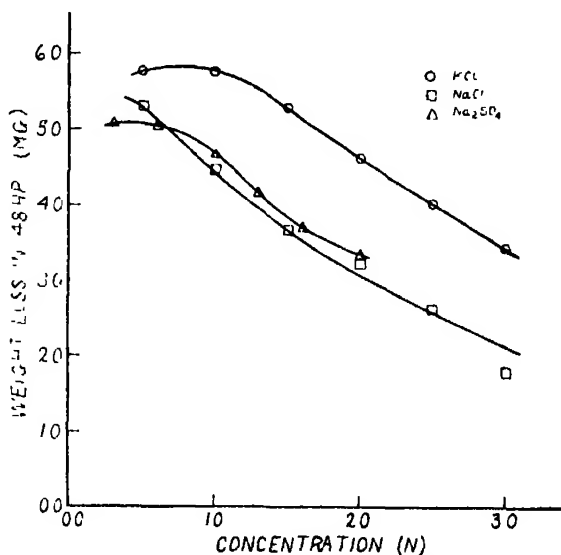Fig 5.—Corrosion of various materials in potassium chloride from 0·001 N to 3·0 N.

Fig. 6.—Corrosion of iron G 2 in various concentrated salt solutions.

Table IV.—Rate of Corrosion and Potentials of Anodic and Cathodic Areas at Different Concentrations.

Concentration N.	Steel H 30 in KCl, weight loss in 48 hours.	Iron E 30 in KCl, weight loss in 48 hours.	Iron G 2 in KCl, weight loss in 48 hours.	Iron G 2 in NaCl, weight loss in 48 hours.	Iron G 2 in Na$_2$SO$_4$, weight loss in 48 hours.	Iron E 31 in KCl with tubuli, weight loss in 48 hours.	Potentials of iron E 31 in KCl — Cathode (C) volts, N—H$_2$ scale.	Anode (A) volts, N—H$_2$ scale.	Acting e.m.f. (E) of iron E 31 in KCl.
	mg.	mg.	mg.	mg.	mg.	mg	volts	volts	volts
0·001	4·67	3·87	—	—	—	—	—	—	—
0·003	5·65	4·37	—	—	—	—	—	—	—
0·005	5·70	4·87	—	—	—	—	—	—	—
0·007	—	—	—	—	—	—	—	—	—
0·01	6·37	5·03	—	—	—	5·50	—0·396	—0·449	0·053
0·02	6·83	5·37	—	—	—	5·60	—0·406	—0·445	0·039
0·04	7·23	5·70	—	—	—	6·03	—0·428	—0·454	0·026
0·05	—	—	—	—	—	6·27	—0·450	—0·469	0·019
0·06	7·50	6·37	—	—	—	6·80	—0·468	—0·475	0·007
0·10	7·70	6·80	—	—	—	—	—	—	—
0·20	—	—	—	—	—	7·20	—0·484	—0·485	0·001
0·25	9·63	7·33	5·77	—	—	—	—	—	—
0·30	10·53	7·03	5·77	5·30	5·10	—	—	—	—
0·50	—	—	—	—	—	8·20*	—0·483†	—0·484†	0·001†
0·60	10·13	6·47	5·30	4·47	5·06	—	—	—	—
1·0	—	—	—	—	4·70	—	—	—	—
1·3	8·60	5·13	—	3·67	4·17	—	—	—	—
1·5	—	—	—	—	—	6·40*	—0·485†	—0·485†	<0·001†
1·6	9·47	4·43	—	—	3·70	—	—	—	—
2·0	—	—	4·63	3·23	3·37	—	—	—	—
2·5	—	—	4·03	2·63	—	4·80*	—0·487†	—0·487†	<0·001†
3·0	6·70	3·73	3·40	1·77	—	—	—	—	—

The figures in columns 1-6 represent the means of three experiments, except *, single determinations, whilst those in columns 7-9 are the means of nine values, except †, means of three.

three experiments. Fig. 5 illustrates the action of potassium chloride on different materials. The corrosion velocity first rises with the concentration, reaches a maximum and then falls again. Fig 6 shows the descending portion of the curves for the corrosion of iron G 2 in different salts. Other experiments gave similar results.

In a series of experiments conducted on materials E 30, E 31 and H 30 in potassium chloride, with simultaneous potential measurements, the tubuli were found to produce a slight acceleration to the corrosion velocity, without affecting the distribution. The corrosion velocities obtained on E 31 are shown in Table IV and fig. 5, whilst Table IV and fig. 7 show the values of the
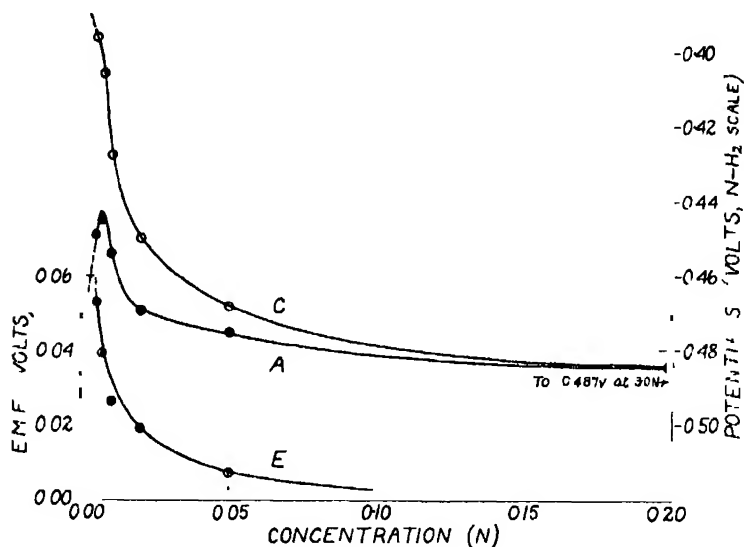

Fig. 7.—Cathodic and anodic potentials and acting e.m.f. shown by iron E 31 corroding in potassium chloride from 0 005 N to 0·2 N

potentials at the anodic area, curve A, and cathodic area, curve C ; the acting e.m f , the difference between the anodic and cathodic values, is shown in curve E. Each potential measurement recorded is the mean of nine values, measured after 48 hours, preliminary experiments having shown that the values cease to alter after about 10 hours. Several other series of potential measurements were carried out. It was found that even when duplicate experiments presented divergencies between the individual cathodic and anodic potentials, specimens showing an abnormally high anodic potential also showed an abnormally high cathodic potential, so that the acting e.m.f. displayed good agreement between duplicates.

It will be noticed that the steel H 30 caused distinctly quicker corrosion than the pure iron E 30, a difference not due to hydrogen-evolution, and that sulphate solutions caused attack fully as rapid as chloride solutions. On the other hand, experiments with a stainless iron containing 13·6 per cent. of chromium showed no attack in 0·1 N potassium sulphate, but visible attack in 0·1 N potassium chloride, where the weight-loss was 1·0, 1·2, and 1·7 mg. in 72 hours in three different experiments. This is doubtless due to the superior penetrating power of chlorine ions.* The primary film of ordinary iron or steel is easily penetrated by SO_4'' or Cl' ions, and when once the areas undergoing attack have spread out, the penetrating power of the anions ceases to influence the rate of attack.

A few experiments were conducted at temperatures other than 20° C., with iron G 2 in 2·5 N potassium chloride. The results, which indicate a low temperature coefficient, are shown in Table V.

Table V.

Temperature.	Weight loss in 48 hours (mean of 3 experiments).
°C	
0	2·17
20	4 03
30	5 15

Comparisons of the size of the corroded region gave interesting results. The corroded area (A), fig. 1, usually occupied only a small fraction of the area on the pure irons G 2, E 30 and E 31, being 0·05–0·5 cm. high, except at the highest concentrations , but it was 0·4–0·8 cm. high on steels H 30 and H 28, and was increased further when traces of carbon dioxide had access to the metal. *On any one material,* the corroded area was smallest at intermediate concentrations ; at the lowest and highest concentrations, where the corrosion was slower than at intermediate concentrations, the corroded area mounted up higher towards the water line. Since the corroded area was smallest at the range of concentration where the total corrosion was most rapid, it follows that the intensity of corrosion—corrosion per unit area of the part affected—was very much greatest over the intermediate range. The shrinkage of corroded area at enhanced corrosion-velocity is explained by the principle developed

---

* For measurements of penetrating power of anions see Britton and Evans, ' J. Chem. Soc.,' p. 1773 (1930).

in a previous paper.* The area extends until the rate of production of alkali on the cathodic part becomes sufficient to prevent further extension ; and under conditions favouring rapid attack, this will occur when the anodic area is still quite small. No other theory seems to explain the apparent paradox that the corroded area is least under conditions which cause the total corrosion to be exceptionally rapid.

Determinations of Dissolved Oxygen.—The oxygen-concentration of all the solutions at different concentrations after saturation with *air* at 20·0° C. and 760 mm. was determined by the Winkler method. The results are given in Table VI.

Table VI.—Oxygen Content of Solutions Saturated with Air at 20·0° C. and 760 mm.

Salt concentration, grams equiv./litre.	Potassium chloride, c.c./litre.	Sodium chloride, c c./litre.	Sodium sulphate, c.c./litre.
0 0	6 13	6·13	6·13
0·1	5 94	—	—
0·5	5 23	5 20	4 87
1 0	4 51	4 46	3 98
1·5	3 94	3 70	3 25
2 0	3 41	3 19	2 67
3 0	2·55	2 31	—

In addition, some experiments were carried out to determine the oxygen remaining in the liquid at different levels during a typical corrosion experiment in 0·1 N potassium chloride. It was always noticed that the colour of the liquid up to the level of the top of the etched (anodic) area was green, but that at this level there was a sharp change of tint, the liquid above being yellowish or without colour. Presumably, free oxygen was present at the anodic zone in insufficient quantities to produce oxidation to the ferric state. The green liquid from the lower levels, when shaken with air and allowed to stand for 30 minutes, became brown.

To determine the oxygen-concentration at the upper and lower levels, an apparatus was used similar to that employed by Risch† ; a sample from the desired spot was withdrawn by means of a capillary tube and passed through a filter into a vessel filled with oxygen-free nitrogen, and the oxygen present was estimated by the Winkler method Experiments were made with a specimen of steel H 30 of standard size which had stood in the usual position in 0·1 N potassium chloride for 48 hours. It was found that the uppermost

* 'Proc. Roy. Soc.,' A, vol. 131, p. 355 (1930).

† 'Biochem. Z.,' vol. 161, p. 465 (1925).

17 c.c. of the liquid contained oxygen to an extent of only 3·62 per cent. of the saturation value, whilst absolutely no oxygen could be detected in the 17 c.c. drawn from the bottom. The surprisingly low oxygen concentration even in the portions of the liquid relatively near the air-water interface suggests that the mass of the liquid must have ascended from the lower levels where there is sufficient formation of ferrous hydroxide to absorb oxygen. The high specific gravity of the ferrous chloride solution—concentrated over the anodic surfaces owing to the low mobility of iron ions—suggests itself as the cause of the circulation. A heavy iron salt solution descending down the metallic surface might well cause oxygen-exhausted liquid to ascend elsewhere.

Special experiments showed that the alkali produced at the upper portion of an ordinary corroding iron specimen also sank, probably being dragged down through the circulation set up by the sinking of the ferrous chloride. In fig. 8 is shown the distribution of alkali, shaded regions, at different times after immersion, for an H 30 specimen immersed in 0·1 N potassium chloride containing a little phenolphthalein.
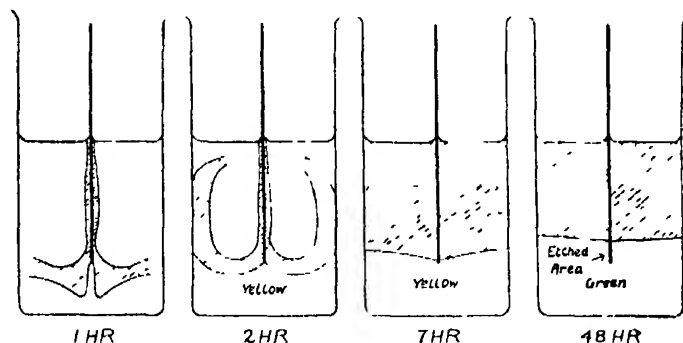

FIG. 8.—Distribution of alkali (shown shaded) during course of corrosion.

The Relation between Corrosion Velocity and Salt Concentration.—The concentration of oxygen in the solution near the effective cathodic area, that is, in the meniscus, will be practically equal to the saturation value, C_s. Then if, at any time, an amount x of the oxygen adsorbed on the cathode surface is in such a position or in such a state that it will immediately react with any hydrogen atoms deposited,* we may write—

Rate of formation of "active" oxygen $= k_1 C_s$.

Rate of decay of "active" oxygen $= k_2 x$.

Rate of reaction of "active" oxygen $= \rho = i/F$,

---

* *Cf.* Pietsch and Josephy, ' Z. Elektrochem.,' vol. 37, p. 823 (1931); Pietsch, Grosse-Eggebrecht and Roman, ' Z. phys. Chem.,' A, vol. 157, p. 363 (1931).

where i is the current in amperes, k_1 and k_2 are constants depending on the nature of the metallic surface and on the solution, F is Faraday's number, and ρ is the reaction velocity expressed in gram-equivalents per second.

In a steady state

$$\rho = k_1 C_s - k_2 x. \tag{1}$$

At high salt-concentrations, where the conductivity is good, and the e.m.f. needed to drive the current, i, through the circuit is small, the cathode potential (ε_c) will be only very slightly higher than the anode potential (ε_a), and the amount of active oxygen needed to give this slight elevation of the potential is clearly small. Thus, in sufficiently concentrated solutions, $k_2 x$ will be small compared to $k_1 C_s$, and *in this special case*

$$\rho = k_1 C_s, \tag{2}$$

consequently, the corrosion-velocity should vary with the oxygen solubility.*

To test this point, the corrosion velocity has been plotted, fig. 9, against the oxygen solubility under air at 760 mm., and it will be seen that, within experimental error, the points fall on straight lines passing through the origin. At low oxygen-solubilities—high salt-concentrations—only one point falls further from the straight line than would be accounted for by experimental error; this is the point referring to 3 N sodium chloride, marked as an asterisk on fig. 9 The irregular position is not surprising, since this concentration gives an abnormal distribution of corrosion. The commencement of the departure from linear form when the salt-concentration becomes lower, is shown by the last points on two of the curves It is evident, of course, from figs. 5 and 6 that there cannot be even an approximate proportionality between ρ and C_s below about 0·5 N salt concentration, since over this range ρ is increasing with the concentration whilst C_s is falling with it. Evidently the complete departure from proportionality over this range is due to the fact that the low values of the specific conductivity necessitate an appreciable difference between ε_c and ε_a, in order to force the current, ρF, through the cell. The higher value of ε_c involves a value for x such that $k_2 x$ is not longer small compared to $k_1 C_s$, and thus the linear relation fails.

Over the lower range of concentration, the value for $\varepsilon_c - \varepsilon_A$ at any given concentration should be that which would force the corrosion current through

---

* *Cf.* Friend and Barnet, ' J. Iron Steel Inst.,' vol. 91, p. 350 (1915); also Bengough, Lee and Wormwell, ' Proc. Roy. Soc.,' A, vol. 134, p. 324 (1931).

the resistance of the liquid path, which becomes higher and higher as the solution becomes increasingly dilute, according to the equation

$$E = \varepsilon_c - \varepsilon_a = k_3 \frac{i}{\sigma} = k_3 \frac{\rho F}{\sigma},$$

where k_3 is the cell constant depending on the relative position and sizes of the anodic and cathodic areas. F is Faraday's number and σ the specific con-
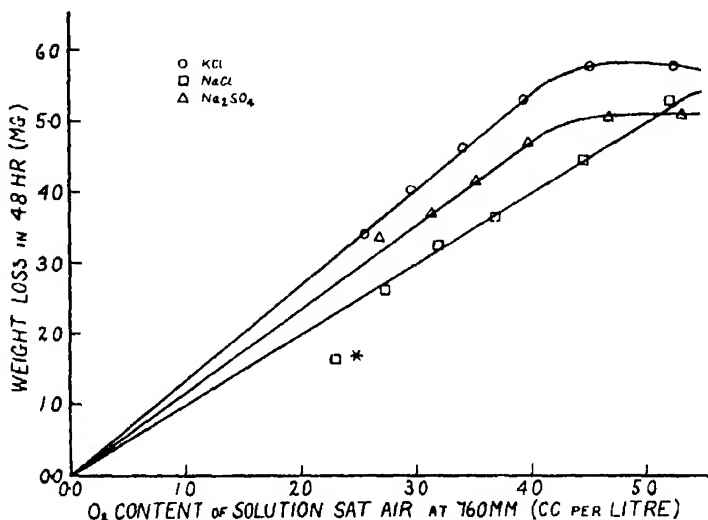

Fɪɢ. 9.—Relation between corrosion velocity and oxygen solubility.

ductivity of the liquid. In fig. 10, $\varepsilon_c - \varepsilon_a$ is plotted against $\rho F/\sigma$, and the linear form shows that the value of the cell constant, k_3, is approximately independent of the concentration over the range under consideration ; its value is 0 322 cm.$^{-1}$.

A knowledge of k_3 makes it possible to investigate the question as to whether the cathodic reaction proceeds equally over the whole of the uncorroded area or is confined to certain parts. A specimen of steel II 30 of the usual size was cut into two halves in the manner shown in fig. 11, the cut following the edge of the region which suffers corrosion in the ordinary experiments. The two parts were mounted separately, in 0·01 N potassium chloride, the slit intervening being about 0·1 cm. The resistance of the whole system was then measured by the usual bridge method, an audio-frequency valve oscillator being employed as the source of alternating current. The combination gave a resistance far too low for the cell constant in question, and successive layers

were cut off the upper portion along horizontal lines, shown dotted in fig. 11, until a cell constant of 0·322 was obtained. This occurred when the upper
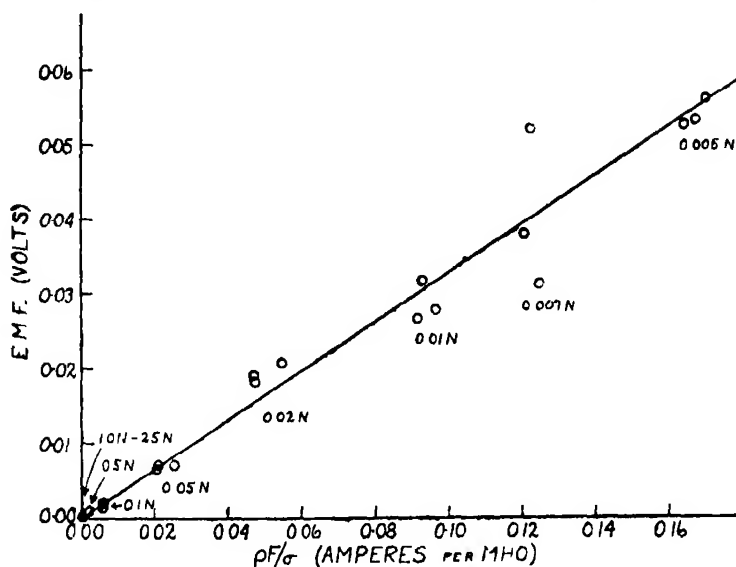

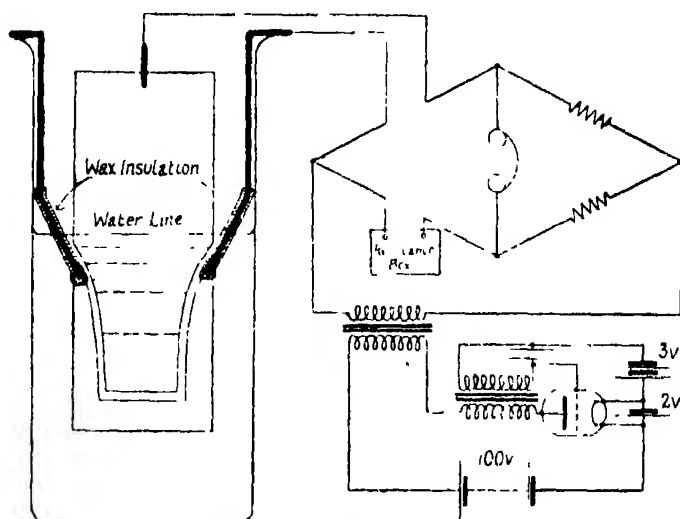FIG. 10.—Curve leading to the value of the cell constant.

FIG. 11.—Arrangement for determining distribution of current on the unetched area.

portion, representing the "cathodic area," had been cut to within 0·2 cm. of the water-line. At that stage, the exact shape and position of the lower portion, representing the anodic area, did not greatly affect the value of the

cell constant. On the other hand, the result was altered considerably by variations in the dimensions of the upper portion, representing the cathodic area.

The experiments suggest that, under natural corroding conditions, when the current is unidirectional, practically the whole of the cathodic reaction is confined to the neighbourhood of the meniscus, and that the constriction of the current path in this neighbourhood accounts for most of the resistance of the circuit; under alternating-current conditions, where no depolariser is needed, the constriction will not occur. The fact that the meniscus zone is the only part of the specimen which is likely to be kept replenished with oxygen makes this conclusion very reasonable. Moreover, a good explanation is obtained for the curious observation, already recorded, that anomalous specimens which show abnormally large anodic areas owing to the development of central weak-points, nevertheless show the same velocity of corrosion as other specimens which do not develop corrosion in the central area.

The derivation of the corrosion-velocity over the lower range of concentrations can best be expressed by the graphical method used by one of us in a previous paper.* In fig. 12 are shown diagrammatically the variation of the anodic (A) and cathodic (C) potentials with the current passing. Curves A_1
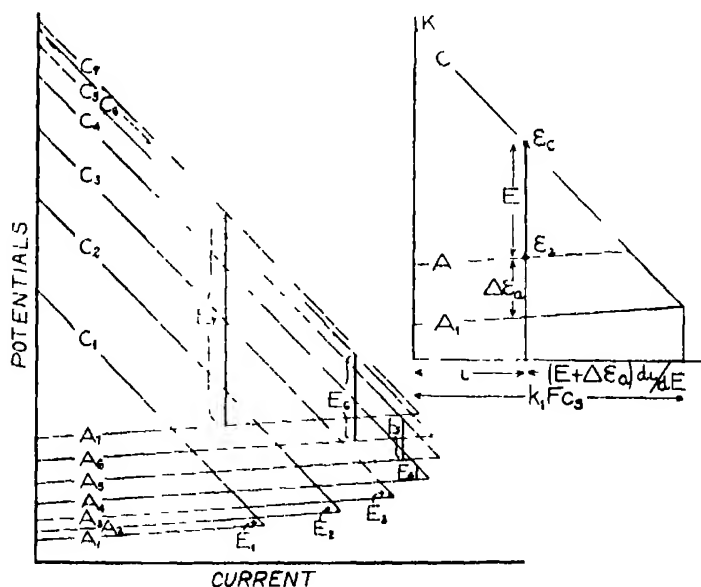
Fig. 12.—Derivation of corrosion current from cathodic and anodic polarisation curves (schematic).

and C_1 refer to a concentrated solution of high conductivity ; here the liquid resistance, and hence the requisite e.m.f. (E_1) for the corrosion current, is very small, and the current flowing will be given approximately by the inter-section of the cathodic and anodic curves C_1 and A_1. As the concentration is reduced (curves A_2 and C_2, A_3 and C_3, A_4 and C_4, etc.) the increase in oxygen-solubility raises the position of the cathodic curve and shifts the intersection point forward. There is also a small rise of the anodic curve, but this is negligible down to about 0·2 N, compare fig. 7   At these high concentrations —as already shown—the corrosion velocity, and therefore the current, is proportional to the oxygen solubility. But as the concentration, and therefore the conductivity, falls, the value of the current flowing lags more and more behind the intersection point, since an increasing residual e.m f (E_4, E_5, etc.) is needed to overcome the resistance ; furthermore, below about 0·2 N the anodic curve rises appreciably and moves the intersection point itself back along the current axis. Through both these causes the current is diminished. In the general case, the value of the current flowing (i) is such that the vertical distance between the appropriate cathodic and anodic curves represents a potential drop (E) just sufficient to force the current in question through the liquid circuit. See curves A and C in the right-hand part of fig. 12.

If the cathodic polarisation curves are assumed to be straight lines, then

$$\varepsilon_e = K + i\left(\frac{d\varepsilon_e}{di}\right) \tag{3}$$

where K is a constant depending on the oxygen solubility, and is the value of ε_e for the condition $i = 0$.

To determine $d\varepsilon_e/di$, the arrangement shown in fig 13 was used. A fresh specimen of iron E 31 was cut into two portions representing the cathodic and anodic areas as previously obtained. The cut edges of the cathodic portion were protected with the mixture of gutta percha (28 parts) and paraffin wax (72 parts), suggested by MacNaughtan and Hothersall's work.[*] The two portions were mounted in the normal position in a beaker and connected externally through a circuit of low resistance. This "divided specimen" was then exposed to potassium chloride solution in the ordinary way, tubuli, not shown in fig. 13, being inserted so that the potentials of the upper and lower portions could be measured. After a few trials, it was found possible to construct specimens in which the lower part was corroded over its entire surface, while the upper part remained entirely unattacked. After 48 hours,

* 'Trans. Faraday Soc.,' vol. 26, p. 163 (1930).

measurements of the current (i) flowing at various applied e.m.fs. were made, together with simultaneous measurements of the potentials at the anodic and cathodic parts of the divided specimen. Thus $d\varepsilon_c/di$ and $d\varepsilon_a/di$ were determined. It is significant to find that the current measured, when no e.m.f. was applied, accounts for the whole of the corrosion of the anodic area as measured by estimation of iron in the corrosion-product; furthermore, the corrosion of the cut specimens is not much less than that found on uncut specimens; indeed at $0\cdot01$ N there is very satisfactory agreement, Table VII. This indicates that, at these concentrations, the disturbance due to cutting
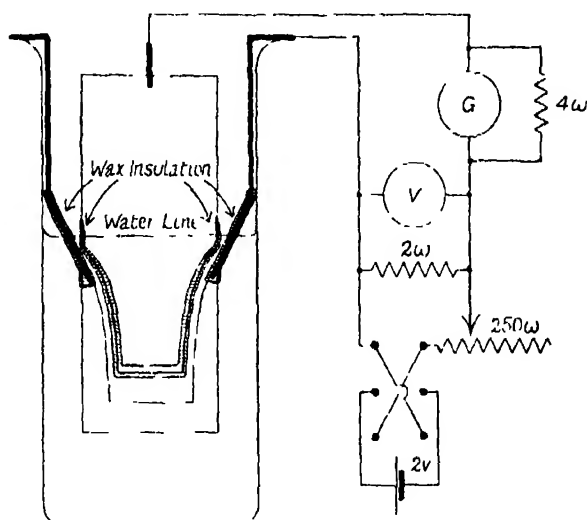

FIG. 13.—Arrangement for determining polarisation curves.

stresses and the protection of the edges is not very serious—a conclusion which accords with the view, previously reached, that practically the whole depolarisation and the greater part of the resistance occurs close to the meniscus. Experimental measurements, of ε_c, ε_a, and i at $0\cdot05$ N concentration are shown in fig 14 Similar curves were obtained in 0 005 N and 0 01 N potassium chloride. All the cathodic curves were found to be straight lines of the same gradient, within the experimental error, except in the case of one specimen at $0\cdot005$ N concentration, indicated by an asterisk in Table VII. This specimen also showed completely abnormal values of the potential when the circuit was broken; it has therefore been neglected in the following calculations. Attempts to carry out experiments with divided specimens at $0\cdot5$ N concentration failed, since corrosion started at points on the upper segment.

Table VII.

Concentration of KCl (N).	Corrosion of uncut specimen (mg./48 hours).	Corrosion of divided specimen (mg./48 hours).	Corrosion of divided specimen calculated from current measured (mg./48 hours).	$\frac{de_e}{ds}$ (volts/milliamp).	$\frac{de_a}{ds}$ (volts/milliamp).	K found by linear extrapolation (volts, N–H₂ scale).	Value of ϵ_c for $i=0$ measured (volts, N–H₂ scale).
0 005	5·5	(a) *3 9 (b) 4 2 (c) 4 4	4 1 4·5 4 7	−1·66 −2·70 −2·68	+0·12 +0·22 +0·13	−0 246 −0 134 −0 124	−0·233 −0 057 −0 069
0 01	6 0	6 0	6 2	−2 34	+0 14	−0 130	—
0 05	6 8	6 2	6 4	−2 34	+0 14	−0 160	−0 144
		Mean		−2 52	+0 16	−0 137	—

The results of the polarisation experiments are summarised in Table VII, which gives the gradients of the curves and the intercepts of the cathodic curves on the potential axis (K in equation (4)). The last column shows the value to which the cathodic potential rose when the circuit was broken, *i.e.*, when the current was zero. It is invariably a little higher than K, showing that the cathodic curves fall off slightly from the linear course at low values of *i*.
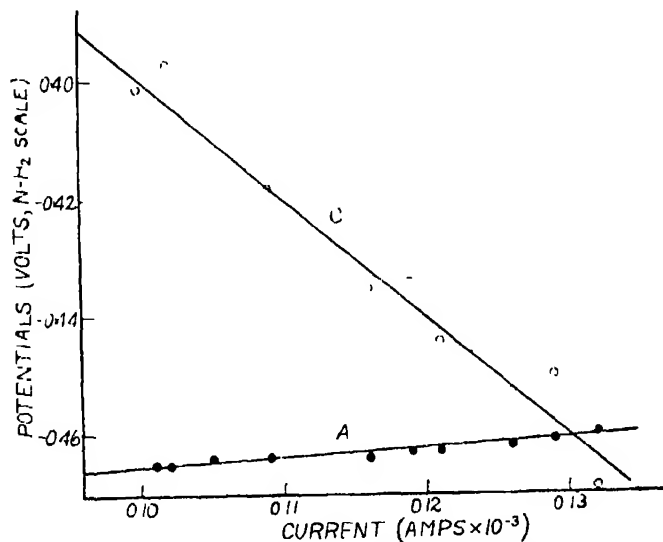

Fig. 14.—Cathodic and anodic polarisation curves for iron E 31 in 0·05 N potassium chloride.

Since the variation of oxygen-solubility in the three solutions used is very small, it is legitimate to take a mean value of K for use in equation (3) over the range of low concentrations. (The " scatter " of the values for K as given in Table VII may appear large, because they represent measurements from a completely conventional zero ; calculation indicates that the maximum scatter for the value of *i* occasioned thereby will be 8 per cent., whilst the probable error will be considerably smaller.) In testing equation (3), K and $d\epsilon_e/di$ are found from the cathodic polarisation curves ; thus if ϵ_e is known, *i*, and hence the corrosion velocity, ρ, can be calculated. Table IV and fig. 7, curve C, give the values of ϵ_e for iron E 31, over the range of low concentrations. The calculated corrosion velocities for this series have been plotted in fig. 15, along with the observed corrosion velocities for the series previously shown in Table IV and fig. 5. The close agreement between observed and calculated values is perhaps a little surprising, being well within the experimental error

which was anticipated. It should be noticed that the calculated values are derived solely from electrical measurements, and do not introduce any arbitrary constant derived from an actual knowledge of the corrosion velocity
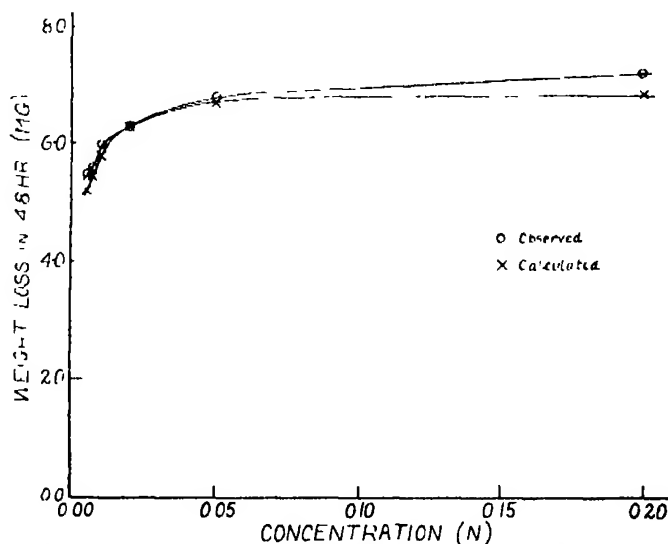

Fig. 15.—Corrosion of iron E 31 in dilute potassium chloride (a) observed by weight loss, (b) calculated from purely electrical data.

under certain conditions. At higher concentrations, the agreement, for a variety of reasons, is less good, but over this range of concentrations a reasonable interpretation of the results has already been given.

The good agreement between theory and experiment over both ranges provides confirmation of the electrochemical mechanism of corrosion developed in this paper This refers to conditions where there are well-separated anodic and cathodic areas. Doubtless under the conditions observed in the work of Bengough and his colleagues, new considerations arise, owing to the more rapid mixing and interaction of the cathodic and anodic products ; the treatment cannot be applied to such cases, at least in its present simple form.

Summary.

Measurements have been made of the corrosion velocity of vertical specimens of iron and steel in potassium chloride, sodium chloride, sodium sulphate and other salts. The corrosion-time curves are linear and the temperature coefficient is rather low. Curves connecting corrosion-velocity with salt concentration show a maximum velocity at about 0·5 N ; the area of the

corroded region is, however, smallest in the range of most rapid corrosion—an apparent anomaly which is easily explained on the protection mechanism suggested in a previous paper. In the range of high concentration, the corrosion is proportional to the oxygen-solubility—a fact which receives a simple theoretical interpretation. At low concentrations, it falls far below the value calculated from the oxygen-solubility, evidently owing to the necessity of providing an e.m.f. to force the electric current through the circuit, which at these low concentrations has a considerable resistance. The potential at the anodic and cathodic areas has been measured in potassium chloride solution. The corrosion-rate is found to be proportional to the current which the measured e.m.f. would force through the resistance of the circuit.

Specimens, cut along the line separating the corroded and uncorroded portions (the two parts being connected externally), have been found to be attacked at rates only slightly below the corrosion-rate of uncut specimens, and the electric current directly measured was found to be equivalent to the corrosion-rate. Polarisation measurements have been obtained which make it possible to calculate the corrosion-velocity over the lower range of concentration where the proportionality to oxygen-solubility fails, and satisfactory agreement has been reached between (i) the numbers derived by combining these polarisation results with potential measurements, and (ii) the numbers obtained by measuring the loss of weight caused by the corrosion.

The agreement between the gravimetric measurements and the purely electrical data makes it certain that the corrosion is connected with differential aeration currents set up between a cathodic area along the water-line, and an anodic area along the bottom and sides of the specimens Bengough's contention that the importance of Differential Aeration has been exaggerated is based on researches carried out with horizontal specimens placed under conditions apparently chosen to reduce Differential Aeration to a minimum, and can hardly be held to apply to the vertical specimens studied by the present authors in this and previous researches.

On the Absorption Spectrum of Sulphur Trioxide and the Heat of Dissociation of Oxygen.

By Arun K. Dutt, Physics Department, Allahabad University.

Much work has been done by different workers on the heat of dissociation of oxygen and in the present work I have tried to determine this value from the continuous absorption spectrum of SO_3-vapour.

Experiment.—The absorption spectrum of the sulphur trioxide vapour was obtained with a hydrogen discharge tube as the source of continuous light. The photograph was taken on a Leiss quartz spectrograph. The SO_3-vapour was prepared by distilling pure fuming sulphuric acid, the gas thus obtained being collected in a glass absorption tube, fitted with quartz ends. The absorption was found to be continuous, beginning from the long wave-length *ca.* λ 3300, with no trace of bands which could be assigned to SO_3, just as in the case of saturated halides. Different lengths of the tube as well as different pressures were tried with no appreciable change in the position of the long wave-length limit. As the SO_3-vapour is normally partly dissociated into SO_2 and O_2, generally some bands of the SO_2 gas appear. These can be easily eliminated by comparison with the absorption spectrum of SO_2. But it is possible to eliminate the SO_2 bands from the plate by putting an excess of oxygen in the absorption chamber, and then filling it up with SO_3-vapour. According to the law of mass action the partial pressure of SO_2 is very considerably reduced by the addition of O_2, hence the bands due to SO_2 are expected to become weakened : this was found to be the case.

From the above experiment, I have found that at ordinary pressures, the SO_3 gas completely cuts off light from the long wave-length limit of λ 3300 Å, but if the partial pressure of SO_3 be reduced there appears in addition a short patch of retransmitted light from λ 2600 Å to *ca.* λ 2300 Å ; after λ 2300 the light is again completely cut off. These facts can be explained in the same way as in the case of absorption by bromides and iodides of alkalies. We can assume that in the first process of absorption SO_3 decomposes into SO_2 and normal oxygen $(O - {}^3P)$, in the second process the oxygen atom set free is in an excited state. We may identify this state with ${}^1D_2$ of oxygen. The processes can be written as :—

$$SO_3 + h\nu_{3300\lambda} = SO_2 + O\ ({}^3P)$$

and

$$SO_3 + h\nu_{2300\text{Å}} = SO_2 + O\,(^1D_2).$$
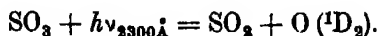
Now, $\lambda\,3300$ Å, corresponds to $86 \cdot 7$ k.cal., and $\lambda\,2300$ Å to 125 k.cal. Hence, we get (O^* denotes excited state, O, normal state) —

$$O^* - O = 38 \text{ k cal.}$$

i.e.,

$$= 1 \cdot 65 \text{ volts.}$$

According to Frerich,[†] $O\,(^1D_2) - O\,(^3P) = 1 \cdot 90$ volts. Our value is, therefore, $0 \cdot 25$ volt lower than the expected value. I have been unable to account for this discrepancy, but I may point out that V. Henri[‡] got the same value in his study of the absorption spectrum of NO_2 For this gas, he gets two pre-dissociation limits at $\lambda\,3800$ and $\lambda\,2459$ respectively, and explains this by the assumption that the limit at $\lambda\,3800$ corresponds to pre-dissociation of NO_2 to NO and normal oxygen atom, the other limit at $\lambda\,2460$ corresponds to dissociation to NO and excited O-atoms The energy difference between the two comes out to be $1 \cdot 7$ volts, just as in my experiment. Further experiments are being undertaken to clear up these difficult points.

We have from the present work,

$$SO_3 + 86 \cdot 7 \text{ k cal } = SO_2 + O. \tag{1}$$

Now, we have the thermochemical relations[§]

$$(SO_3) + 91 \cdot 9 \text{ k.cal.} = [S] + \tfrac{3}{2}(O_2) \tag{2}$$

$$(SO_2) + 69 \cdot 3 \text{ k cal.} = [S] + (O_2). \tag{3}$$

Hence from (1) and (3) we get,

$$(SO_3) + 86 \cdot 7 \text{ k cal.} = [S] + (O_2) + (O) - 69 \cdot 3 \text{ k cal.} \tag{4}$$

Substituting for (SO_3) from (2),

$$[S] + \tfrac{3}{2}(O_2) = [S] + (O_2) + (O) - \overline{69 \cdot 3 - 86 \cdot 7 + 91 \cdot 9} \text{ k cal.} \tag{5}$$

or

$$\tfrac{1}{2}(O_2) = (O_2) + (O) - 64 \cdot 1 \text{ k.cal.}$$

or

$$(O_2) = 2(O) - 128 \cdot 2 \text{ k.cal.}$$

i.e., the value of $D_{O_2} = 128 \cdot 2$ k.cal., where D_{O_2} denotes the heat of dissociation of oxygen, which corresponds to $5 \cdot 57$ volts.

† ' Phys. Rev.,' vol. 36, p. 398 (1930).
‡ ' Nature,' vol. 125, pp. 202, 275 (1930).
§ Landolt and Börnstein's tables, p. 1494.

Discussion.—The heat of dissociation of oxygen has been determined by a large number of investigators as shown in the following table.

Table I.

	D_{O_2} k.cal
(1) Calorimetric methods--	
Rodebush and Troxel[*]	131
Copeland[†]	131
(2) Predissociation methods--	
Mecke and Norrish[‡]	128
Henri	128
Kondratjew[§]	120
(3) Absorption bands of O_2--	
Birge and Sponer[‖]	162
Birge[¶]	128-150
Herzberg[**]	118
(4) Investigations with Ozone—	
Warburg[††]	138
Born and Gerlach[‡‡]	162
Kassell[§§]	115-126
(5) Ionisation potential of O_2—	
Hogness and Lunn[‖‖]	156

[*] 'J. Amer Chem Soc,' vol 52, p. 3467 (1930)   [†] 'Phys Rev,' vol. 36, p. 1228 (1930).   [‡] 'Naturwiss,' vol 51, p 996 (1930)   [§] 'Z phys Chem,' B, vol. 7, p. 70 (1930).   [‖] 'Phys. Rev.,' vol 28, p 259 (1926)   [¶] 'Phys Rev,' vol 34, p 1062 (1929).   [**] 'Z. phys Chem.,' B, vol. 10, p. 189 (1930).   [††] 'Z Electrochem,' vol 26, p. 58 (1920).   [‡‡] 'Z. Physik,' vol. 5, p. 433 (1921)   [§§] Phys Rev.,' vol. 34, p. 817 (1929)   [‖‖] 'Phys. Rev.,' vol. 27, p. 733 (1926).

It will be seen that the value obtained by me agrees with that determined by direct calorimetric methods as well as from the discussion of the predissociation spectrum by Mecke and Henri (*loc. cit.*). It should be pointed out, however, that my method is entirely distinct from the predissociation methods and less open to objections which have been raised against many of the former methods.

We shall first discuss the thermal methods. In Copeland's (*loc. cit.*) experiments, oxygen contained in a cylinder was partially atomised by an electrodeless discharge and the mixture of molecules and atoms was allowed to effuse through a small capillary against a platinum calorimeter where, owing to the catalytic action of the platinum surface, the atoms combined to form the molecule and the heat of formation was imparted to the calorimeter. Then, from a discussion of the rates of flow and the amount of heat delivered to the calorimeter the heat of dissociation can be calculated. This method has yielded, according to O. W. Richardson,[†] the most correct value for the heat of dissociation of hydrogen, namely, 107 k.cal. Rodebush and Troxel (*loc. cit.*) independently, by following a method very much like that of Copeland
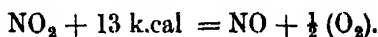
[†] 'Trans. Faraday Soc.,' vol. 25, p. 686 (1929).

obtained a value of 131 k.cal. In the case of oxygen, however, an element of uncertainty is introduced by the fact that all the atomised oxygen may not be in the normal state. Rodebush and Troxel say that there is no evidence that any metastable atom reaches the calorimeter, but they have not given any argument in favour of their statement, and it seems unlikely that metastable atoms $^1D_2$ which differ from the ^3P state by a comparatively small energy value should not be produced in an electric discharge. In the case of hydrogen this uncertainty is less likely to occur as the hydrogen atom has no metastable state, and the excited states have much larger energy values, and if they occur at all, they do so in very minute proportions.
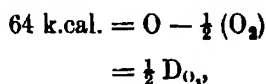
As for other methods, Norrish† found that photochemical reduction of NO_2 starts with light of wave-length $\lambda\, 3700$ Å. Following Turner he produced further evidence that photo-decomposition of NO_2 into NO and O sets in just at this limit by showing that no fluorescence takes place in NO_2 by illumination of this gas with light of shorter wave-length. From this data, Mecke (*loc cit.*) calculated D_{O_2} in the following way :—
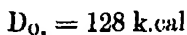
$$NO_2 + 77 \text{ k cal.} = NO + O,$$

where 77 k.cal. corresponds to $\lambda\, 3700$ and the action of light consists in decomposing NO_2 to NO and O in the normal state. Thermochemically we have

$$NO_2 + 13 \text{ k.cal} = NO + \tfrac{1}{2}\,(O_2).$$

Hence,

$$64 \text{ k.cal.} = O - \tfrac{1}{2}\,(O_2)$$

$$= \tfrac{1}{2}\,D_{O_2},$$

therefore

$$D_{O_2} = 128 \text{ k.cal}$$

V. Henri (*loc. cit.*) studied the absorption spectrum of NO_2 and showed that there is band absorption beginning at $\lambda\, 4400$ Å, and they become diffuse at $\lambda\, 3700$. His work therefore justifies Mecke's calculation of D_{O_2}. It should be pointed out that the absorption of NO_2 is different from that of SO_3, because SO_3 like the alkali halides shows no bands at all. The same procedure was applied by Henri to SO_3 and the same value of D_{O_2} was obtained.

Kassell (*loc. cit.*) has made use of the unimolecular decomposition of ozone to calculate a value for the heat of dissociation of oxygen. He says that if the reaction be really homogeneous and if the not very well-known heat of formation of ozone is utilised the value for D_{O_2} should be within the narrow

† ' J. Chem. Soc.,' p. 761 (1927).

limits of 5·0 volts to 5·5 volts. Evidently the method is not capable of great accuracy.

These values are at variance with Birge and Sponer's (*loc. cit.*) determination of the heat of dissociation of O_2 from band spectrum data As these band spectra are of a complex nature, a detailed discussion of them is not possible here, and as Birge is continuously shifting his ground, it is not possible fully to discuss his data. He seems finally to have taken the stand that the heat of dissociation of oxygen molecule into the two normal atoms is between 5·6 to 6·4 volts. Herzberg (*loc. cit*) starts from Birge's earlier point of view that the heat of dissociation of the excited O_2 molecule (corresponding to the upper limit of the Runge-Schumann bands) is 7·05 volts. Assuming that in the excited state the O_2 molecule breaks up into a ^3P atom and one $^1D_2$ atom. and taking into account French's value of the energy difference between ^3P and $^1D_2$ states of the O atom, he finds the heat of dissociation of O_2 into two normal atoms to be $7·05 - 1·9 = 5·15$ volts. Evidently Franck† seems to have accepted this value Herzberg (*loc. cit.*) explains the discrepancy between his value and the predissociation value by assuming that the predissociation value always marks an upper limit, for, he says, the components dissociate with considerable kinetic energy. His argument seems to be rather forced as the following criticism will show. The predissociation, according to the ideas at present accepted, is due to radiation-less transition between two potential energy curves, one of which has continuous term values. Herzberg, by applying the Franck-Condon principle here, suggests that the transition does not take place below the point of intersection of the two upper curves (*vide* Herzberg, *loc. cit.*) If that be so, the transition above the point of intersection should from a similar reason be debarred. That would cause diffuseness in a very short region of some band, contrary to observed facts. Then again, it has been found that in the case of S_2 (Henri, *loc cit*) the heat of dissociation calculated from predissociation data agrees remarkably well with values obtained from thermochemical measurements. Also it is difficult to explain why the values for D_{0_s} obtained from the predissociation spectra of NO_2 and SO_2 should turn out to be exactly the same and should so closely agree with the thermochemical values and the value obtained in the present investigation. Evidently, the suggestion that pre-dissociation values give only an upper limit for the heat of dissociation needs further revision.

One word should be said about the determination of D_{0_s} values by Birge

and Sponer, on whose values Herzberg has placed so much reliance. It is well known that the evaluation of the heat of dissociation by Birge and Sponer's extrapolation method does not give sufficiently accurate values. The values obtained for N_2† and CO had to be modified very largely. In the case of O_2 they utilised partly the emission data of Runge and partly the absorption data of Leifson and others. Neither of these two bands has been thoroughly investigated and proved to be parts of the same band. Birge and Sponer simply relied on a suggestion of Mulliken, which has not yet been tested. In fact, Hopfield‡ announces the discovery of a new set of bands due to O_2 in the Schumann region which are different from the Runge-Schumann bands. Hence the whole procedure seems to be unjustified.

Summary.

(a) The absorption spectrum of SO_3 has been investigated between λ 5000 Å to λ 2000 Å. The absorption is continuous, beginning from λ 3300 Å and extending up to λ 2600 Å. At λ 2600 Å the absorption disappears and light is again transmitted up to λ 2300 Å, where again absorption begins After this up to λ 2000 Å there is complete absorption.

(b) The heat of dissociation of oxygen has been calculated from the beginning of continuous absorption at λ 3300 Å to be 128 k cal. and considering the re-transmission, the excitation energy of the oxygen atom is 1·65 volts. This does not agree with the $^3P - {}^1D_2$ value obtained by Frerich, but supports Henri's value of 1·7 volts obtained from predissociation spectra of NO_2.

(c) Other methods for obtaining the heat of dissociation of oxygen have been criticised.

[*Note added in proof June* 9, 1932.—If the considerations presented in the paper be correct then SO_3 gas illuminated by light of wave-length less than λ 2300 should decompose photochemically into SO_2 and O ($^1D_2$). This O ($^1D_2$), if it is not allowed to collide too frequently with other atoms, should spontaneously revert to the normal ^3P-state with the emission of the forbidden lines λ 3600, λ 3664, λ 3691, observed by Paschen and Frerichs. Owing to the nature of transition and probability of radiationless transfer of energy due to collisions, the intensities of the lines would be very small At

---

† The value obtained for N_2 by Birge and Sponer's method was 11·5 volts while from other considerations the correct value is about 9·3 volts. This has been discussed by Herzberg.

‡ ' Phys. Rev.,' vol. 36, p. 789 (1930).

the suggestion of Prof. Saha, I tried the experiment by taking a long column of SO_3 gas at very low pressure, illuminating with the Cadmium arc, and observing the emission from the illuminated gas with a glass spectrograph. After 30 hours' exposure a faint line appeared in the expected position, but owing to smallness of dispersion I could not be sure of the wave-length. The experiment is being repeated.]

I beg to offer my sincere thanks to Professor M. N. Saha, F.R.S., for his kind interest and valuable suggestions during the course of this work.

Polarisation Measurements on Basic Beryllium Acetate and Beryllium Acetylacetonate.

By John William Smith and William Rogie Angus.

(The Sir William Ramsay Laboratories of Inorganic and Physical Chemistry, University College, London.)

1. *Introduction.*

An investigation of organic beryllium compounds is being carried out by one of us (W. R. A.) with a view to obtaining information regarding their molecular configuration and a study of their molecular polarisations suggested itself as a means of deciding whether or not these compounds are spatially symmetrical. No previous attempts appear to have been made to measure the dipole moment of compounds of this type ; other physical measurements have been made and will be discussed in a later section. In the present investigation measurements have been made in benzene and carbon tetrachloride solution, but in both solvents the compounds are only sparingly soluble.

2. *Purification of Materials.*

Beryllium Compounds.—Small quantities of basic beryllium acetate and beryllium acetylacetonate were very kindly supplied by Professor G. T. Morgan, F.R.S., and Dr. S. Sugden, and our best thanks are due to them. The melting points of the compounds were in accord with the values quoted at

the literature : acetate, m p 285° C ; acetylacetonate, m.p. 108·5° C. Micro-chemical analyses, carried out by Dr. Schoeller, in Berlin, gave the following table .—

Microchemical Analyses

	Beryllium acetate $Be_4O(CH_3COO)_6$		Beryllium acetylacetonate $Be(C_5H_7O_2)_2$	
	Found	Required.	Found	Required
Carbon	35 42	35 46	58 08 57 99	57 94
Hydrogen	4 31	4 46	6 73 6 79	6 81

Benzene.—Benzene of the ' *Extra Pure for Molecular Weight Determination* " grade, supplied by the British Drug Houses, was recrystallised twice and then dried over sodium wire. It was then fractionally distilled and further dried over fresh sodium until the latter retained its bright lustre   No trace of thiophene could be detected

Carbon Tetrachloride.—Pure commercial carbon tetrachloride (Hopkins and Williams) was repeatedly shaken with concentrated sulphuric acid, washed with water, shaken four times with 2N sodium hydroxide and again washed with water. It was allowed to stand over anhydrous potassium carbonate for 24 hours and was then fractionally distilled in an all-quartz distillation apparatus kindly lent by Dr. John Farquharson. The fraction boiling at 76·8° C was collected and dried over stick potash.

The methods given by Newcomb* for detecting small amounts of phosgene, carbon disulphide, sulphur chlorides, aldehydes and other organic substances were applied. No trace of any of these impurities was found. To ascertain whether a minute trace of chloroform was present a sample of the fractionated carbon tetrachloride was heated with Fehling's solution at 60°–70° C for several hours with vigorous shaking from time to time.† There was no reducing action and therefore no trace of chloroform.

3. *Methods of Measurement.*

The dielectric constants of dilute solutions were measured by the resonance method previously described.‡ A double-walled cylindrical glass vessel,

* ' Analyst,' vol 49, p. 225 (1924).
† Ingold and Powell, ' J. Chem. Soc.,' vol. 119, p. 1227 (1921).
‡ Smith, J. W., ' Proc. Roy. Soc.,' A, vol. 136, p. 251 (1932).

heavily silvered on the inside so as to form parallel conducting plates, was used as test condenser. This condenser was connected in parallel with a calibrated Sullivan standard variable air condenser (capacity 50–250 $\mu\mu F$) forming part of the resonance circuit; and against this standard condenser the capacity of the test condenser, containing air, pure solvent, or solution, was measured differentially. The test condenser was placed in a water thermostat and resonance points were determined at different temperatures.

Polarisations for optical wave-lengths were calculated from refractivity measurements on the solvents and solution, and compared with the polarisations for Hertzian wave-lengths calculated from dielectric constant data. The refractive indices were measured for the mercury green line (5461 Å) by a Pulfrich refractometer kindly placed at our disposal by Professor C. K. Ingold, F.R.S.

Density measurements of pure solvents and solutions were made at those temperatures at which resonance points and refractive indices were determined, using a 50 c.c. specific gravity bottle

4 *Dielectric Constant Data for Beryllium Acetylacetonate.*

Owing to the small quantity of this substance at our disposal it has been possible to measure only one solution in carbon tetrachloride. Resonance points were determined at 20°, 25°, 35° and 45° C for the test condenser containing air, pure solvent and solution, and the equivalent capacities were read direct from the calibration curve for the standard condenser. The lead capacities were assumed to be constant and Hartshorn and Oliver's* value of 2·2725 for benzene at 25° C. was taken as the standard dielectric.

The molecular polarisation P_1 of the solute was calculated from the modified Clausius-Mosotti equation applicable to solutions. The significant data are collected in Table I, where f_1 denotes the mol fraction of solute and ε and ρ the dielectric constant and density of the solution, respectively.

Table I.

Temperature :	20°.		25°.		35°.		45°.	
	Carbon tetra-chloride	Solution.	Carbon tetra-chloride	Solution.	Carbon tetra-chloride	Solution.	Carbon tetra-chloride	Solution.
f_1	—	0 00908	—	0 00908	—	0 00908	—	0 00908
ε	2 240	2 254	2 230	2 245	2 207	2·226	2 188	2 206
ρ	1 59309	1·58406	1 58356	1·57370	1·56392	1 55565	1 54232	1 53485
P_1	—	82 1	—	84·6	—	89 5	—	86 9

' Proc. Roy. Soc.,' A, vol. 123, p. 664 (1929).

5. *Dielectric Constant Data for Basic Beryllium Acetate*

Two solutions of basic beryllium acetate in benzene (I and II) and one in carbon tetrachloride (III) have been measured. In both solvents the compound was only sparingly soluble and consequently the possible error in these experimental results is comparatively high. Significant data for measurements at 25° and 45° C. are given in Table II.

Table II.

	f_1	Temperature 25°			Temperature 45°.		
				P_1.			P_1.
Benzene		2 273	0 87381	—	2 234	0 85113	
Solution I	0 00172	2 275	0 87508	132 6	2 238	0 85333	136 6
Solution II	0 00356	2 278	0 87675	133 7	2 243	0 85609	134 0
Carbon tetrachloride		2 30	1 58356	—	2 188	1 54232	—
Solution III	0 00103	2 226	1 58207	126 2	2 187	1 54119	129 1

6. *Refractive Index Data.*

The part of the molecular polarisation arising from induced dipoles may be identified with the molecular refraction R_1 of the solute calculated from the modified form of the Lorentz-Lorenz equation which is applicable to solutions.

In order to compare the polarisations calculated in this way with those calculated from dielectric constant data, the refractive indices of pure solvents and solutions were measured. Refractive index tables for 5461 Å. at 15° C. were given by the makers of the instrument, but in this investigation refractive indices were measured at 25° C. and it was necessary to introduce a temperature correction term for the prism. This term was obtained from correction tables supplied with the instrument by Messrs. Hilger, Ltd.

The values obtained for the pure solvent were compared with values calculated by interpolating the figures quoted in the literature by means of Cauchy's formula

$$n - 1 = A + \frac{B}{\lambda^2} \tag{6}$$

where A and B are constants

Using this formula the values for 5461 Å. interpolated from the figures of Knops[*] and Weegman[†] for benzene at 25° C. are respectively 1·50214 and

---

[*] ' Liebig's Ann.,' vol. 248, p. 175 (1888).

[†] ' Z phys. Chem.,' vol. 2, p. 237 (1888).

1·50230 ; whereas the experimental value obtained was 1·50213, which is in very good agreement.

Table III gives the significant data for the refractive indices and molecular refractions at 25° C. where the solutions I, II, and III are the solutions of basic beryllium acetate referred to in Table II and solution IV is the carbon tetrachloride solution of beryllium acetylacetonate referred to in Table I

Table III

Solution	C_6H_6	I	II.	CCl_4	III	IV
f_1		0 00172	0 00356	-	0 00103	0 00908
n	1 50213	1 50147	1 50109	1 45991	1 45976	1 46135
ρ	0 87181	0 87508	0 87675	1 58356	1 58207	1 57370
R_1	--	95 9	95 9	—	116 5	62 1

7. Discussion.

An examination of the literature revealed the fact that Tanatar* had determined the molecular weight of basic beryllium acetate by the depression of the freezing point of benzene. We, therefore, decided to measure the dielectric constants of benzene solutions, but encountered a surprisingly low solubility. The highest concentration obtainable at 18° C. was just over 1 per cent, approximately equal to that used by Tanatar. In order to obtain more concentrated solutions we next tried carbon tetrachloride as solvent, but unfortunately the solubility was even less. This is very surprising since, according to Wirth,† the solubility of basic beryllium acetate in chloroform at 18° C. is 33 per cent., and as the internal pressures of carbon tetrachloride and chloroform are approximately equal, one might expect a correspondingly close similarity in their solvent powers.

Qualitative determinations of the solubility of basic beryllium acetate have been made in various solvents. It was found to dissolve in toluene, chloroform, and acetone, but appeared to be insoluble in carbon tetrachloride, tetrachlorethane, hexane, and carbon disulphide, all of which are *non*-polar. In the literature it is recorded as soluble also in acetic acid, benzaldehyde, molten monochloracetic acid, phosphorus trichloride, ethyl malonate, ethyl acetate, and nitrobenzene. According to the qualitative determinations made

* ' J. Russ. ges. Chem.,' vol. 36, p. 82 (1904) ; ' Chem. Zlb.,' vol. 1, p. 1192 (1904).

† ' Z. anorg. Chem.,' vol. 87, p. 8 (1914).

and to the previous observations, the solubility appears to be related to the dipolar character of the solvent, and we suggest tentatively that this may account for the sparing solubility in benzene and carbon tetrachloride.

This sparing solubility tends to introduce a fairly large experimental error in the polarisation measurements. In view of this fact the values of the molecular polarisations calculated from the dielectric constant measurements must be regarded as very satisfactory for the solutions of basic beryllium acetate in benzene and of beryllium acetylacetonate in carbon tetrachloride. A molecule which has a permanent electric moment should have a less molecular polarisation at higher temperatures than at lower temperatures. Our results are sometimes slightly greater at higher temperatures, but only by an amount which is well within the limits of possible experimental error. We conclude, therefore, that the molecules of basic beryllium acetate and beryllium acetyl-acetonate possess no permanent electric moment. The solution of basic beryllium acetate in carbon tetrachloride was so very dilute that we feel there is no justification for placing any reliance on the polarisation measurements of this solution, in spite of the fact that the molecular polarisations agree fairly well with those obtained for a solution of the same substance in benzene. The molecular refractivities of basic beryllium acetate in the two benzene solutions (see Table III) agree with one another very closely.

When, however, we compare the molecular polarisations with the molecular refractivities we find that the refractivities are considerably lower both for the basic acetate and for the acetylacetonate as is shown in Table IV, in which mean whole number experimental values are given.

Table IV.

Compound.	Molecular polarisation.	Molecular refractivity.	Difference.
$Be_4O(CH_3COO)_6$	134	96	38
$Be(C_5H_7O_2)_2$	86	62	24

Bragg and Morgan[*] have shown that the crystal structure of basic beryllium acetate is symmetrical; that the four beryllium atoms are situated at the corners of a regular tetrahedron, at the centre of which is situated the unique oxygen atom, and that the six acetyl groups are arranged symmetrically along the six edges. From parachor measurements on basic beryllium propionate,

* 'Proc. Roy. Soc.,' A, vol. 104, p. 437 (1923).

Sugden* has suggested the structural formula, fig 1A, using odd electron link-
ages in preference to the formula, fig. 1B, in which normal two and four electrons
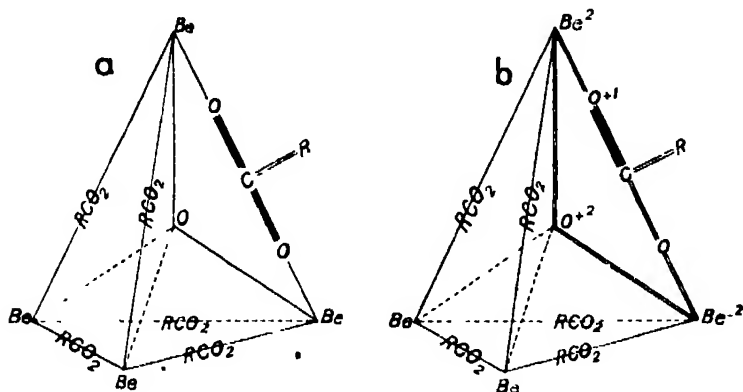linkages are used.   In the figures only one of the six interlocking, six-membered

Fig. 1.

rings is shown in detail and lines joining atoms each indicate a one-electron
linkage.

Both the formulæ answer the requirements of the crystal structure symmetry.
From the symmetrical nature of the molecule it would appear to be most
probable that the difference between the molecular polarisation and molecular
refractivity should be attributed to atomic polarisation.   Atomic polarisations
are more pronounced when atoms are linked by electro-valencies than by
co-valencies.   This is borne out, for example, in the series CCl_4, $TiCl_4$, $SnCl_4$†
where the atomic polarisations increase with the electropositive character of
the central atom.

The high value for the atomic polarisation seems to indicate that the struc-
tural formula in which all the atoms are electrically neutral is not an adequate
representation of the molecule.   From the fact that beryllates exist and in
view of the marked similarity in behaviour between beryllium and aluminium
compounds, it may be supposed that certain beryllium compounds are ampho-
teric in character.   Consequently a charge of -2 on the beryllium atoms
would not be wholly unexpected.

Similar arguments are applicable to the alternative structural formulæ
for beryllium acetylacetonate, figs. 2A and 2B.   Here again polarisation data
favour the second configuration.

* " The Parachor and Valency," p. 145 (1930) ; ' J. Chem. Soc.,' p. 318 (1929).

† ' J. Amer. Chem. Soc.,' vol. 51, p. 2051 (1929).

From considerations of diamagnetic susceptibility measurements,* the same conclusions have been reached regarding the structure of these molecules
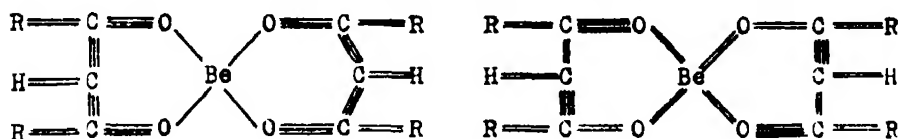

Fig. 2.

8. *Summary.*

The dielectric constants and densities of two solutions of basic beryllium acetate in benzene have been measured at 25° and 45° C and molecular polarisations calculated. Molecular polarisations have been calculated for a solution of beryllium acetylacetonate in carbon tetrachloride from dielectric constant and density measurements at 20°, 25°, 35° and 45° C. Molecular refractivities at 25° C. were determined for each solution. The molecular polarisations do not vary with temperature, but are higher than the molecular refractivities and a tentative explanation is given

* Angus and Farquharson, ' Proc. Roy Soc ,' A, vol 136, p 579 (1932)

The Measurement of Pressures Developed in Explosion Waves.

By COLIN CAMPBELL, WILLIAM BRIAN LITTLER, and CLIFFORD WHITWORTH
(Manchester University).

[PLATE 18]

The measurement of the pressure produced in the " explosion-wave " in gaseous mixtures is difficult because of the rapidity of movement of the wave and the short time for which the pressure over any given area lasts.   In 1894 Dixon and Cain* pointed out that the pressures obtained by firing a mixture in a closed vessel† did not correspond to pressures in the wave front.   Following a suggestion of Mallard and Le Chatelier, they used a method in which glass tubes of known strength were fractured by the explosion-wave, it being assumed that " if a pressure is produced in a glass tube greater than it can stand, the glass will be broken although the pressure may only last for a very short interval of time "   The strength of the glass tubes was found by determining the static pressures required to break similar pieces.   It was found that three lengths from the same piece of glass tubing required respectively 890, 950 and 1220 lbs. per square inch to fracture them : the accuracy of the results was therefore not very great.   Dixon and Cain estimated that the pressure in the explosion-wave in $C_2N_2 + O_2$ lay, probably, between 70 and 120 atmospheres and that in $C_2N_2 + O_2 + 2N_2$ between 63 and 84 atmospheres.

Jones and Bower‡ cast some doubt on the pressures given by Dixon and Cain, and suggested that they were the pressures produced just after detonation had been re-established when the explosion-wave had been damped down at a junction.   The pressure in the wave front of the fully established detonation wave in the mixture $C_2N_2 + O_2$ was estimated by Jones and Bower to be between 58 and 75 atmospheres.

Dixon§ recorded the fact that Jones and Bower found that the mixture $C_2N_2 + O_2 + 2N_2$ produced a pressure between 74 and 93 atmospheres, a higher pressure than for the undiluted mixture $C_2N_2 + O_2$; and he considered their results uncertain.   The discrepancy may perhaps be explained

* ' Mem. and Proc. Manc. Lit. and Phil Soc.,' p. 174 (1894).

† Berthelot and Vieille, ' Ann. Chim. phys.,' vol. 4, p. 14 (1885).

‡ ' Mem. and Proc. Manc. Lit. and Phil. Soc.,' p. 1 (1898).

§ ' Phil. Trans.,' A, vol. 200, p. 338 (1903).

by the observation of Bradley and Browne* that a glass tube which has once been subjected to a high pressure may, owing to deterioration of the glass, break under a much lower pressure, or even spontaneously.

In view of these experiments, the method of measuring explosion pressures by the breaking of glass tubes cannot be regarded as satisfactory.

In the present experiments we have tried to measure the pressure in the explosion-wave by placing across the explosion gallery metal foils of various thicknesses. By choosing two pieces of foil, one of which would stand the force of the explosion and prevent it proceeding along the tube and a second, slightly thinner foil, which was pierced by the explosion, it seemed possible to compare the pressures produced in different mixtures, by calibration of the foils with static air pressure it was also possible to obtain an approximate value for the actual pressure developed in any one mixture

Experimental.

The explosion gallery consisted of a series of glass and metal tubes, 1·5 cm. internal diameter, arranged horizontally The copper diaphragms, usually square pieces, were securely held in the apparatus, shown in fig. 1, between two
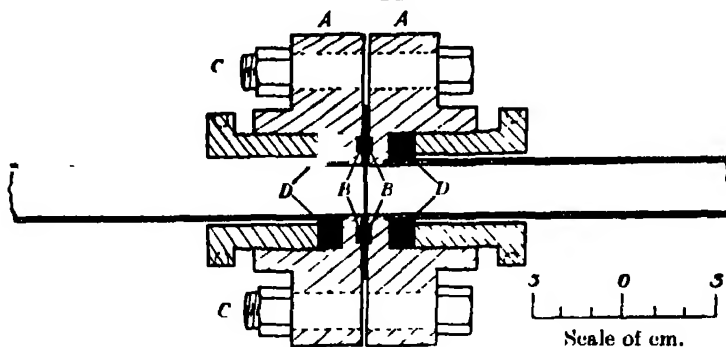
Fig. 1.

cylindrical gunmetal flanges, A, by two leather washers, B, internal diameter 2·2 cm., which could be clamped together by tightening the bolts, C; the glass tubes fitted into these flanges, gas-tight joints being made by means of the stuffing boxes and glands, D. After having been evacuated to a pressure of 0·1 cm. of mercury, or less, by means of a " Hyvac " oil pump, the tubes were filled with the gas mixture. This was ignited near the closed end of the tube system by a spark from the secondary circuit of a coil capable of yielding a ¾-inch spark in air.

* ' J. Phys. Chem ,' vol. 8, p. 37 (1904).

In order that the experimental conditions should be comparable when using different mixtures, it was essential that the explosion-wave should be well established before the flame reached the copper diaphragm, and to make sure that this had taken place the apparatus was erected in front of a rotating-drum camera so that the velocity of the flame before its impact with the diaphragm could be determined from the photograph.

The choice of metal for the diaphragm was carefully considered. Aluminium, tin and silver in thin sheets were found to tear during the setting up or evacuation of the apparatus, but copper was found to be very suitable and all the results given were obtained with this metal   It was found that the static air pressures required to break different samples taken from a long roll of metal agreed with one another, often to within 1 per cent.

During the course of preliminary experiments, the following observations were made —

(1) With a lead-glass gallery, bore 1 5 cm., consisting of 250 cm of lead tubing followed by 50 cm. of glass, the explosion-wave in electrolytic gas $(2H_2 + O_2)$ cut out (" sheared ") a clean hole in a diaphragm 0·003 inch thick ; a slightly thicker diaphragm, 0·0045 inch, was pierced with a very small hole, whilst one still thicker, 0·0057 inch, was merely deformed, a fairly sharp conical depression being produced. When the mixture $C_2H_4 + 3O_2$ was used under the same experimental conditions, a much thicker diaphragm, 0·0063 inch, was sheared. These results suggested that the pressure generated in the ethylene mixture was higher than that in electrolytic gas —a result in accordance with calculations based on the theory of Jouguet.*

(2) The Faraday cement joint between the lead and glass sections of the gallery was often cracked by the explosion, and this led to uncertain results In the later form of apparatus the lead tube was replaced by one of copper, and the metal-glass connection made pressure-tight by means of a stuffing box and gland, similar to that on the diaphragm apparatus

(3) The length of glass tube between the copper tube and the diaphragm was found to affect the breaking power of the mixtures.   Thus with electrolytic gas, the maximum thickness of copper sheared was 0·0045 inch when 18 cm. or 100 cm. of glass were used ; with 150 cm. the maximum thickness sheared was 0·0057 inch, and no further change in the breaking power of the mixture was detected when the length of glass was increased to 240 cm.   A similar type of result was obtained with the mixture $C_2H_4 + 3O_2$.   Thus, it would

---

* ' J. Math. pures appl.,' vol. 1, p. 347 (1905) ; vol. 2, p. 5 (1906).

appear that the force of the explosion is less when the flame has just emerged from a metal tube than when it has travelled some distance in a glass tube ; this is probably due to the greater cooling power of the metal tube.

In view of these observations, the form of apparatus finally adopted was as follows : The metal firing piece forming the closed end of the gallery was screwed into the copper tube, 1·6 cm internal diameter and 300 cm. long , the first 200 cm. of copper formed a smooth curve of radius 300 cm., and the last 100 cm were straight. The copper tube was connected by a stuffing box and gland to a glass tube 1·5 cm. internal diameter and 240 cm. long, which in turn fitted into the apparatus holding the diaphragm. A second glass tube of the same internal diameter and about 150 cm. long, fitting into the far side of the diaphragm apparatus, was filled with the same gaseous mixture as the rest of the system. The appearance of a flame in this tube indicated that the diaphragm had broken and it also gave other information to be discussed below.

Using this apparatus, we have obtained values for the thickness of copper foils which were (*a*) sheared, and (*b*) not sheared, by the explosion-waves in a number of different gaseous mixtures, and the results are given in Table I.

Table I

	Thickness of copper.	
Mixture	Sheared	Unsheared
	inch	inch
$2H_2 + 6O_2$	0 0045	0 0057
$2H_2 + O_2$	0 0057	0 0063
$7H_2 + O_2$	0 0045	0 0057
$C_2H_4 + 2O_2$	0 0103	0 0113
$C_2H_4 + 3O_2$	0 0083	0 0103
$C_2H_4 + 6\frac{1}{2}O_2$	0 0066	0 0080
$C_2H_4 + 19O_2$	0 0057	0 0063
$C_2H_2 + O_2$	0 0103	0 0113
$C_2H_2 + 2\frac{1}{2}O_2$	0 0083	0 0103
$C_2H_2 + 7\frac{1}{2}O_2$	0 0066	0 0080
$C_2H_2 + 10O_2$	0 0063	'
$CH_4 + O_2$	0 0083	0 0103
$CH_4 + 1\frac{1}{2}O_2$	0 0083	0 0103
$CH_4 + 2O_2$	0 0083	0 0103
$CH_4 + 4O_2$	0 0066	0 0080
$CH_4 + 8O_2$	0 0063	0 0066
$2CO + O_2$	0 0063	0 0066

The above table seems to show that whilst electrolytic gas is probably the hydrogen-oxygen mixture with the greatest breaking power, a large excess of either hydrogen or oxygen does not affect this value to any marked extent It will be seen later that this is in accordance with the calculated pressures for these mixtures.   In the case of the ethylene-oxygen mixtures, the breaking power increases from $C_2H_4 + 19O_2$ up to $C_2H_4 + 1\frac{1}{2}O_2$ In some experiments with the latter mixture, the glass tube through which the explosion-wave passed before it reached the diaphragm was shattered, and in this case copper $0 \cdot 0083$ inch was not sheared ; in other experiments where the tube remained intact copper $0 \cdot 0103$ inch was sheared.   The lower breaking power is probably due to a release of pressure behind the wave-front consequent upon the breaking of the glass tube.   (In the particular piece of apparatus used it was not possible to introduce thicker walled glass tubes which would always have withstood the pressure ; and metal tubes were precluded because of their cooling effects, mentioned above, and also because their use would have prevented the photography of the flames)

The breaking power of acetylene-oxygen mixtures increases from $C_2H_2 + 10O_2$ up to $C_2H_2 + O_2$.   In the case of methane-oxygen mixtures, $CH_4 + O_2$, $CH_4 + 1\frac{1}{2}O_2$ and $CH_4 + 2O_2$ all sheared $0 \cdot 0083$-inch copper, but failed to shear $0 \cdot 0103$-inch copper and their breaking powers are evidently not very different.   Some measure of the relative strengths of these mixtures can, however, be obtained from the depth of the conical indentation made on a $0 \cdot 0103$-inch diaphragm by each explosion-wave   On this basis the mixture $CH_4 + O_2$ is a little more powerful than either of the others   In the same way the mixture of equal volumes of acetylene and oxygen was estimated to be more powerful than the mixture of ethylene with twice its volume of oxygen The mixture $2CO + O_2$, shearing, as it does, $0 \cdot 0063$-inch copper, would appear to be stronger than electrolytic gas which does not shear the same thickness

When certain very dilute mixtures such as $C_2H_4 + 18 O_2$, $4CO + O_2$, and $3CO + O_2$ were ignited in the apparatus, detonation was not always established.   In such cases a diaphragm $0 \cdot 002$ inch thick not only remained intact but suffered no appreciable deformation.   These results show the marked difference between the breaking power of a " slow " flame and that of an explosion-wave.

The results given in Table I only permit comparisons to be made between the shearing power of different mixtures, but it seemed possible to estimate the actual pressures by determining the static pressure required to break a given thickness of foil.   For this purpose, air, from a high pressure cylinder, was

applied to one side of a copper foil held in the diaphragm apparatus as already described. Foils as thin as 0·002 inch and 0·003 inch were inclined to tear and did not always shear completely, but the thicker ones sheared in apparently the same way as when hit by an explosion-wave. The static pressure required depended to a slight extent on its rate of application. In calibrating the copper foils it was, therefore, customary to apply the pressure at a constant rate of about half an atmosphere per second ; the reading of the pressure gauge just prior to a sudden " kick " was taken as the breaking pressure. From the typical calibration curve, shown in fig. 2, it is seen that, for all except the thickest foil, a linear relationship exists between the breaking pressures and the
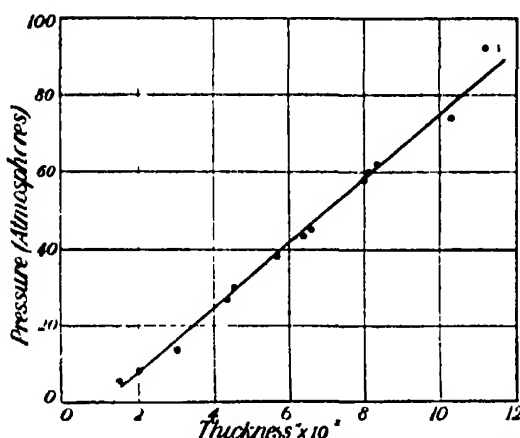

FIG. 2 —Calibration of Copper Foils by Static Air Pressures.

thickness. [The shearing pressures thus obtained do not agree with those calculated from the known physical constants of copper ; the reason for this is that, whilst the diameter of the piece of copper cut out is 1·5 cm., the pressure can act over a wider diameter (see figs. 1 and 7, Plate 18) because the leather washers project some small distance beyond the general level of the shearing edge. When copper was sheared against a perfectly flat edge 1·5 cm. in diameter the pressures required were higher and agreed with those calculated from the physical constants of copper.]

The blow given by the explosion-wave to the foil is of the nature of an impulse and we have photographic evidence, which will be discussed later, that the shearing of the foil occurred over an interval of time of the order of several hundred-thousandths of a second from the time at which the explosion-wave collided with it. It is well known that a load applied suddenly is approximately twice as effective in shearing a given material as when applied gradually.

If the analogy can be applied to the sudden pressure in the explosion-wave acting on the copper foil, then the pressure in the explosion-wave which will break a particular thickness of foil is only half the static (air) pressure which will achieve the same result. It follows, therefore, that the static shearing pressures, corresponding to each thickness of foil employed in the experiments, must be halved in value before being applied to estimate the pressures developed by various explosion-waves. As already shown, it was possible to determine for each mixture two limiting thicknesses of foil, one of which was sheared and the other, slightly thicker, which remained intact after being struck by the explosion-wave. By halving the static shearing pressures corresponding to these two thicknesses it seemed possible to determine the " lower " and " upper " limits between which the actual explosion-wave pressure must lie, a still closer approximation to the latter being obtained by taking the mean of these values. Before detailing the results, we shall discuss the calculation of explosion pressures from theoretical considerations so that the values so obtained may be compared with those determined experimentally.

Theoretical Calculation of Explosion Pressures.

Explosion-wave pressures for several mixtures have been calculated by Jouguet (*loc. cit*) using the specific heat values given by Mallard and Le Chatelier, and later* for a few mixtures according to the specific heat values given by Kast.† The method of calculation is as follows :—

Let C_v be the total molecular specific heat at constant volume of the products of combustion,

Q the heat of reaction,

p_1, p_2 the initial and final pressures respectively,

T_1, T_2 the initial and final temperatures (° K),

s_1, s_2 the initial and final specific volumes,

n_1, n_2 the initial and final numbers of molecules,

R the gas constant, and

γ the ratio of the specific heats of the products at T_2.

From Hugoniot's law for adiabatic dynamic compressions it can be shown that, if the gas laws are obeyed and the chemical reaction proceeds to completion,

$$\int_{T_1}^{T_2} C_v \, dT = Q + \tfrac{1}{2} R \, (\mu - 1 \,)(n_2 T_2 + n_1 T_1 / \mu), \tag{1}$$

* C. R. Acad. Sci. Paris,' vol. 181, p. 546 (1925).

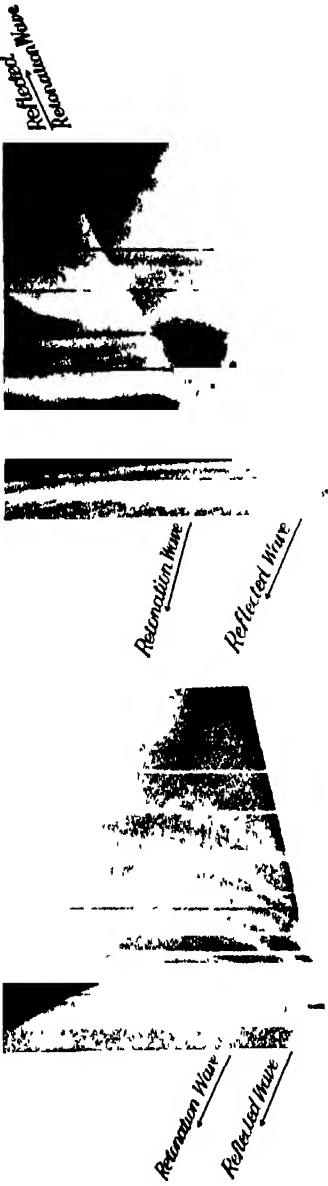† " Spreng-und Zündstoffe," 1921.

Fig. 4

Resonation Wave

Reflected Wave

Reflected
Resonation Wave

Fig. 3

Resonation Wave

Resonation Wave
Reflected Wave

(a)

(b)

(c)

(d)

Fig. 7

Fig. 6

Fig. 5

Reflected
Wave
Resonation
Wave

Reflected Wave
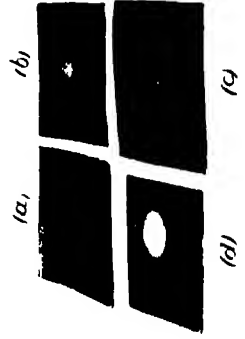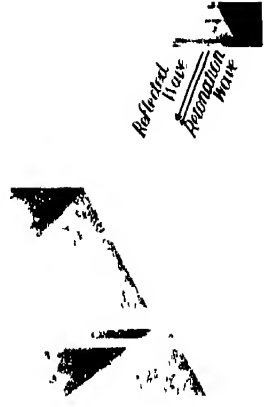
where $\mu = s_1/s_2$. This expression involves T_2 and μ, both unknown, and therefore for a first approximation the second term on the right-hand side of (1) is neglected and one writes

$$\int_{T_1}^{T_2} C_v \, dT = Q. \tag{1A}$$

This equation can be solved and an approximate value obtained for the temperature attained in the wave.

The application of this method of calculation to the reaction $H_2 + \frac{1}{2}O_2 \rightarrow H_2O$ is as follows. The data employed by Jouguet are $Q = 58,000$ calories per gm. mol.; $n_1 = 1 \cdot 5$; $n_2 = 1$; $T_1 = 283°$ K., and C_v (steam) $= 4 \cdot 5 + 0 \cdot 0058\, T$.

Substituting in equation (1A), we have

$$\int_{283}^{T_2} (4 \cdot 5 + 0 \cdot 0058\, T)\, dT = 58,000,$$

whence $T_2 = 3821°$ K. (first approximation).

Before the exact equation (1) can be used, it is necessary to know the value of μ at the temperature T_2. This is obtained by first finding C_v and γ at this temperature. Thus, from the specific heat equation, $C_v = 4 \cdot 5 + 0 \cdot 0058 \times 3821 = 26 \cdot 66$. Hence, since $\gamma = 1 + R/C_v$, at $3821°$ K., $\gamma = 1 \cdot 0746$.

Now the velocity of a shock-and-combustion wave can be shown to be

$$s_2 \sqrt{\frac{p_2 - p_1}{s_1 - s_2}},$$

and is equal to the velocity of sound in the gas at the temperature concerned: therefore,

$$s_2 \sqrt{\frac{p_2 - p_1}{s_1 - s_2}} = \sqrt{\gamma n_2 R T_2}.$$

Since $p_1 s_1 = n_1 R T_1$, $p_2 s_2 = n_2 R T_2$, and $\mu = s_1/s_2$ it follows that

$$\gamma \mu^2 - (\gamma + 1)\, \mu + n_1 T_1/n_2 T_2 = 0. \tag{2}$$

A value for μ can be obtained which on substitution in equation (1) gives a nearer approximation to the temperature. Thus from equation (2),

$$1 \cdot 0746\, \mu^2 - 2 \cdot 0746\, \mu - 0 \cdot 1107 = 0,$$

whence $\mu = 1 \cdot 876$ (first approximation).

Substitution in equation (1) gives

$$\int_{283}^{T_2} (4 \cdot 5 + 0 \cdot 0058\, T)\, dT = 58.000 + \tfrac{1}{2}R\, (\mu - 1)\left(n_2 T_2 + \frac{n_1 T_1}{\mu}\right),$$

i.e., $0 \cdot 0029 \, T_2^2 + 4 \cdot 5 \, T_2 - 59{,}505 = 0 \cdot 876 \, T_2 + 198$ and $T_2 = 3951°$ K. (second approximation).

If the processes to find C_v, γ and μ be repeated, a still closer approximation to T_2 can be obtained. Thus, in the example cited : At 3951° K., $C_v = 27 \cdot 4$; $\gamma = 1 \cdot 0726$; and $\mu = 1 \cdot 879$ (second approximation).

The third approximation for T_2 is thus given by

$$0 \cdot 0029 \, T_2^2 + 4 \cdot 5 \, T_2 - 59{,}505 = 0 \cdot 879 \, T_2 + 199,$$

whence

$$T_2 = 3956° \text{ K.}$$

In practice the above operations are repeated until successive approximations do not differ appreciably (say by 10°). The value for T_2 just obtained is, therefore, the one required.

Knowing T_2, a value can readily be obtained for p_2/p_1, for, from the gas laws, $p_2/p_1 = \mu n_2 T_2 / n_1 T_1$. Since p_1 is in general 1 atmosphere, this equation gives a direct value for p_2. Thus, the explosion-wave pressure for the mixture $2H_2 + O_2$ is given by

$$p_2/p_1 = 1 \cdot 879 \cdot \frac{1 \times 3956}{1 \cdot 5 \times 283}$$

$$= 17 \cdot 5 \text{ atmospheres.}$$

In applying the above method, the initial temperature has been taken as 10° C. ($T_1 = 283°$ K.) and the specific heat values employed are those given by Mallard and Le Chatelier and used by Jouguet, viz. :—

$$C_v \, (H_2, \, O_2, \, N_2, \, CO) = 4 \cdot 5 + 0 \cdot 0012 \, T$$

$$C_v \, (H_2O) \qquad\quad = 4 \cdot 5 + 0 \cdot 0058 \, T$$

$$C_v \, (CO_2) \qquad\quad = 4 \cdot 5 + 0 \cdot 0074 \, T.$$

It is, of course, realised that more recent formulæ (of the type $C_v = A \pm BT \pm CT^2$) are probably more accurate at temperatures up to 2000°, but since the temperatures in the explosion-wave are in many cases between 4000° and 5000° it is very doubtful whether extrapolation is any more reliable on the later formulæ than with the simpler form given above. For convenience, therefore, the above values have been provisionally adopted.

Where modern data for Q (the heat of reaction) differ markedly from those used by Jouguet, the explosion pressures have been re-calculated and are placed in the last column of Table II, the values obtained by Jouguet being placed beside them for purposes of comparison. In the same table are given

the pressures (air-pressures halved as already described) corresponding to the copper foils which were (a) just sheared, and (b) not sheared by the explosion-waves. In most cases the mean of these two values has been taken as the pressure for the mixture ; but in certain cases there are reasons for believing that the real pressures are quite near the lower or higher limit. In each of these cases, the " probable " value is given in brackets.
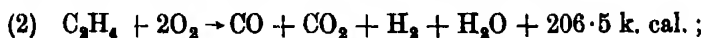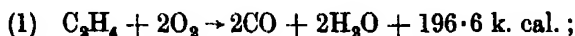
Table II.

	Mixture.	Pressures (atmospheres).		Mean or probable pressure (atms).	Q. (k cal)	Calculated pressures (atmospheres).	
		Copper Sheared.	Copper Unsheared.			Jouguet.	Authors
1	$C_2H_4 + 2O_2$	36 9	46 0	41 5	{ 196 6 / 206 5	- -	41 1 } / 40 4 }
2	$C_2H_4 + 3O_2$	31 0	36 9	34	332 0	- -	31 6
3	$C_2H_4 + 6\frac{1}{2}O_2$	23 0	29 0	26	332 0	—	26 0
4	$C_2H_4 + 19O_2$	19 0	21 8	(19)	332 0	·	18 6
5	$CH_4 + O_2$	31 0	36 9	34	{ 67 5 / 85 3	29 8 / -	— } / 36 3 }
6	$CH_4 + 2O_2$	31 0	36 9	(31)	{ 193 5 / 210 8	27 4 / —	— } / 29·2 }
7	$CH_4 + 4O_2$	23 0	29 0	26	{ 193 5 / 210 8	23 4 / ---	— } / 25 9 }
8	$CH_4 + 8O_2$	21 8	23 0	22 4	210 8	—	21 2
9	$C_2H_2 + O_2$	36 9	46 0	41 5	113 0	54 5	—
10	$C_2H_2 + 2\frac{1}{2}O_2$	31 0	36 9	34	312 0	—	30 0
11	$C_2H_2 + 7\frac{1}{2}O_2$	23 0	29 0	26	312 0	—	25 8
12	$C_2H_2 + 10O_2$	21 8	?	>21 8	307 0	22 0	—
13	$2H_2 + O_2$	19·0	21 8	20 4	58 0	17·5	—
14	$2H_2 + O_2 + 5H_2$	15·0	19 0	(15)	58 0	14 4	-
15	$2H_2 + O_2 + 5O_2$	15 0	19 0	(15)	58 0	14 4	—
16	$2CO + O_2$	21 8	23 0	(23)	68 0	17 2	--

The lower limit has been chosen as more probable than the mean of the lower and higher limits in the case of the mixtures $C_2H_4 + 19O_2$, $CH_4 + 2O_2$, $2H_2 + O_2 + 5O_2$ and $2H_2 + O_2 + 5H_2$ because the explosion-waves in these mixtures seemed only just capable of shearing the thinner copper ; in several experiments the copper disc was not completely severed from the remainder of the piece. In the case of the mixture $2CO + O_2$ the thinner foil was always sheared and the thicker one was occasionally cracked ; this suggested that the pressure was almost equal to the upper limit pressure.

The values of the calculated pressures in those hydrocarbon mixtures

containing insufficient oxygen for complete combustion will first be considered. In the explosion of the mixture $C_2H_4 + 2O_2$, at least two possible reactions may occur :—

(1) $C_2H_4 + 2O_2 \rightarrow 2CO + 2H_2O + 196 \cdot 6$ k. cal. ;

(2) $C_2H_4 + 2O_2 \rightarrow CO + CO_2 + H_2 + H_2O + 206 \cdot 5$ k. cal. ;

and it is uncertain whether either completely represents the mode of burning in the wave-front. Using the value of Q given in (1), the calculated pressure is $41 \cdot 1$ atmospheres compared with $40 \cdot 4$ atmospheres if Q is given the second value ; the corresponding velocities calculated by the formula given below are 2507 and 2490 m.p.s. respectively. Since the observed velocity, 2581 m.p.s., is only slightly higher than either of the calculated velocities, it is probable that the pressure is only slightly greater than either of the figures given above for the calculated pressures and therefore not very different from the mean determined pressure of $41 \cdot 5$ atmospheres.

In the case of the mixture $CH_4 + O_2$ it is generally assumed that the products are $CO + H_2O + H_2$ The recent value of Q ($85 \cdot 3$ k cal.) is much higher than the value used by Jouguet, namely, $67 \cdot 5$ k. cal. The corresponding calculated pressures are $36 \cdot 3$ and $29 \cdot 8$ atmospheres, and the velocities 2682 and 2477 m.p.s. Since the observed velocity, 2528 m.p.s., lies between these two values, it follows that the real pressure lies between the two given pressures and is probably not far from the observed pressure, 34 atmospheres.

Only in the case of the mixture $C_2H_2 + O_2$ is the calculated pressure very much higher than the determined pressure. This difference may be due to a variety of factors. The value of Q, 113 k. cal , used in the calculations was based on the assumption that the reaction is $C_2H_2 + O_2 \rightarrow 2CO + H_2$, but since carbon is always produced during the explosion of this mixture, this equation probably does not accurately represent the reaction occurring in the wave-front. The calculated velocity, 3091 m p.s., is considerably higher than the observed velocity, 2961 m.p.s., and it seems probable therefore that the calculated pressure is also too high. Since the calculated temperature is also much higher than in all the other mixtures, greater uncertainty exists in regard to the probable values for the specific heats. For these reasons it is felt that no reliance should be placed on the figure given for the calculated pressure in this mixture.

While the remaining results in Table II show a very fair agreement between the calculated pressures and the mean (or probable) pressures determined experimentally, the latter are, in general, slightly higher. This applies

particularly to those mixtures, Nos. 2, 6, 10, 13 and 16 in Table II, where the final products are entirely carbon dioxide and/or steam, and may be due to the specific heat formulæ giving too high C_v values for these gases. If this be the explanation, then where excess oxygen is used and appears among the products of combustion, as in the mixture $C_2H_4 + 6\frac{1}{2}O_2 \rightarrow 2CO_2 + 2H_2O + 3\frac{1}{2}O_2$, any errors in the specific heats of CO_2 and H_2O will have less effect on the calculated pressures, provided that the value for C_vO_2 is more nearly correct than that of C_vCO_2 and C_vH_2O. The excess of oxygen will also result in a lower flame temperature at which specific heat values for all the products will be more reliable. This gives an additional reason why calculated and determined pressures should show better agreement in the case of the more dilute mixtures, *e.g.*, Nos. 4, 8 and 12 in Table II.

From his calculations of explosion velocities, Jouguet deduced that the values for the specific heats of gases, as given by the formulæ of Mallard and Le Chatelier, increase too rapidly with temperature. In these calculations, the velocity in m.p.s. is given by $V = (\mu/100)\sqrt{\gamma n_2 R T_2/M}$, where M is the mass of n_2 molecules of products, $R = 84{,}760 \times 981$ ergs, and the other symbols have the same significance as in the previous calculations. In the case of the mixture $2H_2 + O_2$, the calculated velocity of explosion, 2627 m.p.s., is 194 m.p.s. less than the observed velocity, 2821 m.p.s. ; and in the mixture $2CO + O_2$ the calculated velocity, 1664 m.p.s., is 86 m.p.s. below the observed velocity, 1750 m.p.s. ; lower values for C_v would give higher calculated velocities. In this connection we may note that modern values* for the specific heats at 1000° C. and 2000° C. are lower in the case of the diatomic gases and considerably lower in the case of carbon dioxide and steam, than the corresponding values employed by Mallard and Le Chatelier (Table III).

Table III.

Gas.	From Partington and Shilling.		Mallard and Le Chatelier.	
	C_v 1000° C.	C_v 2000° C.	C_v 1000° C.	C_v 2000° C.
O_2	5·45	6 55	6 03	7 23
H_2	5·55	6·25	6 03	7·23
CO	5·45	6·55	6 03	7·23
H_2O	7 90	12 95	11 89	17 69
CO_2	10·18	11 62	13 92	21·32

' Partington and Shilling, " The Specific Heats of Gases," p. 204.

If the specific heats at still higher temperatures, say 4000°, are proportionately less than those employed by Mallard and Le Chatelier, this would easily explain why the calculated pressures in Table II are, in nearly every case, less than the experimentally determined pressures.

Quite recently Jouguet* has recalculated the pressures and rates of explosion for three different mixtures, using specific heat data given by Kast. The results, in which dissociation effects are neglected, are given in Table IV, the determined pressures from Table II being inserted for comparison.

Table IV.

Mixture.	T_2 (° K)	Velocity of explosion		Pressures	
		Calculated. m.p.s.	Observed m p s	Calculated	
$H_2 + O_2$	4780	2907	2821	21 1	20 4
$H_2 + O_2 + 5H_2$	2940	3767	3530	16 1	(15)
$CO + O_2$	6000	2106	1750	26 3	(23)

It is clear that the calculated velocities exceed the observed velocities; from this Jouguet concluded that the specific heats at high temperatures, as given by the Kast formulæ, are too low.

It has been pointed out by Jouguet and also by Lewis and Friauf† that lower values for the calculated velocities are obtained if dissociation is taken into account It is therefore clear that by using slightly higher specific heats than those employed by Kast and/or by taking into account dissociation effects, the calculated velocities would be reduced and could be made to agree well with the observed velocities ; by this procedure the calculated pressures would also be reduced.

It appears then that, in a number of different mixtures, the pressures determined experimentally, by the method described above, lie between the pressures calculated from formulæ for specific heats given by (a) Mallard and Le Chatelier, and (b) Kast, where these have been applied.   Since the former, (a), are believed to give for the calculated pressures too low values, and the latter, (b), too high values, it would appear that the true pressures calculated on Jouguet's theory do not lie far from the determined pressures   In view of uncertainties in the specific heats and the validity of the gas laws at the temperatures of the

* 'C. R. Acad. Sci. Paris,' vol. 181, p. 546 (1925).
† 'J. Amer. Chem. Soc.,' vol. 52, p. 3905 (1930).

reaction, it has not been thought desirable to apply any corrections for possible dissociation, even if reliable data for the latter were available.

The Photographic Records.

The photographs, figs. 3–7, Plate 18, obtained during this research have given some information on the behaviour of the flame before and after collision with the copper diaphragm. Fig. 3 shows the reflected wave produced when the explosion-wave in electrolytic gas strikes foil 0·002 inch thick. Although the latter was sheared, the explosion-wave was reduced to a slow flame and only re-established at a point 35 cm. along the tube. With foil 0·003 inch thick, a similar photograph was obtained, detonation in this case occurring about 40 cm. beyond the diaphragm. When the foil was increased in thickness to 0·0045 inch the explosion-wave made a deep conical bulge in the copper and commenced to shear it at one side ; the flame, however, ignited the mixture in the second glass tube. The photograph obtained, fig. 4, shows that an intense wave is reflected from the foil, that the flame which passed the latter was almost non-luminous, and that detonation was set up about 55 cm. beyond the diaphragm, the resulting retonation wave being reflected by the almost unbroken foil. Both these photographs were obtained during the preliminary experiments, but are in every way typical of those obtained later. With still thicker copper, 0·0057 inch, the explosion-wave in this mixture produced a conical depression in the foil but was not able to penetrate it.

The narrow, dark, vertical lines seen in the flame photographs are due to reference marks, 20 cm. apart, placed on the explosion tubes, whilst the white vertical line was produced by exposing the film, either immediately before or just after the experiment, to a narrow beam of light from a small electric lamp ; this gave the exact direction of the movement of the film as it passed the focus of the camera lens.

The appearance of some of the copper foils after use is shown in fig. 7. When foil 0·002 inch thick was struck by a " slow " flame in the mixture $4CO + O_2$, it was not distorted and only the faint imprint made on it by the leather washers which had held it in position can be seen (a). Opposite sides of the conical bulge produced when an explosion was not strong enough completely to shear the foil are shown in (b) and (c), whilst (d) shows a diaphragm which has been completely sheared. The annular indentation round the edge of the sheared portion (d) indicates that the " pressure effect " of the flame had been spread out over an area extending as far as the leather washers ; this is also visible in (b) and (c).

The photograph of the flame in the mixture $C_2H_4 + 3O_2$, fig. 5, is quite different from those already described for electrolytic gas. The foil in this experiment was 0·0028 inch thick, and the photograph shows clearly the strong wave of reflection produced when the flame struck the copper foil. The velocities of the flame before and after it had passed through the diaphragm apparatus are apparently identical, but the two flame traces are not in alignment : the vertical distance between the second and the extrapolation of the first is about 0·28 cm, and corresponds in this experiment to a time of approximately 0·000045 second. On the original negative, faint "striæ" are visible just beyond the diaphragm ; this suggests that inside the diaphragm apparatus, which was only 5 cm. long, the detonation wave may have been damped down and re-established ; but this is by no means certain. The time 0·000045 second is, therefore, a "maximum" time required to break the diaphragm. When thinner foil, 0·0022 inch, is used, the delay is 0·000033 second, but when thicker foil, 0·0043 inch or more, is used, the explosion-wave is definitely suppressed and is not re-established until the flame has travelled several centimetres in the second glass tube. In general, it appears that for any given mixture, the distance over which the flame must travel before detonation is re-established tends to increase with increasing thickness of foil. This has already been illustrated in the experiments with electrolytic gas given above. When the mixture $C_2H_4 + 1\frac{1}{2}O_2$ is employed and moderately thin foils used, there is no indication of any damping down in velocity of the explosion-wave and the delay therefore probably represents the actual time taken by the explosion-wave to shear the diaphragm. The times required to shear different foils are apparently proportional to the thickness in the case of this mixture, and nearly so in the case of the mixture $C_2H_4 + 3O_2$,

Table V.

Mixture.	Time to shear foil, sec. $\times 10^{-5}$ ($= a$)	Thickness of foil, inches ($= b$)	Delay thi (=
$C_2H_4 + 3O_2$	3 3	0 0022	1 50
$C_2H_4 + 3O_2$	4 5	0 0028	1 61
$C_2H_4 + 1\frac{1}{2}O_2$	4·2	0·0043	(98
$C_2H_4 + 1\frac{1}{2}O_2$	6 2	0 0063	0·98

Table V ; the lack of agreement in this latter case is due possibly to the fact discussed above, that the explosion-wave may have been momentarily damped down.

The Pressure at the Point of Detonation.

The experiments so far described have been attempts to measure the pressure in an explosion-wave which has travelled several metres beyond the point of detonation. Some experiments have been carried out in which it was arranged that detonation was set up much nearer the copper diaphragm. This was made possible by attaching the firing piece directly to the glass tube fitting into the diaphragm apparatus; by using different lengths of glass tube it was possible to vary the position of the point of detonation. The results obtained with the mixture $2H_2 + O_2$, are summarised in Table VI.

Table VI.

Spark-gap to copper foil.	Point of detonation to copper foil.	Thickness of copper.		Corresponding pressures.	
		Sheared.	Unsheared.	Sheared.	Unsheared.
cm.	cm.	in	in.	atmos.	atmos.
175	20–25	0 0057	0 0063*	19 0	21 8
66	10	0·0102	0·0112*	36 9	46·0

* Limiting case, commenced to shear.

In the experiment using foil 0·0112 inch thick, the glass tube was shattered by the force of the explosion, had it remained intact it is very probable that the diaphragm would have been completely sheared. The photograph of this experiment is reproduced in fig. 6. The portion prior to the diaphragm clearly shows (1) the pre-detonation flame, (2) the point of detonation, and (3) the reflected wave from the foil. It will be seen that the early travel of the flame in the second glass tube is not recorded owing to its feeble luminosity after passage through the foil : this, coupled with the fact that detonation was not re-established until after some 80 cm., serves to indicate that the explosion had great difficulty in bulging and cracking the copper foil. Since the explosion-wave in electrolytic gas did not normally shear copper thicker than 0·0057 inch, it is clear from these experiments that the pressure near the point of detonation is much greater than that obtaining when the wave is fully established. This enhanced pressure would seem to be an explanation of the greater destructive effects of gaseous mixtures at the point of detonation noted by other workers, *e.g.*, Dixon, *loc. cit.*, p. 338.

The mixtures were made from gases obtained from cylinders except in the case of carbon monoxide, which was prepared from sodium formate. Mixtures

containing hydrogen, carbon monoxide or methane were stored over water at room temperature and passed directly into the explosion tubes ; those containing acetylene and ethylene were passed rapidly over calcium chloride and stored over mercury. The analyses of the different mixtures used are not given because slight variations in composition had no appreciable effect on the results obtained. The amount of combustible gas was within 2 per cent. of that required by the given molecular proportions ; the remainder was oxygen containing usually 1–2 per cent. nitrogen.

Summary.

(1) Experiments on the shearing of copper foils of various thicknesses by explosion-waves in a number of different gaseous mixtures seem to provide a method of comparing the explosion pressures existing in the flame.

(2) By calibrating these foils by means of static air pressures, direct values of explosion pressures have been determined

(3) These pressures agree fairly well with the pressures calculated by the method suggested by Jouguet, especially in the case of the more dilute mixtures. The effects of the values of the heats of reaction and the formulæ for the specific heats of gases at high temperatures on these calculated pressures are discussed.

(4) Photographs of the flame before and after the copper foils in certain cases give approximate values for the times required to shear them.

(5) Pressures near the point of detonation are higher than in the fully established explosion-wave.

X-Ray Study of Phase Boundaries in Thermal Diagrams of Alloy Systems—Cu-Zn System.

By Professor E. A. OWEN, M.A., D.Sc., and LLEWELYN PICKUP, Ph.D., University College of North Wales, Bangor.

[PLATES 19 and 20]

Within the last 10 years, the study of the diffraction of X-rays by crystal units in metals and alloys has shown that X-ray analysis, apart from giving data on the form and dimensions of the crystalline units, is a powerful method with which to examine the thermal diagrams of alloy systems. Rosenhain* has pointed out, however, that although the X-ray analysis of alloys yields valuable results as to structure and so on, the constitutional diagrams arrived at by this means must necessarily be incomplete, firstly because a very small amount of a second phase in a large mass of another phase cannot be detected by X-ray methods, and secondly, because the parameter measurements have not been accurate enough to determine definitely the boundaries of solid solubility. In view of this statement we felt it would perhaps serve a useful purpose to carry out a careful investigation into the reliability of accurate X-ray methods for establishing thermal equilibrium diagrams of alloy systems. An account of such an investigation is given in this paper, and it may be stated at the outset that, where X-ray data could be compared with data reliably established by other methods, the agreement is as good as, if not better than, that between the data of the various methods amongst themselves. It will be shown that a phase boundary can be determined by the X-ray method from parameter measurements alone, and that an accurate determination can be made irrespective of the amount of the second phase present

It will be necessary to go into the method of measurement and the heat treatment of the alloys in some detail. Precautions have to be taken in the preparation and analysis of the alloys to ensure that the parameter measured is that of the alloy in the equilibrium state, and that its composition is that corresponding to the alloy actually used in the measurement. The paper is therefore divided into two parts ; the first part deals with the method of measurement and the preparation of the alloys, and the second part refers to

* ' J. Inst. Met.,' vol. 42, p. 54 (1929).

the X-ray examination of the alloys with a view to determining the phase boundaries.

Attention is directed to alloys in the copper-zinc system. These were chosen as a considerable amount of work has already been done on them by metallurgical and by X-ray methods; the former have yielded much data concerning the phases and boundaries in the equilibrium diagram, and the latter have resulted in a good general survey of the structures of the various phases. The types of structure given to the different phases in the series[*] appear now to be generally accepted, but the parameters hitherto determined can only be taken as approximate owing to the comparatively low accuracy of the methods employed to obtain them. In the present investigation use is made of the precision camera employed by Gayler and Preston[†] to examine the age hardening of aluminium alloys. By taking various precautions which will be detailed below, the parameters of alloys can be determined to an accuracy of at least 1 in 4000. This accuracy is higher than that which is possible in the ordinary method with the Muller camera or with the X-ray spectrometer, and it enables the small variations in parameter values to be followed which could not be detected by the other methods of measurement.

I.—*Method of Measurement and Preparation of the Alloys.*

In the camera used by Gayler and Preston, the sample under examination, either in the form of a thin flexible sheet or in powder form on a sheet, is placed on the circumference of a cylindrical brass drum and is exposed to a divergent beam of X-rays proceeding from a slit placed at the opposite end of the diameter. A photographic film placed on the drum symmetrically with regard to the slit receives the reflected rays. The conditions are such that the rays come to a focus, producing lines on the film on either side of the slit. If θ is the glancing angle, s the distance between corresponding lines, and r the radius of the drum, then $s/8r = \pi/2 - \theta$, which gives θ when r and s are known. The parameter of the lattice a can then be calculated from Bragg's equation $\lambda = 2\gamma a \sin \theta$, when γ is a function of the Miller indices of the reflecting planes.

It was found that the (420) planes of copper gave with copper radiation a value of about 73° for θ, so that $\tan \theta$ is about 3·3. Thus $\delta a/a = \delta\theta/3\cdot3 = \delta s/26\cdot4r$. Now assuming an experimental measuring error in s of the order

---

[*] Owen and Preston, ' Phys. Soc. Lond.,' vol. 36 (1923), and Westgren and Phragmen, ' Phil. Mag ,' vol. 50, p. 311 (1925).

[†] Gayler and Preston, ' J. Inst. Met.,' vol. 41, p. 218 (1929).

of 0·5 mm.—this is considerably greater than that found by repeated measurements—the error in the parameter, if r is 50 mm., is rather less than 0·04 per cent. Thus very small changes in the lattice parameter can be detected with this instrument. In the actual camera used, the $K\alpha_1$ and $K\alpha_2$ wave-lengths of copper were separated by over 3 mm. when the arc between corresponding lines was about 15·5 cm., and by about 6 mm. when the arc was about 7·5 cm.

The camera was of robust construction. Its outer brass surface was turned in the lathe to ensure that it was truly circular. Its radius was measured by several methods all of which agreed closely with each other giving a mean value of 51·46 mm., but this is not the effective radius because a layer of black paper, 0·08 mm. thick, was placed between the film and the circumference of the camera. Also since the film was double coated, the two images were not exactly superimposed when the film was laid flat. The measured distance between the lines was such that it represented the distance between them if they had been photographed on a single coating of emulsion situated midway between the actual coatings. The thickness of the film before development was 0·23 mm., so that the middle layer of the gelatine was displaced 0·20 mm. radially from the circumference of the camera. Theoretically the contours of the film and the sample examined must have identical radii of curvature. This condition was obtained by fixing a sheet of aluminium foil of thickness 0·20 mm. round the slot to be covered by the sample, thus making the effective camera radius 51·66 mm.

The slit system was incorporated in the camera itself and could be adjusted and fixed in the position to give reflection lines of the best definition. The film and sample were held in position by elastic bands which pressed them lightly and uniformly against the circumference. Precautions were taken to avoid fogging of the film by the use of suitable lead screens. The camera was mounted on a heavy stand furnished with three levelling screws.

Installation.—The X-ray tube, which was of the gas type, was operated on a Schall transformer capable of an output of 30 ma. at 100 kv. It was found that the tube when working steadily over long periods, passed 8 to 10 ma. at 35 to 40 kv. In precision camera work, 1½ to 2 hours' exposure under these conditions was usually sufficient, but for powder spectrum photographs as finally produced, an exposure of 10 hours was required at this input. The latter were occasionally required to check certain points in connection with the structure of the alloys.

Measurement of the Photographs.—All measurements of the films were made with a micrometer screw attached to the carriage of which was a blade pointer.

This pointer was adjusted to move over the film which was supported on a sheet of opal glass, illuminated from below and situated well away from the source of light to avoid undue heating. The micrometer screw was compared with a finely graduated millimetre scale ; over the entire length, the maximum variation in the screw and the scale did not exceed about 0·05 mm. As it was essential for comparative measurements throughout the work periodically to check the micrometer screw, a suitable scale was made by ruling fine lines on the emulsion of an unexposed photographic plate. Periodic checking showed that the variation in the measured distance between the lines was always less than 0·05 mm. in 140 mm. This was considered satisfactory. On this standard, subsequent work gave for well annealed electrolytic copper a parameter of 3·6079 A., which agrees closely with the most accurate determinations made hitherto on the parameter of this element.

Film Shrinkage.—To investigate the shrinkage of the film on developing and fixing, the following method was adopted. A photographic half plate was exposed to light, developed and dried. On the blackened emulsion a fine straight line was cut with a razor edge and two other fine lines cut at right angles to this at about 14·5 cm. apart ; the distance between the cross lines was carefully measured with the micrometer screw. Next a strip of double-coated film, the size used for X-ray exposures, was taken and the cross lines printed on it by super-imposing the glass plate and giving a suitable exposure. The film was then developed in the manner adopted for the standard procedure. On measuring the imprint and comparing with the marks on the plate, any shrinkage could be detected. For instance, four separate readings gave 14·416 cm. as the mean distance between the marks on the blackened plate, while the means of three separate films, cut from different sheets, gave for this distance, 14·394, 14·404 and 14·392 cm. Hence the films showed respectively a shrinkage of 0·15, 0·08 and 0·17 per cent. To allow for this shrinkage fiducial marks were made on the camera so that their imprint appeared on every film exposed ; these marks consisted of small holes bored through the drum near the edge of the slot covered by the film. On development the imprints showed a double edge because the reflected beam did not pass normally through the film, and so two images were produced one on each emulsion. It was easy, however, to decide which edge corresponded to the emulsion adjacent to the hole. To ascertain the true arc between the inside edges of the holes in the drum, a strip of self-toning photographic paper was fixed over the slot and exposed to daylight. Well defined imprints of the holes were thus obtained and the distance between their inside edges measured

with the micrometer screw. Since the paper was not " fixed," this measurement gave the true distance between the holes. The mean value of two measurements each of three separate strips of paper was 14·535 cm., but owing to the thickness of black paper (0·08 mm.) placed between the film and the camera during exposure, a small correction has to be applied to obtain the correct distance of the imprints on the film under experimental conditions. This correction amounted to 0·011 cm., thus making the distance between the inside edges of the imprints on the film to be 14·546 cm.

The measurements of the arcs on each film were corrected by assuming a linear shrinkage throughout the length of the film, calculating its amount by measuring the distance between the two registered spots on the film and comparing with the true distance as derived above. When an abnormally large fiducial length was encountered, this was put down to a bulge in the film from some cause or other and such photographs were discarded. This, however, rarely occurred. By measuring the fiducial distance, arc measurements could always be adjusted to conform to the standard even if measured after a long interval of time.

In the photographs, the $K\alpha_1$ and $K\alpha_2$ lines of copper radiation were always resolved, and in some cases, when conditions were favourable the $K\beta$ line was also registered. The reflected α lines of the copper radiation varied in width from about 0·5 mm. for long arcs to about 0·9 mm. for short arcs. Rather than estimate visually the centre of these lines, it was found more convenient to measure from their edges with the aid of a small power hand lens. The measurements given in Table I were made on a film showing the reflections of the $K\alpha_1$ and $K\alpha_2$ wave-lengths of copper from the (420) planes of annealed copper. The sketch, fig. 1, explains the method of arriving at the arc lengths.
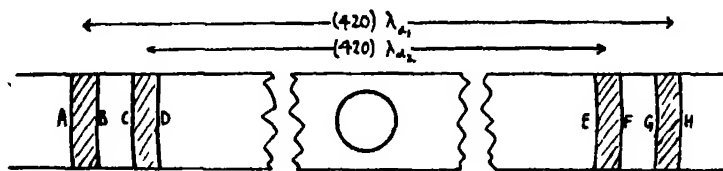

FIG. 1.

Both values for each pair of figures in column 3 of Table I, if the corresponding lines were of equal width, should be the same, but owing to errors in estimating the edges, and also to possible slight differences in the widths, a difference of 0·1 mm. was allowed as the maximum error for arcs longer than about 12 cm.; the actual differences were well under this maximum tolerance.

Table I.

Readings.		Arc length.	Measured mean arc length.	Corrected arc length.	Parameter of copper.
cm.	cm.	cm.	cm.	cm.	Å.
3·562 (A)	16·380 (H)	12·757	12·755	12·747	3·607₉
3·623 (B)	16·315 (G)	12·753			
3·723 (C)	16·201 (F)	12·434	12·432	12·424	3 607₈
3·767 (D)	16·153 (E)	12·430			

For arcs shorter than about 8 cm., the lines of the doublets are broader and their edges are not so well defined, but as the theory of the camera shows, more latitude in measurement is permissible, with the result that even higher accuracy is obtained with these less well defined lines than with those better defined at longer arcs. The most accurate conditions were found to be when the arc was about 8 cm., but owing to the small working range (about 68° to 87°) not even with radiation from targets such as nickel, cobalt, or iron, was it possible to obtain ideal conditions for certain parameter measurements. Under the best conditions the precision of the measurements would not be impaired if the shrinkage correction were entirely neglected.

Conditions for the Production of Reflection Lines.—Owing to the high resolution obtained with the precision camera, well defined reflection lines are not registered on the film unless the spacing of possible reflecting planes is very uniform. Enough cold work is done even with gentle filing so to distort the structure as to make the spacing of the planes irregular enough to spoil the reflections. To obtain sharp lines at large glancing angles it is necessary to eliminate the distortion by annealing the specimen. Experiments showed that there is a minimum annealing temperature below which lines may not be produced and that the higher the annealing temperature is above this minimum, the shorter is the annealing time required to produce the lines. In the process of annealing, however, it is possible that the composition of the alloy may be altered owing to the volatilisation of one of the components. A detailed study was therefore made of the effect of annealing the alloys both in the form of filings and in lump form. Unless precautions are taken to ensure a prolonged cooling from the liquid state, the resulting ingot is in a heterogeneous condition, so that when filings are taken from it, different fragments may have different compositions. Annealing such filings may produce equilibrium in each fragment but unless there is interdiffusion of the components between fragment and fragment, apart from that between the
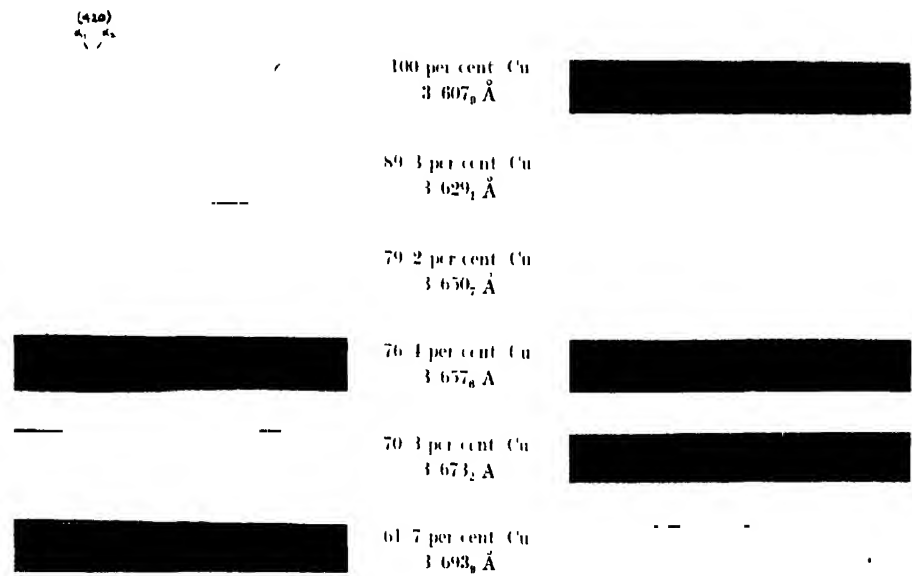
100 per cent Cu
3 607$_9$ Å

89 3 per cent Cu
3 629$_1$ Å

79 2 per cent Cu
3 650$_2$ Å

76 4 per cent Cu
3 657$_8$ A

70 3 per cent Cu
3 673$_2$ A

61 7 per cent Cu
3 693$_9$ Å

Fig 3

62 per cent Cu
$(a + \beta)$
β parameter
2 935 Å

59 5 per cent Cu
$(a + \beta)$
β parameter
2 935 Å

56 9 per cent Cu
(β)
2 949 Å

55 2 per cent Cu
(β)
2 941 Å

52 7 per cent Cu
(β)
2 946 Å

48 4 per cent Cu
$(\beta + \gamma)$
β parameter
2 950 Å

43 2 per cent Cu
$(\beta + \gamma)$
β parameter
2 950 Å

Fig. 6.

43.5 per cent Cu
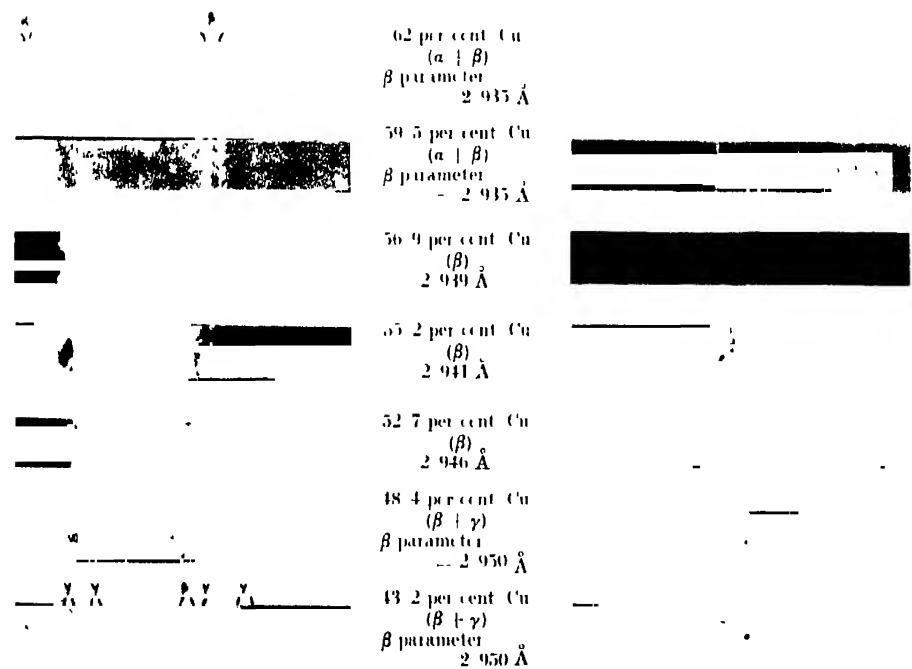710 C

650 C

600 C

550 C

500 C
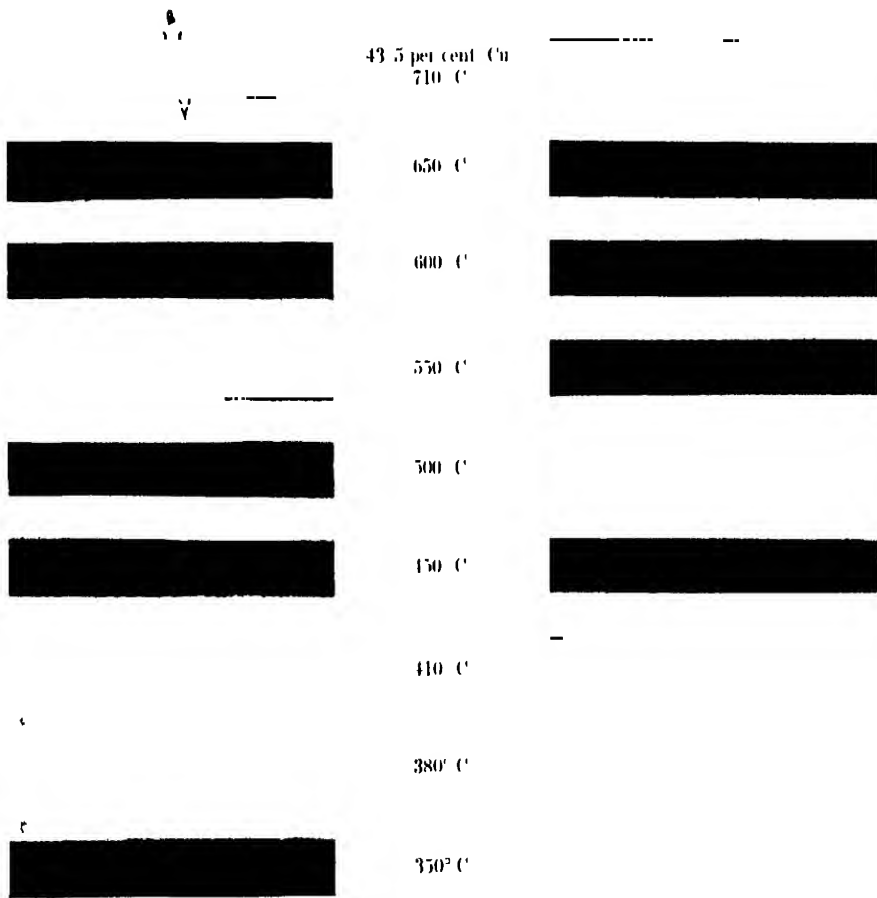
450 C

410 C

380° C

350° C

FIG. 8

components of the same fragment, the mass as a whole will still be hetero-geneous.

To investigate the effect of annealing, six alloys were taken covering a copper range of from 100 per cent. to 56 per cent. Filings of these in the " as cast " condition were first prepared. Then about 1 c.c. of each alloy was lump annealed at 850° to 860° C. for 9 hours, packed in powdered charcoal in a metal container, the ends of which were luted up with alundum cement. After annealing they were allowed to cool slowly in the furnace. Filings were taken after removing the outside surface to a depth of at least 1 mm. These filings together with those taken from the " as cast " specimens, were annealed in evacuated pyrex tubes at 500° C. for 4 hours before their parameters were determined. After the measurement of the parameter, the filings were removed from the aluminium foil on which they were mounted in the camera, and analysed for copper content. Table II gives the results obtained.

Table II.

Alloy marked.	Condition.	Filing analysis (per cent. Cu by weight).	Parameter (Å).	
			α-phase.	β-phase.
897 Z	As cast	89 3	3 629₁	—
897 Z	Lump annealed	90 6	3 627₇	.
752 Z	As cast	74 8	3 662₉	.
752 Z	Lump annealed	76 8	3 657₆	—
673 Z	As cast	67·3	3·679₇	- -
673 Z	Lump annealed	70 3	3 673₂	- -
614 Z	Lump annealed	62·4	3·693₉	—
589 Z	As cast	58·9	3 696₀	2 943₉
589 Z	Lump annealed	59 5	3 696₃	2 944₁
561 Z	As cast	56 1	3 695₇	2·942₃
561 Z	Lump annealed	57 6	3 695₈	2·942₉

These figures are plotted in fig. 2 from which it is observed that the relation between the parameter and composition is the same smooth curve for both the " lump-annealed " and the " as cast " samples* in the pure α region extending down to about 62 per cent. copper. Both the α and the β phase parameters in the (α + β) region are constant.

* The size of ingot cast was about 30 gm   It is probable that this agreement between annealed and " as cast " samples would not obtain if much larger ingots were employed, see Genders and Bailey, ' J. Inst. Met ,' vol. 33, p. 215 (1925).

components of the same fragment, the mass as a whole will still be hetero-geneous.

To investigate the effect of annealing, six alloys were taken covering a copper range of from 100 per cent. to 56 per cent. Filings of these in the " as cast " condition were first prepared. Then about 1 c.c. of each alloy was lump annealed at 850° to 860° C. for 9 hours, packed in powdered charcoal in a metal container, the ends of which were luted up with alundum cement. After annealing they were allowed to cool slowly in the furnace. Filings were taken after removing the outside surface to a depth of at least 1 mm. These filings together with those taken from the " as cast " specimens, were annealed in evacuated pyrex tubes at 500° C. for 4 hours before their parameters were determined. After the measurement of the parameter, the filings were removed from the aluminium foil on which they were mounted in the camera, and analysed for copper content. Table II gives the results obtained.

Table II.

Alloy marked.	Condition.	Filing analysis (per cent. Cu by weight).	Parameter (Å).	
			α-phase.	β-phase.
897 Z	As cast	89 3	$3\ 629_1$	—
897 Z	Lump annealed	90 6	$3\ 627_7$	.
752 Z	As cast	74 8	$3\ 662_9$	.
752 Z	Lump annealed	76 8	$3\ 657_6$	—
673 Z	As cast	67·3	$3\cdot679_7$	- -
673 Z	Lump annealed	70 3	$3\ 673_2$	- -
614 Z	Lump annealed	62·4	$3\cdot693_9$	—
589 Z	As cast	58·9	$3\ 696_0$	$2\ 943_9$
589 Z	Lump annealed	59 5	$3\ 696_3$	$2\ 944_1$
561 Z	As cast	56 1	$3\ 695_7$	$2\cdot942_3$
561 Z	Lump annealed	57 6	$3\ 695_8$	$2\cdot942_9$

These figures are plotted in fig. 2 from which it is observed that the relation between the parameter and composition is the same smooth curve for both the " lump-annealed " and the " as cast " samples* in the pure α region extending down to about 62 per cent. copper. Both the α and the β phase parameters in the (α + β) region are constant.

* The size of ingot cast was about 30 gm   It is probable that this agreement between annealed and " as cast " samples would not obtain if much larger ingots were employed, see Genders and Bailey, ' J. Inst. Met ,' vol. 33, p. 215 (1925).

The lump annealing has altered the composition of each alloy but the alloys in the (α + β) region have not lost as much zinc in proportion to that initially present as the alloys in the pure α region. Thus the presence of the β phase
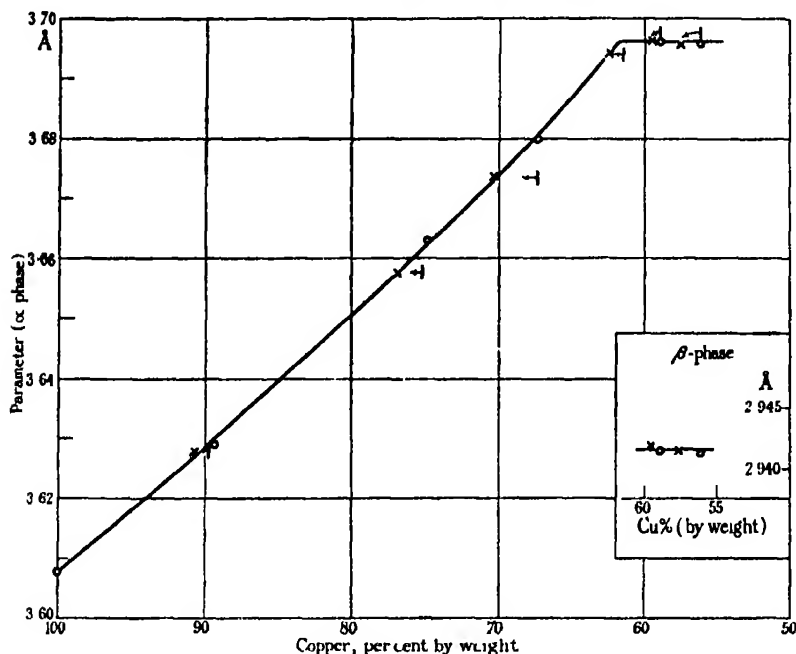

FIG 2.—Cu-Zn Alloys. All samples annealed at 500° C.

O " As cast."   × " Lump annealed."   ×←| Denotes change in composition due to lump annealing of as cast ingot.

appears to prevent zinc from volatilising from the saturated α phase in the (α + β) region so easily as it does from the α phase when it exists alone. This effect is supported by indirect evidence from other sources. For instance Dunn* noticed in the course of an investigation of the diffusion of zinc out of α brass, that the rate of diffusion for an alloy in the (α + β) region was different from that in the case of an alloy in the pure α region. The work of Nadejdin† also shows the same effect.

Having now shown that the " as cast " and the lump annealed samples gave the same results when the actual composition is taken into account and the surface layers of the ingot are discarded, it still remained to find if the full effect of lump annealing had taken place in the one heat treatment. With this aim in view further samples were subjected to lump annealing and their para-

* ' J. Chem. Soc.,' p. 2973 (1926).

† Nadejdin, " Metallung " (1928) ; ' J. Inst. Met. Abs.,' vol. 42, p. 450 (1929).

meters determined after different times of annealing. For this purpose alloys in the (β + γ) region, down to about 48 per cent. copper, were added to those already investigated. Table III contains the results obtained; lump annealing was carried out at 800° to 850° C. for the times stated in the table, filings from each sample being annealed at 500° C. for 4 hours before photographing.

Table III.

Alloy marked.	Parameter (Å).			
	As cast.	After 9 hours annealing.	After 18 hours annealing.	After 36 hours annealing.
ɪ-phase				
897 Z	3 629$_1$	3 627$_7$	3 628$_2$	3 628$_5$
752 Z	3 662$_8$	3 657$_6$	3 659$_3$	3 659$_9$
673 Z	3 679$_7$	3 673$_2$	3 676$_8$	
			3 676$_0$	} 3 674$_9$
614 Z	3 691$_3$	3 693$_9$	3 693$_4$	3·691$_5$
589 Z	3 696$_6$	3 696$_3$	3 695$_4$	3 695$_8$
561 Z	3 695$_7$	3 695$_5$	3 696$_1$	3 692$_8$
523 Z	} No α-phase lines present			
482 Z				
β-phase				
614 Z	No β-phase lines present			
589 Z	2 943$_0$	2 944$_1$	2 942$_0$	2 942$_7$
561 Z	2 942$_8$	2 942$_8$	2 942$_3$	2 942$_4$
523 Z	2 945$_8$	2 945$_9$	2·945$_1$	
482 Z	2 949$_6$	2 948$_7$	2 949$_1$	–

No marked change is shown in the β phase; this is to be expected since it exists within very narrow limits, namely, 2·943 A. to 2·950 A. Slight changes are to be observed in the values of the α phase parameters, but after 18 hours little change takes place; even after 9 hours, the effect is small. The experimental error in determining these parameters was taken to be 1 in 4000 since the reflection lines were far out on the photographic film. The variations observed in the parameters for annealing times greater than 18 hours are therefore mainly due to experimental error. The alloys marked 589 Z and 561 Z are in the (α + β) region, and show that 9 hours annealing is sufficient to produce a constant parameter. This comparatively short time of annealing is attributed as previously stated to the presence of the β phase.

II.—*Determination of Phase Boundaries.*

When the solution of one metal takes place in another, the solute atoms, in most of the cases that have been investigated, replace some of those in the solvent lattice. At the present time, it is not known if this replacement

takes place orderly or at random. There is, however, a change in the lattice dimensions. This may be an increase as when zinc dissolves in copper, fig. 3, Plate 19, or a decrease as when zinc dissolves in silver; the change depends upon the relative " size " of the two kinds of atoms. A saturation point is reached when no more solute atoms can enter the lattice, and at this stage the dimensions or parameters become constant. As in all solution phenomena, this saturation limit will depend upon the temperature.

In the case of alloys when the solute atoms are still further increased beyond the saturation limit, a new constituent or phase is produced. In no case does this second phase consist solely of the solute atoms. This second phase usually has a different lattice form and parameter from those of the first phase, and these exist together with the first phase in mixed regions over a range of composition. To accommodate the change in composition across a region of a pure phase, the lattice parameter must change, if, as is usually the case, the sizes of the two kinds of atoms are different. In the regions consisting of two phases, the mixed regions, it has been found that the parameters of both phases remain constant This indicates that both the lattices are saturated and therefore of fixed compositions, so that to accommodate the change in composition of the alloys across the mixed region, the relative amounts of the two phases must vary. In regard to the two mixed regions on either side of a pure phase, the saturation parameter of this phase depends upon the other phase present. For example, the β phase parameter in the $(\alpha + \beta)$ region in the Cu Zn series is less than that in the $(\beta + \gamma)$ region. The γ and ϵ phases show similar changes in their saturation parameters in the adjacent mixed regions.

The above phenomena relating to the parameters of the phases in pure and mixed regions form the bases of the X-ray method of determining the boundaries of the thermal diagram. The method depends upon the following conclusions, which have been established by experiment when the annealing temperature is constant : (1) When the parameter of a phase, or more strictly the mean atomic volume, changes with composition, a pure phase region is indicated. (2) When the parameter of a phase remains constant with changing composition, this indicates a mixed region ; this is confirmed by the presence in this region of a second phase of constant parameter. (3) In the case of closepacked hexagonal phases the behaviour of the mean atomic volume is taken as the criterion though both the base side (a) and the axial ratio (c) in the Cu-Zn alloys appear to follow independently the behaviour of the parameter as mentioned above.

Hence the boundary of a phase is given by the composition at which the constant parameter in the mixed region meets the curve representing the change in its parameter with composition in the pure region, and the accuracy with which the boundary can be fixed, depends upon the accuracy with which the lattice parameters can be determined.

Having found that the " as cast " alloys gave the same parameters as the " lump annealed " specimens when the composition was taken into account and when the filings were annealed at 500° C., the next step was to investigate what values were obtained with filings annealed at various temperatures. For this purpose a number of alloys in the " as cast " condition was made up to represent the α and the (α + β) regions. Filings from the alloys were annealed *in vacuo* as previously, at 400° C., 500° C., and 800° C. The samples were cooled in air from 400° C. and 500° C., and quenched in iced water after annealing at 800° C. After photographing in the precision camera, the filings were taken off the aluminium foils on which they were mounted and their copper content determined by chemical analysis. Table IV gives the results obtained for parameter and composition at the different temperatures chosen.

Table IV

Alloy marked.	Per cent copper in filings	α-phase parameter ($\mathring{A}$)	Annealing temperature of filings
897 Z	88·7	3·628$_2$	
752 Z	75·2	3·661$_7$	
614 Z	61·5	3·693$_7$	400° C. air cooled.
589 Z	58·9	3·693$_8$	
523 Z	52·3	3·694$_0$	
897 Z	89·3	3·629$_1$	
752 Z	76·4	3·657$_6$	
673 Z	70·3	3·673$_2$	
631 Z	62·8	3·692$_9$	
614 Z	61·7	3·693$_9$	500° C. air cooled.
589 Z	59·9	3·695$_3$	
561 Z	58·1	3·695$_2$	
561 Z	57·6	3·695$_5$	
897 Z	89·8	3·629$_4$	
752 Z	75·3	3·662$_3$	
673 Z	68·0	3·679$_1$	800° C. water quenched.
631 Z	62·8	3·686$_5$	
614 Z	62·9	3·686$_3$	

The figures in Table IV are plotted in the graph shown in fig. 4, in which it is observed that there is no change with temperature of annealing in the value of the α-phase parameter in the pure region, when the composition remains

constant. The annealing treatment given to the filings is therefore sufficient to produce the true equilibrium condition without a prolonged "lump annealing" operation. The saturation parameters for 400° C., 500° C. and 800° C., are slightly different, showing that more zinc can go into solution at 500° C. than at 400° C. and 800° C.

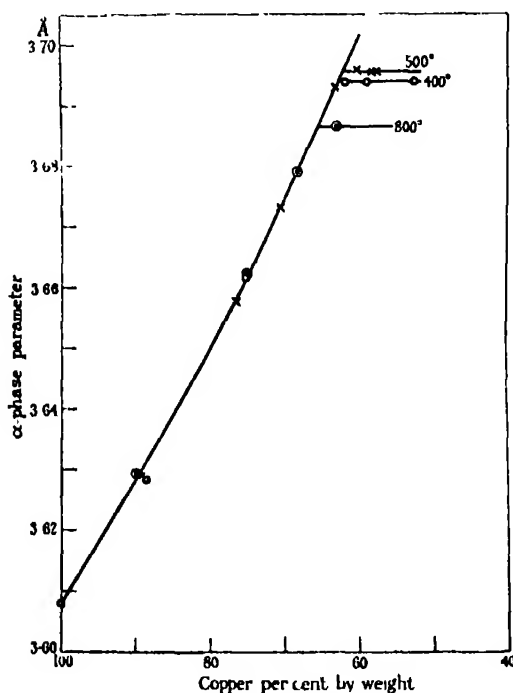In order to determine the saturation parameter at 800° C. attempts were made to obtain a range of composition in the (α + β) region at this temperature,

FIG. 4.—Cu-Zn as cast.

○ Annealed at 400° C.   × Annealed at 500° C.   ⊙ Annealed at 800° C.

but owing to the small range available, and also to the fact that the composition could not be accurately controlled when annealing was carried out at this high temperature, only two photographs were obtained ; these gave the same parameter and the same composition (see Table IV). Since the initial ingot compositions of these two specimens were 63·1 per cent. and 61·4 per cent. copper approximately, but after annealing both became nearly the same, 62·8 per cent. and 62·9 per cent. Cu respectively with parameter values of 3·686₅ and 3·686₃ Å., the saturation parameter at 800° C. may, therefore, be considered to have the value 3·686₄ Å.

The (α) — (α + β) *Boundary.*—To determine the (α) — (α + β) boundary, it was necessary to work with alloys, the compositions of which were in the (α + β) region over the whole range of temperature. In the Cu-Zn system a single alloy with ingot composition of 58·9 per cent. copper by weight sufficed, since with this composition it remained in the mixed region over the whole temperature range. To ensure a true equilibrium state, this alloy was lump annealed at 500° C. for 3 weeks. This prolonged lump annealing was not essential in view of the foregoing results, but it was carried out as an added precaution to ensure homogeneity. Filings were then taken and annealed at various temperatures from 350° C. to 800° C. The samples in thin evacuated silica tubes were water quenched from temperatures of 600° C and above. Rapid air cooling was efficient enough to maintain the state at the lower temperatures.

Chemical analyses were carried out on all the filings to ensure that their composition had not varied unduly from the initial composition of the alloy in the (α + β) range owing to the second annealing process. Data given in Table V were obtained with this alloy (marked 589 Z)

Table V.

Temperature	Parameter	Per cent copper (by weight)	(a) — (a + β) boundary	
			X-ray method.	I.C.T. diagram.
° C.	Å.		Per cent Cu	Per cent. Cu
800	3 686₄	62 9	65 4	65 7
700	3 690₁	60 0	63 9	63 6
650	3 691₈	59 9	63 5	63·4
600	3 694₃	59 2	62 5	62 4
550	3 694₇	59 5	62 3	62 3
500	3 696₀	59 5	61 8	61 7
450	3 696₈	59 2	61·7	61·7
400	3 695₇	59 4	61 9	61·6
350	3 694₂	59 8	62 5	—

The last column shows the reading of the boundary as taken from the Cu-Zn diagram of the International Critical Tables. The agreement over the whole temperature range is very close, the maximum difference being 0·3 per cent. Table VI gives the boundaries at certain temperatures obtained by Gayler and by Genders and Bailey* together with those obtained above.

One advantage, which has already been mentioned, of the X-ray method over the "quenching-microscopical" method adopted by metallurgists is

* 'J. Inst Met.,' vol. 33, p. 222 (1925).

Table VI.

Temperature.	Boundary compositions (per cent Cu by weight)		
	X-ray.	Gayler	Genders and Bailey.
° C.			
600	62 5	62 9	62 5
500	61 8	61 8	61 3
470	—	61·4	61 1
450	61·7	61 1	61 0
400	61·9	61 1	61 0

well illustrated by the above experimental results, namely, that only one alloy is required to determine the boundary over the whole temperature range by this method, while at least two, and not necessarily the same two, are required for each temperature by the metallurgical method. For this latter method the two alloys must be such that one shows a pure region only and the other shows traces of the second phase in addition. If the boundary investigated varies greatly with temperature, a number of alloys of slightly different compositions may be required before two suitable ones are found. The exact composition is then estimated as that at which the second phase first begins to form.

The (α + β) — (β) *and the* (β) — (β + γ) *Boundaries* —To investigate these two boundaries the following five alloys were examined : alloys 589 Z and 561 Z in the (α + β) region, alloy 523 Z in the pure β region, and alloys 453 Z and 432 Z in the (β + γ) region. After lump annealing, filings from these alloys were annealed at different temperatures and the β-phase parameter determined with the precision camera. In most cases the analysis was done on the sample after the annealing operation on the filings, these are indicated on the graph, fig. 5. Other samples were taken to have the ingot composition. Table VII contains the experimental results obtained.

The graph shows that for each temperature, the parameter remains constant over a range of composition, then rises and again becomes constant. The first constant parameter is that of the β-phase in the (α + β) region and the second that of the β-phase in the (β+γ) region, fig. 6, Plate 19. For all temperatures in the pure β region the relation of parameter to composition is the same. From this graph the intersections of the constant parameter lines for each temperature and the sloping line of the pure region give the required boundaries. In Table VIII are tabulated the figures giving the boundaries, and, for comparison, in brackets, those read off the I.C.T. diagram.
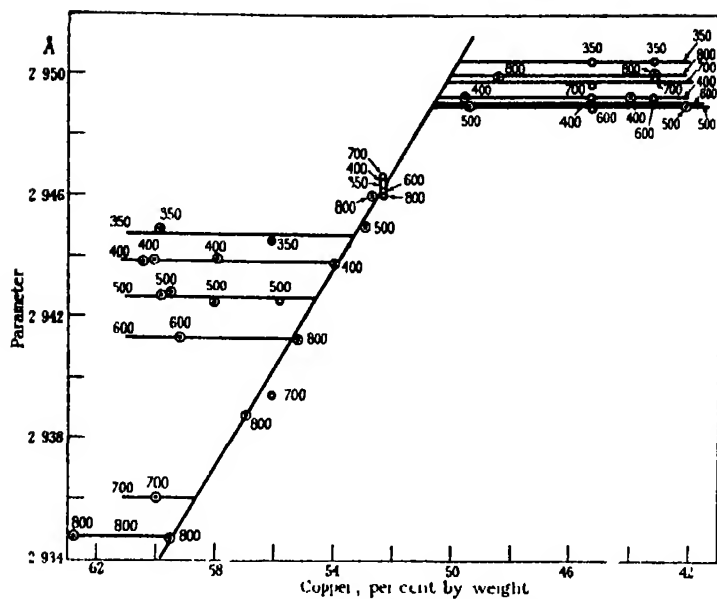
FIG 5.—Cu-Zn. β-phase parameter at different temperatures and compositions. Figures denote annealing temperatures ⊙ Actual filings analysed after annealing. ◯ Ingot analysis before annealing.

Table VII

Temperature of annealing.	Parameter	Composition (per cent Cu by weight)
°C.	Å.	
800	2 934₈	62 7
	2 934₇	59 5
	2 938₈	56 9
	2 941₃	55 2
	2 946₁	52·7
	2 946₁	52 3
	2 049₈	48·4
	2 950₁	43·2
700	2 936₁	60 0
	2 939₄	56·1
	2 946₇	52 3
	2 949₇	45 3
	2 949₉	43 2
600	2 941₃	59 2
	2 946₂	52 3
	2 948₉	45 3
	2 949₃	43 2
500	2 942₇	59 8
	2 942₈	59·5
	2 942₄	58 1
	2·942₀	56·1
	2 945₁	52 9
	2 949₁	49 4
	2·949₁	42·3

Table VII.—(continued).

Temperature of annealing	Parameter	Composition (per cent Cu by weight)
°C.	Å	
400	2·943$_9$	60·4
	2 943$_7$	60·1
	2 943$_9$	57 9
	2 943$_8$	53 9
	2 946$_6$	52 3
	2 949$_2$	49·6
	2 949$_3$	45·3
	2 949$_3$	44·1
350	2 944$_0$	59·8
	2 944$_6$	56·1
	2 946$_4$	52 3
	2 950$_5$	45·3
	2 950$_6$	43·2

Table VIII.

Temperature	Boundary compositions (per cent Cu by weight)	
	$(a + \beta) - (\beta)$.	$(\beta) - (\beta + \gamma)$.
°C		
800	59 4 (61 2)	50·1 (48 3)
700	58 7 (58 7)	50·2 (48 9)
600	55 4 (55 6)	50 6 (50 0)
500	54 6 (54·4)	50·7 (50 6)
400	53·8 (54 4)	50·5 (50 7)
350	53 3 (—)	49 75 (—)

The agreement with the exception of the 800° C. boundaries is quite satisfactory.

The $(\beta + \gamma) - (\gamma)$ *and the* $(\gamma) - (\gamma + \varepsilon)$ *Boundaries.*—Seven alloys were used to derive these boundaries : alloys 453 Z, 432 Z and 414 Z in the $(\beta + \gamma)$ region, alloys 387 Z and 353 Z in the pure γ region, and alloys 304 Z and 245 Z in the $(\gamma + \varepsilon)$ region.

The annealing operations and general procedure were similar to those already employed for the other boundaries. The γ phase parameters were determined from precision photographs and are tabulated for the various temperatures in Table IX.

Table IX.

Temperature.	Parameter	Composition (per cent. Cu by weight)
° C.	Å.	
800	8 830$_7$	43 2
	8·830$_9$	41 4
	8·838$_6$	39·6
700	8 824$_3$	45 3
	8·824$_9$	43 2
	8 831$_1$	41·4
	8 841$_6$	38 7
	8 858$_7$	35 3
600	8 820$_8$	45 3
	8 819$_8$	43 2
	8 831$_0$	41·4
	8 839$_9$	38 7
	8 856$_1$	35 3
500	8 819$_9$	42 2
	8 819$_5$	43 2
	8 829$_4$	41 2
	8 838$_2$	39 6
	8 855$_2$	35 5
450	8 820$_6$	45 3
	8·819$_5$	43 2
	8 829$_5$	41·4
	8 840$_6$	38 7
	8 856$_1$	35 3
400	8 823$_9$	45 3
	8 823$_4$	43 2
	8 829$_7$	41 4
	8 840$_2$	38 7
	8 856$_7$	35 3
500	8 873$_9$	30 4
380	8 874$_6$	30 4
380	8 873$_6$	34 5

The graph of these figures, fig. 7, shows that the relation between the parameter of the γ phase and the composition is somewhat different from those for the α and β phases—it departs to a marked degree from a linear relation in the pure region between 42 and 39 per cent. copper. It is at once seen from the graph that the $(\beta + \gamma) - (\gamma)$ boundary is not parallel to the temperature axis as shown in the I.C.T. diagram, since the parameter of the γ phase in the $(\beta + \gamma)$ region is not constant at all temperatures, fig. 8, Plate 20.

The experimental data on the $(\gamma) - (\gamma + \varepsilon)$ boundary are too few to determine this boundary satisfactorily, but since the parameter at 500° C. and 380° C. for the alloys containing 30·4 per cent. and 24·5 per cent. copper are nearly

identical, this boundary is probably parallel to the temperature axis as given in the I.C.T. diagram at a composition of about 31 per cent. copper.
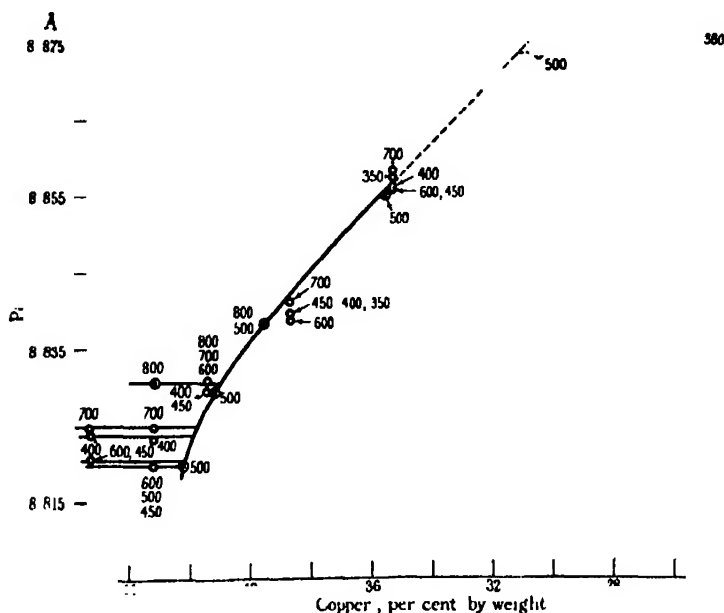
FIG. 7.—Cu-Zn. γ-phase parameter at different temperatures and compositions. Figures denote annealing temperatures. ⊙ Actual filings analysed after annealing. ○ Ingot analysis before annealing.

In Table X are given the boundaries derived from the graph, and in brackets the I.C.T. boundaries.

Table X.

| Temperature | Boundary compositions (per cent. Cu by weight). | |
	$(\beta + \gamma) - (\gamma)$	$(\gamma) - (\gamma - \epsilon)$.
° C.		
800	41 0 (40)	—
700	41 7 (40)	—
600	42 2 (40)	—
500	42 25 (40)	about 31 (31)
450	42 2 (40)	—
400	41·9 (40)	—
380	—	about 31 (31)

The $(\beta + \gamma) - (\gamma)$ boundary, as now determined, shows a slightly higher copper content at all temperatures ; it shows further a small variation from temperature to temperature, as compared to a constant composition over the

whole temperature range as given in the I.C.T. diagram. The accuracy attainable with the precision camera, together with the checking of parameters of different alloys in the ($\beta + \gamma$) region, appears to establish beyond doubt that this boundary is not at a constant composition over the whole range of temperature. With a boundary of this nature, the existence of a true compound of fixed composition (*e.g.*, Cu_5Zn_8) is untenable.

Conclusions.

The experimental results indicate that the method of determining phase boundaries in alloy systems, which is based on parameter measurements by precision X-ray analysis, can be used to establish these boundaries accurately. Apart from the fact that this method is much more expeditious, the accuracy attainable is claimed to be at least equal to that of the metallurgical method of quenching samples followed by microscopical examination, or to that of other methods which make use of data from measurements of certain physical properties, such as thermal expansion, electric resistance, etc , The very close agreement of the X-ray method with other methods for the determination of the (α) — ($\alpha + \beta$) boundary of the thermal diagram, clearly demonstrates that the X-ray method gives true and accurate results since this boundary has been more accurately established by various methods and workers than any other in the system. It is probable therefore that the other boundaries determined here by the X-ray method, are very near to the true values

The phase boundaries of the Cu-Zn alloys are shown in fig. 9, the dotted lines being reproduced from the I.C T. diagram, and the full lines those determined as explained above. The graph displays the following features : (1) The (α) — ($\alpha + \beta$) boundaries are coincident within experimental error and the error of reading the I.C.T. diagram down to 450° C. The X-ray method indicates a slight modification below 400° C. (2) The ($\alpha + \beta$) — (β) boundaries show distinct differences at 800° C. and 400° C. (3) The (β) — ($\beta + \gamma$) boundaries show a decreasing variation from 800° C. down to 500° C. (4) The ($\beta + \gamma$) — (γ) boundary found by X-ray methods is not at a fixed composition over the whole temperature range. It shows a maximum at about 520° C. of 42·25 per cent. Cu ; at 800° C. and 400° C. it corresponds to 41 per cent. and 42 per cent. Cu respectively ; the I C T. tables show a constant composition of 40 per cent. Cu for the boundary The X-ray data therefore indicate that no compound of fixed proportions exists at this composition. (5) The (γ) — ($\gamma + \epsilon$) boundary is most probably vertical between 500° C. and 380° C. as given in the I.C.T. diagram.
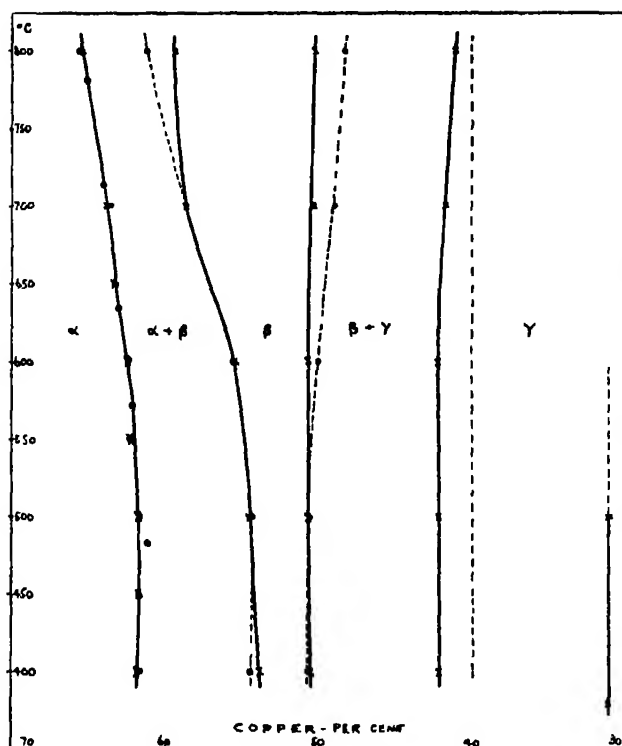
FIG. 9.—Phase boundaries of Cu-Zn alloys.   × By X-ray method.   ⊙ International Critical Tables.   ● Genders and Bailey   —— By X-ray.   . . . I C T.

Summary.

An X-ray precision camera has been employed to determine parameter values of the lattices of the different phases in the Cu-Zn alloy system.   The accuracy attained is at least 1 in 4000.   Small ingots of the alloys were made and all samples before photographing were annealed to eliminate lattice distortion and to produce the equilibrium condition.   The annealing took two forms : the annealing of small lumps (about 1 c.c.) and the annealing of filings. It was found that, provided surface metal was discarded and the actual composition of each reflecting sample was determined by chemical analysis, the annealing of filings from the "as cast" ingot was sufficient to produce the desired condition.

From the composition-parameter relation of each phase, a method of determining the phase boundary compositions has been developed.   This is based on the experimental data obtained with the alloys under investigation, which showed (1) the increase in parameter with composition in a pure phase

region to be independent of temperature, and (2) the parameter values of both phase lattices in a mixed region to be constant with change of composition within the region, but to change with temperature. At a fixed temperature, the constant parameters of a phase in its two mixed regions are different

Alloys down to about 30 per cent. copper were made and annealing treatments over the range 800° C. to 350° C. were carried out.

The copper parameter was found to increase in the pure α-region from $3 \cdot 607_9$ Å. for pure copper to the saturated values $3 \cdot 694_0$ at 400° C., $3 \cdot 695_5$ at 500° C., $3 \cdot 686_4$ at 800° C. The $(\alpha) - (\alpha + \beta)$ boundary was found to be at $65 \cdot 4$ per cent. Cu (800° C.), $63 \cdot 9$ (700° C), $63 \cdot 5$ (650°), $62 \cdot 5$ (600°), $62 \cdot 3$ (550°), $61 \cdot 8$ (500°), $61 \cdot 7$ (450°), $61 \cdot 9$ (400°), $62 \cdot 5$ (350°). The β-phase parameter was found to vary between $2 \cdot 934_8$ Å. at 800° C (62·7 per cent. Cu) and $2 \cdot 950_5$ at 350° C. (43·2 per cent Cu). The $(\alpha + \beta) - (\beta)$ and $(\beta) - (\beta + \gamma)$ boundaries were respectively $59 \cdot 4$ and $50 \cdot 1$ per cent. Cu at 800° C , $58 \cdot 7$ and $50 \cdot 2$ at 700°, $55 \cdot 4$ and 50 6 at 600°, $54 \cdot 6$ and $50 \cdot 7$ at 500°, $53 \cdot 8$ and $50 \cdot 5$ at 400°, $53 \cdot 3$ and $49 \cdot 75$ at 350° The range of the γ-phase parameter was from $8 \cdot 830_7$ Å. at 800° C. (43·2 per cent. Cu) to $8 \cdot 874_6$ at 380° (30·4 per cent. Cu). The $(\beta + \gamma) - (\gamma)$ boundary was found to vary from $41 \cdot 0$ per cent. at 800° C. to $41 \cdot 9$ per cent. at 380° C., with a maximum copper content of $42 \cdot 25$ at about 500°–600° C. With a boundary of this nature, the existence of a true compound of fixed composition ($Cu_5 Zn_8$) is considered untenable Where possible, the boundary compositions found by the X-ray method were compared with those determined by other workers using different methods. The agreement is good and it is concluded that the X-ray method of boundary determination, in addition to being more expeditious, gives data at least as accurate and reliable as those derived from other methods hitherto employed.

A Study of the System Water-Phenol.   Part I.—Densities.

By Owen Rhys Howell, The College of Technology, Manchester.

Introduction.

In order to throw further light on the conditions existing in a system of two partially miscible liquids, it was deemed of interest to measure some physical property of the solutions on both sides of the solubility curve, over the whole range of concentration, at a series of temperatures up to and above the critical solution temperature.

The classical example water-phenol was chosen for study, and the densities of solutions of " phenol in water " and of " water in phenol " have been determined every 10° from 20° to 70°. The densities of the conjugate solutions have also been measured at more frequent intervals near the critical solution temperature.

The viscosities and electrical conductivities have been determined over the same range and the freezing-points have also been examined   These will be the subject of further communications.

Experimental.

Materials.—The phenol was prepared from the purest detached crystals of Messrs. Graesser Monsanto, which contain only very minute traces of cresols. This material was re-distilled in a glass apparatus which had been steeped for a long time in chromic-sulphuric acid mixture before being thoroughly cleaned The whole apparatus was sealed, being open to the atmosphere only through calcium chloride tubes to avoid contamination of the distilled phenol by atmospheric moisture.   The first and last 20 per cent. was neglected, and the middle portion, which distilled at constant temperature, was collected in a series of tubes which were stoppered with corks covered with tin-foil and stored in a desiccator over phosphorus pentoxide.

The setting-point of the distilled phenol, determined from the rate of cooling when bubbling a stream of pure dry nitrogen through the molten material, was $40 \cdot 85° \pm 0 \cdot 50°$.   The purity of the product is proved by the fact that the setting-point remained unaltered after fractional crystallisation from the melt, further distillation and contact with anhydrous sodium sulphate.   It is interesting to note that this phenol, although kept in colourless tubes, remains

absolutely " white," no trace of any pink colour being developed even after more than 3 years.

The values of the melting-point of phenol recorded in the literature cover a very wide range, but the majority lie between 40·5° and 40·8°. These values are slightly low, probably owing chiefly to the presence of traces of water, since phenol is markedly hygroscopic and water has a great lowering effect on the melting-point.

It is remarkable that most text-books on organic chemistry still accept 42° as the melting-point of phenol in spite of the fact that the more reliable measurements are far below this figure, and that Eger* pointed out so long ago that the melting-point of pure phenol is not above 40·9°.

The value now given is almost identical with that of Rhodes and Markley† and very close to that of Hill and Malisoff‡ for their highly purified products, viz., 40·8° and 40·92°, respectively.

The water used was twice distilled in an apparatus of seasoned glass, with precautions to avoid contamination by grease and dust.

Solutions.—All the solutions were made up in flasks of seasoned glass provided with ground stoppers. The requisite number of tubes containing the distilled phenol were carefully warmed to melt the phenol, which was then transferred as quickly as possible to the flask which had previously been counterpoised against another flask of approximately the same size and weight. After having cooled to atmospheric temperature, the phenol was weighed. The weight was corrected to *vacuo*, and the weight of water necessary to obtain the required solution was calculated and corrected to air. Approximately the requisite amount was added, the phenol dissolved by warming slightly and the whole allowed to cool to room temperature again, when the final few drops of water were added to make the correct weight. All concentrations are expressed as percentages by weight of phenol, *i.e.*, grams of phenol per 100 grams of solution.

The conjugate solutions at each temperature were obtained by warming phenol and water to above the critical solution temperature and allowing the mixture to cool with constant shaking to the desired temperature. It was found that separation into two layers was extremely slow, especially at the lower temperatures, the milky liquid showing no sign of separation even after several days. It was, therefore, necessary to add a trace of electrolyte to

---

* ' Pharm. Z.,' vol. 48, p 210 (1903); ' Chem. Z. Rep.,' vol. 27, p. 86 (1903).

† ' J. Phys. Chem.,' vol. 25, p. 527 (1921).

‡ ' J. Amer. Chem. Soc.,' vol. 48, p. 918 (1926).

hasten separation, and in all the experiments three drops of a 1 per cent. solution of pure sodium chloride were added to about 250 c.c. of the milky liquid. This caused complete separation into two perfectly clear layers in a few minutes. The layers were carefully removed by means of a warmed pipette.

Determination of Density.—All measurements were made in a thermostat with a glass back and front, provided with a sensitive toluene regulator and heated by gas from a governed supply. The water in the thermostat was covered with a layer of high-boiling paraffin, which not only prevents evaporation but also helps to maintain a steady temperature. Two standard thermometers recently calibrated at the National Physical Laboratory to the nearest 0·05° were used, and the working temperature was in every case steady to within $\pm 0·01°$.

The densities were determined in the manner already described* and are correct to the nearest figure in the fourth place of decimals. In determining the densities of the conjugate solutions, it was impossible to avoid some separation where the apparatus projected out of the thermostat liquid, but this was kept as small as possible, and the error is not large.

The values adopted for the density of water are those of Thiesen †

Density-Concentration Relation

The densities observed at all concentrations at each temperature are collected in Table I, and the density-concentration curves are plotted in fig. 1. The values for the conjugate solutions are also included in the figure and the boundary curve drawn through them.

The figure bears a striking resemblance to that of the isothermals of a gas near its critical temperature. The curve for 70° is just above the critical solution temperature, and shows the slight inflexion characteristic of the critical isothermal for a gas. Just as there is apparent discontinuity in the gas isothermals in passing from the gaseous to the liquid region, so also there is no obvious continuity between the curves for the water-rich and phenol-rich solutions below the critical solution temperature. Some discontinuity may perhaps be expected if, as is generally supposed, the solutions on one side of the boundary are of phenol in water and those on the other of water in phenol. It will be shown later that the conditions existing in solution are not as simple

---

* Howell, ' J. Chem. Soc.,' p. 158 (1927) ; p. 162 (1929).

† Landolt and Börnstein's " Tables," p. 73 (1923).

Table I.

Density d_4^t.

Conc. phenol per cent.	20° Obs	20° Calc	30° Obs	30° Calc	40° Obs	40° Calc	50° Obs	50° Calc	60° Obs	60° Calc	70° Obs	70° Calc
0	0·9982	0·9982	0·9957	0·9956	0·9922	0·9922	0·9881	0·9881	0·9832	0·9833	0·9778	0·9777
2	1·0001	1·0001	0·9974	0·9973	0·9938	0·9938	0·9894	0·9895	0·9845	0·9845	0·9788	0·9788
4	1·0020	1·0020	0·9990	0·9990	0·9953	0·9953	0·9908	0·9909	0·9857	0·9857	0·9799	0·9799
6	1·0038	1·0038	1·0006	1·0006	0·9967	0·9967	0·9921	0·9921	0·9868	0·9868	0·9808	0·9808
8	1·0055	1·0055	1·0022	1·0021	0·9981	0·9981	0·9934	0·9934	0·9879	0·9880	0·9819	0·9819
10	—	—	—	—	—	—	0·9944	—	0·9889	—	0·9829	—
15	—	—	—	—	—	—	—	—	0·9913	—	—	—
20	—	—	—	—	—	—	—	—	—	—	0·9872	—
30	—	—	—	—	—	—	—	—	—	—	0·9917	—
40	—	—	—	—	—	—	—	—	—	—	0·9962	—
50	—	—	—	—	—	—	—	—	—	—	1·0009	—
60	—	—	—	—	—	—	—	—	1·0138	—	1·0054	—
70	1·0539	(1·0542)	1·0428	1·0428	1·0352	1·0352	1·0273	1·0273	1·0191	1·0191	1·0105	1·0106
75	1·0576	1·0539	1·0462	1·0462	1·0382	1·0382	1·0301	1·0301	1·0218	1·0217	1·0132	1·0132
80	1·0615	1·0576	1·0496	1·0496	1·0413	1·0414	1·0331	1·0331	1·0248	1·0247	1·0161	1·0161
85	1·0655	1·0615	1·0533	1·0533	1·0450	1·0450	1·0367	1·0366	1·0280	1·0280	1·0193	1·0193
90	—	1·0655	1·0572	1·0572	1·0488	1·0488	1·0405	1·0404	1·0319	1·0319	1·0232	1·0233
95	—	(1·0701)	1·0617	1·0617	1·0532	1·0532	1·0448	1·0447	1·0362	1·0362	1·0276	1·0276
100	—	—	—	—	—	—	1·0499	1·0499	1·0413	1·0412	1·0325	1·0325

as this, and it has not been possible to find a general equation to represent the density-concentration curves over their whole range.

One very striking feature of the curve for each temperature is that a portion of it (on the phenol-rich side) is a straight line which, on production, strikes the value for water at that temperature. Evidently, therefore, over this range
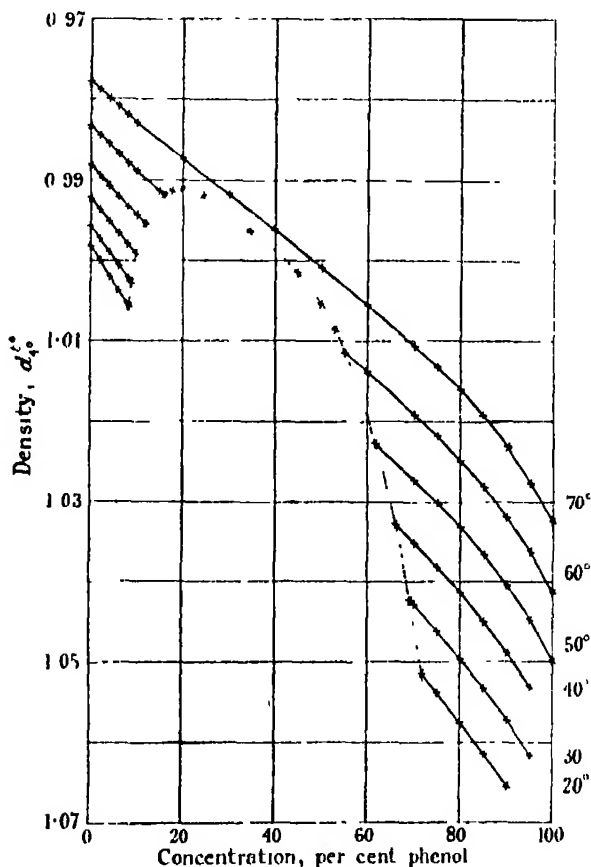
FIG. 1.

the change produced by addition of water to phenol in solution is different from that produced by addition of phenol to water initially. The significance of this will be discussed in a further communication. It may be noted here that this linear relation has been used to calculate the concentration of the phenol-rich conjugate solutions from their densities. The assumption that it holds up to this point is evidently justified from the general form of the curves, and especially that for 70°.

Density-Temperature Relation.

The densities are plotted against the temperature for each concentration in fig. 2. All the curves are perfectly smooth, and each is represented by au equation of the type

$$d_{t^\circ} = d_{20^\circ} - \alpha \, (t - 20) - \beta \, (t - 20)^2,$$
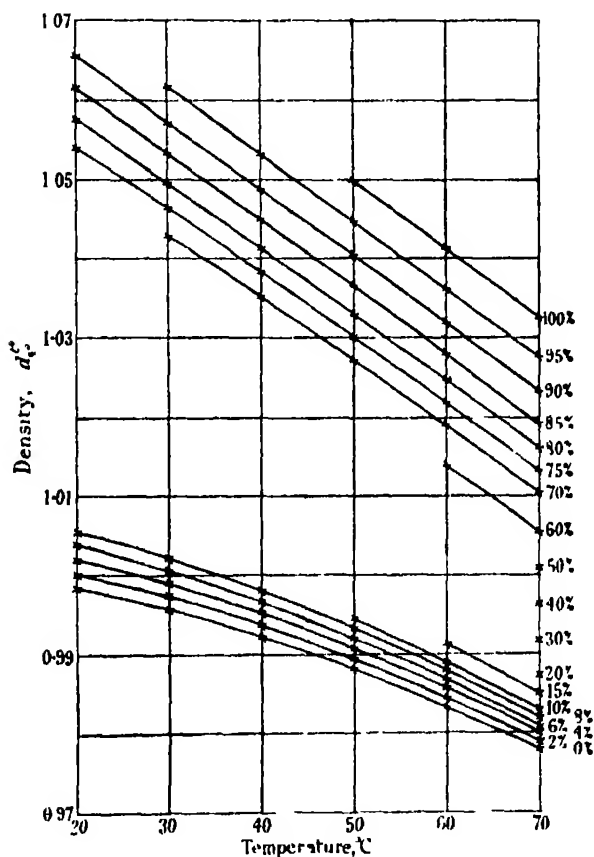
Fig 2.

where α and β are constants, the values for each concentration being given in Table II.

The densities calculated from this relation are given in Table I, and the agreement with the observed values is seen to be very good.

Although both the density-concentration curves and the density-temperature curves are smooth, a very interesting characteristic revealing the conditions existing in solution is brought to light when the values of α and β, the constants

in the density-temperature relation (Table II), are plotted against the concentration, fig. 3.

Table II.

Conc. per cent.	rich solutions		Phenol-rich solutions.		
	$\times 10^4$.	$\beta \times 10^5$.	Conc. per cent.	$\alpha \times 10^4$.	$\beta \times 10^6$.
	2 24	3 70	70	7·23	1 37
	2 44	3 64	75	7 64	1·00
	2 64	3 57	80	7·97	0·67
	2 85	3 50	85	8·12	0·63
	3 02	3 40	90	8 26	0·37
			95	8·42	0·16
			100	8·70	0
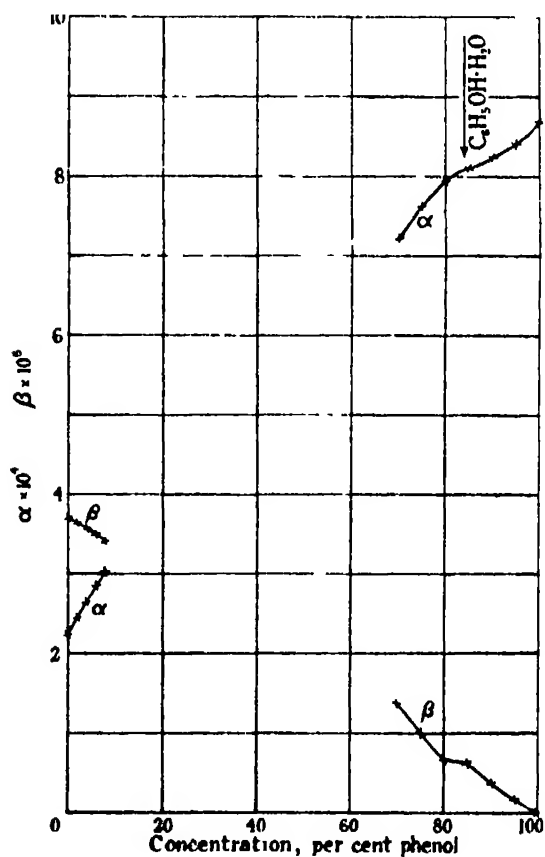
Fig. 3.

As might be expected from the considerations mentioned in discussing the density-concentration relation, the two portions of the α curve, corresponding to the water-rich and phenol-rich solutions, are not continuous, but, in addition, there is a strong inflexion in the later portion at approximately 84 per cent. phenol. Although the β curve is not of the same importance, since a small change in the chosen value of α makes a correspondingly large difference in the value of β, it should be noted that the two portions of the β curve similarly are not continuous and that the later portion exhibits inflexion at the same point as the α curve.

It may be mentioned here that the constants in the viscosity-temperature curves to be discussed in a further communication also show breaks even more marked than these, and at the same concentration. This concentration corresponds to equimolecular quantities of water and phenol, $C_6H_5OH . H_2O$, 83·93 per cent. phenol.

The only known hydrate of phenol is the hemi-hydrate,* $2C_6H_5OH . H_2O$, and this has been confirmed by a further investigation of the freezing-points of the system which will be discussed in a further communication. It is interesting to note that although the hemi-hydrate is a well-defined crystalline compound, none of the density relations (nor, as will be seen later, those of other physical properties) show any indication of its existence in solution. It would therefore seem to be extremely unlikely that the relationship, indicated by the present results, between equimolecular proportions of water and phenol is due to hydrate formation.

There is, however, the alternative possibility that, in highly concentrated solutions of phenol, ionisation occurs in accordance with the scheme :

$$C_6H_5OH + H_2O \rightleftharpoons C_6H_5OH_2{}^{\cdot} + OH'$$
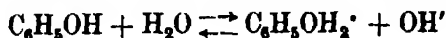
and the discontinuity in question could then arise from the formation of the compound $[C_6H_5OH_2{}^{\cdot}]$ $[OH']$. As the amount of water is increased, there is a transition to the well-known acidity of dilute solutions :

$$C_6H_5OH + H_2O \rightleftharpoons C_6H_5O' + OH_2{}^{\cdot}.$$
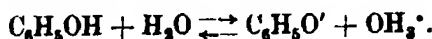
In subsequent papers describing the measurements, it is hoped to adduce direct evidence on this point, and, further, to examine the properties of substitution derivatives of phenol.

---

* Calvert, ' J. Chem. Soc.,' vol. 18, p. 66 (1865); Smits and Maarse, ' Verh. Kon. Akad. Wet. Amst.,' vol. 14, p. 192 (1911); Rhodes and Markley, ' J. Phys. Chem.,' vol. 25, p. 527 (1921).

Line of Mean Density.

The density of a liquid and of the saturated vapour in equilibrium with it, approach with increasing temperature and eventually coincide at the critical temperature.

The densities of the conjugate solutions of phenol in water and water in phenol are analogous. With increasing temperatures the solution of phenol in water becomes richer in phenol, and that of water in phenol becomes richer in water, so that the densities approach and eventually coincide at the critical solution temperature. The curve is shown in fig. 4.
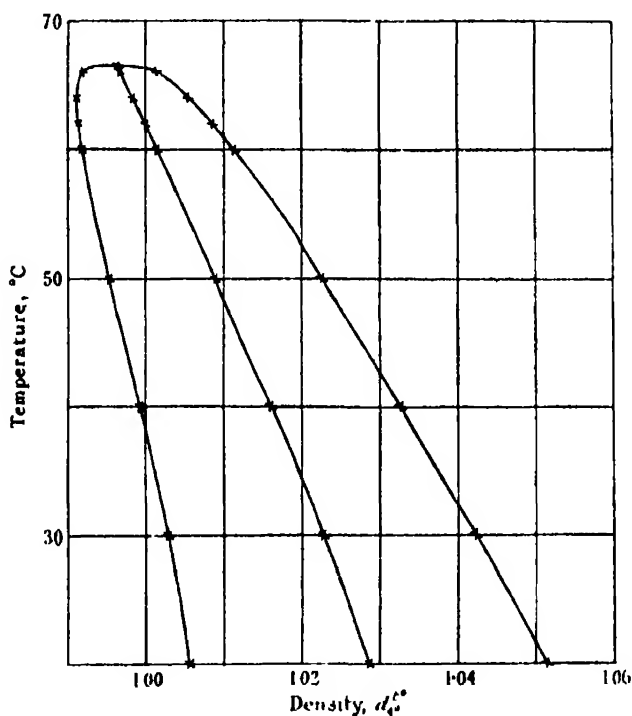
Fig. 4.

For a liquid and its saturated vapour, Cailletet and Mathias* showed that the mean density is a linear function of the temperature : Law of Rectilinear Diameter, but Young† showed that the mean density is more accurately a parabolic function of the temperature.

---

* ' C. R. Acad. Sci. Paris,' vol. 102, p. 1202 (1886) ; vol. 104, p. 1563 (1887)
† ' Phil. Mag.,' vol. 50, p. 291 (1900).

The same relationship has now been found to hold for the conjugate solutions in the phenol-water system. Table III gives the temperatures, the observed

Table III.

Temperature °C.	Density d_4^t.			
	Water layer	Phenol layer.	Mean observed.	Mean calculated.
20	1 0056	1 0515	1 0285$_5$	1 0285$_5$
30	1 0028	1 0423	1 0225$_5$	1 0225$_5$
40	0 9993	1 0328	1·0160$_5$	1·0160$_5$
50	0 9955	1 0226	1 0090$_5$	1 0090$_5$
60	0·9918	1 0114	1 0016$_0$	1 0015$_5$
62	0 9914	1 0087	1·0000$_5$	1 0000$_0$
64	0 9912	1 0056	0 9984$_0$	0 9984$_0$
66	0·9920	1 0015	0 9967$_5$	0 9967$_5$
66·4	—	—	—	0 9965$_0$

densities of the two solutions, the mean of these and also the mean density calculated from the relationship :

$$d_{t^\circ} = d_{20^\circ} - m\,(t - 20) - n\,(t - 20)^2$$

where d is the mean density

$$m = 5 \cdot 75 \times 10^{-4}$$

$$n = 2 \cdot 50 \times 10^{-6}.$$

The agreement is seen to be very good.

It would be of interest to find whether this relationship is true generally for systems of two partially miscible liquids.

The Solubility Curve

Determinations of the mutual solubility of water and phenol have been made by Alexejew,[*] Rothmund,[†] Friedländer,[‡] Scarpa,[§] Timmermans,[||] and Hill and Malisoff.[¶]

The most complete of the earlier investigations is that of Rothmund, whose results have been generally accepted, his curve having been widely reproduced

[*] ' Ann. Physik,' vol. 28, p. 305 (1886)

[†] ' Z. phys. Chem.,' vol. 26, p. 433 (1898)

[‡] ' Z phys. Chem.,' vol. 38, p. 385 (1901)

[§] ' J. Chim. phys.,' vol. 2, p. 447 (1904).

[||] ' Z. phys. Chem.,' vol. 58, p. 129 (1907)

[¶] ' J. Amer. Chem. Soc.,' vol. 48, p. 918 (1926).

in the text-books. The method of measurement was to cool solutions of known concentration until turbidity appeared and to warm again until it disappeared, the mean temperature being taken as that at which the solution is saturated.

The careful measurements of Hill and Malisoff were made with highly purified phenol. Those above 35° were made by the plethostatic method. but those below this temperature " by measuring the volumes of the two phases which result when the two components are put together in two different but known ratios by weight."

The series of density measurements given in the present paper afford a new method of determining the solubility curve. From the density-concentration relations, quadratic for the solutions of phenol in water and linear for those of water in phenol at each temperature, it is possible to calculate the concentration of the conjugate solutions since the densities of these have also been determined. The values are given in Table IV, where those of Rothmund and of Hill and Malisoff are given for comparison and the whole are plotted in fig 5.

<div align="center">Table IV.</div>

Tempera-ture ° C.	Concentration in water layer.			Concentration in phenol layer.		
	Calculated from densities.	Rothmund's values	Hill & Malisoff's values.	Calculated from densities.	Rothmund s values	Hill & Malisoff's values.
20	8 12	8·40	8·36	71·8	72·2	72 2
30	8·86	8 92	9·22	69·2	69·9	69·9
40	9·84	9·78	10·5	66·1	66 8	65·7
50	12·0	12·1	12 5	61·6	62·8	61·6
60	16·1	17·1	16·6	55·1	56 1	55 0
62	17 7	18·8	18·2	52 8	53 8	52·8
64	20·0	20·9	21 4	49·8	51·4	48 6
66	24·6	24·2	—	44·7	46·8	—

The results are in very good agreement with those of Rothmund for the water-rich solutions and with those of Hill and Malisoff for the phenol-rich solutions.

Rothmund's values give a comparatively symmetrical curve with the top smoothly rounded to the critical solution temperature. Hill and Malisoff's curve is much less symmetrical and the top is very flat. The values now found from the densities confirm this ; the curve is unsymmetrical and the top is quite flat over a very wide range of concentration, about 15 per cent.

Line of Mean Concentration.

The relation between the mean concentration of the two conjugate solutions and the temperature has been shown to be approximately linear for a large number of systems of two partially miscible liquids, and its resemblance to the law of Cailletet and Mathias has been discussed by Rothmund.
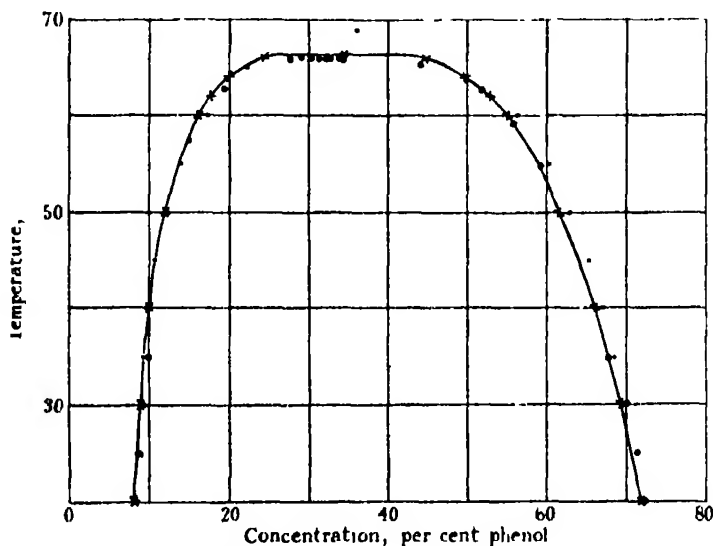

FIG. 5. × Density determinations. ● Rothmund. ⊙ Hill and Malisoff.

Table V.

Temperature °C.	Concentration by weight.				Concentration by volu			
	Water layer.	Phenol layer.	Mean obs.	Mean calc.	Water layer.	Phenol layer	Mean obs.	Mean calc.
20	8·12	71 8	40·0	40 0	8 17	75·5	41·8	41 8
30	8·86	69 2	39·0	39 0	8 88	72·1	40 5	40·5
40	9·84	66 1	38·0	38·0	9 83	68 3	39·1	39 1
50	12·0	61·6	36·8	36·8	12·0	63 0	37 5	37·5
60	16·1	55·1	35 6	35·5	16 0	55·7	35·9	35·8
62	17·7	52·8	35·3	35·3	17 5	53·3	35·4	35·4
64	20 0	49·8	34 9	35 0	19 8	50·1	35 0	35·0
66	24·6	44·7	34·7	34·7	24 4	44 8	34·6	34·6
66 4	—	—	—	34·6	—	—	—	34 5

The values of the concentrations now obtained for the water-phenol system are given in Table V. As with the mean density, the mean concentration is not a linear function of the temperature but is related by the equation :—

$$C_{t^\circ} = C_{20^\circ} - x(t-20) - y(t-20)^2,$$

where C is the mean concentration by weight

$$x = 9 \cdot 0 \times 10^{-2}$$
$$y = 5 \cdot 5 \times 10^{-4}.$$

The calculated values are given and seen to be in good agreement with the observed.

Since the densities of the conjugate solutions are known, the concentration by volume can also be found. The mean concentration by volume is also a parabolic function of the temperature which is given by the equation :

$$C_{t^\circ} = C_{20^\circ} - x' (t - 20) - y' (t - 20)^2,$$

where C is the mean concentration by volume

$$x' = 1 \cdot 21 \times 10^{-1}$$
$$y' = 7 \cdot 6 \times 10^{-4}.$$

The agreement between the calculated and observed values is again satisfactory.

The smoothness of the mean concentration curves is strong evidence of the purity of the materials, since Jones[*] has demonstrated (with the system acetic anhydride-petroleum) that very small amounts of impurity alter the shape of the solubility curve near the critical solution temperature, so that the line of mean concentration exhibits an abrupt bend in this neighbourhood. Hydrate formation[†] may have the same effect, but, as we have already mentioned, this does not obtain in the system water-phenol.

Critical Solution Temperature.

The critical solution temperature (consolute temperature) has been recorded by different observers at various temperatures from 65·3° to 70·7°.

There are at least three reasons for such a wide variation in the values found for this constant. Firstly, the critical solution temperature is profoundly affected by the presence of impurities, and many observers have not employed highly purified materials. Secondly, as Hill and Malisoff have shown, when sealed tubes are used for the determination, high values are obtained if no free space is left. They attribute this to the production of pressure, although the effect of pressure on the critical solution temperature is very small.[‡]

[*] ' J. Chem. Soc.,' p. 1177 (1928).

[†] Jones, ' J. Chem. Soc.,' p. 799 (1929).

[‡] Timmermans, ' J. Chim. phys.,' vol. 20, p. 491 (1923).

Thirdly, on cooling, solutions of water and phenol become opalescent before turbidity appears, and this is especially noticeable at and near the critical solution temperature. Most observers have remarked on this opalescence, which is very striking, and are agreed that it is probably due to the scattering of light owing to slight variations in density due to local inequalities in temperature.* Different observers, however, might not agree as to the exact temperature at which opalescence is replaced by turbidity due to the separation of the conjugate phases.

The value of the critical solution temperature almost universally accepted in the literature is that of Rothmund—viz., 68·4°—but, as Hill and Malisoff have pointed out, this is definitely too high by 2°.

Most observers find the critical solution temperature to be a little above 66°; thus Friedländer gives 66·06° and Timmermans 66·09°. Although Hill and Malisoff record one value above 66°, they accept for the critical solution temperature their mean of several readings, viz, 65·85 ± 0·15°, which is definitely somewhat low, since we have actually determined the densities of the two layers which separate at 66°.

We find the critical solution temperature to be 66·4°.

Critical Solution Concentration.

The critical solution concentration (consolute concentration) has been determined by many observers by producing the line of mean concentration to cut the solubility curve. Since the mean concentration is not a linear function of the temperature, these results must be somewhat in error, especially as the top of the solubility curve is so flat.

The relationship given above between the mean concentration, by weight, and the temperature, affords a method of calculating the critical solution concentration with greater accuracy, see Table V. The value thus found is 34·64 per cent.

An additional and interesting check is obtained from the line of mean density, which enables the density of the critical solution to be calculated, Table III. It has been shown that at each temperature the density-concentration relation for the phenol-rich solutions over a wide range is a straight line on which the value for water itself also lies. By plotting the slopes of these portions of the curves against the temperature, it is possible to find the

* Smoluchowski, ' Ann. Physik.,' vol. 25, p. 205 (1908).

slope at the critical solution temperature and thus calculate the critical solution concentration :—

Density at $66 \cdot 4°$ of the critical solution .... $0 \cdot 99650$

,,   ,,   water .... $0 \cdot 97985$

Difference .... $0 \cdot 01665$

Slope of the straight line at $66 \cdot 4° = 4 \cdot 81 \times 10^{-4}$ per 1 per cent., therefore

$$\text{Conc. of solution} = \frac{1 \cdot 665 \times 10^{-4}}{4 \cdot 81 \times 10^{-4}} \times 100 = 34 \cdot 61 \text{ per cent}$$

This is in excellent agreement with the value obtained from the line of mean concentration. We may, therefore, accept $34 \cdot 6$ per cent. as the critical solution concentration. Hill and Malisoff's value is 34 per cent. and Rothmund's figure, which has formerly been generally accepted, is 36 per cent

Summary.

(1) The densities of a series of solutions of water and phenol of different concentrations suitably spaced over the whole range of miscibility have been measured at $20°$, $30°$, $40°$, $50°$, $60°$ and $70°$.

(2) The density-concentration curve for each temperature is complex, and there is no simple continuity between the portion for the water-rich solutions and that for the phenol-rich solutions. The curves are similar to the isothermals of a gas immediately above and below its critical temperature.

(3) The density-temperature curve for each concentration, on the other hand, is smooth and is represented by the equation :—

$$d_{t°} = d_{20°} + \alpha (t - 20) + \beta (t - 20)^2,$$

the constants α and β having different values for the different concentrations.

(4) The curves of the constants α and β of the density-temperature relation plotted against the concentration exhibit inflexion at approximately 84 per cent. phenol corresponding to equimolecular proportions of water and phenol. No hydrate of this composition is known, and it is therefore suggested that in mixtures of water and phenol, ionisation occurs in two ways :—

$$C_6H_5OH + H_2O \rightleftharpoons C_6H_5OH^{\cdot}{}_2 + OH'$$
$$\rightleftharpoons C_6H_5O' + OH^{\cdot}{}_3$$
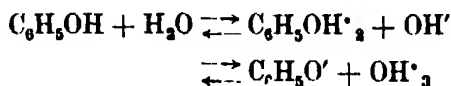
This explains the absence of simple continuity in the physical properties of the water-rich and phenol-rich solutions.

(5) None of the density relations gives any indication of the existence of the known hemi-hydrate of phenol in solution.

(6) The densities of the conjugate solutions have been determined. The line of mean density, as for a gas and its saturated vapour, is parabolic and is accurately expressed over the whole range by the equation :—

$$d_{t^{\circ}}^{mean} = d_{20^{\circ}}^{mean} - 5 \cdot 75 \times 10^{-4} (t - 20) - 2 \cdot 50 \times 10^{-6} (t - 20)^2$$

(7) The concentrations of the conjugate solutions have been calculated from their densities and the solubility curve thus determined is compared with those found by other observers from direct measurements.

(8) The line of mean concentration, like that of mean density, is parabolic. For concentration by weight it is accurately expressed by the equation :—

$$\text{wt. } C_{t^{\circ}}^{mean} = \text{wt. } C_{20^{\circ}}^{mean} - 9 \cdot 0 \times 10^{-2} (t - 20) - 5 \cdot 5 \times 10^{-4} (t - 20)^2.$$

and for concentration by volume by :—

$$\text{vol. } C_{t^{\circ}}^{mean} = \text{vol. } C_{20^{\circ}}^{mean} - 1 \cdot 21 \times 10^{-1} (t - 20) - 7 \cdot 6 \times 10^{-4} (t - 20)^2$$

(9) The critical solution temperature is $66 \cdot 4^{\circ}$.

(10) The critical solution concentration has been calculated both from the line of mean concentration and from the line of mean density, and found to be $34 \cdot 6$ per cent.

A Modified Method of Counting Particles.

By L. H. C. Tippett, M.Sc. (Lond.), British Cotton Industry Research Association.

Introduction and Summary.

Many physical and biological experiments involve the counting of particles which are randomly distributed in space or time. For convenience, the whole of the space or time is divided into a number of zones, and the number of particles in each zone is counted separately. Thus, when using the hæmacytometer, the microscope field is divided into a number of squares, and when counting under the ultramicroscope " snap " readings are taken of a large number of small microscope fields. If a very large number of particles per zone is possible, but the average density is relatively low,* the frequency distribution of zones with 0, 1, 2, etc., particles, as deduced from the laws of probabilities, is described by the Poisson series, and this fact is sometimes used as a test of randomness and as a check on experimental technique.

Assuming the true mean number of particles per zone to be μ and the number of zones counted to be N, the N counts giving an observed mean of $\hat{m}$, the standard error of $\hat{m}$, expressed as a ratio of μ, is well known to be $\sqrt{1/\mu N}$.† Thus, for a given number of zones, the greater the density of particles, the greater is the accuracy of the mean (so long as the Poisson distribution still holds) This is shown by the lowest curve of fig. 1 where the standard error of $\hat{m}$ for a single count ($\sigma_{\hat{m}}$), divided by μ, is plotted against μ.

Sometimes, however, it is inconvenient or impossible to work with high concentrations of particles, because when there are many particles in a zone it may be difficult or impossible to count them accurately. For instance, one particle may tend to obscure others, causing some to be missed in the crowded zones and resulting in departure from the Poisson distribution. Or if the particles are in Brownian motion, as they usually are if of ultra-microscopic size, a " snap " reading of the number has to be taken, and since few observers

---

* These conditions are satisfied if the particles are very small, and the medium in which they are distributed is continuous, relative to the dimensions of the zone. See Rutherford and Geiger, ' Phil. Mag.,' vol. 20, p. 698 (1910); Student, ' Biometrika,' vol. 5, p. 351 (1907); and Wiegner and Russell, ' Kolloid Z.,' vol. 52, p. 189 (1930), for examples.

† True values of constants will be denoted by Greek letters, values estimated from the observations, by assuming the Poisson Law, will be denoted by Latin letters with the ∧ superscript, and crude values obtained from the sample by plain Latin letters.

can estimate at a glance the number of more than three particles, the mean has to be kept so low that very few zones have more than three. Thus it is common to work with a mean of about 0·5 particles per zone, and, with such a low mean as this, a count of even as many as 1000 zones only reduces the standard error of the mean to 4·5 per cent.

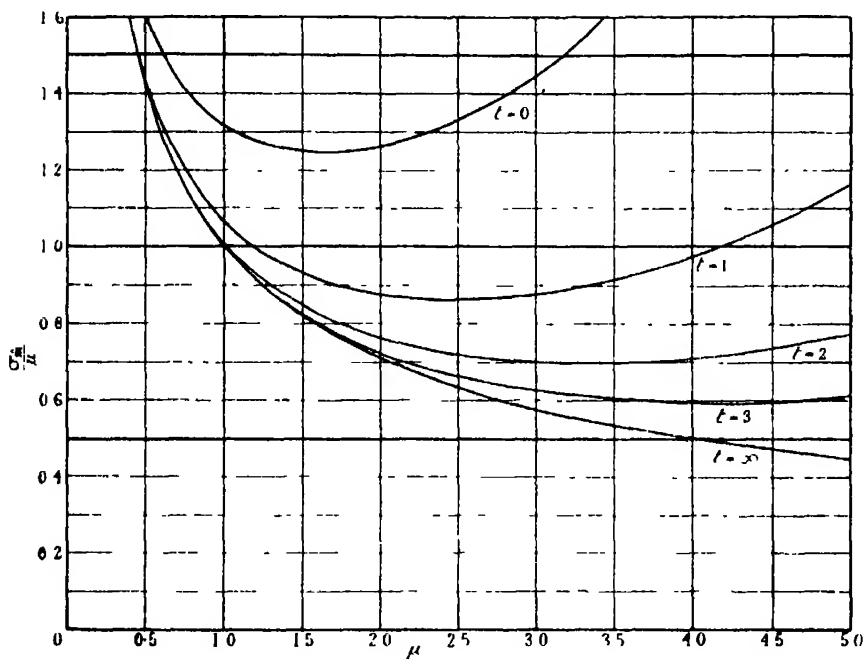There would consequently be a gain in accuracy (or for constant accuracy, an economy of labour) if the technical difficulties of counting the higher

Fig. 1.

densities of particles could be surmounted. This paper suggests a way of achieving this end. The method consists in making counts only on zones with few particles, those zones with more than a certain number of particles being classed together. The mean is estimated from the modified frequency distribution so formed. This method saves time, not only because relatively high concentrations of particles can be used, rendering comparatively few zones necessary for any given accuracy, but also because the numbers of particles in zones with only a few can be counted at a glance, and hence, very quickly. A further advantage arises from the fact that a greater range of particle densities can be investigated than might otherwise be possible.

Modified Method of Estimating Mean.

If all the particles in zones with, say, t or fewer are counted, and the other zones are grouped together as having " more than t," a frequency distribution of the form of Table I can be made, n_0, n_1, etc., being fractions of the total frequency.

Table I.

Number of particles per zone	0	1		s		t	more than t	Total
Proportionate frequency of zones	n_0	n_1		n_s		n_t	n_r	1

Let n_p be the number of zones with t particles or fewer, so that

$$n_p = n_0 + n_1 + \ .. \ n_s + . \quad n_t,$$

and let m' be the mean particles per zone, neglecting zones with more than t, so that

$$m'n_p = 0 . n_0 + 1 . n_1 + ... s . n_s + ... t . n_t.$$

Then if $\hat{m}$ is the estimated mean of the Poisson series that best fits the data, it may be found by solving the following equation, the proof of which is given in the Appendix :

$$m'n_p = \bar{m} \left(n_p - n_r \frac{\hat{n}_t}{\hat{n}_r} \right)$$

The factors $m'n_p$, n_r and n_p are obtained from the observations ; $\hat{n}_t$ and $\hat{n}_r$ involve only $\hat{m}$ as an unknown and can be calculated directly from it , values may be obtained from Soper's[*] tables of the Poisson distribution. For $t = 1$, 2 and 3, $\hat{n}_t/\hat{n}_r$ has been calculated from Soper's tables, and is given in Table IV. Values of $\hat{m}$ which nearly satisfy the equation may be obtained by trial or from the nomograms mentioned later, and a more accurate value may be determined by interpolation. An example is worked out below.

When $t = 0$, that is, when the zones are divided into two classes, those with particles and those with none, the value of $\hat{m}$ corresponding to any value of n_0 may be found directly from Soper's tables. For $t = 1$, 2 or 3, $\hat{m}$ may be determined accurately enough for many practical purposes from the nomograms of figs. 2, 3 and 4. The nomogram has three scales, n_r, $m'n_p$ and $\hat{m}$, and each

---

[*] Pearson, " Tables for Statisticians and Biometricians," Camb. Univ. Press (1914).
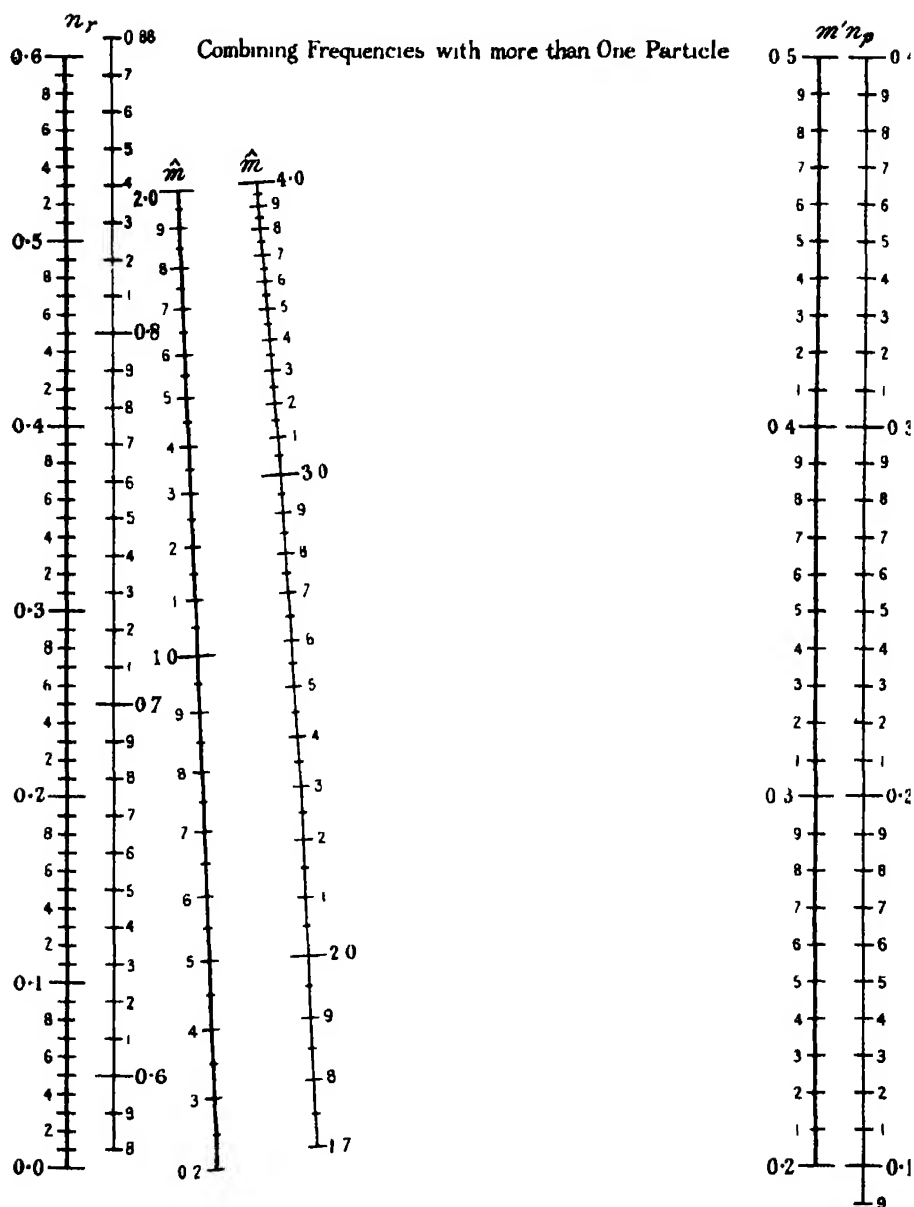
Fig. 2

figure has two such nomograms covering different ranges of $\hat{m}$. The corresponding scales of each pair are drawn consistently in thick or thin lines, and

Combining Frequencies with more than Two Particles

Fig. 3.

Combining Frequencies with more than Three Particles

Fɪɢ 4
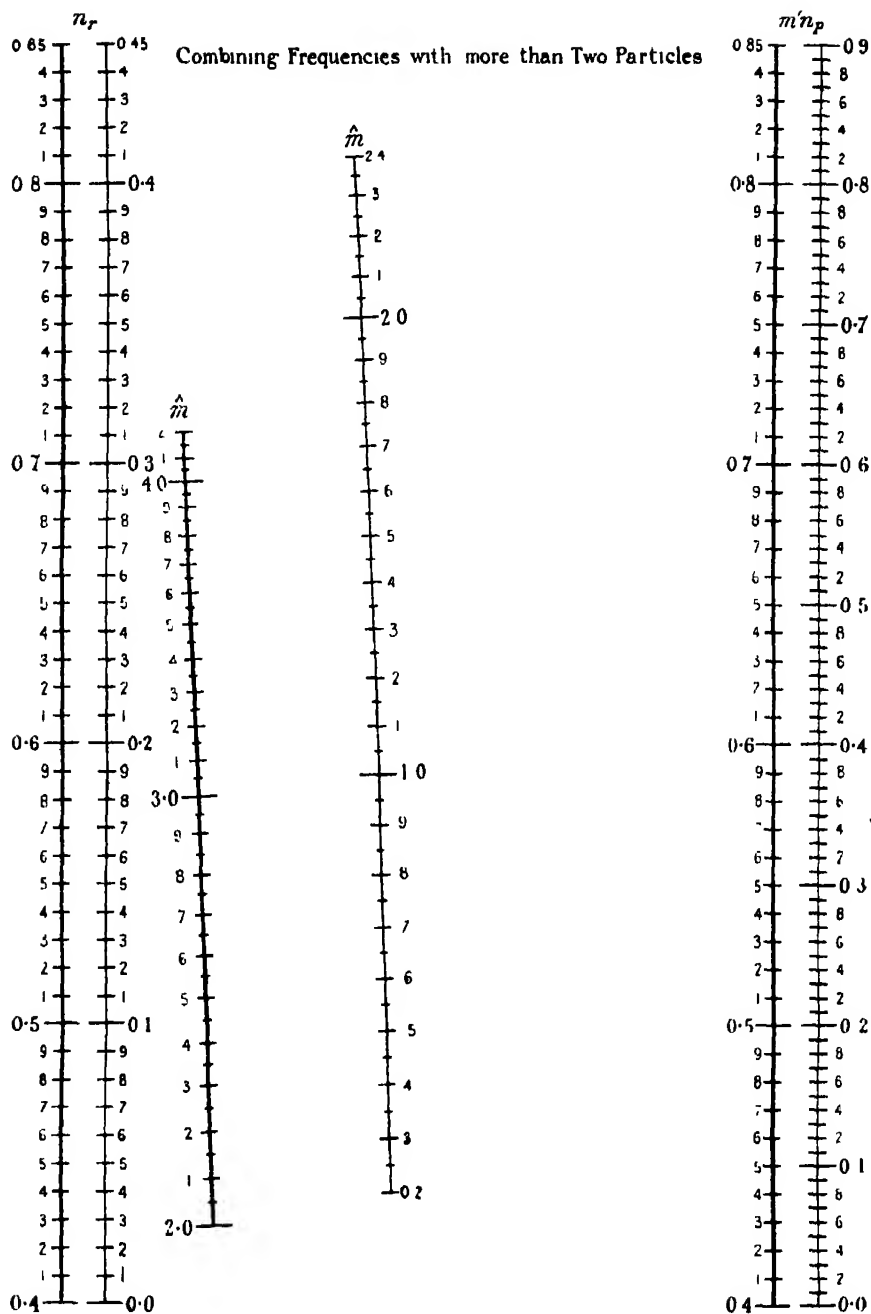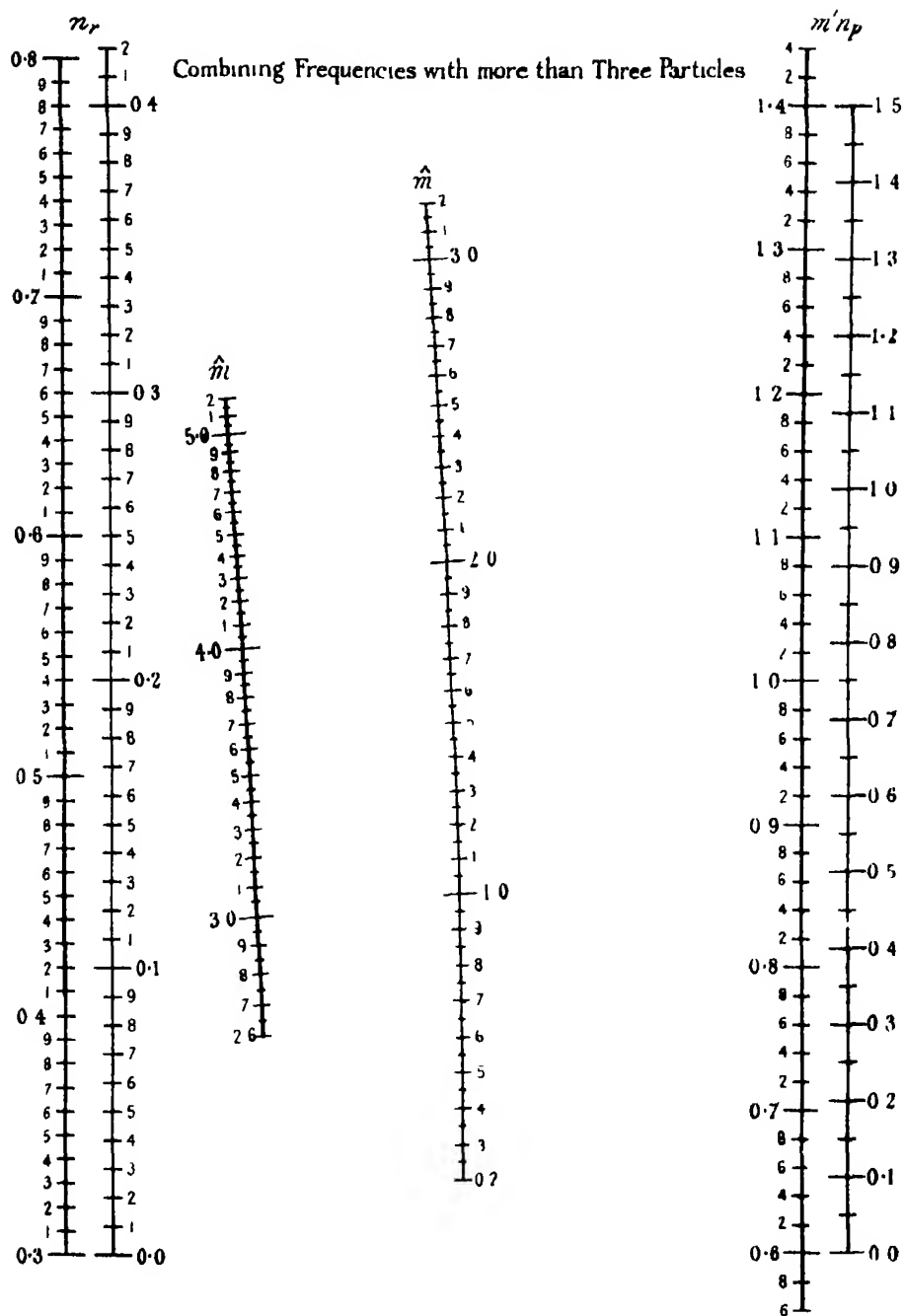
it will be seen that if the left-hand scale of $\hat{m}$ covers the appropriate range, the left-hand scales of n_r and $m'n_p$ must be used in conjunction. In few places are imperfections of draughtsmanship likely to cause errors in $\hat{m}$ greater than 0·02 particle, while most determinations should be correct to 0·01 particle.

Since the nomograms and tables only cover a limited range of conditions, experimenters may often need to solve the equation from the beginning, and the following example illustrates the process. The data, given by Rutherford and Geiger (*loc. cit.*), are numbers of α-particles emitted in intervals of 1/8 minute and from them the distribution of Table II is obtained. Now, the proportionate

Table II.

No of α-particles per interval	0	1	2	3	4	more than 4	Total.
Frequency of intervals	57	203	383	525	532	908	2608

frequency of intervals with zero particles is $57/2608 = 0·0227$, and, assuming the Poisson distribution, the nearest value of $\hat{m}$ in Soper's tables which has this frequency with zero particles is 3·8. Hence, to obtain $\hat{m}$ more accurately, the right-hand side of the equation will be calculated for $\hat{m} = 3·7$, 3·8, 3·9 and 4·0. From Table II, the following constants are obtained :—

$$m'n_p = \frac{4672}{2608} = 1·7914,$$

$$n_r = \frac{908}{2608} = 0·34816, \text{ and } n_p = 0·65184.$$

The first three columns of Table III are obtained from Soper's tables, and from them and from the above constants, the values in the other columns are deduced. The last column contains values of the term on the right-hand

Table III.

$\hat{m}$.	$\hat{n}_4$.	$\hat{n}_r$.	$\dfrac{\hat{n}_4}{\hat{n}_r}$.	$n_r \dfrac{\hat{n}_4}{\hat{n}_r}$.	$n_p - n_r \dfrac{\hat{n}_4}{\hat{n}_r}$.	$\hat{m}\left(n_p - n_r \dfrac{\hat{n}_4}{\hat{n}_r}\right)$
3·7	0·193066	0·312780	0·617258	0·21490	0·43694	1·6167
3·8	0·194359	0·332156	0·585144	0·20372	0·44812	1·7029
3 9	0·195119	0·351634	0·554892	0·19319	0·45865	1·7887
4 0	0·195367	0·371162	0 526366	0·18326	0·46858	1·8743

side of the equation, and the value of $\hat{m}$ which satisfies it is a little greater than $3\cdot9$, and by linear interpolation between $3\cdot9$ and $4\cdot0$ it is calculated to be

$$3\cdot9 + \frac{1\cdot7914 - 1\cdot7887}{1\cdot8743 - 1\cdot7887} \times 0\cdot1 = 3\cdot903.$$

Now, using another arrangement by counting only up to three particles per interval, $m'n_p = 0\cdot9755$, $n_r = 0\cdot5521$, and from the nomogram of fig. 4, $\hat{m} = 3\cdot91$. If all the particles are counted, Rutherford and Geiger give the full distribution, the mean equals $3\cdot871$. The difference in the results given by the three methods is much less than the standard error of the mean.

Standard Error of Mean

Let the standard error of a mean, determined from the above equation, be $\sigma_{\hat{m}}$, and let μ and ν (with appropriate suffixes) be true values of $\hat{m}$ and $\hat{n}$; then $\sigma_{\hat{m}}$ for a single zone may be obtained from the following equation:

$$\frac{\mu^2}{\sigma_{\hat{m}}{}^2} = \mu\nu_p - \mu^2\nu_{t-1} + \mu\nu_t\left(\mu\frac{\nu_r \mid \nu_t}{\nu_r} - 1\right).$$

As usual, when the true values of the constants are unknown, estimates obtained from the sample are substituted as a first approximation. In fig. 1, $\sigma_{\hat{m}}/\mu$ is plotted against μ for $t = 0, 1, 2, 3$ and ∞; if there is a total of N zones, these values of $\sigma_{\hat{m}}/\mu$ must be divided by $\sqrt{\mathrm{N}}$.

As might be expected, the standard errors of the means obtained by the modified method are greater than those of means obtained from the full distribution. For each value of t, there is an optimum density. When $t = 3$, this density is at about $4\cdot2$ particles per zone, when $\sigma_{\hat{m}}/\mu$ is $0\cdot59$ If now all particles are counted, with a mean of $0\cdot5$ (a common case of ultra-microscope observations), $\sigma_{\hat{m}}/\mu = 1\cdot43$, and to obtain an accuracy by this method equal to that of the modified method with $t = 3$, nearly six times as many zones need to be counted, the number of zones for constant accuracy varying inversely as the square of $\sigma_{\hat{m}}/\mu$.

Goodness of Fit.

Before any modified method is used, it is obviously necessary to test the basic assumption that the Poisson distribution applies. This may be done directly for a few representative test cases where all particles can be counted, or indirectly by using different concentrations of particles bearing known

relations to each other, and seeing if the means estimated by the modified method bear the same relations.

Where this is not possible, the estimated frequencies in the modified distribution may be found with the aid of Soper's tables, and compared with the observed frequencies by means of the well-known P, χ^2 test for goodness of fit. Since the total and mean are both estimated from the sample, the " degrees of freedom "[*] are two less than the number of frequency groups (*i.e.* $= t$), or Elderton's tables[†] should be entered at n' equal to one less than the number of frequency groups ($n' = t + 1$).

The estimated frequencies for a mean of $3 \cdot 903$ and total of 2608 are given in Table IV, and when these are compared with the observed frequencies of Table II, $\chi^2 = 2 \cdot 36$, $n' = 5$, and (from Elderton's tables), $P = 0 \cdot 7$. When

Table IV.

No. of particles per zone	0	1	2	3	4	More than 4	Total
Expected frequency per zone ($\hat{m} = 3 \cdot 903$)	52 6	205 4	400 9	521 5	508·9	918 7	2608

the Poisson series is fitted to the full distribution ($\hat{m} = 3 \cdot 871$) and the same final grouping is adopted for comparison, $\chi^2 = 2 \cdot 97$. The difference between the two values of χ^2 is of no importance.

It will be noted that when the mean is found by the modified method, no errors in χ^2 are introduced by combining the tail frequencies, as is the case when the combination is done after the theoretical distribution has been fitted, see Sheppard,[‡] and Neyman and Pearson.[§]

Applications

The saving in labour resulting from the adoption of the modified method of counting when applied to the ultramicroscope has been shown to be considerable. Even when it is possible to count every particle, time may be

---

[*] Fisher, R. A., " Statistical Methods for Research Workers," 3rd ed. Oliver and Boyd (1930).

[†] Pearson, *loc. cit.*

[‡] Sheppard, W. F , ' Phil Trans ,' A, vol 228, p. 115 (1929).

[§] Neyman, J., and Pearson, E. S., " Further Notes on the χ^2 Distribution," ' Biometrika,' vol. 22, p. 298 (1931).

saved by adopting the modified method. With a density of $4 \cdot 2$ particles per zone, $\sigma_{\hat{m}}/\mu = 0 \cdot 49$ when all are counted, and 100 zones give the same accuracy as 140 counted by the modified method when $t = 3$. With the standard method, zones containing many particles take some time to count, while with the modified method they can all be estimated at a glance, and it may well be that 140 counted in this way take less time than 100 with every particle counted. The method could usefully be explored in places where a large amount of routine work is done, *e.g.*, bacteriological laboratories.

Where the counting is difficult, and involves eye-strain, it has been found advantageous to use the modified method with $t = 1$. Where there is considerable risk that the presence of even one particle may interfere with the observation of a second which may be present, the modified method may be used with $t = 0$. When the true mean is $1 \cdot 6$, the standard error of the mean so estimated (expressed as a ratio of that mean) is only $1 \cdot 24$, and this is less than the corresponding standard error for $\mu = 0 \cdot 5$, when all particles are counted, that is, the accuracy of the modified method with $t = 0$ is greater than that with which many ultra-microscopists have to be satisfied.

Besides resulting in a possible saving in time, these modified methods enable a wider range of particle concentrations to be used than is sometimes possible with the standard method

Appendix

Deduction of Formulæ and Construction of Nomograms.

Table V is a frequency distribution of zones, n_s being the observed proportionate frequency with s particles, and $\hat{n}_s$ being the corresponding frequency in the estimated Poisson series. If the estimated mean is $\hat{m}$, then

$$\hat{n}_s = \frac{\hat{m}^s}{s!} e^{-\hat{m}}, \quad \text{and} \quad \hat{n}_r = 1 - \sum_{s=0}^{s=t} \frac{\hat{m}^s}{s!} e^{-\hat{m}}.$$

Table V

No. of particles per zone	0	1		s		t	More than t	Total.
Frequency of zones— Observed Poisson series	n_0 $\hat{n}_0$	n_1 $\hat{n}_1$		n_s $\hat{n}_s$		n_t $\hat{n}_t$	n_r $\hat{n}_r$	1 1

Estimation of Mean

The mean of the series, $\hat{m}$, may be estimated by the Method of Maximum Likelihood,[*] and this is done by determining the value of $\hat{m}$ which makes the quantity,

$$\sum_{s=0}^{s=r} n_s \log \hat{n}_s \tag{1}$$

a minimum, the summation extending over all frequency groups, including the "more than t" group.

Now

$$\frac{\partial}{\partial \hat{m}} n_s \log \hat{n}_s = \frac{sn_s}{\hat{m}} - n_s \quad \text{for} \quad s = 0 \quad \text{to} \quad s = t$$

and

$$\frac{\partial}{\partial \hat{m}} n_r \log \hat{n}_r = \frac{n_r}{\hat{n}_r} \left[\sum_{s=0}^{s=t} \hat{n}_s - \sum_{s=0}^{s=t} \hat{n}_{s-1} \right] = n_r \frac{\hat{n}_t}{\hat{n}_r} \tag{2}$$

Hence, the differential of (1) with respect to $\hat{m}$, equated to zero, yields the equation

$$\frac{1}{\hat{m}} \sum_{s=0}^{s=t} sn_s - \sum_{s=0}^{s=t} n_s + n_r \frac{\hat{n}_t}{\hat{n}_r} = 0 \; ;$$

or, putting $\sum_{s=0}^{s=t} n_s = n_p$ ($=$ the proportion of zones with t particles or fewer)

and $\sum_{s=0}^{s=t} sn_s = m'n_p$ (m' = mean particles per zone for zones containing t particles or fewer),

$$m'n_p = \hat{m} \left(n_p - n_r \frac{\hat{n}_t}{\hat{n}_r} \right). \tag{3}$$

Since $\hat{n}_t$ and $\hat{n}_r$ involve only $\hat{m}$ as an unknown, and $m'n_p$, n_p and n_r are determined from the observations, equation (3) can be solved for $\hat{m}$. A general solution has not been discovered, but it was found that a nomogram could be formed and three are given in figs. 2–4. The two sets of side scales in figs. 2–4 are linear scales of n_r and $m'n_p$. The points on the scale of $\hat{m}$ were determined empirically by assuming successive values of $\hat{m}$ and finding pairs of values of $m'n_p$ and n_r which would satisfy equation (3); lines were drawn cutting the side scales at appropriate values, and their intersection gave the position of $\hat{m}$ on the central scale. Three or more such lines for one value of $\hat{m}$ always intersected at one point. The ultimate choice of dimensions of the nomograms was made after several trials. It was found that the points forming the scale of $\hat{m}$ fell on lines which were nearly straight, and the final nomograms were

---

[*] Fisher, ' Phil. Trans.,' A, vol. 222, p. 309 (1922).

made by determining accurately 2, 3 or 4 points covering the range of the $\hat{m}$ scale, joining these by one, two or three straight lines, and thus forming the backbone. Then for intermediate values of $\hat{m}$, corresponding population values of $m'n_p$ and n_r were found from Soper's tables, and the intersections with the backbone of lines joining these values on the side scales were marked. Thus, errors of draughtsmanship are least for the values of $m'n_p$ and n_r which are most frequently encountered. This was found to be more satisfactory than the method of finding the points of $\hat{m}$ separately and joining them with a curve drawn by eye to smooth out small irregularities.

Standard Error of Estimated Mean.

If $\sigma_{\hat{m}}$ is the standard error of the mean, estimated by the method of maximum likelihood,

$$-\frac{1}{\sigma_{\hat{m}}^2} = \overline{\sum_{s=0}^{s=r} \frac{\partial^2}{\partial \hat{m}^2} n_s \log \hat{n}_s}, \tag{4}$$

where the bar indicates the mean value of the quantity in all samples that can be drawn from the population.

Differentiating equations (2) again,

$$\frac{\partial^2}{\partial \hat{m}^2} n_s \log \hat{n}_s = -\frac{sn_s}{\hat{m}^2} \text{ for } s = 0 \text{ to } s = t,$$

and

$$\frac{\partial^2}{\partial \hat{m}^2} n_r \log \hat{n}_r = \frac{n_r}{\hat{n}_r}\left(\hat{n}_{t-1} - \hat{n}_t - \frac{\hat{n}_t^2}{\hat{n}_r}\right),$$

whence, substituting in (4),

$$-\frac{1}{\sigma_{\hat{m}}^2} = -\frac{m'n_p}{\hat{m}^2} + \frac{n_r}{\hat{n}_r}\left(\hat{n}_{t-1} - \hat{n}_t - \frac{\hat{n}_t^2}{\hat{n}_r}\right). \tag{5}$$

The mean values of the terms of (5) are the population values (denoted by corresponding Greek letters), and they must also satisfy equation (3). Hence the following equation may be obtained,

$$\frac{\mu^2}{\sigma_{\hat{m}}^2} = \mu\nu_p - \mu^2\nu_{t-1} + \mu\nu_t\left(\mu\frac{\nu_r + \nu_t}{\nu_r} - 1\right). \tag{6}$$

Since the frequencies in (6) are fractions, the standard error obtained is for a count on a single zone.

When $t = 0$,

$$\sigma_{\hat{m}}^2 = \left(\frac{1}{\nu_0} - 1\right) = e^\mu - 1,$$

and when $t = \infty$ (*i.e.*, when all the particles are counted),

$$\sigma_{\hat{n}}^2 = \mu.$$

The points for fig. 1 were obtained from equation (6) with the aid of Soper's tables.

Table VI.—Values of $\hat{n}_t/\hat{n}_r$.

$\hat{n}$.	$t = 1.$	$t = 2.$	$t = 3.$	$\hat{n}$	$t = 1.$	$t = 2.$	$t = 3$
				2 6	0 26359	0 52131	0 82414
				2 7	0 24151	0·48376	0 77112
				2·8	0 22144	0·44930	0 72220
				2 9	0 20316	0 41761	0·67698
0 5	3·3620	5 269	7 21	3 0	0 18650	0·38842	0·63510
0 6	2·7013	4 274	5·88	3 1	0·17129	0 36147	0 59622
0·7	2 23106	3 5634	4·934	3 2	0 15738	0 33656	0·56007
0·8	1 87996	3 0320	4 223	3·3	0·14466	0·31351	0·52640
0·9	1 60829	2·6197	3·671	3 4	0 13300	0 29215	0·49501
1 0	1 39220	2 2906	3 229	3 5	0·12231	0 27234	0 46569
1·1	1 21659	2 0223	2 869	3 6	0·11250	0 25394	0·43828
1 2	1 07132	1 7995	2 5687	3 7	0 10350	0 23683	0·41262
1 3	0 94939	1·6117	2 3156	3·8	0 09524	0 22092	0 38857
1 4	0 84582	1 45142	2 0992	3 9	0 08764	0·20611	0·36602
1·5	0 75693	1 31319	1 9120	4 0	0 08065	0·19232	0·34485
1 6	0 67997	1 19289	1·7488	4 1	0 07422	0·17946	0·32496
1·7	0·61285	1 08733	1·6052	4 2	0 06831	0·16747	0 30626
1 8	0 55391	0 99408	1 4780	4·3	0 06287	0 15628	0 28867
1 9	0·50186	0 91120	1·36460	4 4	0 05786	0 14585	0·27212
2 0	0·45568	0·83715	1 26296	4·5	0 05324	0 13610	0 25653
2 1	0 41452	0·77067	1·17139	4 6	0·04900	0 12700	0 24184
2·2	0 37768	0·71072	1 08853	4·7	0·04509	0·11851	0 22799
2·3	0·34461	0·65646	1 01323	4 8	0 04148	0·11057	0 21403
2 4	0·31483	0 60719	0 94458	4 9	0 03816	0·10315	0 20261
2 5	0 28793	0 56231	0·88177	5 0	0 03511	0 09622	0 19099

The Collision of α-Particles with Atomic Nuclei.

By H. S. W. MASSEY, B.A , M.Sc., Exhibition of 1851 Senior Student, Trinity College, Cambridge.

Since the introduction of the concept of nuclear potential barriers by Gurney and Condon* and by Gamow† a great deal of attention has been concentrated on the behaviour of such systems As a consequence of this there has been a considerable increase of knowledge of nuclear phenomena, particularly in so far as these are concerned with α-particles. As a great proportion of experimental investigations in nuclear physics are concerned with the observation of effects due to impacts of α-particles on nuclei, the theoretical investigation of such collisions is of great interest.   In this connection difficulties arise owing to the strong perturbation of the α-particle wave by the nuclear potential barrier This renders the ordinary theory of collisions, due to Born,‡ inapplicable and this failure of the usual theory was not realised for some time. A more suitable theory has never been developed explicitly, though formulæ which one would expect to derive from such a theory have been used.   In this paper a suitable theory is developed   Besides establishing the validity of the above formulæ, this theory is also applied to the consideration of the probability of α-particle exchange on impact and to the elastic scattering by light nuclei (Mg, Al, etc).

It is shown that α-particle exchange is of considerable importance when the energy of the incident α-particle coincides with that of a virtual level of the nucleus and will have the effect of broadening the level

We will now consider the general theory

1. General Theory.

Let us consider the impact of an α-particle of mass M on a nucleus of mass M' such that MM'/(M + M') is nearly equal to M.   Denote the aggregate of co-ordinates of the nuclear particles by r_N, of the incident α-particle by r. The wave equation for the combined system is

$$\left[\frac{h^2}{8\pi^2 M} \nabla^2 + H(r_N) + E - V(r, r_N) \right] \Psi = 0, \tag{1}$$

* ' Nature,' vol. 122, p 439 (1928).

† ' Z. Physik,' vol. 51, p. 204 (1928).

‡ ' Z. Physik,' vol. 38, p 863 (1926).

where H is the Hamiltonian describing the internal motion of the nuclear particles, $V(r, r_N)$ the interaction energy between the incident particle and the nucleus, and E the total energy of the system. We require a solution of this equation which is finite throughout space and has the asymptotic form

$$e^{ikz} + \Sigma \, \psi_s \, (r_N) \frac{e^{ik_s r}}{r} f_s \, (\theta, \phi), \tag{2}$$

for large r. Here $\psi_s \, (r_N)$ are the wave functions of the various nuclear states and the wave numbers k_s are such that the conservation of energy is satisfied, i.e.

$$k^2 = \frac{8\pi^2 M}{h^2} E_i, \quad k_s^2 = \frac{8\pi^2 M}{h^2} \{E_i - (E_s - E_0)\},$$

where E_s is the energy of the sth state of the nucleus, and E_i that of the incident α-particle. Having obtained a solution in this form, the probability of excitation of a given nuclear level becomes

$$Q_s = \frac{k_s}{k} \iint |f_s \, (\theta, \phi)|^2 \sin \theta \, d\theta \, d\phi. \tag{3}$$

To obtain an approximate solution with these properties we expand the function Ψ in the form

$$\Psi = \Sigma \, \psi_s \, (r_N) \, F_s \, (r). \tag{4}$$

Substituting (4) in (1) we find

$$\Sigma_s \left[\frac{h^2}{8\pi^2 M} \nabla^2 + (E - E_s) \right] F_s \, (r) \, \psi_s = V \, (r, r \,) \, \Psi. \tag{5}$$

Multiply (5) on both sides by $\bar{\psi}_s$ and integrate over all co-ordinates of the nuclear system. This gives, from the orthogonal properties of the functions ψ_s,

$$\left[\frac{h^2}{8\pi^2 M} \nabla^2 + (E - E_s) \right] F_s = \Sigma_u \int V \, (r, r_N) \, \psi_u \, \bar{\psi}_s \, dv_N \, F_u. \tag{6}$$

In order to obtain a satisfactory approximation to the solution of this system of equations, we neglect the non-diagonal matrix elements of V with respect to the nuclear wave functions, except those associated with F_0 (the incident and elastically scattered wave). We then obtain

$$\left[\frac{h^2}{8\pi^2 M} \nabla^2 + (E - E_s) \right] F_s = \int V \, (r, r_N) \, \psi_s \bar{\psi}_s \, dv_N \, F_s + \int V \, (r, r_N) \, \psi_0 \bar{\psi}_s \, dv_N \, F_0$$
$$s = 1, 2, \ldots$$

$$\left[\frac{h^2}{8\pi^2 M} \nabla^2 + (E - E_0) \right] F_0 = \int V \, (r, r_N) \, \psi_0 \bar{\psi}_0 \, dv_N \, F_0. \tag{7}$$

Before considering the solution of these equations we will consider how the ejection of protons with α-particle capture, and also α-particle exchange, can be brought into the scheme.

A solution in the form (4) above must include these possibilities and, just as for collisions of electrons with atoms where electron exchange may take place, they arise from the terms of Ψ representing excitation of nuclear states such that F_s corresponds to a negative energy of the α-particle. In order to obtain approximate equations for proton emission and α-particle exchange it is, however, not convenient to use the expansion above, but to expand in terms of the wave functions of the final system. We take instead of (4)

$$\Psi = \Sigma \, \psi_t \, (r_N') \, G_t \, (r'), \tag{8}$$

where $\psi_t \, (r_N')$ is a wave function of the nucleus formed by the collision, and r_N', r' denote the aggregate of co-ordinates of the nuclear and outgoing particles respectively. If we are concerned with proton emission, the probability of finding the nucleus in the state t after the collision is given by

$$Q_t = \frac{k_t}{k} \int |g_t \, (\theta, \, \phi)|^2 \sin \theta \, d\theta \, d\phi, \tag{9}$$

if

$$G_t \sim \frac{e^{ik_t r}}{r} \, g_t \, (\theta, \, \phi).$$

For α-particle exchange we must proceed as shown in section (2c), as the final nuclear states are then indistinguishable from those which occur in an inelastic collision without exchange.

Proceeding as before, we obtain the equations

$$\left[\frac{h^2}{8\pi^2 M'} \, \nabla'^2 + (E - E_t) \right] G_t = \Sigma_v \int V \, (r', \, r_N') \, \Psi \overline{\psi}_v \, dv_N' \, G_v \tag{10}$$

In order to approximate to the solution of this system of equations we neglect non-diagonal elements of V with respect to the wave functions of the final nucleus, and take

$$\Psi = G_t \, (r') \, \psi_t \, (r_N') + F_0 \, (r) \, \psi_0 \, (r_N), \tag{11}$$

for the calculation of G_t. This gives

$$\left[\frac{h^2}{8\pi^2 M'} \, \nabla'^2 + (E - E_t) \right] G_t = \int V \, (r', \, r_N') \, \psi_t \, (r_N') \, \overline{\psi}_t \, (r_N') \, dv_N' \, G_t$$
$$+ \int V \, (r', \, r_N') \, F_0 \, (r) \, \psi_0 \, (r_N) \, \overline{\psi}_t \, (r_N') \, dv_N'. \tag{12}$$

Having now obtained the differential equations for the various scattered waves, we will investigate the solutions of the equations and the formulæ these solutions lead to.

Solution of Equations —The equations occurring are all of the form[*]

$$[\nabla^2 + k^2 - V(r)]\chi = \Sigma a_n(r) P_n(\cos\theta). \tag{13}$$

We require solutions of these equations satisfying the following conditions :—

(1) For large r they must tend to $\dfrac{e^{ikr}}{r} f(\theta)$;

(2) They must be finite and single valued everywhere.

Expanding χ in the form

$$\chi = \Sigma \chi_n(r) P_n(\cos\theta), \tag{14}$$

we find

$$\frac{d^2}{dr^2}(r\chi_n) + \left| k^2 - V(r) - \frac{n(n+1)}{r^2} \right| (r\chi_n) = ra_n(r). \tag{15}$$

Now if L_n^c, L_n^e are two independent solutions of the homogeneous equation

$$\frac{d^2}{dr^2}(r\chi_n) + \left\{ k^2 - V(r) - \frac{n(n+1)}{r^2} \right\} r\chi_n = 0, \tag{16}$$

the general solution of the inhomogeneous equation (15) takes the form

$$\chi_n = \frac{L_n^c}{k} \int_{c_1}^r a_n(r') L_n^e(r') r'^2 dr' + \frac{L_n^e}{k} \int_{c_2}^r a_n(r') L_n^c(r') r'^2 dr', \tag{17}$$

c_1, c_2 being arbitrary constants. Then, if we choose the solutions L_n^c, L_n^e so that χ_n^c is finite everywhere, and tends asymptotically to

$$\frac{1}{r} \cos\{kr - \tfrac{1}{2}(n+1)\pi + \delta_n\}, \tag{18}$$

and L_n^e tends asymptotically to

$$\frac{1}{r} e^{i(kr - \frac{1}{2}n\pi + \delta_n)}, \tag{19}$$

a solution of (16) satisfying the required conditions, will clearly be

$$\chi_n = \frac{1}{k} \left\{ L_n^c \int_\infty^r a_n(r') L_n^e(r') r'^2 dr' + L_n^e \int_0^r a_n(r') L_n^c(r') r'^2 dr' \right\}, \tag{20}$$

---

[*] This form is strictly correct only when the final nucleus is in an s state and so has a spherically symmetrical field. When it is not we may imagine the field as averaged over all orientations before solving the equation.

80

$$\chi_n \qquad \frac{e^{i(kr - \frac{1}{2}n\pi + \delta_n)}}{kr} \int_0^\infty a_n(r') L_n^c(r') r'^2 dr'. \qquad (21)$$

Substituting in the expansion (14) we find then

$$\chi \sim \frac{1}{kr} \Sigma_n e^{i(kr - \frac{1}{2}n\pi + \delta_n)} \int_0^\infty a_n(r') L_n^c(r') r'^2 dr'. \qquad (22)$$

In order to obtain this sum in a closed form as an integral it is easy to see that, if we write

$$\Sigma_n a_n(r) P_n(\cos\theta) = H(r, \theta),$$

then

$$\chi \sim \frac{1}{4\pi} \frac{e^{ikr}}{r} \int H(r', \theta') \overline{F}(r', \Theta') dv', \qquad (23)$$

where $F(r, \Theta)$ is the solution of the homogeneous equation which tends asymptotically to

$$\frac{1}{k} \Sigma_n e^{-i\delta_n} i^n (2n+1) \cos\{kr - \frac{1}{2}(n+1)\pi + \delta_n\} P_n(\cos\Theta), \qquad (24)$$

i.e., is the wave function representing the motion of α-particles in the field, so normalised as to correspond to an incident plane wave of unit amplitude and an associated *converging* spherical wave. The angles θ', Θ' are the angles the directions of the incident and outgoing plane waves, respectively, make with a fixed axis. Solutions normalised in the same way as $F(r, \Theta)$ will be denoted by German script as $\mathfrak{F}(r, \Theta)$.

2 *Application of the Solutions.*

(a) *Inelastic Collisions without Exchange or Proton Emission.*—For these we have the differential equations

$$\left[\nabla^2 + k_s^2 - \frac{8\pi^2 M}{h^2} \int V(r, r_N) \psi_s \overline{\psi}_s dv_N \right] F_s - \frac{8\pi^2 M}{h^2} \int V(r, r_N) \psi_0 \overline{\psi}_s dv_N F_0 \quad (25)$$

Using (23), the required asymptotic expansion of the solution is simply

$$F_s \sim \frac{2\pi M}{h^2} \frac{e^{ik_s r}}{r} \int V(r, r_N) \psi_0(r_N) \overline{\psi}_s(r_N) F_0(r) \overline{\mathfrak{F}}_s(r) dv_N dv, \qquad (26)$$

where $\mathfrak{F}_s$ is the solution of the homogeneous equation corresponding to motion of α-particles in the field of the excited nucleus.

Substituting in (3) the cross section corresponding to this excitation is simply

$$Q_s = \frac{8\pi^3 M^2}{h^4} \frac{k_s}{k} \int \left| \int V(r, r_N) \psi_0(r_N) \overline{\psi}_s(r_N) F_0(r) \mathfrak{F}_s(r) dv_N dv \right|^2 \sin\theta\, d\theta \qquad (27)$$

This formula is just the one used without proof by Gamow in Chapter IV of his book,* for F_0, $\mathfrak{F}_s$ are the incident and final wave functions of the colliding α-particle in the fields of the initial and final nuclei respectively. They are functions already perturbed by the interaction energy. It is perfectly clear from this formula that the first approximation of Born's theory would be completely inadequate as $F_0(r)$, $\mathfrak{F}_s(r)$ differ very greatly from plane waves in the region of the nucleus from which comes the main contribution to the integral above.

The order of magnitude of Q_s has already been estimated by Gamow and will not be investigated here.

(b) *Proton Emission with α-particle Capture.*—For this we have

$$\left\{ \nabla'^2 + k_t^2 - \frac{8\pi^2 M}{h^2} \int V(r', r_N') \psi_t(r_N') \bar{\psi}_t(r_N') \, dv_N' \right\} G_t(r')$$
$$= \frac{8\pi^2 M}{h^2} \int V(r', r_N') F_0(r) \psi_0(r_N) \bar{\psi}_t(r_N') \, dv_N'. \quad (28)$$

Using (23), the asymptotic expression of G_t becomes

$$G_t \sim \frac{2\pi M'}{h^2} \frac{e^{ik_t r'}}{r'} \int V(r', r_N') F_0(r) \psi_0(r_N) \bar{\psi}_t(r_N') \bar{\mathfrak{G}}_t(r') \, dv_N' \, dv, \quad (29)$$

so the probability of excitation with proton emission is

$$Q_t = \frac{8\pi^3 M'^2}{h^4} \frac{k_t}{k} \int_0^\pi \left| \int V(r' r_N') F_0(r) \psi_0(r_N) \bar{\psi}_t(r_N') \bar{\mathfrak{G}}_t(r') \, dv_N' \, dv \right|^2 \sin\theta \, d\theta. \quad (30)$$

This is the formula used by Gamow on p. 96 of his book, $F_0(r) \psi_0(r_N)$ and $\psi_t(r_N') \mathfrak{G}_t(r')$ being the initial and final wave functions respectively. As Gamow has already estimated the value of Q_t, we will not proceed any further with this.

(c) *α-particle Exchange.*—In this case we have an exactly similar formula to that above with $M' = M$. However, the effect of this α-particle exchange cannot be represented by the addition of the corresponding cross section to that of the non-exchange process, for we must obtain the wave function of the system of nuclear plus incident α-particles, symmetric in all the α-particle co-ordinates.

If N is the number of nuclear α-particles the co-ordinates of which we denote by $r_1, \ldots, r_N$, the incident α-particles being distinguished by the suffix $N + 1$,

* "Atomic Nuclei and Radioactivity," Oxford University Press.

the wave function $\Psi(r_1, \ldots, r_N, r_{N+1})$ obtained above will have the asymptotic form

$$\Psi(r_1, \ldots, r_N, r_{N+1}) \sim \Sigma_s \psi_s(r_1, \ldots, r_N) \frac{e^{ik_s(r_{N+1})}}{r_{N+1}} f_s(\theta, \phi)$$

$$+ \Sigma_s \Sigma_t \psi_s(r_1, \ldots, r_{p-1}, r_{p+1}, \ldots, r_{N+1}) \frac{e^{ik_s r_p}}{r_n} g_s(\theta, \phi) \qquad . (31)$$

$$+ \psi_0(r_1, \ldots, r_N) e^{ikz_{N+1}}$$

The wave function symmetric in all the α-particles will then be

$$S\Psi = \frac{1}{\sqrt{(N+1)}} \Sigma_p \Psi(r_1, \ldots, r_{p-1}, r_{p+1}, \ldots, r_{N+1}, r_p). \tag{32}$$

Using this function to compute the ratio of scattered current to incident, we find for the total cross section corresponding to the excitation of the sth nuclear state,

$$Q_s = \frac{k_s}{k} \int |f_s(\theta, \phi) + Ng_s(\theta, \phi)|^2 \sin\theta \, d\theta \, d\phi \tag{33}$$

For the moment we will restrict ourselves to the case of elastic scattering only. Then, taking $s = 0$, we have, using (29) above,

$$g_0(\theta, \phi) = \frac{2\pi M}{h^2} \int V(r', r_N') F_0(r) \psi_0(r_N) \bar{\psi}_0(r_N') \bar{\mathfrak{F}}_0(r') \, dv_N' \, dv', \tag{34}$$

for in this case $\mathfrak{G}_s$ is simply equal to $\mathfrak{F}_0$, both the incident and ejected α-particles moving in the same field. The functions are normalised to represent an incident wave of unit amplitude and the associated scattered wave.

3. *Estimation of the Exchange Effect.*

In order to estimate the magnitude of the exchange effect we use a method very similar to that used by Gamow (*loc. cit.*) in considering the emission of protons.

We expand F_0 and $V(r', r_N)$ in a series of spherical harmonics and take the ground state of the nucleus to be an S state. Then

$$\left.\begin{array}{l} F_0 = \Sigma_n i^n (2n+1) e^{i\delta n} F_0^n(r) P_n(\cos\theta) \\ \mathfrak{F}_0 = \Sigma_n i^n (2n+1) e^{-i\delta n} F_0^n(r) P_n(\cos\theta) \\ V(r', r) = \Sigma_n V_n(r', r) P_n(\cos\gamma) \end{array}\right\}, \tag{35}$$

where γ is the angle between the vectors r', r. Substituting in (34) we find

$$g_0(\theta, \phi) = \frac{2\pi M}{h^2} \Sigma_n e^{2i\delta_n} P_n(\cos\theta) \int\int V_n(r', r) F_0^n(r) F_0^n(r') \bar{\chi}_0(r) \chi_0(r') r_1'^2 r^2 \, dr \, dr', \tag{36}$$

where χ_0 is the wave function of a single α-particle in the ground state. It is clear that, since $\chi(r)$, $\chi_0(r')$ are negligible outside the nucleus of radius r_0, the only appreciable contribution to the integral arises from the region inside the nucleus. As a consequence we need only consider the form of the various wave functions in this region. These may be written in the form

$$F_0{}^n(r) = \frac{1}{kr_0}\, \xi_n(r)\, e^{\pm I_n}, \quad \chi_0 = \frac{1}{\Omega^{\frac{1}{2}}}\, \zeta(r), \tag{37}$$

where Ω is the volume of the nucleus and I_n is given by*

$$I_n = \frac{4\pi^2 Z e^2}{hv} - \frac{4\pi e\sqrt{2M}}{h}\, \sqrt{2Zr_0}\left(1 + \frac{h^2}{4\pi^2 M}\, \frac{n(n+1)}{r_0}\right). \tag{38}$$

The plus sign is to be taken only at a resonance level, the negative sign in all other cases. ξ_n represents a wave of approximately unit amplitude and χ_0 is normalised in the usual manner.

Substituting these expressions we find

$$g_0(\theta, \phi) \simeq \frac{2\pi M}{h^2 \Omega k^2 r_0{}^2} \Sigma_n e^{2i\delta_n}\, P_n(\cos\theta)\, e^{\pm 2I_n} \int V_n\, \xi_n(r)\, \xi_n(r')\, \overline{\zeta}(r)\zeta(r')\, r^2 r_1{}^2\, dr\, dr'. \tag{39}$$

The integral is a certain mean of the interaction energy, which we may denote by $\overline{V}_n$, giving finally

$$g_0(\theta, \phi) \simeq \frac{2\pi M}{h^2 \Omega k^2 r_0{}^2} \Sigma_n e^{2i\delta_n} e^{\pm 2I_n}\, \overline{V}_n\, P_n(\cos\theta). \tag{40}$$

The chief interest of this formula is that it shows that the probability of α-particle exchange is very small except at a resonance level, owing to the presence of the term

$$e^{\pm 2I_n}.$$

At a resonance level one must take the positive sign for the exponential and the formula (40) cannot then be regarded as valid. It shows, however, that the effect of exchange will be large under these conditions. This would be expected since it is clear that exchange will only take place with appreciable probability if the wave functions of the two exchanging particles overlap. At a resonance level the overlap will be considerable and so we expect the above result.

---

* This formula holds provided n is not too large. When n is large then $\overline{V}_n$ will be very small and such terms may be neglected.

The most interesting effect of α-particle exchange is that it will result in a broadening of the level, as may be seen from the following considerations. The breadth of a level is inversely proportional to the time that the α-particle stays in the level. If there is a considerable probability of the α-particle exchanging places with another in a lower state this time will be reduced and the level correspondingly broadened.

The effect of a resonance level on the direct elastic scattering has been investigated by Mott.* Any deviations from the results which he obtains must be due to α-particle exchange, and it would thus be of interest to investigate experimentally the deviations from classical scattering under these conditions.

4. *Anomalous Scattering.*

The anomalous scattering of α-particles has excited considerable interest, as it appears to offer a means of determining the nuclear field of force. Thus on classical theory it was possible to derive the form of the law of force which would give rise to the observed scattering, but it soon became clear that laws deduced in this way were of little significance. The classical theory could not be expected to hold. A number of attempts were then made to use the first approximation of Born's quantum theory of collisions in order to derive the law of force. Such methods gave results of as little significance as those given by the classical theory. This is due to the fact that the first approximation of Born's theory calculates the scattering by integrating the amplitude of the spherical waves scattered from each element of a plane wave and neglects the contribution from the scattered waves themselves. For the case of particles moving in a powerful repulsive field this approximation is a very poor one, for the effect of the field is to prevent the wave penetrating within a certain effective diameter so giving no contribution to the scattered amplitude integral from the enclosed region. In Born's first approximation this is just the region which gives rise to the greatest contribution to the integrals concerned. As a consequence the first approximation gives much too great scattering and this was exhibited by the very small nuclear radius obtained with its use.

It is therefore necessary to obtain a more exact solution of the equation (7) representing the elastic scattering. Beck† considered this equation in general terms and showed how a qualitative interpretation of the experimental observa-

* ' Proc. Roy. Soc.,' A, vol. 133, p. 228 (1931).

† ' Z. Physik,' vol. 62, p. 331 (1930).

tions could be made in terms of the nuclear radius. The quantitative application of this method is very lengthy, but has been carried out by Taylor[*] for the scattering by hydrogen and helium with very interesting results. For the heavier light elements such as aluminium the complication of calculation is very much greater, and in any case it is clear that it is not possible to determine the nuclear field from the observations, for the following reasons. All that we can hope to obtain is the height of the potential barrier and a rough idea of the rate of fall of the potential near this peak.

Consider the impact of an α-particle on the nuclear potential field. Slow α-particles will not be affected by the field as their density in this region is, in any case, very small. Unless the α-particle penetrates appreciably the deviations from Rutherford scattering will not be great and can be considered merely as a small perturbation of that due to the Coulomb field. Measurements of such deviations will only give the radius of the nucleus and practically no information as to the internal field. When the α-particle penetrates considerably we may neglect the effect of the Coulomb field and the problem of the scattering of α-particles becomes precisely similar to the scattering of slow electrons by atoms. Owing to the overlap of the wave functions of nuclear and incident α-particles, α-particle exchange becomes important and also the perturbation of the nuclear field by the incident particle, just as in the case of the scattering of slow electrons by atoms. The introduction of these effects prevents any significant determination of the nuclear internal field. It is true that a field may be obtained which gives the observed results, but such a field is not of any great physical significance.

It appears then that it is only possible to determine the nuclear radius and this may be done by means of an approximate method which will now be described. This method only applies when the perturbation of the incident wave (by this is meant the wave incident in the Coulomb field, not a plane wave) is small and the scattering does not deviate greatly from classical scattering.

The equation for the elastic scattering without exchange is

$$\left[\nabla^2 + k^2 - \frac{8\pi^2 M}{h^2} V(r) \right] F_0 = 0, \tag{41}$$

where

$$V(r) = \int V(r, r_N) |\psi_0(r_N)|^2 \, dv_N, \tag{42}$$

---

[*] ' Proc. Roy. Soc.,' A, vol. 134, p. 103 (1931); ' Nature,' vol. 129, p. 56 (1932); and in course of publication.

and is the potential of the static field of the nucleus. We then write (41) in the form

$$\left(\nabla^2 + k^2 - \frac{8\pi^2 M}{h^2} \frac{Ze^2}{r} \right) \psi = \frac{8\pi^2 M}{h^2} V'(r) \psi, \qquad (43)$$

where $V'(r)$ represents the deviation of the potential from the Coulomb value. A solution of this equation is required which will tend asymptotically to the sum of an incident and scattered wave. To obtain this we expand the function ψ in the form

$$\psi = \Sigma_s A_s \psi_s(r) P_s(\cos \theta), \qquad (44)$$

giving

$$\frac{d^2}{dr^2}(r\psi_s) + \left[k^2 - \frac{8\pi^2 M}{h^2} \frac{Ze^2}{r} - \frac{s(s+1)}{r^2} \right](r\psi_s) = \frac{8\pi^2 M}{h^2} V'(r)(r\psi_s). \qquad (45)$$

In order to solve this equation approximately we consider the right-hand side as a known function by neglecting the effect of $V'(r)$ on the wave function ψ_s in the first approximation. Now it has been shown by Gordon* that solutions of the equation with $V'(r)$ zero may be obtained which have the asymptotic form

$$r L_s{}^c(r) \sim \cos \{kr - n \log 2kr - \tfrac{1}{2}(s+1)\pi + \sigma_s\}$$

$$r L_s{}^e(r) \sim \exp \pm i \{kr - n \log 2kr - \tfrac{1}{2}(s+1)\pi + \sigma_s\}, \qquad (46)$$

respectively. Here

$$n = \frac{4\pi^2 M e^2 Z}{kh^2} = \frac{2\pi Ze^2}{hv} \quad \text{and} \quad \sigma_s = \arg \Gamma(in + s + 1).$$

The first of these solutions is finite throughout space, and so is the solution which represents the scattering of waves by the Coulomb field. Gordon showed that

$$\Sigma_s A_s L_s{}^c(r) P_s(\cos \theta),$$

represents a plane wave of unit amplitude and the corresponding scattered wave, if

$$A_s = \frac{i^s}{k}(2s+1) e^{i\sigma_s}. \qquad (47)$$

Accordingly we take for the function on the right-hand side of (45)

$$\psi_s = \frac{i^s}{k}(2s+1) e^{i\sigma_s} L_s{}^c(r). \qquad (48)$$

---

* ' Z. Physik,' vol. 48, p. 180 (1928).

We then have to solve the equation

$$\frac{d^2}{dr^2}(r\psi_s) + \left(k^2 - \frac{8\pi^2 MZe^2}{r}\right)(r\psi_s) = \frac{8\pi^2 M}{kh^2} V'(r)\, i^s\,(2s+1)\, e^{i\sigma_s}\, r L_s^c(r). \tag{49}$$

The solution of this inhomogeneous equation may be obtained by using exactly the same methods as were used in Section 1, the functions $L_s^c(r)$, $L_s^e(r)$, corresponding to these functions $L_n^c(r)$, $L_n^s(r)$ of formula (17). We thus have for the solution

$$\psi_s = A_s L_s^c(r) + \frac{8\pi^2 M}{kh^2}\left\{ L_s^e(r)\int_0^r V'(r')\, L_s^c(r')\, L_s^c(r')\, A_s\, r'^2\, dr' \right.$$
$$\left. + L_s^c(r)\int_r^\infty V'(r')\, L_s^e(r')\, L_s^c(r')\, A_s\, r'^2\, dr'. \right\} \tag{50}$$

Using the asymptotic expressions (46) for $L_s^c(r)$, $L_s^e(r)$, we find for the asymptotic form of the approximate solution of (45), satisfying the required boundary conditions

$$\psi \sim \frac{1}{kr}\,\Sigma_s e^{i\sigma_s}\,(2s+1)\,[i^s\cos\{kr - n\log 2kr - \tfrac{1}{2}(s+1)\pi + \sigma_s\}$$
$$+ \frac{8\pi^2 M}{h^2}\exp i(kr - n\log 2kr)\, i^{-s}\int_0^\infty V'(r')\, L_s^c(r')\, L_s^c(r')\, A_s\, r'^2\, dr']\, P_s\cos\theta). \tag{51}$$

In order to sum this series we make use of parabolic co-ordinates as was first suggested by Gordon (*loc. cit.*) and carried out by Temple.* Using these co-ordinates it was shown that

$$\frac{1}{k}\,\Sigma_s e^{i\sigma_s}\, i^s\,(2s+1)\, L_s^c(r)\, P_s(\cos\theta) = e^{-\frac{1}{2}\pi n}\,\Gamma(1+in)\, e^{ikr\cos\theta}\, L(2ikr\sin^2\tfrac{1}{2}\theta, in), \tag{52}$$

where the function $L(u, n)$, has been expressed in the form

$$L(u, n) = \frac{e^u}{\Gamma(1+n)}\int_0^\infty x^n e^{-v}\, I_0\,(2\sqrt{ux})\, dx, \tag{53}$$

by Sommerfeld,† and has the asymptotic form

$$e^{ikr\cos\theta}\, L(u, n) \sim \frac{e^{\frac{1}{2}\pi n}}{\Gamma(1+in)}\left\{ e^{i(kr\cos\theta + n\log 2kr\sin^2\frac{1}{2}\theta)} \right.$$
$$\left. - \frac{n}{4kr\sin^2\frac{1}{2}\theta}\, e^{i(kr - n\log 2kr\sin^2\frac{1}{2}\theta + 2\sigma_s)} \right\}. \tag{54}$$

* 'Proc. Roy. Soc.,' A, vol. 121, p. 673 (1928).

† 'Ann. Physik,' vol. 5, p. 257 (1931).

In order to complete the summation we require also

$$\frac{1}{k} \Sigma_s e^{i\sigma_s} n^{-s} (2s + 1) L_s^c (r) P_s (\cos \theta),$$ (55)

which may be obtained from (52) by changing θ into $\pi - \theta$. We therefore obtain for (55)

$$e^{-\frac{1}{2}\pi n} \Gamma (1 + in) e^{-ikr \cos \theta} L (2ikr \cos^2 \tfrac{1}{2}\theta, in).$$

It is then easy to see that the series (51) may be summed to give

$$\psi \sim e^{i(kr \cos \theta + n \log 2kr \sin^2 \frac{1}{2}\theta)} - \frac{n}{2kr \sin^2 \tfrac{1}{2}\theta} e^{i(kr - n \log 2kr \sin^2 \frac{1}{2}\theta + 2\sigma_s)}$$

$$- \frac{2\pi M}{rh^2} e^{i(kr - n \log 2kr) - n\pi} \{\Gamma (1 + in)\}^2$$

$$\times \int V' (r') L (2ikr' \sin^2 \tfrac{1}{2}\theta', in) L (2ikr' \cos^2 \tfrac{1}{2}\Theta_1', in) e^{ik(n_s - n_1)} r' dv',$$ (56)

where n_0 and n_1 are unit vectors in the direction of incidence and observation respectively and θ', Θ', are polar angles measured with respect to these vectors as axes   The first term represents the incident wave, the second the wave scattered by the Coulomb field, the third that scattered by the "anomalous" field.   The ratio of the scattering to the classical value will then be given by

$$1 + \frac{k^2 \sin^2 \tfrac{1}{2}\theta}{4\pi Z e^2} e^{i(n \log \sin^2 \frac{1}{2}\theta - 2\sigma_s) - n\pi} \Gamma(1 + in)^2 \int V' (r') L\bar{\Omega} e^{ik(n_s - n_1)} r' dv' \Bigg|^2.$$ (57)

For $n = 0$ this degenerates into the ordinary first Born approximation.   To show how large n really is, its value for α-particles of velocity 2×10^9 cm. per second in the fields of various nuclei are given in the table.

Table I.

Element.	n.	Element.	n.
Aluminium	2 8	Beryllium	0 86
Magnesium	2·6	Helium	0 43
Carbon	1 3	Hydrogen	0 21
Boron	1 08		

The fact that the Born first approximation gives the correct formula for scattering by a pure Coulomb field is purely a coincidence owing to the quantity in disappearing from the actual expression for the scattered amplitude when

the intensity is obtained from it. This will not be the case when the field deviates from the Coulomb value.

5. *Calculation for an Exponential Form for* V'(r).

For simplicity we will take the case of

$$V'(r) = -\frac{Ae^{-\mu r}}{r}, \tag{58}$$

which is a reasonable form to represent the probable nuclear field near the top of the potential barrier. Choosing now parabolic co-ordinates

$$\xi = r'(1 + \cos\theta'), \quad \eta = r'(1 - \cos\theta'), \quad \phi,$$

the integral occurring in (57) takes the form

$$I = \frac{A}{2} \iiint e^{-\frac{1}{2}\mu(\xi+\eta)} L(ik\eta, in) L(ik\xi', in) e^{ik(\xi-\xi'+\eta'-\eta)} d\xi \, d\eta \, d\phi. \tag{59}$$

Here ξ', η' are parabolic co-ordinates with respect to the direction n_1 as axis and are connected with ξ, η by the relations

$$\xi' = \xi\cos^2\tfrac{1}{2}\theta + \eta\sin^2\tfrac{1}{2}\theta + 2\sqrt{\xi\eta}\sin\tfrac{1}{2}\theta\cos\tfrac{1}{2}\theta\cos\phi,$$

$$\xi' + \eta' = \xi + \eta. \tag{60}$$

Substituting in (59) the integral expression (53) for L $(ik\eta, in)$ we have

$$I = \frac{A}{2} \iiiint v^{in}e^{-v}I_0\{2(ik\xi'v)^{\frac{1}{2}}\} u^{in}e^{-u}I_0\{2(ik\eta u)^{\frac{1}{2}}\} e^{-\lambda(\xi+\eta)} du \, dv \, d\xi \, d\eta \, d\phi, \tag{61}$$

where $\lambda = \tfrac{1}{2}\mu - ik$.

In view of the expression (60) for ξ' we may expand

$$I_0\{2(ik\xi'v)^{\frac{1}{2}}\}$$

in the form[*]

$$I_0\{2(ik\xi'v)^{\frac{1}{2}}\} = \Sigma_m I_m\{2(ik\eta v)^{\frac{1}{2}}\sin\tfrac{1}{2}\theta\} I_m\{2(ik\xi v)^{\frac{1}{2}}\cos\tfrac{1}{2}\theta\}\cos m\phi \tag{62}$$

The integration over the ϕ co-ordinates reduces this sum to the first term only and we have

$$I = \pi A \iiint v^{in}e^{-v}I_0\{2(ik\xi v)^{\frac{1}{2}}\cos\tfrac{1}{2}\theta\} I_0\{2(ik\eta v)^{\frac{1}{2}}\sin\tfrac{1}{2}\theta\}$$

$$u^{in}e^{-u}I_0\{2(ik\eta u)^{\frac{1}{2}}\} e^{-\lambda(\xi+\eta)} du \, dv \, d\xi \, d\eta. \tag{63}$$

---

[*] Watson, " Theory of Bessel Functions," p. 358, Camb. Univ. Press (1922).

Using now the integrals*

$$\int_0^\infty e^{-\lambda\xi} I_0 \{2 (\imath k\xi v)^{\frac{1}{2}} \cos \tfrac{1}{2}\theta\} \, d\xi = \frac{1}{\lambda} e^{-\frac{\imath k v \cos^2 \frac{1}{2}\theta}{\lambda}},$$

$$\int_0^\infty e^{-\lambda\eta} I_0 \{2 (\imath k\eta u)^{\frac{1}{2}}\} \, I_0 \{2 (\imath k\eta v)^{\frac{1}{2}} \sin \tfrac{1}{2}\theta\} \, d\eta = \frac{1}{\lambda} e^{-\frac{\imath k}{\lambda}(v \sin^2 \frac{1}{2}\theta + u)} I_0 \left\{ \frac{\imath k}{\lambda} (uv)^{\frac{1}{2}} \sin \tfrac{1}{2}\theta \right\}, \tag{64}$$

we have, putting $v = \lambda x$, $u = \lambda y$,

$$I = \pi A \lambda^{2\imath n} \int_0^\infty \int_0^\infty e^{-\imath k (x + y)} (xy)^{\imath n} e^{-\lambda (x + y)} I_0 (\imath k \sqrt{xy} \sin \tfrac{1}{2}\theta) \, dx \, dy. \tag{65}$$

Expanding $I_0 (\imath k \sqrt{xy} \sin \tfrac{1}{2}\theta)$ in the power series

$$I_0 (\imath k \sqrt{xy} \sin \tfrac{1}{2}\theta) = \sum_r \frac{x^r y^r \sin^{2r} \tfrac{1}{2}\theta (\imath k)^{2r}}{(r\,!)^2}, \tag{66}$$

enables us to complete the integration term by term. The general term is then

$$\pi A \lambda^{2\imath n} \frac{(-k^2 \sin^2 \tfrac{1}{2}\theta)^r}{(r\,!)^2} \int_0^\infty \int_0^\infty e^{-(\lambda + \imath k) x} e^{-(\lambda + \imath k) v} x^{\imath n + r} y^{\imath n + r} \, dx \, dy$$

$$= \pi A \lambda^{2\imath n} (-k^2 \sin^2 \tfrac{1}{2}\theta)^r \left\{ \frac{\Gamma (r + \imath n + 1)}{r\,!} \right\}^2. \tag{67}$$

This gives finally for the integral, remembering $\lambda = \tfrac{1}{2}\mu - \imath k$,

$$4\pi A (\tfrac{1}{2}\mu - \imath k)^{2\imath n} \{\Gamma (1 + \imath n)\}^2 F \left(\imath n + 1, \imath n + 1, 1, -\frac{4k^2 \sin^2 \tfrac{1}{2}\theta}{\mu^2} \right) \tag{68}$$

and the ratio of observed to classical scattering

$$1 - \frac{A k^2 \sin^2 \tfrac{1}{2}\theta}{Ze^2} e^{\imath [n \log (\sin^2 \frac{1}{2}\theta (\frac{1}{4}\mu^2 + k^2))] - 2n (\frac{1}{2}\pi - \arctan 2k/\mu)}$$

$$\times |\Gamma (1 + \imath n)|^2 F \left(\imath n + 1, \imath n + 1, 1, \frac{-4k^2 \sin^2 \tfrac{1}{2}\theta}{\mu^2} \right) \tag{69}$$

since

$$(\tfrac{1}{2}\mu - \imath k)^{2\imath n} = e^{\imath n \log (\frac{1}{4}\mu^2 + k^2) + 2n \arctan 2k/\mu}. \tag{70}$$

This formula reduces to that given by the Born first approximation if one puts $n = 0$. It is clear from (69) that one would expect the anomalous scattering to increase more rapidly with increase of velocity than with increase of angle of scattering, a behaviour observed with aluminium. The detailed numerical application of the formula (69) will be carried out in a later paper.

* *Ibid.*, pp. 393, 395.

6. *Validity of Approximations.*

In order to consider the conditions under which the above discussed theory is valid, one may follow a method similar to that used in discussing the validity of the first approximation of Born's theory. The deviation of the scattering from Coulombian scattering may be represented in terms of the differences of phase between the scattered waves of various orders and the corresponding wave scattered by a purely Coulomb field. If this difference of phase is small compared with unity for all, then the above theory will be accurate. For the scattering of α-particles by helium the phases have been calculated by Taylor (*loc. cit.*) for the anomalously scattered waves of zero order, these alone being of importance. In the case of the low velocity particles (velocities from $1 \cdot 1$ to $1 \cdot 4 \times 10^9$ cm. per second) the phases are quite small, being approximately $0 \cdot 1$ radians. It thus appears that the above theory is applicable for these velocities in helium and so will be applicable to the collisions of still faster particles with heavier nuclei.

In order to obtain a condition of validity in mathematical form it is only necessary to relate our formula (51) with the one given by Taylor (*loc. cit.*) when only the zero order wave is disturbed. If K_0 is the phase difference from the Coulomb scattered wave, Taylor shows that the asymptotic form of the anomalously scattered wave is

$$\frac{(e^{2iK_0} - 1)}{2ikr} e^{i(kr - n \log 2kr + 2\sigma_0)}. \tag{71}$$

This is to be compared with our formula (51) which gives for the zero order wave

$$\frac{8\pi^2 M}{kh^2 r} \int_0^\infty V'(r') L_0^c(r') L_0^c(r') r'^2 dr' \, e^{i(kr - n \log 2kr + 2\sigma_0)}. \tag{72}$$

The condition of validity of the approximate theory is then that

$$K_0 = \frac{8\pi^2 M}{h^2} \int_0^\infty V'(r') L_0^c(r') L_0^c(r') r'^2 dr' \ll 1. \tag{73}$$

By analogy with the corresponding criterion for the validity of Born's first approximation in its application to the scattering of electrons by atoms it is probable that K_0 does not have to be much less than $0 \cdot 5$ in order that the above criterion be satisfied.[*]

---

[*] J. McDougall, 'Proc. Roy. Soc.,' A, vol. 136, p. 549 (1932).

Summary.

The collision of α-particles with atomic nuclei is discussed, using a quantum theory of collisions which allows for the disturbance of the incident wave by the Coulomb repulsive field of the nucleus. In particular, the probability of α-particle exchange is considered and shown to be large at a resonance level.

The theory is also applied to the anomalous scattering of α-particles by light nuclei and its range of applicability to such cases considered. In connection with experimental results the theory should provide a means of accurately determining the radii of light nuclei.

The Surface Ionisation of Potassium by Tungsten.

By P. B. Moon and M. L. E. Oliphant.

§ 1. It is well known that atoms of low ionisation potential may be ionised by contact with a hot metal surface. If, for instance, a positively charged hot tungsten filament be surrounded by the vapour of potassium, rubidium or cæsium the filament will lose positive charge at a rate governed by the vapour density of the alkali metal and very nearly independent of the temperature of the filament if this temperature be not too low. From this independence the conclusion is drawn that all (or very nearly all) atoms which strike the filament evaporate in the ionic state ; in other words, the efficiency of the surface as an ionising agent is nearly perfect. The objection might perhaps be raised that this conclusion is not strictly justified by the experimental evidence which merely shows the efficiency to be *constant*. It would, of course, be remarkable if the constant were other than unity, but further evidence is clearly desirable and has been given by Langmuir and Kingdon[*] in their discussion and extension of Saha's theory of the equilibrium of ions. electrons and atoms. Their calculations account for the low efficiency and its large temperature variation in cases where the " electron work-function " of the surface is less than the ionisation potential of the atom, and predict perfect efficiency when the work-function greatly exceeds the ionisation potential. A

---

[*] ' Proc. Roy. Soc.,' A, vol. 107, p. 61 (1925).

direct verification that the efficiency of surface ionisation is, in a favourable case, indeed unity, is provided by the observation made by one of us* that no net current flows to a sufficiently hot nickel surface bombarded by slow Cs^+ ions For fast ions, however, the efficiency was found to decrease.

It is the purpose of this paper to show how surface ionisation may provide the source of a beam of positive ions which has great intensity, steadiness and length of life, and to describe some experiments in which we have used this source for the more detailed investigation of the drop in ionisation efficiency which occurs (as already noted in the case of Cs^+) when *fast* K^+ ions strike a hot target   Moon's previous observation dealt only with the equilibrium state of the re-emission from the target ; in the present work we have studied the building up and breaking down of this equilibrium when the incident beam is switched on or off   It should be stated at once that we have found the process to be complicated and have attempted no more than a qualitative study of its more important features. Tungsten was chosen as the target material on account of the ease with which it may be cleaned by flashing to a high temperature, while K^+ ions were used in preference to Cs^+ because the temperatures at which the phenomena under investigation occur are higher and more readily measured by optical pyrometry.

Apparatus.

§ 2. The experimental tube was constructed as follows.   A vertical tube AB, fig. 1, of pyrex glass, was divided into two portions by a glass partition into which was sealed a nickel plate pierced with a slit 4 mm. × 0·3 mm.   The seal was made by spot-welding a spiral of tungsten wire round the cylindrical collar to which the plate was also spot-welded   Pyrex adheres much more satisfactorily to tungsten than to nickel, and the corrugated nature of the surface is a further advantage in this connection.   Parallel to the slit and less than a millimetre above it was a tungsten strip 8 mm. × 2 mm. × 0·08 mm. welded to stout nickel leads and carried on a heavy-current pinch at the upper end of the tube.   This strip was heated to about 1000° C. by alternating current.   The upper part of the tube carried a side-tube into which a small quantity (about 1/10 gram) of potassium was eventually introduced.   The side-tube originally ended in a series of bulbs which served as stills for the purification of the potassium ; as each stage of the distillation was completed the corresponding bulb was sealed off and removed so that eventually only a

* Moon, ' Proc. Camb. Phil. Soc.,' vol. 27, p. 570 (1931).

short side-tube remained as at V. The upper half of the tube AB was maintained at a temperature of about 120° C., while the side-tube was at about 80° C., so that the vapour pressure of potassium in the upper half of AB was in the neighbourhood of 3×10^{-6} mm The hot tungsten strip then acted as a surface-ionisation source of K^1 ions, the total emission under normal working conditions being a few microamperes. By raising the potassium vapour

pressure it was easy to increase the emission to a milliampere, and there seems to be no reason, apart from space-charge limitation, why it should not be increased still further if desired. The source was maintained at a positive potential of 20–200 volts with respect to the neighbouring nickel plate, and a few per cent. of the total emission passed through the slit S_1 into the lower half of AB, which constituted the experimental chamber. The intensity of this beam was, of course, mainly determined by the temperature of the side tube containing the potassium, but variation of the accelerating voltage between the strip and the slit system provided an intensity control useful over a three- or four-fold range, for if this voltage be reduced the current from the strip becomes limited by space-charge. It is unwise to reduce the accelerating voltage too far or the parallelism of the beam may be much impaired. The source was found to work very steadily and consistently when temperature equilibrium
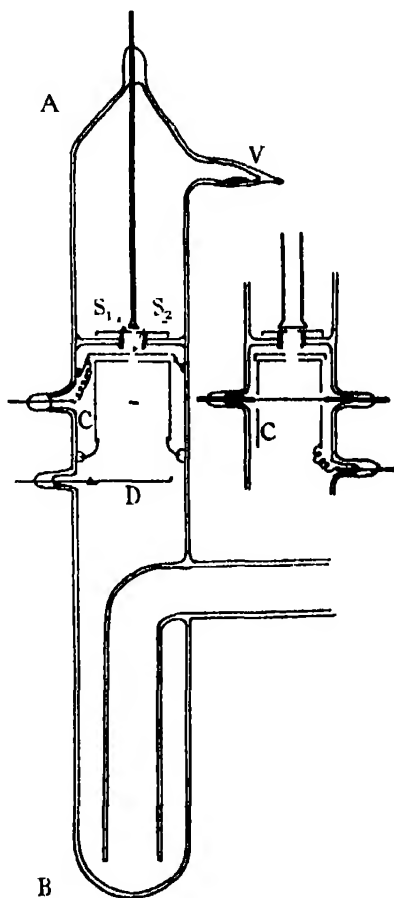
FIG. 1.

had once been attained; we have not so far had the opportunity of testing either its purity or its life, but it may be remarked that the only impurities likely to be present are ions of those elements (Rb and Cs) whose ionisation potentials are less than the electron work-function of tungsten,[*] and that the

---

[*] Oliphant, in recent unpublished experiments, finds a few per cent of Na^+ ions always present with commercial potassium. The significance of this, especially in connection with the "ageing" of a clean target, has not yet been determined.

distillation in ionic form of a gram of potassium requires the passage of nearly 2500 coulombs of electricity.

In addition to the K^+ beam the strip will emit some neutral potassium atoms, particularly if the slit system be positively charged with respect to the source. This neutral beam, whose general direction was downwards through the slit, was useful as a weak source of potassium atoms ; the ionic beam could have been separated from it, if required, by an electric field. On the other hand, any atoms which pass through S_1 from the glass walls of the tube will necessarily travel obliquely and will not strike the target. They are objectionable not only as a waste of potassium but also because it is desirable that the vapour-pressure of potassium in the lower half of the apparatus should be as low as possible ; their number was kept small by using a strip wider than the slit and close to it, so that the glowing tungsten, from which the emission was mainly of positive ions, occupied nearly the whole " field of view " of the slit S_1.

The ionic beam was ultimately defined by a slit S_2, parallel to the first and of the same dimensions, in a second nickel plate about a centimetre from S_1. The beam next passed through a wider slit in the circular closed end of the nickel cylinder C, which formed the experimental chamber. It then struck the target, which consisted of a strip of tungsten $1 \cdot 3$ mm. wide and $0 \cdot 08$ mm. in thickness stretched diametrically across the cylinder and passing through holes in its walls to tungsten seals in the walls of the tube. The lower end of the cylindrical experimental chamber was partially covered with a grid of nickel wires ; at about a centimetre below this grid was a nickel disc D whose purpose was to catch any positive ions which might by mischance fail to strike the target, and to prevent them from charging the glass walls of the tube and so distorting the electric field within the experimental chamber.

The gap between the cylinder and the beam-catching plate enabled the target to be viewed through an optical pyrometer. The pyrometer was used to find the temperature of the target in terms of the heating current which was then used as a measure of the temperature ; this procedure was employed because changes of temperature which are, for the purposes of these experiments, of more importance than actual temperatures, were most reliably estimated by the changes in heating current required to produce them. The usual emissivity correction was made.

The extreme lower end of the tube formed a mercury trap of " reversed " design, cooled in liquid nitrogen, which led to the pumps and the McLeod gauge ; by this means the pressure of all vapours—including potassium—in

the lower half of the tube was reduced to a very low value. All metal parts were glowed *in vacuo* by an eddy-current heater after assembly in the apparatus, and the glass was thoroughly baked before the introduction of the potassium into the end bulb, which latter operation was performed as quickly as possible. The distillation of the potassium from one bulb to another was done slowly with the pumps working meanwhile, after the distillation was complete the apparatus was pumped for some hours before the experiments were started. With both strips hot and the source chamber at its working temperature the McLeod gauge read zero. It was found that the main source chamber could be kept at about 120° C. by the heat developed in the source strip provided that the upper half of the tube were suitably lagged ; a small heating coil was provided to maintain the side-tube V at the appropriate temperature.

The target strip was heated by a battery of accumulators so controlled by switches and variable resistances that, by the simple operation of the switches, it could be heated to any one of three temperatures previously determined by the settings of the resistances. All such apparatus in electrical connection with the target was thoroughly insulated and surrounded by earthed shields ; a lead was taken from it to the amplifier and oscillograph which served to measure the current reaching or leaving the target. The design of the current measuring system and of the photographic recording arrangements will not be discussed here ; their interest is mainly technical. The oscillograph had a natural frequency of about 50 per second and the system had an overall sensitivity of $3 \cdot 08 \times 10^{-9}$ amperes per millimetre. The currents measured were of the order of 10^{-7} amperes. The more important electrical connections are shown in fig. 2 ; the current measuring apparatus and such subsidiary details as shielding arrangements are omitted. The slit S_2 and the disc D were kept slightly positive with respect to the cylinder so that slow secondary electrons set free from them should not reach the experimental chamber. The positive ion beam was accelerated between S_1 and S_2, when required, by a voltage, variable between 0 and 10,000 volts, derived from cells or from a transformer-rectifier set. The beam could be cut off by opening the switch Q. By means of the double-contact key K the target could be made either 20 volts positive or 20 volts negative with respect to the surrounding cylinder, the emission of positive ions from the tungsten being thus either allowed or prevented.

The Evaporation of K¹ Originally Deposited as very Slow Ions.

§ 3. The source was made hot, but was electrically isolated from S_1 ; there was then no appreciable positive ion beam but only a small beam of atomic

potassium striking the target. The target was cleaned by flashing to about 2000° C.; its temperature was then lowered to, say, 750° C. and its potential was made 20 volts negative with respect to the surrounding cylinder so that
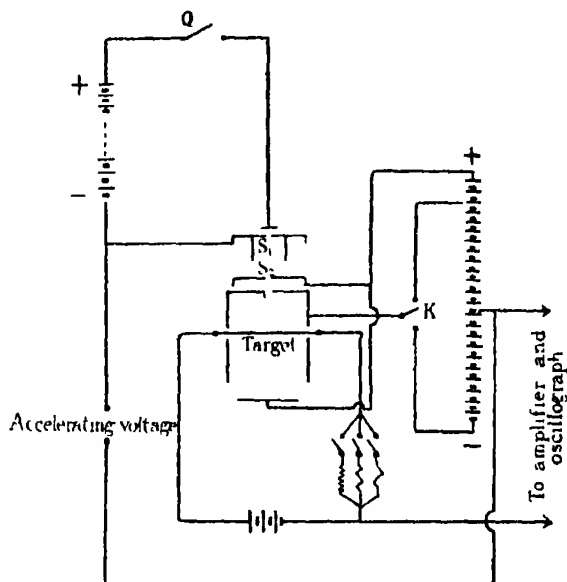
Fig. 2.

no positive ions could leave it. The field was now suddenly reversed, thus releasing the ions, and after a few seconds the target was raised to a temperature of 1250° C. Let us consider what we may expect to happen.

The clean target at 750° will receive a small atomic beam ; the atoms which strike it will, after a short stay on the surface, evaporate again, a few as neutral atoms but the great majority as K^+ ions. The ions, having only thermal energies, will be turned back by the opposing field and will strike the target again with the energies with which they left it. As time goes on more and more potassium reaches the surface by way of the atomic beam ; the amount of potassium in the surface layer will therefore increase until the rate of evaporation *in the atomic form* ($i^{\times}$) is sufficient to balance the rate of arrival of atoms in the beam. When this state is reached, however, the majority of the atoms in the layer have made many ineffectual attempts to leave the target and therefore last struck the surface as slow positive ions. The rate of arrival of slow ions will in fact exceed that of neutral atoms in the ratio of the rates of evaporation of ions and atoms—a ratio which in the present experiments was always large. Even long before equilibrium has been reached the greater

part of the potassium on the surface will have made its most recent collision with the surface not as an atom but as an ion. On the reversal of the electric field the departure of ions is no longer prevented and the target will immediately lose positive charge at a rate i^1 which will decrease with time as the concentration of the potassium layer sinks to the low equilibrium value at which the arrival rate is equal to $(i^\times + i^+)$ Fig. 3 illustrates in an exaggerated manner what we should anticipate and what is, in fact, found. The current i^+ leaving the target*—zero while the target is negative—is of amount AC immediately
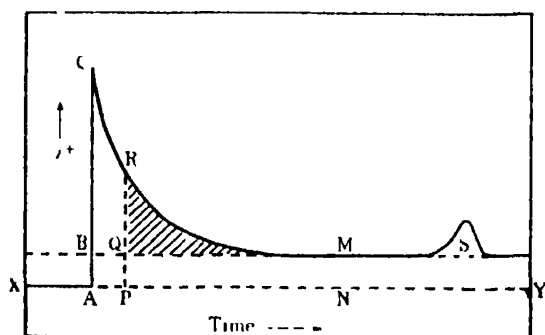
FIG. 3.

on reversal of the field, it decreases with time until it finally reaches a steady value AB. The rate AB plus the rate of evaporation of atoms from the surface in the same new equilibrium conditions will together equal the rate of arrival of potassium in the beam, so that if we neglect $i^\times$ in comparison with i^+ we may regard AB as representing the arrival rate. If we knew the final equilibrium amount of potassium on the surface we should be able to deduce from the experimental curve the relation between i^+ and the surface concentration; if, in fact, we draw any ordinate PQR then PR represents the value of i^1 at a surface concentration given by the sum of this equilibrium concentration and the shaded area QRM. This may be seen on considering that the concentration at the time N is (very nearly) the equilibrium concentration, the amount of potassium which has arrived during the time PN is given by PQMN, while the amount evaporated as ions during this time is given by PRMN, the net loss during the time PN is, therefore, QRM. We can obtain at least an upper limit to the equilibrium concentration by finding the area S of the " throw " obtained when the target is suddenly flashed to 1250°, for at so high a temperature the equilibrium layer

---

* In this and all subsequent figures an upward displacement of the curve from the dotted zero line XY indicates that the target is losing positive charge.

will be negligible and the sudden rise of temperature will cause the almost complete evaporation of the existing layer. The glowing of the target strip will also increase the length of strip which is hot enough to emit positive ions at a measurable rate, and a portion of the observed throw will be due to evaporation in the ionic form of potassium which had accumulated (owing to diffusion from the centre of the strip or to stray atoms from the original neutral beam) on the cooler parts of the strip. It is possible, too, that a small amount of potassium may diffuse into the metal and be retained there until the moment of flashing. Subject to these uncertainties, which are relatively only of importance at low surface concentrations, we may obtain from the experimental evaporation curve the relation between i^+ and surface concentration for all values of i^+ between AC and AB.
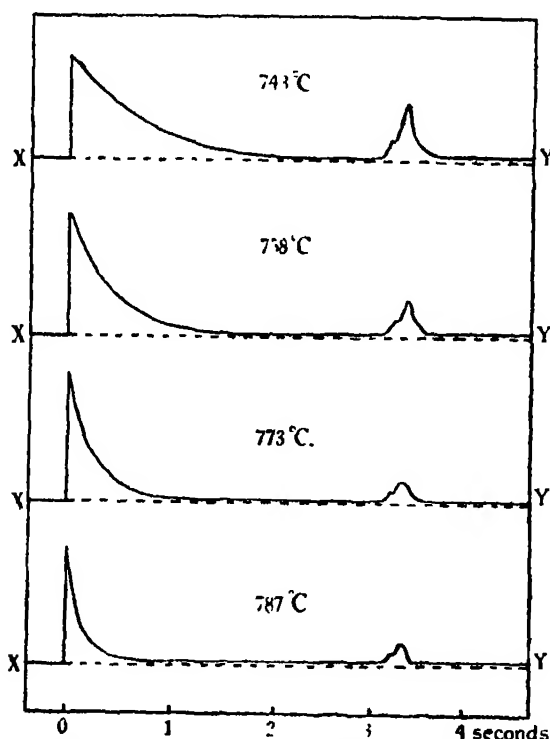
Fig. 4.—Evaporation curves for K$^+$ ions deposited with thermal energies on W.

Fig. 4 shows the results of such experiments made at target temperatures of 743° C., 758° C., 773° C., and 787° C. In order to avoid delay a set of records such as this was taken on a single sheet of photographic paper, and the superimposition of the four records gives a misleading impression of complexity.

The curves reproduced in fig. 4 and subsequent figures are for this reason (and for economy of reproduction) drawings carefully made to scale from the originals. All measurements were, of course, made on the photographs themselves.

In fig. 5 we give in graphical form the results of the analysis of these four experimental curves. It will be seen that in each case the rate of evaporation of positive ions (i^+) is a linear function of the surface concentration. That
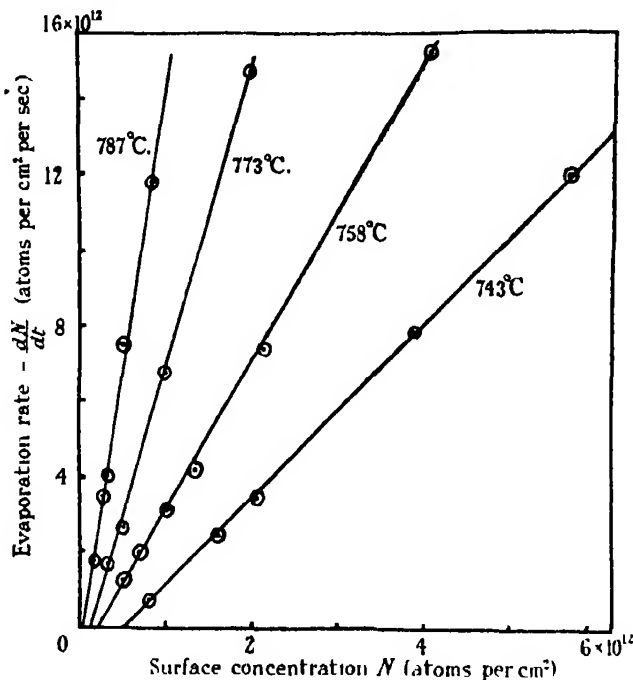
Fig. 5 —Analysis of curves of fig. 4.

the lines do not pass through the origin may be due to one or both of the uncertainties already discussed ; we see no significance in their convergence towards a point on the axis of i^+. The lines of fig. 5 show that over the ranges of temperature and concentration investigated, the mean time of life of a potassium ion upon a tungsten surface before its evaporation in the ionic state is uninfluenced by the addition of more potassium to the layer already on the surface. We are therefore almost certainly justified in concluding that our results represent the evaporation characteristics of isolated ions.* The concentrations dealt with in these experiments are, of course, very low, the greatest

* It is, of course, conceivable that we are dealing with *clusters* of ions each evaporating as an entity.

concentration shown in fig. 5 being less than 1 per cent. of that in a monatomic layer of potassium.

Some interest attaches to the variation with surface temperature of the rate of evaporation per unit concentration, for if this quantity, which is given by the slope of a line such as those of fig 5, varies, over a small range of temperature, as $e^{-\phi/\kappa\tau}$, where T is the absolute temperature and K is Boltzmann's constant, we may probably identify ϕ with the energy required to remove a K^+ ion from the surface.

The four points of fig. 6 show the logarithms of the slopes of the four lines of fig. 5 plotted against the reciprocals of the corresponding absolute temperatures. The straight line drawn among these points leads to a value of $4 \cdot 4$
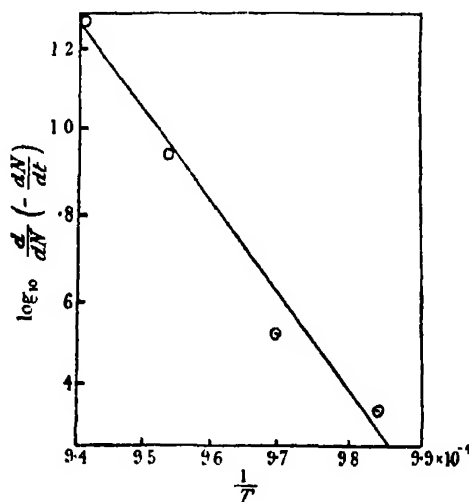
Fig. 6.—Temperature dependence of slopes of lines of fig. 5.

electron-volts for ϕ; none of the points lies further from the line than would correspond to an error of $4°$ in the temperature measurement, but it is plain that the measurements were taken over a range of temperature insufficient to give more than a very rough value of ϕ. Much the same value for ϕ was obtained from other evaporation curves.

The Ionic Evaporation of Potassium Deposited as Fast Positive Ions.

§ 4. Experiments for the study of the influence on the evaporation characteristics of the speed with which the ions hit the surface were carried out as follows :—

A positive ion beam was allowed to fall upon the target for any desired period and was then suddenly removed by opening the switch Q. The variation in the current to the target was recorded.

By this means we obtain a curve showing the rate at which ions are leaving the surface at various times after the removal of the beam. It was found that the evaporation curves were functions not only of the target temperature and of the velocity of the impinging ions but also of the length of time for which the beam had been striking the target before being cut off. The intensity of the beam had a slight influence upon the form of the curve. The evident complexity of the phenomenon rendered impossible, for the time being, anything more than a general qualitative investigation; it also leads to difficulty in the clear presentation of the results We have thought it best to give diagrams of a few only of the many curves obtained; the examples are chosen with a view to setting forth what appear to be the more important features of the experimental results.

The first point of interest is the magnitude of the sudden change in current to the target which occurs at the instant of cutting off the beam. This was found to differ from the beam itself (as measured by the current reaching the. target when cold or, better, by the total current reaching target plus surrounding cylinder at any temperature) by not more than a few per cent. It is an immediate conclusion that nearly all the potassium ions which leave the target do so not as a result of instantaneous reflection but by means of thermal evaporation, for any reflected current would be cut off with the beam and the net sudden change would be less than the beam by the corresponding amount.

Fig. 7 (1) shows the result of cutting off a beam of 230-volt ions which had been striking the target for a long time. The final current to the target is, of course, to be taken as zero, and it will be seen that in the initial equilibrium state (with the beam on) the target is receiving a net positive charge which is an appreciable fraction of the beam. The decay of the rate of evaporation after removal of the beam is roughly, but not quite, exponential. Fig. 7 also shows corresponding curves at the same temperature but at higher voltages. The number of ions which evaporate positively charged* is smaller at these higher voltages, while the evaporation curves depart still more from the exponential form. The remarkable feature now appearing is the very slow rate of change of the evaporation rate near the beginning of the process It will be observed that for a time the rate may even increase slightly.

---

* The ratio of this number to the number arriving will be called the "ionisation efficiency."
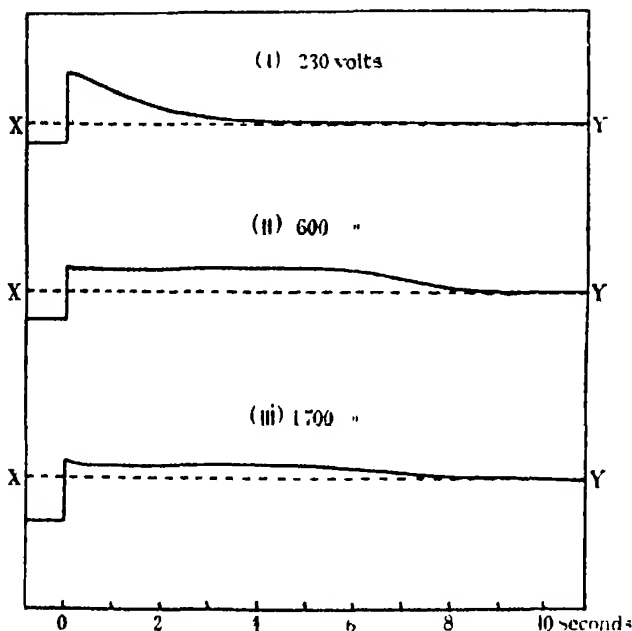
FIG. 7.—Evaporation curves at 767° C

The influence of target temperature at a fixed voltage is shown in fig. 8. It will be seen that, roughly, an increase in temperature has a similar effect to a decrease in voltage. The first curve, taken at a relatively high temperature, shows an ionisation efficiency of 94 per cent.

All the above experiments were made after the target had been exposed for some minutes to the beam in question. Fig. 9 illustrates the influence of the length of time for which the target, after being cleaned by flashing to 2000° C and allowed to cool to the experimental temperature of 793° C, had been exposed to a beam of 940 volt ions. It will be seen that a considerable time of exposure to the beam (long compared with the time scale of the evaporation process) is required before the target is capable of re-emitting K^+ ions. It was verified that the essential requirement was exposure to the *beam* and not merely to the " vacuum."

When the surface has thus been brought to a condition in which it can re-emit positive ions the removal of the beam does not cause it to return to the original state of a freshly cleaned surface. This is illustrated by fig. 10, which represents the effect of switching the beam on and off when the target had previously been subjected to long bombardment by the ions. The influence of time of exposure before removal of the beam is again very marked, but the
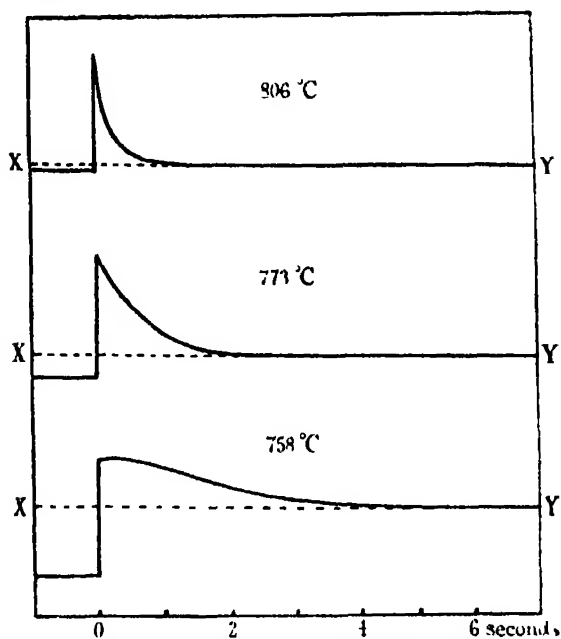
FIG. 8.—Evaporation curves at 340 volts
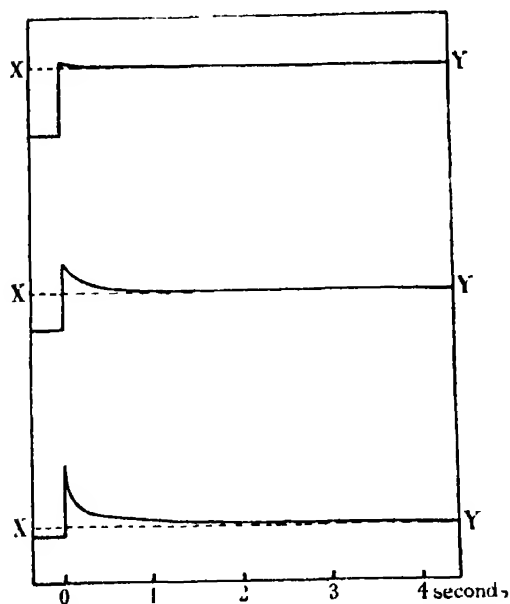
FIG. 9.—Effect of time of exposure to 940 volt beam; target previously cleaned by glowing at 2000° C. Experimental temperature, 793° C. Exposures of 2 seconds, 15 seconds and 100 seconds respectively.

initial stage of fig. 9, in which re-emission of K^+ is almost zero, is not repeated. The bombardment must, therefore, cause some change in the target which time
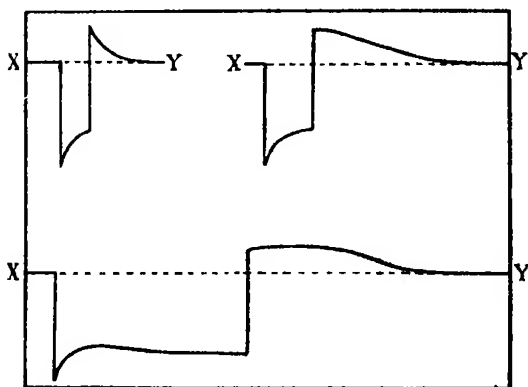
Fig. 10 —Beam switched on and off.   Target rested but not flashed between exposures.
758° C., 365 volts.

alone will not eradicate completely.   One would anticipate, perhaps, that if slow and fast ions were to fall simultaneously upon the target the rate of evaporation of the slow ions would also be governed by this change in the properties of the target.   It is easy to test this experimentally.   If, while the high-speed ion beam is striking the target, we reverse for a moment the field between the target and the surrounding cylinder we shall accumulate upon the target surface a layer of potassium which (although originally derived from the high-speed beam) last struck the target with thermal velocities only. When we restore the field to its original direction these ions will be able to leave the target, but they evaporate from a surface which is—and has been throughout the experiment—bombarded by high-speed ions   Fig. 11 (ii) shows the result of such an experiment , on comparing this curve with the evaporation characteristics at the same temperature of the high-speed ions themselves, fig. 11 (i), and with those of slow ions* in the absence of the high-speed beam, it will be seen that bombardment of the target by fast ions does not affect the evaporation of slow ions   It seems, therefore, that the complicated laws of evaporation of fast ions are not due to changes in the properties of the surface.   We had at one time a fear that some ions might find their way past the plate D and communicate a charge to the glass walls of the tube, and that some of our results might be due to the variation of this charge with the voltage of the beam and with time.   Mr. R. C. Evans, who is studying surface

* Obtained as in § 3.

ionisation problems at the Cavendish Laboratory, very kindly repeated some of our experiments with a slightly modified apparatus in which this possibility was entirely absent. His results are in substantial agreement with ours and show that such an effect is not the cause of the phenomena which we have described. We are grateful to Mr. Evans for permission to mention this unpublished work.

Fast Ions (940v)

Slow Ions

Slow Ions in presence of Fast Ions
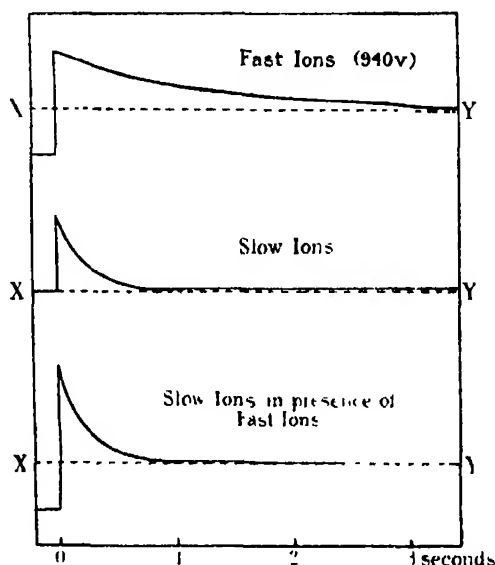
Fig 11.—764° C

Summary and Discussion of Experimental Results.

We have found that—

(i) K^+ ions of thermal velocities are re-emitted from a hot tungsten target in a manner consistent with the thermal evaporation of isolated particles.

(ii) If the target be sufficiently hot, 780° C. or more, the result (i) extends approximately to ions of energies in the neighbourhood of 300 volts. A positively charged target in this case receives only a small net current, the efficiency of surface ionisation being near unity.

(iii) At higher energies, or, if the temperature be below about 780°, even below 300 volts, this behaviour is departed from in two ways :—

(a) Only a fraction of the incident beam evaporates in ionic form.

(b) Those ions which are re-emitted as ions yield, on the removal of the incident beam, " evaporation curves " differing markedly from the

exponential form associated with cases (i) and (ii). The most striking feature which may appear is an almost constant evaporation rate which persists for some time before the drop towards zero commences.

(iv) The phenomena of (iii) are much influenced by the amount of previous bombardment undergone by the target.

(v) The ratio of evaporation of potassium deposited as slow ions is not influenced by the simultaneous bombardment of the target by high-speed ions.

(vi) On the sudden removal of the incident beam the net current to the target changes by an amount equal to the beam.

We draw the following conclusions :—

(α) The re-emission of K^+ ions from a hot tungsten surface on which they impinge with high velocity is, as for slow ions, a process of evaporation ("surface ionisation") rather than instantaneous reflection. This follows from (vi).

(β) Since, by (v), the properties of the metal *surface* as an ionising agent are unaltered by the high-speed beam, the altered form of the evaporation curve for fast ions must be a property either of the ions themselves or of the interior of the metal as influenced by the bombardment. Now the evaporation process occupies a time of the order of a second, and the only trace of its previous history which an ion on or in a metal can retain for such a time is its position. It would seem to follow that the observed phenomena are due to the penetration of fast ions below the surface of the metal. It is interesting in this connection to note that Brewer[*] has found that the deposition of K^+ ions upon an iron surface affects the photoelectric properties of the surface somewhat less at 270 volts than at lower energies of the ions. This observation suggests that fast ions do not remain on the surface but, of course, gives us no hint as to whether they remain inside the surface or leave the target entirely.

(γ) Since the failure of a proportion of fast ions to evaporate again as ions is always associated with a non-exponential evaporation curve, it is likely that the same ultimate cause is responsible for both phenomena. The observation that the ionisation efficiency for fast ions is greater at oblique than at normal incidence[†] would be in accordance with this view. We can conceive of only

---

[*] 'Phys. Rev.,' vol. 38, p. 401 (1931).

[†] Moon, *loc cit.*

three ways in which the ionisation efficiency can fall below unity.   The missing ions must either—

    (i) remain on or in the metal surface ;

    (ii) be reflected as neutral atoms ; or

    (iii) evaporate as neutral atoms.

It should not be difficult to distinguish experimentally at least the first of these possibilities from the other two, and it seems inappropriate to discuss the matter until such discriminatory experiments have been made.   We would, however, suggest that if the first of these three alternatives should prove correct an explanation will probably have to be sought in terms of the diffusion back to the surface of those ions whose initial energies suffice to carry them through the surface into the body of the metal   If it be assumed that potassium diffuses through hot tungsten in accordance with the usual diffusion law, and if, furthermore, all atoms which diffuse further into the metal than a certain distance from the surface are permanently retained and take no further part in the diffusion process, we calculate evaporation curves whose forms are very similar to the experimental curves such as are illustrated in figs. 7 and 8.   The correlation of the form of the evaporation curve with the efficiency of surface ionisation is given in a manner which is qualitatively correct   The calculations do not at the moment rest on any secure experimental basis and we do not stress what may well be a quite fortuitous agreement ; we allude to them only to show that penetration of the surface may lead to very considerable complication of the simple law of ionic evaporation which holds for isolated atoms or ions deposited at low velocity.

    (δ) It remains to consider the possibility that, in those experiments with fast ions in which the target had been exposed to the beam for some time, the surface concentration had become so high that the ions were not evaporating as independent ions from a clean surface.   It is known[*] that at surface concentrations of the order of one-tenth of a monatomic layer the evaporation rate is no longer proportional to the number of ions present and at higher concentrations it actually decreases.   We have shown that such deviations are inappreciable up to surface concentrations of 6×10^{12} atoms per cm.^{2}, but it should be mentioned that in some of the experiments with fast ions the total area beneath the evaporation curve corresponds to as much as three times this concentration.   Reference to fig. 11 will, however, show that even the

* J. A. Becker, ' Phys. Rev.,' vol. 28, p. 341 (1926).

end of the evaporation curve for fast ions differs markedly from that for slow ions at the same temperature, so that although the phenomena of the initial stages of the curves may be connected with departure from proportionality of surface concentration and rate of evaporation, there yet remains the definite difference between the evaporation characteristics of slow and fast ions.

The Condensation of Bromal with Urea.

By Frederick Daniel Chattaway, F.R.S., and Eric John Francis James.

Urea condenses readily with 1 or 2 molecules of bromal forming respectively *monobromal urea* (I), and *dibromal urea* (II)

$$CBr_3 . CH(OH) . NH . CO . NH_2$$

I

$$CBr_3 . CH(OH) \quad NH . CO . NH . CH(OH) . CBr_3$$
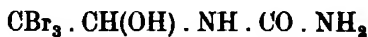
II

The condensation proceeds somewhat less readily than does the corresponding reaction with chloral When, for example, the compounds are left in aqueous solution, monobromal urea only is formed, even when excess of the aldehyde is used.

The monobromal urea thus produced condenses normally with a second molecule of bromal only when the two compounds are melted together and heated for a time at 100°.

When monobromal urea is heated with one equivalent of chloral, an identical condensation occurs and bromal chloral urea (III),* is produced, the same compound being also formed when monochloral urea is similarly heated with an equivalent of bromal.
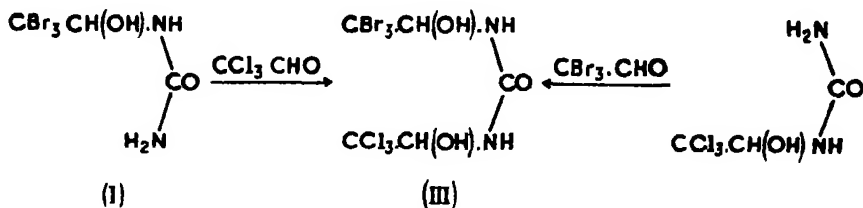
All these condensation products behave very similarly to the corresponding chloral compounds.

* *Cf.* 'Central,' vol. 1, p. 547 (1902).

They react with acetic anhydride and yield well-crystallised *diacetyl derivatives.*

$$CBr_3 CH(OAc) NH \diagdown CO \diagup AcHN$$

$$CBr_3 CH(OAc).NH \diagdown CO \diagup CBr_3.CH(OAc).NH$$

$$CBr_3.CH(OAc).NH \diagdown CO \diagup CCl_3.CH(OAc).NH$$
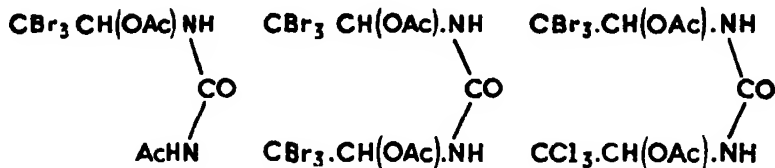
Bromal urea, dibromal urea, and bromal chloral urea, all dissolve readily in aqueous alkalis, giving solutions from which on the addition of acetic anhydride dimolecular *anhydro compounds* of ether-like structure separate. For example, monobromal urea yields bis-(α-*carbamido*-$\beta\beta\beta$-*tribromo ethyl*) *ether* (IV), and dibromal urea yields the compound (V).

$$CBr_3CH \, NH \, CO \, NH_2 \diagdown O \diagup CBr_3CH \, NH \, CO \, NH_2$$

(IV)

$$CBr_3CH \, NH \, CO \, NH.CH \, CBr_3 \diagdown O \qquad O \diagup CBr_3 CH \, NH \, CO \, NH \, CH \, CBr_3$$

(V)
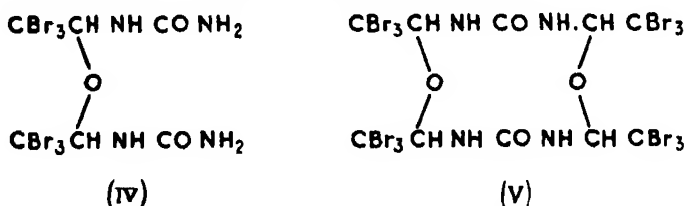
When any one of these ethers is added to a solution of a sodium alkoxide in the appropriate alcohol, it reacts exactly as the corresponding chloral compound, but rather more rapidly. Fission occurs at the ether linkage, and the corresponding *alkoxy compound* results, the other half of the molecule decomposing into bromoform, sodium formate, and urea. Series of compounds of the general formula (VI) and (VII) are thus produced.

$$CBr_3 . CH . NH . CO . NH_2$$
$$|$$
$$OR$$

(VI)

$$CBr_3 . CH . NH . CO . NH . CH . CBr_3$$
$$| \qquad\qquad\qquad |$$
$$OR \qquad\qquad\quad OR$$

(VII)
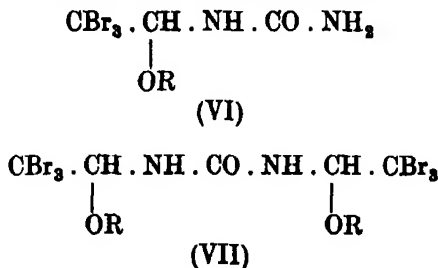
The anhydro compound formed by bromal chloral urea yields similarly dialkoxy compounds of the constitution

$$CBr_3 . CH . NH . CO . NH . CH . CCl_3$$
$$| \qquad\qquad\qquad |$$
$$OR \qquad\qquad\quad OR$$
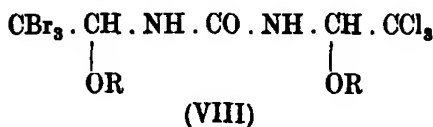
(VIII)

In this case the dialkoxy compounds of the type (VIII) and also those containing two different alkoxy groups, can be obtained by condensing the bromal monoalkoxy compounds (VI), with anhydrous chloral, forming the anhydro compound of the resulting N-(α-alkoxy-βββ-tribromoethyl)-N′-(α-hydroxy-βββ-trichloro ethyl) carbamide (IX), and decomposing this anhydro compound with a sodium alkoxide dissolved in the appropriate alcohol.

$$
\begin{array}{c}
\underset{\text{ÓR}}{\text{CBr}_3 \,\overset{|}{\text{CH}}\, \text{NH CO NH}_2} \xrightarrow{\text{CCl}_3\,\text{CHO}} \underset{\text{ÓR}}{\text{CBr}_3 \,\overset{|}{\text{CH}}\, \text{NH CO NH}\, \overset{|}{\text{CH}}.\text{CCl}_3} \\
\text{(VI)} \qquad\qquad \text{(IX)}\quad \text{OH}
\end{array}
$$

(VI) → CCl₃ CHO → CBr₃ CH NH CO NH CH.CCl₃ (with OR, OH) (IX) | NaOHaq. + Ac₂O

CBr₃ CH NH CO NH CH CCl₃ (OR, OR′) (VIII) ← NaOR′ ← CBr₃ CH NH.CO NH.CH CCl₃ (OR) / O \ OR / CBr₃ CH NH CO.NH CH CCl₃
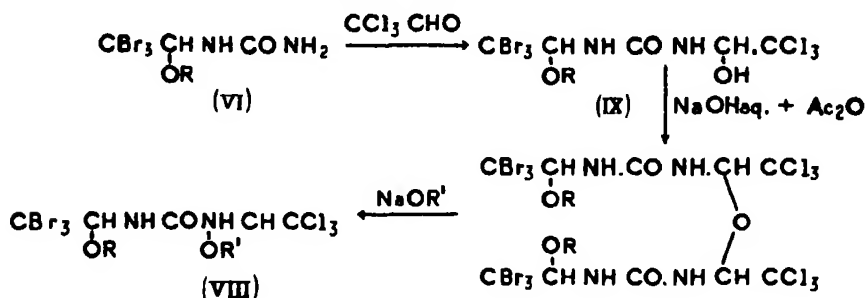
In this way the isomeric compounds

$$
\underset{\text{OCH}_3}{\text{CBr}_3 . \overset{|}{\text{CH}} . \text{NH} . \text{CO} . \text{NH} . \overset{|}{\text{CH}} . \text{CCl}_3}
$$
$$
\qquad\qquad\qquad\qquad \underset{\text{OC}_2\text{H}_5}{}
$$

and

$$
\underset{\text{OC}_2\text{H}_5}{\text{CBr}_3 \; \overset{|}{\text{CH}} . \text{NH} . \text{CO} \;\; \text{NH} \; \overset{|}{\text{CH}} . \text{CCl}_3}
$$
$$
\qquad\qquad\qquad\qquad \underset{\text{OCH}_3}{}
$$
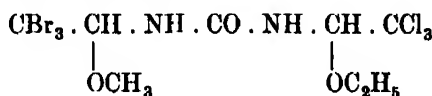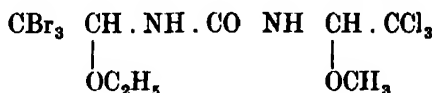
have been prepared As would be expected, they resemble each other closely in properties, but differ somewhat in melting point, the compound having the methoxy group contiguous to the tribromomethyl group melting some 9° higher than its isomer.

Although chloral condenses readily with the α-alkoxy-βββ-tribromoethyl-carbamides (VI), yielding the well-crystallised N-(α-alkoxy-βββ-tribromoethyl)-N′-(α-hydroxy-βββ-trichloroethyl) carbamide (IX), similar compounds containing a bromal group have not been obtained. Bromal apparently condenses with both α-ethoxy-βββ-tribromoethyl carbamide, and with α-ethoxy-βββ-trichloroethyl carbamide, but the product in each case is a viscid liquid, which has not been obtained crystalline, and which is decomposed very easily by alkaline solutions.

Experimental.

Monobromal urea, (α-hydroxy-βββ-tribromoethyl carbamide),

$$\text{CBr}_3 . \text{CH(OH)} . \text{NH} . \text{CO} . \text{NH}_2 \quad \text{(I)}.$$

10 g. of bromal hydrate and 4 g. (1 mol. + excess) of urea were dissolved in 30 c.c. of water, and the solution allowed to stand for 3 days. During this time *monobromal urea* separated as a colourless, crystalline solid.

It separates from boiling water in fern-like clusters of small plates, m.p. 136° (decomp.). (Found : Br, 70·2 ; $C_3H_5O_2N_2Br_3$ requires Br, 70·4 per cent.) When warmed with acetic anhydride, containing a trace of sulphuric acid, monobromal urea yields N-(α-*acetoxy-*βββ-*tribromoethyl*)-*N'-acetyl carbamide*, which separates from boiling aqueous acetic acid in compact rhombic prisms, m.p 184° (decomp). (Found Br, 56·8 ; $C_7H_9O_4N_2Br_3$ requires Br, 56·5 per cent.)

Dibromal urea, (sym-*di-*(α-*hydroxy-*βββ-*tribromoethyl*) *carbamide*),

$$CBr_3 . CH(OH) NH CO . NH . CH(OH) . CBr_3 (II).$$
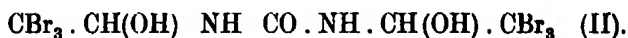
5 g. of monobromal urea and 5 g. (1 mol. + slight excess) of bromal hydrate were warmed together on the water-bath for 15 minutes On stirring the molten mass with water dibromal urea separated as a colourless solid. It crystallises from boiling aqueous alcohol in colourless four-sided plates, m p. 178° (decomp.). (Found : Br, 77·3 ; $C_5H_6O_3N_2Br_6$ requires Br, 77·2 per cent) When warmed with acetic anhydride containing a trace of sulphuric acid it yields sym-*di-*(α-*acetoxy-*βββ-*tribromoethyl*) *carbamide*, which separates from boiling, slightly diluted acetic acid in slender colourless prisms, m.p. 180° (decomp.). (Found . Br, 67·6 ; $C_9H_{10}O_5N_2Br_6$ requires Br, 67·9 per cent.)

Bis-(α-*carbamido-*βββ-*tribromoethyl*) *ether* (IV).

6·8 g. of monobromal urea (I) were dissolved in 40 c.c. of ice-cold N/1 sodium hydroxide (2 mols.), and 2 g. of acetic anhydride added drop by drop with vigorous shaking, the temperature being kept at 0°–5° Bis-(α-*carbamido-*βββ-*tribromoethyl*) *ether* (IV), separated as a colourless flocculent solid on each addition of acetic anhydride. It crystallises from boiling aqueous alcohol in slender, rather flattened, prisms, which decompose without previously melting at about 211°. (Found : N, 8·3 ; Br, 72·3 ; $C_6H_8O_3N_4Br_6$ requires N, 8·5 ; Br, 72·3.) When warmed with acetic anhydride it yields bis-(α-*N'-acetyl-carbamido-*βββ-*tribromoethyl*) *ether*, $O(CH . CBr_3 . NH . CO . NHAc)_2$, which crystallises from boiling, slightly dilute, acetic acid in colourless rhombs, m.p. 219° (decomp.). (Found : Br, 63·1 ; $C_{10}H_{12}O_5N_4Br_6$ requires Br, 63·2 per cent.)

α-ethoxy-βββ-tribromoethyl carbamide,

$$CBr_3 . CH(OC_2H_5) . NH . CO . NH_2 \quad (VI).$$

To a solution of 3·4 g. of *bis*-(α-carbamido-βββ-tribromoethyl)-ether (IV) in 20 c.c. of ethyl alcohol a solution of 0·24 g. (1 mol.) of sodium in ethyl alcohol was added. The solution was at first clear, but in a few seconds sodium formate separated, the solution at the same time developing a strong odour of bromoform. After 10 minutes 200 c c of water were added, when *α-ethoxy-βββ-tribromoethyl carbamide* (VI) separated as a colourless crystalline solid (1·6 g. ; 90 per cent. theoretical). It crystallises from boiling aqueous alcohol in colourless large lustrous plates, m.p. 162° (decomp.) (Found : Br, 65·2 ; $C_5H_9O_2N_2Br_3$ requires Br, 65·05 per cent) When warmed with acetic anhydride it yields *N-α-ethoxy-βββ-tribromoethyl-N'-acetyl carbamide*, which separates from boiling aqueous acetic acid in colourless plates, m p. 177° (decomp.). (Found : Br, 58·7 ; $C_7H_{11}O_3N_2Br_3$ requires Br, 58·4 per cent.) In a similar way, using the appropriate alcohol, were prepared the following :—

α-methoxy-βββ-tribromoethyl carbamide, large colourless plates from aqueous alcohol, m.p. 184° (decomp.). (Found : N, 7·7 ; Br, 67·8 ; $C_4H_7O_2N_2Br_3$ requires N, 7·9 ; Br, 67·6 per cent)

α-n-propoxy-βββ-tribromoethyl carbamide, large, glistening plates from aqueous alcohols, m p. 144° (decomp.) (Found · Br, 63·0 ; $C_6H_{11}O_2N_2Br_3$ requires Br, 62·7 per cent.)

Sym-*di-(α-ethoxy-βββ-tribromoethyl) carbamide,*

$$CBr_3 . CH(OC_2H_5) . NH . CO . NH . CH(OC_2H_5) . CBr_3 \quad (VII).$$
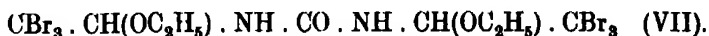
4 g. of dibromal urea (II) were dissolved in 25 c.c of ice-cold N/1 sodium hydroxide (4 mols) and 1·3 g. of acetic anhydride added with shaking. On each addition anhydro dibromal urea (V) separated as a colourless flocculent solid, which was collected and cautiously dried. The crude material, which could not be obtained crystalline, melted at 92° (decomp.). It was dissolved in 30 c.c. of ethyl alcohol, and a solution of 0·5 g. (excess) of sodium in 25 c.c. of ethyl alcohol added. After 10 minutes, during which time sodium formate separated, water was added to the liquid, which smelt strongly of bromoform, when sym-*di-(α-ethoxy-βββ-tribromoethyl) carbamide* (VII) separated as a colourless crystalline solid. It was repeatedly crystallised from boiling aqueous alcohol, from which it separates in small, slender, colourless flattened prisms, m.p. 196° (decomp) (Found : Br, 70·5 ; $C_9H_{14}O_3N_2Br_6$ requires Br, 70·8 per cent.)

Sym-*di-(α-methoxy-βββ-tribromoethyl) carbamide*, prepared in a similar way, using sodium methoxide in methyl alcohol, crystallises from boiling aqueous alcohol in very slender, colourless flattened prisms, m.p. 215° (decomp.). (Found : Br, 74·1 ; $C_7H_{10}O_3N_2Br_6$ requires Br, 73·8 per cent.)

Bromal chloral urea, N-(α-hydroxy-βββ-tribromoethyl)-N'-(α-hydroxy-βββ-trichloroethyl) carbamide.

$$CBr_3 . CH(OH) . NH . CO \quad NH . CH(OH) . CCl_3. \quad (III)$$

10 g. of monochloral urea and 15 g. (1 mol.) of bromal hydrate were warmed on the water-bath for 30 minutes. On stirring the resulting semi-solid mass with water, *bromal chloral urea* (III) was obtained as a colourless crystalline solid. It crystallises from boiling aqueous alcohol in thin, colourless, six-sided plates, m.p. 186°. (Found : Cl, 22·2 , Br, 49·4 ; $C_5H_6O_3N_2Cl_3Br_3$ requires Cl, 22·1 ; Br, 49·2 per cent) When warmed with acetic anhydride, it yields *N-(α-acetoxy-βββ-tribromoethyl)-N'-(α-acetoxy-βββ-trichloroethyl) carbamide*, which separates from boiling aqueous acetic acid in slender, colourless prisms, m.p. 185° (decomp.) (Found : Cl, 18·9 ; Br, 42·0 ; $C_9H_{10}O_5N_2Cl_3Br_3$ requires Cl, 18·6 ; Br, 41·9 per cent.)

N-(α-ethoxy-βββ-tribromoethyl)-N'-(α-ethoxy-βββ-trichloroethyl) carbamide,

$$CBr_3 . CH(OC_2H_5) . NH . CO . NH . CH(OC_2H_5) . CCl_3 \quad (VIII).$$
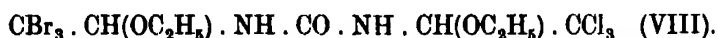
8 g. of bromal chloral urea (III) were dissolved in 32 c.c. of ice-cold N/1 sodium hydroxide (4 mols) and 3·3 g. of acetic anhydride were added with shaking. *Anhydro bromal chloral urea* separated as a colourless solid, which was collected, cautiously dried, and dissolved in 30 c c of ethyl alcohol. To this solution 0·5 g. of sodium, dissolved in 30 c c. of ethyl alcohol were added. After standing for 10 minutes 200 c.c. of water were added, when *N-(α-ethoxy-βββ-tribromoethyl)-N'-(α-ethoxy-βββ-trichloroethyl) carbamide* (VIII) separated as a colourless crystalline solid It was repeatedly crystallised from boiling aqueous alcohol, from which it separates in very slender, colourless flattened prisms, m.p. 203° (decomp.). (Found : Cl, 19·4 ; Br, 43·9 , $C_9H_{14}O_3N_2Cl_3Br_3$ requires Cl, 19·5 , Br, 44·1 per cent.)

N-(α-ethoxy-βββ-tribromoethyl)-N'-(α-hydroxy-βββ-trichloroethyl) carbamide,

$$CBr_3CH(OC_2H_5) . NH . CO . NH . CH(OH) . CCl_3 \quad (IX).$$
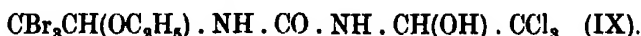
2 g. of α-ethoxy-βββ-tribromoethyl carbamide (VI) and 5 g. (1 mol. + excess) of anhydrous chloral were warmed together on the water-bath for 15 minutes. The viscid mass was then stirred with water, when *N-(α-ethoxy-βββ-tribromo-*

ethyl)-*N'*-(α-*hydroxy*-βββ-*trichloroethyl*) *carbamide* (IX) was obtained as a colourless, semi-solid mass which rapidly became granular and crystalline. It crystallises from warm, slightly diluted alcohol in long, slender, colourless flattened prisms, m.p. 144° (decomp.). (Found: Cl, 20·4; Br, 46·3; $C_7H_{10}O_3N_2Cl_3Br_3$ requires Cl, 20·6; Br, 46·5 per cent) When warmed with acetic anhydride it yields *N*-(α-*ethoxy*-βββ-*tribromoethyl*)-*N'*-(α-*acetoxy*-βββ-*trichloroethyl*) *carbamide*, which crystallises from boiling aqueous alcohol in slender, colourless prisms, m.p. 192° (decomp). (Found: Cl, 19·1; Br, 43·0, $C_9H_{12}O_4N_2Cl_3Br_3$ requires Cl, 19·1; Br. 43 0 per cent)

In a similar way was prepared *N*-(α-*methoxy*-βββ-*tribromoethyl*)-*N'*-(α-*hydroxy*-βββ-*trichloroethyl*) *carbamide*, long, slender, colourless, flattened prisms from aqueous alcohol, m p 193° (decomp.). (Found: Cl, 21·4; Br, 48·0; $C_6H_8O_3N_2Cl_3Br_3$ requires Cl, 21·2; Br, 47·8 per cent.)

N - (α-*ethoxy*-βββ-*tribromoethyl*) - *N'* - (α-*ethoxy*-βββ-*trichloroethyl*) *carbamide* (VIII) from *N*-(α-*ethoxy*-βββ-*tribromoethyl*)-*N'*-(α-*hydroxy*-βββ-*trichloroethyl*) *carbamide* (IX)

7 g of N-(α-ethoxy-βββ-tribromoethyl)-N'-(α-hydroxy-βββ-trichloroethyl) carbamide (IX) were dissolved in 30 c.c. of ice-cold N/1 sodium hydroxide, and 1·5 g. of acetic anhydride were added On each addition bis-(α-*N'*-α-*ethoxy*-βββ-*tribromoethyl-carbamido*-βββ-*trichloroethyl*) *ether* separated as a colourless semi-solid mass, which on stirring became granular. It crystallises with difficulty, and could not therefore be obtained perfectly pure. It was dissolved in 25 c c. of ethyl alcohol, and 0·5 g. of sodium dissolved in ethyl alcohol were added. After standing for 10 minutes water was added to the mixture, when *N*-(α-*ethoxy*-βββ-*tribromoethyl*)-*N'*-(α-*ethoxy*-βββ-*trichloroethyl*) *carbamide* (VIII) separated as a colourless solid. It crystallises from boiling aqueous alcohol in colourless flattened prisms, m p. 203° (decomp), identical in every way with the specimen prepared from bromal chloral urea. In a similar way the two following isomers were prepared.

N-(α-*methoxy*-βββ-*tribromoethyl*)-*N'*-(α-*ethoxy*-βββ-*trichloroethyl*) *carbamide*, colourless, flattened prisms from aqueous alcohol, m p. 206° (decomp.). (Found: Cl, 20·3; Br, 45·0; $C_8H_{12}O_3N_2Cl_3Br_3$ requires Cl, 20·1; Br, 45·2 per cent)

N-(α-*ethoxy*-βββ-*tribromoethyl*)-*N'*-(α-*methoxy*-βββ-*trichloroethyl*) *carbamide*, slender, colourless, flattened prisms from aqueous alcohol, m.p. 197° (decomp.). (Found: Cl, 20·1, Br, 45·3; $C_8H_{12}O_3N_2Br_3Cl_3$ requires Cl, 20·1; Br, 45·2 per cent.)

Summary.

Urea condenses with 1 or 2 molecules of bromal yielding *monobromal urea*,

$$CBr_3 . CH(OH) . NH . CO . NH_2,$$

and *dibromal urea*,

$$CBr_3 . CH(OH) . NH . CO . NH . CH(OH) . CBr_3,$$
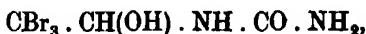
respectively. Monobromal urea also condenses with 1 molecule of chloral yielding *bromal chloral urea*,

$$CBr_3 . CH(OH) . NH . CO . NH . CH(OH) . CCl_3.$$

These compounds dissolve easily in aqueous alkalies giving solutions from which, on the addition of acetic anhydride, dimolecular *anhydro compounds* of ether-like structure separate

These anhydro compounds react with solutions of sodium alkoxides in the corresponding alcohols, fission occurs at the ether linkage, and mono- and di-alkoxy compounds are formed.

The monoalkoxy compounds themselves condense with anhydrous chloral, producing compounds of the structure

$$CBr_3 . \underset{\underset{OR}{|}}{CH} . NH . CO . NH . \underset{\underset{OR}{|}}{CH} . CCl_3$$
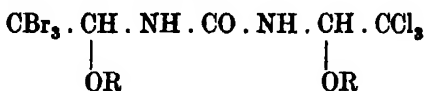
which also similarly dissolve in alkalies and react with acetic anhydride, yielding anhydro compounds. These, on treatment with a sodium alkoxide, yield dialkoxy compounds of the general formula

$$CBr_3 . \underset{\underset{OR}{|}}{CH} . NH . CO . NH . \underset{\underset{OR}{|}}{CH} . CCl_3.$$
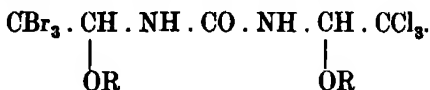
When the two alkoxy groups are the same the compounds are identical with the corresponding compounds prepared directly from bromal chloral urea. When they are different two isomers are possible which can be prepared by introducing the group R or R′ into bromal urea, condensing the alkoxy compound thus obtained with chloral, and then, through the anhydro compound, introducing the group R′ or R. These isomers resemble each other closely in properties, but differ somewhat in melting point.

The Action of Halogens upon the Arylazoacetoacetates and Related Compounds.—Part II.

By Frederick Daniel Chattaway, F.R.S., and Reginald Jack Lye.

It has recently been shown* that the action of halogens upon the arylazo-acetoacetates is not so simple as was formerly supposed, but varies according to the experimental conditions. When the nucleus is already fully substituted, halogen atoms may enter or replace the acetyl group, and may even, in some cases, replace the carbethoxy group. For example, the following compounds were obtained by the action of bromine upon ethyl 2.4:6-tribromophenyl-azoacetoacetate.
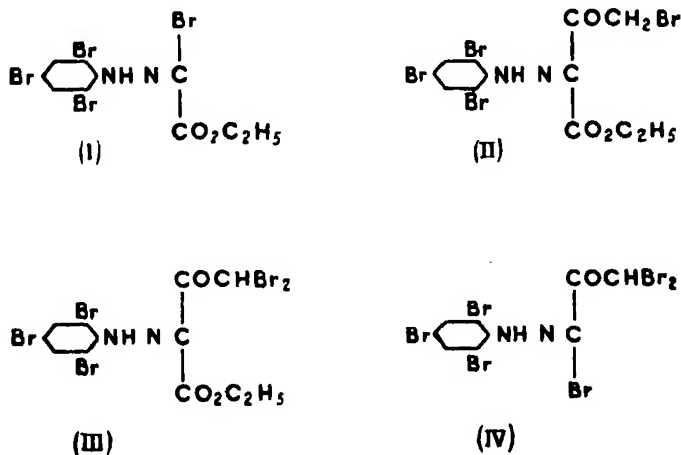
The more energetic action of chlorine upon ethyl 2:4:6-trichlorophenyl-azoacetoacetate, although it yields stages (I) and (II) at the ordinary temperature, causes breaking down of the molecule when the higher temperature, which would be necessary to bring about stages (III) and (IV), is employed

In the case of those arylazoacetoacetates in which the nucleus is less fully substituted, the action of halogens is even more complicated, since, in addition to the replacement or substitution of the acetyl or carbethoxy group by halogen atoms, nuclear substitution may also take place.

Not more than two halogen atoms are introduced into the aryl nucleus, even when excess of halogen is used. Hence the action of either chlorine or

bromine upon ethyl 2 : 4-dichloro- or ethyl 2 : 4-dibromophenylazoacetoacetate is similar to its action upon the corresponding ethyl 2 : 4 : 6-trihalogenphenyl-azoacetoacetates under the same conditions.

Chlorination of ethyl 2 : 4-dichlorophenylazoacetoacetate in acetic acid at the ordinary temperature, causes replacement of the acetyl group by a chlorine atom, with the formation of ethyl α-chloroglyoxalate-2 4-dichlorophenyl-hydrazone (V).

$$Cl\text{—}\langle\ \rangle\text{—}NH.N{:}C \begin{array}{c} Cl \\ | \\ C \\ | \\ CO_2C_2H_5 \end{array}$$
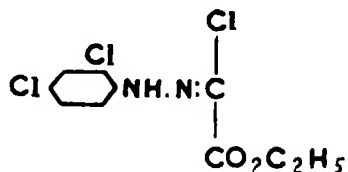
If, however, the chlorination be carried out in dry chloroform previously saturated with hydrogen chloride, ethyl 2 : 4-dichlorophenylazo-γ-chloroaceto-acetate (VI), identical with the compound formed by coupling 2 · 4-dichloro-phenyldiazonium chloride with γ-chloroacetoacetic ester, is obtained

$$\underset{\underset{CO_2C_2H_5}{|}}{\overset{\overset{COCH_3}{|}}{Cl\langle\ \rangle NH\,N{:}C}} \xrightarrow{Cl_2} \underset{\underset{CO_2C_2H_5}{|}}{\overset{\overset{COCH_2Cl}{|}}{Cl\langle\ \rangle NH\,N{\cdot}C}} \longleftarrow Cl\langle\ \rangle N_2Cl + \underset{\underset{CO_2C_2H_5}{|}}{\overset{\overset{COCH_2Cl}{|}}{CH_2}}$$

(VI)
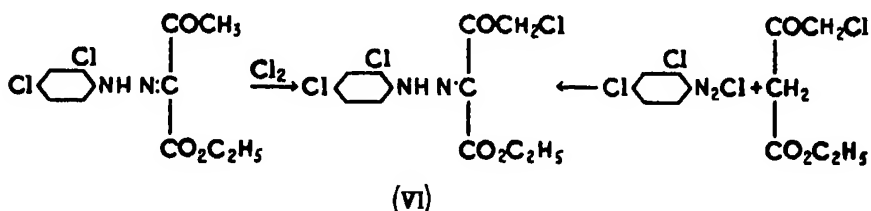
Ethyl 2 . 4-dichlorophenylazo-γγ-dichloroacetoacetate cannot be obtained by direct substitution of ethyl 2 : 4-dichlorophenylazoacetoacetate, since, at the ordinary temperature, action ceases when one chlorine atom has been introduced into the acetyl group, whilst, at a higher temperature, the molecule breaks down under the action of the halogen.

Bromine replaces the acetyl group as a whole, when an equivalent amount is added, at the ordinary temperature to a solution of ethyl 2 : 4-dibromophenyl-azoacetoacetate in acetic acid containing either water or sodium acetate (fused or crystalline), with the formation of ethyl α-bromoglyoxalate-2 : 4-dibromo-phenylhydrazone* (formula as (V)).

---

* Since, however, ethyl 2 : 4-dibromophenylazoacetoacetate is only sparingly soluble in cold acetic acid, and the suspension is not readily attacked, ethyl α-bromoglyoxalate-2 : 4-dibromophenylhydrazone is more conveniently prepared by the further action of bromine upon ethyl α-bromoglyoxalate-p-bromophenylhydrazone.

When, however, the action takes place in hot glacial acetic acid, progressive substitution of the acetyl group occurs, with the formation of ethyl 2 : 4-dibromophenylazo-γ-bromoacetoacetate (VII), (identical with the product obtained by coupling 2 : 4-dibromophenyldiazonium chloride with γ-bromo-acetoacetic ester), and of ethyl 2 : 4-dibromophenylazo-γγ-dibromoacetoacetate (VIII).

The action of excess of bromine at 100° does not further substitute either the nucleus or the acetyl group, but causes the slow replacement of the carbethoxy group by a bromine atom, until, finally, ββω-tribromo-α-ketopropaldehyde-2 : 4-dibromophenylhydrazone* (IX) is the sole product.

$$ \text{(VII)} \qquad \text{(VIII)} \qquad \text{(IX)} $$
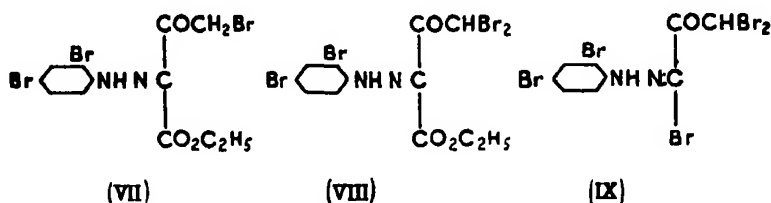
When either chlorine or bromine reacts with ethyl phenylazoacetoacetate, similar reactions occur, but it is difficult to isolate the products successively formed.

Chlorination in glacial acetic acid at the ordinary temperature yields finally ethyl α-chloroglyoxalate-2 : 4-dichlorophenylhydrazone (V), and though the reaction can be stopped approximately at the ethyl α-chloroglyoxalate-*p*-chlorophenylhydrazone stage, the separation of this compound from the product of the action is difficult.

Similarly, although chlorine substitutes both the phenyl nucleus and the acetyl group when a limited amount is allowed to act upon ethyl phenylazo-acetoacetate dissolved in anhydrous solvents, ethyl phenylazo-γ-chloroaceto-acetate and ethyl *p*-chlorophenylazo-γ-chloroacetoacetate (formulæ as (VI)), cannot easily be isolated from the mixture of compounds produced. They can, however, readily be obtained by coupling the corresponding diazonium salts with γ-chloroacetoacetic ester.

Bromine also substitutes the phenyl nucleus, and replaces or substitutes the acetyl group in ethyl phenylazoacetoacetate, and the products can be more easily isolated than the corresponding chlorine compounds.

---

* This compound is also obtained by the action of 3 mols. of bromine upon α-keto-propaldehyde 2 : 4-dibromophenylhydrazone.

When two molecular equivalents of bromine react at the ordinary temperature* with ethyl phenylazoacetoacetate in acetic acid containing either water or an equivalent amount of sodium acetate, an almost quantitative yield of ethyl α-bromoglyoxalate-p-bromophenylhydrazone (X) is obtained, and the same compound is quantitatively formed when ethyl p-bromophenylazoacetoacetate is similarly brominated. The action of one molecular equivalent of bromine upon ethyl phenylazoacetoacetate dissolved in acetic acid containing an equivalent amount of sodium acetate, whilst leaving a portion of the unsubstituted compound unattacked, gives a mixture of ethyl α-bromoglyoxalate-phenyl and p-bromophenylhydrazones.†

Excess of bromine carries the reaction no further than the ethyl α-bromoglyoxalate-p-bromophenylhydrazone stage at the ordinary temperature, though in boiling acetic acid the aryl nucleus of this latter compound is further substituted, and ethyl α-bromoglyoxalate-2 : 4-dibromophenylhydrazone (XI) is formed
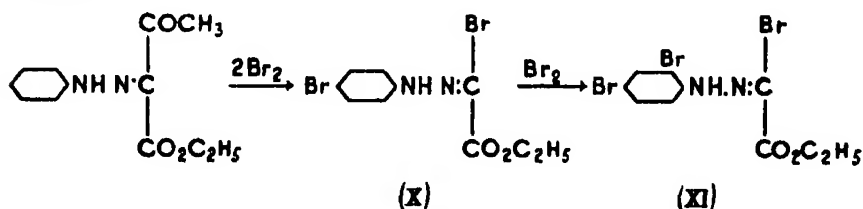
The action of three molecular equivalents of bromine upon ethyl phenylazoacetoacetate, dissolved in glacial acetic acid at the ordinary temperature, causes substitution in the para position of the phenyl nucleus, and the acetyl group is at the same time substituted, two atoms of bromine being successively introduced, with the formation of ethyl p-bromophenylazo-γγ-dibromoacetoacetate (XII).
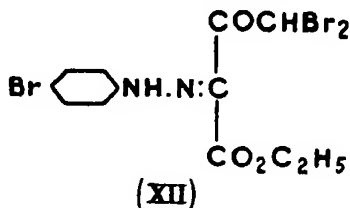
When less than three molecular equivalents of bromine react with ethyl phenylazoacetoacetate, no single product is formed, and the mixtures resulting

---

* As the temperature at which bromination is carried out is raised, the reaction proceeds less and less cleanly, with a corresponding diminution in yield of ethyl α-bromoglyoxalate-arylhydrazone.

† As observed previously by Bowack and Lapworth, 'J. Chem Soc.,' vol. 87, p. 1854 (1905).

are difficult to separate. The lower bromination products, ethyl phenylazo-γ-bromoacetoacetate and ethyl *p*-bromophenylazo-γ-bromoacetoacetate (XIII) can, however, easily be made by coupling the corresponding diazonium salts with γ-bromoacetoacetic ester.
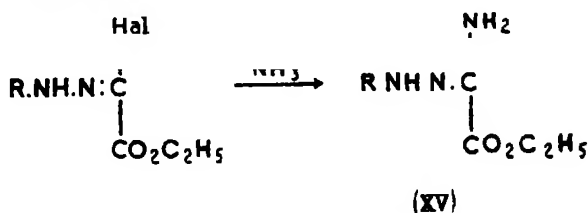
$$Br\langle\ \rangle N_2Cl + \begin{matrix} COCH_2Br \\ | \\ CH_2 \\ | \\ CO_2C_2H_5 \end{matrix} \longrightarrow Br\langle\ \rangle NH\ N.\begin{matrix} COCH_2Br \\ | \\ C \\ | \\ CO_2C_2H_5 \end{matrix}$$

(**XIII**)
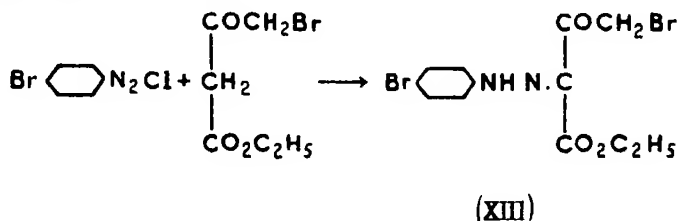
The action of excess of bromine at the ordinary temperature causes no further substitution, either in the phenyl nucleus or in the acetyl group, but when the temperature at which bromination is carried out is raised, the carbethoxy group is first hydrolysed and finally replaced by bromine Thus *p*-bromophenylazo-γγ-dibromoacetoacetic acid (XIV) is the chief product obtained when three molecular equivalents of bromine are allowed to react with ethyl phenylazoacetoacetate at 60°, whilst the action of excess of bromine in boiling acetic acid leads to the quantitative formation of ββω-tribromo-α-ketopropaldehyde-2 : 4-dibromophenylhydrazone (IX)

$$Br\langle\ \rangle NH\ N:\begin{matrix} COCHBr_2 \\ | \\ C \\ | \\ CO_2H \end{matrix}$$

(**XIV**)
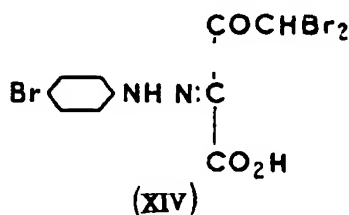
All the substituted arylazoacetoacetates and α-halogenglyoxalate arylhydrazones when heated in acetic acid solution with tin and concentrated hydrochloric acid are reduced to halogen-substituted anilines, the constitution of which establishes the extent of nuclear substitution

The ethyl α-halogenglyoxalate-arylhydrazones react readily at the ordinary temperature with alcoholic ammonia, giving the corresponding hydrazidines or ethyl α-aminoglyoxalate-arylhydrazones (XV)

$$R.NH.N:\begin{matrix} Hal \\ | \\ C \\ | \\ CO_2C_2H_5 \end{matrix} \xrightarrow{\ NH_3\ } R\ NH\ N.\begin{matrix} NH_2 \\ | \\ C \\ | \\ CO_2C_2H_5 \end{matrix}$$

(**XV**)

As in the case of the similar compounds obtained from ethyl 2 : 4 : 6-tri-halogenphenylazoacetoacetates, the azo-γ-halogen and γγ-dihalogenaceto-acetates readily lose the elements of hydrogen halide when heated with an alcoholic solution of potassium acetate, ring closure takes place, and corresponding derivatives of 4-hydroxypyrazole result. Thus ethyl 2 : 4-dibromo-phenylazo-γ-bromoacetoacetate yields 4-hydroxy-1-(2' : 4'-dibromophenyl)-3-carbethoxypyrazole (XVI). When this compound is brominated, it yields 4-hydroxy-1-(2' : 4'-dibromophenyl)-3-carbethoxy-5-bromopyrazole (XVII), which is also produced when ethyl 2 : 4-dibromophenylazo-γγ-dibromoaceto-acetate is heated with an alcoholic solution of potassium acetate.
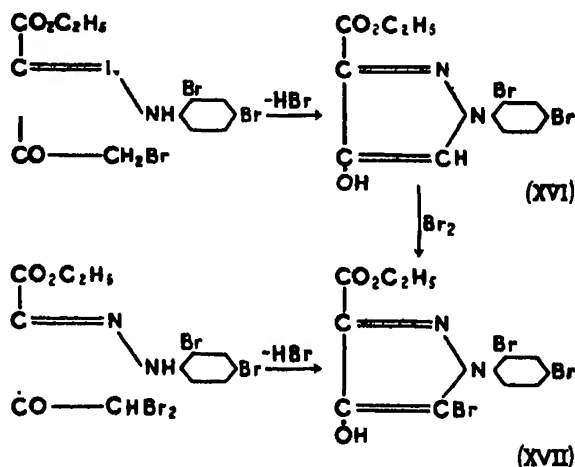
These 4-hydroxypyrazoles are well-crystallised, colourless compounds, which form colourless acetyl and benzoyl derivatives, the pyrazolyl-4-acetates and pyrazolyl-4-benzoates.

Experimental.

Ethyl α-bromoglyoxalate p-bromophenylhydrazone.

9·6 g. of bromine (2 mols.) in 10 c.c. of acetic acid were added slowly to a cooled solution of 7 g of ethyl phenylazoacetoacetate (1 mol.), and 8 g. of crystallised sodium acetate (2 mols.) in 30 c.c. of acetic acid. After standing and careful addition of 50 c.c. of water, *ethyl α-bromoglyoxalate-p-bromophenyl-hydrazone* separated out. Colourless, long, slender prisms from alcohol, m.p., 149–150°. (Yield : 80 per cent. theoretical.) (Found : Br, 45·5. Calculated for $C_{10}H_{10}O_2N_2Br_2$ Br, 45·7 per cent.)

Ethyl α-bromoglyoxalate-p-*bromophenylhydrazone* was similarly formed, in practically theoretical amount, when 1·6 g. of bromine (1 mol.) was added to

a solution of 3·1 g. of ethyl *p*-bromophenylazoacetoacetate (1 mol.) and 1·4 g. of crystallised sodium acetate (1 mol.) in 10 c.c. of acetic acid.

Ethyl α-aminoglyoxalate-p-bromophenylhydrazone.

5 g. of powdered ethyl α-bromoglyoxalate-*p*-bromophenylhydrazone were added, in small portions, to a cooled saturated solution of ammonia in alcohol (10 c.c.). After standing for 30 minutes, *ethyl α-aminoglyoxalate-p-bromophenylhydrazone*, which is formed in almost theoretical amount, separated. It crystallises from boiling alcohol in colourless, flattened prisms, with domed ends, which become green on exposure to light, m.p. 154°–155°. (Found : Br, 28·0. $C_{10}H_{12}O_2N_3Br$ requires Br, 28·0 per cent.)

Ethyl α-bromoglyoxalate-2 · 4-dibromophenylhydrazone.

4·8 g. of bromine (3 mols.) in 5 c c. of acetic acid were added slowly to a cooled solution of 2·3 g. of ethyl phenylazo-acetoacetate (1 mol) and 2·7 g. of crystalline sodium acetate (2 mols.)* in 15 c.c. of acetic acid. The mixture was allowed to stand for 30 minutes to ensure complete formation of the intermediate ethyl α-bromoglyoxalate-*p*-bromophenylhydrazone, and then heated on a water-bath at about 70° for an hour On cooling and adding water *ethyl α-bromoglyoxalate-2 : 4-dibromophenylhydrazone* separated as a rather viscid solid. It crystallises from boiling alcohol in colourless, long, slender, flattened prisms, m.p. 120°. (Yield : 60 per cent. theoretical) (Found : Br, 55·8. $C_{10}H_9O_2N_2Br_3$ requires Br, 55·9 per cent.)

Ethyl α-bromoglyoxalate-2 : 4-dibromophenylhydrazone was also obtained practically pure and in almost theoretical amount, when 5 g. of ethyl α-bromoglyoxalate-*p*-bromophenylhydrazone (1 mol) and 2·4 g of bromine (1 mol.) dissolved in 30 c.c. of acetic acid were heated on a water-bath at 70°–80° for an hour.

Ethyl α-aminoglyoxalate-2 : 4-dibromophenylhydrazone is quantitatively formed when ethyl α-bromoglyoxalate-2 : 4-dibromophenylhydrazone is stirred with a saturated solution of ammonia in alcohol. It crystallises from boiling alcohol in large, compact, colourless prisms, m p. 108°–109°. (Found : N, 11·4 ; Br, 44·0. $C_{10}H_{11}O_2N_3Br_2$ requires N, 11·5 ; Br, 43·8 per cent.)

Ethyl α-bromoglyoxalate 2 : 4-dichlorophenylhydrazone.

1·6 g. of bromine (1 mol.) in 3 c.c. of acetic acid was added to a solution of 3 g. of ethyl 2 : 4-dichlorophenylazoacetoacetate (1 mol.) and 1·4 g. of crystalline sodium acetate (1 mol.) in 40 c.c. of acetic acid at the ordinary temperature.

---

* If more than 2 mols. of sodium acetate are used, the solution darkens in colour during the subsequent heating, and the yield of ethyl α-bromoglyoxalate-2 : 4-dibromophenylhydrazone is diminished.

After standing for an hour and then adding water, *ethyl α-bromoglyoxalate-2 : 4-dichlorophenylhydrazone* separated out. It crystallises from boiling alcohol in colourless, flattened prisms, which become yellow on exposure to light, m.p. 117°. (Found : Cl, 21·0 ; Br, 23·7. $C_{10}H_9O_2N_2Cl_2Br$ requires Cl, 20·9 ; Br, 23·5 per cent.)

Ethyl α-chloroglyoxalate p-chlorophenylhydrazone.

2·3 g. of sodium N-chloro-*p*-tolylsulphonamide (1 mol.) were added in portions to a cooled solution of 2·7 g. of ethyl *p*-chlorophenylazoacetoacetate (1 mol.) in 5 c.c. of acetic acid. After standing for 30 minutes, *ethyl α-chloroglyoxalate* p-chlorophenylhydrazone began to separate. It crystallises from boiling alcohol in long, flattened, colourless prisms, m.p. 146°–147°. (Found : Cl, 27·4 Calculated for $C_{10}H_{10}O_2N_2Cl_2$, Cl, 27·2 per cent)

Ethyl α-chloroglyoxalate p-bromophenylhydrazone, which was similarly prepared, crystallises from boiling alcohol in colourless, long, flattened prisms, m.p. 163°. (Found : Cl, 11·7 ; Br, 26·4 Calculated for $C_{10}H_{10}O_2N_2ClBr$, Cl, 11·6 ; Br, 26·2 per cent.)

Ethyl α-chloroglyoxalate 2 · 4-*dichlorophenylhydrazone*

3 g. of ethyl 2 : 4-dichlorophenylazoacetoacetate were suspended in 15 c c. of acetic acid, and chlorine passed in until the liquid was saturated The excess of chlorine and hydrogen chloride were aspirated off, and water carefully added, when *ethyl α-chloroglyoxalate-*2 : 4-*dichlorophenylhydrazone* separated as a yellowish solid. It crystallises from boiling alcohol in colourless, flattened prisms, m.p. 98°. (Found : Cl, 36·1 $C_{10}H_9O_2N_2Cl_3$ requires Cl, 36·0 per cent.)

Ethyl α-chloroglyoxalate 2 : 4-*dibromophenylhydrazone*, prepared similarly by the action of chlorine upon ethyl 2 : 4-dibromophenylazoacetoacetate, crystallises from boiling alcohol in felted, colourless needles, m.p. 108° (Found . Cl, 9·3 ; Br, 41·8. $C_{10}H_9O_2N_2ClBr_2$ requires Cl, 9·2 ; Br, 41·6 per cent.)

Ethyl p-bromophenylazo-γ-bromoacetoacetate (*ethyl* γ-bromo-αβ-*diketobutyrate-*α-(p-*bromophenylhydrazone*)).

8·5 g. of *p*-bromoaniline (1 mol.) were diazotised at 0°, using 40 c.c. of concentrated hydrochloric acid and 3·5 g. of sodium nitrite (1 mol.). The resulting diazonium solution was slowly added at 0°, with constant stirring, to a solution of 12 g. of ethyl γ-bromoacetoacetate (1 mol. + excess) in 50 c.c. of alcohol, containing in suspension 70 g. of crystallised sodium acetate The stirring was continued for 2 hours, and the mixture then left at the ordinary temperature for 12 hours to ensure complete separation of the *ethyl* p-*bromophenylazo-γ-bromoacetoacetate.* It crystallises from boiling benzene in long, slender, pale

yellow prisms, m.p. 113°–114°. (Found . Br, 40·7. $C_{12}H_{12}O_3N_2Br_2$ requires Br, 40·8 per cent.)

Ethyl phenylazo-γ-bromoacetoacetate, which was similarly prepared, crystallises from boiling alcohol in long, slender, golden-yellow prisms, m.p. 81°. (Found . Br, 25·5. $C_{12}H_{13}O_3N_2Br$ requires Br, 25·5 per cent.)

Ethyl 2 : 4-dibromophenylazo-γ-bromoacetoacetate, similarly prepared, separates from boiling benzene in golden-yellow, elongated prisms, m.p. 144°–145°. (Found : Br, 51·2. $C_{12}H_{11}O_3N_2Br_3$ requires Br, 50·9 per cent.)

The following arylazo-γ-chloroacetoacetates were obtained in the same way from ethyl γ-chloroacetoacetate and the corresponding diazonium salts.

Ethyl phenylazo-γ-chloroacetoacetate, flattened, golden prisms from alcohol, m.p. 92°. (Found : Cl, 13·2. Calculated for $C_{12}H_{13}O_3N_2Cl$, Cl, 13·2 per cent.)

Ethyl p-chlorophenylazo-γ-chloroacetoacetate, flattened, yellow prisms from alcohol, m p. 102°–103°. (Found Cl, 23·5. $C_{12}H_{12}O_3N_2Cl_2$ requires Cl, 23·4 per cent.)

Ethyl 2 : 4-dichlorophenylazo-γ-chloroacetoacetate, long, slender, pale yellow, flattened prisms from alcohol, m.p. 105°. (Found : Cl, 31·7. $C_{12}H_{11}O_3N_2Cl_3$ requires Cl, 31·5 per cent)

Action of bromine (3 mols) on ethyl phenylazoacetoacetate in cold acetic acid Formation of ethyl p-bromophenylazo-γγ-dibromoacetoacetate.

24 g. of bromine (3 mols) in 10 c c. of glacial acetic acid were added in portions to a cooled solution of 11·7 g. of ethyl phenylazoacetoacetate in 30 c.c. of glacial acetic acid. *Ethyl p-bromophenylazo-γγ-dibromoacetoacetate* began to separate almost at once as a yellow solid It was collected after standing for 2 hours, and after washing with a little acetic acid was practically pure. It crystallises from alcohol in bright yellow, flattened prisms, m.p. 135°–136°. (Yield : 80 per cent. theoretical.) (Found : Br, 51·0. $C_{12}H_{11}O_3N_2Br_3$ requires Br, 50·9 per cent.)

On reduction with tin and hydrochloric acid in boiling acetic acid solution, it yielded *p*-bromoaniline.

Action of bromine (3 mols) on ethyl phenylazoacetoacetate in hot acetic acid. Formation of p-bromophenylazo-γγ-dibromoacetoacetic acid.

48 g. of bromine (3 mols) in 30 c.c. of glacial acetic acid were added to a solution of 23 g. of ethyl phenylazoacetoacetate in 30 c.c. of glacial acetic acid, the temperature during addition being kept at 60°–70°. The colour of the bromine at once disappeared, and hydrogen bromide was copiously evolved. On cooling, a yellow solid was deposited, consisting chiefly of p-*bromophenylazo-*

γγ-*dibromoacetoacetic acid*   It is rather sparingly soluble in boiling acetic acid, from which it separates in beautiful golden-yellow, flattened prisms, m p. 205° (decomp.). (Yield : 60 per cent. theoretical.) (Found : N, 6·4 ; Br, 54·3. $C_{10}H_7O_3N_2Br_3$ requires N, 6·3 ; Br, 54·2 per cent.)

On reduction with tin and hydrochloric acid in boiling acetic acid solution, it yielded *p*-bromoaniline.

Ethyl 2 : 4-*dibromophenylazo-γ-bromoacetoacetate.*

4·8 g of bromine (1 mol.) dissolved in 5 c.c. of glacial acetic acid were added cautiously to a hot solution of 11·7 g. ethyl 2 : 4-dibromophenylazoacetoacetate (1 mol.) in 25 c.c. of glacial acetic acid. On cooling, *ethyl* 2 : 4-*dibromophenylazo-γ-bromoacetoacetate* separated as a yellow solid. It crystallised from boiling benzene, in golden-yellow, elongated prisms, m.p. 144°–145°, and was in every respect identical with the compound prepared above by coupling 2 : 4-dibromophenyldiazonium chloride with ethyl γ-bromoacetoacetate. The yield was almost quantitative.

Ethyl 2 : 4-*dichlorophenylazo-γ-bromoacetoacetate* was similarly prepared by acting upon ethyl 2 : 4-dichlorophenylazoacetoacetate in glacial acetic acid solution, with 1 mol. of bromine. Long, slender, flattened, pale yellow prisms from benzene, m.p. 113°. (Found : Cl, 18·75 ; Br, 21·0. $C_{12}H_{11}O_3N_2Cl_2Br$ requires Cl, 18·6 ; Br, 20·9 per cent.)

Ethyl 2 . 4-*dibromophenylazo-γγ-dibromoacetoacetate.*

3·2 g. of bromine (2 mols.) dissolved in 3 c.c. of glacial acetic acid were added to a solution of 3·9 g. of ethyl 2 : 4-dibromophenylazoacetoacetate (1 mol) in 10 c.c. of glacial acetic acid at about 100°. *Ethyl* 2 : 4-*dibromophenylazo-γγ-dibromoacetoacetate* separated immediately from the hot solution as a yellow solid. It crystallises from boiling acetic acid, in which it is rather sparingly soluble, in long, yellow needles, m.p. 153°–154°   (Yield : 90 per cent. theoretical.)   (Found : Br, 58·4. $C_{12}H_{10}O_3N_2Br_4$ requires Br, 58·2 per cent.)

Ethyl 2 : 4-*dichlorophenylazo-γγ-dibromoacetoacetate*, similarly prepared by the action of 2 mols. of bromine upon ethyl 2 : 4-dichlorophenylazoacetoacetate dissolved in acetic acid, crystallises from acetic acid in lemon-yellow needles, m.p. 128°. (Found : Cl, 15·5 ; Br, 34·9. $C_{12}H_{10}O_3N_2Cl_2Br_2$ requires Cl, 15·4 ; Br, 34·7 per cent.)

Action of chlorine upon ethyl 2 : 4-*dichlorophenylazoacetoacetate in chloroform.*
Formation of ethyl 2 : 4-*dichlorophenylazo-γ-chloroacetoacetate.*

5 g. of ethyl 2 : 4-dichlorophenylazoacetoacetate were dissolved in 20 c.c. of dry chloroform which had been previously saturated with dry hydrogen chloride, and a slow stream of chlorine was bubbled through, at the ordinary

temperature, until the liquid was saturated. The excess of chlorine and hydrogen chloride was then aspirated off, and the bulk of the chloroform allowed to evaporate at the ordinary temperature. The resulting yellow, viscid mass was repeatedly crystallised from boiling alcohol, when *ethyl* 2 : 4-*dichlorophenylazo-γ-chloroacetoacetate*, m p. 105°, was obtained, though in very poor yield It was identical, in every respect, with the compound obtained as above by coupling 2 : 4-dichlorophenyldiazonium chloride with ethyl γ-chloroacetoacetate.

Action of excess of bromine upon ethyl phenylazoacetoacetate   Formation of βββ*ω-tribromo-α-ketopropaldehyde-2 4-dibromophenylhydrazone.*

$$(C_6H_3Br_2 . NH \quad N \cdot CBr . COCHBr_2.)$$
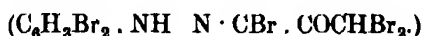
24 g. of bromine (7 mols.) in 20 c c of acetic acid were added to a solution of 4·7 g of ethyl phenylazoacetoacetate in 30 c.c. of acetic acid, at 100°, the solution being then heated on a water-bath for an hour. Hydrogen bromide was freely evolved, and βββ*ω-tribromo-α-ketopropaldehyde-2 : 4-dibromophenylhydrazone* (8·4 g.) separated from the hot solution as a yellow solid. It crystallises from boiling acetic acid in deep yellow needles, m.p. 140°–141°. (Found : Br, 71·7. $C_9H_5ON_2Br_5$ requires Br, 71·8 per cent) When reduced in boiling acetic acid with tin and hydrochloric acid it yielded 2 : 4-dibromoaniline.

βββ*ω-tribromo-α-ketopropaldehyde-2 4-dibromophenylhydrazone* is also formed by the action of excess of bromine at an elevated temperature upon any of the lower bromination products.

α-ketopropaldehyde-2 . 4-dibromophenylhydrazone

20 g. of 2 : 4-dibromoaniline (1 mol.) were diazotised using 6 g. of sodium nitrite (1 mol.) and 80 c.c. of concentrated hydrochloric acid. The resulting diazonium solution was slowly added, at 0°, to a solution of 10 g. of acetoacetic acid* (1 mol. + excess) in 250 c c. of water During the addition of the diazonium solution, 150 g. of crystalline sodium acetate (1 mol. + excess) were added in portions. The stirring was continued for several hours after the addition of the diazonium solution, and the *α-ketopropaldehyde-2 : 4-dibromophenylhydrazone* which had separated, was collected after standing at the ordinary temperature for 12 hours. It crystallises from boiling alcohol, in very pale yellow, long, slender prisms, m.p. 165°. (Found : Br, 49·7. $C_9H_8ON_3Br_2$ requires Br, 50·0 per cent.)

---

* Japp and Klingemann, ' Ann Chem.,' vol. 247, p. 190 (1888).

Action of bromine (3 *mols.*) *upon* α-*ketopropaldehyde*-2 : 4-*dibromophenyl-hydrazone. Formation of* ββω-*tribromo*-α-*ketopropaldehyde*-2 : 4-*dibromophenyl-hydrazone.*

4·8 g. of bromine (3 mols.) dissolved in 6 c.c. of acetic acid were added to a solution of 3·2 g of α-ketopropaldehyde-2:4-dibromophenylhydrazone in 20 c.c. of hot glacial acetic acid. On cooling, ββω-*tribromo*-α-*ketopropalde-hyde*-2 : 4-*dibromophenylhydrazone* separated quantitatively as a yellow solid. It crystallised from boiling acetic acid in deep yellow needles, m.p. 140°–141°, and is identical in every respect with the compound obtained by the action of excess of bromine upon ethyl phenylazoacetoacetate (see above).

All the arylazo-γ-halogenacetoacetates and arylazo-γγ-dihalogenacetoacetates described above, yield derivatives of 4-*hydroxypyrazole*, in almost quantitative amount, when heated with an alcoholic solution of potassium acetate

4-*hydroxy*-1-(2′ : 4′-*dibromophenyl*)-3-*carbethoxypyrazole.*

4·7 g. of powdered ethyl 2 : 4-dibromophenylazo-γ-bromoacetoacetate (1 mol.) were added in portions to a boiling solution of 2 g of potassium acetate (1 mol. + excess) in 60 c.c of alcohol   At each addition of the ethyl 2 : 4-dibromophenylazo-γ-bromoacetoacetate a red colouration developed momentarily, and potassium bromide separated   The boiling was continued for a few minutes.   On cooling and adding water 4-*hydroxy*-1-(2′ : 4′-*dibromophenyl*)-3-*carbethoxypyrazole* separated as a colourless solid   It crystallises from boiling alcohol in small, colourless, hair-like needles, m.p. 160°. (Found . Br, 41·3. $C_{12}H_{10}O_3N_2Br_2$ requires Br, 41·0 per cent)   When heated with acetic anhydride containing a drop of concentrated sulphuric acid it gave 1-(2′ : 4′-*dibromophenyl*)-3-*carbethoxypyrazolyl*-4-*acetate*   Long, colourless prisms from alcohol, m.p. 103°–104°. (Found : Br, 37·2. $C_{14}H_{12}O_4N_2Br_2$ requires Br, 37·0 per cent.)

1-(2′ : 4′-*dibromophenyl*)-3-*carbethoxypyrazolyl*-4-*benzoate*, obtained by the Schotten-Baumann method, crystallises from boiling alcohol, in long, slender, colourless prisms, m.p. 137°. (Found : Br, 32·6. $C_{19}H_{14}O_4N_2Br_2$ requires Br, 32·4 per cent.)

4-*hydroxy*-1-(2′ . 4′-*dibromophenyl*)-3-*carbethoxy*-5-*bromopyrazole.*

0·5 g. of bromine (1 mol.) in 2 c c of acetic acid was added to a solution of 1·3 g. of 4-hydroxy-1-(2′ : 4′-dibromophenyl)-3-carbethoxypyrazole (1 mol.) in 10 c.c. of boiling acetic acid.   The colour of the bromine at once disappeared, and, on cooling, 4-*hydroxy*-1-(2′ : 4′-*dibromophenyl*)-3-*carbethoxy*-5-*bromopyra-zole* separated as a colourless solid.   It crystallises from boiling alcohol in long, colourless, flattened, obliquely truncated prisms, m.p. 189°. (Found :

Br, 51·4. $C_{12}H_9O_3N_3Br_3$ requires Br, 51·2 per cent.) This compound was also obtained when ethyl-2 : 4-dibromophenylazo-γ-dibromoacetoacetate was heated with an alcoholic solution of potassium acetate.

Its *acetyl derivative* forms compact prisms from alcohol, m.p 91°–92°. (Found : Br, 46·9. $C_{14}H_{11}O_4N_2Br_3$ requires Br, 47·0 per cent.)

By similar methods the following derivatives of 4-hydroxypyrazole were also prepared.

4-hydroxy-1-phenyl-3-carbethoxypyrazole, * obtained from ethyl phenylazo-γ-chloroacetoacetate and from ethyl phenylazo-γ-bromoacetoacetate, crystallises from alcohol in colourless compact prisms, m.p. 85°. (Found . N, 12·0. $C_{12}H_{12}O_3N_2$ requires N, 12·1 per cent.)

4-hydroxy-1-(p-bromophenyl)-3-carbethoxypyrazole, separates from boiling alcohol in colourless, flattened prisms, m.p 136°–137°. (Found Br, 25·6. $C_{12}H_{11}O_3N_2Br$ requires Br, 25·7 per cent.)

4-hydroxy-1-(p-bromophenyl)-3-carbethoxy-5-bromopyrazole is moderately easily soluble in boiling alcohol, from which it crystallises in slender, colourless prisms, m p. 103°. (Found : C, 36·9 ; H, 2·6 ; N, 7·0 ; Br, 41·2. $C_{12}H_{10}O_3N_2Br_2$ requires C, 36·95 , H, 2·6 , N, 7·2 ; Br, 41·0 per cent.)

Its *acetyl derivative* crystallises from alcohol in shining, colourless leaflets, m.p. 134°. (Found · Br, 37·0. $C_{14}H_{12}O_4N_2Br_2$ requires Br, 37·0 per cent.)

4-hydroxy-1-(p-chlorophenyl)-3-carbethoxypyrazole, elongated, slender, colourless prisms from alcohol, m p. 137°–138° (Found : Cl, 13·2. $C_{12}H_{11}O_3N_2Cl$ requires Cl, 13·3 per cent.)

4-hydroxy-1-(2′ : 4′-dichlorophenyl)-3-carbethoxypyrazole was prepared from both ethyl 2 : 4-dichlorophenylazo-γ-chloroacetoacetate and ethyl 2 : 4-dichlorophenylazo-γ-bromoacetoacetate It crystallises from boiling alcohol in long, colourless, flattened prisms, m.p. 154°–155°. (Found : Cl, 23·7. $C_{12}H_{10}O_3N_2Cl_2$ requires Cl, 23·6 per cent.) Its *acetyl derivative* separates from boiling alcohol in felted, colourless needles, m.p. 85°. (Found : Cl, 20·6. $C_{14}H_{12}O_4N_2Cl_2$ requires Cl, 20·7 per cent)

4-hydroxy-1-(2′ : 4′-dichlorophenyl)-3-carbethoxy-5-chloropyrazole was prepared by chlorinating 4-hydroxy-1-(2′ : 4′-dichlorophenyl)-3-carbethoxypyrazole in

---

* This description of 4-hydroxy-1-phenyl-3-carbethoxypyrazole (m.p. 85° C.) agrees with the observation of Wolff (' Ann. Chem.,' vol. 313, p. 1 (1900)), who first obtained this compound from ethyl phenylazo-γ-bromoacetoacetate. Favrel (' C. R. Acad. Sci.,' Paris, vol. 156, p. 1912 (1913)), who states that he obtained the compound from ethyl phenylazo-γ-chloroacetoacetate, gives its melting point as 258°–260° C. The compound he describes cannot have been 4-hydroxy-1-phenyl-3-carbethoxypyrazole.

acetic acid solution at the ordinary temperature.　It crystallises from boiling alcohol in long, slender, flattened, colourless prisms, m.p. 161°.　(Found : Cl, 31·7.　$C_{12}H_9O_3N_2Cl_3$ requires Cl, 31·7 per cent.)

4-*hydroxy*-1-(2' : 4'-*dichlorophenyl*)-3-*carbethoxy*-5-*bromopyrazole* was obtained both by eliminating hydrogen bromide from ethyl 2 : 4-dichlorophenylazo-γγ-dibromoacetoacetate, and by brominating 4-hydroxy-1-(2' : 4'-dichloro-phenyl)-3-carbethoxypyrazole.　Colourless, flattened, obliquely truncated prisms from alcohol, m.p 176°–177°.　(Found : Cl, 18·7 ; Br, 21·0. $C_{12}H_9O_3N_2Cl_2Br$ requires Cl, 18·7 , Br, 21·05 per cent.)

Summary

The action of chlorine or bromine upon arylazoacetoacetates, in which the cyclic group is not already fully substituted, causes both substitution in the nucleus and replacement or substitution of the acetyl group or carbethoxy group

Two halogen atoms only enter the phenyl nucleus, even when excess of halogen is used　Hence the action of either chlorine or bromine upon ethyl 2 : 4-dichloro- or ethyl 2 · 4-dibromophenyl-azoacetoacetate is similar to its action upon the corresponding ethyl 2 · 4 : 6-trihalogenphenylazoacetoacetates.

According to conditions, bromine either replaces or substitutes the acetyl group, and finally replaces the carbethoxy group, yielding the compounds,
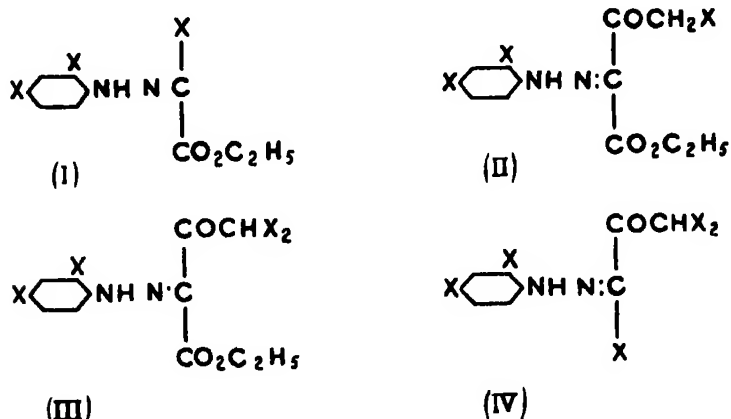
X = Cl or Br.

With chlorine only stages (I) and (II) are realised, since the molecule breaks down when the more vigorous action required to bring about stages (III) and (IV) is attempted.

The action of chlorine and bromine on unsubstituted or partially substituted ethyl phenylazoacetoacetate is similar, but halogen atoms also enter the nucleus. As these various substitutions and replacements do not, however, occur in strict succession, mixtures are generally obtained, from which individual compounds can only be isolated with difficulty.

When heated with alcoholic potassium acetate, the arylazo-γ-halogenacetoacetates and arylazo-γγ-dihalogenacetoacetates lose hydrogen halide, with ring closure, and formation of derivatives of 4-hydroxypyrazole.

The Apparent Conductivity of Oxide Coatings used on Emitting Filaments

By R. H. FOWLER, F.R.S., and A. H. WILSON

§ 1. Recent experiments by Reimann and Treloar* among others have thrown further light on the way in which the electrical current supplying the filament emission passes through the coating of barium- or strontium-oxide, used to render the filament a low-temperature emitter. They have studied in particular the variation of the current flowing with applied potential and with temperature. Though these phenomena have been elaborately discussed already by these authors and also by Reimann and Murgoci,† by Becker‡ and by Lowry,§ it seems to us possible that something new can be said in the light of the more detailed theory of semi-conductors and rectifying contacts now available.‖ It is possible that in return for the study of conductivity some light may be thrown on the most perplexing feature of thermionic emission from oxide-coated cathodes—its failure to saturate properly for moderate voltages.

---

* ' Phil. Mag.,' vol. 12, p. 1073 (1931).

† ' Phil. Mag.,' vol. 9, p. 440 (1930).

‡ ' Phys. Rev.,' vol. 34, p. 1323 (1929); ' Trans. Amer. Electro-chem. Soc.,' vol. 59, p. 207 (1931).

§ ' Phys. Rev.,' vol. 35, p. 1367 (1930).

‖ Wilson, ' Proc. Roy. Soc.,' A, vol. 136, p. 487 (1932). Substantially the same theory has been proposed independently by Frenkel and Joffe, ' Phys. Z. Sowjetunion,' vol 1, p. 60 (1932), and Nordheim, ' Z. Physik,' vol. 75, p. 434 (1932).

The recent experimental work of Reimann and Treloar need only be shortly summarised here. The conductivity measurements were made by measuring the current between two oxide-coated nickel filaments twisted tightly together and recoated after twisting. [The two twisted wires were used jointly as a single cathode for thermionic measurements.] The conductivity as measured is therefore derived from the current flowing from metal electrode to metal electrode for given potential difference between the electrodes, deeply immersed in the oxide and separated by a thickness of oxide of the order of 0·02 mm.

The conductivity grows during a *forming* process and suffers oxygen poisoning in very much the same way as the thermionic emission; as a consequence of these forming and poisoning processes it is agreed that some amount of electrolysis is going on, which may well account for the greater part of the conductivity in the earliest stages of *forming*. We shall see later in discussing the time-effects of the conduction currents that we must suppose that part of the current is carried electrolytically throughout the life of the filament. But we shall also be driven to conclude from the same time-effects that the current must be composite and cannot be purely electronic or purely electrolytic. There is no longer any difficulty in supposing that the major part of the current is electronic so far as concerns the temperature-variation of the current for given voltage. This variation is that typical of electronic semi-conductors. It is our object here to examine whether the current-voltage-temperature relationship for the formed coating may not be simply (but of course only roughly) explained on the supposition that the current is *mainly* electronic, provided we bear in mind the peculiar properties of semi-conductors and semi-conductor-metal contacts. We conclude that such an explanation is possible, but no precise and elegant account is to be expected of such a complex phenomenon.

§ 2. *Ideal Current-voltage Relationships for the System Metal-semi-conductor-metal.*—The current-voltage relationship observed by Reimann and Treloar is a composite one built up out of three sections which must be discussed separately—the nickel/oxide interface, the oxide itself, and the oxide/nickel interface. The whole system might be asymmetrical and have a rectifying effect, but it is more reasonable and probably correct to assume that the mean properties of the two contacts are the same, since they were treated identically, so that the system is symmetrical and cannot rectify.

The voltage V applied between the nickel filaments may be thought of as broken up into three parts

$$V = V_1 + V_2 + V_3, \tag{1}$$

applied respectively to the metal/oxide interface, the oxide layer and the oxide/metal interface. Then according to the proposed theory of semi-conductors and rectifying metal/semi-conductor contacts, we have approximately

$$I = Ae^{-W/kT} \{e^{\epsilon V_1/kT} - 1\} e^{-\epsilon V_1/kT_0} \quad \text{(metal/oxide)} \quad (2)$$

$$I = Be^{-W/kT} V_2 \quad \text{(Ohm's law } in \text{ oxide)} \quad (3)$$

$$I = Ae^{-W/kT} (1 - e^{-\epsilon V_3/kT}) e^{\epsilon V_3/kT_0} \quad \text{(oxide/metal).} \quad (4)$$

These formulæ provide only a rough approximation to the exact formulæ of the theory, but they should suffice for a first survey. A and B are constants; they include really powers of T whose variation may be ignored compared with that of other factors. The factor $e^{-W/kT}$ comes from the number of conducting electrons in the oxide provided by the thermal excitation. The factor $\exp(\pm \epsilon V/kT_0)$ represents the variation of the mean transmission coefficient of the metal/oxide contact with the voltage applied across the contact; kT_0 being merely a constant representing the properties of this layer. The factor will over-estimate the effect of V on the transmission coefficient for values of V greater than kT_0. In general kT_0 may be expected to be fairly large compared with kT.

Formula (4) gives the current-voltage relationship for a rectifying contact when the current flows in the direction of *high* resistance. It is obvious by inspection that the current tends to saturate at the value $A \exp(-W/kT)$ and later increases again owing to the increased transmissibility Formula (2) gives the similar current voltage relationship in the direction of *low* resistance. There is here a rapid exponential increase of current, somewhat affected at later stages by the diminishing transmissibility. Formula (3) is merely Ohm's law for the oxide itself.

In order to obtain I as a function of V from formulæ (1)–(4) it is only necessary in principle to assign suitable values to the constants, plot I as a function of V_1, of V_2, of V_3, on three separate diagrams, read off V_1, V_2 and V_3 for a given value of I, thus obtaining $I = f(V_1 + V_2 + V_3) = f(V)$. Various devices can be used to shorten the work, into which we need not go. The curves shown in fig. 1 are the result of this process, using the values of T_0 and A/B there stated. These are the only structural parameters in the equations which affect the form of the curves. The remaining constant, which may be taken to be $A \exp(-W/kT)$, is a common factor in each expression for I. Since we cannot compare absolute values of I calculated and observed, this common

factor does not concern us except for its temperature variation, which merely alters the scale of I from one temperature to another.

§ 3. *Characteristics of the I–V Curves and their Comparison with Observed Values.*—It is easily seen that the curves are of much the same characteristic shape at all temperatures, the principal change being in the scale factor $\exp(-W/kT)$. The only other factors in which the temperature occurs are $(\exp \varepsilon V_1/kT - 1)$ and $\{1 - \exp(-\varepsilon V_3/kT)\}$. Of these the first is comparatively
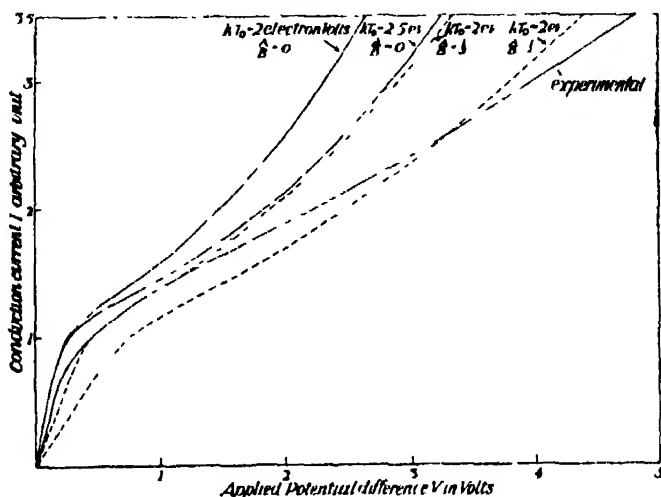
FIG. 1.—Showing calculated and observed current-voltage curves $I = f(V) = f(V_1 + V_2 + V_3)$ for different values of the parameters and a temperature of 922° K.

unimportant, since V_1 is small and adjusts itself to V_3. The second factor is practically constant for large values of V_3, and so, if we remove the scale factor $\exp(-W/kT)$, the various current-voltage curves will differ somewhat for small values of V, but will tend to become the same for values of V much larger than kT. The general similarity of shape means that, if any particular voltage V is chosen (it does not much matter what) and log I is plotted against $1/T$ for constant V, a good straight line will be obtained whose slope will determine W. This should occur in spite of the peculiar shape of the I–V curve and its failure to show saturation. It was, in fact, found by Reimann and Treloar that good straight line plots of log I against $1/T$ are so obtainable.

The calculated curves at all temperatures show a considerable amount of "character," differentiating them from the ohmic straight line. They all show the initial sharp rise and the tendency to saturate, followed later by a further increase. The character is naturally more marked for larger values

of T_0, which delay the breakdown of the attempt to saturate to higher voltages and for larger values of B/A, that is, for a smaller ohmic part of the total resistance. Except that the final rate of increase, in the neighbourhood of 5 volts or so, is too rapid, the calculated curves give a very good representation of the observed I–V curve at 922° K. given by Reimann and Treloar, in their fig. 3, curve I. It is, however, interesting to record that their observed curves at lower temperatures show distinctly less "character" and cannot be imitated by any of the calculated curves using constants in any way comparable to those used at 922° K. In the particular curves of this figure again, the ratio of the currents at 922° K. and 793° K. and at 793° K. and 652° K. are quite inconsistent with a constant value of W, especially at the higher voltages. Now a variation with temperature like $\exp(-W/kT)$ is to be expected of the current at a given voltage, whether it is electronic or electrolytic. We are, therefore, forced to conclude, if the electronic theory we are using is in any way correct and if the experiments may be taken at their face value, that the current is a mixed one, mainly electronic at the higher temperature, mainly electrolytic at the low. This is in agreement with the results of Becker,[*] who finds a conductivity of the type

$$\alpha_1 e^{-\beta_1 T} + \alpha_2 e^{-\beta_2 T},$$

and who interprets these terms as electronic and electrolytic respectively with $\beta_1 > \beta_2$, $\alpha_1 \gg \alpha_2$. The change in "character" of the curves for different temperatures appears to us by itself as necessitating some such interpretation as that the current is a mixture of two different effects.

So far we have not considered how the electrolytic part of the current should vary with voltage, but this can readily be done, if we use the model proposed by Gurney[†] in his paper on the quantum mechanics of electrolysis, and assume, rather boldly perhaps, that it is applicable also to the electrolysis of the solids. The current is then carried through the oxide coating by Ba^+ (or Ba^{++}) and O^- (or O^{--}) ions which are discharged at the metal electrodes by extracting an electron from or surrendering one to the metal. The relationship between the voltage drop and the current across either interface is for this current of the form

$$\frac{d \log I}{dv} = \frac{\varepsilon}{ykT} \qquad (y \gg 1)$$

or

$$I = I_0 \, e^{\varepsilon |V|/ykT},$$

\hfill (5)

[*] *Loc. cit.* (1931).

[†] 'Proc. Roy. Soc.,' A, vol. 134, p. 137 (1931).

provided the voltage is not too great, the sign of V being, of course, that required to drive the electron current. The relationship for the oxide itself is perhaps roughly ohmic, but comparatively more important than the ohmic part of the electronic current owing to the much shorter free path of an ion. The electrolytic current according to equation (5) plus an ohmic section will show no tendency to saturate at moderate voltages; without the ohmic section it would increase exponentially over the whole voltage range, for which (5) is valid, which is of the order of a few volts. With an ohmic section the exponential rate of increase will be steadily slowed down until the current-voltage curve approximates to a straight line at the higher voltages. The voltage at which this occurs will, of course, depend on the temperature and also on the relative importance of the interface and ohmic potential drops. The ohmic section will also, of course, be required to take up the greater part of the total voltage drop, so that the voltage drops across the interfaces will probably remain in the region of validity of (5) for comparative large total voltages. The electrolytic current-voltage curves will therefore show none of the " character " found at 922° K. (fig. 1). They are therefore just exactly of the general type required to explain the curves found by Reimann and Treloar at lower temperatures.

To attempt any more detailed analysis of the I–V curves on these lines would be a mistake, as there are too many constants at our disposal to make any fitting of the curves obtained significant. But if we may suppose that the electronic current is dominant at 922° K., we may conclude that the theory gives an excellent account of the observed curve, except at the higher voltages. But here the too sharp rise of the theoretical curve is due to the faulty approximations we have used for the actual theory.

§ 4. *Time-changes in the Current-voltage Relationship.*—If the proposed explanation of a mixed conductivity is accepted, we believe that a satisfactory explanation can be given of the time-changes in the current voltage relationship, observed especially at low temperatures. At such temperatures it is found that on imposing a new voltage the current only slowly reaches its new equilibrium value. In particular if the voltage, having been steady at V_1 with a current I_1 is reduced to V_2 (with a final equilibrium current I_2), the current rapidly falls to a value I_2' ($> I_2$) which may be more than twice as great as I_2. Now suppose the current is mixed. Besides the electron current there is then an electrolytic current, positive Ba ions going one way and negative O ions the other, both being discharged on the filament electrodes. Besides the steady accumulation of discharged atoms, there will tend to be a concentration

gradient of Ba^{++} and O^{--} with an associated back potential gradient opposing the electrolytic current characteristic of the current flowing. This potential gradient will, of course, also oppose the electron current. But the modification of the potentials in the surface layers, by the Ba^{++} in the oxide *to* which the electron has to jump *from* the metal and by the O^{--} in the oxide *from* which the electron has to jump *to* the metal, will assist the electron current, and if the ohmic part of the resistance is small this effect can easily outweigh the polarisation effect in the oxide itself. Thus, after a decrease of voltage, and until the concentration of heavy ions has fallen by diffusion to the correct new value, an electron current will flow which is greater than the equilibrium value for the new voltage, thus accounting for the observations

It must not be supposed that we could yet give a satisfactory quantitative account of the observations in this simple way. We have suggested that at low temperatures the electrolytic current becomes a significant fraction of the whole current, or even dominates it. At the same time we propose to explain the time effects by changes in the electronic current due to changes in the heavy ion concentrations. It has yet to be shown in numerical detail that these two effects are consistent, and this is not possible without a more elaborate theory.

§ 5. *Forming, Poisoning and Reviving.*—We now comment shortly on the special features of oxide-coated cathodes enumerated in the heading, for they seem to provide some of the strongest evidence that the coating is an electronic semi-conductor with an impurity conductivity, the important impurity being free barium or strontium. In "forming" a filament the formation or activation proceeds much more rapidly if electron currents are drawn from the coating than if the coating is merely heated. When currents are flowing the barium ions will move through the coating, thus beginning to supply the necessary electron sources for the conduction. Activation proceeds with oxygen emission, and poisoning is the reverse process proceeding when oxygen can be supplied to the filament. All these features point to the necessity of free barium in the coatings, which is even more forcibly supported by the fact that free barium activates a filament when directly supplied by distillation. There is thus quite unambiguous evidence that the active state of the filament (when the filament coating both conducts current and emits electrons efficiently) is a state in which free barium is present as an impurity and probably (but this is only an inference) present both on the surface as a monatomic film and in the bulk of the material. That an active coating is in such a state that it will conduct electronically as an impurity semi-conductor is therefore no *ad hoc*

hypothesis, but a necessary consequence of its other properties. It seems to be fair to conclude that the observed current-voltage relationships are to be accounted for in the way we have suggested.

§ 6. *The Thermionic Emission.*—When we come to consider the thermionic emission, and in particular its variation with anode voltage, it must at once be admitted that any existing theory fails completely. In spite of this we wish to point out some significant facts in the hope that they may in the future lead to a better understanding of the underlying processes. The most striking feature of the thermionic current is its failure to saturate, and the curves of thermionic current against anode potential show an extraordinary resemblance to the curves of conduction current against voltage, which we have discussed above. This failure to saturate is not confined to oxide-coated filaments, but occurs whenever the emitting surface is composite, even when there is less than a monatomic surface layer of foreign matter present. It is reasonable, therefore, to ascribe the failure to saturate to the presence of a film of barium on the surface of the oxide, but we can give no reasonable explanation of the effect of this film. The only way in which the thermionic current can be made to imitate the conduction current seems to be to assume that the passage of the electrons through the composite surface layer to the vacuum requires a potential drop V_3 and has a current-voltage relationship (I, V_3) similar to that for the oxide/metal interface. We are then required to assume further that there is a current-voltage relationship (I, V_4) for the gap between the outside of the film on the cathode and the metal anode itself. Since there are no significant space charge effects in such cases, one is tempted to say that $\partial I/\partial V_4 = 0$. But the problem then becomes indeterminate—that is, there is no unique (I, V) relationship where $V = V_1 + V_2 + V_3 + V_4$, unless one other equation can be found such as $V_4 = 0$. If we might assume $V_4 = 0$ and the proper features for the oxide/vacuum interface, then the observed thermionic current-voltage curves could be reproduced. For these assumptions we have no theoretical justification at present, but we believe a search for a solution along these lines might be profitable.

Summary.

Recent experiments have established peculiar forms for the electrical conductivity of an oxide coating as applied to a metal wire to make it a good low temperature thermionic emitter. The current flowing has been studied as a function of voltage and temperature. By applying Wilson's theory of semiconductors and rectifying contacts, and Gurney's theory of electrolytic conduction, it is possible to give a satisfactory analysis of the observations and to conclude that the current is a mixed one, mainly electronic at high temperatures, mainly electrolytic at low. The marked resemblances between the behaviour of the conduction current as a function of voltage and temperature and the behaviour of the thermionic emission, and one of the outstanding difficulties of thermionic theory, are commented on.

The Influence of Foreign Gases on the Lower Critical Oxidation Pressure of Carbon Disulphide.

By A. Ritchie, R. R. H. Brown, and J. J. Muir

The study of gaseous reactions has recently acquired additional interest, since it has been found that a considerable number of reactions can be explained on the basis of a chain hypothesis   In 1923 Christiansen and Kramers[*] studied the kinetics of a unimolecular reaction and found that explosion is possible if the total change of energy resulting from the reaction is greater than the energy of activation. Since that time the mechanism of chain reactions has been carefully investigated and some of the conditions for the continued propagation of the reaction have been ascertained.

Thus, if we have two gases mixed together without any chemical change taking place, a reaction *may* commence when even a very small quantity of a third molecule is added, or if one of the original molecules receives energy of activation (from whatever cause). Designating the original molecules for simplicity by A and B and the new molecule by C, which we will suppose reacts

[*] ' Z. phys. Chem.,' vol. 104, p. 451 (1923).

with A, giving a fourth molecule D (and possibly other molecules also), we have

$$A + C \rightarrow D.$$
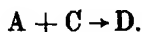
If then D reacts with B, producing more C (as well as other products) :

$$B + D \rightarrow C + \text{etc.,}$$
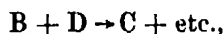
C and D are continually produced and form links in a chain, enabling the reaction to proceed.   If the amount of C and of D formed in unit time is greater than the amount destroyed, the chain will have many branches, *i e*, the reaction auto-accelerates and explosion occurs.   The active centres C and D may be destroyed in two ways : (*a*) by collision in the gas phase, (*b*) by collision with the surface of the vessel.   These considerations show that the amount of C and D formed and destroyed in unit time varies with the concentration of the gases A and B.   There may be a definite range of concentration in which the rate of formation of the active centres exceeds the rate at which they are destroyed, *i e.*, in which " explosion " can occur.   Many reactions are satisfactorily explained by this hypothesis   Phosphorus vapour and oxygen, sulphur vapour and oxygen, hydrogen and oxygen, carbon disulphide and oxygen, are found to unite explosively only between certain limits of pressure, and Semenoff[*] showed that this is explicable by means of the theory of chains.   He investigated the effect of the presence of foreign gas and the effect of varying the diameter of the reaction vessel on the lower oxidation limit and obtained the following relation :

$$p_{P_4}{}^{\frac{1}{2}} p_{O_2} \left(1 + \frac{p_X}{p_{P_4} + p_{O_2}} \right) d^2 = K$$

p_{P_4} is the pressure of phosphorus vapour, p_X the pressure of foreign gas, p_{O_2} is the critical oxidation pressure, d the diameter of the reaction vessel, and K a constant over a considerable temperature range.   Dalton and Hinshelwood[†] found that this equation also held when phosphine was substituted for phosphorus vapour

The equation can be derived theoretically by the assumption that below the critical pressure the chains are being broken so efficiently by the walls that the concentration of active centres remains stationary.   The foreign gas molecules impede the chains reaching the wall and so lower the critical oxida-

* ' Z. Physik,' vol. 46, p. 109 (1927) ;   vol. 48, p. 571 (1928) ;   also Hinshelwood and Thompson, ' Proc. Roy. Soc.,' A, vol. 118, p. 170 (1928).

† ' Proc. Roy. Soc.,' A, vol. 125, p. 294 (1929).

tion pressure. The equation should hold for all similar chain reactions, but it must be noted that it is only approximately true. Melville and Ludlam* investigated the effect of a large number of gases and organic vapours on the oxidation of phosphorus, and although they found that straight lines were obtained when $1/p_{O_2}$ was plotted against $1 + p_X/p_{P_4} + p_{O_2}$ (p_{P_4} being kept constant), these lines had not the same slope d^2/K as is expected from the above equation. Melville and Ludlam showed that the differences were, in the main, due to the different rates of diffusion of the chain propagators into the foreign gases. Melville† has recently given a theoretical equation for this foreign gas effect. He finds that p_X should be multiplied by a factor inversely proportional to the diffusion coefficient of the chain propagators into the gases present.

The factor is

$$f D_X^{-1} = \sigma_{AX}^2 \left(\frac{1}{M_A} + \frac{1}{M_X} \right)^{-\frac{1}{2}} \Big/ k,$$

where M_A and M_X are the molecular weights of the diffusing molecules A and of the foreign gas X respectively σ_{AX} is the sum of the radii of A and X. M_A and σ_A will be mean values, as they represent the effect of two chain propagators. Thompson‡ has recently found that the foreign gases change the lower critical explosion pressure of hydrogen-oxygen mixtures in the same order as was found by Melville and Ludlam. In this case active centres were introduced by an electric spark.

The critical pressure limits of the carbon disulphide oxygen explosion have been investigated by Thompson.§ His researches show that the active centres of the chain are principally formed at a hot wall.

In the present investigation the carbon disulphide and oxygen were kept at room temperatures and the hot wall furnished by a glass-covered or ordinary tungsten filament. It was found that this method gave the pressure of foreign gas at the lower critical oxidation pressure to within 1 mm. of mercury. The object of the present work was to investigate the effect of several gases and organic vapours on the lower critical oxidation pressure for $CS_2 : 3O_2$ mixtures with a view to testing the applicability of Semenoff's equation with Melville and Ludlam's correction.

* 'Proc. Roy. Soc.,' A, vol. 132, p. 108 (1931).
† 'Trans. Faraday Soc.,' vol. 28, p. 308 (1932).
‡ 'Trans. Faraday Soc.,' vol. 28, p. 299 (1932).
§ 'Z. phys. Chem.,' B, vol. 10, p. 273 (1930); Thompson and Kearton, 'Z. phys. Chem.,' B, vol. 14, p. 359 (1931).

Apparatus and Procedure.

The apparatus is shown diagrammatically in fig. 1. R is the reaction tube, which is 25 cm. in length and 2·5 cm in diameter. The filament F is mounted on a degassed nickel support, which is attached to borated copper wire, which in turn passes to the outside of the vessel through a pinch seal. The whole arrangement is mounted on the ground glass joint of the reaction tube. The
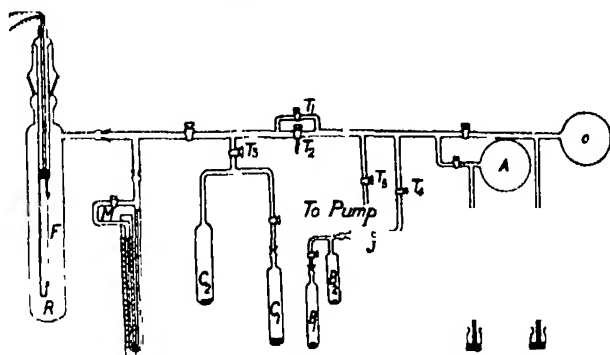

FIG. 1.—Diagram of the reaction tube R showing connections to oxygen reservoir O, to the foreign gas reservoir A, and to the CS_2 reservoir C_2.

glass filament is prepared as follows. Pyrex tubing is drawn down to a fine capillary which is threaded with 0·1 mm. tungsten wire and the glass melted on to the wire electrically in vacuo. Glass ends are now fitted on and filled with lead into which pass copper wires. This type of filament was first used by Melville in connection with the stable chain oxidation of phosphorus. Actually most of our experiments were conducted using a plain tungsten filament. This was only heated to a dull redness and so practically no oxidation took place. The results show that there is little difference in the behaviour of the two filaments M is a sulphuric acid manometer with scale attached. C_1 contains the carbon disulphide, A and O are reservoirs for foreign gas and oxygen respectively. When organic liquids are used they are placed in B_1, which is then connected to the rest of the apparatus at J.

The procedure is as follows. C_1 is immersed in liquid air and the apparatus is evacuated, using an electrically driven oil-pump. Tap T_3 is closed and some carbon disulphide distilled into C_2. The taps T_1 and T_5 are now closed and A and O filled with the foreign gas and oxygen to a pressure of about 20 mm. of mercury through tap T_4. Carbon disulphide vapour is now introduced into the reaction vessel to the desired pressure as read from the manometer. Oxygen is then admitted to about three times that pressure. The filament is switched on for 1 or 2 seconds. If the pressure is below the critical value no flash is seen and

the manometer reading remains the same. The foreign gas is now admitted in small quantities by means of the tap-pipette T_2 and the filament heated after each addition. At a certain pressure of foreign gas an explosion takes place and the pressure falls. The explosion is accompanied by a blue luminescence.

Organic liquids were distilled *in vacuo* from B_1 to B_2 and their vapours admitted by the tap-pipette into the reaction vessel. In the case of hydrogen the oxygen had to be introduced afterwards for reasons which will appear later. The oxygen, nitrogen, argon, hydrogen and carbon dioxide were all obtained from cylinders and were dried by passing them over phosphorus pentoxide. Sulphur dioxide was obtained from a syphon of the liquid. The carbon disulphide was previously distilled and the middle fraction used. The carbon tetrachloride was sulphur free The table below shows some of the experimental results. All pressures are in millimetres of mercury.

Table I.

Inert gas X.	p_{CS_2}	p_{O_2}	p inert gas	$1/p_{CS_2} p_{O_2}$	$1 + \dfrac{p_X}{p_{CS_2} + p_{O_2}}$
Carbon dioxide	3 7	16 9	0	0 0162	1 00
	3 0	12 5	+ 9	0 0205	1 30
	3 8	11 4	6 9	0 0231	1 45
	3 4	10 2	11 0	0 0288	1 81
	2 7	8 1	23 8	0 0457	3 20
Sulphur dioxide	3 7	16 8	0	0 0163	1 00
	4 1	12 9	3 7	0 0192	1 22
	3 5	11 2	9 6	0 0253	1·65
	3 2	10 3	12 6	0 030	1·93
	3 0	9 3	16 8	0 0359	2 36
Nitrogen	4 0	15 7	0	0 0159	1 00
	4 0	12 4	10 1	0 0204	1 62
	3 7	15 1	4 3	0 0181	1 23
	3 5	10 8	21·9	0·0263	2 53
	3 0	9 3	35·2	0 0359	3 86
Argon	3·6	16 6	0	0 0169	1 00
	4·2	12 6	4 2	0 0189	1 25
	3 8	11 8	9 9	0 0224	1 63
	3 2	9 7	19 1	0 0317	2 47
Argon, using a glass - covered filament	3 4	10 3	8 2	0 0287	1 ··
	2 7	8 1	12 8	0 0456	2 18
	2 3	7 3	16 1	0 0596	2 68
Hydrogen	3·9	16 4	0	0 0156	1 00
	3 8	20 3	13 8	0 0130	1 57
	3 7	27 4	27 0	0 0100	1 87
	3 5	31·4	38 2	0 0090	2 09
	4 0	18·1	11·3	0 0138	1 51
	3 9	24 1	5 0	0·0106	1·18
	3·7	26 5	12·3	0 0104	1 41

Discussion.

As shown in fig. 2, when $1/p_{CS_2} p_{O_2}$ is plotted against $\left(1 + \dfrac{p_X}{p_{CS_2} + p_{O_2}}\right)$ satis-factory lines are obtained except in the case of hydrogen. The slopes of the lines given by argon, nitrogen, carbon dioxide and sulphur dioxide follow the
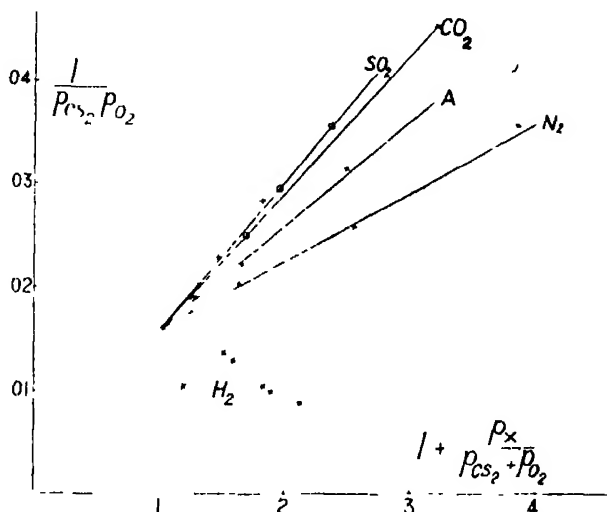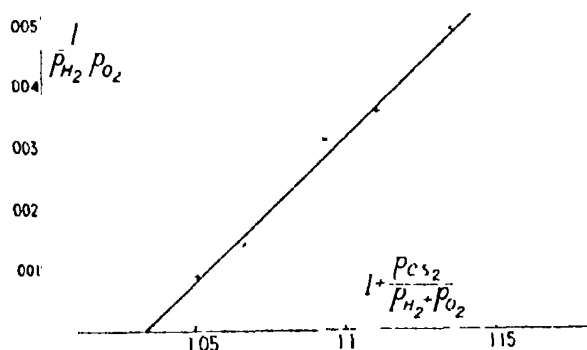

Fig. 2 —The graph obtained by plotting $1/p_{CS_2} p_{O_2}$ against $1 + \dfrac{p_X}{p_{CS_2} + p_{O_2}}$. p_{O_2}, p_{CS_2}, and p_X being the critical oxidation pressure, the pressure of CS_2 and the pressure of foreign gas respectively.

same order as was found by Melville and Ludlam (*loc. cit.*) for the $P_4 : O_2$ explosion. Assuming

$$p_{CS_2} p_{O_2} \left(1 + \frac{fD_X^{-1} p_X}{p_{CS_2} + p_{O_2}}\right) = \text{constant}$$

($= p_{CS_2} p_{O_2}$ when no foreign gas is present), the above experimental results give the following values for fD_X^{-1}.

Foreign gas.	Nitrogen.	Argon	Carbon dioxide.	Sulphur dioxide
fD_X^{-1}	0·42	0 64	0 83	0·92

These values are not sufficiently accurate to enable a calculation of the molecular weight of the chain propagator to be made, using the expression

$$\frac{\sigma_{AX}^2 (1/M_A + 1/M_X)^{-\frac{1}{2}}}{k} \text{ for } fD_X^{-1}.$$

Hydrogen gives an abnormal result. The presence of hydrogen, instead of reducing the value $p_{CS_2} p_{O_2}$, actually increases it. This result is accounted for in the following way. In all the other experiments, the change of pressure after exploding was always about 80 to 90 per cent. of the original pressure of carbon disulphide. This means that the main reaction gives sulphur dioxide and carbon dioxide. When hydrogen was present the change of pressure after explosion was approximately one and a half times the pressure of the hydrogen. The main reaction is therefore the formation of water from hydrogen and oxygen. It therefore appears probable that we were dealing with the $H_2 : O_2$ explosion and that CS_2 was behaving as an inert gas by preventing the $H_2 : O_2$ chain propagators reaching the wall.

<div align="center">Table II.</div>

p_{H_2}	p_{O_2}	p_{CS_2}	$1/p_{H_2} p_{O_2} \times 10^2$	$1 + \dfrac{p_{CS_2}}{p_{H_2} + p_{O_2}}$
13 8	26 3	3 8	0 357	1 11
27 0	27 4	3 7	0 137	1 07
38 2	31 4	3 5	0 083	1 05
11 3	18 1	4 0	0 489	1 14
5	24 1	3 9	0 830	1 13
12 3	25 5	3 7	0 307	1 09

When $1/p_{H_2} p_{O_2}$ is plotted against $1 + \dfrac{p_{CS_2}}{p_{H_2} + p_{O_2}}$ as shown in fig. 3 a straight line is obtained, if the value obtained for a very small pressure of hydrogen is excluded. A peculiar fact about this line is that it appears to show that the

FIG. 3.—The graph obtained by plotting $1/p_{H_2} p_{O_2}$ against $1 + \dfrac{p_{CS_2}}{p_{H_2} + p_{O_2}}$. p_{O_2}, p_{CS_2} and p_{H_2}, being the critical oxidation pressure, the pressure of CS_2 and the pressure of hydrogen respectively.

$H_2 : O_2$ explosion is impossible under the experimental conditions unless carbon disulphide is present. It is therefore very probable that CS_2 acts as an explosion sensitisor for the $H_2 : O_2$ reaction. The propagator of the $CS_2 : O_2$ explosion chain may give on colliding with H_2 an active centre, which can start the propagation of the $H_2 : O_2$ chain. Carbon disulphide therefore can be looked upon as a catalyst of the reaction under the special conditions of these experiments.

The effect of carbon tetrachloride and of benzene on the lower critical pressure was complicated as neither of these vapours acted as " inert " gases. When a certain pressure of benzene or of carbon tetrachloride was reached, on heating the filament a cloud of white particles was formed and a deposit was left on the walls. This pressure was just about where explosion would be expected if these vapours behaved as inert gases. It is probable that the active centres are decomposed on colliding with the organic molecules to give sulphur or complicated compounds.

Thompson* found that it was difficult to get reproducible results for the explosion limit owing to variations of the surface of the reaction vessel. There was no difficulty of this kind in the above experiments, as after one or two explosions, which yielded high values, steady results were obtained. The explosion gave no apparent deposit on the walls, but it is very probable that the surface is covered with a thin layer of sulphur or a compound of sulphur, so that further explosions do not change the nature of the surface. The fact that the explosion limit changes with the surface is evidence that chains can be reflected from a surface as well as broken by that surface.

Below the lower critical limit a blue luminescence could be seen round the hot filament, but no change of pressure was observed. This luminescence is taken as evidence of a *stable* chain reaction below the critical limit similar to the $P_4 : O_2$ stable chain found by Melville and Ludlam.† The luminescence observed by Thompson during the induction period is probably due to this type of stable chain. Further examination of the luminescence below the lower limit will shortly be carried out.

Summary.

The lower critical oxidation pressure of carbon disulphide vapour in presence of " inert " gases has been found to obey the expression

$$p_{CS_2} p_{O_2} \left(1 + \frac{f D_x^{-1} p_x}{p_{CS_2} + p_{O_2}} \right) = \text{constant,}$$

* ' Z. phys. Chem.,' B, vol. 10, p. 273 (1930).

† ' Proc. Roy. Soc.,' A, vol. 135, p. 315 (1932).

where p_{cs_1} and p_{0_1} are the lower critical explosion pressures in the presence of pressure p_X of inert gas. D_X is the diffusion coefficient of the chain propagator into the foreign gas.

The effects of hydrogen, carbon tetrachloride and benzene, which do not behave as " inert " gases, are discussed.

The Recovery of Proportional Elasticity in Overstrained Steel.

By S. L. SMITH, D Sc., A.C.G.I., and J. V. HOWARD, D Sc.

When a metal is pulled beyond its yield point, the total extension is partly a plastic permanent set and partly elastic in the sense that some of the strain disappears on the removal of the stress. But this elasticity differs from the primitive elasticity of the material in that the stress plotted against the strain during the unloading period gives a curved line instead of a straight one. On immediately reloading the material, the stress-strain line is again curved, but in the opposite direction ; so that, during the unloading and reloading, the stress-strain curve forms a loop of what may be termed mechanical hysteresis

Bauschinger was the first to observe that the limit of proportional elasticity could be lowered by overstraining the metal ; and that, by resting the test-piece for a period of 50 hours, the elastic limit was restored to a value sometimes above its initial or primitive value.

The questions which at once present themselves are :—

(1) Can the property of proportional elasticity always be restored to the overstrained metal by resting it at ordinary temperatures ?

(2) Is the period of 50 hours used by Bauschinger sufficient to allow the new limit of proportional elasticity to reach its highest possible value, or will a longer rest period permit a greater degree of elastic recovery and a still higher value for the new elastic limit ?

(3) In what way do variations in the composition of the metal affect its power of recovery ?

(4) Would the recovery of proportional elasticity be prevented if the metal carried a constant stress during the pause between testing instead of resting under no load as in the Bauschinger experiments ?

It seems possible that the answer to these questions might throw some light on the behaviour of metal subjected to stress-repetition.

Some 9 years ago the authors made an investigation of the factors which determined the formation of the hysteresis loops.* A number of the test pieces used in this work were severely overstrained but not broken. These have been stored away since that time and have now been re-tested. For this investigation the load-extension instrument devised by Professor Dalby† was used, in which the load-extension line for a tension test is traced out by a spot of light moving over a photographic plate.

1 *Scope of the Investigation.*

The present research has been confined to the study of steels of different types.

The steels tested comprise :--

(i) A series of straight carbon steels ranging from mild steel of $0 \cdot 10$ per cent. carbon content to steel of eutectoid composition, $0 \cdot 85$ per cent carbon, and including one case of bright-drawn cold-rolled mild steel.

(ii) A series of steels similar to the above as regards carbon content but containing about three times as much phosphorus, namely $0 \cdot 1$ per cent. instead of $0 \cdot 03$ per cent.

(iii) Low-carbon nickel steels of the case-hardening type.

(iv) A 3 per cent. nickel steel of forging grade.

(v) Nickel-chrome steels including an air-hardening steel.

All these steels were given various heat treatments before the original overstraining, the particulars of which are stated in the Table of Results.

---

* 'Proc. Roy. Soc.,' A, vol. 107, p. 113 (1925).

† 'Phil. Trans.,' A, vol. 221, p. 117 (1921).

2. *The Original Overstraining.*

This was carried out in a special manner. Each test-piece was first pulled to a point beyond its yield-point, the line of primitive elasticity being recorded. The load was then removed and immediately re-applied, thus causing the load-extension line to describe a loop The looping operation was repeated at intervals of permanent set of about 0·03 inch, but only every fourth loop was recorded. This process was continued until the maximum load for the test-piece was reached.

Fig. 1 shows two typical records and also, to the left hand, the load-extension diagrams obtained from a breaking test on a piece of the same material.

The upper diagrams refer to a nickel steel of forging grade. The load-extension diagram for the break test has all the characteristics associated with a normal steel, namely, a load peak at the yield point, followed by a yield period link during which the load is nearly constant, followed again by the curve of plastic deformation. The primitive limit of proportional elasticity, scaled off the record of the looping test, occurs at 24·5 tons per square inch.

The lower diagrams were obtained from a nickel-chrome steel. The load-extension diagram differs fundamentally from the previous one in that it has no yield point in the usually accepted sense. It also possesses a very low primitive elastic limit. A high elastic limit and a definite yield-point can be conferred on the steel by suitable heat-treatment. (See tests Nos 44 and 45 in the Table of Results.)

Instead of the above method of overstraining, some of the test-pieces were subjected to continuous looping at constant load.

3. *The Re-test for Elastic Recovery*

Each test-piece was pulled to a predetermined load and immediately unloaded, the load-extension lines for loading and unloading being recorded. This process was carried out with a number of loads ranging up to the final load reached in the original overstraining.

The object of this procedure was to enable any curvature of the load-extension line to be readily detected.

If the metal had recovered its proportional elasticity, the loads for ascending and descending loads would be coincident.

If the metal had not recovered, the load-extension lines would be curved and the record would show a loop.

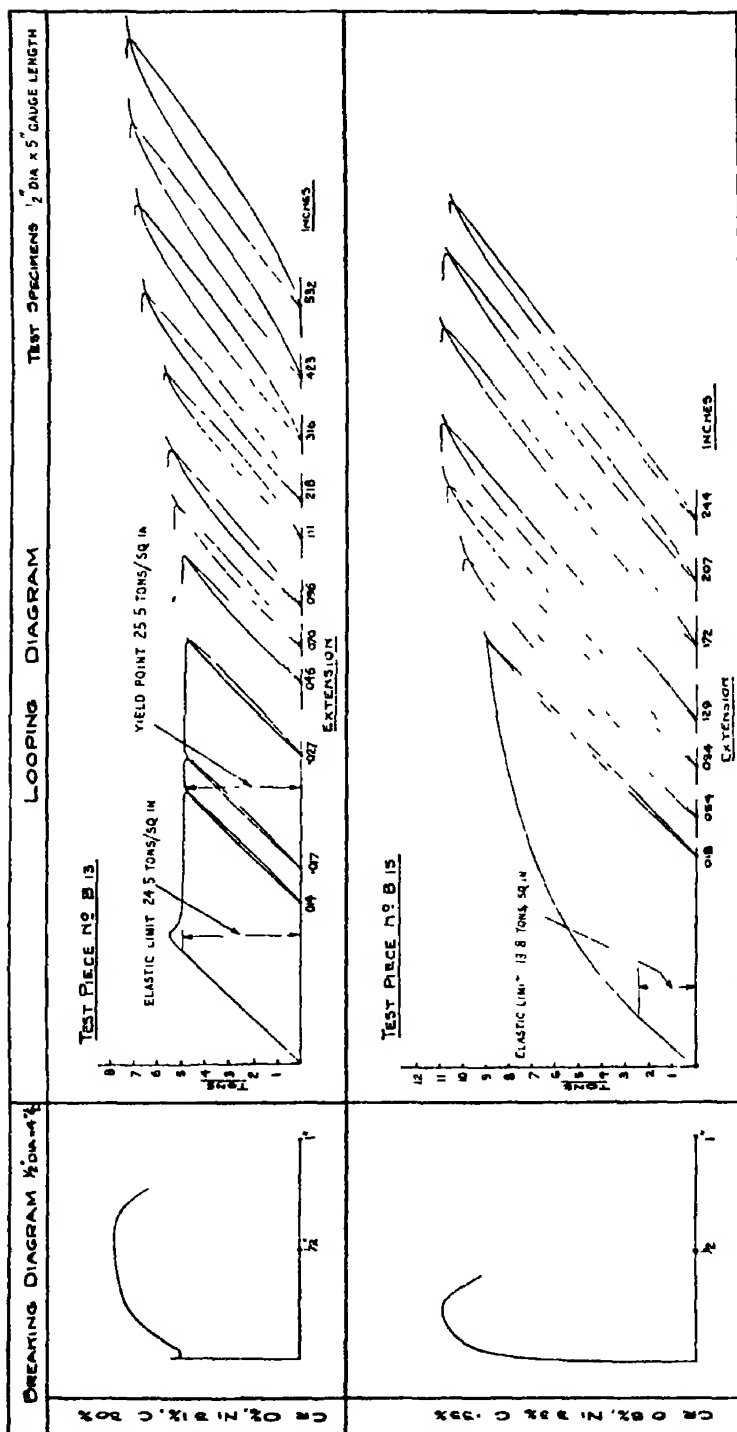Figs. 2, 3 and 4 show some of the records obtained in the re-tests.

FIG. 1.

4. *Types of Re-test Record*

The records can be classified into three groups.

(i) *Complete Elastic Recovery* —Fig 2, test-piece No. B.8 is an example of this type of record. The primitive elastic limit occurred at 5·1 tons, and the maximum load originally reached was 8·5 tons
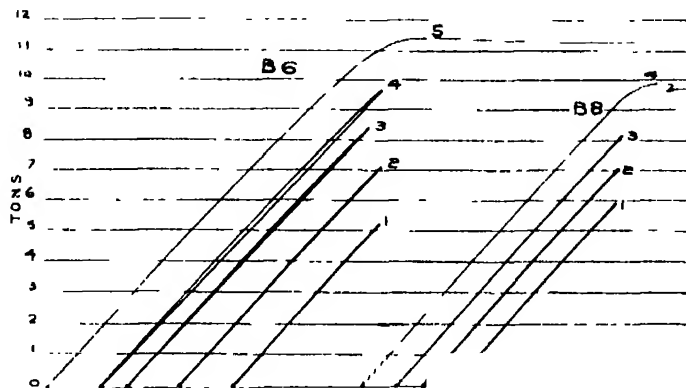

Fig. 2.—Typical re-test records.

The load-extension lines for loading and unloading in the re-test are coincident up to the maximum load applied in the original overstraining, showing that the metal had completely recovered its property of proportional elasticity and that the limit of proportionality had been raised right up to the last stress previously applied.

The test-piece was finally pulled until it definitely yielded. The record of this pull is marked " 4 " and shows the yield-point occurring at 10·0 tons.

(ii) *Partial Elastic Recovery.*—Fig. 2, test-piece B.6 is an example. (See test No. 39 in the Table of Results.) The primitive elastic limit occurred at a load of 2·8 tons and the steel had no definite yield point, the load-extension diagram from the original test being of the same type as that of test-piece B.15 shown in fig. 1. The maximum load applied in the original test was 10·8 tons.

The loading and unloading lines traced at the lower loads on re-testing are coincident, but loops develop at the higher loads before the previous maximum load is reached.

The first two pulls of the re-test afford evidence of elastic recovery   Pull No. 3 gives a small but definite loop showing that the limit of proportional elasticity has been passed, but that the metal is non-proportionally elastic since the loop closes at the bottom and no permanent set is recorded.

The final pull, No. 5, gives a yield-point on re-testing at 11·3 tons.

Fig. 3, obtained with a nickel-chrome steel (test No 46 in the Table of Results) is a re-test record of the same type.
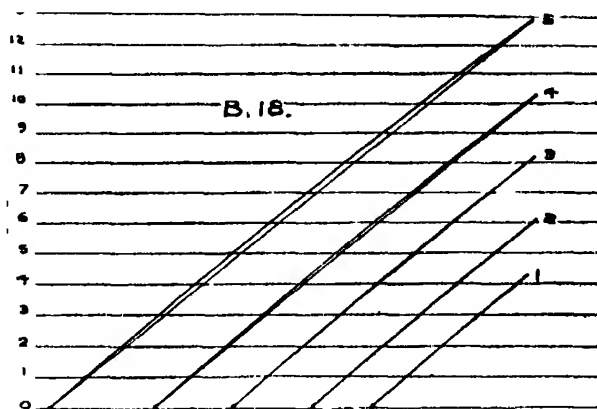

FIG. 3.—Re-test of nickel-chrome steel.

(iii) *No Elastic Recovery.*—Fig. 4 shows two records of this type.

In both cases loops are traced even at the lowest loads applied in the re-test, showing that there has been no recovery of proportional elasticity although the metal possesses complete non-proportional elasticity.
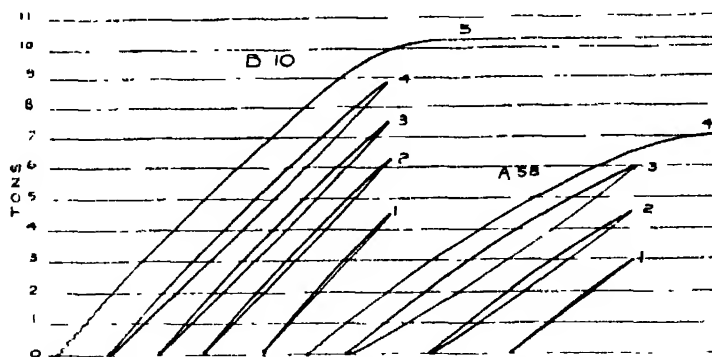
FIG 4.—Typical re-test records : non-recovery type.

Test-piece B.10 had a primitive elastic limit at 8·0 tons and the maximum load applied in the original test was 10·2 tons, which pull No. 5 shows to be the new yield-point.

Test-piece A.58 had been looped at a constant load of 6·1 tons. Pull No. 3 of the re-test, to a load of 6·1 tons, gives a loop which is absolutely identical with the last loop recorded in the original looping test 9 years previously.

5. *The Effect of Resting under Load.*

Two steels were used to investigate the effect of imposing a constant stress on the metal during the interval between the original overstraining and the re-test.

The first was a steel containing 0·63 per cent. carbon (test-piece No. A.58, test No. 27 in the Table of Results).

After looping at a constant load of 6·1 tons, the test-piece was set up in a single-lever testing machine of the ordinary type under the same load and allowed to remain for 18 days. No extension or creep occurred during this period and the beam of the machine remained floating without attention.

On re-testing at the end of the 18 days, the test-piece afforded loops which were identical, load for load, with those recorded in the original test. The steel had undergone no elastic recovery during the period of rest under load.

The same test-piece was then rested *under no load* for 9 years. On re-testing identical loops were again obtained The material therefore had no inherent power of elastic recovery and the fact that it did not recover under load is immaterial. This is corroborated by test No. 26 in the Table carried out on the same steel.

The second steel was a mild steel of 0 2 per cent. carbon content. Two test-pieces of this steel (R.2 and R 3, tests Nos. 49 and 50 in the Table) were overstrained in the usual manner and then rested for 22 days under stresses of 25·0 and 6·5 tons per square inch respectively.

On re-testing, both test-pieces were found to have completely recovered their property of proportional elasticity right up to the maximum load previously applied.

In this case recovery had taken place in spite of the load carried during the rest period and the inference is that recoverability is an inherent physical property and is unaffected by the condition of stress.

6. *Minimum Time for Recovery.*

The mild steel referred to in the previous paragraph is evidently one that readily recovers its proportional elasticity. A test-piece of this material was therefore overstrained and re-tested at intervals of a few hours in order to determine how soon the recovery took place.

Figs. 5, 6 and 7 form a complete record of the test history of this specimen.

Fig. 5 is the record obtained during the original overstraining, the maximum load reached being 7·5 tons.
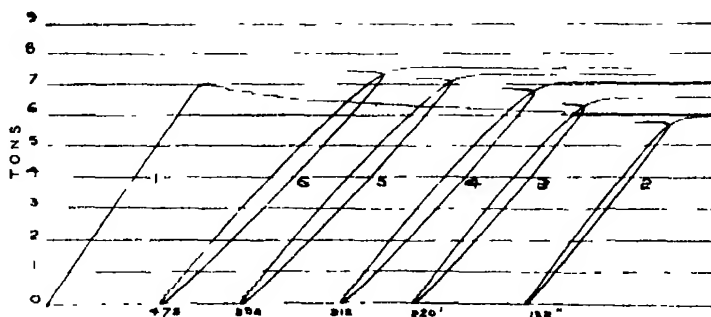
FIG. 5.—Original test : mild steel.

Immediately after this overstraining the test-piece was again loaded and at once unloaded. The record of this pull is shown at the left of fig. 6. Not only are the loading and unloading lines curved, but they do not meet at the bottom at no load, showing that the metal is in a partly plastic condition.
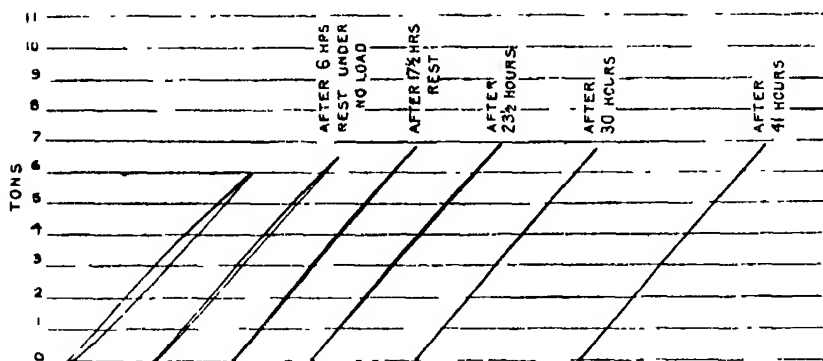
FIG. 6.—Re-test of mild steel showing progressive recovery

The test-piece was then rested under no load for 6 hours and again pulled. The record was a closed loop as shown in the figure. The steel was no longer plastic, but its elasticity was still non-proportional.

Subsequent pulls after increasing periods of rest afforded loops of gradually decreasing width until, after a rest of 30 hours, the lines of ascending and descending load were coincident At some time between 24 and 30 hours the metal had recovered its proportional elasticity. The record obtained after 41 hours serves as a confirmation.

The specimen was then re-tested in the normal manner.   Fig. 7 is the record of this re-test, which is of the complete elastic recovery type, p. 523.
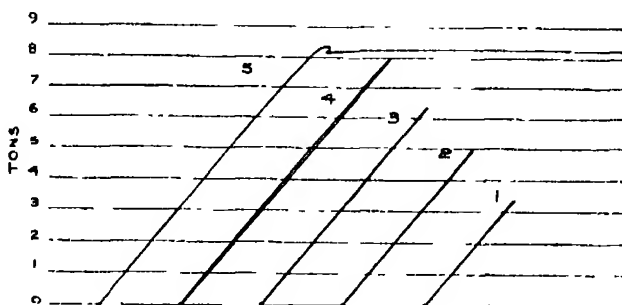

Fig 7

7. *Conclusions.*

(1) Mild steel, of carbon content up to about $0 \cdot 2$ per cent., possesses the power of complete elastic recovery up to the maximum stress previously applied irrespective of the variations in structure brought about by different heat treatments and irrespective of its previous mechanical history.

Thus all the tests numbered 1 to 10 in the Table gave records similar to B 8, fig. 2, with the exception of No. 7, test-piece H.28, which will be referred to again later.   This low-carbon series includes steels in the pearlitic condition, quenched and re-heated sorbitic steels ; and one, No 8, test-piece A 40, which had undergone severe mechanical cold-working during manufacture.

(2) Steels of a higher carbon content, $0 \cdot 3$ per cent. to $0 \cdot 7$ per cent., possess this power of recovery to a more limited extent.   Some of the steels in this category were found to have a considerable power of recovery and the elastic limit on re-testing was sometimes higher than the primitive elastic limit.   Others showed no recovery at all.   The two factors which appear to suppress, partially or even entirely, the power of elastic recovery are :—

(a) The presence of an abnormal amount of phosphorus.

For example, test No. 11 refers to a steel containing $0 \cdot 30$ per cent. carbon and $0 \cdot 04$ per cent. phosphorus.   This steel recovered completely. Test No. 13 was made on a steel of similar carbon content and heat-treatment, but which contained $0 \cdot 10$ per cent. phosphorus.   This steel did not recover.   Comparison of tests Nos. 19 with 17 and 21 with 26 gives similar results.

The inference is that phosphorus in excess of the amount usually permitted in steel specifications not only produces the condition of " cold-shortness " but may have even more serious effects when the material has to withstand a series of repeated loads.

(b) The change produced by quenching followed by re-heating to about 600° C.

    An example of this is steel No. 3A containing 0·50 per cent. carbon. Test No. 19 in the Table was made after annealing at 900° C. The re-test showed a considerable degree of elastic recovery. Test No. 20 relates to the same steel after a double heat-treatment. In this condition there was absolutely no elastic recovery.

    Tests Nos. 35 and 36 on a steel containing 2·2 per cent. nickel and tests Nos. 39 and 40 on a similar steel containing 4·6 per cent. nickel give similar results.

    Tests Nos. 43 to 48 refer to nickel-chrome steels. These show the same change in the power of elastic recovery with the different heat-treatments.

In general, the results of the present tests show that annealing at 900° C. develops the maximum power of elastic recovery in a steel, whereas quenching and re-heating reduces, and may possibly entirely destroy, its self-healing property.

A reasonable explanation is thus afforded for the apparently anomalous result of test No. 7, referred to in the previous paragraph. This is a low-carbon steel which might be expected to have a high degree of recoverability. But not only is the phosphorus content high, but the steel has been quenched and re-heated ; and these two factors, operating in conjunction, appear to have sufficed to prevent any return to a condition of proportional elasticity.

(3) Carbon steels of eutectoid composition, 0·85 per cent. carbon, have no power of recovery, whatever heat-treatment they have received.

    Test No. 30 refers to such a steel in the normal pearlitic condition. Tests Nos. 31 and 32 were made on the same steel after it had been given prolonged annealing treatments to produce partial and complete divorce, with the pearlite in the spheroidised condition. Tests Nos. 33 and 34 relate to sorbitic eutectoid steel. In none of these cases was there any trace of elastic recovery observable.

Table of Results.

Test No.	Test piece No.	Steel No.	C.	P.	Ni.	Cr.	Heat treatment.	Primitive elastic limit. tons/sq. in.	Primitive yield point. tons/sq. in.	Maximum stress applied in original test. tons/sq. in.	Date of original test.	Date of re-test.	Remarks.
1	B.4	C.H.S.	0·15	0·09	0	0	900° C., 1½ hours, F.	16·3	16·8	25·1	12.7.22	18.1.32	Complete elastic recovery.
2	B.9	C.H.S.	0·15	0·09	0	0	880° to 800° n hour, Q.	26 1	26 1	32 2	18.1.32	18.1.32	Complete elastic recovery.
3	C.H.S.	C.H.S.	0·16	0·02	0	0	1100° C., 1100 hours, F.	26 1	26 0	32 2	29.9.22	20.1.32	Complete elastic recovery. (Tested up to 20 1 tons/sq. in.)
4	1A	1A	0·16	0·02	0	0	880° C., 2 hours, F.	16 7	16 7	26 1	18.7.22	20.1.32	Complete elastic recovery. (Tested up to 16 6 tons/sq. in.)
5	1A	1A	0·19	0·11	0	0	880° C., 2 hours, F.	16 1	16 0	25 8	14.1.32	20.1.32	No elastic recovery.
6	H.10	1A	0·19	0·11	0	0	900° C., 2 hours, F.	18·3	18·3	25 8	14.1.32	7.1.33	Elastic recovery up to 12 8 tons/sq. in.
7	H.28	3484	0·19	0·11	0	0	900° C., 2 hours, F.	17 8	21 8	36 8	19.7.22	20.1.32	Elastic recovery up to 21 3 tons/sq. in. Loop recorded at 27 6 tons/sq. in.
8	H.1	B.D.S.	0·18	0·10	0	0	None. Steel bright-drawn	29 0	28	39 0	19.7.22	15.1.32	No elastic recovery. Definitely yielded at 24 8 tons/sq. in.
9	A.40	B.D.S.	0·20	0·11	0	0	Steel bright-drawn	29 0	28	38 8	15.1.32	15.1.32	Complete elastic recovery. (Tested up to 39 0 tons/sq. in.)
10	A.62	2A	0·20	0·04	0	0	900° C., ½ hour, F.		28	39 0	22.7.22	17.1.32	Complete elastic recovery. (Tested up to 30 1 tons/sq. in.)
11	H.14	2A	0·20	0·04	0	0	850° C., ½ hour, F.	12 4	12 4	29 4	17.1.32	17.1.32	No recovery. (Tested up to 32 8 tons/sq. in.)
12	H.20	2A	0·30	0·04	0	0	900° C., 2 hours, F.	19 0	19 0	34 8	14.1.32	14.1.32	Elastic recovery up to 32 8 tons/sq. in. Loop recorded at 27 6 tons/sq. in.
13	H.17	3465	0·33	0·10	0	0	900° C., 2 hours, F.	21 3	24 1	36 5	18.1.32	18.1.32	Definitely yielded at 24 8 tons/sq. in. Loop recorded at 34 8 tons/sq. in.
14	H.32	3465	0·33	0·10	0	0	850° C., ½ hour, F.	17·8	24 1	36 1	18.7.22	18.1.32	No elastic recovery. Definitely yielded at 38 4 tons/sq. in. Loop recorded at 63 0 tons/sq.
16	A.34	F.T.S.	0·43	0·05	0	0	850° C., ¼ hour, Q.		38 8	68 0	26.7.22	20.1.32	Elastic recovery up to 18 9 tons/sq. in.
17	H.18	3A	0·60	0·10	0	0	900° C., 2 hours, F.	20 0	20 5	44 0	18.7.22	18.1.32	No elastic recovery. Definitely yielded at 40 0 tons/sq. in.
18	H.16	3A	0·40	0·10	0	0	900° C., 2 hours, F.	22 5	30 0	44 3	14.1.32	18.1.32	No elastic recovery. Definitely yielded at 41 0 tons/sq. in.
19	H.30	3A	0·40	0·10	0	0	600° C., 2 hours, F.	13 7	14 0	39 5	14.1.32	18.1.32	No elastic recovery.
20	H.27	4A	0·60	0·03	0	0	600° C., ½ hour, F.	16 4	25 0	44 0	12.7.22	14.1.32	Elastic recovery up to 43 0 tons/sq. in.
21	H.19	4A	0·63	0·03	0	0	810° C., ½ hour, F.	19 0	25 6	44 2	20.12.22	14.1.32	Elastic recovery up to 6 tons/sq. in.
22	H.31	4A	0·63	0·03	0	0	810° C., ½ hour, F.	19 0	28 0	46 2	15.1.72	14.1.32	Loop at constant load in original test.
23	A.77	4A	0·63	0·02	0	0	900° C., ½ hour, Q.	31 0	35 0	44 3	9.12.22	18.1.32	Loop at constant load in original test.
24	A.80	4A	0·63	0·02	0	0	900° C., ½ hour, F.	18 0	28 0	46 3	18.1.32	18.1.32	Loop at constant load in original test.
25	A.55	4A	0·63	0·03	0	0	900° C., ½ hour, F.	19 0	20 3	38 1	17.1.32	16 1 32	No recovery.
26	H.22	3487	0·63	0·11	0	0	850° C., ½ hour, F.	20 3	20 5	37 1	18.1.32	17.1.32	No elastic recovery. Loop recorded at 46 3 tons/sq. in.
27	H.6S	3187	0·63	0·11	0	0	900° C., ½ hour, F.		21 5	34 8	13.12.22	9 1 23	Small loop recorded at 34 8 tons/sq. in.
28	H.34	3487	0·63	0·11	0	0	600° C., 2 hours, F.	30 6	36 2	66 5	29.9.22	12 1 32	No elastic recovery after 9 years' rest under no load.
29	H.32	5A	0·74	0·03	0	0	600° C., 2 hours, F.	25 0	36 5	51 1	19.7.22	13.1.32	Yield-point on re-testing, 50 0 tons/sq. in.
30	H.30	5A	0·83	0·02	0	0	None. Steel as received		28 1	60 0	20.7.22	15.1.32	Elastic recovery up to 36 0 tons/sq. in.
31	A.31	D	0·83	0·05	0	0	650° C., 31 hours, F.	20 6	20 6	44 0	17.1.23	30.1.32	No elastic recovery.
32	A.32	D	0·83	0·02	0	0	800° C., 20 minutes, cooled to 650° C. in 3 hours, 14	15 9		44 6	7.1.23	30.1.32	No elastic recovery.
33	H.33	6A	0·85	0·04	0	0	hours at 650° C., F.	28 1	32·1	48·5	30.1.32	30.1.32	Definitely yielded at 39 5 tons/sq. in. Yield-point on re-testing, 48 5 tons/sq. in.
34	H.36	3490	0·83	0·11	0	0	800° C., ½ hour, Q.	30 6		60 2	17 1 23	17 1 23	No elastic recovery
35	H.8	C.H.N.S.1	0·20	0·10	2 2	0	800° C., 2 hours, F.	16 8	20 5	38 7	17 1 23	17 1 23	No recovery.
36	B.10	C.H.N.S.1	0·20	0·01	2 2	0	920° C. to 860° C. in ½ hour, Q.	28 1	39 0	39 0	17 1 23	17 1 23	Yield-point on re-testing, 32 5 tons/sq. in. Yield-point on re-testing.
37	B.5	C.H.N.S.2	0·10	0·02	2 9	0	800° C., ½ hour, Q.	19 0	19 0	33 0	17 1 23	20.1.32	No recovery. Yield-point on re-testing.
38	B.6	C.H.N.S.3	0·10	0·02	2 9	0	14° C. to 832° C. in ½ hour, Q.	29 1	25 1	37 3	17 1 23	30.1.32	Complete elastic recovery. (Tested up to 33 0 tons/sq. in.)
39	H.0	C.H.N.S.3	0·15	0·02	4 8	0	800° C., ½ hour, F.			39 8	17 1 23	30.1.32	Elastic recovery up to 33 0 tons/sq. in. and upwards.
40	C H N.S.3	C H N.S.3	0·15	0·05	4 6	0	940° C. to 848° C. in ½ hour, Q.	12 1		47 0	12.7 22	(a) 20.1.32	Elastic recovery at 20·5 tons/sq. in. Definitely yielded at 31·6 tons/sq. in. Yield-point, 41 5 tons/sq. in.
41	N.S.	N.S.	0 30	0 03	4 6	0	850° C., ½ hour, F.	24 8	25 5	43 2	17.7 22	(a) 20.1.32	No recovery. Definitely yielded at 46 8 tons/sq. in. Yield-point on re-testing, 37 0 tons/sq. in.
43	B.14	N.S.	0 30	0·03	3·1	0	900° C., Q. (oil).	37·7	40·8	52 8	26 9.22	(b) 17.1 23	Complete elastic recovery up to 43 5 tons/sq. in. Yield-point on re-testing, 54 5 tons/sq. in.
44	B.16	N.C.S.	0 33	0 02	3·3	0 8	850° C., (oil).	40·8	63·5	67 0	11.1.23	(b) 20.1.32	Elastic recovery up to 28 4 tons/sq. in. Loop recorded from 34·5 to 49 0
45	B.16	N.C.S.	0 33	0 02	3·3	0 8	830° C., (oil).	43·3	62·6	66·4	9.1.23	(b) 20.1.32	Elastic recovery up to 28 0 tons/sq. in. Loop recorded up to 58 0 tons/sq. in.
46	B.17	N.C.A.S.	0·30	0·02	3·3	1·2	810° C., Q. F. at 2° C. per min.	77·4		67·4	5.3.23	(b) 20.1.32	Elastic recovery up to 42 2 tons/sq. in. Loop recorded up to 66·5 tons/sq. in.
47	B.19	N.O.A.S.	0·30	0·03	3·5	0·8	830° C., ½ F. at 2° C. per min.	11·2	55·1	69 1	6.3.23	20.1.32	No recovery.
48	B.30	M.S.	0·20	0·03	1·2	0·2	810° C., Q. (water)	35·7	66	68·1	6.3.23	20.1.32	No recovery. Loop recorded at 27 6 tons/sq. in. and upwards.
49	B.32	M.S.	0·20	0	1·5	0·2	650° C., F. at 2° C. per min.	17·9	52·1	66·0	6.3.23	20.1.32	Elastic recovery up to 68·0 tons/sq. in.
50	R.3	M.S.	—	—	—	—	None.	17·9	20·5	28·6	12.1.32	12.1.32	Rested under stress of 25·0 tons/sq. in. Complete elastic recovery up to maximum stress originally applied.

(4) The recovery of proportional elasticity in overstrained steel at ordinary temperatures is not solely dependent on the length of the rest period. The power of elastic recovery is an inherent physical property of some steels. Others have no such power. Recovery, if it takes place at all, may be complete in the course of a few hours. In the case of steels which have not the power of recovery, a very prolonged rest has no effect in bringing about the change from non-proportional to proportional elasticity.

> The mild steel referred to in § 6 above underwent complete recovery in 30 hours. In other cases re-testing after 14 days (test No. 25), 18 days (tests Nos. 23 and 24), and 32 days (tests Nos. 49 and 50), showed complete recovery which probably occurred sooner.

> Some test-pieces were re-tested twice, once after a rest of from 2 to 6 months, and again after a further rest of 9 years (tests Nos. 27, 30, 31, 32, 33, 36 and 40). In all these latter cases the re-tests furnished loops identical, load for load, with those recorded in the original tests

(5) The power of recovery is unaffected by the condition of stress in the metal. A steel which is capable of recovering its elastic property will do so even if it is stressed during the rest period very nearly to its breaking stress.

8. *Table of Results.*

For the purpose of reference, data relating to the test-pieces, numerical values obtained in the tests, and remarks based on an examination of the re-test records are set out in the Table of Results.

As regards composition, in addition to the carbon, phosphorus, nickel, and chromium, the steels were also analysed for sulphur, manganese and silicon, the amounts of which did not vary sufficiently from steel to steel to cause variations in the mechanical properties.

Heat treatment.—The first temperature recorded in the column headed " heat treatment " is the temperature attained at the end of the heating period, which was maintained constant for the period stated.

The letter " Q " denotes immediate quenching in water.

The letter " F " denotes cooling in and with the furnace.

In the case of bars which were given a tempering or re-heating treatment, this is indicated in the Table in the same way.

Stresses.—The values given in the Table of the yield-point were reckoned from the constant-load yield period and not on the peak load at the commencement of yielding as indicated in fig. 1, test-piece No. B.13.

The maximum stress attained in the original test and also the stresses applied on re-testing were computed on the reduced cross-sectional area as measured after testing.

Summary.

When a metal test-piece is pulled beyond its primitive yield-point, its extension is partly plastic and partly non-proportionally elastic. Unloading and immediately re-loading causes the load-extension line to trace a loop of mechanical hysteresis. Bauschinger first observed that a rest of 50 hours under no load at ordinary temperatures caused a recovery of proportional elasticity with a new elastic limit in some cases higher than the primitive limit.

This paper records an investigation made to determine whether all steels possess this power of recovery to the same extent; whether Bauschinger's 50-hour rest is sufficient to develop the maximum recovery or if a longer period will result in a further raising of the elastic limit; and whether recovery is impeded by the imposition of stress during the rest period.

About 50 different steels, severely overstrained and rested for 9 years, were re-tested for elastic recovery, others were rested under stress before re-testing, and an investigation was made of the minimum time required for elastic recovery of mild steel.

Test-records were made with the Dalby Autographic Load-extension Recorder and the disappearance or persistence of the hysteresis loops used as an indication of the extent of recovery. The records are of three types: complete elastic recovery up to the load previously applied; partial recovery; and total non-recovery.

The steels examined are classified on this basis and it is shown that composition and the heat-treatment received influence the power of recovery. Some steels are inherently incapable of recovery and remain non-proportionally elastic even after 9 years. Mild steel recovers readily and records are given showing recovery progressing to completion in 30 hours. Recovery is unaffected if the metal is stressed during the rest period.

The seven figures are reproduced from photographic records made with the Dalby instrument.

On the Mass Rate of Reactions in Solids.

By R. S. BRADLEY, J. COLVIN, and J. HUME, the University, Leeds.

In a previous paper, Hume and Colvin* showed that the mass rate of decomposition occurring in crystalline particles was a function of three quantities, namely, the rate of nucleation, the rate of linear propagation and the size and shape of the particle. For a study of the energetics of the reaction, the second of these quantities is of primary importance, so that special attention was directed to the derivation of this quantity, under such conditions that a knowledge of the nucleation rate was unnecessary. In the case of the dehydration of certain salt hydrates in vacuo,† the rate of nucleation is so large that the entire surface of all the crystals is rapidly covered and the subsequent mass rate can be predicted from simple geometrical considerations. On the other hand, if the rate of nucleation is not so large that this simplification can be made, then the whole course of the reaction will be determined by the progressive formation of nuclei as the reaction proceeds.

In many cases it is possible by visual observation to obtain qualitative information as to the manner of nucleation. For example, it might be found that decomposition proceeded from points on the surface or at the corners or edges of the crystals. The question can be treated generally if it is assumed that in a mass of crystalline particles the total number of points capable of becoming nucleation centres is n_0 and that each of these points has the same probability of becoming active. At time t, let there be n_t points still unaffected. Then the number of nuclei formed during the time interval dt is given by $- dn_t = kn_t . dt$, where k is a constant. Hence $n_t = n_0 e^{-kt}$ and the number of points where nucleation has occurred is $n_0 (1 - e^{-kt})$. If the reaction spreads with a constant velocity u from the nuclei which are formed, the rate of the mass reaction will be given by

$$dm/dt = n_0 . f(k, t, u)$$

The form of the function will depend on the shape of the crystalline particles and on the form of the advancing interface. In the sequel, an attempt is made to evaluate the effect of nucleation in the reactions

$$CaCO_3 . 6H_2O \longrightarrow CaCO_3 + 6H_2O$$
$$KHC_2O_4 . \tfrac{1}{2}H_2O \longrightarrow KHC_2O_4 + \tfrac{1}{2}H_2O.$$
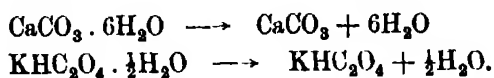
* 'Phil. Mag.,' vol. 8, p. 589 (1929).

† Hume and Colvin, 'Proc. Roy. Soc.,' A, vol. 132, p. 548 (1931).

The Decomposition of Calcium Carbonate Hexahydrate.

In a previous investigation of the decomposition of calcium carbonate hexahydrate, Topley and Hume* were able to derive the linear rate from restricted regions of the percentage decomposition time curves. At the same time, the more or less protracted induction period during which the velocity of decomposition increased, clearly indicated a relatively small rate of nucleus formation. For this reason, a reinvestigation of this reaction was desirable.

Details of the mode of preparation of calcium carbonate hexahydrate and of the method of measuring the velocity of decomposition are to be found in previous papers *† Preliminary microscopic observations of the decomposition of various specimens under water were made in the hope that some information might be gained regarding the manner of nucleation. For this purpose the thin plates which predominate during the early stages of crystallisation are most convenient, not only because of their extreme transparency, but also because of the avoidance of excessive stabilisation by sugar decomposition products, which results if the crystals are exposed for too long a time to the mother liquor, Topley and Hume (*loc. cit.*). It was observed that, after the lapse of time, a slight cloudiness spread over the surface of the crystals, spreading being completed in less than a minute. No further change was then appreciable for some time in the crystal itself, but in the water around it appeared small dots which later grew and showed themselves to be crystals of calcite. Finally the cloudy crystal, which had become more and more attenuated in thickness, disappeared completely

The fact that the crystal did not appear to diminish in length or breadth indicates either that nucleation does not spread to the narrow faces parallel to the microscope axis or, more probably, that the interface proceeding from the upper and lower faces has completely traversed the thin crystal before spreading from the vertical faces has occurred to a noticeable extent. The observation that the cloudiness did not increase during the reaction admits of several explanations.

(1) The reaction proceeds by solution of the hexahydrate and crystallisation of calcite. This hypothesis is untenable in view of the microscopic observation that the incidence of cloudiness, so far as one can judge, obeys a probability law, instead of occurring simultaneously in all the crystals.

* 'Proc. Roy. Soc.,' A, vol. 120, p. 211 (1928).

† Hume and Topley, 'Proc. Leeds Phil. Soc.,' vol. 1, p. 169 (1927).

(2) The reaction proceeds by liberation of the six molecules of water from the hexahydrate lattice at the interface. A reasonable explanation of this mechanism is that in the lattice a calcium ion, a water molecule and a carbonate ion attain, by vibration, positions which enable the calcium and carbonate ions to combine to form a molecule of calcium carbonate, whereupon the six molecules of water surrounding the calcium ion are liberated. This results in the formation of adsorbed calcium carbonate molecules as the first formed layer of decomposition product, which presumably promotes the decomposition of the next layer of hexahydrate. As the calcium carbonate molecules become more remote from the interface by the progress of the reaction the forces of adsorption are weakened and allow aggregation to finely divided crystalline calcite, which subsequently either dissolves or becomes detached from the parent crystal. Thus no pseudomorph of the original crystal remains.

As a consequence of the views outlined above, an expression for the mass rate of reaction can be derived as follows. Let there be n_0 crystals of uniform size and shape, thin plates of thickness θ, with upper and lower parallel faces of area A. It is assumed that nucleation occurs simultaneously on the upper and lower faces of a crystal and that the time interval from the incidence of nucleation until the whole face is involved is negligible. Even if nucleation spreads to or occurs on the vertical faces, the effect can be minimised by using crystals of such dimensions that the area of the parallel major faces is great compared with the total area of the other faces. The reaction then proceeds by the movement of the interface with linear velocity u in a direction perpendicular to the major faces. The number of crystals nucleated at time t from the start of the reaction in the interval dt is $k \cdot n_0 e^{-kt} \cdot dt$. Now consider a crystal which nucleated at time t from the start. At time t_2 the volume of resultant (dv) produced from this particle will be given by

$$dv = 2A \cdot u \cdot (t_2 - t),$$

and thus for the n_t particles nucleated at time t,

$$dV = 2A \cdot u \cdot n_0 \cdot k \, (t_2 - t) \, e^{-kt} \cdot dt.$$

Hence the total volume decomposed (V_t) at time t_2 will be given by the equation

$$V_t = 2A \cdot u \cdot n_0 \cdot k \int_0^{t_2} (t_2 - t) \, e^{-kt} \, dt$$

$$2A \cdot u \cdot n_0 \cdot \left(t_2 + \frac{e^{-kt_2} - 1}{} \right.$$

But the fractional decomposition $\alpha_{t_2} = \dfrac{V_{t_2}}{n_0 A \theta}$, hence

$$\alpha_{t_2} = \frac{2u}{\theta}\left(t_2 + \frac{e^{-kt_2}-1}{k}\right).\qquad\text{(I)}$$

Equation (I) is valid until time $t_2 = \theta/2u$, when a crystal which nucleated at zero time will be completely decomposed. After this time the values given by the equation will be in excess of the true values, the excess at time t_3 (greater than $\theta/2u$) being equal to the decomposition occurring in the time interval

$$t = 0 \rightarrow t = t_3 - \frac{\theta}{2u},$$

i.e., the excess equals

$$\frac{2u}{\theta}\left(t_3 - \frac{\theta}{2u} + \frac{e^{-k\left(t_3 - \frac{\theta}{2u}\right)}-1}{k}\right).$$

Thus the fractional decomposition at time t_3 will be given by

$$\alpha_{t_4} = \frac{2u}{\theta}\left(t_3 + \frac{e^{-kt_3}-1}{k}\right) - \frac{2u}{\theta}\left(t_3 - \frac{\theta}{2u} + \frac{e^{-k\left(t_3 - \frac{\theta}{2u}\right)}-1}{k}\right)$$

$$= \frac{2u}{\theta}\left[\frac{\theta}{2u} + \frac{e^{-kt_3}\left(1 - e^{\frac{k\theta}{2u}}\right)}{k}\right],$$

or

$$\alpha_{t_4} - 1 = \frac{2u}{k\theta}\left(1 - e^{\frac{k\theta}{2u}}\right)e^{-kt_3}.\qquad\text{(II)}$$

Equation (II) is applicable only at times greater than $\theta/2u$.

Experimental.

Crystals of calcium carbonate hexahydrate were prepared by saturating lime-sucrose solution with carbon dioxide. About 36 hours after carbonation the crystals had attained a suitable form and were then washed and sized by falling through ice-cold water. Duplicate measurements of the rate of decomposition at two temperatures were then made dilatometrically. The thermostats were maintained at $7\cdot07°$ and at $10\cdot07°$ by means of a stream of water cooled by an Electrolux refrigerator unit. The mean thickness ($\theta = 0\cdot0005$ cm.) of the crystals was measured microscopically. The results are given in Table I.

Table I.—Decomposition of Calcium Carbonate Hexahydrate.

Run 1 at 7 07°.		Run 2 at 7 07°.		Run 3 at 10 07°		Run 4 at 10·07°.	
t in mins.	100 a	*t* in mins	100 a	*t* in mins	100 a.	*t* in mins.	100 a.
0	0 00	0	0 00	0	0 00	0	0 00
39	1 87	40	1 76	27	1 36	22	1·64
59	3 49	80	5 61	37	2 85	32	3 20
89	6·63	110	9·22	57	7 20	52	7 13
109	8·92	150	14 73	77	12 84	72	12 46
149	14·16	190	21·44	97	20 92	92	20·41
209	24·28	220	27 25	117	31 05	112	30 66
254	33 67	255	35 22	137	42 74	132	42 54
290	42·17	291	44 31	157	54 63	102	59 91
330	52 41	331	54 62	167	60 39	182	70·49
363	60·91	364	63 37	187	70 65	202	78 59
400	69 88	401	72 36	207	78 81	212	81 95
451	80 54	452	82 49	249	89 61	242	89 23
529	90·72	530	91·58	281	93 76	276	93 60
559	95·13	600	95·52	331	97 14	310	96 54
∞	100 00	∞	100·00	∞	100 00	∞	100 00

Discussion

Derivation of k, *the Nucleation Constant* —Equation (II), applicable at times greater than $\theta/2u$ may be written

$$1 - \alpha_{t_3} = k'e^{-kt_3},$$

where

$$k' = \frac{2u}{k\theta}\left(e^{\frac{k\theta}{2u}} - 1\right),$$

so that

$$\log_{10}(1 - \alpha_{t_3}) = \log_{10} k' - 0\cdot4343\, kt_3,$$

i.e., $\log_{10}(1 - \alpha_{t_3})$ is a linear function of t_3.

Fig. 1 shows the graph $\log_{10}(1 - \alpha_{t_3})$ against t_3 for run 4. In every case an equally satisfactory line is obtained, whose slope gives directly the value of k, the nucleation constant. Prior to t_3 the linear relationship breaks down, so that the value of $\theta/2u$ can thus be approximately determined.

Derivation of u, *the Linear Rate.*—Having obtained the value of k, equation (I) can be used to derive values of u, the linear rate of propagation. Unfortunately, in all solid reactions uncertainty exists as to the true zero time, which may not coincide with the apparent experimental zero. Let $t_e = t_3 - t_{obs}$, where t_{obs} is the time of observation from the experimental zero. On substitution, equation (I) becomes

$$\alpha_t = \frac{2u}{\theta}\left(t_{obs} + t_e + \frac{e^{-k(t_{obs} + t_e)} - 1}{k}\right.$$

The zero correction in this case is made by altering the time reference point on the assumption that the whole of the volume change has been observed experimentally. If, on the other hand, reaction had begun before the initial observation it would have been necessary to use the method employed in the latter part of this paper. The introduction of t_0 does not invalidate the above calculation of k. By taking two points on the experimental curve representing the fractional decomposition plotted against time of observation, values for
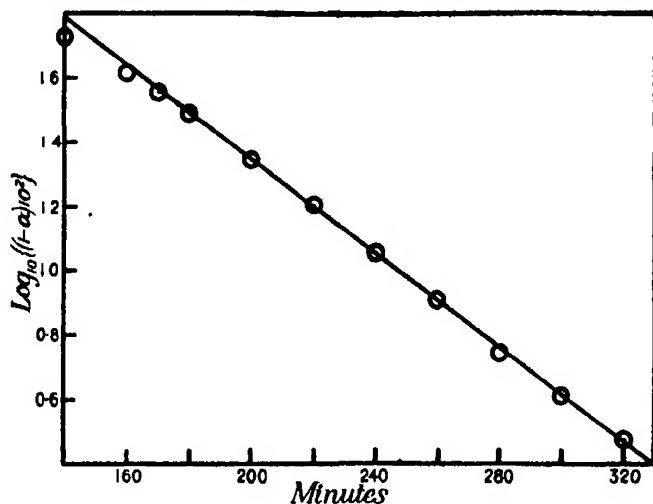
Fig 1.

t_0, $2u/\theta$ and hence $\theta/2u$ can be obtained by graphical solution Thence values of α, the fractional decomposition, can be calculated for any time and compared with the experimental values. Fig. 2, which is typical of the results obtained, shows this comparison for run 1. The agreement between the experimental and the theoretical curves is very good except in the early stages. This small discrepancy is due to the assumption that nucleation once begun spreads instantaneously over the surface of a single crystal. The results are summarised in Table II.

Table II.

Run No.	Temperature $^\circ$ C.	$-t_c$ in mins.	$2u/\theta \times 10^3$ min.$^{-1}$.	$k \times 10^3$ min.$^{-1}$.	$u \times 10^7$ cm.min.$^{-1}$.
1	7·07	26 0	2·54	9·69	6 36
2	7·07	26 4	2·58	9·89	6·48
3	10 07	22·3	6·65	17·4	16·62
4	10 07	15 8	6·50	16·8	16·26

From these values the energies of activation E_u and E_k are respectively 49,500 calories and 29,300 calories. The former value is discrepant from that given by Topley and Hume, namely 38,000 calories. Since the values have been derived by different methods, detailed consideration of their relationship will be published elsewhere. It is intended to make a further study of the energy of activation over a wider range of temperature.
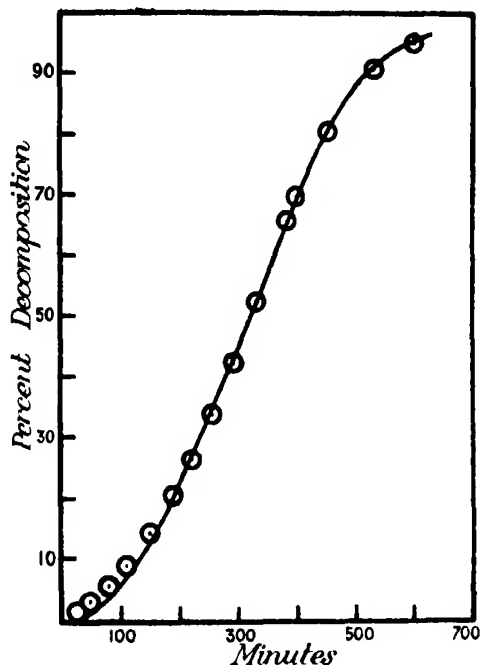
Fig. 2.

O = Experimental Point.
Continuous Line = Theoretical Curve

The Decomposition of Potassium Hydrogen Oxalate Hemihydrate.—Hume and Colvin[*] showed that a mass of crystals of potassium hydrogen oxalate hemi-hydrate decomposes according to a sigmoid curve and analysed the last part of the curve by assuming that the march of the interface across the crystal corresponded to a contracting circle. In this way they obtained a value for the linear velocity of the interface in agreement with the observed values for single crystals. In this section the first part of the curve will be analysed allowing for the nucleation rate.

As nucleation nearly always proceeds at the crystal boundary the possibility

---

[*] ' Proc. Roy. Soc.,' A, vol. 125, p. 635 (1929).

arises that the nucleation rate is proportional to the perimeter of the undecomposed part of the crystal. This leads to a definite result as follows.

For a single crystal let the initial perimeter available for nucleation be l_0. The perimeter at time t, l_t, the initial number of points available for nucleation n_0 and the number unaffected at time t, n_t. Then the number of points at which reaction has started at time t is $(n_0 - n_t)$. Let u be the mean velocity of the interface. The properties of the crystal chosen are, of course, a mean of those of the mass ; in other words, equations referring to one crystal on multiplication by the total number of crystals refer to a perimeter length equal to the total length and an area equal to the total area. In this way fractional nucleation for a single crystal becomes intelligible.

On the above assumption $-\dfrac{dn_t}{dt} = kl_t$, where k is the nucleation constant. Assume that semicircles of resultant spread out from each nucleus. During an interval dt the radius of the semicircular area round each nucleus increases by $u \cdot dt$, and consequently the length of crystal perimeter available for nucleation decreases by $2u \cdot dt$. Hence

$$\frac{dl_t}{dt} = -2\left(n_0 - n_t\right)u.$$

During this interval dt, $-dn_t$ nuclei have been formed, but the effect of these on the perimeter is of the second order and therefore negligible. Hence

$$-\frac{d^2 n_t}{dt^2} + 2k\left(n_0 - n_t\right)u = 0,$$

or

$$n_0 - n_t = l_0 \left(\frac{k}{2u}\right)^{\frac{1}{2}} \sin\left\{(2ku)^{\frac{1}{2}} t\right\},$$

since $n_0 - n_t = 0$ when $t = 0$ and $\left(\dfrac{dn_t}{dt}\right)_{t=0} = -kl_0$. Those nuclei formed between t and $t + dt$, $-\dfrac{dn_t}{dt} dt$ in number, will have produced an area of resultant equal to $-\tfrac{1}{2}\pi u^2 (t_1 - t)^2 \dfrac{dn_t}{dt} \cdot dt$ at the time t_1 $(t_1 > t)$. Hence the area of resultant at any time t_1 is

$$\int^{t_1} \tfrac{1}{2}\pi u^2 (t_1 - t)^2 kl_0 \cos\left\{(2ku)^{\frac{1}{2}} t\right\} \cdot dt.$$

The fractional decomposition is obtained by dividing this result by the area of the crystal. On performing the integration, the fractional decomposition

is found to be proportional to $\sin\{(2k \cdot u)^{\frac{1}{2}}t\}$. This does not accord with the experimental results and another basis must be found for the theory.

In the above treatment of nucleation the emphasis has been laid on the crystal edges. There are, however, three systems of points capable of developing nuclei, the lattice points of the plane faces, those along the edges and those at the corners. The activation energies of the nucleation rates for these three systems may be so different that only one system contributes appreciably to the reaction. At the corners the asymmetry is greatest and the greatest nucleation rate would be expected.

Let there be on the average n_0 points per crystal capable of becoming nucleation centres. At time t let there be n_t points still unaffected. Then the number of nuclei formed during the interval dt is $-dn_t = k \cdot n_t \, dt$, where k is the nucleation constant. Hence $n_t = n_0 e^{-kt}$. Suppose that from each point the sector of a circle spreads out. The average angle of the sector will be $\pi\left(1 - \dfrac{2}{n_0}\right)$ if the points are corners.

Then, as before, the area of the resultant formed at any time t_1 is

$$A_{t_1} = \int_0^{t_1} \tfrac{1}{2}\pi\left(1 - \frac{2}{n_0}\right) k n_0 u^2 (t_1 - t)^2 e^{-kt} \cdot dt,$$

or

$$\frac{A_{t_1}}{\tfrac{1}{2}\pi n_0 u^2 \left(1 - \dfrac{2}{n_0}\right)} = t_1^2 - \frac{2t_1}{k} + \frac{2}{k^2} - \frac{2e^{-kt_1}}{k^2}.$$

A zero correction must be applied in the following way. Let the experimental zero be t_e seconds after the true zero, and let the time t_{obs} become t_2 referred to the true zero, or $t_2 = t_{obs} + t_e$. At t_e the area of resultant is

$$\int_0^{t_e} \tfrac{1}{2}\pi k n_0 u^2 \left(1 - \frac{2}{n_0}\right) e^{-kt} (t_e - t)^2 \cdot dt.$$

At t_2 the area of resultant is

$$\int_0^{t_2} \tfrac{1}{2}\pi k n_0 u^2 \left(1 - \frac{2}{n_0}\right) e^{-kt} (t_2 - t)^2 \cdot dt.$$

The difference gives the increase in area between t_e and t_2, *i.e.*, during the observation time t_{obs}. With the above value of t_2 this difference is given by

$$\frac{A_{t_{obs}}}{\tfrac{1}{2}\pi n_0 u^2 \left(1 - \dfrac{2}{n_0}\right)} = t^2_{obs} + 2t_{obs}\left(t_e - \frac{1}{k}\right) + \frac{2e^{-kt_e}}{k^2}(1 - e^{-kt_{obs}}).$$

If A_0 is the area of the crystal, the fractional decomposition observed is obtained by dividing A_t by

$$A_0 - \int_0^{t_c} \tfrac{1}{2}\pi n_0 k u^2 \left(1 - \frac{2}{n_0}\right)(t_c - t)^2 \, dt.$$

It was found that the observed values of the fractional decomposition could be fitted to a curve of the above type in which the last term is omitted. With $2(t_c - 1/k) = 1800$ seconds the effect of the last term is negligible. This is shown on the graph, fig. 3, where the fractional decomposition read off from
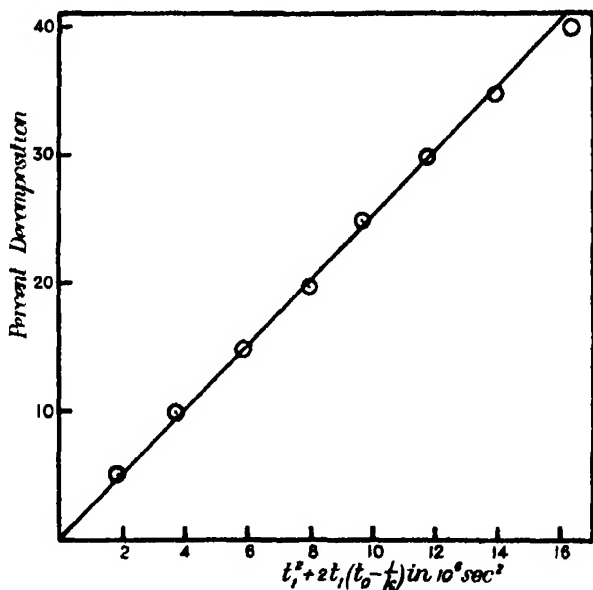
Fig. 3.

the smoothed curve A in fig. 4 of Hume and Colvin's paper (*loc. cit.*) is plotted against $t^2_{\text{obs}} + 2t_{\text{obs}}(t_c - 1/k)$. A straight line is obtained up to 35 per cent. decomposition, and the line passes as it should through the origin. Above 35 per cent. decomposition the areas of resultant meet one another or reach the opposite side of the crystal.

The area A_0 is given by Hume and Colvin as $1\cdot04 \times 10^{-3}$ cm.². The correction to A_0 is only about 2 per cent. From the graph we find that

$$\tfrac{1}{2}\frac{\pi}{A_0} n_0 u^2 \left(1 - \frac{2}{n_0}\right)$$

is $2\cdot55 \times 10^{-8}$. This gives the following values for u: $n_0 = 6$, $u = 2\cdot0 \times 10^{-6}$ cm. sec.$^{-1}$; $n_0 = 5$, $u = 2\cdot4 \times 10^{-6}$ cm. sec.$^{-1}$; $n_0 = 4$, $u = 2\cdot9 \times 10^{-6}$

cm. sec.$^{-1}$. The experimental mean velocity is $2 \cdot 72 \times 10^{-6}$ cm sec.$^{-1}$. Hence n_0 lies between 4 and 5, a reasonable value.

Summary

An analysis has been made of the form of the mass decomposition curves encountered in the dehydration of salt hydrates, with a view to evaluating the effect of progressive nucleation. The method has been applied to the reactions,
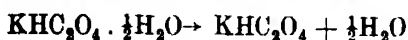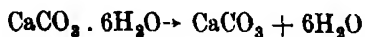
$$CaCO_3 . 6H_2O \rightarrow CaCO_3 + 6H_2O$$

$$KHC_2O_4 . \tfrac{1}{2}H_2O \rightarrow KHC_2O_4 + \tfrac{1}{2}H_2O$$

The Nuclear Spin of Arsenic.

By S. Tolansky, B.Sc., Ph.D.* (Physikalisch-Technische Reichsanstalt, Berlin-Charlottenburg).

(Communicated by A. Fowler, F.R.S.—Received April 21, 1932)

Introduction.

No fine structure has yet been recorded in any of the lines of the spectra of arsenic. The present paper gives an account of the fine structures of the majority of the visible lines of As II. This spectrum is very rich in strong lines and has been observed here in the region $\lambda\lambda$ 6400–4300 with high resolving power. The gross structure multiplet analysis of As II has been made by K. R. Rao,† and the fine structure observations recorded here support this analysis. The terms expected and found in this spectrum are shown in Table I.

<p style="text-align:center">Table I.</p>

Electron configurations.	Terms.					
$4s^2 . 4p^2$	^1S		^1D		^3P	
$4s^2 . 4p . 5s$		^1P		^3P		
$4s^2 . 4p . 5p$	$^1(S$	P	$D)$	$^3(S$	P	$D)$
$4s^2 . 4p . 4d$	$^1(P$	D	$F)$	$^3(P$	D	$F)$
etc.						

All lines involving the $4s^2 . 4p^2$ configuration lie in the deep ultra-violet region ; therefore this configuration will be disregarded in the present investigation. According to the vector coupling scheme of White and Ritschl* it will be expected that the $4s^2 . 4p . 5s$ configuration will show wide hyperfine structure separations, since it involves an unpaired penetrating s electron ; this is actually verified here with some modification. As the $4s^2 . 4p . 5p$ configuration has no penetrating s electron, only narrow structures are to be expected, but this, however, is not observed, since structures occur in this configuration which are of the same order as those found in the previous case. This has important theoretical significance and will be discussed later. The intervals in the $4s^2 . 4p . 5s$ triplet terms which are $^3P_0-^3P_1 = 397$ cm.$^{-1}$ and $^3P_1-^3P_2 = 2382$ cm^{-1} show that the electron coupling is by no means pure (LS) since the interval ratio deviates widely from the Landé interval rule. In the $4s^2 \ 4p . 5p$ and in the $4s^2 . 4p^2$ terms the deviations are much less marked. This incomplete (LS) coupling affects the structure and will be considered later.

Experimental.

In order to reduce the Doppler and Stark widths of the lines, an attempt was made to produce the As II spectrum in a hollow cathode tube cooled with liquid air. The efficiency of this tube depends upon the sputtering action of the positive rays striking the material to be investigated, which lies in a cooled hollow cathode. If the material does not sputter easily then the source is weak and of little use. The sputtering increases with increase in mass of the positive rays, so that the heavier the gas used the more efficient in general is the tube. Helium, neon and argon were employed in turn, and in each case the pure gas was continuously circulated through the tube at a pressure of about a millimetre. The lines of the As II spectrum were indeed obtained, but so faintly as to be quite useless for observational purposes. Water cooling

instead of liquid air cooling gave very little increase in intensity since the vapour pressure of the arsenic is still very low at 20° C. It appears that arsenic is very difficult to sputter.[*]

A different source was tried and this time very successfully. The tube was a simple quartz Geissler-tube with thick iron rods as electrodes sealed in with hard vacuum sealing wax, fig. 1. The tops of the electrodes were completely covered with powdered arsenic. Pure helium was circulated continuously through the tube at a pressure of 1 mm. and the tube was excited by means of a transformer, a small current being used. The observations were carried out end-on, the window being kept clear by means of a minute flame. A little arsenic was distilled into the capillary, which was 4×2 mm., being oval in section for maximum efficiency on the spectroscope slit, and on starting the discharge a very rich strong As II spectrum was emitted. The capillary was at a lower temperature than 100° C. and the lines emitted were surprisingly sharp. No doubt this is due to helium being the main carrier of the current, and also in part to the rapid flow of the gas helping to cool the arsenic vapour in the capillary.
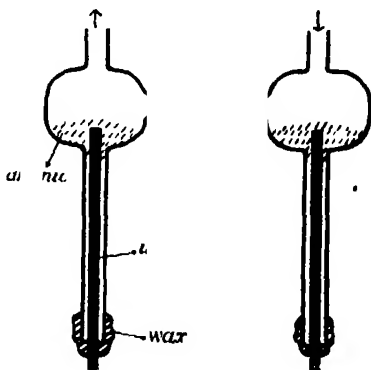
Fig. 1.

The lines were examined for fine structure with a silvered Fabry-Perot interferometer having plate separations varying regularly from 5 to 25 mm. A large Zeiss three-prism spectrograph was used for preliminary dispersion, the interferometer being placed in the parallel beam Agfa Andresa, Perutz Persenso and Ilford Soft Gradation Panchromatic plates were used and exposure times varied from 10 minutes to 2 hours. Each line was measured with at least two different separations of the interferometer plates, and except in the faintest poorly resolved components, the agreement was always good.

The wave-lengths and intensities of the lines observed agree with those given by Kayser.[†] From the viewpoint of fine structure, the lines can be divided into four broad classes, shown in Tables II and III. The lines in the upper part of Table II are quite single, showing no trace of structure even with a

---

[*] In this connection it is of interest to note that Dr. Badami, who is working here with antimony, has found the same difficulty. Antimony is, of course, very closely related to arsenic.

[†] " Handbuch der Spektroskopie," vol. 7.

high resolving power approaching $2\frac{1}{2}$ millions. On the other hand, the lines in the lower part show a quite distinct broadening indicative of a very narrow structure which it is impossible to resolve.

Table II.

Wave-length.	Intensity	Allocation.
6402 6	3	
6338 2	5	
5837 9	2	
5496 8	20	
5363·5	3	
5196 2	2	
5141 0	5	
5121 3	5	
4888 5	5	$4p \ 5s . {}^3P_0 - 4p . 5p . {}^1P_1$
4799 4	5	
4543 6	12	
4494 4	20	
4466 5	20	
4458 7	20	
4447 6	8	
4431 7	10	
4427 2	8	
4412 3	15	
4315 5	15	
4242 4	15	
6110 3	6	$4p \ 5s \ {}^1P_1 - 4p . 5p \ {}^1P_1$
5451 3	3	
5130 8	5	
4707 7	5	$4p . 5s . {}^1P_1 - 4p . 5p . {}^1S_0$
4602 5	10	
4590·8	13	
4539 9*	10	
4437 6	30	
4421·0*	15	

* Very broad

Table III gives the list of lines in which structure has been measured, and these are of two kinds, namely, regular series degrading to the violet in both intensity and interval, and lines which show a general complex structure. The regular series lines are indicated by an asterisk. The line λ 6022·6 shows a perfectly regular series triplet, but along with λ 4549·0 is an exception in that it degrades to the red and not to the violet, a fact which is in complete accord with the analysis given later. The visually estimated intensities are given in brackets below each component and the reliability of the observations indicated by a remark in the last column. The poor lines are due either to the structure being very narrow or else because of the fact that the line in question

Table III.—As II Lines with Fine Structure.

Wave-length.	Int.	Structure.					Allocation.	Remarks.
6170·6	10	118 (5)	0 (20)	76 (2)	124 (1½)	201 (15) +	$4p \cdot 5s \cdot {}^3P_1 - 4p \cdot 5p \cdot {}^3D_1$	Good.
6022·6*	8	198 (1)	120 (2)	0 (3) +			$4p \cdot 5s \cdot {}^3P_0 - 4p \cdot 5p \cdot {}^3D_1$	Good.
5657 0*	2	0 (4)	117 (3)	195 (2)	225 (1) +		$4p \cdot 5s \cdot {}^3P_2 - 4p \cdot 5p \cdot {}^1P_1$	Medium.
5651 3*	20	0 (3)	74 (2)	112 (1) +				Poor.
5558 1	20	85 (4)	0 (20)	37 (5)	112 (10)	158 (5) +	$4p \cdot 5s \quad {}^3P_1 - 4p \cdot 5p \cdot {}^3D_2$	Good.
5331·3*	10	0 (3)	88 (2)	119 (1) +			$4p \cdot 5s \quad {}^3P_2 - 4p \cdot 5p \cdot {}^3P_2$	Poor.
5231 4*	9	0 (3)	197 (2)	326 (1) +				Good.
5107 6	10	0 (1)	41 (1) +				$4p \cdot 5s \cdot {}^1P_1 - 4p \cdot 5p \cdot {}^1D_2$	Poor.
5105 5	10	0 (3)	95 (1)	144 (2)	171 (2) +		$4p \cdot 5s \cdot {}^3P_2 - 4p \cdot 5p \cdot {}^3S_1$	Poor.
4985·4*	5	0 (3)	194 (2)	311 (1) +			$4p \cdot 5s \cdot {}^3P_1 - 4p \cdot 5p \cdot {}^1P_1$	Good.
4730 6*	8	0 (3)	139 (2)	230 (1) +			$4p \cdot 5s \cdot {}^3P_1 - 4p \cdot 5p \cdot {}^3P_2$	Good.
4552·2*	4	0 (3)	171 (2)	261 (1) +			$4p \cdot 5s \cdot {}^3P_1 - 4p \cdot 5p \cdot {}^3S_1$	Medium.
4552·2*	4	0 (3)	171 (2)	261 (1) +			$4p \cdot 5s \cdot {}^3P_1 - 4p \quad 5p \cdot {}^3S_1$	Medium.
4549 0*	30	127 (1)	82 (2)	0 (3) +				Poor.
4413 6*	25	0 (3)	70 (2)	127 (1) +				Poor.
4340 4*	15	0 (4)	276 (3)	513 (2)	666 (1) +			Good.
4336·6*	15	0 (4)	160 (3)	274 (2)	321 (1) +			Medium.

* Regular degraded series.

lies in a region unfavourable for a silvered interferometer. In the table the strongest component of each line is made the null line and the separations of the rest are given in cm.$^{-1} \times 10^{-3}$. In the good lines the separations are

probably accurate to about 1 or 2 units and in the worst to about 10 units, the latter figure holding only for the very badly resolved components. The line allocations are those given by Rao.

Analysis of the Structures.

The analysis is simplified by the fact that arsenic only possesses one isotope, namely 75, so that no isotopic complications are at all possible. Two separate methods of analysis are employed, according to the nature of the line in question. The first method is used for a complex line that is well resolved. Such a line is, of course, a tiny multiplet and is simply analysed by means of constant differences in the usual manner, giving both upper and lower term fine structures. The gross structure transitions of the lines measured are shown in fig. 2 and it is seen that most of the terms involve more than one line, so that a check on the analysis is often possible.
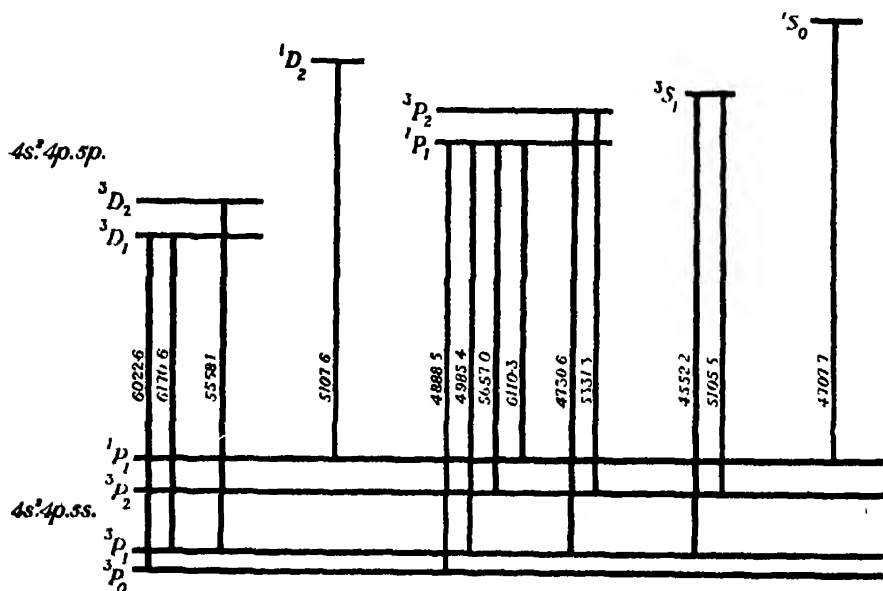
Fig. 2.—Transition investigated.

The second method of analysis is that proposed by Fisher and Goudsmit* and has been used successfully by the author in analysing the fine structures in the bromine and iodine arc spectra. For this method the nuclear spin and the J values of upper and lower terms must all be known. It is briefly illus-

trated in fig. 3 for the case of $4p . 5s . {}^3P_1 — 4p . 5p . {}^3P_2$, the nuclear spin being taken as ⅔. It is assumed that the interval rule holds exactly in the term fine structures, that is to say, the interval between two terms with fine structure quantum numbers f and $f + 1$ is $A(f + 1)$ where A is the interval factor and is a constant for any given gross multiplet term. The value of A depends primarily upon the coupling between the optical electron and the nuclear spin, and being different in upper and lower terms produces the complex fine structure patterns usually met with. The graph is built up as follows. Both upper and lower terms are given the same interval factor and the resulting line complex plotted as points along the line AB, which is therefore the line structure observed when the ratio of upper to lower interval factor is +1. The upper term is then inverted, retaining, however, the same value of A, and the line complex now formed by all the possible transitions is plotted at EF, which therefore shows the structure when the ratio of the upper to lower interval factors is —1. The corresponding transitions in AB and EF are then joined by lines, which for clarity are drawn with thickness roughly proportional to the intensities of the lines concerned. The selection rule employed is, of course, $\Delta f = \pm 1$ (0 → 0 excluded), and the absolute intensities of the components are calculated from the formulæ given by Hill.[*]

A horizontal line drawn at any particular point between AE gives the appearance of the structure for that particular ratio of the upper to lower interval factors. Thus at CD, the exact centre of AE, the upper term structure is zero and the resulting line pattern is a sharp triplet degrading to the violet, and in which the interval rule is exactly obeyed. The graph is particularly useful in the case when the upper factor is small compared with the lower. In this case the line still appears as a fairly sharp triplet, and in order to fit such a line into the graph, the following is employed. Through each of the centre points on CD dotted lines are drawn along the optical centres of gravity of the lines coming to that point, and it is seen that for a fair distance on either side of CD the line complex appears as a triplet, the lines becoming broader and the intervals altering as AB or EF is approached. The observed line is found to fit only one horizontal position and this position gives the values of both upper and lower interval factors. If the ratio of the factors is not very large, *i.e.*, the horizontal line is a good distance from CD, then other centre of gravity lines have to be constructed. Below the graph in fig. 3 are shown at (*a*) the predicted pattern of the line considered, for an upper to lower ratio

of 100 : 17. At (b) is the resulting triplet which is all that can be experimentally observed because of resolving power difficulties, whilst (c) shows the triplet observed. There is very good agreement both in intervals and in intensities.

The detailed analyses of individual lines will now be considered. The sharp regular series triplets and quartets show the number of fine structure components in one of the terms of the line concerned, usually the $4p \cdot 5s$ term.
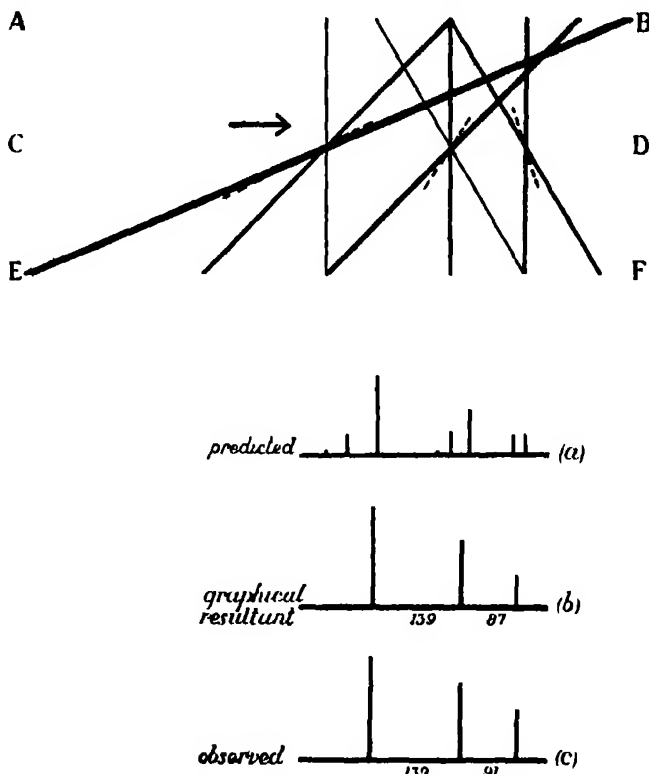
Fig 3.—Graphical method of analysis. Structure of $\lambda\,4730\cdot6$ $4p \cdot 5s \cdot {}^3P_1 - 4p \cdot 5p \cdot {}^3P_2$.

since a sharp regular series can only arise when the structure in one term is relatively small compared with that in the other. The maximum series observed is a quartet, this being clearly shown by three lines, only one of which, however, has been allocated. Since the term multiplicity is $2I + 1$ or $2J + 1$ according to which is the smaller, then I must be $\tfrac{3}{2}$ in order to account for the quartet lines. The allocated quartet is $4p \cdot 5s \cdot {}^3P_2 - 4p \cdot 5p \cdot {}^1P_1$, which would give a quintet if I were greater than $\tfrac{3}{2}$, and it is probable that the strongest of the unallocated quartets has a J value of three. It will be shown later

that the intervals in the term $4p \cdot 5s \cdot {}^3P_1$ strongly support the value of $\frac{3}{2}$ for I.

The lines will now be considered in the order convenient for analysis.

$\lambda\, 6022 \cdot 6.$ $4p \cdot 5s \cdot {}^3P_0 - 4p \cdot 5p \cdot {}^3D_1.$

This line is a well-resolved very sharp regular triplet degraded to the red. The lower term having a J value of zero remains single $(2J + 1 = 1)$ so that the triplet line structure is identical with the term structure of $4p \cdot 5p \cdot {}^3D_1$. Since this term has a J value of 1 a triplet is predicted, as observed. The term and line structure are shown in fig. 4, *a*.

$\lambda\, 4888 \cdot 5.$ $4p \cdot 5s \cdot {}^3P_0 - 4p \cdot 5p \cdot {}^1P_1.$

This line is quite sharp, showing no trace of structure even with $2\frac{1}{2}$ millions resolving power. As the lower term is single $(J = 0)$, it follows that the structure in the upper term must be very minute and not at all observable.

$\lambda\, 4985 \cdot 4.$ $4p \cdot 5s \cdot {}^3P_1 - 4p \cdot 5p \cdot {}^1P_1.$

This is an extremely sharp regular triplet degrading to the violet. The absence of structure in the previous line shows that the upper term has practically no structure, hence it follows that, as in the first line considered, the line structure gives a term structure, the term in this case being $4p \cdot 5s \cdot {}^3P_1$, fig. 4, *b*.[*]

$\lambda\, 6170 \cdot 6.$ $4p \cdot 5s \cdot {}^3P_1 - 4p \cdot 5p \cdot {}^3D_1.$

A complex line showing five components. Because the structures of the $4p \cdot 5s \cdot {}^3P_1$ and $4p \cdot 5p \cdot {}^3D_1$ terms have both been obtained from previous lines, it is possible to predict the fine structure of this line, and this is shown in fig. 4, *c*. Owing to the fact that the upper interval 120 is so close to the lower interval 117, the lines $\frac{5}{2} \to \frac{3}{2}$ and $\frac{3}{2} \to \frac{1}{2}$ fall practically on top of one another. Similarly, since the sum of the upper intervals is 198, and as one of the lower intervals is 194, then $\frac{3}{2} \to \frac{5}{2}$ and $\frac{1}{2} \to \frac{3}{2}$ also superpose. The respective intensities of these pairs have been summed in forming the predicted pattern and, as seen in the diagram, the observational agreement both as to intensities and intervals is remarkably exact. This exact agreement confirms both the analysis of the previously discussed terms and also indicates the reliability of the gross structure multiplet allocations.

---

[*] In a preliminary note to 'Nature' (vol. 129, p. 652 (1932)) on the nuclear spin of arsenic, the allocation of this line was mistakenly given as $4p \cdot 5s \cdot {}^3P_1 - 4p \cdot 5p \cdot {}^3P_1$. This error has no effect on the conclusions there stated.

(a)

(b)

(c)
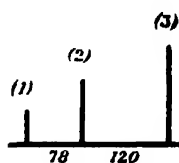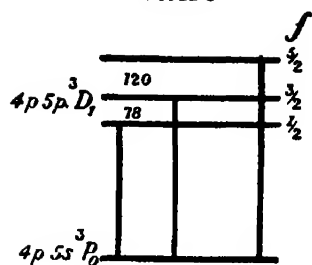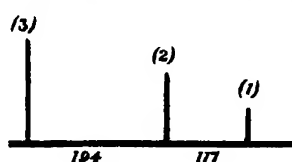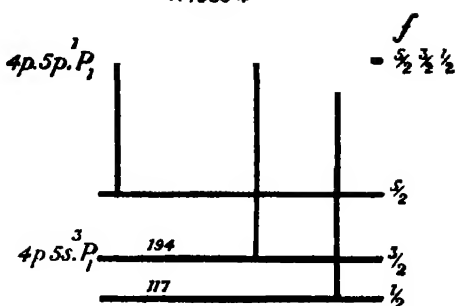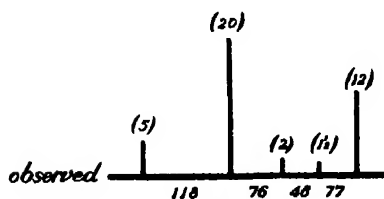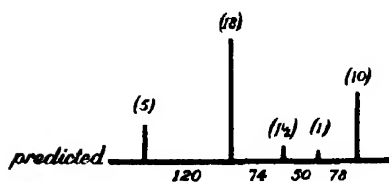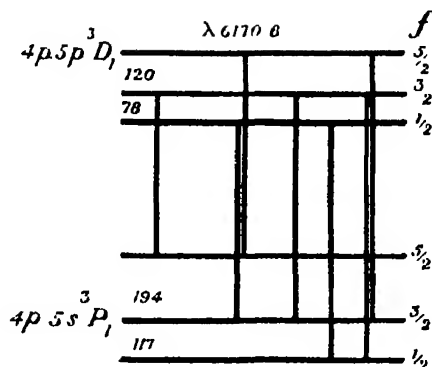
λ 4730·6. $4p \cdot 5s \cdot {}^3P_1 - 4p \cdot 5p \cdot {}^3P_2$.

This is a regular triplet fairly well resolved, but in a region where maximum resolution is not attainable, so that the separation of the last pair of components is not as good as that of the first pair. The line fits into its graph at a ratio of lower to upper interval factor of 100 . 17, fig. 3. The observed intervals are 139, 91 and those predicted 139, 87, which is very good agreement. Of course, the line is adjusted in the graph to make the first predicted and observed intervals equal. In this line there is a check on the graph since the structure of the $4p \cdot 5s \cdot {}^3P_1$ term is already known. Assuming the interval rule holds in the upper term, then the term structure of $4p \cdot 5p \cdot {}^3P_2$ is thus also obtained from this line.

λ 4552·2. $4p \cdot 5s \quad {}^3P_1 - 4p \cdot 5p \cdot {}^3S_1$.

The present line is similar to the previous line and was also analysed graphically. The observed pattern is 171, 90, and a ratio of 4 : 1 gives 171, 99, which is good considering the fact that the tail end of the triplet is not well resolved. The ratio values obtained in this and the previous lines are not affected by the lack of resolution since they are really obtained from the first more accurate interval. The predicted, resultant observable, and the actually observed patterns are shown in fig 6, *a*.

λ 5558·1. $4p \cdot 5s \cdot {}^3P_1 - 4p \cdot 5p \cdot {}^3D_2$.

This line is complex, showing five components, and, as the structure of the lower term is already determined, that of the upper can be calculated even although the resolution is incomplete. Both methods of analysis can be used, and assuming that the interval rule holds in the upper term the structure shown in fig. 5, *a*, is obtained. This gives the resultant pattern, fig. 5, *b*, the observed pattern being shown at fig. 5, *c*. The agreement is quite good, although the very weak component $\frac{1}{2} \rightarrow \frac{3}{2}$ was missed. The middle observed component (intensity 5) is somewhat displaced from the predicted position, but since it lies asymmetrically between two strong lines it is not completely resolved from the stronger.

λ 5657·0. $4p \cdot 5s \cdot {}^3P_2 - 4p \cdot 5p \cdot {}^1P_1$.

This is a regular quartet degraded to the violet, the lines being sharp. The last two components are quite clearly resolved, but rather too close for accurate measurement. Previous data have shown that the upper term has a negligible

structure, therefore the line structure should be the term structure of $4p \cdot 5s \cdot {}^3P_2$. This being so, the interval rule should hold. The observed intervals are 117, 78, 30, the error in the first two being ± 4 units and that in the last much more. If the Landé rule holds exactly, the intervals should be 117, 83, 50. The first two agree reasonably well, so that it is fairly safe to assume that in

4p 5s terms the interval rule is valid, and that the latter values give the actual structure of the term. The term and line structures are shown in fig. 6, b.

$\lambda 5331 \cdot 3$. $4p \cdot 5s \cdot {}^3P_2 - 4p \cdot 5p \cdot {}^3P_2$.

Since the lower term structure, which is given above, is only medium, and as in this particular case the upper term has also a reasonably wide structure, as deduced from $\lambda 4730 \cdot 6$, the line is therefore complex, narrow and very difficult indeed to resolve. It was observed as a poor triplet, the components being both broad and badly resolved. The resultant predicted pattern and that observed are shown in fig. 6, c, and the bad agreement is no doubt entirely due to lack of resolution. The line at least does not contradict any previous analysis, since it is predicted to be complex.

$\lambda 5105 \cdot 5$. $4p \cdot 5s \cdot {}^3P_2 - 4p \cdot 5p \cdot {}^3S_1$.

Like the previous line, this is also a badly resolved very unreliable group. Both the upper and lower structures have been deduced from other lines so that the line structure can be built up. Fig. 6, d, shows the result, and it is seen that agreement is poor.

Fig. 5.

$\lambda 6110 \cdot 3$. $4p \cdot 5s \cdot {}^1P_1 - 4p \cdot 5p \cdot {}^1P_1$.

This line is single, showing a slight broadening to the red, which is just noticeable. As the upper term is known to be narrow the lower term must also be the same, but since the line degrades to the red, then this lower term structure is inverted.

FIG 6.

$\lambda 4707 \cdot 7.$ $4p \cdot 5s \cdot {}^1P_1 - 4p \cdot 5p \cdot {}^1S_0.$

This is identical with the previous line, being single and degraded to the red. The upper term, having a J value zero, is single; therefore this line checks the above, both giving the $4p \cdot 5s \cdot {}^1P_1$ term as having a very narrow inverted structure

$\lambda 5107 \cdot 6.$ $4p \cdot 5s \cdot {}^1P_1 - 4p \cdot 5p \cdot {}^1D_2.$

This is a very narrow complex line appearing as a close doublet with high resolution, the components being 41 units apart and of similar intensity. As the lower term is so narrow the structure must be due to the upper term. It should then be a quartet, but with a narrow quartet and with poor resolution, the last three components will group together and the resultant appearance is a doublet, the intensities of the two being about the same. It follows, therefore, that a rough idea of the interval factor of $4p \cdot 5p \cdot {}^1D_2$ can be obtained and this turns out to be 12 units.

In addition to the structures of all of these allocated lines, those of a number of unclassified lines have also been measured and these are all given in Table III. Attention may be drawn to the line $\lambda 4340 \cdot 4$, which is a perfectly resolved quartet having a much coarser structure than any other line, namely intervals of 276, 237, 153. For a J value 3 these should be in the ratio 9 : 7 : 5 and actually they are in the ratio $9 \times 31 : 7 \times 34 : 5 \times 31$. This is suggestive of a term with J value 3 and interval factor 62 Further, the regular quarter $\lambda 4336 \cdot 6$ shows the intervals 150, 114, 47, the last separation not being very accurate. These are in the ratio $7 \times 23 : 5 \times 23 : 3 \times 16$, which, when the poor measurement of the last component is considered, are in the ratio 7 : 5 : 3, the value demanded by a J value of 2. Since both lines degrade to the violet, these J values are to be attributed to the lower terms.

Discussion.

The structures and interval factors of the various terms are given in Table IV. Only the data for the terms ${}^3P_0$, ${}^3P_1$, ${}^1P_1$, of the $4p \cdot 5s$ and the ${}^3D_1$, ${}^3S_0$ terms of $4p \cdot 5p$ are *exactly* determined. From fig 2 it is seen that most of the term interval factors have been obtained from more than one line. The interval ratio in the $4p \cdot 5s \cdot {}^3P_1$ term is exactly 5 : 3, which is the correct value required for a nuclear spin of $\frac{5}{2}$. However, the ratio in the $4p \cdot 5p \cdot {}^3D_1$ term, which should be the same if the interval rule holds, is 5 : 3·25 and the measure-

Table IV.—Term Fine Structures and Term Interval Factors.

Terms.		Term structures.	Interval factors.
$4p \cdot 5s$	$^3P_0$	Zero	Zero
	$^3P_1$	194 117	78
	$^3P_2$	117 83 50	33
	$^1P_1$	Small, inverted	Small, inverted
$4p \cdot 5p$	$^3D_1$	120 78	50
	$^3D_2$	84 60 36	24
	$^1D_2$	—	12
	$^3P_2$	46 33 20	13
	$^1P_1$	Small	Small
	$^3S_1$	48 29	14
	$^1S_0$	Zero	Zero

ments are sufficiently exact to show that this deviation is real. It is possible that the exact interval rule fails in the other $4p \cdot 5p$ terms, but since the deviation is relatively small in $^3D_1$, any effect cannot be destructive upon the preceding analysis. It is, of course, impossible to detect deviations in any of the other terms since the interval rule was assumed in deducing their structures. This breakdown of the interval rule will be mentioned again later.

The relative observed values of the interval factors will now be compared with those predicted by the vector coupling method of White and Ritschl (*loc. cit.*).

This coupling method is illustrated in fig. 7, for the $4p \cdot 5s$ configuration. At the left at A are the $4p \cdot {}^2P_{1\frac{1}{2}}$ terms of As III on which the ^3P and ^1P terms of As II are built. The $4s^2$ electron group, being closed, exerts no influence on the fine structures and so is completely neglected. The l value of the $4p$ electron is shown by a long thin arrow, and the spin by a short thick black arrow. The As II terms formed by the addition of a $5s$ electron, in (LS) coupling, are shown at B, the small hollow arrow representing the spin of the added s electron. The effect of compounding a nuclear spin $I = \frac{3}{2}$ is shown at C. Since the total spread of the fine structure, *i.e.*, the interval factor, is proportional to cos (IS) when cos (IJ) = 1, White and Ritschl (*loc. cit.*), then the relative interval factors are proportional to the angles made by I and S when I is placed parallel to J. The resulting relative patterns shown at C hold only for strict (LS) coupling. At the extreme right of the diagram the observed interval factors are recorded, and the main difference between the two is that the observed A for $^3P_1$ is greater than that for $^3P_2$, whilst in the predicted diagram this is reversed.

However, fig. 7 holds only for strict (LS) coupling, and actually the gross multiplet analysis indicates a stage intermediate between (LS) and (JJ). Fig. 8 shows the structures obtained with pure (JJ) coupling and with respect to this the following point is of importance. Breit* has shown, that in heavy elements, a $p_{\frac{1}{2}}$ electron, *i.e.*, a p electron with l and s opposing, behaves as if it were a penetrating electron and should therefore produce wide structures.
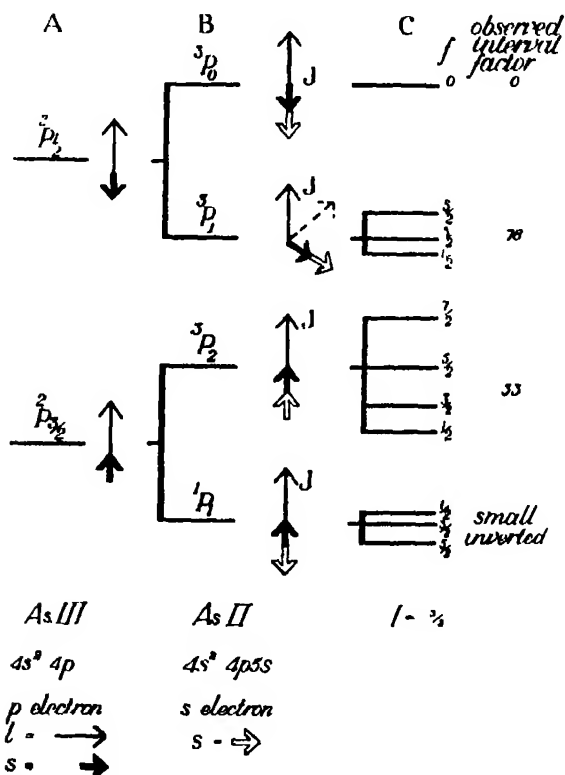
FIG. 7.—Fine structure vector couplings. (LS) coupling.

Since the $^3P_1$ term in fig. 8 is built up out of a $p_{\frac{1}{2}}$ electron and an s electron coupled parallel, then it should show the largest interval factor of all the terms in this configuration. It is seen that the observed results fit in very well with the predictions of fig. 8. The interval factor for $^3P_0$ is zero, the factor for $^3P_1$ is greater than that for $^3P_2$ and $^1P_1$ is small and inverted. These are all predicted so that the structures can fit a coupling scheme intermediate between (LS) and (JJ) but having a strong tendency towards (JJ).

* 'Phys. Rev.,' vol. 37, p. 1182 (1931) and vol. 38, p. 462 (1931).

The data for the $4p \cdot 5p$ configuration are not exact enough for conclusions to be drawn about the coupling processes.

The penetrating property of the $p_\frac{1}{2}$ electron, which explains the wide structure of $^3P_1$, also succeeds in accounting for the abnormally large structure found in the $4p \cdot 5p \cdot {}^3D_1$ term. Since this term is built up out of two $p_\frac{1}{2}$ electrons coupled parallel, then on this view it should possess a structure comparable
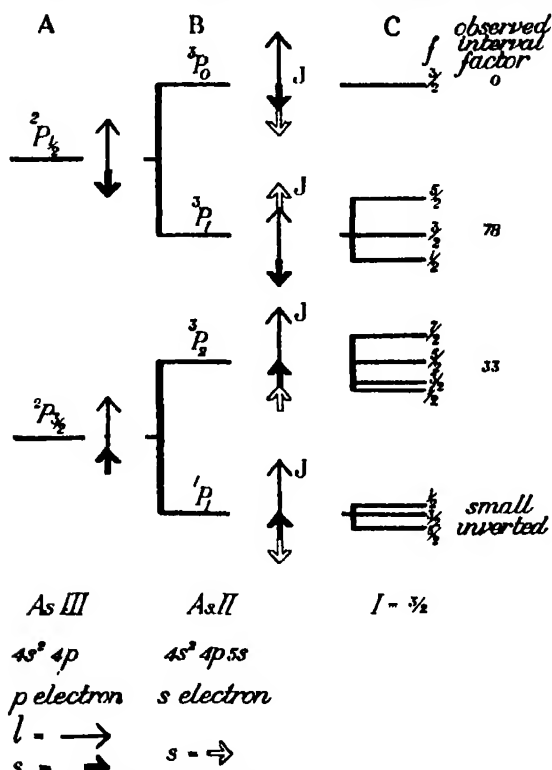
FIG. 8.—Fine structure vector couplings. (JJ) coupling.

with that produced by a penetrating s electron, and experimentally this is found to be the case. It is to be observed that the interval rule does not hold exactly in this term, which is possibly associated with the fact that the orbital motions of the $p_\frac{1}{2}$ electrons affect the coupling so that the simple cosine law of interaction is not valid.

Concerning the list of single and broad lines which are not allocated, and are given in Table II, all that can be said is that they probably represent transitions between the $4p \cdot 5p$ and $4p \cdot 4d$ configurations, whilst the coarse line λ 4340·4 may come perhaps from the $4s \cdot 4p^3$ group. It is to be observed that the fine structure observations confirm the gross structure multiplet analysis.

Summary.

The fine structures in the majority of the strong visible lines in the spectrum of As II have been observed and analysed. Most of these lines involve the $4p . 5s$ and the $4p . 5p$ electron configurations. The source used was a Geissler tube containing arsenic and helium, and the structures were observed with a Fabry-Perot interferometer having varying plate separations.

The structures can be completely explained by taking the nuclear spin as $\frac{3}{2}$.

The term structures of all the four $4p . 5s$ terms and those of seven of the $4p . 5p$ terms have been determined, and the former can be accounted for if the electron coupling in As II is taken to be intermediate between (LS) and (JJ) but with a strong tendency towards (JJ).

The analysis shows that a $p_{\frac{1}{2}}$ electron is to be considered as if it were penetrating, and experimentally such an electron is found to produce wide fine structures.

Twenty-six unallocated lines are found to be either quite single or else just broadened a little, and these probably represent $4p . 4d — 4p . 5p$ transitions.

The fine structure observations confirm the gross structure multiplet analysis in detail.

The Elastic Limit of Metals Exposed to Tri-Axial Stress.

By Gilbert Cook, D.Sc.

§ 1. *Introduction.*

The numerous investigations which have been carried out since the opening of the present century into the elastic breakdown of metals have resulted in the formulation of several hypotheses concerning the conditions of stress and strain necessary for its occurrence. The methods generally employed in the investigations have consisted in the application of combinations of tension and compression with torsion, and of bending with torsion, to solid bars and thin tubes, and of tension and compression combined with internal and external pressure to thin tubes ; so that the stress system produced in the metal was essentially bi-axial in character, the third principal stress being either very small or zero. The results of these experiments have given general support to the shear stress hypothesis of Guest,* although with deviations which in some cases are not insignificant.

Experiments employing a tri-axial stress system, in which the relation to each other of the component stresses could be varied, have been comparatively few in number. Tests by Turner† on thick walled cylinders of mild steel exposed simultaneously to internal pressure and axial tension, were inconclusive, possibly owing to the irregularity of the tubes. Those by Cook and Robertson,‡ also on thick-walled tubes of varying dimensions, showed a reasonably constant value of the maximum shear stress at the instant of elastic breakdown at the internal surface ; this stress was, however, considerably higher than the shear stress observed in the uni-axial state of stress in a simple tensile test of the same material, a result confirmed in more recent tests of a similar kind by the author.§ The newer hypotheses of Haigh‖ and of von Mises¶ require an effect of this kind ; but it has been suggested by the author that the observed effect may nevertheless be associated more directly with the non-uniform character of the stress distribution, rather than as an indication of the

* ' Phil. Mag.,' vol. 50, p. 69 (1900).

† ' Engineering,' vol. 92, p. 115 (1911).

‡ ' Engineering,' vol. 92, p. 786 (1911).

§ ' Phil. Trans.,' A, vol. 230, p. 103 (1931).

‖ Haigh, ' Rept. Brit. Assn.,' p 486 (1919), and p. 324 (1921).

¶ von Mises, ' Nachr. Ges. Wiss. Gottingen,' p. 582 (1913).

inapplicability of the hypothesis which regards failure as due to the existence of a critical value of the shear stress.

The investigation described in the present paper is a further attempt to ascertain more definitely which of these three hypotheses most closely represents the conditions at the elastic limit in certain metals when exposed to a tri-axial stress system. If p_x, p_y, p_z are the principal stresses, then according to the Guest hypothesis of constant shear stress at least one of the equations

$$p_x - p_y = \pm f, \quad p_y - p_z = \pm f, \quad p_z - p_x = \pm f, \qquad (1)$$

must hold, f being a constant equal to the stress at the elastic limit in a uni-axial system. The Haigh hypothesis of constant strain energy is represented by the equation

$$p_x^2 + p_y^2 + p_z^2 - 2\sigma (p_y p_z + p_z p_x + p_x p_y) = f^2, \qquad (2)$$

where σ is Poisson's ratio, while the relation proposed by von Mises is

$$(p_z - p_y)^2 + (p_y - p_z)^2 + (p_z - p_x)^2 = 2f^2, \qquad (3)$$

which, as shown by Hencky,[*] is also the condition of constant energy of shear strain.

Regarding the principal stresses as co-ordinates, the surfaces represented by the above equations have been discussed in detail by Haigh (*loc. cit.*), Westergaard,[†] and Schleicher.[‡] Equations (1) and (3) represent the surface of a hexagonal prism and its circumscribing cylinder respectively, both extending indefinitely in the axial direction, which is equally inclined to the positive directions of the co-ordinate axes. Equation (2) is that of a prolate spheroid whose major axis also lies in this direction.

It will thus be seen that the hypotheses of Guest and of von Mises, as distinct from that of Haigh, require that the liability of a material to elastic breakdown under a given stress system should not be affected by the addition of a fluid stress. On the other hand, variations in the value of the intermediate principal stress will be without effect on the conditions of failure only if the Guest hypothesis is valid. The two lines of attack thus suggested are described in § 2 and § 3 below.

§ 2. *The Effect of Fluid Stress on the Elastic Limit.*

There is little definite knowledge available as to the behaviour of materials under fluid *tensile* stress. No method of imposing this kind of stress in any

---

[*] ' Z. angew. Math. Mech.,' vol. 4, p. 323 (1924).

[†] ' Franklin Inst.,' vol. 189, p. 627 (1920).

[‡] ' Z. angew. Math. Mech.,' vol. 6, p. 199 (1926).

considerable intensity and in such a manner that it can be measured even approximately has been discovered , and although there is reason to believe that such states of stress exist under particular circumstances, and give rise to brittle fractures in otherwise ductile materials, little is known as to the intensity of stress which produces such fractures. It is probably very high compared with the elastic limit in uni-axial tension.

The available knowledge regarding the effect of high fluid *compressive* stress on metals is chiefly due to the researches of Bridgman. The general conclusion to be drawn from them is that the application of a pure hydrostatic pressure, even of extreme intensity, produces no permanent change in the metal. It is, of course, inconceivable that plastic flow would occur in an isotropic material under simple fluid stress, either tensile or compressive. It does not, however, necessarily follow from the absence of an observed permanent effect that a critical state is not reached during the application of the fluid stress which might make possible a permanent change of shape under the action of a distorting stress which, applied alone, would be within the elastic limit   In this connection an observation made by Bridgman* in an investigation of the effect of pressure on the rigidity of metals is of interest. A number of metals in the form of helical springs were exposed to torsional stress simultaneously with hydrostatic pressure up to 12,000 atmospheres. With one exception, all the metals tested had high elastic limits, and no permanent change in the dimensions of the springs made from these metals could be detected   The exception was that of the metal palladium, whose elastic limit was rather low. As no numerical data are given by Bridgman for this case, his own remarks upon it may be quoted :—" The original spring " . . . [as extended] " was not far from its elastic limit, and under pressure there was an effect which amounted to an increase of set or lowering of the elastic limit   . . . After the termination of the experiment " [involving applications of pressure up to 12,000 atmospheres] " the palladium spring was found to have received considerable permanent elongation   The effect of pressure on the elastic limit has apparently never been determined , what we have here is virtually a qualitative observation that the limit is lowered by pressure, an unexpected result."

It seemed important, therefore, to the author that a critical test on this point should be performed, a metal of sufficiently low elastic limit being used so that a fluid pressure many times greater than the shear stress at the elastic

---

* ' Proc. Amer. Acad. Arts Sci.,' vol. 64, p. 39 (1929).

limit could be imposed. The method adopted was similar to that employed by Bridgman. The material chosen was soft iron wire 0·0275 inch in diameter. It was coiled into the form of a helical tension spring of about 25 coils having a mean diameter of 0·560 inch, and was then annealed in a vacuum furnace. Reference marks were made on the spring in two pairs separated by 17 coils, each mark of a pair being at opposite ends of a diameter. By this means the axial extension while under load in the atmosphere, and any permanent set which occurred, could be measured by observation through the telescope of a cathetometer.

The spring was first extended by successive loads at atmospheric pressure in order to determine the position of the elastic limit. The observations are given in Table I, and the load-extension curve in fig. 1.

Table I.

Total load	Mean distance between reference marks	Extension
lb.	mm.	mm.
Zero	48·38	—
0·054	56·21	7 83
0·104	63 37	14·99
0 114	64·84	16 46
0·124	66 43	18 05
0 134	68·31	19 93

It will be seen that there is a fairly well defined elastic limit at a load of 0·114 lb., corresponding to a maximum shear stress in the wire of 3·5 tons per square inch. The spring was now re-annealed, and a load of 0·104 lb., slightly below that corresponding to the elastic limit as determined above, was applied and removed as described in part (1), Table II. The small permanent set produced by the first two applications of this load is seen to remain unaltered after a further 48 hours' continuous application of the same load ; thus, although the material is exposed to a stress little less than that which would cause considerable plastic flow, it appears to be quite stable.

The spring was now suspended vertically in a pressure vessel, fig. 2, consisting of a thick-walled tube of high tensile steel, filled with glycerine. A load equivalent to that previously imposed, 0·104 lb., was suspended from the spring, due allowance being made for the density of the glycerine. The pressure was raised to 21·5 tons per square inch by means of an intensifier, and was allowed to remain at this figure for a period of 48 hours. The spring

was then removed from the apparatus, particular care being taken to avoid imposing any strain upon it in doing so. A measurement on the unloaded
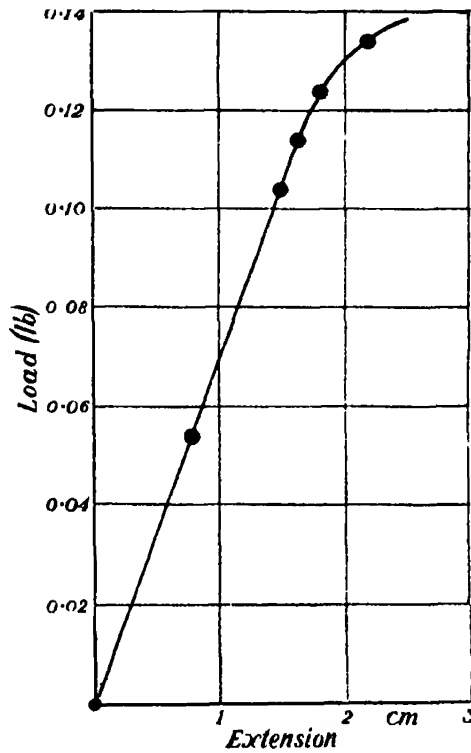
Fig 1

Table II.

Load applied and removed		Duration of application.	Mean distance between reference marks after removal of load	Permanent extension.	
Axial load.	Fluid pressure			]	Per-centage.
lb.	tons/sq. in.	hours	mm.	mm.	
		--	50 81	—	—
0 104	—	2	51 08	0 27	0·54
0·104	—	16	51 13	0 32	0·64
0·104	—	48	51 13	0 32	0 64
(11)					
0·104	21·5	48	51 03	0·22	0·44

spring now gave the figures shown in part (ii), Table II. The small permanent extension previously observed has apparently been diminished slightly,
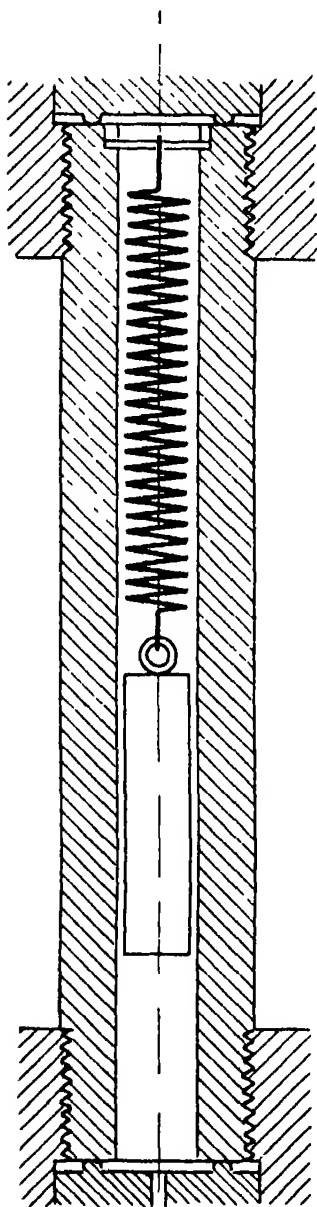
but it is considered that the difference is probably due to the unavoidable handling of the spring in placing it in, and withdrawing it from, the pressure apparatus. It is, in any case, in the opposite direction to that which would be found if the elastic limit were lowered by the application of the fluid pressure. It will be noted that the fluid pressure imposed in this test was more than six times as great as the shear stress at the elastic limit observed under atmospheric conditions, and the absence of any appreciable effect due to its application justifies the conclusion that the addition of such pressure does not increase the liability of this material to elastic breakdown. Although it cannot with certainty be inferred that other ductile materials would behave in a similar manner, it seems highly probable that the effect observed by Bridgman in the case of palladium is due to some other cause.

§ 3 *Effect of Variations in the Magnitude of the Intermediate Principal Stress*

If the conclusion is accepted that the position of the elastic limit is independent of the intensity of the fluid stress, it follows that stress differences alone will be found in the expression of any theory which can be applicable. The shear stress theory of Guest, and the shear strain energy theory of von Mises-Hencky comply with this condition. The question as to which of these two hypotheses is preferable may be examined by observing whether the maximum shear stress, or, what is equivalent, the difference between the extreme principal stresses,

Fig. 2.

prevailing in the material at the elastic limit, is affected by the value of

the intermediate principal stress. This has been the method used in recent investigations where, however, the enquiry has been confined to the conditions necessary to set up and maintain a condition of plasticity in material which has already received a considerable amount of plastic deformation. The work of Lode* on thin tubes of iron, nickel, and copper exposed to combinations of internal pressure and longitudinal tension ; of Hohenemser† on thin steel tubes subjected to combined tension and torsion, and particularly the recent work of Taylor and Quinney‡ on tubes of copper, aluminium and iron, have shown that the onset of plastic flow under such conditions is undoubtedly affected by the value of the intermediate principal stress, and to an extent, moreover, which is in good agreement with the hypothesis of constant energy of shear strain   The experiments to be described in this section were undertaken in order to discover whether a similar effect was observable in regard to the elastic limit in previously unstrained materials

The case of compound stress chosen for this study was that which exists at the inner surface of a thick-walled cylinder exposed simultaneously to internal pressure and longitudinal tension   In a cylinder in which the longitudinal stress is due solely to the internal pressure, the principal stresses at a point in the inner surface are, from the well-known theory

$$
\left.
\begin{aligned}
p_x &= p \; \frac{1}{k^2 - 1} \\[2mm]
p_y &= p \; \frac{k^2 + 1}{k^2 - 1} \\[2mm]
p_z &= - p
\end{aligned}
\right\}
\tag{4}
$$

where p is the numerical value of the internal fluid pressure, and k the ratio of external to internal diameter   In this the axis of x is taken parallel to the axis of the cylinder, and those of y and z in the tangential and radial directions respectively, tensile stresses being positive   The relative values of p_y and p_x may be varied over a considerable range by varying k, but p_x, although dependent also on k, is comparatively small except in very thin tubes. It may, however, be varied independently of p_y and p_z, by applying an additional axial load, and it is the intermediate principal stress so long as the additional axial stress is less than $p \cdot k^2/(k^2 - 1)$.   By choosing a suitable value for k we may

* ' Ver deuts Ing Forschrft ,' vol. 303 (1928).

† ' Z angew Math Mech ,' vol. 11, p 15 (1931).

‡ ' Phil. Trans.,' A, vol 230, p 323 (1931)

examine by this method the effect of the intermediate stress extending, from a comparatively low value, over a range greater than the internal pressure applied, without altering the disposition of any of the principal stresses

Two varieties of mild steel, containing 0·21 per cent. C and 0·35 per cent C respectively were used in the investigation. These were specially prepared and supplied by Messrs. Thos Firth & Sons. The analyses are given in Table III.

Table III —Analysis of Steels.

Reference	C.	Si.	Mn	S.	P.	Ni	Cr
C	0 21	0·09	0 05	0 018	0 018	0·11	—
J	0·35	0 22	0 66	0 020	0 020	0 46	0 05

A considerable amount of information was available from a previous investigation in regard to the behaviour of the 0·21 per cent C steel under other non-uniform stress systems

Stress-strain diagrams obtained from tests in simple tension on specimens of the same shape and with the same heat treatment as the cylinders, are shown in fig. 5, and it will be seen that no deviation from a linear relation between stress and strain is perceptible up to the yield point, which thus coincides with the elastic limit.

The cylinders used in the tests under tri-axial stress were machined to the form shown in fig. 3. It was decided to keep the dimensions the same in all
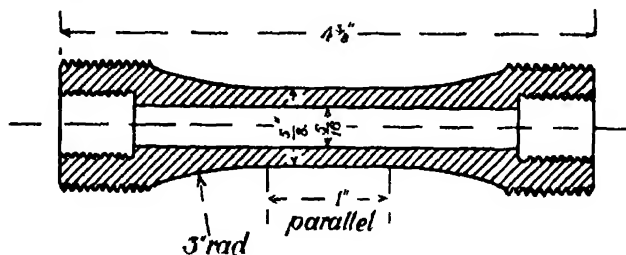
Fig. 3.

cases, so that no variation in the ratio of the transverse principal stresses would occur. The external diameter of the central parallel portion was made twice the internal diameter, and this portion was connected to the screwed ends by fillets of large radius to avoid concentrations of stress due to the axial load. The specimens were carefully machined internally and externally and were then heat treated *in vacuo* to remove initial stresses. The temperatures employed were 900° C. for the 0·21 per cent C steel, and 870° C. for the 0·35

per cent C steel, the specimens being allowed to remain for 20 minutes at this

temperature The specimens of 0·21 per cent. C steel were allowed to cool in the furnace, as it was desired to compare the results of the tests applied to this material with others in which the same heat treatment had been given, while those of 0·35 per cent. steel were removed from the furnace to cool by radiation *in vacuo*

The method used for applying the combination of fluid pressure and axial stress is shown in fig 4. The longitudinal tension, applied through axial loading grips of the ball type from a special straining gear, is measured by the elastic extension as recorded by a mirror extensometer, of a weigh bar A of high tensile steel coupled in series with the specimen B. Fluid pressure was transmitted to the interior of the test piece through a fine bore steel tube C from an intensifier and was measured by means of a steel tube Bourdon gauge with jewelled bearings reading to 20 tons per square inch, and graduated in divisions of 0·1 ton per square inch. The gauge was calibrated against a dead weight tester at the makers' works in the presence of the author.

In order to observe the strains produced in the specimen two extensometers were used   The radial extension of the external surface was measured by means of a Lamb diametral extensometer,* and for the axial extension a mirror extensometer embodying the Martens principle was employed   The purpose of both extensometers was to indicate when any departure occurred from a linear relation between the strains and applied stresses, and it was unnecessary therefore to convert scale readings into actual strains.

The method generally employed in carrying out a test was first to strain the cylinder axially to a stress such as, with the addition of the stress due to the estimated internal pressure, would give approximately a predetermined
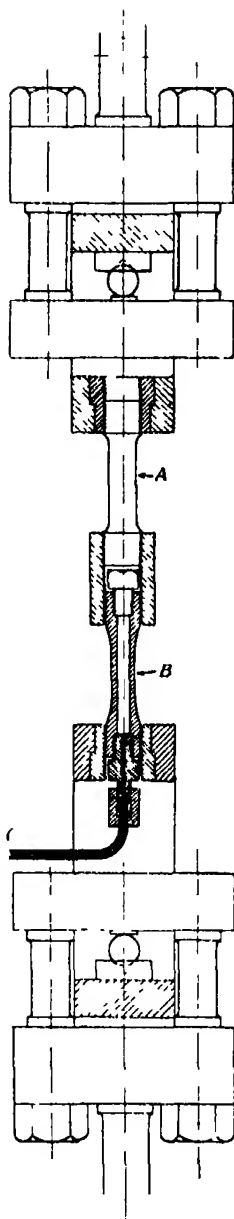
Fig. 4.

* For a description of this extensometer, see ‘ Engineering,’ vol. 119, p. 207 (1925).

value of the total axial stress. The fluid pressure was now raised, and readings on both extensometers attached to the specimen, and also on that on the weigh bar, were taken, the intervals being reduced to 0·1 or 0·05 ton per square inch as the point of breakdown was approached. As the pressure was raised the extensions, both radial and axial, were almost exactly proportional to the increase in pressure. A period of at least 1 minute was allowed to elapse
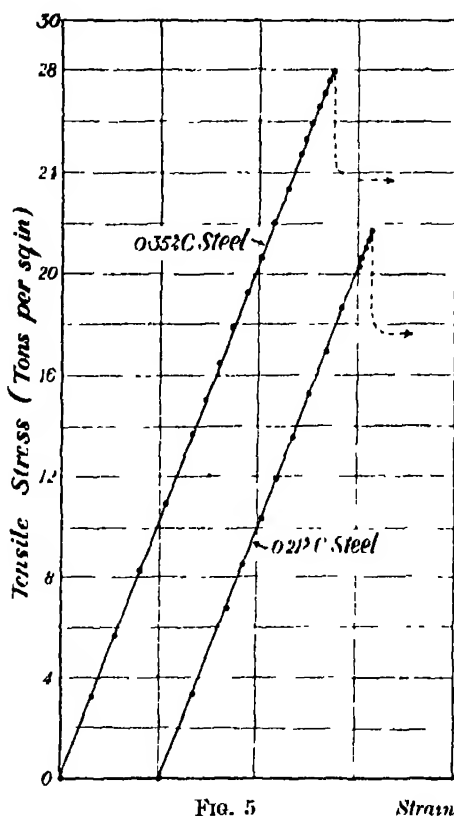
FIG. 5   *Strain*

at each value of the pressure during which the extensometers were carefully observed for any sign of creep, or departure from the proportional increment in extension. The elastic limit was marked by a much larger increment in the radial strain than had previously occurred, or in a contraction, both being accompanied by a slow creep.*

* The contraction in diameter frequently observed is not due, as might be supposed, to an increase in the axial strain, but to the initial localisation of the breakdown causing the external surface to become slightly elliptical. The effect has been discussed in detail elsewhere by the author (*loc. cit.*).

In an investigation of this nature it is desirable to obtain as large a number of test results as possible, and for this purpose one or other of the following courses may be adopted :—

(1) A considerable number of specimens may be used, and a single test only carried out on each specimen   Where a large amount of machining is required, as in the present case, this method is expensive, and there is also the possibility of variations in properties from specimen to specimen due to variations in composition.   It is, however, probably the best method, and was employed for the tests of the 0·35 per cent. C steel, but it was not possible, owing to the cost, to use a large number of specimens.

(2) By immediately relieving the pressure on the first sign of elastic breakdown the amount of overstrained material would be small and probably localised in a small area.   A second test would produce breakdown at another point, and in this way the same specimen could be used for a number of tests with different amounts of axial stress   This method was employed for the 0·21 per cent C steel   It is not altogether free from objection, but repeat tests under the same conditions show that the effects of previous tests are inappreciable

(3) The specimens may be renormalised or re-annealed after each test. This method was, however, not used owing to the possibility of structural changes following the process when repeated many times.

Fig 6 shows the character of the stress strain diagrams.   The ordinates represent the internal pressure, while the abscissæ represent, to an arbitrary scale, the radial extension   The whole of the diagrams for the tests with 0·35 per cent. C steel are shown, but for reasons of space the series for one specimen only (No. 4) of the 0·21 per cent C steel is given

The numerical results are contained in Tables IV and V.   The radial and tangential principal stresses are obtained from the second and third of equations (4), while the axial principal stress is given by the equation

$$p_{s} = p_{x_0} + \frac{p}{\lambda^2 - 1}$$

where p_{x_0} is the externally applied axial stress as measured by the weigh bar. In order more readily to see the effect of variations in the intermediate principal stress, the tests are tabulated in order of increasing axial stress.   The
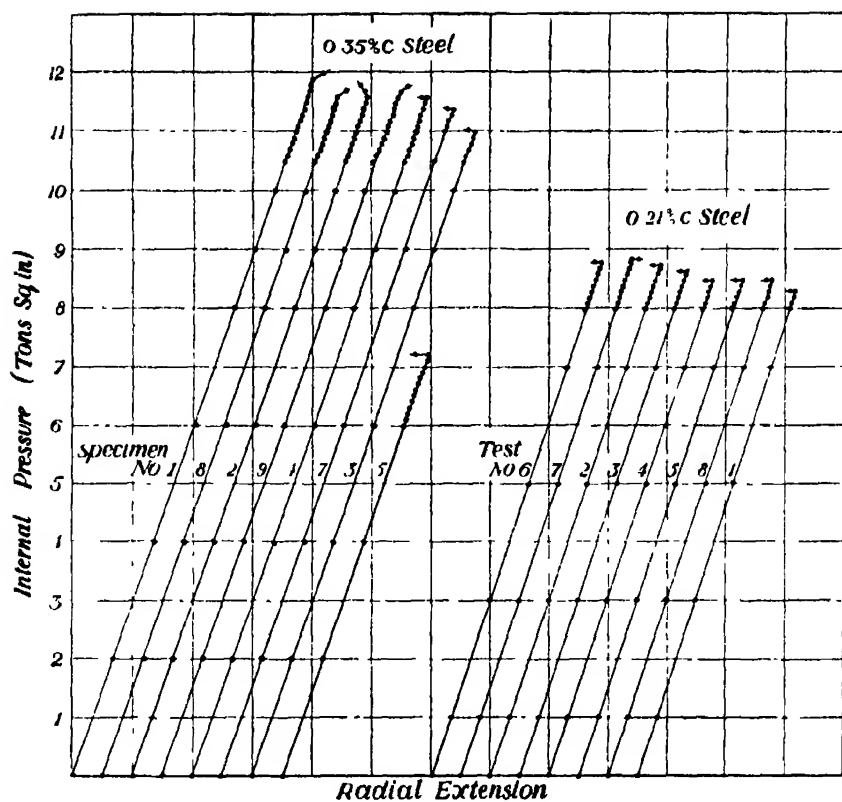
Fig. 6.

Table IV.—Tests on 0·35 per cent. C Steel Cylinders

Elastic Limit and Yield-point in Simple Tension, $f = 27 \cdot 9$ tons per square inch.

Ratio, external to internal diameter, $2 \cdot 1$

Speci-men No.	Principal stresses at elastic limit			Equivalent uni-axial stress for same value of		f_s/f	f_e/f
	Axial (p_x).	Tangential (p_v)	Radial (p_z)	Maximum shear stress (f_s).	Maximum shear strain energy (f_e)		
	tons/sq. in	tons/sq. in	tons/sq. in.	tons/sq. in.	tons/sq. in.		
1	4 00	19·90	—11 95	31 85	27 60	1 140	0 990
8	4 40	19·30	—11 60	30·90	26·75	1·105	0·960
2	8 90	19 50	—11 70	31·20	27·45	1·115	0 982
9	14 05	19 40	—11·65	31 05	28 75	1·110	1·030
4	17·80	19 30	—11·60	30·90	30·10	1 105	1·075
7	19·00	19·00	—11 40	30 40	30·40	1 090	1·090
3	20·20	18·33	—11 00	31 20	30 30	1 115	1·085
5	24·05	12·00	— 7 20	31·25	27·30	1 120	0·975
6	27 95	0	0	27·95	27 95	—	—
Mean						1·112	1 023
Maximum variation (per cent)						4·5	13 0
Mean variation from mean (per cent.)						1·0	4·6

Table V.—Tests on 0·21 per cent. C Steel Cylinders.
Elastic Limit and Yield-point in Simple Tension, $f = 21\cdot6$ tons per square inch.
Ratio, external to internal diameter, 2 : 1

Speci-men No.	Test No.	Principal stresses at elastic limit.			Equivalent uni axial stress for same value of		f_s/f	f_e/f
		Axial (p_x)	Tangential (p_y)	Radial (p_z)	Maximum shear stress (f_s)	Maximum shear strain energy (f_e)		
		tons/sq. in.	tons/sq. in.	tons/sq in	tons/sq in.	tons/sq in.		
1	(1)	3 25	14·60	−8 75	23 35	20 20	1 080	0 935
	(4)	3 70	14 60	−8·75	23 35	20 20	1 080	0 935
	(5)	7 70	14 50	−8 70	23·20	20 65	1 075	0 955
	(3)	13 40	14 50	−8 70	23·20	22 70	1 075	1 052
	(2)	15 05	14·00	−8 40	23 45	22 95	1·087	1 063
	(6)	16 05	14 00	−8 40	24 45	23 50	1 132	1·089
2	(1)	3 50	14 65	−8 80	23·45	20 30	1 087	0 940
	(5)	3·70	14·60	−8·75	23 35	20 20	1 080	0·935
	(3)	10 35	14 50	−8 70	23 20	21 40	1 075	0 990
	(4)	13·85	14·15	−8 50	22 65	22 50	1 050	1 042
	(2)	14 60	13 65	−8·20	22 80	22 40	1 057	1·037
3	(1)	3 40	14 65	−8 80	23 45	20 35	1 087	0 942
	(4)	12 00	14 65	−8 80	23 45	22 25	1 087	1 030
	(2)	14·40	14 00	−8 40	22·80	22 60	1 057	1 047
	(3)	14·65	14 30	−8 60	23·25	23 00	1 078	1 065
	(5)	16·60	13 40	−8 05	24 65	23 25	1 140	1·077
4	(6)	3·55	14 65	−8 80	23 45	20 35	1 087	0 942
	(7)	3·95	14 75	−8 85	23 60	20 45	1 092	0·948
	(2)	4·55	14 60	−8 75	23 35	20 30	1 080	0 940
	(3)	7 05	14 40	−8 65	23 05	20 40	1 069	0 945
	(4)	10 10	14 15	−8 50	22 65	20 90	1 050	0 968
	(5)	13 05	14 15	−8 50	22 65	22 10	1 050	1 023
	(8)	14 25	14 15	−8·50	22·75	22 70	1 054	1 051
	(1)	14 55	13 85	−8 30	22·85	22·50	1 060	1 041
5	(1)	3·00	14 50	8 70	23 20	20 10	1 075	0 930
	(2)	9 05	14 40	−8·65	23 05	20 90	1 069	0 968
	(3)	14 80	14 00	−8 40	23 20	22 80	1 075	1 057
	(4)	18 65	10·20	−6 10	24 75	21 80	1 146	1 010
6	(1)	5·45	14 50	−8 70	23·20	20 20	1 075	0 935
	(2)	21·80	4 85	−2 90	24 70	21 90	1 143	1·014

Mean							1 082	0 997
Maximum variation (per cent.)							8 9	15 9
Mean variation from mean (per cent.)							1 6	5·0

equivalent uni-axial stress, that is, the value of f calculated from the tabulated values of the principal stresses by means of equations (1) and (3), and the ratios of this to the stress at the elastic limit observed in the simple tensile test, are given in the last four columns.

The results are also shown graphically in fig. 7. The ratio k being constant throughout the present series makes it possible to represent them on a two-dimensional diagram in which the internal pressure is plotted against the total axial stress. On the same diagram are plotted, by means of broken lines,
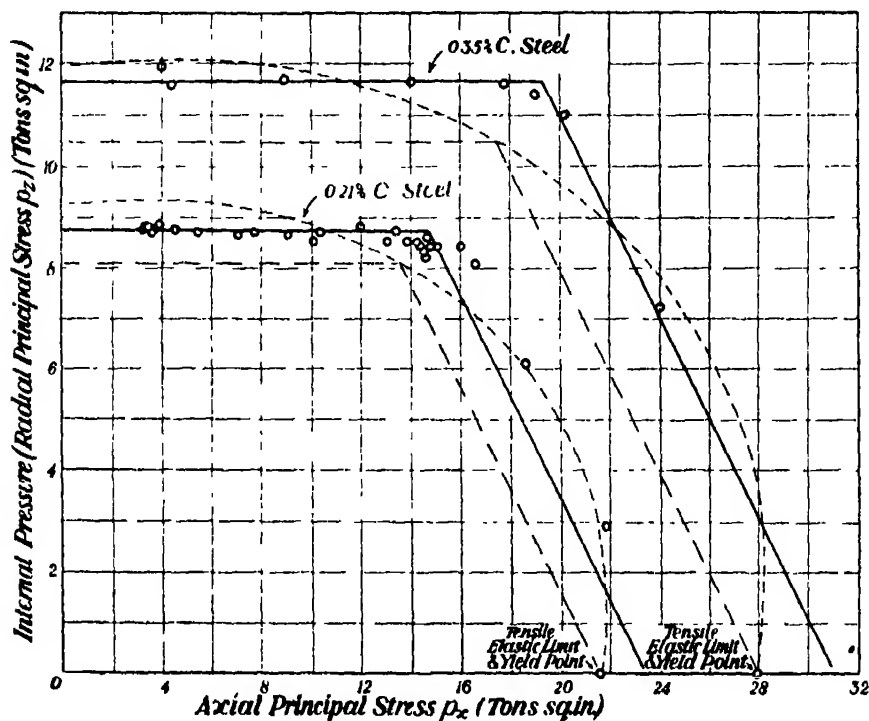
Fig. 7.

— --   Constant shear strain energy ⎫ equal to value observed at tensile yield
—. -.—   Constant shear stress   ⎬   point.
—   -   Constant shear stress, equal to mean of observed values

the theoretical relations according to the two hypotheses, based upon the observed value of the tensile elastic limit ; that is to say, the lines are made to pass through the point on the axis of p_x representing that stress. These lines are part of the intersection of the surfaces corresponding to equations (1) and (3) with the plane

$$p_y + p_z \ (k^2 + 1)/(k^2 - 1) = 0$$

The full line in each case is drawn for a constant value of the shear stress equal to the mean value observed in the tests.

The mean value of the ratio given in the last column in Tables IV and V is much closer to unity than that obtained from the figures in the previous column, which might suggest that failure under tri-axial stress is better correlated with that in simple tension on the basis of the hypothesis of constant shear strain energy rather than on that of constant shear stress. But it may be observed that the individual variations in value of the ratio from test to test is much less for the shear stress hypothesis than for the shear strain energy hypothesis, and it will be noticed that in the value of the latter ratio there is a progressive variation which is absent from the former If we exclude those cases in which the axial stress is appreciably greater than the tangential principal stress, the shear stress figures will be seen to be in still closer agreement , and since, under these conditions, the axial stress is the intermediate principal stress, the conclusion appears to be unavoidable that it is without appreciable effect upon the conditions under which the elastic limit is first reached in these materials

It is interesting to note that the average value of the maximum shear stress observed in the present tests on the 0·21 per cent C steel, namely 11 7 tons per square inch, is in close agreement with the values 11·9 tons per square inch and 12·1 tons per square inch previously obtained with the same material in torsion and flexure respectively

The evidence therefore favours the view that as regards the initial elastic breakdown in mild steel, the maximum shear stress is the critical factor , that the Guest hypothesis is true to the extent that, for the same kind of stress distribution, the values of the principal stresses at the elastic limit are such as to give a constant value of the maximum shear stress But, further, in this material the critical value of the shear stress depends on the character of the stress distribution, so that the results obtained from the ordinary tensile test, in which the stress distribution is uniform, are not strictly comparable with systems of combined stress where, as is generally the case, the distribution is not uniform.

Summary

The paper describes an investigation carried out to determine the relation holding between the principal stresses at the elastic limit in certain ductile materials when exposed to stresses in three dimensions, and to examine the applicability of the hypotheses of constant maximum shear stress (Guest), constant total strain energy (Haigh), and constant energy of shear strain (von Mises-Hencky).

An observation by Bridgman, suspecting an effect upon the elastic limit under distorting stresses by the superposition of high hydrostatic pressure, was examined by exposing an annealed iron wire to torsional stress (*a*) at atmospheric pressure, and (*b*) under hydrostatic pressure of 21·5 tons per square inch. No lowering of the elastic limit was observed, a result which suggests that the Haigh hypothesis does not hold.

To discriminate between the two remaining hypotheses, tests were carried out on thick-walled cylinders of mild steel, exposed to combinations of internal pressure and axial tensile stress. It is shown that variations in the axial stress, provided that it remains the intermediate principal stress, have a negligible effect on the internal pressure required to cause initial failure at the internal surface ; and therefore for the same kind of stress distribution the values of the principal stresses at the elastic limit are such as to give a constant value of the maximum shear stress.

Intensity Distributions in Molecular Spectra : The Swan System (C_2).

By R. C. Johnson, M A , D Sc , and N. R. Tawde, B.A., M.Sc., University of London, King's College

(Communicated by E V Appleton, F.R.S —Received April 28, 1932)

1 *Introduction*

The problem of obtaining accurate measurements of the relative intensities of spectral lines or bands when these cover a considerable wave-length range is one of the most difficult in experimental spectroscopy. These difficulties have been enumerated by many writers, *e g* , in a recent paper by Read and L W. Johnson,[*] and it is not proposed to enter into a detailed discussion here. The problem is much simpler when a small spectral range only is being investigated, such as, for example, the fine structure of an individual band or the intensity within a line multiplet, and a large amount of experimental work has been done within these limits The desirability of quantitative data on intensity distributions within band systems is apparent from the theoretical work of Condon[†] published in 1926, explaining the general characteristics of such distributions. The cases to which Condon's theory has been applied by way of illustration have been almost all naked-eye estimates of band intensities on an arbitrary scale (0–10) An exception to this is the α-system of BO on which Elliot[‡] has made accurate measurements In the present paper we have made preliminary observations on the well-known " Swan " system of the C_2 molecule. This system has the advantage, from an experimental standpoint, of lying wholly within the visible region of the spectrum, and, further, that its intensity distribution is characteristic of a large class of band systems, and that it can be produced under a variety of experimental conditions.

2. *Experimental Methods.*

The Swan system has been produced and studied from five sources, differing widely both in temperature and in electrical conditions ; the cone of the Bunsen flame, the cone of the Oxy-coal gas flame, the Carbon arc in hydrogen, the discharge tube containing a trace of carbon impurity in the presence of 30 mm.

[*] ' Phil. Mag.,' vol. 11, p. 1152 (1931).

[†] ' Phys. Rev.,' vol. 28, p. 1182 (1926) ; vol. 32, p. 858 (1928).

[‡] " The Optical Determination of the Relative Abundance of Isotopes," Utrecht, 1930.

pressure of argon, and the condensed spark under glycerine. A Hilger glass prism constant deviation spectrograph was used for photography. Ilford Rapid Process Panchromatic plates were used through the work, and with due precautions in the matter of exposure and development were found when photometered to give an exceptionally clear and uniform background with very little " grain effect." Two plates were taken of each source, one exposed a longer time for the benefit of the fainter bands, the other one a shorter time for the sake of accuracy in measuring the strongest bands   Correlation of the two plates was made by measuring a number of bands of intermediate intensity on both plates   On each plate a set of seven strips of continuous spectra was photographed adjacent to the band system, for the purpose of determining the Blackening-Intensity curves of the plate at any desired wave-length.   For this purpose a step-slit* having seven steps of widths 2 26 mm , 1·53 mm., 1·05 mm , 0·74 mm., 0·48 mm , 0·26 mm , and 0·13 mm , was mounted in the collimator tube in place of the normal long slit.   The step slit was illuminated by a special 12-volt gas-filled tungsten spiral-filament lamp, supplied by a battery of large capacity   It was placed about 1 metre distant and accurately in line with the collimator, no lens being used   This lamp had been previously calibrated by means of a thermopile, Paschen galvanometer and quartz mono-chromator, so that its E_λ λ relation was known   The dispersion curve $d\lambda/dm$ λ of the glass prism spectrograph having previously been obtained, an $E_\lambda d\lambda : \lambda$ curve was constructed appropriate to the standard lamp when used in conjunction with this particular spectrograph   The value of the light energy falling on a given interval of the plate at any desired wave-length was therefore known on a relatively correct scale.   It was proportional to (slit width w) $\times$ $E_\lambda d\lambda$.   Reflection and absorption losses in the spectrograph do not produce any error in the final results since these are the same for both the calibration spectra and the band system itself.

Microphotometer records were obtained of the band system and of the calibration spectra opposite each band head.   Plotting optical density $\log_{10}(i_0/i)$ of the calibration spectra (deduced from the microphotometer record) against light intensity (known as explained above), the intensity corre-sponding to the optical density of the band could be read.   With this procedure it was necessary to construct a separate Blackening-Intensity curve for each band head, and though laborious, it was found to be essential on account of the rapidly varying sensitivity of the plate with wave-length

A second method of intensity determination was also examined, viz., the neutral wedge method developed by Merton and Nicholson.* In this case the wedge spectrum of the band system and also of the standard lamp were photographed on the same plate. After development and fixing of the plate it was " cut " with potassium ferricyanide solution to give sharp end points. The heights " h " of the band heads and of the corresponding points of the wedge spectrum of the lamp were measured on a micrometer, and from these, using the customary formula, $I_{Ph} \propto$ antilog $(d_\lambda h/m)$, the photographic intensities of both may be calculated. d is the optical density gradient of the wedge and is a function of λ. Its determination is discussed later. m is the magnification of the lens system of the spectrograph and is also a function of λ. (It is determined by the simple procedure of photographing a line spectrum through a collimator slit of known length and measuring the lengths of the lines.) The " photographic " intensities of the bands of a system differ from true relative intensities on account of the varying sensitivity of photographic plate with wave-length. The correcting factor by which the " photographic " intensity of each band is then multiplied is $\dfrac{w \times E_\lambda \cdot d\lambda}{(I_{Ph} \text{ of lamp})_\lambda}$. The bands are thus brought to a relatively correct scale.

For purposes of comparison the (0, 0) band of the system was called 100 and the other bands calculated accordingly

We may here anticipate the discussion of these two methods so far as to say that we consider that with certain precautions the first method is the more accurate

3. *Peak Intensity and True Band Intensity.*

Ideally the intensity of a band should be determined by a summation of the intensities of the fine structure components, which presupposes complete resolution of the band on an instrument of high resolving power. For a complete band system the intensities of many thousands of lines would need to be measured, certainly in many cases an almost impossible procedure. A fairly accurate estimate may probably be made by comparing the intensities of corresponding fine structure lines in different bands. Since, however, the rotational energy distribution is dependent on the moment of inertia—which varies slowly with vibrational quantum number—this cannot be absolutely accurate Another method used by Elliot, although very laborious, is applicable to unresolved bands in cases where the overlapping is not excessive.

* ' Phil. Trans.,' vol. 217, p. 237 (1917).

The microphotometer record is enlarged, and the optical densities of a large number of points on the contour are calculated. The intensities corresponding to these are read from the Blackening-Intensity curves, and, finally, a new contour can be constructed of which the ordinates represent intensities. An integration of the area under this contour should now give a quantity proportional to the " weight " of the band.

The point of maximum intensity in an unresolved band is in many cases fairly close to the head. This " peak " intensity is experimentally easy to determine, although from a theoretical standpoint it is doubtful how far it may be taken as proportional to the band intensity. If the moment of inertia of the molecular varies but little with vibrational quantum number, then the band head will occur in every case at nearly the same j-value, and the peak value will probably be approximately proportional to band " weight." In the present communication we have dealt entirely with peak intensities and— at least to a first approximation—we believe that results of some value have been obtained.

4. Discussion of the Microphotometric Method.

In fig. 1 is represented diagrammatically the intensity distribution in the Swan system as deduced by eye-estimates from a spectrogram of the blue cone
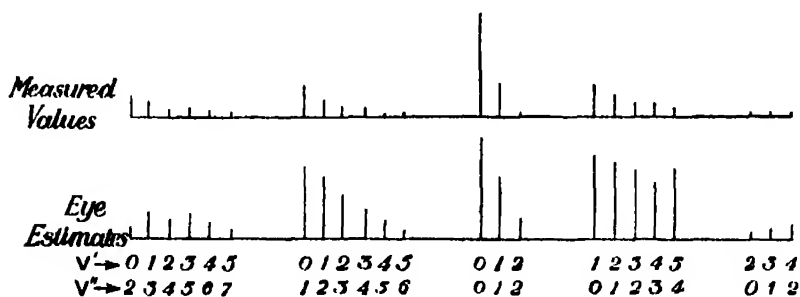
FIG. 1.—Eye estimates and measured intensity values of the Swan system photographed from a Bunsen flame.

of the Bunsen flame and by microphotometric measurement of the same plate. A personal element necessarily enters into the former, but it is apparent how very considerable is the range of error in eye estimations of photographed spectra. If visual observations are made directly on the spectrum, then apart from variations in the intensity of the source there will be physiological factors leading to error, and their magnitude is difficult to assess. Confining ourselves therefore to eye-estimates of spectrograms the errors arise from two sources :

(1) the nature of the characteristic Blackening-Intensity relation of the photographic plate ; (2) the variation of this relation—and therefore of the so-called " sensitivity "—with wave-length. These factors are well known to all workers in this field, but for the sake of clarity in subsequent discussion it would seem desirable to present them in a little more detail.

Blackening-Intensity Relations.—By blackening (B), or optical density of the photographic image, we mean $\log_{10} (i_0/i)$, where i is the light transmitted through the image, corresponding to i_0 incident upon it. In fig. 2 we have constructed the characteristic curves for four different wave-lengths deduced,
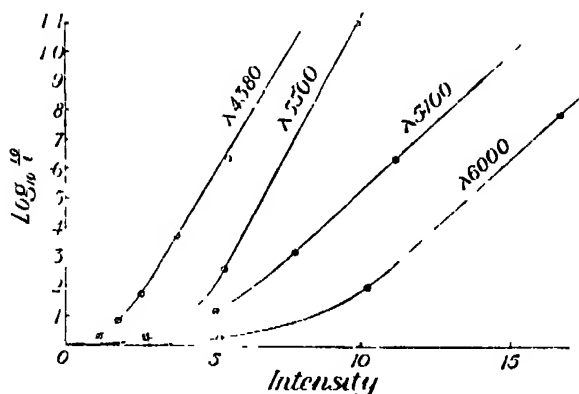
Fig. 2 —Characteristic Blackening-Intensity values

of course, from the same plate. A notable feature of each curve is that the approach to the origin is for a considerable distance almost parallel to the I-axis. This is especially pronounced at the less refrangible end. There are three practical consequences of this. Firstly, eye-estimates of spectrograms, which take cognisance of *blackening* only, and merely infer intensity, will in this region considerably under-estimate the intensity values, indeed many lines of considerable strength will not be observed at all. Secondly, the effect of a very slight chemical fog of varying amount in different parts of the plate will give rise to considerable error, and thirdly, eye estimates of bands or lines superposed on other band structure, or continuous spectrum, will also be in error. This latter effect is particularly applicable to band sequences where all heads succeeding the first one are superposed on the fine structure of preceding bands. The method of allowing for this in microphotometric work is explained by fig. 3. In each case the optical density of the structure work immediately preceding a head was measured, and from this the corresponding intensity was determined ; the difference between this and the intensity of the succeeding

head was taken as the true intensity of the latter. Where the peak value was not located at the head, the microphotometer curve of the preceding structure work was extrapolated to deduce the intensity value directly under the peak. This procedure is not the same as taking the difference of the optical densities of the peak and the background and reading the equivalent
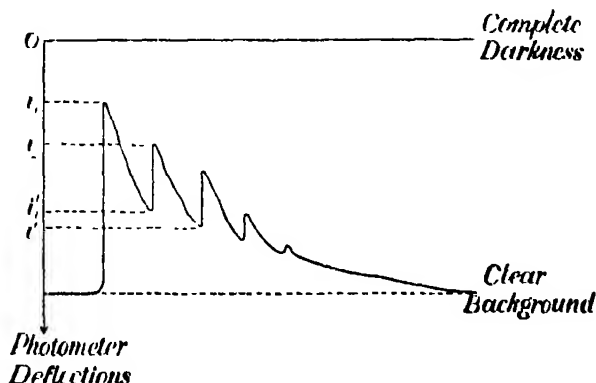
FIG. 3.

value from the characteristic curve. It can be shown that these procedures are identical only over the linear part of the curve. Thus let $I = f(B)$, say, and let I_1 and I_2 be intensities corresponding to two successive peaks, and I_1' the intensity produced by the structure work of the first band on which the second head is superposed. Then

$$I_1 = f(B_1) = f\left(\log_{10} \frac{i_0}{i_1}\right),$$

$$I_1' = f(B_1') = f\left(\log_{10} \frac{i_0}{i_1'}\right),$$

$$I_2 = f(B_2) = f\left(\log_{10} \frac{i_0}{i_2}\right).$$

We have

$$I_2 - I_1' = f\left(\log_{10} \frac{i_0}{i_2}\right) - f\left(\log_{10} \frac{i_0}{i_1'}\right).$$

If $f(B) = kB$ then this is equal to

$$f\left(\log_{10} \frac{i_1'}{i_2}\right) = f(B_2 - B_1').$$

We have seen that the flatness of the characteristic curve in its approach to the origin is liable to be a source of error in intensity determination. It is

therefore suggested that in all microphotometric work preliminary experiments should be made to determine the degree of fogging necessary to bring the plate into a condition represented by the linear part of the characteristic curve, and that such fogging should precede exposure to the spectrum.

Another point of practical importance follows from the departure from linearity in the region of large density values. Such curves as those of fig 2 above a density of 1·2–1·5 begin to flatten out and ultimately approach a constant value of B. One would expect this, in that complete photochemical change of the emulsion obviously provides a maximum limit to the blackening. As a result of this, eye estimates of the intensities of strong bands will tend to be too low.

Plate Sensitivity Variation.—It is easy to construct curves which show how the light intensity, in arbitrary units, required to produce a given optical density varies with wave-length. The curves show that there is a pronounced peak of relatively poor sensitivity in the green region, also that above λ 5700 in the yellow region, the sensitivity gradually falls off This variation is, of course, not considered in eye estimates.

5. *Discussion of the Neutral Wedge Method.*

The neutral wedge method of Merton and Nicholson has the merit of extreme simplicity in principle The characteristic curves of the plate and the use of a microphotometer are not involved. It is, however, necessary to give the plates special treatment after development in order to define more clearly the end points of the lines or bands photographed This may be done by making successive contact prints on other plates till the required degree of contrast is obtained, or by careful " cutting " of the plate with potassium ferricyanide solution. This process removes a certain optical density from the background and from the line contour, but as the wedge spectrum of the standard lamp receives the same treatment it can be shown* that within reasonable limits no appreciable error should arise. To " cut " a wedge spectrum to the necessary extent it is in practice necessary to give a time of exposure many times as great as that which would be required for an ordinary spectrogram. A further slight disadvantage is the increase in length at the base of each line due to halation or irradiation. This has to be allowed for in measuring the lengths of the lines and with some experience it can usually be done fairly accurately. A point arising out of the wedge method seems to have escaped

---

* ' Phil. Mag ,' vol. 2, p. 596 (1926)

notice hitherto and will be explained in reference to fig. 4. The clear glass wedge is for convenience omitted and only the neutral glass wedge is represented. It is of length L and angle α. A line of intensity I is reduced by the thickness x of absorbing material to the small critical value I_e which will just produce appreciable blackening of the plate. The corresponding line of height h on the plate corresponds to a length h/m of the neutral wedge if m is the magnification of the lens system of the spectrograph. If we assume the absorption at the thin end is not zero, but a definite small quantity, then the "ideal" wedge may be regarded as of length L + l, say.
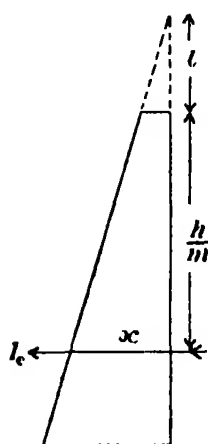
We then have

$$I_e = I e^{-kx} = I e^{-k \left(l + \frac{h}{m} \right) \tan \alpha}$$

Fig. 4.   therefore

$$0.434 \, k \, \tan \alpha \left(l + \frac{h}{m} \right) = \log_{10} \frac{I}{I_e}.$$

If D_λ is the optical density of the thick end of the wedge

$$0.434 \, k \, (\text{L} + l) \tan \alpha = D_\lambda$$

or

$$0.434 \, k \tan \alpha = d_\lambda,$$

where d_λ is the optical density gradient of the wedge. Hence

$$\log_{10} \left(\frac{I}{I_e} \right) = d_\lambda \left(l + \frac{h}{m} \right)$$

or

$$I = I_e \, 10^{l d_\lambda} . \text{antilog} \left(\frac{d_\lambda h}{m} \right).$$

Now d_λ is a function of wave-length, and thus if the value of l can be determined it should be possible to assess the variable factor $10^{l d_\lambda}$. In practice the factor $I_e \, 10^{l d_\lambda}$ should cause no difficulty in that it will be the same for both the band system under investigation and the standard lamp spectrum. As the *ratio* of these is involved in calculating the true intensities of the bands the factor is eliminated.

We have attempted to use the wedge method for the Swan system as produced in the five sources mentioned, but we do not use these data in this paper, being disposed to place greater confidence in those obtained by use of the microphotometer.

6. *Potential Energy Functions of the* C_2 *Molecule—Transition Probabilities.*

In the papers by Condon to which reference has been made, it has been shown that if we write the nuclear potential energy as a power series

$$U(r) = u_2 (r - r_0)^2 + u_3 (r - r_0)^3 + u_4 (r - r_0)^4 + \dots$$

the coefficients u_2, u_3, u_4, etc, may be evaluated for both initial and final electronic states from the constants of vibrational and fine structure analysis. Shea* has derived these coefficients from the known data of the Swan system. In a paper by Morse† a function is suggested which expresses the nuclear potential energy remarkably well over a wide range :

$$U(r) = A + D\,e^{-2a(r-r_0)} - 2D\,e^{-a(r-r_0)}.$$

Here D is the energy of dissociation and is given approximately by $(\omega_e^2/4\omega_e x)$. A is a constant and $a = 0\cdot2454 \sqrt{\mu \omega_e x}$, μ being the reduced mass of the molecule. The Swan band origins are given by

$$\nu = 19300\cdot18 + [1792\cdot77\,(v' + \tfrac{1}{2}) - 19\cdot35\,(v' + \tfrac{1}{2})^2]$$
$$- [1641\cdot55\,(v'' + \tfrac{1}{2}) - 11\cdot67\,(v'' + \tfrac{1}{2})^2],$$

from which we have derived the constants of the Morse formula for both electronic states.

$$A' = 61717 \quad D' = 41525 \quad a' = 2\cdot643 \quad (r_0' = 1\cdot265)$$
$$A'' = 58545 \quad D'' = 57727 \quad a'' = 2\cdot053 \quad (r_0'' = 1\cdot311)$$

The functions are plotted to scale in fig 5, and the vibrational energy levels are marked. By Condon's graphical method we have derived the parabola which represents maximum probability of transition. This is superposed in its correct position upon the data of figs. 6 to 10 which give the transition probabilities derived from experiment. It should be remembered that the graphical derivation of the parabola is sensitive to small changes in the constants of the formula, and, making reasonable allowance for this, the agreement may be considered satisfactory.

* ' Phys. Rev.,' vol. 30, p. 825 (1927).
† ' Phys. Rev.,' vol. 34, p. 57 (1929).

7. *Experimental Data.*

In Tables I to V the experimental data of intensities are given. These are on a relatively correct scale taking the $(\frac{1}{2}, \frac{1}{2})$ band as 100. Now the intensity of a transition is proportional to ν^4 (where ν is the resulting frequency), to the

Fig. 5.—Scale diagram U (r); r for the initial and final states of the Swan system.

number of molecules in the initial state, and to the probability of transition. Each intensity has therefore been divided by a number proportional to ν^4 (the wave-numbers of the band origins were taken),* and these values are given in the tables below the intensities. The sum of such values of (I/ν^4) for each v'' progression is placed adjacent to the corresponding value of v' and is

* 'Phil. Trans.,' vol. 226, p. 180 (1927).

Fig. 6.—Transition probabilities   Swan bands—Bunsen flame.

Table I.—Values of I and I/ν^4.   Cone of Bunsen Flame.

Weight.	v' / v''	0	1.	2	3	4.	5	6.	7.
130 4	0	100	29 4	20 4					
		71	29 5	29 9					
73 2	1	31 9	31 0	17 2	13 6				
		16 0	21 4	16 7	19 1				
30 8	2	1 9	20 7	3 0	10 4	6 0			
		0 7	10 2	2 0	9 8	8 1			
27 9	3		3 4	18 5	0 6	8 0	7 7		
			1 2	9 0	0·4	7 3	10 0		
15 3	4			4 0	11 9		2 4	4 8	
				1 4	5 7		2 2	6 0	
7 7	5					6 5*		1 5	2 7
						3 1		1 3	3 3
1 7	6						2 5*		0·6
							1 2		0·5

* Values calculated by extrapolation.   The *sum* was observed experimentally.
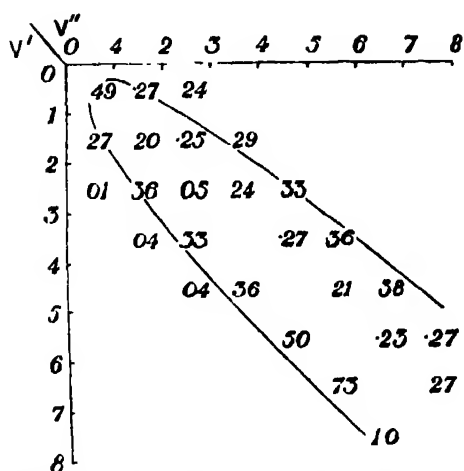
Fig. 7.—Transition probabilities.   Swan bands—Oxy-coal gas flame.

Table II.—Values of I and (I/v^4).   Cone of Oxy-Coal Gas Flame.

Weight.	v'' / v'	0.	1.	2	3	4.	5.	6.	7
145 2	0	100 71 0	38 5 38·7	24 2 35·5					
85 6	1	45 6 22 9	24 8 17·1	21·7 21·1	17 5 24·5				
47 3	2	1 9 0 7	34·9 17 2	3 7 2 5	12 3 11·6	11·4 15 3			
34 6	3		4 1 1 5	23 6 11 4		10·1 9·2	9·6 12·5		
19 9	4			2 3 0 8	15·1 7 2		4 7 4 2	6·1 7·7	
9 0	5					9·5* 4 5		2·4 2·1	2·0 2·4
3·5	6						5·5* 2·6		1 1 0·9
1·3	7							2·8* 1·3	

* Values calculated by extrapolation.   The *sum* was observed experimentally.

FIG. 8.—Transition probabilities.   Swan bands—Carbon arc in H₂.

Table III.—Values of I and I/v⁴.   Carbon Arc in Hydrogen.

Weight.	v'' / v'	0.	1	2.	3	4	5	6.
115 7	0	100 71·0	25 3 25 4	13 2 19 3				
81 3	1	33·3 16 7	28 4 19 6	15 6 15 1	21·3 29 9			
50 5	2	4 1 1 5	30 2 14 9	4 9 3 3	10 1 9 5	15 8 21·3		
30 4	3		6 4 2 3	25 5 12 4		8 1 7 4	6·4 8 3	
15·9	4			10·3 3 7	16 7 8 0		3 3 2 9	1 0 1·3
5·7	5					10 0* 4 7		1 1 1 0
2 4	6						5* 2 4	
0·5	7							1* 0 5

* Values calculated by extrapolation.   The *sum* was observed experimentally.
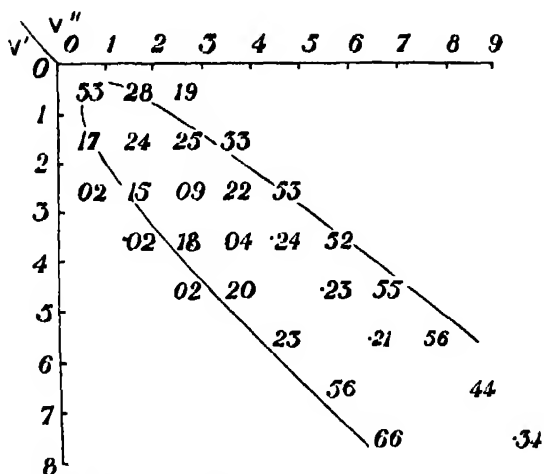
Fig. 9.—Transition probabilities.   Swan bands—Argon tube.

Table IV.—Values of I and (I/v⁴)   Argon Tube.

Weight	v'' / v'	0	1.	2	3	4	5.	6	7	8
133 4	0	100	36 6	17 5						
		71 0	36 8	25 6						
1.36 8	1	47·4	47 8	35 7	32·3					
		23 8	33·0	34 7	45·3					
137 0	2	6 7	41 3	17 6	31·6	54 0				
		2 5	20 3	11·8	29·7	72 7				
101 8	3		5 6	37 4	5 9	27 3	40·7			
			2 0	18 1	3·9	25 0	52 8			
79·6	4			3 5	32 9		20 8	35 0		
				1 3	15 8		18 5	44·0		
55 6	5					26 5*		13 6	25·5	
						12 6		11·9	31 1	
17 8	6						21·5*		9*	
							10 1		7 7	
10 0	7							14*		4*
								6·6		3·4

* Values calculated by extrapolation.   The *sum* was observed experimentally.
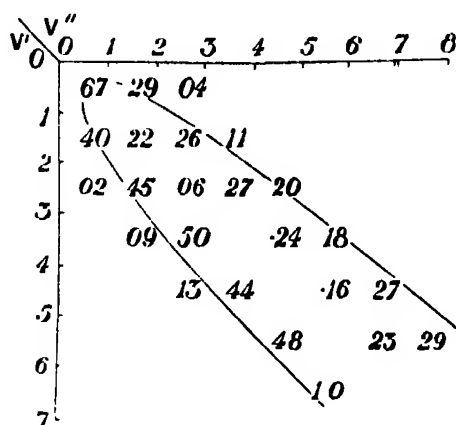
Fig. 10.—Transition probabilities.   Spark under Glycerine.

Table V.—Values of I and $(1/v^4)$ Condensed Spark in Glycerine.

Weight	v'' / v'	0	1	2	3	4	5.	6	7.
	0	100	29 9	3*					
105 5		71 0	30 1	4 4					
	1	63 2	25 5	20 6	6 4				
78 3		31 7	17 6	20 0	9 0				
	2	3 3	43 2	4 6	13 6	7 0			
47 8		1 2	21 3	3 1	12 8	9 4			
	3		8 0	34 4		8 8	4 7		
33 7			2 9	16 7		8 0	6 1		
	4			8 6	22 3		4 4	5 3	
24 4				3 1	10 7		3 9	6 7	
	5					15*		3 8	3 5
14;7						7 1		3 3	4 3
	6						7*		
3 3							3·3		

* Values calculated by extrapolation.   The *sum* was observed experimentally.

proportional to the number of molecules in the initial state (v'), or, as we may say briefly, to the weight of this state. By taking the quotient of the (I/v^4) value of a band and the weight of the initial state we have a number proportional to the transition probability. These probabilities are given in figs. 6 to 10. In view of all the inherent difficulties of spectro-photometry the data of Tables I to V may be in considerable error, perhaps within limits of 25 per cent., but this represents a considerable advance upon the available data based on eye-estimates which may be in error by several hundred per cent. In the absence of several repetitions of the same work one therefore hesitates to draw conclusions, but tentatively it may be suggested that experimental conditions of excitation seem to have an influence on the distribution of probability. We note, for example, the unusually strong probabilities in the $\frac{1}{2}$, $2\frac{1}{2}$ sequence in the argon tube, and in the $1\frac{1}{2}$, $\frac{1}{2}$ sequence in the spark under glycerine.

8. *The Vibrational Energy Distribution. Effective Temperatures.*

The first column of Tables I to V gives on an arbitrary scale the numbers of molecules in the various initial vibrational states. *Assuming* that it is a distribution in thermal equilibrium at temperature T we should expect $N_{v'} = N_0 e^{-(E^{v}/KT)}$, so that

$$hc \left[\omega'_e (v' + \tfrac{1}{2}) - \omega'_e x'_e (v' + \tfrac{1}{2})^2 \right] = KT \log_e \frac{N_0}{N_{v'+\frac{1}{2}}},$$

and here

$$1792 \cdot 77 \, (v' + \tfrac{1}{2}) - 19 \cdot 35 \, (v' + \tfrac{1}{2})^2 = 1 \cdot 6083 \, T \log_{10} \frac{N_0}{N_{v+\frac{1}{2}}}.$$

By plotting vibrational energy against $\log (N_0/N_{v'+\frac{1}{2}})$ we obtain the absolute temperature directly. We have thus derived the following temperatures : Bunsen flame 4700°, oxy-coal gas flame 4700°, carbon arc in hydrogen 5000°, and spark in glycerine 6100°. These clearly bear no relation to the true temperature of the source and are evidence that there is no statistical equilibrium of the excited molecules with their surroundings under any of the exciting conditions. This may be connected with the fact that the C_2 molecule is produced in every case by the breakdown of another more complex molecule— probably in every case a hydrocarbon molecule—and the energy changes of these processes are quite obscure. When these processes are known precisely the above effective temperatures may prove to be a consequence of the energy equations of the dissociative processes. The vibrational distribution in Table IV is of an unusual character, and, if genuine, it would seem that it cannot be

explained on the classical statistics.   In this field of work, however, a great deal of experimental data on other band systems is desirable before definite conclusions can be drawn.

We should like, in conclusion, to thank Professor A. Fowler for permission to use the microphotometer of the Imperial College, and also Mr. Simmonds for help and advice in this connection.

Summary.

(1) The sources of error arising in photographic spectro-photometry over wide spectral ranges are summarised, and it is generally shown to be desirable to fog the plate on to the linear part of the characteristic curve.

(2) The neutral wedge method is discussed   The effect of appreciable absorption at the thin end of the wedge is shown to be eliminated by the usual procedure.

(3) Peak intensities of the Swan system have been measured from calibrated photographs of the spectrum produced under five different conditions of excitation.

(4) The vibrational transition probabilities are derived from these data and compared with the Condon " parabola " of maximum probability.   The latter was derived by use of Morse's formula.

(5) Study of the experimental data of the populations of the various initial vibrational states has shown that under none of the conditions studied is thermal equilibrium approached.   Certain " effective " temperatures are derived and discussed.

The Motion of a Point-Charge as the Shortest Path in a Moving Medium.*

By H. F. Biggs, Demonstrator in Physics, Oxford University.

(Communicated by E A. Milne, F.R.S.—Received May 3, 1932.)

§ 1. *The Fermat Principle in a Moving Medium, and its Application to Electrodynamics.*

The motion of a charge in an electromagnetic field can be described by a rather suggestive model. Put roughly, the world-line for a particle of charge e and mass m may be described as a four-dimensional " shortest path " relative to a medium whose velocity (varying from point to point) is $-\dfrac{e}{mc^2} \mathbf{A}$, where $\mathbf{A}$ is the four-dimensional electromagnetic potential, whose components are a_x, a_y, a_z, $i\phi$; (a_x, a_y, a_z) being the three-dimensional vector potential and ϕ the scalar potential.

The analogy with a " ray of sound " may make the meaning clearer; in a wind that varies from point to point, sound actually travels from one fixed point to another by the path of shortest time. Some details of the analogy are :—

Path of sound.	Path of charged particle.
Ordinary time, t	Proper time, or interval, s
Constant velocity of sound.	Constant four-dimensional " velocity " of particle, of magnitude i and components dx/ds, dy/ds, dz/ds, $icdt/ds$, where $ds^2 = - dx^2 - dy^2 - dz^2 + c^2dt^2$.
Co-ordinates of sound-pulse, x, y, z.	Co-ordinates of particle, x, y, z, ict.

Let us first imagine an n-dimensional ($n = 3$ or 4 in our applications) euclidean space with an independent time τ and suppose, filling this space, a

---

medium with velocity $\mathbf{V}$; that is to say, if a particle of the medium has co-ordinates x_λ relative to some fixed axes, $\partial x_\lambda / \partial \tau = V_\lambda$. Suppose now that something identifiable, which we shall call a disturbance, travels through the medium with a constant velocity c relative to the medium (in the case of sound of course c is the ordinary velocity of sound, in the electromagnetic case, as hitherto, the fundamental velocity). Then in a time $d\tau$, if the disturbance has travelled from $(x_1, x_2, \ldots)$ to $(x_1 + dx_1, x_2 + dx_2, \ldots)$ or, as we shall write it, from (x_λ) to $(x_\lambda + dx_\lambda)$, the displacement relative to the medium will be $(d\xi_\lambda) = (dx_\lambda - V_\lambda d\tau)$.

But we may now put $d\tau = ds/c$ where ds is the displacement *relative to the medium*, such that $ds^2 = \sum_\lambda d\xi_\lambda^2$, and we have then

$$d\xi_\lambda = dx_\lambda - \frac{V_\lambda}{c} ds = dx_\lambda - v_\lambda ds,$$

where $\mathbf{v} = (v_\lambda) = \mathbf{V}/c$ is the ratio of the velocity of the medium to that of the disturbance, or the value of the velocity of the medium when the unit of τ is so chosen that $c = 1$.

We have therefore

$$ds^2 = \sum_\lambda (dx_\lambda - v_\lambda ds)^2. \tag{1}$$

Now let us develop the equation for the shortest path relative to the medium, which by Fermat's principle gives the actual path in the case of sound, namely

$$\delta \int ds = 0 \quad \text{or} \quad \int \delta ds = 0,$$

the end-points of the integral being taken as fixed. Equation (1) then gives

$$2ds\, \delta\, ds = \tfrac{1}{2} \delta \sum (dx_\lambda - v_\lambda\, ds)^2$$

$$\delta\, ds = \tfrac{1}{2} \delta \sum \left(\frac{dx_\lambda}{ds} - v_\lambda \right)^2 ds,$$

so that

$$\tfrac{1}{2} \int \delta \sum \left(\frac{dx_\lambda}{ds} - v_\lambda \right)^2 ds = 0.$$

Developing this in the usual way (as for instance in Eddington, "The Mathematical Theory of Relativity," p. 60) we find

$$\int \delta \left(\frac{dx_\lambda}{ds} \right) \left(\frac{dx_\lambda}{ds} - v_\lambda \right) ds - \int \delta v_\lambda \left(\frac{dx_\lambda}{ds} - v_\lambda \right) ds = 0, \tag{2}$$

where we omit the Σ by the usual summation convention.

But for the first integral we have

$$\int \delta\left(\frac{dx_\lambda}{ds}\right)\left(\frac{dx_\lambda}{ds} - v_\lambda\right) ds = \int \frac{d}{ds}\, \delta x_\lambda \left(\frac{dx_\lambda}{ds} - v_\lambda\right) ds,$$

which becomes on integrating by parts, since $\delta x_\lambda = 0$ at the limits,

$$-\int \delta x_\lambda \frac{d}{ds}\left(\frac{dx_\lambda}{ds} - v_\lambda\right) ds. \tag{3}$$

In evaluating the second integral of (2) we have

$$\delta v_\lambda = \delta x_\mu \frac{\partial v_\lambda}{\partial x_\mu},$$

so that the term gives

$$-\int \delta x_\mu \frac{\partial v_\lambda}{\partial x_\mu}\left(\frac{dx_\lambda}{ds} - v_\lambda\right) ds,$$

which becomes on interchanging dummy suffixes λ and μ

$$-\int \delta x_\lambda \frac{\partial v_\mu}{\partial x_\lambda}\left(\frac{dx_\mu}{ds} - v_\mu\right) ds. \tag{4}$$

Adding (3) and (4), we then have

$$\int \delta x_\lambda \left[\frac{d^2x_\lambda}{ds^2} - \frac{dv_\lambda}{ds} + \frac{\partial v_\mu}{\partial x_\lambda}\left(\frac{dx_\mu}{ds} - v_\mu\right)\right] ds = 0,$$

whence we deduce, since the δx_λ are arbitrary,

$$\frac{d^2x_\lambda}{ds^2} = \frac{dv_\lambda}{ds} - \frac{\partial v_\mu}{\partial x_\lambda}\left(\frac{dx_\mu}{ds} - v_\mu\right)$$

$$= \frac{\partial v_\lambda}{\partial x_\mu}\frac{dx_\mu}{ds} - \frac{\partial v_\mu}{\partial x_\lambda}\left(\frac{dx_\mu}{ds} - v_\mu\right)$$

$$= \left(\frac{\partial v_\lambda}{\partial x_\mu} - \frac{\partial v_\mu}{\partial x_\lambda}\right)\frac{dx_\mu}{ds} + v_\mu \frac{\partial v_\mu}{\partial x_\lambda}. \tag{5}$$

But, going back to electrodynamics, we may write for the four-dimensional force-vector **K** acting on a point-charge e, in our present notation,

$$K_\lambda = e\frac{u_\mu}{c} F_{\lambda\mu}, \tag{6}$$

where $K_{1,\,2,\,3}$ is the ordinary force, $F_{23,\,31,\,12} = H$ and $F_{14,\,24,\,34} = -iE$, and the first three components of **u** give the velocity of the charge in the ordinary sense.

We now replace K_λ and u_μ by the true (special) relativity vector components. Since

$$K_\lambda = m \frac{d^2 x_\lambda}{dt^2}, \qquad (\lambda = 1, 2, 3), \qquad (7)$$

approximately, we write

$$K_\lambda = c^2 m_0 \frac{d^2 x_\lambda}{J^2}, \qquad (\lambda = 1, 2, 3, 4), \qquad (8)$$

where m_0 is the resting mass.

Also

$$\frac{u_\mu}{c} = \frac{dx_\mu}{ds}, \qquad (9)$$

while

$$F_{\lambda\mu} = \frac{\partial A_\mu}{\partial x_\lambda} - \frac{\partial A_\lambda}{\partial x_i}. \qquad (10)$$

Substituting, therefore, from (8), (9) and (10) in (6), we find for the four-dimensional equation of motion of a point-charge

$$\frac{d^2 x_\lambda}{ds^2} = -\frac{e}{m_0 c^2} \frac{dx_\mu}{ds} \left(\frac{\partial A_\lambda}{\partial x_\mu} - \frac{\partial A_\mu}{\partial x_\lambda} \right). \qquad (11)$$

This is equivalent to the *terms of the first order in* v_μ in (5) if we put[*]

$$v_\lambda = -\frac{e}{m_0 c^2} A_\lambda. \qquad (12)$$

To verify that equation (8) is the correct form according to the classical relativity theory, and that we are justified in generalising from (7) to (8), we consider the electrostatic case where the only component of A is $A_4 = \imath\phi$. We then have, putting $\lambda = 1$ and $\mu = 4$ only, for $\dot{x} \to 0$

$$\frac{d^2 x}{c^2 dt^2 (1 - \beta^2)} = -\frac{e}{m_0 c^2} \frac{\imath c\, dt}{c\, dt \sqrt{1 - \beta^2}} \left(-\imath \frac{\partial\phi}{\partial x} \right),$$

where

$$\beta^2 = (dx^2 + dy^2 + dz^2)/c^2 dt^2$$

or

$$\frac{m_0}{\sqrt{1 - \beta^2}} \frac{d^2 x}{dt^2} = eE_x,$$

thus checking with the well-known relativity expression for the transverse mass,

$$m =$$

---

[*] It should be noticed here that the "medium" moves like a four-dimensional incompressible liquid, since the four-dimensional divergence of A, and therefore of v, is zero.

The analogy expounded above is perhaps only a curiosity. Certainly there can be nothing very like an absolute velocity representing the vector A, since electrons and protons react to a given A not only to vastly different extents but in opposite directions.

We must here make clear exactly what is supposed given, and what is determined by the minimum principle in the two cases. For sound we suppose the end-points given only in space ; the minimum principle then determines the trajectory of the waves, including, of course, the initial direction, and when this is found, the length of the trajectory gives to a first approximation the time taken by the sound. In the electromagnetic case, the end-points are given in *space and time* The trajectory is then given by the minimum principle, both as to space and time, *i e.*, the four co-ordinates are given as functions of a single variable* s, the proper time, or the interval *measured along the trajectory* ; the initial four-dimensional direction gives the initial velocity in the ordinary sense ; and finally we get the proper time along the whole path, $\int_A^B ds$, analogous to the time in the sound case. This interval, or proper time, between the end-points is not, of course, equal to the interval in the usual sense given by $s^2 = c^2 t^2 - AB^2$, except in the case of a straight trajectory, *i e*, for zero field, for a neutral particle or a particle of infinite mass. It is, in fact, proportional to the *action*, and this whole treatment has points of resemblance with Schrodinger's† paper on the Hamiltonian principle of minimum action.

The analogy to the fixing of the initial *direction* of the sound-path is the fixing not only of the spatial direction but also of the magnitude of the particle's velocity. For instance, if A and B are two points in a plane S normal to a given uniform magnetic field H, an electron may be made to travel from A to B in any given time-interval t, the velocity and direction of aim being completely determined. The path is a circle in the plane S, whose centre is the point where AB subtends the angle $\omega t = \dfrac{eHt}{mc}$. This determines geometrically the initial direction, and also the radius r, which in turn determines the velocity $r\omega$

---

* Since, as we see in the next section, we must take the absolute magnitude of the four-dimensional velocity to be unaltered by the field, an element of four-dimensional trajectory will have the same value as the corresponding ds, the displacement relative to the medium as dealt with above. It does not seem worth while, therefore, to use a different symbol such as ds' for the element of trajectory, though the meaning of ds is here rather different from what it was before.

† 'Ann. Physik,' vol. 79, p. 361 (1926).

§ 2. *Discussion of the Term of the Second Order in the Velocity of the Medium in* (5).

The last term in (5) for the case of sound seems to have no counterpart in the electrical case. This term may be written as grad $v^2/2$ and is the acceleration of the air in the case of steady flow. In the electrical case it would give a term in the ordinary acceleration equal to $-\frac{1}{2}e^2 \operatorname{grad}(\phi^2)/(m^2c^2)$ cm./sec.^{2} since $v_4 = e/(mc^2) i\phi$, but it would seem to be too materialistic a view of the medium to suppose that it had an acceleration which it imparted to the particle. Besides, the value of this term depends on the zero of potential, which hitherto has been considered as placed at infinity only by arbitrary choice. Moreover, the effect of this term could hardly have escaped notice since in actual experiments on electronic deflection it is of the same order as the relativity correction. It is true that determinations of e/m for the electron shows a discrepancy,[*] Wolf's[†] accurate deflection method giving a value half a per cent. *higher* than the spectroscopic method. But Wolf's observation chamber was earthed, so that if the earth is at zero potential, the effect of the term in question would have been an increased velocity and therefore too *small* a value for e/m when the velocity is calculated in the usual way. Thus the term is of the wrong sign to account for the discrepancy. The effect of the extra term on the determination of e/m from the comparison of the Rydberg constants of H and He$^+$ cancels out in the working, and the effect on the Zeeman shift would obviously be zero.

If then we regard (11), or (5) without the last term, as the true equation, the acceleration will always be normal to the velocity, since we have for the scalar product

$$\frac{dx_\lambda}{ds}\frac{d^2x_\lambda}{ds^2} = \left(\frac{\partial v_\lambda}{\partial x_\mu} - \frac{\partial v_\mu}{\partial x_\lambda} \right)\frac{dx_\lambda}{ds}\frac{dx_\mu}{ds},$$

which will vanish identically. Thus the velocity will still be of constant magnitude and the field can change only its direction.

§ 3. *Simple Deduction of Curvature of Path for Two-dimensional Motion.*

The first-order terms of (5) which are perhaps the only true terms in the electrical case, and give a very close approximation in the case of sound, may be given a very easy geometrical interpretation, which we shall follow out for

[*] R. T. Birge, ' Phys. Rev.,' vol. 33, p. 265 (1929).
[†] ' Ann. Physik,' vol. 83, p. 884 (1927).

the simplest case of a sound-wave. Suppose there is a wind blowing horizontally in a fixed direction, but with constant velocity-gradient upwards. Let sound be travelling directly down the wind and therefore in a vertical plane. Then if the x and y axes are taken tangential and normal to the path at any point P, the curvature of the path is by (5) given by the single term

$$\frac{d^2y}{ds^2} = \left(\frac{\partial v_y}{\partial x} - \frac{\partial v_x}{\partial y}\right)\frac{dx}{ds},$$

omitting the second order terms in (5) as negligible, by hypothesis, or, since $ds = dx$

$$-\frac{1}{\rho} = \frac{d^2y}{dx^2} = \frac{\partial v_y}{\partial x} - \frac{\partial v_x}{\partial y} = |\text{curl } \mathbf{v}| = -\frac{dv_X}{dY} = \text{const.}, \tag{13}$$

where X and Y are horizontal and vertical directions.

The quasi-geometrical reason for this is as follows If an arc of length s and curvature $1/\rho$ is given a constant displacement dn normal to itself along almost its whole length, while its ends are kept fixed, the increase of length is $s\,dn/\rho$ (as familiar in the theory of the bent beam) or

$$\int ds = \delta\mathrm{A}/\rho, \tag{14}$$

where δA is the area swept out. But when s is the actual path, this excess of length is balanced by the greater drift down the wind along the displaced path. For the increase of drift will be $\int_A^B \mathbf{v}\,.\,\mathbf{ds}' - \int_A^B \mathbf{v}\,.\,\mathbf{ds}$ or $\oint \mathbf{v}\,.\,\mathbf{ds}$ round the area, or, by Stokes's theorem

$$|\text{curl } \mathbf{v}|\,\delta\mathrm{A}. \tag{15}$$

Remembering that the units have been appropriately chosen, we may equate (14) and (15), thus finding (13).

§ 4. *Larmor Precession and Spin Energy.*

In the case considered (curl $\mathbf{v}$ = const.), the path of sound is a circle, in close analogy with the circular path of a charge travelling in a plane normal to a uniform magnetic field. The angular velocity of the sound-pulse or the charge respectively in its circular path is equal to the curl of the velocity of the medium, or *twice* the local angular velocity of the medium itself. Thus in ordinary units, electrodynamics gives for the angular velocity ω of the charge

$$\frac{e\mathbf{u} \times \mathbf{H}}{} = m\omega^2 r \text{ in magnitude,}$$

where u is the velocity of the charge in centimetres per second, or

$$\frac{e\mathbf{u} \times \mathbf{H}}{c} = -\, m\mathbf{u} \times \boldsymbol{\omega},$$

therefore

$$\boldsymbol{\omega} = -\frac{e}{mc}\,\mathbf{H} = -\frac{e}{mc}\,\text{curl A},$$

$$= c\,\text{curl v}$$

where v is the velocity of the medium given by (12).

Half of this, or

$$o = -\frac{e}{2mc}\,\mathbf{H},$$

is the angular velocity of the Larmor precession, and we then have

$$o = \tfrac{1}{2}c\,\text{curl v},$$

where the right-hand side is, by elementary hydrodynamics, the *local angular velocity of the medium* The factor c only appears because o and v are referred to different units of time. Thus the plane of a precessing orbit is, as it were, carried round by the medium.

Again, the energy of a spinning electron or proton when oriented parallel or antiparallel to a field H, has its counterpart in the model. For the magnetic moment is

$$\mu = \frac{h}{2\pi}\frac{e}{2mc},$$

where m is the mass of the electron or the proton, so that the energy in the field is

$$\pm\,\mu H = \frac{h}{2\pi}\frac{e}{2mc}\,H = \frac{ho}{2\pi} = h\nu,$$

where ν is the frequency of rotation of the medium corresponding to the local angular velocity o. It must, of course, be borne in mind that the velocity and angular velocity of the medium depend on the mass of the particle we are considering.

The accelerated motion of a charge down an electric field can, of course, also be considered as a path in which the " direction of motion " is changing at a uniform rate ; for if we regard a uniform ordinary velocity as an angular *displacement* of the four-dimensional velocity from the time-axis, a uniform acceleration will give a constant angular *velocity*, in the same sense, but since these components of angular velocity are imaginary (mathematically), there

are no corresponding frequencies, and therefore no energy of orientation in the *electric* field. It is therefore not necessary to suppose, as had been suggested from considerations of relativity symmetry,[*] that an electron possesses an electric moment as well as a magnetic moment.

§ 5. *Connection with the de Broglie Waves.*

The analogy we have traced, of course, suggests that the physical basis for the principle of the minimum path may be the same in the two cases, and therefore invites us to connect the path of a charge with wave-mechanics. First we must get clearer what is the exact analogy with the velocity of the sound-waves. Though the treatment at first sight seems to imply that the fundamental four-dimensional velocity is that of the waves at whose point of reinforcement the particle exists, a more consistent picture is got by imagining that the " waves " are stationary in the field-free case (not standing waves in the usual sense, but a configuration fixed in space-time), and that any particle or any point of three-dimensional space of necessity moves through this world across the wave-grid with the fundamental velocity Thus the de Broglie frequency $\nu = m_0 c^2/h$ for a stationary particle m_0 is regarded as the frequency with which a point, stationary in space, but necessarily " moving through time " with the same velocity as the particle, crosses the " lines " (really three-dimensional continua) of the grid. If we have a system of space-axes (x', y', z') relative to which the particle is moving slowly in the ordinary sense, *i.e.*, a space-time system in which the world-line of the particle is inclined at a small angle to the time-axis, the wave-grid is still normal to the world-line of the particle, and hence the space $x'y'z'$ in which the particle lies, *i.e.*, the plane space $t'(p) = t'$(particle), crosses the grid at a small angle, and, moving across it with the same fundamental velocity in a slightly different direction, cuts any given crest of the grid in a *two*-dimensional locus which has a *great* velocity inversely proportional to the angle of intersection and therefore to the velocity of the particle. That is, the phase velocity is $u = c^2/v$ in ordinary units. To treat this velocity u as a true velocity of propagation is to follow a false analogy ; it is more closely analogous to the great velocity with which a wave-crest on water is seen to run along a wall inclined at a small angle to the wave-front. The fact of having an apparent velocity greater than that of light therefore does not seem to be a valid objection to the reality of the waves.

* Frenkel, ' Z. Physik,' vol. 37, p. 243 (1926) ; vol. 47, p. 786 (1928).

The tracing out of the path of a particle by Fermat's principle may now be described as follows. First, in a force-free region, the particle must travel through space-time with velocity of constant absolute magnitude. The *direction* of this velocity is what is determined by the Fermat principle.

Given the direction at any moment, we construct the stationary wave-grid, ruling parallel, three-dimensional spaces at the interval

$$\Delta s = c \Delta t = \frac{c}{\nu} = c \frac{h}{m_0 c^2} = \frac{h}{m_0 c} \text{ cm.}$$

(the interval is always time-like, though its unit is here the centimetre or light-centimetre). Having got this grid, we vary the conditions slightly by varying the initial direction of motion and varying the grid at the same time, keeping it always normal to the varied direction. The locus of reinforcement of the grid will then be the normal trajectory of the original grid, which in the force-free case is the straight line in the original direction.

In an electromagnetic field, the grid itself is to have a velocity $- eA/m_0 c^2$ and if this varies from point to point, the grid will be distorted, but the particle will still travel along the distorted line of reinforcement with constant velocity relative to the grid.

§ 6. We can now proceed to find the differential equation for the wave-function, which has a remarkable resemblance to Dirac's equation for the electron, but involves no symbols other than those denoting ordinary four-dimensional vectors and scalars.

For a system of plane waves we write the wave-function

where $\omega/2\pi$ is the frequency, $n/2\pi$ the wave-number, **n** a vector normal to the waves, of magnitude n, **ρ** the position vector (x, y, z) and **n** . **ρ** the three-dimensional scalar product. But in a field-free region the frequency of the de Broglie waves is E/h and the wave-number is M/h where E and M are the energy (mc^2) and momentum (mV) of the particle, so that u becomes

$$u = ae^{\frac{2\pi i}{h}(Et - M \cdot \rho)}.$$

The exponent can now be written

$$- \frac{i}{\chi}(imc \, ict + mV \cdot \rho) \qquad \left(\chi = \frac{n}{2\pi}\right.$$

or

$$- \frac{i}{\chi} \mu \cdot \sigma,$$

where the scalar product is four-dimensional in this last expression, and μ, σ, are the four-dimensional vectors formed by supplementing $m\mathbf{V}$ and ρ respectively by components imc, ict in the time dimension.

But μ is m_0c times the fundamental velocity-vector drawn in the direction of the particle's motion or world-line. We shall, as before, regard the latter as a unit vector and denote it by $\hat{\mathbf{s}}$ so that we write

$$\mu = m_0c\,\dot{\mathbf{s}}.$$

Thus

$$u = ae^{-\frac{m_0\vec{r}\,\mathbf{s}}{\chi}\,\sigma}.$$

The differential equation for u will then be

$$\operatorname{grad} u = -\frac{i}{\chi}\,um_0c\operatorname{grad}(\vec{\mathbf{s}}\,.\,\sigma)$$

(four-dimensional grad)

$$= -\frac{i}{\chi}\,um_0c\,\dot{\mathbf{s}}.$$

For the case where there is a field, we shall keep $\vec{\mathbf{s}}$ to mean the velocity of the particle, which we have found to remain of unit magnitude, but in the equation we must replace $\vec{\mathbf{s}}$ by $\dot{\mathbf{s}} - \mathbf{v}$, the velocity relative to the medium, where $\mathbf{v}$ is given by (12).

We thus find

$$\operatorname{grad} u - \frac{i}{\chi}\,m_0c\mathbf{v}u = -\frac{i}{\chi}\,m_0c\,\vec{\mathbf{s}}u$$

or

$$\operatorname{grad} u + \frac{i}{\chi}\frac{e}{c}\,\mathbf{A}u = -\frac{i}{\chi}\,m_0c\,\vec{\mathbf{s}}u$$

or

$$\mathbf{k}_\lambda\left(\frac{\partial}{\partial x_\lambda} + \frac{i}{\chi}\frac{e}{c}\,\Lambda_\lambda\right)u + \frac{m_0c}{\chi}\,i\,\vec{\mathbf{s}}u = 0, \tag{16}$$

where $\mathbf{k}_\lambda$ are the ordinary unit vectors in the four co-ordinate directions. For comparison we write down in similar notation Dirac's equation as made symmetrical by Sommerfeld (" Wave Mechanics," ch. 2, p. 10, equation (5)):

$$\alpha_\lambda\left(\frac{\partial}{\partial x_\lambda} + \frac{i}{\chi}\frac{e}{c}\,\mathrm{A}_\lambda\right)u + \frac{m_0c}{\chi}\,u = 0,$$

where α_λ are symbols which denote neither vectors nor scalars, but have rules of combination of their own. I have not, however, succeeded in connecting the angular momentum of spin with equation (16) as Dirac does with his.

Summary.

In § 1 an analogy is traced between the equation of motion of a point-charge in the electromagnetic field and that of a sound-pulse in a medium moving with varying velocity, both being derived by the same development from similar Fermat principles. The (four-dimensional) " velocity of the medium " in the electromagnetic case is found to be $-e\mathbf{A}/m_0 c^2$ where $\mathbf{A}$ is the well-known four-dimensional electromagnetic potential.

§ 2. This model, however, introduces a term $\operatorname{grad}(\mathbf{A}^2)$ into the expression for the acceleration of e; a discussion shows that this term probably has no physical meaning and must be omitted.

§ 3. It is shown that for two-dimensional motion the curvature of the path can be deduced very simply from the Fermat principle.

§ 4. It is shown that the Larmor precessional velocity is equal to the " local angular velocity of the medium " and that the energy of the spinning electron in a magnetic field is equal to h times the corresponding " frequency of rotation of the medium "

§ 5. The Fermat principle is explicitly connected with the de Broglie waves, these waves being considered stationary in space-time while any particle moves across them with the fundamental velocity.

§ 6. A differential equation is derived for the wave-function of a point-charge, analogous to Dirac's differential equation but containing only vector and scalar quantities.

The Kinetics of Electrode Processes. Part I.—Depolarisation Effects by Hydrogen and Oxygen at Platinum Electrodes.

By J. A. V. Butler, D Sc., and G. Armstrong, B.Sc., University of Edinburgh.

Introduction.

Tafel in 1905[*] observed that the hydrogen overvoltage could be expressed as a function of the current density by the equation $i = ke^{-bV}$, and that the constant b was approximately equal to $F/2RT$, where R is the gas constant and F the electrochemical equivalent. Bowden[†] has recently shown that the dependence of the constant b on the temperature required by the relation $b = F/2RT$ holds for the liberation at the anode and cathode respectively of both oxygen and hydrogen.

In a recent paper Gurney has examined the quantum mechanics of the transfer of electrons between a metal and ions in the solution and has shown that a relation of this kind, with the observed factor, may arise from the conditions of this transfer [‡] He gives as the necessary conditions for the transfer of electrons from the electrode to positive ions in the solution, or from negative ions to the electrode as $E_+ > \Phi + V$[§], $E_- < \Phi + V$, respectively, where Φ is the thermionic work function of the metal and E_+, E_- the neutralisation potentials of the ions. In the extended form of the theory these are defined as $E_+ = I_+ - W_+ - R_+$, $E_- = I_- + W_- + R_-$, where I_+, I_- are the ionisation potentials of the ions, W_+, W the hydration energies, and R_+, R_- quantities representing the repulsive potential energy between the solvent and the ion at the instant after its neutralisation. By integrating the probabilities of transfer between ions for which these conditions are satisfied he

[*] ' Z. phys. Chem.,' vol. 50, p. 641 (1905).

[†] ' Proc. Roy. Soc.,' A, vol. 126, p. 107 (1929)

[‡] ' Proc. Roy. Soc.,' A, vol. 134, p. 137 (1931). Earlier expressions for the rate of transfer of electrons from a metal to ions in solution were given by Butler, ' Trans. Faraday Soc.,' vol. 19, p. 734 (1924), and by Erdy-Grüz and Volmer, ' Z. phys. Chem.,' A, vol. 150, p. 203 (1930). These were, however, incapable of giving the required factor 2 in the expression $b = F/2RT$; in Gurney's theory this arises from a consideration of the forces between the neutralised ion and the solvent molecules.

[§] The sign of V used here is the reverse of Gurney's. We shall throughout give V the sign of the potential of the electrode with respect to the solution.

obtains, on certain assumptions, the expression $i = k'Te^{\pm FV/2RT}$ where the positive (negative) sign applies to the discharge of negative (positive) ions.

According to this calculation the rate of transfer of electrons from the electrode to hydrogen ions at the reversible potential V_0 is $i = k'Te^{-FV_0/2RT}$. When an electrode remains at the reversible potential without the passage of any current it is evidently necessary that there shall be some other process whereby electrons (or the equivalent charge) are transferred in the opposite direction at the same rate. This flow of electricity may come from (1) the ionisation of hydrogen molecules in the solution, (2) the ionisation of hydrogen adsorbed on the surface of the electrode, (3) atomic hydrogen dissolved in the metal yielding positive hydrogen ions to the solution by the process $H \rightleftharpoons H^+$ (solution) $+ \varepsilon$. Mechanisms of the reversible hydrogen potential could be constructed on the basis of either of these processes, but that which is actually operative can only be discovered by an investigation of the energy relations underlying each or by experimental study of the conditions under which such processes take place.

The condition for the transfer of an electron from molecular hydrogen in solution to the electrode, according to Gurney's theory, is $\Phi + V > I - W$, where W is the negative potential energy of the ion H^+_2 at the instant of formation. The first stage ionisation potential of the hydrogen molecule is $15 \cdot 3$ volts, and W can hardly be greater than 6 ε-volts. It thus appears to be improbable that molecular hydrogen can give electrons to the metal when V is less than $\varepsilon_H = + 4$ volts. There is no information available as to the energy levels of adsorbed atoms and molecules. The considerable heats of adsorption observed by Taylor and others in cases of " activated adsorption " would probably imply a corresponding reduction in the ionisation potentials, which may enable Gurney's condition to be satisfied at more negative values of V for substances adsorbed in this way.

The experiments to be described were designed to elucidate the electromotive behaviour of hydrogen and oxygen at electrodes. Bowden* has recently investigated the anodic and cathodic polarisation of platinum electrodes in dilute sulphuric acid saturated with hydrogen and oxygen, using mainly current densities greater than 10×10^{-3} amps./cm.² It will be desirable to give at the outset a brief summary of his observations.

Hydrogen Saturated Solutions.—If the current density is sufficiently large, on anodic polarisation the potential changes linearly with time from near the

* 'Proc. Roy. Soc.,' A, vol 125, p. 446 (1929).

reversible hydrogen potential to near the potential at which oxygen is liberated. The quantity of electricity required for this linear change is 3×10^{-3} coulombs for electrodes having an actual area estimated at $3 \cdot 3$ cm.[2]. With electrodes which have been previously used, the potential may remain constant for a time at the reversible hydrogen potential before the linear change occurs. There is also a small kink in the linear part at $\varepsilon_H = + 0 \cdot 62$ volts. When the current is reversed after the anodic polarisation the potential rises linearly to $\varepsilon_H = + 0 \cdot 62$ volts, remains constant for a time at this value and then passes linearly to near the reversible hydrogen potential. The total quantity of electricity required for the two linear changes is also constant at 3×10^{-3} coulombs.

Oxygen Containing Solutions.—The potential of a platinum electrode in oxygen saturated solutions is about $\varepsilon_H = + 0 \cdot 87$. After anodic polarisation it returns, at open circuit, very slowly to this value and after cathodic polarisation it remains for a short time near the reversible hydrogen potential and then falls quickly to the same value. When the electrode is polarised anodically and the current is then reversed, the passage of about 1×10^{-3} coulombs brings the potential to $+ 0 \cdot 62$ volts, at which an arrest occurs similar to that in hydrogen saturated solutions. After a time the potential rises linearly to near the reversible hydrogen potential, about 2×10^{-3} coulombs being required.

Bowden regarded $+ 0 \cdot 87$ volts as the potential of platinum oxide in solutions saturated with oxygen, and $+ 0 \cdot 62$ volts as the potential of this oxide in solutions saturated with hydrogen (probably representing the reduction potential of the oxide to platinum and water). He suggested that the constant quantity of electricity, viz , 3×10^{-3} coulombs, required for the linear changes of potential in the passage from the reversible hydrogen potential to that at which oxygen is evolved is a measure of the amount of electrolysis required to replace a mono-molecular layer of hydrogen at the electrode surface by one of oxygen.

Experimental Methods.

Rapidly varying potential differences were recorded by means of a Cambridge Einthoven string galvanometer, used in conjunction with a thermionic valve, as shown in fig. 1. The movable contact C, which could be placed in either of the mercury caps A, B, enabled either the electromotive force of the experimental cell or known electromotive forces from the potentiometer P to be applied to the grid of the valve V. An Osram HL 210 valve was employed,

with a grid bias G of 3 volts and a plate voltage of 56 volts. The anode current passed through the string S of the galvanometer which was heavily shunted by the resistance R. The movements of the string, together with time marks at intervals of 0·04 second, produced by the Cambridge Instrument Company's time-marker controlled by an electrically maintained tuning fork, were photographed on strips of bromide paper in the paper camera of the same firm. This arrangement has the advantage that the sensitivity can be varied enormously by varying the shunt resistance R, and also, if necessary, the plate voltage and the grid bias G, and it is possible to obtain a high sensitivity without unduly increasing the period of vibration of the string. As normally used when the range of variation of the applied potential difference was about 2 volts, the sensitivity on the film was 2–3 mm. per 0·1 volt, and when the applied potential
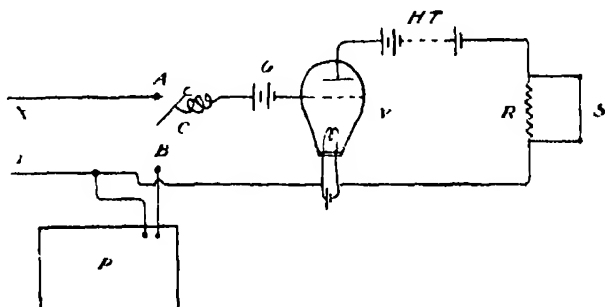
FIG. 1.—Valve Circuit.

difference was suddenly changed from 0 to 1·7 volts the time required for the string to take its new position was less than 1/200 second. The displacement of the string does not vary exactly linearly with the potential difference. A calibration was therefore obtained on the record during each experiment by connecting the movable contact C with the cup B and turning the voltage dial of the potentiometer. A series of steps were thus obtained on the record, corresponding to intervals of 0·1 volt. The grid current of the valve with the grid bias employed is of the order of 10^{-9} amps., and is negligible compared with the polarising currents.

For the observation of slowly varying potential differences a Lindemann electrometer was used in conjunction with a potentiometer. With this arrangement potential differences could be determined with an error of about ± 0·002 volts.

The experimental vessel is shown in fig. 2. The vessel B contains the electrodes which are to be experimented upon (only one, D, is shown in the diagram).

The tube C, which is connected with B by a bent tube, contains the auxiliary electrode E between which and the experimental electrode D the electrolysing current is passed. The solution is freed from oxygen and saturated with hydrogen in another vessel by alternately pumping out and filling with pure hydrogen. The electrode vessel and its connecting tubes are carefully swept out with hydrogen, and the solution introduced through the tube Y by suction applied at the trap T or at V. S is a standard electrode by reference to which the potential difference of D is measured. Contact with this electrode is established by sucking up the solution from the vessel B above the tap U and then running the solution from the reservoir R until it makes contact with it. A mercurous sulphate electrode in normal sodium sulphate solution was usually employed as the standard electrode. Its potential difference on the standard hydrogen scale is $\varepsilon_H = + 0 \cdot 66$ volts.

The electrolysing current was obtained from a high-tension battery with suitable resistances in series. The current was measured during or immediately after each experiment by determining by means of the potentiometer the fall of potential down a known resistance through which the current passed. It was found to be essential to have every part of the apparatus, and particularly everything connected with the high-tension battery, carefully insulated on sheets of glass supported by paraffin blocks.

Fig. 2.—Electrode Vessel.

The Behaviour of Platinum Electrodes in Dilute Sulphuric Acid.

(1) *Experiments with Platinum Electrodes in Hydrogen Saturated Solutions.*— We have usually worked with current densities between 1 and 30 milliamperes/ cm.², *i.e.*, with somewhat smaller currents than those used by Bowden. The electrolyte was N/10 sulphuric acid, and the platinum electrodes employed had an apparent area of approximately 1 cm.². Experiments on the quantity of electricity required to establish the hydrogen overvoltage, in solutions

carefully freed from oxygen, showed that about 1.5×10^6 coulombs were required to raise the potential by 100 millivolts. The effective area, by comparison with Rideal and Bowden's value[*] for mercury electrodes (6×10^{-7} coulombs per cm.²), which we have confirmed, is about 2.5 cm.².

Some typical examples of the behaviour of the electrodes are shown in fig. 3. The various electrodes employed are distinguished by the letters D, F, etc.
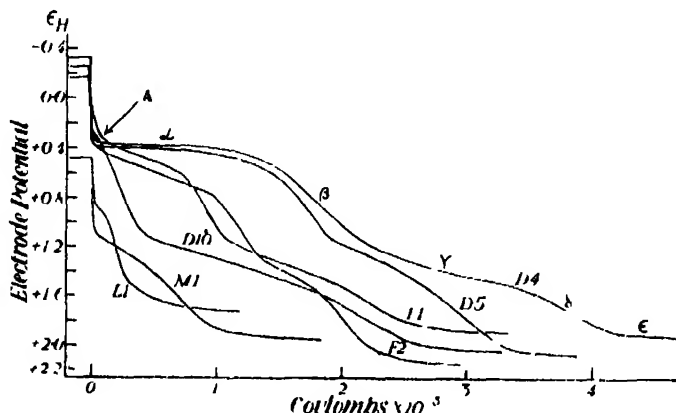
Fig. 3 —Anodic polarisation of platinum electrodes in hydrogen saturated solutions.

D4	1.95×10^{-3} amps.	F1.	3.7×10^{-3} amps.
D5.	11.4×10^{-3} amps.	F2.	13.8×10^{-3} amps.
D10	8.2×10^{-3} amps	M1.	0.37×10^{-3} amps.
L1.	0.006×10^{-3} amps.		

The electrode D was a small piece of platinum foil having both sides exposed to the solution and the electrode F was coated with paraffin wax on one side, the side exposed measuring 1 cm.². This electrode was placed horizontally in the solution with its uncovered side downwards, fig 2. In the experiments D_4, D_5, D_{10}, F_1, F_2 the electrode was first polarised negatively until the hydrogen overvoltage was established and the current was then reversed. The curves D_4 and F_1 were obtained with electrodes which had never previously been anodically polarised, while D_5, D_{10} and F_2 were obtained by similar subsequent polarisations of the same electrodes.

The potential of the reversible hydrogen electrode in this solution is $\varepsilon_H = -0.06$ volts. After the preliminary cathodic polarisation, but before the anodic current was started, the potential of the electrode was usually between -0.2 and -0.3. On restarting the current, making the electrode the anode, the potential falls very rapidly, at a rate which agrees with the

figure given above for the establishment of the hydrogen overvoltage, to *below the reversible hydrogen potential*. The potential at which this rapid fall comes to an end is displaced more towards positive potentials the greater the current density, as can be seen from the values listed under A in Table I.

Table I —Platinum in N/10 Sulphuric Acid Saturated with Hydrogen.

Experiment	Current (amps).	A.	B.
D_4	$1\ 95 \times 10^{-2}$	$+0\ 31$	$ca\ +0\ 5$
D_9	$5\ 6 \times 10^{-3}$	$+0\ 36$	—
D_{10}	$8\ 2 > 10^{-3}$	$+0\ 46$	$+0\ 35$
D_6	$11\ 4 \diagup 10\ 3$	$+0\ 38$	$+0\ 36$
D_7	$13\ 0 \diagdown 10^{-3}$	$+0\ 40$	$+0\ 3$
D_8	$36\ 0 \times 10^3$	$ca\ +0\ 66$	$+0\ 2$

In the subsequent course of the curves five stages can be distinguished which are developed to different extents —

(α) A stage in which the potential remains nearly constant as in D_4, D_5, or falls linearly at a slow rate as with the wax-coated electrode in F_1, F_2. In D_{10} this stage is very short.

(β) This leads to a more rapid, almost linear, fall of potential from about $+0\cdot6$ to $1\cdot0$ volts   The amount of current required to produce this linear change (about $0\cdot7 \times 10^{-3}$ coulombs per volt) is approximately independent of the current density, increasing somewhat as the current density is increased.

(γ) Between $+1\cdot0$ and $+1\cdot4$ volts the rate of fall of the potential decreases again.   The length of this slower stage is shorter the greater the current density.   In an experiment with the current of 36×10^{-3} amps. this stage was inconspicuous.

(δ) The rate of fall of the potential again increases giving once more an approximately linear slope, which is greater the greater the current density.

(ε) The rate of change then diminishes, and a constant value is finally reached at the potential at which oxygen is steadily evolved.

For comparison with these curves L_1 and M_1 show the anodic polarisation of electrodes which have not been given a preliminary cathodic polarisation. The initial potential is low, viz., about $+0\cdot5$, owing to the presence of traces of oxygen.   The potential falls quickly at first, and only stages (γ), (δ) and (ε) appear.

In most of these experiments the current was again reversed when the electrode potential had reached a steady value, corresponding to the liberation of oxygen. During the momentary stoppage of the current the potential rises to about $+1 \cdot 6$ volts. Its course on making the electrode the cathode again is shown for some typical cases in fig. 4 Except at the smallest current
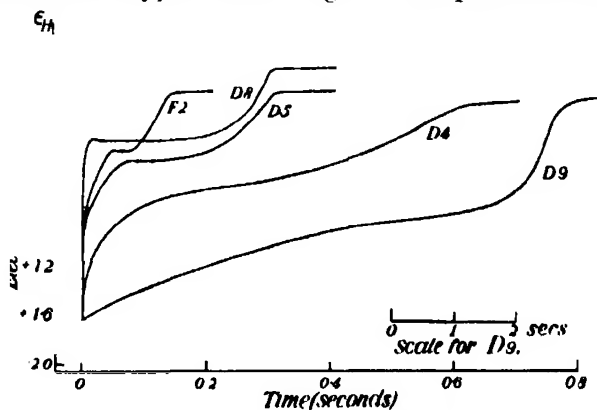
Fig 4 —Cathodic polarisation of electrodes after previous anodic polarisation

D4.	$1 \cdot 95 \times 10^{-3}$ amps.	
D5	$11 \cdot 4 \times 10^{-4}$ amps.	
D9	No current	
D8	$3 \cdot 6 \times 10^{-3}$ amps	
F2	$13 \cdot 8$ 10^{-3} amps.	

density the potential rises extremely rapidly to about $+1 \cdot 6$ and the curves show marked breaks at potentials between $+0 \cdot 2$ and $+0 \cdot 5$ volts. The position of this break also depends on the current density, being displaced further towards negative potentials the greater the current The position for different current densities is given under B in Table I. After this the potential rises almost linearly to somewhat above the reversible hydrogen potential and soon reaches a constant value It may be observed that at high current densities the potential rises initially a little higher than the position of the break and returns to a lower value. At low current densities a definite break is not observed, but is represented by a point of inflection in the curve. The curve D_9, which is plotted on a longer time scale, represents the natural recovery of the potential when no current is passed. Its slope is greatly dependent on the length and intensity of the previous anodic polarisation, and a more detailed study of it will be given at a later stage. The particular example shown was obtained with electrode D, in an experiment in which the anodic current was stopped as soon as the potential had reached $+2 \cdot 0$ volts. After longer anodic polarisation the initial rise of the potential is steeper and the break at about $+0 \cdot 86$ more marked.

In order to elucidate the effect of the current density on the position of the arrest the following experiment was carried out. An electrode was given 10 seconds anodic polarisation with a current of 13·6 milliamperes. An equal current was then passed in the opposite direction for a time sufficiently long to take the potential on to the arrest, at about +0·43 volts, when it was stopped. The potential immediately fell to +0·85 and remained constant. On starting the current again, still cathodically, the potential rose to near the original value of the arrest. The same changes of potential were repeated on stopping and restarting the current again. It thus appears that the arrest observed on returning from positive to negative polarisations is due to a process which gives rise at zero current to a constant potential at about +0·85 volts. The positions observed during the passage of current, fig 4, must be regarded as displacements from this position produced by the current

The apparent potential of the arrest would be displaced towards the negative by the inclusion in the measured value of part of the fall of potential due to the passage of current through the electrolyte   We have examined the effect of varying the position of the tip of the tube L with respect to the electrode D, fig. 2, but no significant displacements of the potential, with the current densities used here, could be obtained even when the tip of L was brought below the electrode. The alignment of the electrode was also without influence, for similar curves were obtained with vertical electrodes having both sides exposed to the solution and horizontal electrodes having the upper side waxed.

(2) *Experiments with Platinum Electrodes in Oxygen Saturated Solutions —* Platinum electrodes in M/10 sulphuric acid saturated with oxygen usually had a potential about +0·85 volts. On the first anodic polarisation the potential often falls comparatively slowly (curve I, fig. 5), but in subsequent anodic polarisations obtained after the potential has risen at open circuit to about. +1·2 volts, much steeper and concordant slopes are obtained (curve II). When the current is reversed after the anodic polarisation, the potential rises at first linearly at the same rate (curve III). As a result of a number of concordant experiments with electrode D, we found that in these linear changes $0·85 \times 10^{-5}$ coulombs were required to change the potential by 0·1 volt. If the effective area had not changed since the experiments in hydrogen containing solutions, it follows that $0·34 \times 10^{-5}$ coulombs per 0·1 volt are required for each square centimetre of accessible surface in the establishment of the oxygen overvoltage. This quantity is considerably smaller than that found by Bowden, namely, $3·8 \times 10^{-5}$ coulombs for an electrode having an estimated accessible area of 3·3 cm.², or $1·1 \times 10^{-5}$ coulombs per cm.² of

accessible surface. The accessible area of the electrode does not appear to change during anodic polarisation, for the same value was obtained after a considerable amount of such treatment.

When, after anodic polarisation, the current is reversed the potential rises at first linearly at the rate given above and then more slowly, giving with the larger current densities a lengthy arrest between 0·4 and 0·45 (curves V, VI) The position of this arrest is somewhat displaced towards negative potentials
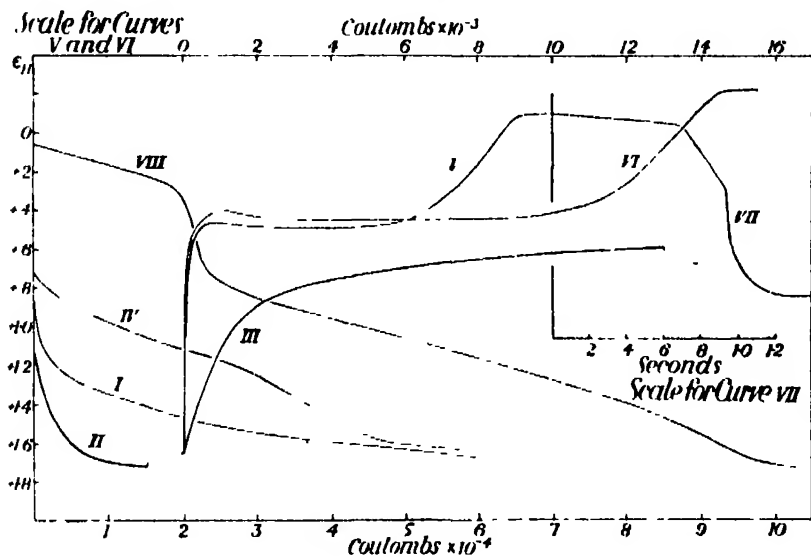
Fig. 5.—Behaviour of platinum electrodes in oxygen saturated solutions   (Electrode D.)

Curve I.   4 3 × 10⁻³ amps.   Curve VI   29 × 10⁻³ amps.
Curves II, III, IV   0 49 × 10⁻³ amps.   Curve VII.   Open circuit.
Curve V.   4 3 × 10⁻³ amps   Curve VIII. 4·3 × 10⁻³ amps.

the greater the current density. With large current densities there is a small maximum in the curve before the horizontal part is reached. After the arrest the potential begins to rise again and a nearly linear rise changes sharply to a constant value just above the reversible hydrogen potential. Curve VII shows the course of the potential when the current is now stopped. The length of the initial slow change to the vicinity of the reversible hydrogen potential is greatly dependent on the length of the previous cathodic polarisation, but the other two stages are approximately independent thereof. The potential finally reaches a value +0·83 close to the original value.

When after a short cathodic polarisation the current is reversed the potential falls slowly and linearly to +0·3, rapidly to about +0·7 and finally approxi-

mately linearly to between $+1 \cdot 6$ and $+2 \cdot 0$ according to the current density (curve VIII). After a prolonged cathodic polarisation this curve is preceded by a very slow change from about $-0 \cdot 05$ to $+0 \cdot 1$, but the subsequent parts of the curve are practically independent of the current density.

When, after anodic polarisation, the electrode is made the cathode for a short time, so that the potential reaches a position on or near the arrest and the current is then reversed (curve IV, obtained immediately after curve III), the potential falls comparatively slowly, and similarly to the lower part of curve VIII. If the circuit is then opened and after the potential has risen to about $+1 \cdot 2$ the electrode is again made the anode a rapid and linear change like curve II is again obtained.

Discussion.

When no transfer of electrons (or ions) occurs across the electrode boundary during the passage of a current, so that the whole of the current is employed in changing the charge of the double layer, the change of the potential difference with time is given by the equation,

$$idt/dV = B, \tag{1}$$

where i is the current flowing to the electrode, and B, which may be called the capacity of the double layer, is the rate at which the charge of the double layer increases with the potential difference. If i is given in amperes, t in seconds, and V in volts, B is the number of coulombs required for the increase of the potential difference, per volt. It is reasonable to suppose that in the linear changes of potential observed in the establishment of the hydrogen overvoltages in the absence of oxygen, and in the establishment of the oxygen overvoltage after a previous anodic polarisation, curve III, fig. 5, the whole of the current is employed in changing the charge of the double layer. The value of B for the electrodes used in this paper is then $1 \cdot 5 \times 10^{-5}$ between $\varepsilon_H = 0$ and $-0 \cdot 5$ and $8 \cdot 5 \times 10^{-5}$ between $\varepsilon_H = +1 \cdot 5$ and $2 \cdot 0$. We have no information as to its value for intermediate potentials, but there seems no reason to suppose that it does not lie between these two values.

When, during the passage of current, the transfer of electrons (or ions) across the double layer occurs, we have

$$B \, . \, dV/dt = i - i', \tag{2*}$$

* In these equations anodic currents must be regarded as positive and cathodic currents negative, and V given its proper sign as the potential of the electrode with respect to the solution.

where i' is the current employed in this transfer. We may call i' the *depolarisation current*. It follows that when dV/dt differs from i/B, there must be a depolarisation current due to some process whereby the transfer of electrons (or ions) across the double layer can occur

In the anodic curves shown in fig 3 the initial fall of potential is in agreement with the equation $dV/dt = i/B$, and therefore is due to the decrease in the charge of the double layer, the depolarisation current being negligible In the other parts of the curves dV/dt is comparatively so small compared with i/B (giving B its larger value at the positive end) that the value of i' must everywhere approach that of i.

We will consider first the general effect of an anodic depolariser. Suppose that the depolarisation process is the transfer of electrons from molecules of the depolariser in the solution to the electrode. If c is the effective concentration of the depolariser at the electrode, the depolarisation current might be expected to be governed by an equation of the type

$$i' = kce^{aV}. \tag{3}$$

Consequently when an anodic current i is passed the potential will fall rapidly according to (2) until this term becomes comparable with i, and when $i' = i$, dV/dt will be zero. An exponential expression like (3) would give rise in (2) to a very sudden transition from a very rapid fall of potential to a constant value of V. Also, for equal concentrations of the depolariser, the greater the value of i the greater will be the value of V when the state $dV/dt = 0$ is reached.

Now if the concentration of the depolariser at the electrode diminishes as the current is continued through the depletion of the amount originally present, or if the depolariser is used up at the anode faster than it can diffuse up from the solution, the constant value of the potential cannot be maintained With the moderately large currents employed in these experiments, the fraction of the current which is used in producing the changes of potential is small, and the rate of change of the potential will be governed by the rate of change of c in (3), i' remaining practically equal to the current i

We can now discuss the changes of potential in the typical anodic curve D4, fig. 3, for platinum in hydrogen saturated solutions. The potential first falls very rapidly according to (1) and at the point A the first depolarisation process is encountered. At this point the depolarisation current i' increases rapidly from approximately zero to a value approaching i and the rate of change of the potential becomes nearly zero. We have seen that the position of this point is lower the greater the current density, which is in accordance

with (3). As the concentration of the depolariser at the electrode surface decreases, the potential falls off at first very slowly and then more quickly (stages α, β), until the second slow stage γ is reached. This marks a second depolarisation process giving rise to the stages γ, δ, which are similar to α, β. Finally the potential reaches values at which oxygen can be liberated and the final constant potential of the stage ε is due to continuous depolarisation by the discharge of negative ions at the rate $i' = i$.

It is not possible to identify with certainty the two depolarisation processes which occur, at these current densities, at about $+0\cdot4$ and $+1\cdot2$ volts. The discharge of negative ions, resulting in the liberation of oxygen, cannot occur continuously until the potential $+1\cdot65$ is reached. At this potential according to Bowden's* measurements, a current density of 10^{-7} amps./cm.² is possible for this process. The large depolarisation currents observed at higher potentials must arise from some other cause. The arrest α appears to be dependent on the amount and extent of the previous polarisation of the electrode. It appears after cathodic polarisation of electrodes which have never previously been anodically polarised and is apparently due to the hydrogen produced in the previous cathodic polarisation.

Since it is improbable that molecular hydrogen dissolved in the solution can give up electrons to the metal at these potentials, the depolarising action observed must be ascribed to hydrogen adsorbed at the surface or dissolved in the metal.

The stage γ appears in all the curves for hydrogen saturated solutions, being less marked the greater the current density. It also appears in oxygen saturated solutions after cathodic polarisation, curve VIII, fig. 5, but that it cannot be due to hydrogen is shown by the fact that it also appears after a short cathodic polarisation in which the potential rises only to $+0\cdot9$, at which hydrogen cannot have been liberated, curve IV. The remaining possibilities are that it is due to (1) the passage into solution of platinum ions, (2) the discharge of negative ions. If we regard the second as more probable we have to enquire why, when negative ions can be discharged at a rate nearly equal to the current density at $\varepsilon_{II} = +1\cdot0$, it is necessary for the potential to fall to about $+1\cdot8$ before their discharge can continue at a steady rate.

It may be suggested that the formation of an adsorbed layer of oxygen, held at the surface of the electrode by considerable forces, would require a smaller expenditure of energy, and therefore take place at a more negative

---

* 'Proc. Roy. Soc.,' A, vol. 126, p. 107 (1929).

potential than that required for the liberation of free oxygen in the solution. On this view the depolarisation observed in the stage γ is due to the formation of an adsorbed layer of oxygen. As this becomes more complete the potential falls steadily, until when the steady state is reached we may suppose that the surface is completely covered and that the further production of oxygen is by the discharge of negative ions in the solution at a short distance from the electrode, by the process investigated by Gurney.

On this view the difference of the anodic curves II and IV, fig. 5, is easily explained. When the potential is allowed to recover at open circuit after anodic polarisation the adsorbed layer of oxygen is not destroyed and when the electrode is made anodic again the current is employed entirely in changing the charge of the double layer, until the potential is reached at which oxygen can be discharged in the solution. But we may suppose that in the cathodic polarisation, curve III, the oxygen layer is partly destroyed during the slow change between $+0\cdot8$ and $+0\cdot6$ and in the subsequent anodic polarisation, curve IV, it must be reformed before oxygen can be freely liberated.

Turning now to the cathodic curves V, VI, fig. 5, showing the forced recovery from positive to negative potentials in oxygen saturated solutions, the initial rate of change of the potential is in accordance with the value of B given above.* At about $+0\cdot8$ volts the effect of depolarisation begins to be apparent, and after rising more slowly, at higher currents to a slight maximum, the potential remains nearly constant for a time. In this condition we must suppose that depolarisation occurs according to (2), i' being equal to i. As the depolariser at the electrode becomes depleted the potential begins to rise again, and the slope of the curve increases gradually from zero to an approximately constant value. Finally depolarisation by the discharge of hydrogen ions can take place and the curve changes its direction sharply, becoming horizontal. It has been shown that the position of the intermediate arrest is displaced upwards by increase of the current density, and at zero current is at about $+0\cdot86$ volts in both hydrogen and oxygen.

On the hypothesis suggested above this potential must be regarded as that of platinum covered with an adsorbed layer of oxygen, and the cathodic arrest marks the destruction of this film owing to the transfer of electrons from the electrode to the oxygen atoms converting them into ions which are neutralised by the hydrogen ions present in the solution. Bowden (*loc. cit.*) has suggested

---

* Similar curves are also obtained with hydrogen saturated solutions, fig. 4, but the initial rate of rise is greater. This is no doubt connected with the fact that the presence of hydrogen causes the potential to rise at open circuit fairly rapidly.

that a definite oxide. PtO_2, is formed during anodic polarisation, which may, after long polarisation, be several molecules in depth. It is necessary to see if the observed lengths of the cathodic arrest can be reconciled with the hypothesis suggested above, or whether it is necessary to postulate the formation of such a layer of oxide.

To this end we have made observations of the variation of the length of the cathodic arrest with the quantity of electricity passed during the previous anodic polarisation. In fig 6 the number of coulombs required for the cathodic
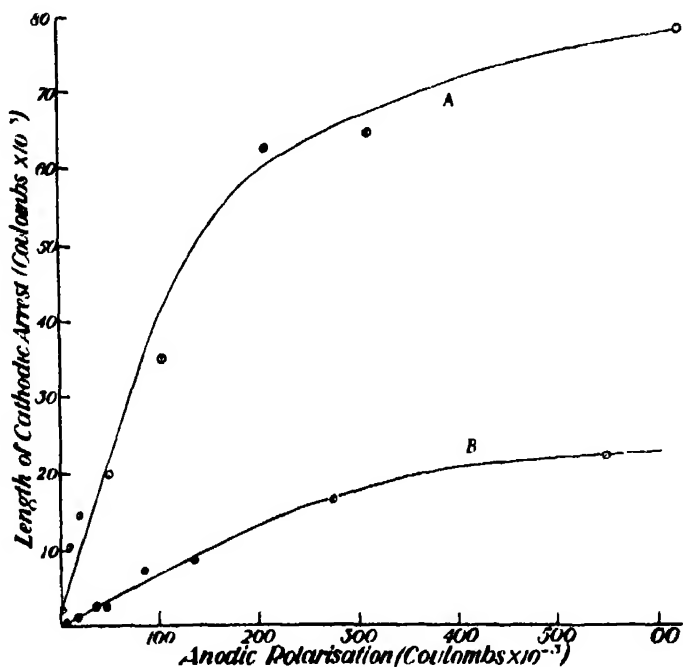
FIG. 6.—Variation of length of the cathodic arrest with the amount of anodic polarisation.

arrest is plotted against the number of coulombs passed during the anodic polarisation, excluding the quantity required to change the potential to its steady value on the positive side. The curve A refers to oxygen saturated solutions and the curve B to hydrogen saturated solutions. The smaller values were obtained at a variety of current densities and are reasonably concordant; the larger values with a current of 5×10^{-3} amps./cm.^{2}.

In oxygen saturated solutions the length of the arrest increases at first linearly with the amount of anodic polarisation, reaching a value of about 60×10^{-3} coulombs for an anodic polarisation of 200×10^{-3} coulombs.

After greater amounts of anodic polarisation the length of the arrest increases more slowly, reaching a value of 94×10^{-3} coulombs after the passage of 3700×10^{-3} coulombs. This value is sufficient for the reduction of 280×10^{15} atoms of oxygen. Taking the true area of the platinum as about $2 \cdot 5$ times the apparent area, it may be estimated that $4 \cdot 5 \times 10^{15}$ atoms of oxygen would completely cover the surface if spaced one to each atom of platinum, or 9×10^{15} if two atoms of oxygen are attached to each platinum atom at the surface. It is evident that if the arrest is due to a film of oxide, the greatest value must be ascribed to a film at least 30 molecules in thickness. Since there is no change in the appearance of the platinum, which remains perfectly bright even after continued anodic polarisation, it is difficult to regard such an oxide film as a possibility

On one occasion it was observed that when a stream of oxygen was bubbled through the solution during the experiment the length of the arrest was much reduced Some observations of the effect of stirring the solution were then made. It was found that whereas in an unstirred solution, after 40 seconds anodic polarisation with a current density of $5 \cdot 2 \times 10^{-3}$ amps., the length of the arrest was 12 seconds, when the solution was stirred by a rotating glass stirrer at 2, 4 and 8 revolutions per second, under the same conditions, the lengths of arrest were $1 \cdot 8$, $1 \cdot 6$ and $1 \cdot 4$ seconds respectively. When after an anodic polarisation of 40 seconds the electrode was taken out of the solution, washed and replaced before being cathodically polarised the arrest was also reduced to about $1 \cdot 2$ seconds. It thus appears that the substance causing depolarisation is not firmly attached to the electrode, and can be removed to a large extent by even gentle stirring. It is perhaps significant that the amount remaining after washing and replacing in a fresh solution corresponds fairly closely with that expected for a single layer of oxygen atoms spaced one to each platinum.

These facts are accounted for on the hypothesis that there is a single layer of adsorbed oxygen atoms at the surface, if it be supposed that as the oxygen atoms in this surface layer are reduced they are replaced from the solution. So long as this replacement can occur the potential remains nearly constant on the arrest, but when the supply of available oxygen is depleted the potential will begin to rise as the surface layer is destroyed. Since the molecular oxygen present in an oxygen saturated solution does not appear to be very active in this way, it must be supposed that some part of the oxygen liberated in the anodic polarisation in an active, possibly monoatomic state. In order to test whether any such active form of oxygen could be detected we added potassium

iodide to the solution in the anode chamber immediately after electrolysis, but observed no liberation of iodine. However, very minute quantities would be sufficient to produce the observed effects.

The curve for hydrogen saturated solutions is also linear for the smaller values, but its slope is only about one-fifth that of the oxygen curve. Even after long anodic polarisation the length of the arrest is much less than that observed under similar conditions in oxygen. This may be due to several causes : (1) the depolarising action of the oxygen present in the oxygen saturated solutions may be added to that of the oxygen formed during the electrolysis, (2) the oxygen formed during the electrolysis may diffuse away from the electrode more rapidly in hydrogen than in oxygen saturated solutions, (3) part of the oxygen liberated in the hydrogen saturated solutions may react with hydrogen, thus diminishing the quantity which can act as depolariser. It is possible that all three effects play a part in producing the observed result, but the effect of (1) is small, since the length of the arrest in oxygen saturated solutions with no previous anodic polarisation is about 2×10^{-3} coulombs, and (2) should tend to disappear as the anodic polarisation is increased, so that it is probable that (3) is mainly responsible. In order to ascertain if hydrogen peroxide is formed in this reaction, we polarised an electrode anodically in M/10 sulphuric acid saturated with hydrogen for 20 hours with a current of about 5×10^{-3} amps., but we were unable to detect any hydrogen peroxide in the solution.

In view of the effect of hydrogen in reducing the length of the arrest, it is not surprising that when both electrodes between which the electrolysing current passes are in the same vessel, the length of the arrest is considerably reduced. That comparatively small quantities of hydrogen are effective in this way is shown by the fact that the arrest is appreciably shorter even after short polarisations, when only a small quantity of hydrogen has been liberated in the solution.

Some experiments have been carried out on the anodic polarisation of a platinum electrode in N sodium hydroxide solutions. The curves are similar in form to those obtained in sulphuric acid, but are displaced towards negative values by 0.7–0.8 volt. This displacement corresponds to the difference between the reversible potentials of the oxygen and hydrogen electrodes in the two solutions, and shows that all the processes occurring in the course of the curves are governed by the p_H of the solution.

Summary.

(1) A study has been made of the anodic and cathodic polarisation of platinum electrodes in solutions saturated with hydrogen and with oxygen, using current densities mainly between 0.5 and 30×10^{-3} amps./cm^2. The observed behaviour is interpreted on the basis of a theory of the effect of depolarisation processes on the rate of change of the potential.

(2) On the anodic polarisation of electrodes, which have previously been cathodically polarised in hydrogen saturated solutions, two depolarisation processes are observed at potentials more negative than that at which the steady liberation of oxygen occurs They are ascribed respectively to the electrolytic solution of adsorbed or dissolved hydrogen, and to the formation of a layer of adsorbed oxygen. On cathodic polarisation of an electrode which has previously been anodically polarised one such process is observed which marks the removal of the adsorbed layer of oxygen.

Investigations in the Infra-Red Region of the Spectrum. Part VI.—The Absorption Spectra of the Dioxides of Chlorine and Sulphur.

By C. R. BAILEY and A. B. D. CASSIE, The Sir William Ramsay Laboratories of Inorganic and Physical Chemistry, University College, London, W.C.

The infra-red spectrum of chlorine dioxide has not been previously determined, although its photochemical properties and its electronic band spectrum have been the subject of recent extensive enquiry.* From the latter attempts have been made to interpret the band spectrum, and to assign values to the characteristic frequencies of the fundamental modes of vibration in the ground electronic state. It will be seen from the following that the values so deduced are incorrect, and it is probable that in no case of a polyatomic molecule is a complete determination of its fundamental frequencies possible without resort to its infra-red spectrum.

Experimental.

The method of preparation described by Goodeve and Stein (*loc. cit.*) was followed. The gas passed under water-pump vacuum to a trap immersed in a carbon dioxide-acetone freezing mixture; it was then distilled through phosphoric oxide tubes and condensed in a second trap cooled by liquid air. This trap could be removed from the generating system by means of a glass seal and a spherical glass joint; the ground joint was of universal pattern and the trap containing the dioxide could therefore be readily transported and connected to the absorption tube system. The latter was of as small capacity as possible, and no manometer was included, pressure in the absorption tube being regulated by immersing the dioxide trap in a freezing mixture of known temperature. The greatest pressure used during the investigation was the vapour pressure of the gas at 0° C., or approximately 630 mm. The length of the absorbing column of gas was in all cases 45 cm.; the lubrication of taps

* Mayer, 'Z. phys. Chem.,' vol. 113, p. 220 (1924); Booth and Bowen, 'J. Chem. Soc.,' vol. 127, pp. 342, 510 (1925); Goodeve and Stein, 'Trans. Faraday Soc.,' vol. 25, p. 738 (1929), Nagai and Goodeve, *ibid.*, vol. 27, p. 508 (1931), Wallace and Goodeve, *ibid.*, p. 648; Finkelnburg and Schumacher, 'Z. phys. Chem.,' Bodenstein Festb., p. 704 (1931), Urey, 'Ind. Eng. Chem.,' vol. 23, p. 1241 (1931); Urey and Johnston, 'Phys. Rev.,' vol. 38, p. 2131 (1931).

and of joints between the rocksalt end plates and the absorption tubes was effected by chlorinated vaseline.

The monochromator method described in Part IV* of the present series of investigations was used throughout without essential modification, and a pressure sufficient to give some 50 per cent. absorption was aimed at for detailed examination of any band. The tubes were painted a dead black, and no evidence of rapid decomposition was observed, the selective absorption of near infra-red radiation producing no appreciable decomposition of chlorine dioxide.

The Observed Data.

The results are summarised in Table I. The relative intensities are approximate estimates for the slit width employed The last two columns give the suggested origin together with the calculated frequency ν_c.

Table I.

Band.	Band centre		Maxima.	P–R separation	Relative intensity.	Slit width.	Origin.	ν_c calculated.
	$\lambda(\mu)$.	ν_0.						
		cm^{-1}	cm^{-1}	cm^{-1}		cm^{-1}		
B	10 57	946	932	31	20	5		
C	9 017	1109	1095 1106 1123	28	50	7		
E	5 307	1884	1870 1884 ? 1900	30	2	10		1892
F	4·916	2034	—	—	4	15	$\nu_1 + \nu_3$	2055

There is much evidence (Goodeve and Stein, Urey and Johnston (*loc. cit.*)) from the electronic band spectrum that the third fundamental vibrational frequency associated with the ground state is approximately 527 cm.$^{-1}$. A search was made for this band without success, the failure to detect the band was, as the result of other experiences in the neighbourhood of 19–22 μ, attributed to the existence of scattered radiation of shorter wave-length which could not be excluded from the thermopiles. Conversion of the apparatus into a double manochromator confirmed this suspicion, since beyond 18 μ no galvanometer deflection was observed when the radiation traversed the

empty tube. With the apparatus as at present constructed 19 μ appears to be the approximate long wave limit for experimentation, even with the sylvine prism ; all residual radiation appears to be absorbed by the rocksalt plates of the absorption tubes and thermopiles. The stops inserted in the absorption tubes during the measurements on CS_2 and COS* were not used during the present work ; their position was found to be difficult to adjust, and they were omitted since stray radiation causing galvanometer deflections on changing over from the empty to the full tube had been otherwise eliminated. Clearly they eliminate much of the shorter wave-length radiation emitted by the Nernst filament and scattered within the spectrometer, for with them in position we were able to detect the COS band at 18·96 μ ; even this procedure is not entirely satisfactory, however, since this band should show a Q branch which was not observed. We have consequently suspended investigation in the region 18 to 20 μ until some more satisfactory method had been developed.

The preliminary double monochromator was built up from monochromators of two types : the first employed the chromatic foci method first used in the long wave region by Rubens and Wood ; the second was the prism spectrometer monochromator previously described   Fig. 1 indicates the arrangement of the first type , it was of an experimental nature and could almost certainly
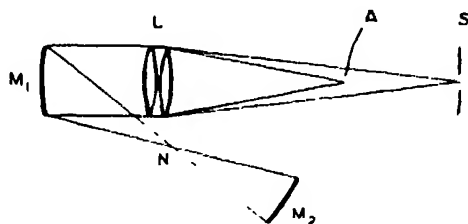
Fig. 1

be improved upon, the only lenses available being of rocksalt, and of somewhat small focal aperture. N is the Nernst filament, M_1 a stainless steel mirror, L the lenses, S the spectrometer slit, and A is a stop just larger than the visible image of the filament which appears inside the focus S for radiation of wavelength 19 μ M_1 was inserted to provide as large a solid angle of radiation falling on S as possible. The ratio of the distances LS : LA is equal to the ratio of $(\mu - 1)$ for 0·5 μ to $(\mu - 1)$ for 19 μ ; this is surprisingly large, LS/LA being approximately 1·5. The stop A, which is placed nearer to S than the visible focus, cuts out most of the shorter wave-length radiation. Lenses

* Part IV, *loc. cit.*

and plates of sylvine or potassium bromide would be required for the region beyond 18 μ, but the method might be used with advantage for shorter wavelengths where scattered radiation of still shorter wave-length must falsify results to some degree.

The Individual Bands.

Band B (the bands are lettered to correspond with those previously determined for sulphur dioxide in Part II)[*]—10·57 μ, $v_3 = 946$ cm.$^{-1}$ (fig. 2). This fundamental was investigated with the rocksalt prism and a slit width containing 5 cm.$^{-1}$; resolution into P and R branches was achieved with a
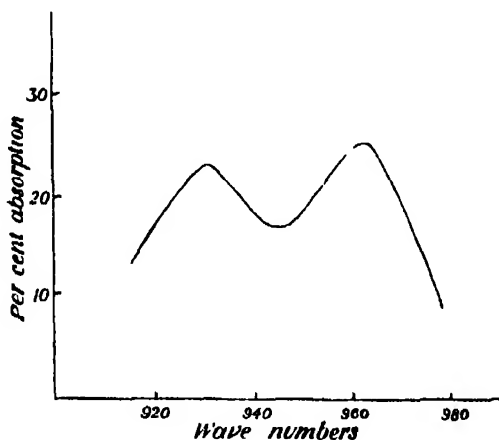
FIG. 2.

separation of 30–31 cm.$^{-1}$. No difficulty was experienced in the repeated detection of the band or in the determination of the shape of the contour of the envelope; these remarks apply equally well to the fundamental band C, and it follows that absorption of radiation through these fundamental modes of vibration produces zero or negligible decomposition of the molecule. The intensities and positions of the two bands confirm their choice as fundamentals; the corresponding frequencies selected by Urey and Johnston (*loc. cit.*) from the ultra-violet spectrum were 727 and 858 cm.$^{-1}$, and, for a molecule of this weight and probable force constants, obviously too low.

Band C.—9·017 μ, $v_1 = 1109$ cm.$^{-1}$, fig. 3. The rocksalt prism was used with a slit width enclosing 6–7 cm.$^{-1}$. It is by far the most intense band observed, and the shape of its envelope has always indicated the presence of a

[*] 'Proc. Roy. Soc.,' A, vol. 130, p. 144 (1930).

Q branch, although no complete separation of the three branches was possible; the P-R separation is again 30 cm.$^{-1}$.

Band E.—5·307 μ, $2\nu_3 = 1884$ cm.$^{-1}$. With the fluorite prism, the slit width employed included some 10 cm.$^{-1}$. It is the first harmonic of band B; as will be seen from the discussion below, the presence or absence of a Q branch is of great importance in fixing the structure of the chlorine dioxide molecule, and many attempts were made to obtain definite evidence on this point. The resolution required is just within the theoretical limit of the instrument, and
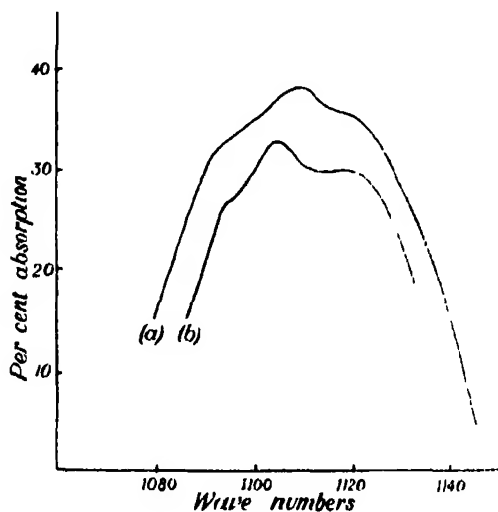
Fig. 3.

the shape of the contours observed when this condition holds must be accepted with caution. On the whole, the experimental evidence favours the existence of a Q branch, and we shall assume this to be the case. At a pressure of approximately 630 mm , 45 cm. of ClO$_2$ absorbed approximately 50 per cent. of the incident radiation.

Band F.—4·916 μ, $\nu_1 + \nu_3 = 2034$ cm.$^{-1}$. No resolution was obtained with the fluorite prism, but it is hoped to reinvestigate the contour with a grating instrument. It is a summation tone, and once again the shape is of importance for the structure of the molecule. At 630 mm. the maximal absorption was approximately 90 per cent., the slits containing 10 cm.$^{-1}$.

The Molecules of ClO$_2$ and SO$_2$: Qualitative Discussion.

The outstanding feature of the spectra of the two substances is their very close similarity. This is clearly indicated in fig. 4, which shows the positions

and approximate intensities of the bands in the two spectra, together with the resolution so far achieved   The SO_2 and ClO_2 bands at 525 and 527 cm.$^{-1}$ have not been completely observed in the infra-red and no estimate of their relative intensities can be given.   Part II of the present series reports a band at 606 cm.$^{-1}$ for SO_2 and this was adopted by us as a fundamental frequency ; it seems probable that this is to be interpreted as $\nu_3 - \nu_2$; the envelope reproduced on p. 144 of that communication indicates that the absorption falls to some low value at about 18 μ ; this is precisely the long wave limit of the apparatus, and consequently too great stress is not to be laid upon either the shape of the envelope or the maximal separation observed.   The work of Strong* in the far infra-red shows that considerable absorption exists beyond this point, and the most reasonable value for the long wave fundamental from
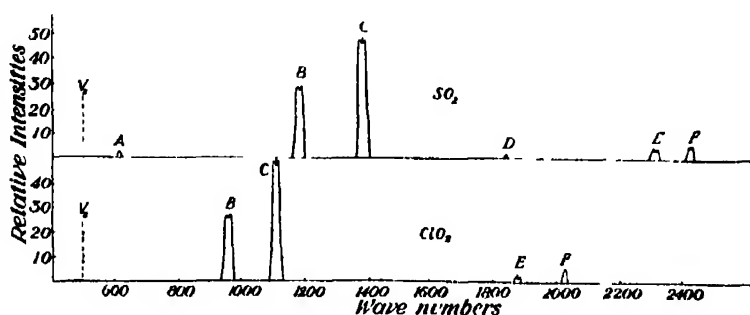
Fig. 4.

measurements of the Raman spectrum by Dickinson and West,† and others, and from the ultra-violet by Henri,‡ seems to be 525 cm.$^{-1}$.   The corresponding value for ClO_2 of 527 cm.$^{-1}$ is taken from Goodeve and Stein, and from Urey and Johnston (*loc cit.*).

As we propose to utilise the great similarity between these two spectra to amplify and correct our earlier results for SO_2, we will emphasise this feature by referring once more to fig. 4 ; the relative intensities of the observed bands for the two substances show that for both of them, a column of gas 45 cm. long and at the same pressure absorbs the same percentage of the incident radiation for any given mode.   The agreement is carried through into the contours of the bands.

These contours are determined by the orientation of the electric doublet,

* ' Phys. Rev.,' vol. 37, p. 1484 (1931).

† ' Phys. Rev.,' vol. 35, p. 1126 (1930).

‡ See Placzek, ' Ber. sächs. Ges (Akad.) Wiss. Leipzig, vol. 84, p. 98 (1931).

effective in the vibration concerned, relative to the different axes of the various moments of inertia of the molecule. For SO_2 the observed envelopes have been shown to be consistent with a triangular structure, and we are justified in assuming a similar construction for the ClO_2 molecule. The assumption of the triangular form is also supported by other evidence : for SO_2 by the high value of the permanent dipole moment, by the Kerr effect as shown by Stuart,[*] and by the presence of lines corresponding to all three fundamentals in the Raman spectrum ; for both molecules by the absence from their infra-red spectra of the peculiarities characteristic of the rectilinear triatomic molecules CO_2, CS_2 and SCO. For such substances we expect the following features : if the resultant electronic angular momentum be zero, only the longest wavelength fundamental should have a Q branch, and this should be of low intensity. Secondly, if any fundamental vibrational level has a frequency approximately twice that of another fundamental, splitting of the former into sublevels takes place ; and finally, for the symmetrical molecules, no absorbing frequency active in the infra-red should be the sum of any two other frequencies there observed. It will be seen in the case of both the substances now studied that the shortest fundamental bands possess Q branches too intense to be due to any resultant angular momentum ; whilst for ClO_2, two of the fundamental bands have frequencies nearly twice that of the third fundamental, but no doubling of the fundamental levels occurs.

Constants of the Triatomic Molecule.

Taking the triangular structure of the two substances as qualitatively established, we will now determine the various molecular constants, and of these we will first consider the vertical angles. The normal modes of vibration of the atoms in a molecule of type XY_2 have been evaluated by a number of workers.[†] Assuming the triangle to be isosceles, and the force constants for the two equal sides to be equal, we have two distinct vibrating systems to be discussed, namely, one in which a central restoring force acts between the base particles, and another where this restoring force is replaced by a restoring couple acting about an axis normal to the plane of the triangle and passing through the vertex. In both systems central restoring forces act between the mass at the vertex of the triangle and either mass at the base. We propose to apply Bjerrum's calculations to the observed spectra, and to show how the

---

[*] ' Z. Physik,' vol. 55, p. 358, and vol. 59, p. 13 (1929).

[†] See III, ' Proc. Roy. Soc.,' A, vol. 132, p. 245 (1931).

lengthy computations demanded by the normal method of application may be considerably shortened.

Bjerrum takes as the three representative co-ordinates the projections of the extensions of either side on the original direction of side ; these appear to be the simplest and, using them, Radakovic has deduced for a system of central forces expressions for the normal frequencies and modes in the general case of three unequal masses at the vertices of a scalene triangle. Sidgwick* repeats the original suggestion of Langmuir that sulphur dioxide has the structure $O = S - O$; this would necessitate unequal force constants and presumably unequal sides to the triangle. This is believed to be the case with NO_2, but the heats of linking of the two oxygen atoms differ very greatly, much more so than for SO_2. The experimental results for the latter substance are satisfied by the simpler assumption, and we shall restrict ourselves to this.
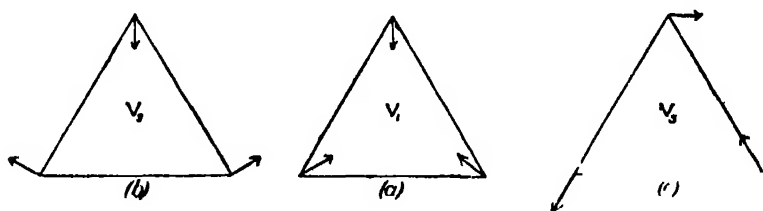
FIG. 5.

There are, corresponding to the three degrees of vibrational freedom, three normal modes, two of which are symmetrical about the bisector of the vertical angle, and a third unsymmetrical about this line, fig. 5. We shall refer to these as the symmetrical and unsymmetrical modes respectively, and, in conformity with Dennison's classification,† characterise them as v_1, v_2, v_3.

The frequency equation from which the semi-vertical angle and the force constants are deduced is a cubic in the squares of the normal frequencies ; relations between the roots of the equation and its coefficients give three equations that determine the three above unknowns. These equations as usually written are cumbersome, and the arithmetical calculations involved are readily susceptible to error. Furthermore, there is normally no indication from the experimentally observed frequencies as to which is the unsymmetrical, and the general method for its determination is to try each of the three frequencies in turn, and to note which of the three gives real solutions for the required quantities. When the complete Raman spectrum is available, it is possible to

* ' Ann. Rep. Chem. Soc.,' p. 400 (1931).
† ' Rev. Mod. Phys.,' vol. 3, p. 289 (1931).

apply the selection rules deduced by Placzek (*loc. cit.*); if, of the two short wave fundamentals, one is symmetrical and the other unsymmetrical, the more intense scattered line is to be attributed to the former. We shall revert to this point below. The simplest method of determining possible unsymmetrical frequencies is to eliminate the force constants, and so obtain an equation for the semi-vertical angle; the correct unsymmetrical frequency is that which gives a real value for this angle.

The frequency equation for the central force system may be written

$$\left[p^2 - K_1 \left\{ \frac{1}{m} + \frac{2}{M} (\sin^2 \alpha) \right\} \right] \middle| \middle| p^4 - \left\{ \frac{2K_2}{m} + \frac{K_1}{m} + \frac{2K_1}{M} \cos^2 \alpha \right\} p^2$$
$$+ \frac{2K_1 K_2}{m^2} \left(1 + \frac{2m}{M} \right) \cos^2 \alpha \right] = 0, \quad (1)$$

where m is the mass of the base particles, M the mass of that at the vertex; α is the semivertical angle; K_1 is the force constant referring to the equal sides of the triangle, and K_2 to the base; $p = 2\pi \nu c$, where ν is the normal frequency in cm.$^{-1}$.

If p_3 refers to the unsymmetrical frequency, and p_1 and p_3 to the symmetrical frequencies, then on eliminating K_1 and K_2 from the three equations relating p_1, p_2 and p_3 to the coefficients of equation (1), we obtain

$$\frac{4}{\left(1 + \frac{2m}{M} \right)} \cdot \frac{m^2}{M^2} \cdot \frac{p_1^2 p_2^2}{p_3^2} + \frac{2m}{M} (p_1^2 + p_2^2 + p_3^2) \quad \sin^2 \alpha$$

$$+ \quad \frac{4}{1 + \frac{2m}{M}} \cdot \frac{m}{M} \cdot \frac{p_1^2 p_2^2}{p_3^2} + \left(1 - \frac{2m}{M} \right)(p_1^2 + p_2^2 + p_3^2) - 2\left(1 + \frac{m}{M} \right) p_3^2 \quad \sin^2 \alpha$$

$$+ \quad \frac{1}{1 + \frac{2m}{M}} \cdot \frac{p_1^2 p_2^2}{p_3^2} - (p_1^2 + p_2^2 + p_3^2) + 2\left(1 + \frac{m}{M} \right) p_3^2 \quad = 0, \quad (2)$$

which is an equation determining α. It is convenient to handle, since large multiples of 10 are eliminated, and the observed frequencies are readily interchanged.

For the valence force system we have as frequency equation

$$\left[p^2 - K_1 \left\{ \frac{1}{m} + \frac{2}{M} \sin^2 \alpha \right\} \right] \left[\frac{m}{2} p^4 - \left[\left\{ \left(1 + \frac{2m}{M} \sin^2 \alpha \right) \cos^2 \alpha \right\} K' \right. \right.$$
$$\left. \left. + \left(\frac{1}{2} + \frac{m}{M} \cos^2 \alpha \right) K_1 \right] p^2 + K_1 K' \left(\frac{1}{m} + \frac{2}{M} \right) \cos^2 \alpha \right] = 0, \quad (3)$$

where m, M, K_1 and α are as in equation (1), and

$$K' = \frac{K_\theta}{4\cos^2\alpha}.$$

K_θ is the tangential restoring force per unit arc displacement of the vertical angle, that is, the potential energy due to a displacement $d\theta$ of this angle is $\frac{1}{2}K_\theta l^2 (d\theta)^2$, where l is the length of either equal side. Performing the operations on equation (3) that we applied to equation (1), we have

$$\frac{p_1^2 p_2^2}{p_3^2} \cdot \frac{x^3}{1 + \frac{2m}{M}} - (p_1^2 + p_2^2 + p_3^2)\,x + 2p_3^2\left(1 + \frac{m}{M}\right) = 0, \qquad (4)$$

where $x = 1 + \frac{2m}{M}\sin^2\alpha$. (4) is a cubic of reduced form to be numerically solved for x, and permutation of p_3 among the observed frequencies is comparatively simple.

When the possible unsymmetrical frequencies and the corresponding semi-vertical angles have been determined by means of formulæ (2) and (4), the force constants can be calculated as follows :—

$$K_1 = \frac{m p_3^2}{\left(1 + \frac{2m}{M}\sin^2\alpha\right)}, \qquad (5)$$

$$K_2 = \frac{m}{2}(p_1^2 + p_2^2) - \left(1 + \frac{2m}{M}\cos^2\alpha\right)K_1, \qquad (6)$$

$$K_\theta = 2\frac{p_1^2 p_2^2}{p_3^2} \cdot \frac{m\left(1 + \frac{2m}{M}\sin^2\alpha\right)}{\left(1 + \frac{2m}{M}\right)}. \qquad (7)$$

It should be noticed that equation (5) determines K_1 for both the central and valence force systems.

The Molecules of ClO_2 and SO_2 : Quantitative Discussion.

On applying the above considerations to the observed spectra for SO_2 and ClO_2, we obtain the molecular characteristics displayed in Tables II (*a*) and (*b*) ; these give the possible unsymmetrical frequencies with their corresponding semi-vertical angles, and the force constants for the two systems.

Table II.

(a) Central Force System for SO_2 and ClO_2.

Molecule.	Possible unsymmetrical frequency ν_2.	Semi-vertical angle.	K_1.	K_2.
	cm.$^{-1}$	°	dynes/cm. $\times 10^{-5}$	dynes/cm. $\times 10^{-5}$
SO_2	1152	32	9 6	1 7
SO_2	1152	57	7·25	5·2
ClO_2	946	33	6·7	1·8
ClO_2	946	48	5 7	3·0

(b) Valence Force System for SO_2 and ClO_2.

SO_2	1152	32	9 6	4 6
SO_2	1361	61	9·8	3·3
ClO_2	946	29	6·7	4·5
ClO_2	1109	70	6·1	3·6

The problem now is to determine which of these solutions is consistent with other observed data, and in effect to decide between the acute and obtuse angled triangles. At this point we can stress another similarity between the two molecules ; the electronic band spectra have been explored in the ultra-violet region, for SO_2 recently by Watson and Parker,[*] and for ClO_2 as already cited. The two spectra are very much alike ; in particular, in both cases the plot of the frequency difference between successive band heads against integers gives a straight line up to a definite integer, when the curve breaks to a second straight line inclined to the first. This phenomenon is of very rare occurrence, and Urey has attributed this discontinuity to the swinging of the isosceles triangle with a large vertical angle through a linear model to a second isosceles triangle with an acute vertical angle, the former corresponding to the ground electronic state. However, as we have seen, this hypothesis depends upon the assumption of incorrect values for the fundamental frequencies, and we have consequently no definite evidence from the ultra-violet upon the size of the vertical angle ; the remaining data from the infra-red provide (i) the relative intensities of the observed bands, and (ii) the contours of the envelopes, which indicate the presence or absence of a Q branch. We shall consider the latter feature in some detail.

In Part II, the presence or absence of Q branches was shown to depend upon the orientation of the electric doublet effective in a given vibration relative to the axes of the three moments of inertia, and quantum mechanical investigations (Dennison, *loc. cit.*) give this orientation for the fundamental and combination tones. The results may be summarised thus : if the frequency of any observed infra-red band be given by $(n_1\nu_1 + n_2\nu_2 + n_3\nu_3)$, where ν_1 and ν_2 are the frequencies of the symmetrical modes, fig. 5, a and b, and ν_3 is the frequency of the unsymmetrical mode, fig. 5, c, then the electric doublet effective in the vibration is parallel to the bisector of the vertical angle when n_3 is even, and normal to this line when n_3 is odd ; n_1 and n_2 may assume any value, and when n_3 is zero the effective doublet is always parallel to this bisector. Knowing the orientation relative to the bisector, we also know it with regard to the axis of least inertia, since this is either parallel or perpendicular to the former. Which of these cases holds depends finally upon the vertical angle and upon the masses of the atoms composing the molecule. The three moments of inertia are $A < B < C$, and since we are dealing with a plane molecule, $A + B = C$. Furthermore, the moment of inertia about the bisector of the vertical angle 2α is $2ml^2 \sin^2 \alpha$, and that about an axis perpendicular to this line, passing through the centre of mass, and lying in the plane of the triangle is $(2mM/(M + 2m))l^2 \cos^2 \alpha$. Hence the axis of least inertia will be parallel or perpendicular to the bisector of the vertical angle according as $(M/(M + 2m)) \cos^2 \alpha >$ or $< m \sin^2 \alpha$, *i.e*, as $\tan^2 \alpha <$ or $> M/(M + 2m)$. For SO_2 and ClO_2 the critical value is found to be 35°. Hence if α is less than this value, the axis of least inertia is parallel to the bisector of the vertical angle, and perpendicular to it if α is greater than 35°.

This inequality, together with the selection rules derived from quantum mechanics and quoted above, gives the orientation of the electric doublet effective in the various bands relative to the axes of inertia for the various possible models. These are summarised in Table III , where the direction of vibration of the doublet is shown as either parallel or perpendicular to the least axis of inertia, since for the planar molecule there can be no vibrating doublet along the axis of greatest inertia, Table III specifies the orientation completely.

In the discussion in Part II referred to above, we also deduced qualitatively that if the effective electric doublet be perpendicular to the axis of least inertia, the observed band should consist only of P and R branches, whilst if the doublet be parallel to this axis, the band should show a Q branch in addition ; this

Table III.—The Orientation of the Effective Electric Doublet relative to the Least Axis of Inertia for the various possible Molecular Models of SO_2 and ClO_2.

(a) The unsymmetrical frequency ν_3 is taken as 1152 and 946 cm.$^{-1}$ respectively.

Band.	Mode *	Frequency.		Force system.			
		SO_2.	ClO_2.	Central.		Valence.	
				$a < 35°$	$a > 35°$	$a < 35°$	$a > 35°$
		cm $^{-1}$	cm $^{-1}$				
C	ν_1	1361	1109	Parallel	Perpendicular	Parallel	No solution
—	ν_2	524	527	,,	,,	,,	,,
B	ν_3	1152	946	Perpendicular	Parallel	Perpendicular	,,
A	$\nu_3 - \nu_2$	606	—	,,	,,	,,	,,
D	$\nu_1 + \nu_2$	1871	—	Parallel	Perpendicular	Parallel	,,
E	$2\nu_2$	2305	1184	,,	,,	,,	,,
F	$\nu_1 + \nu_3$	2499	2034	Perpendicular	Parallel	Perpendicular	,,

(b) The unsymmetrical frequency ν_3 is taken as 1361 and 1109 cm.$^{-1}$ respectively.

Band.	Mode *	SO_2	ClO_2	Central $a<35°$	Central $a>35°$	Valence $a<35°$	Valence $a>35°$
B	ν_1	1152	946	No solution	No solution	No solution	Perpendicular
—	ν_2	524	527	,,	,,	,,	,,
C	ν_3	1361	1109	,,	,,	,,	Parallel
A	$\nu_1 - \nu_2$	606	—	,,	,,	,,	Perpendicular
D	$\nu_2 + \nu_3$	1871	—	,,	,,	,,	Parallel
E	$2\nu_1$	2305	1884	,,	,,	,,	Perpendicular
F	$\nu_1 + \nu_3$	2499	2034	,,	,,	,,	Parallel

* See fig. 5, p 629.

criterion has been quantitatively investigated by Dennison with the aid of the quantum mechanics, and he arrives at the same conclusion.

In applying these principles to the observed spectrum, it must be remembered that the accuracy of the deduction depends upon the degree of resolution obtainable, and that further examination by a grating spectrometer is necessary before finality is reached. Meyer, Bronk and Levin* explored band F in this way, and found no evidence of a Q branch of any intensity, while our own results for band B in both SO_2 and ClO_2 show P and R branches only. Table III renders this consistent with a vertical angle of less than 70° on both the force systems ; the envelopes of band C are identical for the two substances,

* 'J. Opt. Soc. Amer.,' vol. 15, p. 257 (1927).

and although complete resolution has not been attained, nevertheless the available evidence points to the existence of a powerful Q branch, thus denying the possibility of a central force system with vertical angle greater than 70° if C is a symmetrical frequency. On the other hand, the valence force system with the larger angle permits the presence of this Q branch when band C is taken as the unsymmetrical frequency. Now band E for ClO_2 occurs at some 400 cm.$^{-1}$ on the longer wave side for the corresponding band for SO_2 and the resolution obtained for the former is slightly better ; the envelope shows traces of a Q branch in this band for ClO_2 which may be concealed in the broad P branch of the SO_2 band. If this is so, the only possible solution demands a central force system with an angle α of $< 35°$

While the present work has been in preparation, Dadieu and Kohlrausch[*] have published a paper on the Raman effect and molecular structure of simple triatomic molecules. They adopt the obtuse angled triangle for SO_2, with 1361 cm.$^{-1}$ as the unsymmetrical frequency, and suggest that the Q branch observed by us in this band is due to the presence of water vapour. Whenever we have obtained the water vapour band in this region, we have always obtained easy resolution of the band into the two widely separated maxima ; furthermore, the corresponding ClO_2 band has exactly the same shape but occurs some 260 cm.$^{-1}$ on the long wave side at 1109 cm.$^{-1}$. However, reference to Table III will show that the structure put forward by Dadieu and Kohlrausch requires the presence of a Q branch, and the suggestion of the presence of an impurity is thus inconsistent with their own deductions.

Dennison has demonstrated that the fine structure of the vibration-rotation bands in the infra-red is intimately bound up with the numerical ratio of the least to the intermediate moment of inertia, and some estimate of the shape of the envelope for a given band can be made from the extremely useful chart in his paper ; this shows the variation in the fine structure as the above ratio changes from unity to zero. When the vertical angle is 35°, the two smaller moments are equal and our molecules are symmetrical tops , in that case the bands B and C would show the same envelope, contrary to observation. If A/B is 0·65 ($\alpha = 30°$), the chart indicates that band C should possess a considerable Q branch, while band B should have none. These points are emphasised to illustrate the considerable change to be expected in the spectrum for comparatively small changes in the vertical angle.

The degree of resolution obtained in the case of ClO_2 is, with the exception

* ' Phys. Z.,' vol. 33, p. 165 (1932).

noted, not so satisfactory as in the previous work on SO_2. The slightly coarser outline of the bands is perhaps to be attributed to the isotope effect, and although it is not sufficient to produce any actual separation of maxima for the dioxide, it may well produce a broadening of the bands, and so render the observed maxima less distinct. In the case of the monoxide the effect may be expected to be considerable for certain bands.

Molecular Dimensions.

When Part II of the present series was written, in default of other evidence, band A at 606 cm.$^{-1}$ was chosen as a fundamental frequency; the existence of a frequency difference of this value had been previously recognised by Coblentz,[*] and peculiarly enough in two cases where we had failed to isolate the bands. The temptation to adopt this as a fundamental frequency was too great, and the assumption that the separation of 9 cm.$^{-1}$ observed corresponded to the greatest moment of inertia led to abnormally large values for the interatomic distances. Probably no great reliance is to be placed on the observed separation since the readings were taken at the extreme limit of usefulness of the spectrometer. The maximal P and R branch separations recorded for the other bands prove to be the same for both molecules. We accordingly have to associate these more accurately observed separations with the moments of inertia concerned; for this we must have recourse once more to the considerations propounded by Dennison in the paper cited.

We have seen that if the semi-vertical angle is 35°, the molecules become symmetrical tops with electric doublets vibrating in the plane normal to the symmetry axis or axis of greatest inertia, and observed bands have only P and R branches, while the separation of the two maxima corresponds to the greatest moment of inertia. Reference to Dennison's paper and to those of Kramers and Ittmann[†] shows that a top whose motions are governed by quantum mechanics behaves differently from a top moving according to classical mechanics; in particular, as the top changes from a symmetrical to an asymmetrical rotator, there is no abrupt change in its motions such as was demanded by the older system,[‡] where the top may spin about its axis of greatest or of least inertia, and where its motions depend upon the axis of spin. According to the new system, the transitions for an asymmetrical top

[*] "Investigations of Infra-red Spectra," Part I, p. 52.

[†] 'Z. Physik,' vol. 60, p. 663 (1930); et ante.

[‡] Bailey, Cassie and Angus, 'Trans. Faraday Soc.,' vol. 26, p. 197 (1930).

change continuously from the limit where the smaller moments of inertia are equal to that where the least moment of inertia vanishes. At the first limit observed bands have only P and R branches whose separation gives the greatest moment of inertia, and at the second limit the band due to vibrations of the doublet parallel to the least axis of inertia has P and R branches with a Q branch vanishing because of the Boltzmann factor, whilst that due to vibrations parallel to the intermediate axis of inertia consists of lines which tend to become infinitely far apart, the separation corresponding to the vanishing least moment of inertia. Hence near the first limit the P and R branches approximate to those of a diatomic molecule whose moment of inertia equals the greatest moment for the triangular molecule. Near the second limit, the band due to vibrations parallel to the intermediate axis will have separations corresponding to those of a diatomic molecule with a moment of inertia equal to the least moment for the triatomic.

The models deduced for ClO_2 and SO_2 approximate to the first limit, and the P and R branch separation should give a moment of inertia rather less than the greatest. The frequency difference of 30 cm.$^{-1}$ corresponds to a moment of inertia of 4.7×10^{-39} g. cm.^{2}; if this were the greatest moment and the vertical angle 60°, the length of each side of the triangle would be $1.2A$. Wierl[*] using the electron diffraction method, found that the sulphur and oxygen nuclei in SO_2 were separated by 1.37 A., and this value is consistent with the qualitative infra-red estimate of slightly greater than 1.2 Å. It is interesting to compare these measurements with the interatomic separation in sulphur monoxide, SO; Henri and Wolff obtained the rotational fine structure of this substance in the ultra-violet,[†] and found 1.34 Å. for this distance.

The same dimensions may be expected to hold good for the chlorine compound. The spectroscopic similarity leads one to enquire whether the phenomenon persists in other physical properties; we find the melting points, boiling points, surface tensions, and molecular volumes, of the ascertainable physical data, much the same in both cases. The cause of the similarity is probably to be found in the electronic structure of the two substances. The "odd" electron in the chlorine compound confers paramagnetic properties upon the dioxide, and is presumably responsible for its chemical instability; it appears, however, to be incorporated in the structure in such a way that,

* 'Phys. Z.,' vol. 31, p. 1028 (1930).

† 'J. Phys. Radium,' vol. 10, p. 81 (1929).

although necessarily unpaired, it takes no part in structure formation, and the two substances are almost isosteres.

The recent work of Slater,[*] Pauling,[†] and Hund[‡] exemplifies the quantum and wave mechanical significance of directed valence. Hund has extended and modified the conception; directed valences, equivalent to the valence stroke as written by chemists, are characterised by localisation of the electronic proper-functions concerned; he shows that localisation is obtained if there exist proper-functions of single electrons from each atom for binding purposes, and also sufficient electrons to fill the resulting proper-functions of the molecule. The most important case of non-localised bonds then arises when the electrons present are too few to satisfy each possible directed bond with two electrons. Hund's paper should be consulted for examples, but the general procedure in molecule formation is as follows : if localised bonds are possible, σ bonds take energetic preference over π bonds, while a double bond in all cases is a $\sigma\pi$ bond ; the subsequent formation of triple bonds and the various spatial arrangements need not be discussed here, but it may be pointed out that when, for example, in a q^4 atom space considerations such as occur in the cyclo-paraffins prevent the formation of localised bonds, these are replaced by non-localised bonds with a smaller stability betrayed in a larger heat of combustion. In other cases where we have an electron deficiency we may have localised σ bonds with superimposed non-localised π bonds. In the case of sulphur dioxide, where for each atom, two electrons are lacking from a complete outer shell, the " holes " may be treated as electrons,[§] the energy expression being the same as for the presence of two electrons outside a closed shell. The simplest picture of the formation of the molecule from the individual atoms would then suppose the formation of a σ bond between the sulphur and each oxygen atom, thus involving four " electrons " of probably the (2, 1, 0) type ; the remaining electrons on the oxygen atoms (one each, of (2, 1, 1) or (2, 1, —1) type) may be deemed to occupy a proper-function giving a non-localised π bond. Proper-functions for two double bonds, which would consist each of a localised σ and a localised π bond, cannot be obtained from the two " electrons " of the sulphur, and would apparently necessitate a rectilinear structure in any case. The first structure suggested meets with confirmation from the value

[*] ' Phys. Rev.,' vol. 37, p. 481, and vol. 38, p. 1109 (1931).

[†] ' J. Amer. Chem. Soc.,' vol. 53, p. 1367, and p. 3237 (1931).

[‡] ' Z. Physik,' vol. 73, p. 1, and p. 565 (1931).

[§] Heisenberg, ' Ann. Physik,' vol. 10, p. 888 (1931).

of the force constant K_1, which is approximately 9×10^5 dynes/cm., intermediate between the values for a single and a double bond.

Turning to the chlorine compound, we have five holes of a p type to allocate ; it is important to note that in the allotment of electrons to the molecular proper-functions we must consider the molecule as a whole, and fill up the proper-functions with the available electrons ; this procedure renders it likely that we have σ type single bonds between the chlorine atom and each oxygen, while the odd electron incompletely fills a non-localised proper-function, and thus accounts for the instability of the substance. The force constant is approximately 6×10^5 dynes/cm , and confirms the choice of the single bond plus an incompletely filled non-localised proper-function.

Reverting finally to the preference of the acute over the obtuse angled structure, we would emphasise that the choice of the former rests upon the assumptions that Dennison's selection rules are correct and that complete resolution has been obtained in the critical bands ; the equilateral triangle also seems the most plausible structure for a triatomic molecule with a non-localised proper-function, and gives the correct interatomic separation, whereas the obtuse angled form gives a distance of some $2 \cdot 3$ Å. between the sulphur and oxygen atoms Against this interpretation we have to set the fact that band B is the most intense in the Raman spectrum, and Placzek's selection rules indicate this as the symmetrical frequency of the two short wave fundamentals, while the change of electric moment, and consequently the intensity in the infra-red, is usually greatest for the unsymmetrical frequency, which should then be band C. It is possible that the introduction of the non-localised proper-function may contravert Placzek's rules, and we have in addition little knowledge of the actual amplitudes of vibration in the various fundamentals. Because of the difficulty of reconciling the diverse evidence, it may be best to leave the question open and to summarise the two possible structures as in Table IV. We have recently completed an examination of the infra-red absorption spectrum of chlorine monoxide, and propose to leave any discussion of the thermochemistry of the dioxide until we can collate the results for the two substances.

Summary.

(1) The infra-red absorption spectrum of chlorine dioxide has been examined and compared with that of sulphur dioxide.

(2) The two substances are spectroscopically and physically alike, and have similar structures.

Table IV.—The Molecular Characteristics of SO_2 and ClO_2 for the Acute and Obtuse Angled Forms.

(a) The Acute Angled Structure.

(Central forces provide the possible solution in each case.)

SO₂.		ClO₂.	
Fundamental frequencies.	Force constants.	Fundamental frequencies.	Force constants.
cm⁻¹.	× 10⁻⁵ dynes/cm.	cm.⁻¹	× 10⁻⁵ dynes/cm.
$\nu_1 = 1361$	K_1 9 6 (S — O)	$\nu_1 = 1109$	K_1 6 7 (Cl — O)
$\nu_2 = 524$	K_2 1·7 (O — O)	$\nu_2 = 527$	K_2 1 8 (O — O)
$\nu_3 = 1152$		$\nu_3 = 946$	
$O\widehat{S}O = 60°$, S—O and O—O = 1 37 Å.		$O\widehat{Cl}O = 60°$, Cl—O and O—O = 1·4 Å.	

(b) The Obtuse Angled Structure.

(Valence forces provide the possible solution in each case.)

cm.⁻¹	× 10⁻⁵ dynes/cm.	cm.⁻¹	× 10⁻⁵ dynes/cm.
$\nu_1 = 1152$	K_1 9 6 (S — O)	$\nu_1 = 946$	K_1 6 7 (Cl — O)
$\nu_2 = 524$	K_ϕ 3 3 (O — O)	$\nu_2 = 527$	K_ϕ 3 6 (O — O)
$\nu_3 = 1361$		$\nu_3 = 1109$	
$O\widehat{S}O = 122°$, S—O = 2 3 Å., O—O = 3 9 Å.		$O\widehat{Cl}O = 140°$, Cl—O = 2 4 Å., O—O = 4·2 Å.	

(3) The available evidence permits of two possible structures with vertical angles of approximately 60° and 120° respectively, the weight of probability being slightly in favour of the acute angled form.

(4) The electronic structure has been discussed, and values for the molecular characteristics have been derived.

Perturbations and Rotation Constants of some First Negative Nitrogen Bands.

By W. H. J. Childs, B.Sc , Ph.D., Davy-Faraday Research Laboratory.

(Communicated by Sir William Bragg, F.R S —Received May 12, 1932.)

[Plate 21.]

During the course of a systematic programme of intensity measurements of band spectra it was considered advisable to include some measurements of the first negative nitrogen bands. These bands are emitted by the ionised nitrogen molecule and show very clearly the interesting phenomenon of alternating intensities. It was soon found, however, that the particular source employed possessed a number of useful properties, not least of which was its ability to excite in a selective manner the negative bands so that they were practically free from the usually troublesome second positive group. In addition, the bands were excited to such unusually high rotational levels that in this way a number of large and hitherto unobserved perturbations were revealed. It is the purpose of this paper to discuss these perturbations in detail ; the other characteristics of this type of excitation will be discussed elsewhere.

Experimental.

The bands were excited in an ordinary Pointolite lamp, that is, in a comparatively low voltage (70 v.) tungsten arc in pure nitrogen at about 10 cm. pressure. Under these circumstances the 0, 0 ; λ 3914 band was obtained entirely unobscured, whilst the 0, 1 ; λ 4278 band contained but slight traces of the 1, 2 ; λ 4237 band. They were photographed in the second order of a 21-feet concave grating of the Physikalisches Institut, Bonn ; in the case of λ 3914 two satisfactory plates being obtained with exposure times of 6 hours whilst for λ 4278 only one plate was obtained with an exposure of 10 hours. The plates were measured in the usual way, precautions being taken to eliminate any possible errors of the screw of the measuring micrometer. Intercomparison of the several sets of measurements (four) for each plate shows that the relative accuracy attained is about 0·06 cm. ⁻¹—this is the mean error for a large number of lines—whilst the two plates of λ 3914 indicate that for this band the absolute accuracy is also of the same order. For the purposes of this paper, however, the absolute accuracy is of lesser importance, since the information to be discussed is derived from measurements within a single band. Intensities were obtained from plates taken in the first order using the "raster"

method of Frerichs.* Since this paper is concerned primarily with the perturbations it will suffice to say that these plates were photometered with a Moll type recording microphotometer and the intensities evaluated from the density records in the usual manner. These intensity measurements will form the subject of a separate communication. A portion of the 0, 0 band is reproduced in Plate 21 with below it for comparison a photograph of the band as it appears when excited at the hollow cathode of a Geissler tube. The remarkable change in the appearance of the band is at once evident ; the branches can be followed to about K = 80 (in a plate taken under smaller dispersion to K = 100) and this extension combined with freedom from extraneous lines makes the band under high dispersion a very fine example of its kind.

The results of the measurement of these two bands are given in Tables I and II. The bands have already been measured to K = 30 by Fassbender† and more recently by Coster and Brons,‡ and use has been made of Fassbender's measurements to supplement the tables for R(0) and R(1) which were too faint to measure, and for the lines P(1) to P(12), *i.e.*, from the origin to the head, which were unresolvable owing to their Doppler width caused by the high effective temperature of the source. It is due to this width that the close doublets of which these bands are composed were not fully resolved until K = 20 approximately, although with the Geissler tube source and similar resolving power they can be resolved at K = 14 or less.

Table I.—The numbering is according to the modern notation. The high frequency component of the doublets is associated with $(K + \frac{1}{2})$ except in the perturbed regions, where the assignments are given at the side.

	R branch.			P branch.	
K.	λ (air).	ν (vacuum).	K.	λ (air)	ν (vacuum).
0	3909 71 F	25570 10	0		
1	09 04 F	74 54	1	3910 94 F	25562 10
2	08 298	79 37	2	11 48 F	58 58
3	07 533	84 38	3	11 97 F	55 34
4	06 703	89 81	4	12 43 F	52 38
5	05 841	95 46	5	12 82 F	49 79
6	04 927	25601 45	6	13 18 F	47 44
7	03 969	07 73	7	13 50 F	45 40
8	02 956	14 38	8	13 76 F	43 69

F = Fassbender's measurement.

* ' Z. Physik,' vol. 31, p. 305 (1925).

† ' Z. Physik,' vol. 30, p. 73 (1924).

‡ ' Z. Physik,' vol. 73, p. 747 (1932).

Table I—(continued).

	R branch.			P branch.	
K.	**λ (air)**	**ν (vacuum).**	**K.**	**λ (air)**	**ν (vacu**
9	3901 915	25621 21	9	3913 96 F	25542 34
10	00 829	28 34	10	14 15 F	41 14
11	3899 713	35 68	11	14 25 F	40 44
12	98 499	43 66	12	14 34 F	39 91
13	97 267	51 77	13	14 34 F	39 91
14	95 996	60 13	14	14 331	39 94
15	94 675	68 84	15	14 249	40 48
16	93 309	77 84	16	14 136	41 22
17	91 900	87 14	17	13 969	42 30
18	90 451	96 71	18	13 770	43 60
	90 422	96 90	19	13 516	45 26
19	88 964	25706 53	20	13 215	47 23
	88 932	06 74	21	12 878	49 43
20	87 428	16 69	22	12 511	51 82
	87 389	16 95		12 471	52 08
21	85 833	27 24	23	12 072	54 69
	85 801	27 46		12 037	54 92
22	84 213	37 97	24	11 582	57 89
	84 170	38 26		11 542	58 15
23	82 529	49 14	25	11 051	61 36
	82 490	49 40		11 015	61 60
24	80 825	60 44	26	10 473	65 14
	80 780	60 74		10 427	65 44
25	79 057	72 18	27	09 842	69 27
	79 016	72 46		09 804	69 51
26	77 266	84 09	28	09 172	73 65
	77 218	84 41		09 127	73 94
27	75 414	96 41	29	08 454	78 35
	75 376	96 66		08 414	78 61
28	73 540	25808 89	30	07 694	83 32
	73 481	09 28		07 647	83 63
29	71 601	21 82	31	06 882	88 64
	71 556	22 12		06 836	88 94
30	69 633	34 95	32	06 034	94 19
	69 577	35 32		05 980	94 54
31	67 621	48 39	33	05 130	25600 12
	67 572	48 71		05 085	00 41
32	65 554	62 21	34	04 187	06 30
	05 519	62 44		04 137	06 63
33	63 485	76 06	35	03 198	12 79
	63 421	76 49		03 145	13 14
34	61 351	90 36	36	02 180	19 47 (K −½)
	61 289	90 77		02 119	19 87 (K +½)
35	59 362	25903 71 (K −½)	37	01 286	25 34 (K −½)
	59 134	05 23 (K +½)		01 054	26 86 (K +½)
36	56 933	{ (19 93) (K +½)	38	3899 953	34 10 (K +½)
		(20 17) (K −½)		99 922	34 30 (K −)
37	54 854	33 99 (K −½)	39	98 948	40 71 (K +
	54 717	34 91 (K −½)		98 801	41 67 (K −½)
38	54 160	38 66 (K +½)	40	99 378	37 88 (K +½)
	52 609	49 11 (K +½)		97 791	48 32 (K −
	51 453	56 89 (K +½)		96 613	56 07 (K +
39	49 767	68 26 (K −½)	41	95 996	60 13 (K −
	49 708	68 66 (K +½)		95 964	60 34 (K +)

Fassbender's measurement

Table I—(continued).

R branch.			P branch.		
K.	λ (air)	ν (vacuum).	K.	λ (air).	ν (vacuum)
40	3847 510	25983 49 (K−½)	42	3894 830	25667 82 (K−½)
	47 432	84 02 (K+½)		94 753	68 32 (K+½)
41	45 114	99 68 (K−½)	43	93 509	76 52
	45 114	99 68 (K+½)		93 509	76 52 (K+½)
42	42 658	26016 30	44	92 106	85 78
	42 482	17 49		91 930	86 94
43	40 154	33 27	45	90 667	95 28
	40 028	34 12		90 535	96 15
44	37 625	50 42	46	89 182	25705 09
	37 503	51 25		89 066	05 86
45	35 041	67 97	47	87 652	15 21
	34 930	68 73		87 534	15 99
46	32 410	85 81	48	86 073	25 66
	32 313	86 53		85 962	26 39
47	29 759	26103 93	49	84 447	36 42
	29 656	04 63		84 346	37 09
48	27 067	22 29	50	82 779	47 48
	26 960	23 02		82 675	48 17
49	24 323	41 03	51	81 065	58 85
	24 227	41 69		80 963	59 53
50	21 548	60 01	52	79 314	70 48
	21 447	60 70		79 209	71 17
51	18 738	79 26	53	77 513	82 45
	18 642	79 92		77 414	83 10
52	15 884	98 84	54	75 671	94 70
	15 790	99 49		75 573	95 35
53	12 971	26218 85	55	73 795	25807 19
	12 889	19 42		73 687	07 91
54	10 079	38 75	56	71 858	20 10
	09 981	39 43		71 758	20 77
55	07 121	59 14	57	69 883	33 28
	07 026	59 80		69 792	33 89
56	04 122	79 84	58	67 870	46 72
	04 025	80 51		67 773	47 37
57	01 098	26300 75	59	65 821	60 42
	00 999	01 43		65 713	61 14
58	98 030	21 99	60	63 730	74 42
	97 936	22 65		63 629	75 09
59	94 934	43 47	61	61 580	88 82
	94 839	44 13		61 494	89 40
60	91 801	65 23	62	59 402	25903 43
	91 710	65 87		59 323	03 96
61	88 641	87 22 (K−½)	63	57 202	18 21
	88 547	87 88 (K+½)		57 109	18 83
62	85 368	26410 04 (K+½)	64	54 877	33 84 (K+½)
	85 239	10 94 (K −½)		54 740	34 76 (K−½)
63	82 325	31 29 (K−½)	65		
	82 171	32 36 (K+½)		52 609	49 11 (K+½)
64	79 149	53 50	66	50 519	63 19
	79 049	54 20		50 413	63 90
65			67	47 472	83 76
	3775 083	81 99 (K+½)		47 355	84 54
66	72 111	26502 85	68	45 298	98 44
	71 992	03 69		45 186	99 20
67	68 774	26 32	69	42 885	26014 77
	68 708	26 78		42 795	15 37

Table I—(continued).

	R branch			P branch	
K.	λ (air)	ν (vacuum)	**K.**	λ (air).	ν (vacuum).
68	3765 390	26550 16	70	3840 392	26031 65
	65 251	51 14		40 253	32 59
69	61 954	74 41	71		
	61 842	75 20		Weak	Weak
70	58 496	98 86	72	35 274	66 39
	58 388	99 62		35 166	67 12
71	55 000	26623 62 (K + ½)	73	32 664	84 14 (K + ½) ?
	54 887	24 42 (K - ½)		32 555	84 88 (K − ½)
72	51 467	48 69	74	29 993	26102 33
	51 368	19 40		29 887	03 05
73	Weak	Weak	75	Weak	Weak
74	44 320	99 56	76	24 558	39 42
	44 223	26700 25		24 450	40 16
75	Weak	Weak	77	Weak	Weak
76	37 032	51 63	78	18 976	77 63
	36 945	52 25		18 875	78 32
77	Weak	Weak	79	Weak	Weak
78	29 653	26804 55	80	13 236	26217 03
	29 568	05 16		13 150	17 62
79	Weak	Weak	81	Weak	Weak
80	22 151	58 58	82	07 334	57 62
	22 102	58 93			
81	Weak	Weak			
82	14 048	26917 17			

Table II.—The numbering is according to the modern notation. The **high frequency** component of the doublets is associated with (K + ½), **except** in the perturbed regions, where the assignments are given at the side.

	R branch			P branch	
K	λ (air)	ν (vacuum)	K	λ (air)	ν (vacuum)
0	4273 14 F	23395 43	0		
1	72 32 F	99 93	1	4274 60 F	23387 46
2	71 458	23404 65	2	75 23 F	84 00
3	70 543	09 66	3	75 80 F	80 88
4	69 507	15 34	4	76 31 F	78 09
5	68 442	21 18	5	76 76 F	75 65
6	67 310	27 40	6	77 13 F	73 59
7	66 111	33 98	7	77 46 F	71 79
8	64 865	40 83	8	77 72 F	70 38
9	63 545	48 08	9	77 90 F	69 39
10	62 176	55 62	10	78 04 F	68 65
11	60 740	63 52	11	78 11 F	68 28
12	59 247	71 74	12	78 11 F	68 28
13	57 689	80 33	13	78 103	68 29
14	56 974	80 24	14	77 949	69 14

F = Fassbender's measurement.

Table II—(continued).

	R branch.			P branch	
K.	λ (air).	ν (vacuum).	K.	λ (air).	ν (vacuum).
15	4254 390	23498 54	15	4277 744	23370 26
16	52 659	23508 11	16	77 521	71 47
17	50 881	17 94	17	77 191	73 28
18	48 996	28 37	18	76 843	75 18
19	47 081	38 98	19	76 426	77 48
20	45 086	50 04	20	75 920	80 22
21	43 066	61 25	21	75 364	83 26
	43 040	61 40	22	74 738	86 69
22	40 998	72 74	23	74 053	90 44
	40 952	73 00			
23	38 841	84 74	24	73 305	94 53
	38 797	84 98			
24	36 637	97 00	25	72 494	98 97
	36 591	97 26	26	71 642	23403 64
25	34 371	23609 63		71 588	03 93
	34 300	10 03	27	70 713	08 73
26	32 048	22 59		70 658	09 03
	31 991	22 91	28	69 719	14 18
27	29 668	35 88		69 658	14 51
	29 614	36 18	29	68 655	20 01
28	27 236	49 48		68 603	20 30
	27 175	49 82	30	67 544	26 11
29	24 742	63 44		67 483	26 45
	24 684	63 77	31	66 360	32 61
30	22 201	77 68		66 299	32 95
	22 126	78 11	32	65 127	39 39
31	19 580	92 39		65 060	39 75
	19 527	92 69	33	63 815	46 60
32	16 928	23707 29		63 758	46 91
	16 868	07 63	34	62 467	54 01
33	14 204	22 62		62 399	54 39
	14 159	22 87	35	61 038	61 88
34	11 471	38 01		60 984	62 18
	11 389	38 47	36	59 583	69 89 (K−½)
35	08 864	52 71 (K−½)		59 508	70 31 (K+½)
	08 581	54 31 (K+½)	37	58 267	77 15 (K−½)
36	05 741	70 35' (K+½)		57 988	78 68 (K+½)
	05 695	70 61 (K−½)	38	56 430	87 28 (K+½)
37	02 980	85 96 (K+½)		56 371	87 60 (K−½)
	02 833	86 80 (K−½)	39	54 945	95 48 (K+½)
				54 766	96 46 (K−½)
38	01 924	91 94 (K+½)	40	55 184	94 16 (K+½)
	00 073	23802 43 (K−½)		53 290	23504 62 (K−½)
	4198 701	10 21 (K+½)		51 886	12 38 (K+½)
39	96 447	22 99 (K−½)	41	50 881	17 94 {(K−½) / (K+½)}
	96 364	23 47 (K+½)			
40	93 485	39 82 (K−½)	42	49 195	27 27 (K−½)
	93 392	40 35 (K+½)		49 099	27 80 (K+½)
41	90 372	57 53 (K−½)	43	47 325	37 63 (K−½)
	90 372	57 53 (K+½)		47 325	37 63 (K+½)
42	87 168	75 79	44	45 358	48 53
	86 960	76 97		45 146	49 71
43	83 919	94 33	45	43 335	59 76
	83 765	95 21		43 179	60 63
44	80 610	23913 24	46	41 250	71 34
	80 473	14 02		41 108	72 13

Table II—(continued).

	R branch.			P branch.	
K.	**λ (air).**	**ν (vacuum).**	**K.**	**λ (air).**	**ν (vacuum).**
45	4177 257	23932 43	47	4239 098	23583 31
	77 128	33 17		38 971	84 01
46	73 845	52 00	48	36 896	95 56
ᵖᵘ	73 707	52 79		36 770	96 27
47	70 378	71 91	49	34 631	23608 18
	70 264	72 56		34 495	08 95
48	66 857	92 16	50	32 302	21 18
	66 724	92 93		32 180	21 86
49	63 281	24012 77	51	29 922	34 47
	63 158	13 48		29 798	35 16
50	59 658	33 69	52	27 468	48 20
	59 540	34 37		27 359	48 80
51	55 986	54 92	53	24 983	62 09
	55 865	55 62		24 863	62 77
52	52 272	76 44	54	22 430	76 40
	52 155	77 11		22 307	77 09
53	48 511	98 26	55	19 816	91 07
	48 399	98 91		19 691	91 77
54	44 699	24120 43	56	17 149	23706 05
	44 591	21 06		17 033	06 70
55	40 987	43 05	57	14 410	21 46
	40 720	43 60		14 315	21 99
56	36 918	65 79	58	11 637	37 07
	36 806	66 45		11 517	37 75
57	32 954	88 97	59	08 797	53 09
	32 851	89 57		08 691	53 69
58	28 962	24212 36	60	05 904	69 43
	28 849	13 02		05 804	69 99
59	24 915	36 11	61	02 980	85 96
	24 811	36 72		02 833	86 80
60	20 810	60 25	62	4199 962	23803 06
	20 716	60 81		99 853	03 67
61	16 700	84 47 (K−½)	63	96 919	20 31
	16 591	85 12 (K+½)		96 809	20 94
62	12 644	24309 66 (K+½)	64	93 733	38 41 (K+½)
	12 436	10 49 (K−½)		93 573	39 32 (K−½)
63			65		
	08 277	34 26 (K+½)		90 637	56 02 (K+½)
64	05 836	58 07	66	87 691	72 75
	04 261	58 77		87 570	73 49
65			67	83 662	95 79
	4099 052	89 03 (K+½)		83 492	96 77
66	95 114	24412 48	68	80 610	23913 24
	94 986	13 24		80 473	14 02
67	90 763	38 44	69	77 257	32 43
	90 653	39 10		77 128	33 17
68	86 328	64 97	70	73 845	52 00
	86 165	65 94		73 707	52 79
69	81 842	91 85	71	70 378	71 91
	81 708	92 66		70 264	72 56
70	77 320	24519 02	72	66 857	92 16
	77 174	19 89		66 724	92 93
71	72 753	46 51			
	72 916	45 53			

The system of levels for these bands is shown schematically in fig. 1, which serves to make clear the evaluation of the initial term differences from R(K) and P(K), and the final term differences from R(K − 1) and P(K + 1). These differences are given in Tables III and IV. Since the initial state is common to both bands they should give identical values; Table III is therefore an additional check on the accuracy of the measurements.
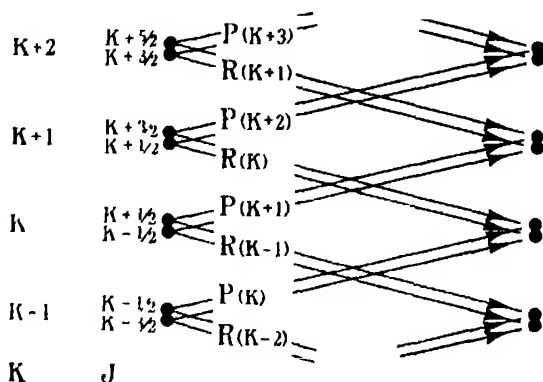
FIG. 1.—System of transitions for the N_2^+ bands. The $J \to J$ transitions have been omitted.

The Rotational Constants.

The extended rotational structure of the bands should make possible the determination of the rotational constants of the molecule with some considerable degree of accuracy. The rotational levels, if the doubling be for the moment neglected, might be expected to a close approximation to be spaced according to the expression

$$F = B_v \cdot K(K+1) + D_v \cdot [K(K+1)]^2.$$

It is quite possible to represent the $v'' = 0$ state by an expression of this form, but the $v'' = 1$ state requires an additional term whilst the $v' = 0$ state is so violently disturbed that it cannot be fitted by any simple function of powers of (K), as is clearly shown by fig. 2. The expressions which have been found best to fit the levels are as follows :—

$$v'' = 0 \quad F = 1 \cdot 9224 \cdot K(K+1) - 5 \cdot 92 \cdot 10^{-6} [K(K+1)]^2$$

$$v'' = 1 \quad F = 1 \cdot 9016 \cdot K(K+1) - 6 \cdot 21 \cdot 10^{-6} [K(K+1)]^2 + 4 \cdot 14 \cdot 10^{-5} (K)^3$$

$$v' = 0 \quad F = 2 \cdot 0725 \cdot K(K+1) - 6 \cdot 85 \cdot 10^{-6} [K(K+1)]^2 + 5 \cdot 77 \cdot 10^{-5} (K)^3$$

$$\left. \right\} \quad (1)$$

Table III.—Term differences for the $v' = 0$, $^2\Sigma_u$ levels. The values are derived from $R(K) - P(K)$ and are therefore the term differences $F'(K+1) - F'(K-1)$

K.	3914	4278	K	3914	4278
1	12 44	12 47	39	326 59	326 53
2	20 76	20 78		327 95	327 99
3	29 03	29 06	40	335 17	335 20
4	37 37	37 34		346 14 }	346 19 }
5	45 64	45 66		327 95 }	327 97 }
6	53 97	53 89	41	339 55	339 59
7	62 29	62 24		339 34	
8	70 52	70 53	42	348 48	348 52
9	78 78	78 75		349 17	349 17
10	87 22	87 06	43	356 75	356 70
11	95 43	95 34			
12	103 71	103 57	44	364 64	364 71
13	111 79	111 78		364 31	364 31
14	120 19	120 10	45	372 69	372 67
15	128 36	128 28		372 58	372 54
16	136 62	136 64	46	380 72	380 66
17	144 84	144 66		380 67	380 66
18	153 20	153 10	47	388 72	388 60
19	161 38	161 50		388 64	388 55
20	169 59	169 82	48	396 63	396 60
21	177 92	178 07		396 63	396 66
22	186 15	186 18	49	404 61	404 59
	186 18			404 60	404 53
23	194 45	194 42	50	412 53	412 51
	194 47			412 53	412 51
24	202 55	202 60	51	420 41	420 45
	202 59			420 39	420 46
25	210 82	210 86	52	428 36	428 24
	210 86			428 32	428 31
26	218 95	218 95	53	436 40	436 17
	218 97	218 98		436 32	436 14
27	227 14	227 15	54	444 05	444 03
	227 15	227 15		444 08	443 97
28	235 24	235 30	55	451 95	451 98
	235 34	235 31		451 89	451 83
29	243 47	243 43	56	459 74	459 74
	243 51	243 47		459 74	459 75
30	251 63	251 57	57	467 47	467 51
	251 70	251 66		467 54	467 58
31	259 75	259 78	58	475 27	475 29
	259 78	259 74		475 28	475 27
32	268 02	267 90	59	483 05	483 02
	267 90	267 88		482 99	483 03
33	275 94	276 02	60	490 81	490 82
	276 07	275 96		490 78	490 82
34	284 06	284 00	61	498 40	498 51
	284 15	284 08		498 48	498 32
35	290 92	290 83	62	507 51	507 43
	292 09	292 13		506 08	505 99
36	300 70	300 72	63	513 08	
	300 06	300 04		513 31	513 32
37	309 57	309 65	64	518 74	518 75
	307 13	307 28		520 36	520 36
38	314 81	314 83	65		
	304 56 }	304 66 }		532 88	533 01
	322 79 }	322 93 }			

Table III—(continued).

K.	3914.	4278	K.	3914.	4278
66	539 66	539 73	73	Weak	
	539 79	539 75	74	597 23	
67	542 56	542 65		597 20	
	542 24	542 33	75	Weak	
68	551 72	551 73	76	612 21	
	551 94	551 92		612 09	
69	559 64	559 42	77	Weak	
	559 83	559 49	78	626 92	
70	567 21	567 02		626 84	
	567 03	567 10	79	Weak	
71	Weak	574 60 ?	80	641 55	
		572 97 ?		641 31	
72	582 30		81	Weak	
	582 28		82	659 55	

When two values are given the first is the $(K - \frac{1}{2})$, the second the $(K + \frac{1}{2})$ difference.

Table IV.—Term differences for the $v'' = 0$, $v'' = 1$, $^2\Sigma_g$ levels. The values are derived from $R(K - 1) - P(K + 1)$ and are therefore the values of $F''(K + 1) - F''(K - 1)$

K.	3914.	4278.	K.	3914.	4278.
	11 52	11 43	26	202 91	200 90
	19 20	19 05		202 95	201 00
3	26 96	26 69	27	210 44	208 41
4	34 58	34 29		210 47	208 40
5	42 31	41 84	28	218 06	215 87
6	50 03	49 52		218 05	215 88
7	57 72	57 10	29	225 57	223 37
8	65 35	64 64		225 65	223 37
9	73 07	72 26	30	233 18	230 83
10	80 68	79 86		233 18	230 82
11	88 45	87 43	31	240 76	238 29
12	95 96	95 23		240 78	238 36
13	103 72	102 60	32	248 27	245 79
14	111 29	110 07		248 30	245 78
15	118 91	117 77	33	255 91	253 28
16	126 54	125 26		255 81	253 24
17	134 24	132 93	34	263 27	260 74
18	141 88	140 46		263 35	260 69
19	149 58	148 15	35	270 89	268 12
20	157 20	155 72		270 90	268 16
21	164 87	163 35	36	278 37	275 56
	164 87			278 37	275 63
22	172 55	170 89	37	285 87	283 01
	172 54			295 83	283 07
23	180 08	178 34	38	293 24	290 34
	180 11			293 28	290 48
24	187 78	185 89	39	300 79	297 81
	187 80			300 78 }	297 78 }
25	195 30	193 36		300 82	297 83
	195 30	193 33	40	308 13	305 22
				308 32	

Table IV—(continued).

K.	3914.	4278	K	3914.	4278.
41	315 67	312 55	61	461 80	457 19
	315 70	312 55		461 91	457 14
42	323 16	319 90	62	469 01	464 16
				469 05	464 18
43	330 52	327 26	63	476 18	471 17
	330 55	327 26		476 20	471 25
44	337 99	334 57	64		
	337 97	334 58		483 25	478 24
45	345 33	341 90	65	490 31	485 32
	345 39	341 89		490 30	485 28
46	352 76	349 12	66		
	352 74	349 16		497 45	492 26
47	360 15	356 44	67	504 41	499 24
	360 14	356 52		504 49	499 22
48	367 51	363 73	68	511 55	506 01
	367 54	363 61		511 41	505 93
49	374 81	370 98	69	518 51	512 97
	374 85	371 07		518 55	513 15
50	382 18	378 30	70	Weak	519 94
	382 16	378 32		Weak	520 10
51	389 53	385 49	71	532 47	526 86
	389 53	385 57		532 50	526 96
52	396 81	392 83	72	539 54	
	396 82	392 85		539 48	
53	404 14	400 04	73	546 36	
	404 14	400 02		546 35	
54	411 66	407 19	74	Weak	
	411 51	407 14	75	560 14	
55	418 65	414 38		560 09	
	418 66	414 36	76	Weak	
56	425 86	421 59	77	574 00	
	425 91	421 61		573 93	
57	433 12	428 72	78	Weak	
	433 14	428 70	79	587 52	
58	440 33	435 88		587 54	
	440 29	435 88	80	Weak	
59	447 57	442 93	81	600 96	
	447 56	443 03		Weak	
60	454 65	450 15			
	454 73	449 92			

When two values are given the first is the $(K - \frac{1}{2})$ and the second the $(K + \frac{1}{2})$ difference.

The general expression is thus of the form .—

$$F = B_v \cdot K(K+1) + D_v \cdot [K(K+1)]^2 + \phi(K)^3.$$

The small additional term $\phi(K)^3$ is probably to be attributed to a slight distortion of the molecule, arising in the one case from vibration and in the other from excitation. The way in which the expressions fit the experimental values is shown in fig. 2 ; the constants have been grouped together for convenience in Table VII and exhibit some interesting regularities. The trend

of the B_v and D_v values* with increasing v is in the expected direction. If we assume that

$$B_v = B_e + \alpha\,(v + \tfrac{1}{2}); \qquad D_v = D_e + \beta\,(v + \tfrac{1}{2})$$

we obtain for the values of B_e and α the values $1 \cdot 9328$ and $-0 \cdot 0208$ respectively, and for D_e and β respectively $-5 \cdot 75 \cdot 10^{-6}$ and $-0 \cdot 29 \cdot 10^{-6}$. It is
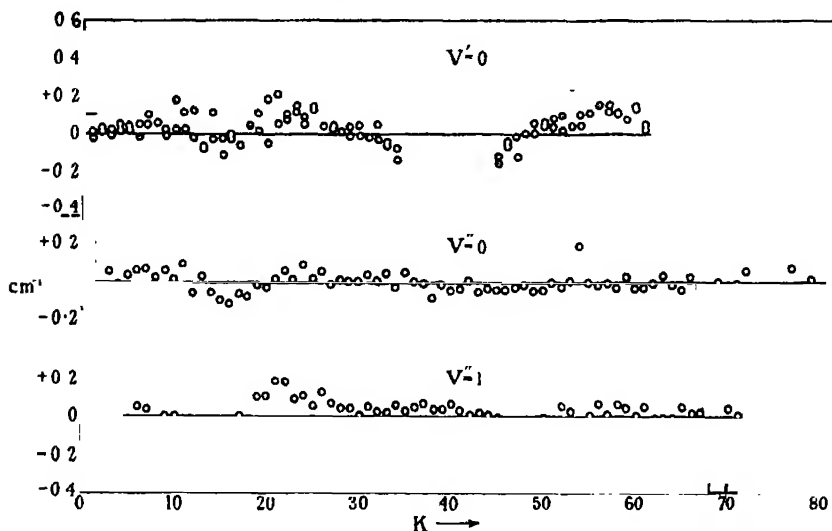
Fig. 2.—Deviations of the measured term differences from those calculated from expressions (1).

interesting to compare the inter-relations between these constants by means of the well-known expressions

$$\alpha = 6B_e{}^2/\omega_e,$$
$$D_e = 4B_e{}^3/(\omega_e)^2.$$

Adopting 2208 cm.$^{-1}$ for the value of ω_e we obtain $\alpha = 0 \cdot 010$ and $D_e = 5 \cdot 93 \cdot 10^{-6}$ in satisfactory agreement with the experimental values.

The Spin Doubling.

In deriving the values of the rotational constants no account has been taken of the fact that the rotational levels are closely doubled, due to the fact that the electron spin vector is slightly coupled to the nuclear angular momentum, so that two slightly different values of the rotational term are possible, according as the spin sets itself parallel or anti-parallel. The levels have

---

* B_v is inversely proportional to the moment of inertia. The term with the coefficient D_v is added to take account of the swelling of the molecule under centrifugal forces.

been treated as single and, strictly speaking, the constants just derived are only valid for their "centres of gravity." The scheme of fig. 1 shows that the two components resulting from the doubling belong to two distinct families the members of which do not inter-combine, so that it is impossible from direct measurement to decide anything about the relative displacement of the two families. It is usual to take account of the doubling by adding to the rotational energy terms a small spin-coupling factor which is assumed to have the form $\pm \gamma$ (K), so that the completed term is of the form*

$$\text{F} = \text{B}_v \text{K} (\text{K} + 1) + \text{D}_v \ [\text{K} (\text{K} + 1)]^2 + \phi (\text{K})^3 \pm \gamma (\text{K})$$

As a way out of the difficulty Ornstein and van Wijk† have assumed that the coupling factor is of the form γ (K) given above, and, supposing that the coefficients for the initial and final states have the values γ_i and γ_f respectively, have endeavoured to find the numerical values by plotting the values of the doublet separation of the successive lines of a branch against (K) The points should lie on a straight line ; the intersection of this line with the v axis gives the value of γ_f and the slope of the line gives $(\gamma_i - \gamma_f)$ As evidence that they have correctly assigned the values of $(\text{K} + \frac{1}{2})$ and $(\text{K} - \frac{1}{2})$ to the components of the doublet (they associate $(\text{K} + \frac{1}{2})$ with the high frequency, $(\text{K} - \frac{1}{2})$ with the low frequency component of each doublet) they point out the fact that it is the high frequency component in each case which has the greater intensity, and that since the intensity expressions contain the statistical weight factor $(2\text{J} + 1)$ so that the relative intensities of the $(\text{K} - \frac{1}{2})$ and $(\text{K} + \frac{1}{2})$ components will be as $\text{K} : \text{K} + 1$, it is clear that their assignment is the correct one. The same point has been made by Coster and Brons (*loc. cit.*). In the opinion of the writer too much weight should not be placed on these intensity differences. Where they can be measured they are always much greater than is to be expected from the simple explanation just given. In the region $\text{K} = 70$ where they should be of the order of 1 per cent., *i.e.*, not measurable, they are indeed of the order of 13 per cent. and very evident It may be that the phenomenon is similar in nature, though smaller in magnitude, to that exhibited by other $^2\Sigma \rightarrow {}^2\Sigma$ bands, for example in the C bands of CaH one component can under certain circumstances be entirely missing, and again in some of the HgH bands one component is several times the strength of the

---

* Actually the factor for the $(\text{K} - \frac{1}{2})$ term is $- \gamma(\text{K} + 1)$, and for the $(\text{K} + \frac{1}{2})$ term it is $+ \gamma(\text{K})$, but the form given above is amply sufficient for practical purposes.

† 'Z. Physik,' vol. 49, p. 315 (1928).

other.[*] It is clear therefore that the assignment of $(K + \frac{1}{2})$ to the high frequency component must remain, although plausible, an assumption. Plotting the values of the doublet separation with this assumption against (K) leads to the following results for the spin-coupling factor. The accuracy is not sufficient to be able to distinguish between the $v'' = 0$ and $v'' = 1$ states.

Rotational energy level (spin-doubling) separations—[†]

for the $v' = 0$ state $\qquad + 0 \cdot 013$ (K) cm.$^{-1}$ $\qquad (+ 0 \cdot 013),$

for the $v'' = 0$, $v'' = 1$ states $\qquad + 0 \cdot 002$ (K) cm.$^{-1}$ $\qquad (- 0 \cdot 002).$

The actual values themselves are probably not very accurate ; it is only the difference $0 \cdot 011$ which has any pretensions to accuracy. The measurements of Coster and Brons when treated in a similar manner yield the values given in brackets, so that it is probable that the splitting of the v'' states is extremely small.

These values are not in agreement with those of Ornstein and van Wijk (*loc. cit.*), who give no estimation of the relative accuracy of their measurements. It is probable, however, that these permitted only a rough estimate of the size of the constants.

The Perturbations.

Before discussing the perturbations in any detail it will be advisable to give some account of the present point of view regarding them. The question of when disturbances in the normal spacing of the rotational energy levels of a molecule may be expected to occur has been investigated by Kronig,[‡] who finds that two states will mutually perturb each other if they possess the following necessary peculiarities :—

(1) Their energies are equal.

(2) They both have the same total angular momentum J.

(3) If both states have the same multiplicity.

(4) If the values of Λ do not differ by more than 0, $+1$, -1.

---

[*] E. Hulthen, ' Phys. Rev.,' vol. 29, p. 97 (1927) ; ' Z. Physik,' vol. 50, p. 332 (1928).

[†] These values may be compared with those of the very similar CN bands. For the $^2\Sigma$ ground state, $v'' = 2$, the spin-doubling can be represented by $+ 0 \cdot 0082$ $(K + \frac{1}{2})$, *i.e.*, the $(K + \frac{1}{2})$ levels are above the $(K - \frac{1}{2})$ levels as in the N_2^+ bands.

[‡] ' Z. Physik,' vol. 50, p. 347 (1928).

(5) Both must possess the same symmetry properties, *i.e.*, both positive or both negative, and if the nuclei are equal, symmetric or anti-symmetric, gerade or ungerade.

The perturbations in the He_2 spectrum investigated by G. H. Dieke[*] bear out the postulated conditions very well. The subject has been carried a stage farther by Ittmann,[†] who has applied the methods of Kronig's paper to the special case of $^2\Sigma$, $^2\Pi$, mutually perturbing levels, since it is for this case that we have in practice the most precise information. Ittmann finds that for a case (*a*) $^2\Pi$ level (inverted) and a case (*b*) $^2\Sigma$ level the perturbations should have the general characteristics of fig. 3. Confining attention to the $^2\Sigma$ level, and supposing that the levels intersect at the angle shown in the diagram, we
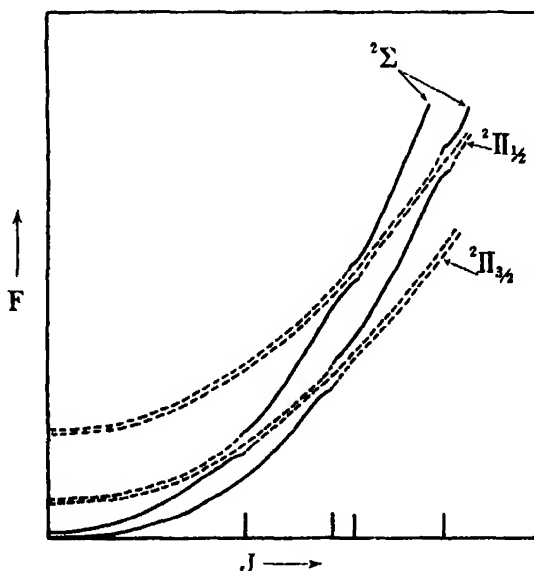
Fɪɢ. 3.—Mutual perturbation of $^2\Sigma$ and $^2\Pi$ levels.

note the following sequence. The first perturbation, going from low to high rotational levels, affects only the one member of the doublets, the other member behaving quite normally. Next follow two perturbations in close proximity to one another, and both doublet components are affected. Finally, there is a fourth perturbation in which again only one of the doublet components is affected. In each case the levels before the disturbance are deflected in the

* ' Phys. Rev.,' vol. 38, p. 646 (1931).

† ' Z. Physik,' vol. 71, p. 616 (1931).

direction of lower energy, whilst those following are deflected in the opposite direction. In the neighbourhood of each perturbation extra lines may appear due to the fact that the perturbed levels acquire some of the properties of the perturbing levels, and *vice versa*, so that transitions may occur which are normally prohibited. It has been possible to check these conclusions from the CN bands, where the perturbations have been dealt with by Rosenthal and Jenkins,[*] Ittman (*loc. cit.*) and recently by Jenkins, Roots and Mulliken.[†] The measure of agreement between experiment and theory is very satisfactory. Another recent and very interesting example, in which a $^2\Pi_{\frac{1}{2}}$ and a $^2\Pi_{\frac{1}{2}}$ are the perturbing states has been found by Rydberg[‡] in the HgH bands.

In the case of CN the perturbing levels are the $a^2\Sigma$ lower state of the molecule ($v'' = 11$) and the inverted $^2\Pi$ upper state, written $^2\Pi i$, of the red CN bands ($v' = 6$). The $b^2\Sigma$ upper state of the violet CN bands ($v' = 12$) is also perturbed, but this does not seem to have been discussed. In the case of the N_2^+ bands the situation is a little different. It is the upper $^2\Sigma$ level ($v = 0, 1, 3,$ 5 ?, 8 ?, 9 ?) which is perturbed, and the perturbing level is unknown, though it is a very plausible assumption that by analogy with the very similar CN molecule we have also in this case a $^2\Pi_i$ level. The upper level of the N_2^+ bands is probably $^2\Sigma_u^+$ and the ground level, $^2\Sigma_g^+$, so that there are two possibilities for the $^2\Pi$ level. It could be $^2\Pi_g$ and in the neighbourhood of the upper level, the transition $^2\Sigma_u^+ \to {}^2\Pi_g$ being in the infra-red ($^2\Pi_g \to {}^2\Sigma_g^+$ is, of course, prohibited) or it could be $^2\Pi_u$ and in the neighbourhood of the ground states with the transition $^2\Pi_u \to {}^2\Sigma_g^+$ in the infra-red. That it is actually $^2\Pi_u$ is more likely from electron configurations, whilst it is definitely required by the mere presence of the perturbations (see rule 5 above). We are now in a position to discuss the perturbations of this paper, and to endeavour to link them up with those of the $v' = 1$ and $v' = 3$ levels treated by Coster and Brons (*loc. cit.*).

The presence of the perturbations is apparent from a mere glance at the bands, Plate 21, the disturbance in the neighbourhood of P(40) being especially obvious. A closer inspection reveals the expected perturbation at R(38) a somewhat similar disturbance close to P(67) and R(65), and a number of irregularities in the doublet spacings. All these are identical in both bands so that it is clear that it is the $v' = 0$ state which is affected. The perturbed levels were found by a process of continuous extrapolation An example

---

[*] 'Proc. Nat. Acad. Sci.,' vol. 15, p. 896 (1929).

[†] 'Phys. Rev.,' vol 39, p. 16 (1932).

[‡] 'Z. Physik,' vol. 73, p. 74 (1932).
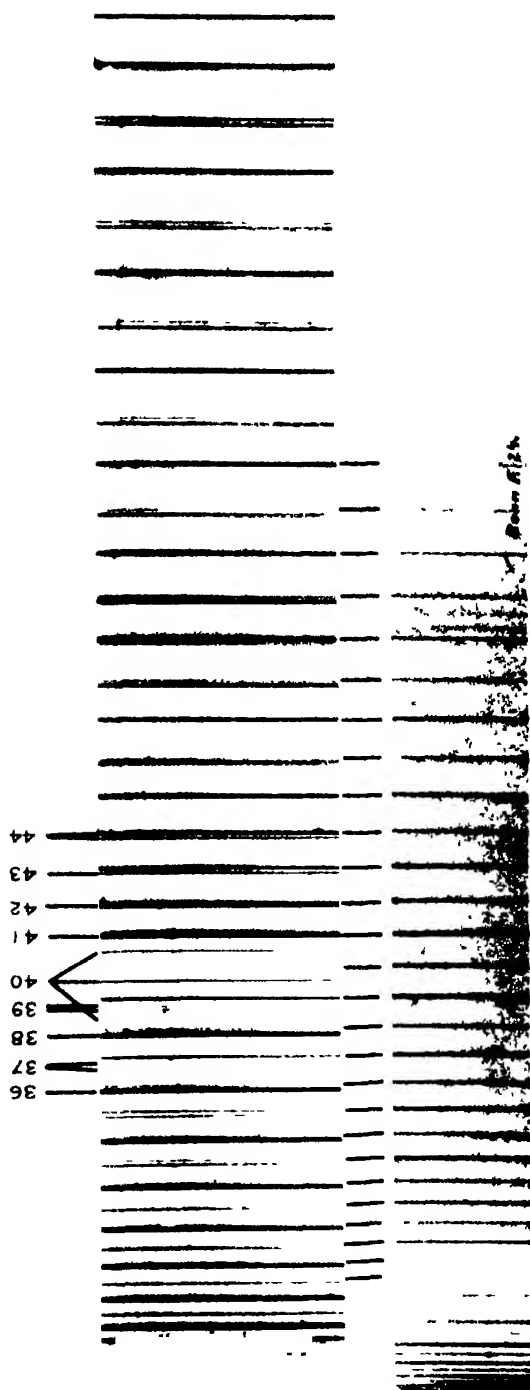
The upper strip shows the band in an arc discharge, the lower strip under Geissler tube conditions. The marks below the upper strip indicate the R branch proceeding from the origin, whilst those above show the perturbation

will make this clear. It is supposed that the progress of the initial levels has been determined as far as K = 37 and it is desired to locate the levels K = 39. The lines proceeding from this level are R(38) and P(40) ending on the levels K = 38 and K = 40 respectively. These are unperturbed and may be predicted with some certainty to be separated 300·82 cm.$^{-1}$ for $v'' = 0$ and 297·79 cm.$^{-1}$ for $v'' = 1$. There are three P and three R lines in each band which give differences of 300·78, 300·79, 300·82 and 297·78, 297·81, 297·83 respectively. If these are the lines sought the R lines should give, when combined with P(38), identical values for each band. When this test is applied the 0, 0 band gives 304·36, 314·81, 322·59, compared with 304·34, 314·83, 322·61, from the 0, 1 band, which is fairly conclusive evidence that the levels have been located. In this manner the gaps were filled in, accounting for all the lines in the disturbed regions in the major perturbation of both bands. It is now possible to determine the extent to which the levels depart from a regular spacing. The results of a comparison with expressions (1) in the region of the perturbations are given in Tables V and VI and are also shown

Table V.—Observed and calculated levels in the neighbourhood of the perturbation at K = 39.

The calculated levels are based on the level K = 30   For the observed levels the assumption is made that F (31) — F (30) = 127·84 cm.$^{-1}$. A similar assumption has had to be made at K = 44, where it has been assumed that the separation of the (K — $\frac{1}{2}$) and (K + $\frac{1}{2}$) sub-levels is 0·86 cm.$^{-1}$.

K.	F (calc.).	Observed. (K — $\frac{1}{2}$)	O — C	Observed. (K + $\frac{1}{2}$).	O — C.
30	0	0	0 00	30	0 30
31	127 84	(127 84)	0 00	128 14	0 30
32	259 75	259 77	0 02	260 06	0 31
33	395 74	395 80	0 06	396 03	0 29
34	535 79	535 75	—0 04	536 08	0 29
35	679 89	679 83	—0 06	680 15	0 26
36	828 05	826 63	—1 42	828 19	0·14
37	980 27	980 54	0 27	980 20	—0 07
38	1136 52	1136 24	—0 28	1135 40	—1·12
39	1296 79	1295 36	—1 43	1284 80	—11·99
				1303 05	6 26
40	1461 11	1462 80	1 69	1463 37	2·26
41	1629 46	1630 54	1 08	1630 96	1·53
42	1801 82	1802 37	0 55	1802 71	0·89
43	1978 18	1979 04	0 86	1980 16	1 98
44	2158 56	2159 10	0 54	2159 96	1·40
45	2342 93	2343 72	0 79	2344 47	1·54
46	2531 28	2531 78	0 50	2532 52	1·24
47	2723 62	2724 41	0 79	2725 14	1 52
48	2919 95	2920 44	0 49	2921 12	1·17

Table VI.—Observed and calculated levels in the neighbourhood of the perturbation at K = 66.

The levels are based on that of K = 60. The additional assumptions are made that (a) F(61) − F(60) = 247·28 cm.$^{-1}$; (b) at K = 68 the separation of the (K − ½) and (K + ½) sub-levels is 0·62 cm.$^{-1}$.

K.	F (calc.).	Observed. (K − ½).	O. − C.	Observed. (K + ½).	O. − C.
60	0	0	0 00	62	0·62
61	247 28	(247 28)	0 00	(247 90)	0 62
62	498 38	498 46	0 08	499 02	0 64
63	753 34	754 75	1 41	753 94	0·60
64	1012 12	1011 54	−0 58	1012 34	0 22
65	1274 75	1273 50	−1 25	1274 30	−0 45
66	1541 20	1544 35	3 15	1545 29	4 09
67	1811 43	1813 27	1 84	1814 07	2 64
68	2085 46	(2086 96)	1 50	2087 58	2 12
69	2363 28	2365 00	1 72	2366 00	2 72
70	2644 87	2646 49	1 62	2647 24	2 37
71	2930 21	2932 12	1 91	2933 07	2·86
72	3219 30	3221 09	1·79	3220 35 ?	1 05 ?
73	3512 15	3514 40	2 25	3515 35	3 20
74	3808 71				
75	4108 98	4111 63	2 65	4112 55	3·57
76	4412 96				
77	4720 64	4723 84	3 20	4724 64	4 00

in fig. 4. It is clear from this diagram that in both perturbations it is both components which have been affected. This is comparable with the perturbation of the $v' = 12$, $b\,^2\Sigma$ upper level of CN, but is in sharp contrast with that of the $v' = 1$ level of N_2^+ where, as in the $v'' = 11$ level of CN, the first perturbation extends only to the one doublet component. At first sight it appears that several additional lines have put in an appearance. It is suggested, however, that what has really happened is that each component has been perturbed twice in rapid succession, the course of the levels in the region of the perturbation being roughly that of fig. 4. According to this view the disturbances at K = 39 and K = 66 are due to successive vibrational levels of the $^2\Pi$ state, and should thus have very similar appearances. It is difficult to pronounce an opinion upon this, as the band lines are fading out at K = 66 and it is quite possible that some faint lines have been missed, but it is significant that the two levels which one would expect to see affected, viz., the K − ½ component of K = 63 and the K + ½ component of K = 69, are indeed both displaced. If this interpretation is correct then the perturbation at $v' = 1$, K = 13 and that just discussed at $v' = 0$, K = 69 are caused by

one and the same vibrational level of the $^2\Pi$ state. A somewhat uncertain extrapolation from the perturbations lends support to this view. Extrapolating from the K = 39 perturbation indicates that the $^2\Pi$ state involved is located some 900 cm.$^{-1}$ above the $v' = 0$ $^2\Sigma$ state with a value for B_v of approxi-
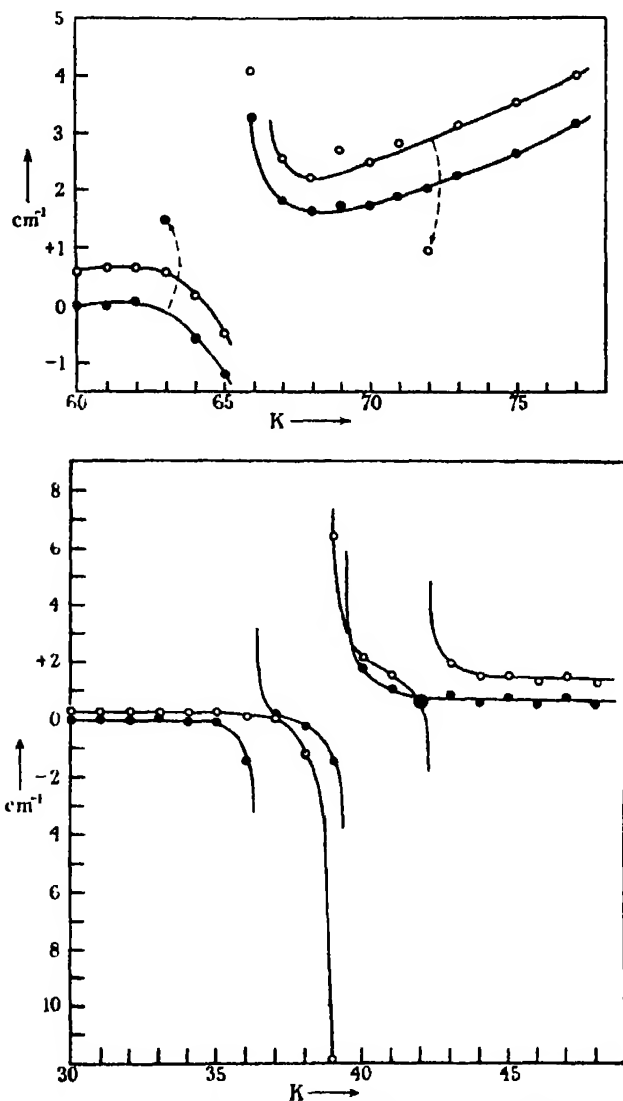
Fig. 4, *a* above, and *b* below.—Showing the displacement of the *levels* in the region of the perturbations. This diagram is plotted from the results of Tables V and VI. The full circles represent the $(K - \frac{1}{2})$ levels, the open circles the $(K + \frac{1}{2})$ levels.

2 x 2

mately 1·50. Using this value of B_v and extrapolating from the $K = 66$ perturbation shows that the next vibrational level of the $^2\Pi$ state is situated at approximately 2430 cm.$^{-1}$ above the $v' = 0$ $^2\Sigma$ state, and crosses the $v' = 1$ levels at $J = 14$. The relative disposition of the perturbing levels is thus that of fig. 5.
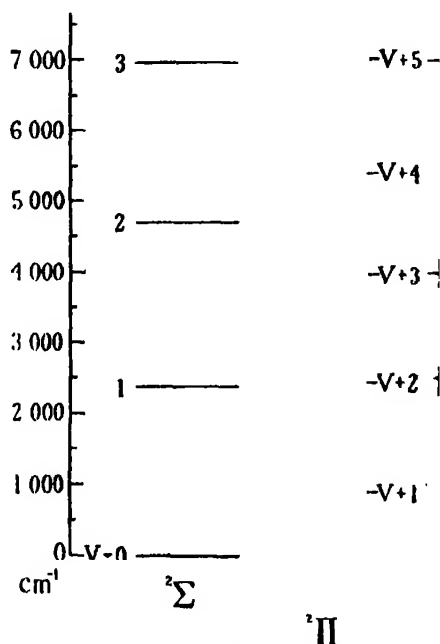
FIG. 5.—The relative positions of the $^2\Sigma$ and $^2\Pi$ vibrational levels indicated by the perturbations.

An interesting detail for which no explanation is put forward is the " stagger " of the levels from $K = 43$ onwards, shown in fig. 4. This may be connected with the fact that the doublet separations, from the point at which they become measurable until the perturbation sets in, are alternately larger and smaller

Table VII.

State.	B_v.	D_v.	ϕ.	B_e.	a.	D_e.	β.
		$\times 10^{-6}$	$\times 10^{-5}$			$\times 10^{-6}$	$\times 10^{-6}$
$v'' = 0$	1·9224	−5·92	0 00 ⎫	1·9328	−0 0208	−5 75	−0·29
$v'' = 1$	1·9016	−6·21	4·14 ⎬		(0 010)	(5 93)	
			⎭		calc.	calc.	
$v' = 0$	2·0725	−6·85	5·77				

than the mean value. This latter phenomenon is barely discernible, but is thought to be real.

Summary.

The 0, 0 and 0, 1 first negative nitrogen bands emitted from an arc have been examined under high dispersion The structure has been followed to high values of the rotational quantum number, and this has permitted an accurate estimation of the rotation constants of the $v'' = 0$, $v'' = 1$ $^2\Sigma_g{}^+$ ground states and the $v' = 0$ $^2\Sigma_u{}^+$ upper state Values for the spin-doubling constant have also been obtained. The extension of the band structure has brought to light two perturbations of the $v' = 0$; $^2\Sigma$ upper state which are related to those already known to exist in the $v' = 1$ and $v' = 3$ states. With the information derived from the new perturbations, tentative estimates of the position of the hypothetical $^2\Pi$ perturbing levels can be made.

The Energy Distribution among the Positive Ions at the Cathode of the Glow Discharge through Gases.

By R. M. Chaudrhi and M. L. Oliphant.

The energy distribution among the positive ions which strike the cathode of the glow-discharge through gases is of some importance in the theory of the phenomenon,[*] and as very little is known about the mean-free-paths of ions in gases it is difficult to make an estimate of this distribution. Attempts have been made in the past to measure this quantity by perforating the cathode and applying retarding potentials to the ions which penetrate through.[†] The positive ion photographs obtained by the parabola method of Sir J. J. Thomson[‡] give information concerning the distribution in a strongly abnormal discharge. These last, and observations of the Doppler effect[§] in canal-rays, suggest that there are particles present with energies corresponding with a fall through the full potential drop across the dark-space, while the retarding potential measurements of Von Hippel show a sharp upper limit to the energy at between 0·3 and 0·5 of the total cathode fall. The dark-space stretches over 20 to 100 molecular free-paths, so that if ions are present with the full energy corresponding to the cathode fall they must have relatively long free-paths in the dark-space.

We have carried out measurements of the energy distribution among the positive ions which penetrated through a slit in a plane cathode into an evacuated space beyond, by a retarding potential method and by the method of focussing at 127° 17′ in an inverse first power electrostatic field.[||]

The Retarding Potential Measurements.

The apparatus was designed to avoid as far as possible the effects produced by the secondary electrons set free from the collector and from slits, etc.,

[*] Compton and Morse, 'Phys Rev.,' vol. 30, p. 305 (1927); Morse, 'Phys. Rev.,' vol. 31, p. 1003 (1928).

[†] E.g., Von Hippel, 'Ann. Physik,' vol. 81, p. 1046 (1926).

[‡] "Rays of Positive Electricity," Longmans, Green & Co. (1921).

[§] Johnson, 'Proc. Phys. Soc.,' vol. 39, p. 26 (1926).

[||] Hughes and Rojansky, 'Phys. Rev.,' vol 34, p. 291 (1929).

while ionisation was avoided by keeping the pressure at a very low value. It is shown diagrammatically in fig. 1.

The nickel anode A and cathode C are plane parallel electrodes about 3·5 cm. in diameter and 8 cm. apart. The cathode is in the form of a cap of thin copper fitting tightly over the end of a glass tube and tied on firmly by binding the overlap with copper wire. At the centre of the cathode there is a slit, 10 mm. long by 0·5 mm wide. Immediately behind this is a Faraday cylinder
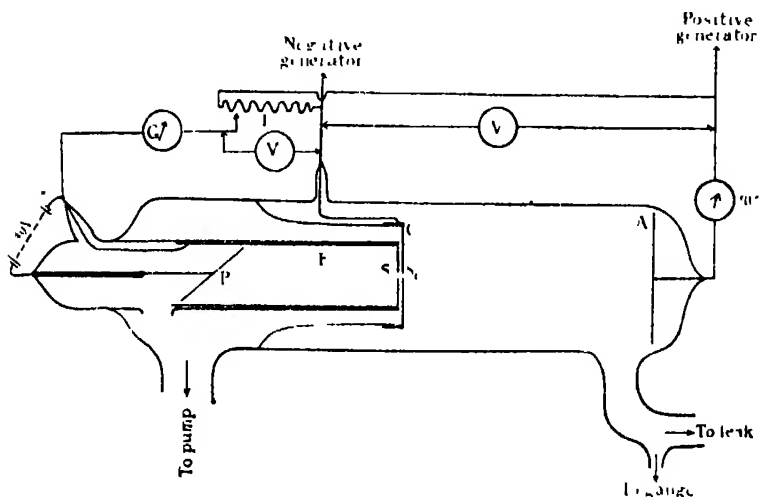
Fig 1

F with a slit in the front surface somewhat wider than the slit in the cathode and placed as close to the back surface of the cathode as possible. A plate P, inside the Faraday cylinder, was charged to a potential of about 40 volts; this prevented the escape of secondary electrons. Varying retarding potentials could be applied between C and F by means of a potentiometer L, which was placed across the terminals of the discharge itself. The electrode system was set up inside a glass tube about 4·5 cm in diameter. Air or any other gas could be let into the tube through a leak, and the pressure adjusted to any desired value as measured with a McLeod gauge. The gas which leaked in through the hole in the cathode was pumped away with a steel diffusion pump and the pressure on this side of the diaphragm could be kept at a very low value. The discharge potential was obtained from a high voltage generator and the current was adjusted by alteration of the filament temperature of a two-electrode valve in series with the apparatus.

Results.

The retarding potential curves obtained under a variety of conditions are typified by those given in fig. 2.   The apparent positive ion current falls from a maximum with zero retarding potential on the Faraday cylinder to zero at a potential corresponding to 0·3 to 0·5 of the discharge potential.   After that it reverses and with a retarding potential equal to the full potential across
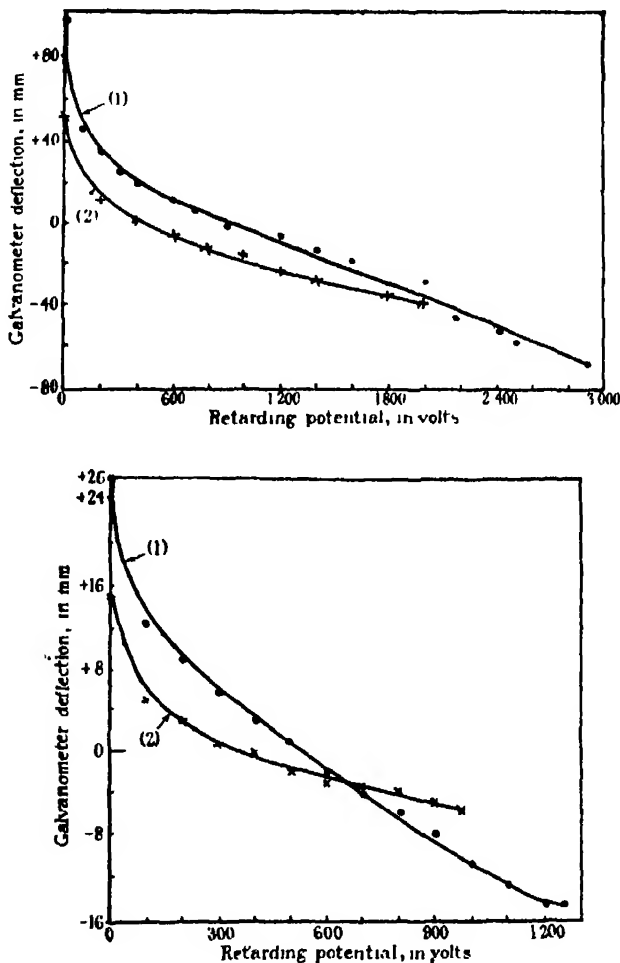
FIG. 2.

(a) Above (1) $i = 0·6$ m.a., $v = 2900$ volts, $P = 0·033$ mm. Hg.; (2) $i = 1·0$ m.a., $v = 2000$ volts, $P = 0·05$ mm. Hg.   (b) Below (1) $i = 0·6$ m.a., $v = 1270$ volts, $P = 0·05$ mm. Hg.; (2) $i = 0·2$ m.a., $v = 1000$ volts, $P = 0·05$ mm. Hg.

the discharge an electron current of the same order of magnitude as the original positive ion current flows to the Faraday cylinder. This electron current does not saturate but increases continually with increasing positive potential applied to the collector. It may arise from several causes :—

(1) The penetration of the field between the cathode and the Faraday cylinder through the slit in the cathode may result in electrons from the discharge in the immediate neighbourhood of the slit being drawn to the Faraday cylinder.

(2) Radiations and metastable atoms may penetrate through the slit and give rise to electrons from all the surfaces which they strike.* This gives a current which reverses with the potential and which it is very difficult to allow for.

(3) Positive ions are retarded by the field between the cathode and Faraday cylinder and the slower ions return to the back surface of the cathode and may there set free electrons which then travel to the Faraday cylinder.

Experiments of Oliphant† show that excited atoms travel in large numbers through a hole in a canal in a negatively charged Langmuir probe, and it seems likely that these will also be present in the stream passing through the slit in the cathode used in these experiments. Ratner‡ has shown that reversible currents of very large magnitude flow between electrodes placed inside a large cathode so constructed that no charged particles could possibly reach them from the discharge itself, but to which radiations and metastable atoms could readily penetrate. Also positive ions with energies of one or two hundred volts can set free electrons from gas-covered surfaces, such as those used in the present experiments, with an efficiency approaching 100 per cent., so that retarded positive ions might account for a relatively large electron emission from the back of the cathode. It is impossible to make any estimate of the magnitude of the electron currents which might arise from (1). In any case the variation of this electron current completely masks the variation of the positive ion current with variation of the retarding potential

An attempt was made to prevent the electrons from leaving the surfaces at which they were generated and reaching the Faraday cylinder by applying

---

* Oliphant, ' Proc. Roy. Soc.,' A, vol. 124, p. 228 (1929).

† Oliphant, *loc cit.*

‡ ' Proc. Nat. Acad. Sci. Wash ,' vol. 15, p. 318 (1929).

a transverse magnetic field. The width of the dark-space was much reduced thereby, but the electron current still persisted. To prevent penetration of the field through the slit and also in an attempt to reduce the secondary emission from the back of the cathode, a grid was placed between the slit and the Faraday cylinder and charged to a potential of —2 to —410 volts with respect to the cathode. This produced a marked change in the shape of the curve for low retarding potentials, possibly owing to capture of some positive ions by the grid, but beyond 100 volts the curve was very little changed, even with the addition of a magnetic field.

Experiments designed to find the energy distribution among the positive ions striking the cathode have been described by Von Hippel (*loc. cit.*). Using a retarding potential method he obtained a curve of exactly the same form as those given in fig. 2, but he appears to have cut off the curve quite arbitrarily at the point where the positive ion current fell to zero, and does not mention the reversed current. His conclusion that the maximum positive ion energy was 0·3 to 0·5 of the total energy corresponding to free fall through the dark-space is therefore untenable

The Focussing Method.

A magnetic velocity analysis of the ions which penetrate through the hole in the cathode is not easily carried out, for the ions have different masses and it is difficult to shield the discharge itself from the strong fields required. An electrostatic analysis was therefore made by the method of bending the particles through 127° 17' in an inverse first power electrostatic field (Hughes and Rojansky, *loc. cit.*) and focussing upon the slit of a Faraday cylinder. This method avoids the troubles produced by secondary electrons from the discharge and slits, for these are bent in the opposite direction and can never reach the collector. This latter was made narrow and long to reduce secondary emission, and a small electric field was applied for the same purpose between the defining slit in front of the Faraday cylinder and the collector itself

The Apparatus.

The discharge took place between the anode A and cathode C, fig. 3, placed about 8 cm. apart in a pyrex tube 5 cm. in diameter. Ions passed through the slit S_1 into the evacuated space beyond where they were bent round in the arc of a circle of 5·25 cm. mean radius by means of an electrostatic field between the two curved plates P turned from an alloy of aluminium and zinc. These plates were geometrically secured 5 mm. apart by screwing the upper one to

the back of the cathode, while the lower plate was fastened concentric with it by means of insulating strips of mica held by screws. The angle turned through between the first slit S_1 and the defining slit S_2 was carefully arranged to be 127° 17'. Ions which were focussed upon S_2 entered the Faraday cylinder F. Secondary emission from S_2 was prevented from reaching F by applying a small electron retarding potential between S_2 and F. The cathode was fastened into the glass tubes by winding para-rubber strip about the joints LL and painting with cellulose enamel. These joints were kept cool by the water jacket shown in the figure.
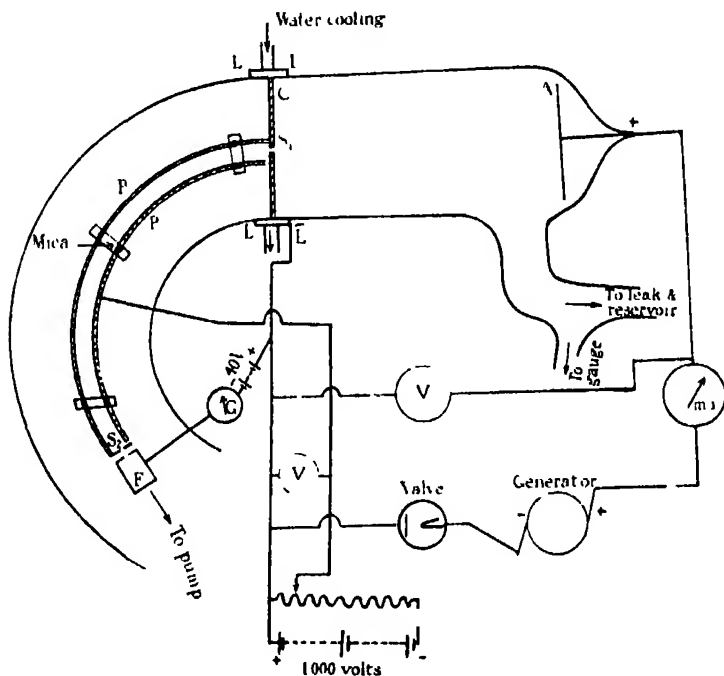
FIG. 3.

The slit S_1 was about 0.5 mm. $\times$ 1.0 mm., while S_2 was 10 mm. $\times$ 1.0 mm. A large four-stage Gaede diffusion pump together with a trap of low resistance was used for evacuating the analysing side of the apparatus where the pressure was kept below 10^{-4} mm. of Hg. The gas used entered by way of a fine leak from a reservoir at a suitable pressure. The tube containing the deflecting plates and Faraday cylinder was silvered to prevent disturbances arising from charges on the glass walls.

The current to F was measured with a galvanometer of sensitivity about 10^{-10} amp./mm. The bending potential between the plates P was obtained

from a battery of small accumulators giving 1000 volts, and was applied
through a potentiometer.   This potential and the potential across the discharge
itself were measured with suitable electrostatic voltmeters, and on account of
the inherent weaknesses of this type of instrument are subject to rather large
errors.

<div align="center">

The Results.

</div>

In order to obtain reproducible results it was necessary to keep the pressure
in the analysing side of the apparatus at a very low value, for the proportion
of slow ions reaching the Faraday cylinder decreased rapidly with increase in
pressure.   For instance, neglect to apply liquid air to the trap gave a pressure
of mercury vapour sufficient to prevent all slow ions from ever reaching the
collector.   However, when liquid air was applied and the pumps were running
well the curves obtained were strictly reproducible.

Fig. 4 shows a typical curve obtained with air.   It will be seen that ions are
present with all energies from practically zero up to the full energy corre-
sponding to the potential across the discharge.   There is a maximum in the
curve in the region of low energies and a relatively sharp fall off in the number
of ions at an energy very nearly that given by the cathode fall of potential,
assumed equal to the potential across the discharge.   There is a " tail " to
the curves on the high velocity side, but we have assumed that this is experi-
mental, and take as our maximum energy that given by the point of inter-
section of the tangent to the steep end part of the curve with the volt-axis.

A series of curves taken with air at the same pressure as in fig. 4 is given
in fig 5.   The different curves correspond to different discharge currents,
and, since the discharge is abnormal, to different potentials.   The curves
are similar to one another, and it is seen that the energy corresponding to the
maximum number of ions does not depend on the discharge potential or current.
It is a function of pressure alone.   In figs. 6 and 7 two further series of curves
for air are given, taken at different constant pressures, one lower and one
higher than in fig. 5.   The curves are of the same general shape in different
series.   The small differences will be discussed later.

The curves obtained at a considerably higher pressure and shown in fig. 8
exhibit, however, a different character.   The maximum of the curve occurs
at or near zero energy.   It is thus obvious that the maximum of the curve
shifts towards zero energy as the pressure increases, while the relative number
of ions with energy near that corresponding with the discharge potential
decreases with the increase in pressure.   At lower pressures the maximum is
broad, while at higher pressures it becomes sharper.

In fig. 9 we have given curves taken at a constant voltage, but with different pressures and hence different discharge currents. It will be seen that the slope of the curves for energies greater than that corresponding with the maximum increases with increase of pressure. Increase of the discharge current leads
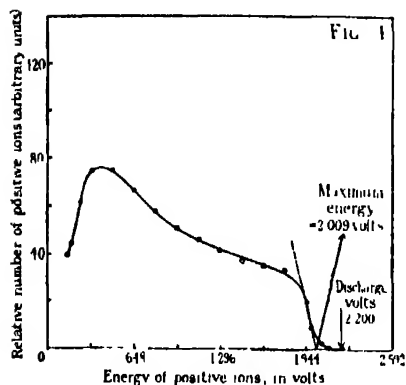
FIG. 4.—Gas = air, P = 0·0345 mm Hg, v = 2200 volts, i = 0·50, 0·58 m.a
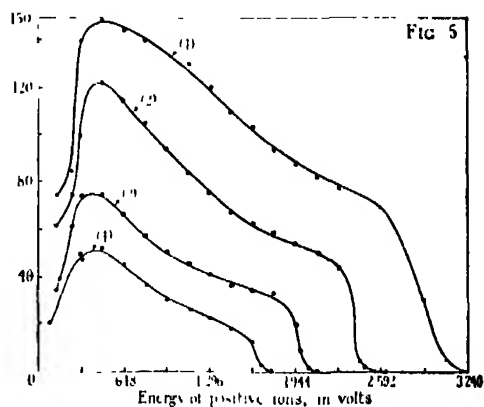
FIG. 5.—Gas = air, P = 0 0345 mm. Hg. (1) i = 1 2 m a , v = 3700 volts ; (2) i = 1·0 m a , v = 2850 volts, (3) i = 0·50, 0·58 m a , v = 2200 volts , (4) i = 0·25, 0·30 m.a., v = 1680 volts.
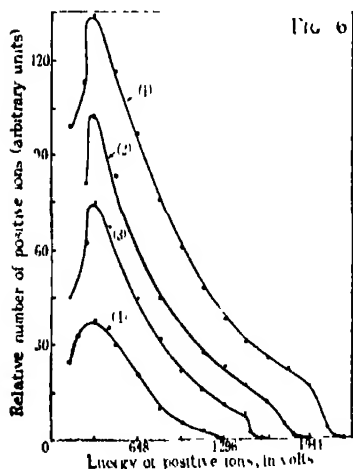
FIG. 6.—Gas = air, P = 0·0565, 0·0575 mm. Hg. (1) i = 2·0 m.a., v = 2075 volts ; (2) i = 1·5 m.a., v = 1750 volts ; (3) i = 1·0 m.a., v = 1480 volts ; (4) i = 0 5 m.a., v = 1200 volts.
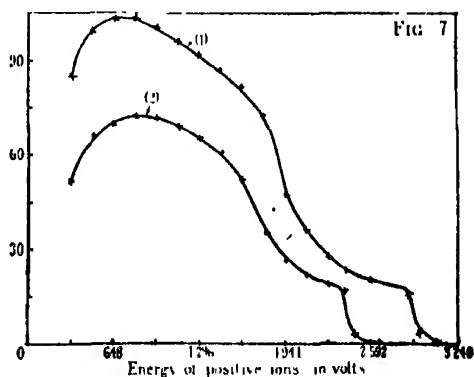
FIG. 7.—Gas = air, P = 0·020 mm. Hg. (1) i = 0·8 m.a., v = 3500 volts ; (2) i = 0·45 m.a., v = 3050 volts.

to a greater increase in the number of ions with energies in the neighbourhood of the maximum of the curve than of ions with greater energies.

The curves given are typical of a large number obtained in these experiments, for a range of pressure from 0·02 mm. to 0·12 mm. of mercury, this being the range over which a discharge could be maintained easily with a low enough pressure behind the cathode.
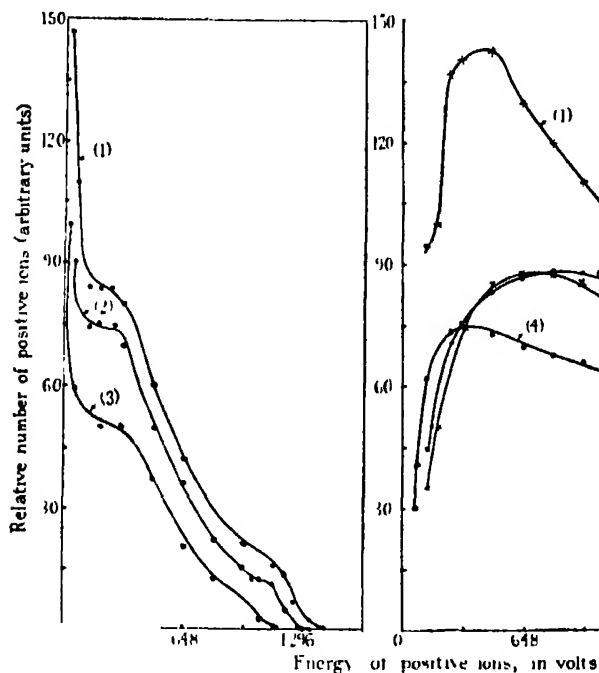
FIG. 8.—Gas = air, P = 0·124 mm. Hg. (1) ι = 4·0 m.a., v = 1100 volts; (2) ι = 3·0 m.a., v = 990 volts; (3) ι = 2·0 m.a., v = 870 volts.
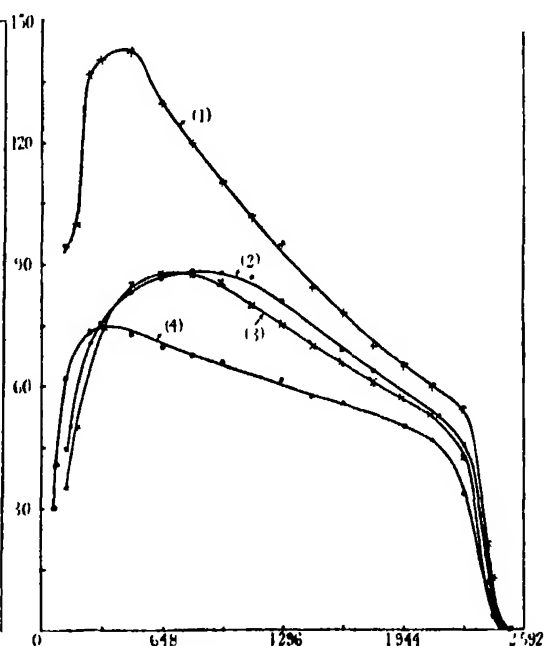
FIG. 9.—Gas — air, discharge volts = 2800. (1) ι = 2·0 m.a , P = 0·0415 mm. Hg; (2) ι = 1 0 m.a , P = 0·033 mm. Hg; (3) ι = 0·8 m.a., P = 0·0305 mm. Hg, v = 2750 volts; (4) ι = 0·6 m.a., P = 0·0265 mm. Hg.

Similar curves were taken with hydrogen and with argon. Experiments could not be performed with hydrogen over as great a range of pressure as with air, owing to its high sparking potential and to the rapid diffusion through the slit giving a high pressure behind the cathode. The curves obtained and given in fig. 10 are, however, similar to those obtained in air. The maximum lies in the neighbourhood of zero energy for all pressures used. The positive ion currents obtained with hydrogen were always much larger than those obtained with the same discharge currents in air or argon at similar pressures. Typical curves for argon are given in fig. 11, and it is evident that they are of
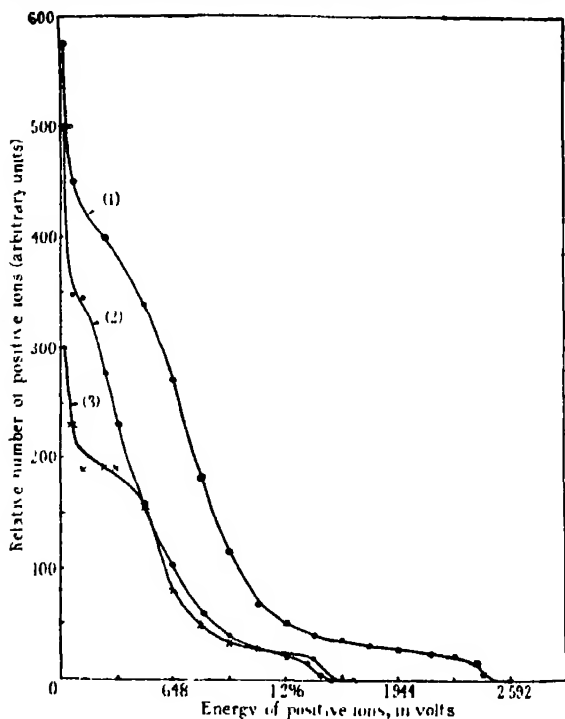
Fig. 10.—Gas = hydrogen. (1) $i = 0.4$ m.a., $v = 2650$ volts, P = 0.103 mm. Hg ; (2) $i = 2.0$ m.a., $v = 1410$ volts, P = 0.196 mm. Hg. (3) $i = 1.0, 0.9$ m.a., $v = 1520$ volts, P = 0.161 mm. Hg.
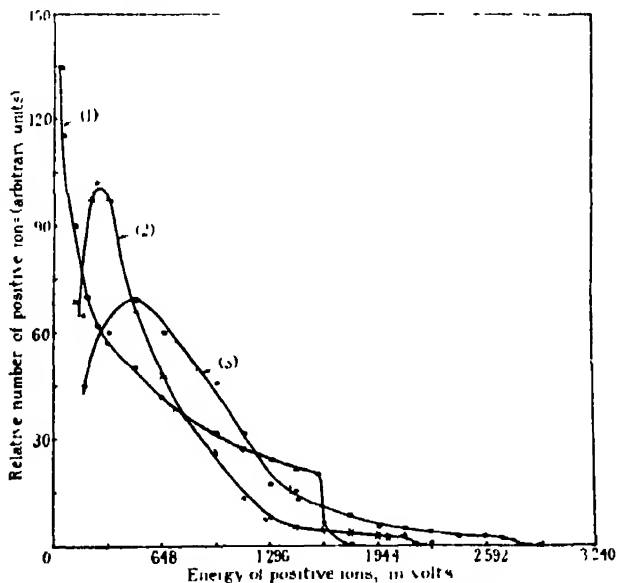
Fig. 11.—Gas = argon. (1) $i = 7.0$ m.a., $v = 1670$ volts, P = 0.134 mm. Hg ; (2) $i = 0.6$ m.a., $v = 2475$ volts, P = 0.0565 mm. Hg ; (3) $i = 0.35, 0.30$ m.a., $v = 3225, 3250$ volts, P = 0.0395 mm. Hg.

the same general character as those found for air and hydrogen, but the currents obtained to the Faraday cylinder for a given discharge current and pressure were smaller than for those gases.

It is obvious from all these results that in air, hydrogen and argon, the maximum energy of the positive ions which strike the cathode, at all pressures and current densities which have been used, corresponds with the full potential on the discharge tube, within 10 to 15 per cent. The results are collected in Table I.

Table I.

Gas	Pressure	Discharge current	Discharge potential.	Maximum energy of positive ions.
	mm of Hg	m a.	volts	volts
Air	0·124	2 0	870	907
	0 085	1 0	1030	1036
	0 124	4 00	1100	1198
	0 056	0 5	1200	1231
	0 056	1 0	1480	1458
	0 034	0 25	1680	1684
	0 056	1 5	1750	1782
	0 047	1 35	1940	1800
	0 056	2 0	2075	2041
	0 034	0 50	2200	2009
	0 028	0·90	2550	2268
	0 030	0 80	2750 {	2462 / 2430
	0·026	0 60	2800	2462
	0 033	1 0	2800	2462
	0 041	2 0	2800	2462
	0 034	1 0	2850	2462
	0 020	0 45	3050	2500
	0 037	1 7	3300	2754
	0 020	0 8	3500	2950
	0 034	1 2	3700	3142
H₂	0 196	1 0	1150	1231
	0·196	2 0	1420	1425
	0 161 {	1 0 / 0 9	} 1520	1523
	0·103	0 2	2200	1976
	0·103	0·4	2650	2397
Ar	0·134	4 2	1370	1393
	0·134	7 0	1670	1588
	0 056	0 6	2475	2170
	0 039 {	0 35 / 0·30	} 3225	2689

Discussion.

It is seen from the above results that the energy distribution among the positive ions striking the cathode of a glow discharge between plane parallel electrodes is, in any one gas, a function of pressure alone. At any particular

pressure the number of ions possessing any one energy is approximately proportional to the discharge current.

The maintenance of the glow discharge is generally assumed to be effected by the liberation of electrons from the surface of the cathode by the impact or neutralisation of positive ions. If n positive ions are required on the average, to produce one electron from the cathode, then the electron set free must produce a mean number of ions, n, sufficient to reproduce itself when they reach the cathode. These ions will be produced throughout the dark-space and, in the absence of loss of energy by collision with gas atoms, will strike the cathode with energy corresponding to the potential difference between the place of origin and the cathode surface. According to Aston* the field in the dark-space is a linear function of the distance from the edge of the negative glow, but observation of the Stark effect† shows that the field exhibits a maximum in the immediate neighbourhood of the cathode, and falls off rapidly between there and the surface. The number of ions produced by an electron per centimetre of its path through a gas is a function of the energy. It is zero for energies smaller than the ionisation energy, increases linearly from that value to twice the ionisation potential and then more slowly to a maximum at an energy which lies, in general, between 50 and 100 volts, thereafter decreasing. The existence of this maximum affords a qualitative, though not quantitative, explanation of the normal cathode fall of potential.‡ Let us see what energy distribution among the positive ions would follow from these facts.

Electrons set free from the cathode surface will not produce ions till they have fallen through the ionisation potential of the gas. Thus, in the absence of collisions, there would be no ions colliding with the cathode with energy less than this value. At reasonably low pressures in air and argon the number of ions with energies less than about 300 volts falls off rapidly with decrease in energy and appears to be very small indeed for low energies, as shown in fig. 4. It is difficult to make any quantitative estimate of the way in which the ionisation will vary with distance from the cathode, for the field is varying, while the original electrons will be mixed with the new-born ones resulting from the ionisation along the path. It can be shown (J. J. Thomson, *loc. cit.*) that Aston's linear variation of the field is consistent with the assumption of uniform ionisation throughout the dark-space. Hence we would assume that

* 'Proc. Roy. Soc.,' A, vol. 84, p. 526 (1911).
† Brose, 'Ann. Physik,' vol. 58, p. 731 (1919).
‡ Steinbeck, 'Z. Physik,' vol 53, p. 192 (1929).

the number of ions with any given energy would increase rapidly above the ionisation potential, approaching a constant value which would be maintained, in the absence of collisions, up to the potential corresponding to the cathode fall, and would then drop suddenly to zero.   The experimental energy distribution curves show a maximum, however.

The cathode dark-space is of the order of 20 to 100 molecular free-paths in thickness, but, owing to lack of knowledge of the relation this bears to the mean-free-paths of positive ions, we cannot calculate the loss of energy of the ions as they pass across the dark-space.   Experiments on the mean-free-path of positive ions in gases have been made by several investigators,* but the results obtained have little application to the discharge since they have practically all been carried out with ions moving in some different gas.   There is also the difficulty that there are two different processes by which the energy of the positive ions may be degraded.   Firstly, ordinary collisions between the ions and the atoms of the gas, which have the same mass, will lead to loss of energy and to deviation from the original path.   Secondly, a process of electron exchange may take place between the ion and neighbouring atoms, by which the ion is neutralised and a fresh ion produced without there being, necessarily, any exchange of kinetic energy.   This process has been investigated by Kallman and Rosen,† who found that the probability of this transfer depended very markedly on the relation between the neutralisation energy of the ion, N, and the ionisation potential of the neutral atoms, I.   When the difference (N — I) is large the probability of transfer of the electron is small, but it increases rapidly as (N — I) decreases to small values, approaching a finite maximum when (N — I) is zero.   Now in the discharge in simple gases we are concerned with the passage of ions through the gas from which they originated by simple ionisation, so that N and I are identical.   It follows that the process of capture of electrons will be very marked, and that fresh slow ions will be produced throughout the dark-space by the neutralisation of the original ions.   It is impossible to make any quantitative estimate of the frequency of the exchange, as it is certain that the presence of a large electric field will considerably modify the value found in a field-free space.   However, it is possible that this process would account for the presence of the peak found in the experimental energy distribution curves given in this paper, with the resulting preponderance of slow-moving ions.

---

* Dempster, 'Proc. Nat. Acad. Sci., Wash.,' vol. 12, p. 96 (1926).
† 'Z. Physik,' vol. 61, p. 61 (1930).

Under the conditions which exist in most discharge tubes the number of electrons set free from the cathode by the impact of a positive ion increases with the energy of the ions. The cathode fall of potential is much reduced if the efficiency of liberation of electrons by the ions is increased. For instance, in the same gas the cathode fall is much greater with the negative electrode made of a metal such as clean platinum than it is when that electrode is covered with an alkali metal. It is known that the impact of a positive ion of given energy sets free many more electrons in the latter case than it does in the former. Now if the ions which traverse the dark-space lose much energy by collision we would expect that a reduction of the length of the path of the ions through the gas before they reached the cathode would increase their average energy, and hence decrease the cathode fall by increase of the number of electrons liberated. A magnetic field applied to the discharge parallel to the cathode surface reduces the width of the dark-space by curving the paths of the electrons which probably traverse the same length of path through the gas in travelling to the negative glow as they did in the absence of the field. However, the positive ions will be scarcely affected by the small field required, and will now traverse a much smaller path through the gas before colliding with the cathode. We would expect a reduction of the cathode fall of potential under these conditions. Holm* has shown that the width of the dark-space may be reduced to one-tenth of its original value without appreciably altering the cathode fall. This would indicate that the energy distribution of the ions was unaffected by the presence of the field and the reduction in the length of path through the gas. We must conclude that the ions make few, if any, collisions with gas molecules which result in a loss of kinetic energy as they traverse the dark-space. On this account it is perhaps not surprising that we find some ions present which have the full energy corresponding to the cathode fall of potential, as shown in the curves given in this paper.

We have tested the conclusions of the last paragraph by applying a magnetic field parallel to the surface of the cathode of the second form of apparatus, and determining the energy distribution among the positive ions. It was found that the mean of two distribution curves taken with the field in each of two opposite directions was identical with the distribution found without the field, even when the dark-space was reduced to one-half or less of its former value. We are thus led again to believe that positive ions do not lose energy by collision in the dark-space. This experiment also shows that the small

* ' Phys. Z ,' vol. 16, p. 20 (1915).

slit in the cathode can have no perceptible influence on the energy distribution among the positive ions which strike it, an influence which might be expected on account of the reduced electron current outwards, for with a magnetic field the ions come from a part of the dark-space and negative glow which is effectively over another portion of the cathode.

The experimental results show that the number of ions with a given energy increases proportionally with the current at any particular pressure. However, if the voltage is kept constant and the current is varied by varying the pressure, it is found that the number of slow ions increases with the current, *i.e.*, with the pressure, more rapidly than the number of faster ions, as shown in fig. 9. This is possibly due to increase in the probability of electron exchange with increase in the pressure of the gas.

Summary.

(1) The energy distribution among the positive ions which strike the cathode of the glow discharge through gases has been determined by the retarding potential method and by an electrostatic focussing method. It is found that the distribution is independent of the current and the voltage across the dark space within the rather large errors of measurement. It is a function of pressure alone.

(2) The maximum energy of the positive ions is equal, within the experimental error, to the cathode fall of potential

(3) At a constant pressure the number of positive ions with any particular energy increases proportionally with the current density in the discharge.

(4) At a particular voltage the number of positive ions with small energy increases more rapidly than the number with higher energy as the pressure, and hence the current density, is increased.

(5) A partial explanation of the distribution found is offered in terms of the variation of the efficiency of ionisation by electrons with change in their energy, and of the process of electron exchange between the ions and the neutral atoms of gas. This discussion leads to the conclusion that the positive ions do not make an appreciable number of collisions with gas molecules which result in a loss of energy, in spite of the fact that the dark-space is from 20 to 100 molecular free-paths in thickness.

The Scattering of Alpha Particles at small Angles by Helium.

By P. WRIGHT, Ph D., Fellow of the University of Wales.

(Communicated by Lord Rutherford, F R.S.)

(Received June 10, 1932)

It has been shown by Mott[*] on the basis of the wave mechanics, that in the case of collisions between identical particles the scattered particles should interfere with the projected particles travelling in the same direction. When α-particles are scattered in helium, if the scattered α-particles and projected helium nuclei of similar velocity are identical in all respects, there will be interference between the two streams of particles For collisions in which the particles act upon each other with forces varying as the inverse square of the distance between them, the interference results in the scattering intensity varying above and below the classical value and rising to double the classical numbers at 45°. At small angles the scattering predicted by the quantum mechanics does not differ greatly from that given by the classical theory.

An experiment carried out by Chadwick[†] showed quite definitely that for sufficiently slow α-particles the amount of scattering at 45° was double that of the classical theory. For these α-particles of low velocity the results showed that the forces varied very little from Coulomb forces ; hence it was evident that the discrepancy was due to the failure of the classical theory. The scattering of slow α-particles by helium has also been investigated by Blackett and Champion[‡] by means of an expansion chamber. The observed scattering was in good agreement with the wave mechanical scattering. These experiments verify the assumption upon which Mott's theory is based, namely, that it is impossible to distinguish between an α-particle and a nucleus of helium travelling at the same velocity. Thus the helium nucleus has no spin or vector quantity associated with it ; its field of force is perfectly spherical.

The distance of collision for the slowest α-particles used in Chadwick's experiments on the scattering at 45° was about $7 \cdot 8 \times 10^{-13}$ cm. and the results suggested that a true change in the law of force takes place at smaller collision distances. From previous observations by Rutherford and Chadwick[§]

[*] ‘ Proc. Roy. Soc ,’ A, vol. 126, p. 259 (1930).

[†] ‘ Proc. Roy. Soc.,’ A, vol. 128, p. 114 (1930).

[‡] ‘ Proc. Roy. Soc.,’ A, vol. 130, p. 380 (1931).

[§] ‘ Phil. Mag.,’ vol. 4, p. 805 (1927).

of the scattering at small angles, it appears that the distance of approach between the centres of colliding particles must be nearer 15×10^{-13} cm. before inverse square numbers are reached. The effects of polarisation would not account for the departure from classical scattering at these comparatively great distances of collision.

In the experiments[*] on the scattering at small angles the low velocity α-particles were produced by placing absorbing sheets of mica in the path of a beam of particles of initial range 6·9 cm. from a source of radium active deposit. It is probable that these measurements were unreliable owing to the heterogeneity of the incident beam brought about by the passage of the α-particles through the absorbing sheets of mica. In the present series of experiments the measurements of scattering at small angles were repeated and extended to scattering of α-particles of low velocity by using α-particles of smaller initial range, 3·9 cm., from polonium. The scattering was measured for the ranges of angles 8° to 12° and 12° to 18°, so without involving any appreciable error the results may be taken to represent the scattering at 10° and 15° respectively. Shortly after these experiments had been completed, a wave mechanical solution of the problem of the anomalous scattering by helium and hydrogen was put forward by H. M. Taylor.[†] The scattering deduced from this theory is in close agreement with the observed scattering by hydrogen and is in fair general agreement with the observed scattering in helium.

The anomalous scattering is explained by the wave mechanics as a consequence of the scattering by the non-Coulombian fields of force. Taylor[‡] points out that, without any specific model of the nucleus, the anomalous scattering at any given velocity can be deduced in terms of a single parameter which determines the amplitude of the spherically symmetrical wave scattered by the region where the interaction energy differs from the Coulomb value. For scattering in helium, the ratio R of the number of particles scattered through an angle ϕ to the classical Coulombian number is given by

$$ R = \frac{|\operatorname{cosec}^2 \phi \cdot e^{-i a \log \sin^2 \phi} + \sec^2 \phi \, e^{-i a \log \cos^2 \phi} + 2i \, (e^{2iK_0} - 1)/a^2|^2}{\operatorname{cosec}^4 \phi + \sec^4 \phi}, $$

where K_0 is the single parameter referred to, and $a = 8\pi e^2/vh$, v being the velocity of the incident α-particles.

The experimental value for R at any one given value of ϕ and v determines

* 'Phil. Mag.,' vol. 4, p. 605 (1927).
† 'Proc. Roy. Soc.,' A, vol. 134, p. 103 (1931).
‡ 'Nature,' vol. 129, p. 56 (1932).

K_0 for that velocity, and the formula will then predict R for other angles. If the values of K_0 are calculated for two or more different velocities, they can be used to determine a model for the nuclear field. The model determined by Taylor from the observed scattering in helium is of the type postulated by Gamow to account for radioactive phenomena.

In the more complete treatment of the problem a series of phase constants K_0, K_2, K_4, ..., K_{2n}, should be considered, though good reasons are produced to show that only the first term involving K_0 is of importance. However, the term in K_2 becomes zero for $\phi = 27° 23'$ so that it would be possible to calculate K_0 exactly from the experimental scattering at this angle, provided that the remaining terms of the series are negligible. Using values of K_0 calculated from the observed scattering at 27°, it would then be possible to deduce the corresponding values of K_2 from the observed scattering at another angle. With this object in view, measurements of the scattering at 27° (angular limits 23° to 31°) were made. It has been found, however, that the theory cannot be extended with advantage beyond a consideration of the single parameter K_0.

The Experimental Method.

The experimental arrangement used in these experiments was the annular ring method as adapted for the observation of scattering of α-particles in a gas by
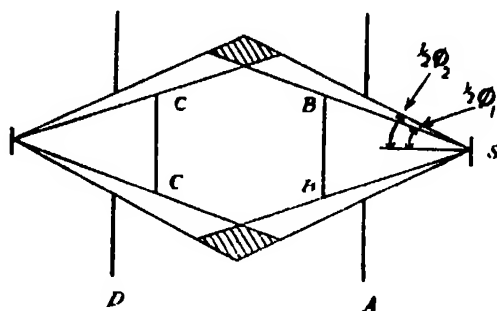
FIG. 1.

Rutherford and Chadwick (*loc. cit.*). The incident beam of α-particles proceeding from a source S was an annular ring of limits $\phi_1/2$, $\phi_2/2$, fig 1, defined by the diaphragms A and B, while a similar pair C and D defined the scattered beam received by the counting area Z. The region of the gas effective in scattering particles to Z was an annular ring, shown shaded in fig. 1.

For helium, the number of α-particles scattered per second to unit area at Z, on classical theory and for Coulomb forces, is given by

$$\frac{Q\,nt\,b^2}{16r^2}(\cosec^2\phi_1 - \cosec^2\phi_2),$$

where

$Q =$ number of α-particles emitted per second by source,

$n =$ number of helium atoms per cubic centimetre,

$t =$ mean scattering path in the gas,

$r =$ mean distance from source to scattering region,

$b = \dfrac{2E^2}{MV^2}.$

Similarly the number of projected helium nuclei reaching unit area at Z per second should be

$$\frac{Q\,nt\,b^2}{16r^2}(\sec^2\phi_2 - \sec^2\phi_1).$$

These projected helium nuclei correspond to α-particles scattered between angles $\pi/2 - \phi_1$ and $\pi/2 - \phi_2$.

As in the experiments of Rutherford and Chadwick (*loc. cit.*) and of Chadwick (*loc. cit.*) the number of particles to be expected at Z according to the above formulæ was determined by comparing the scattering in helium with the scattering in argon under the same conditions. To calculate the numbers directly from the formulæ it would be necessary to have theoretically exact geometrical conditions in the apparatus and to know the efficiency of the counter, and the values of Q and of V. It is difficult to estimate V directly in cases where absorbing sheets of mica are placed over the source to produce incident α-particles of lower velocity. By adjusting the pressure of the argon to give the same stopping power as the helium, the velocity distribution of the α-particles in the scattering region can be made the same in both cases even if the beam is heterogeneous. It has been shown by Rutherford and Chadwick that in collisions between the α-particle and the argon nucleus the forces obey Coulomb's Law. For scattering in argon, the number of α-particles arriving on unit area of the counting aperture Z per second is

$$\frac{Q\,n_1t_1\,b_1^2}{64r^2}(\log\tan\phi_2/4 - \log\tan\phi_1/4 + \cot\phi_1/2\,\cosec\,\phi_1/2$$
$$- \cot\phi_2/2\,.\,\cosec\,\phi_2/2)$$

where

n_1 = number of argon atoms per cubic centimetre,

$t_1 = t \cos \phi/2$, and t = mean scattering path in the gas,

$$\phi/2 = \frac{\phi_1/2 + \phi_2/2}{2}$$

$b_1 = 36e \cdot E/MV^2$.

The apparatus employed is shown in fig. 2 and was similar to that used by Rutherford and Chadwick except that the scintillation screen was replaced by the window of a Geiger proportional counter. The needle of the detector was
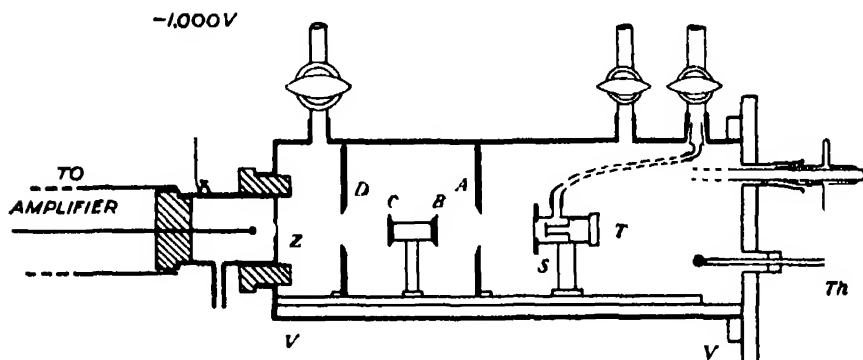
Fig. 2.

connected to a four-stage valve amplifier and the impulses recorded by means of headphones. The counter was mounted in a large ebonite plug fixed in the end plate of the scattering chamber VV, and presented an aperture of diameter 0·56 cm., covered with a mica window of 0·7 cm. stopping power, for the reception of the scattered particles. The counting area was tested and found to be uniformly efficient for the recording of α-particles entering the counter in the direction normal to the plane of the window. The case of the counter was charged negatively to about 1000 volts and the air in the counter was at the critical pressure of 10 cm. of mercury. Under these conditions the current from the detector was proportional to the ionisation; hence disturbances due to β- and γ-radiation were usually small.

The source, a disc of 5 mm. diameter, was enclosed in a brass tube T the end of which was covered with a thin sheet of mica or, in some cases, a film of collodion. This tube was provided with a separate connection, via a U-tube in liquid air, to the pump system, in order to avoid contamination of the scattering chamber.

The diaphragms A and D consisted of graphite sheets having circular apertures of diameter 9 mm. and the diaphragms B and C were graphite discs of the same diameter. The source and diaphragms were carried on a brass plate fixed to the base of a cylindrical brass vessel VV. The source, diaphragms and counting aperture Z, were carefully centred on a common axis.

To reduce extraneous scattering all metal surfaces were covered with paper. The apertures A and D and discs B and C had the same diameter 9 mm., the diameter of the source being 5 mm., so that the scattering to Z from graphite edges was usually negligible. The amount of contamination together with the natural effect could be determined at any time during an experiment by rotating in front of the source a graphite screen carried by the ground joint G. By rotating the ground joint still further a sheet of mica could be introduced in the path of the incident α-particles so that the scattering of two different ranges of α-particles could be compared in the course of one experiment. Usually, the same mica screen was used throughout a series of experiments at any one angle of scattering and further reduction in the range of the α-particles was brought about by placing sheets of mica or films of collodion over the end of tube T in addition to the fixed mica or collodion window.

For α-particles of range greater than about 3 cm. the active deposit of radium on a 5 mm. button of polished nickel was used as a source, and for ranges shorter than 3 cm. a platinum disc of diameter 5 mm. coated with polonium was used. The source was fixed in the tube T and the carrier inserted in the scattering chamber which was then slowly evacuated. A good vacuum was necessary in order to prevent discharges from the case of the Geiger counter to the scattering chamber. The amount of extraneous scattering was then determined from the number of α-particles entering the counter.

Pure helium was admitted slowly into the scattering chamber through a U-tube containing charcoal which was immersed in liquid air. After completing the observations of the scattering in helium, the gas was pumped back into the container and the apparatus evacuated. Argon was then introduced and corresponding observations carried out.

Results and Discussion.

Each point on the graphs given below represents the mean of the results of several experiments in the cases where Ra (B + C) was used as the source of α-particles. With helium as the scattering gas, it was usually possible to count several hundred particles, and with argon several thousand, in each experiment.

The error due to probability fluctuations is less than 5 per cent. for the mean values given.

In general, the argon scattering was found to obey the Coulomb Law. Apparent deviations were, however, observed with incident α-particles of low initial range. With the method of counting used in these experiments it was not feasible to carry out observations with α-particles, of energies at the scattering region, corresponding to ranges less than about 1·5 cm. Owing to the heterogeneity of the beam, due to straggling effects, and to the fact that the α-particles pass through the absorbing screens at different angles, many of the particles fail to penetrate the mica window of the Geiger counter. This was evident from the observations of the scattering in argon, particularly in the experiments at larger angles of scattering. A marked deficiency of scattering was observed at 27° with incident α-particles of low initial range. The angular limits in this series of experiments were 23° and 31°, the distance between source and counter was only 5·9 cm. compared with the distance of 16 cm. for scattering at 10°, and the diameters of the source and counter window were not small compared with the diameters of the diaphragms. Thus many of the particles arriving near the circumference of the counter window are those scattered through angles greater than 31°. They enter the mica window obliquely and many of them fail to be recorded.

When an α-particle is scattered through a large angle by collision with a helium nucleus it loses energy. It is possible that with the α-particles of smallest initial range dealt with in these experiments, the efficiency of counting was less in the helium observations than in those with argon. The difference, which should be small for the angles at which scattering was observed in this investigation, would tend to make the observed ratios smaller than they should be.

The pressures of helium used varied from about 5 cm. to 45 cm. according to the range of the α-particles and the angle of scattering. In order to reduce the absorption of the scattered particles in the gas the pressure of helium was adjusted as low as was sufficient to give a convenient number of particles for counting.

The scattering was observed at mean angles of 10°, 15° and 27° for several ranges of α-particles between 1·4 cm. and 6 cm. The ratio R of the observed to classical scattering in helium was determined by dividing the ratio of the observed scattering in helium to the observed scattering in argon by the calculated ratio of scattering in helium to scattering in argon. The mean values of R, and the average range of the α-particles at the point of scattering,

for the series of experiments at each of the above angles of scattering, are tabulated below.

Scattering at 10°.   (Angular limits 8° to 12°.)
Ra (B + C) source.

Range.	5·6	4 9	4·4	3·7	3·1	2·5
R	0 90	0 65	0 51	0 42	0 53	0 82

Po source

Range.	3 4	3 3	3 2	3 0	2 6	2 5	1·6	1·4
R	0 61	0 58	0 60	0 64	0 78	0 86	0 87	0·87

Scattering at 15°.   (Angular limits 12° to 18°.)
Ra (B + C) source.

Range	5 9	5·2	4 9	4 8	4·2	3·7
R	2·5	1·7	1 4	1 3	0 63	0·40

Po source.

Range.	2 8	2 1
R	0 67	0 87

Scattering at 27°.   (Angular limits 23° to 31°.)
Ra (B + C) source.

Range.	6 1	5 25	4 7	4 3	3 8	3 3	2 8
R	3 7	2 83	2 26	2 0	1 56	1·23	1·00

Po source.

Range.	3 0	2 55	2·0	1 6
R.	0·97	0·97	1 00	1·2

In figs. 3, 4, and 5 the values of R predicted by Taylor's theory are shown by the broken lines. They are calculated from the formula involving the single
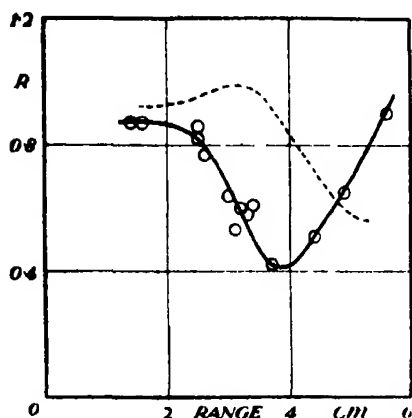
FIG. 3.—Scattering at 10°.
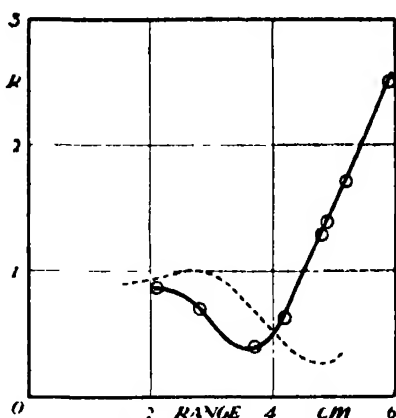
FIG. 4.—Scattering at 15°.

parameter K_0. The numerical values of K_0 used for the calculation were those deduced by Taylor (*loc cit*) from the observed scattering at 45°, on the assumption that the remaining phase constants K_2, K_4, , K_{2n} may be
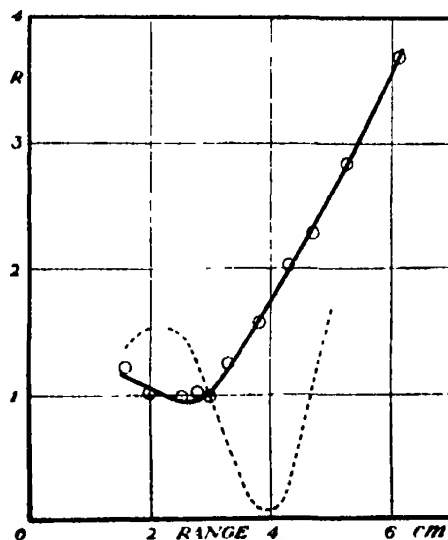
FIG. 5.—Scattering at 27°.

neglected. It will be shown later that it is not possible to obtain from the observed scattering at 27° a set of values of K_0 which can be used to predict the scattering at other angles.

The theoretical curves do not extend to ranges of α-particles beyond about 5·4 cm. The equation for K_0 has no real solution at higher velocities, that is, the phase change K_0 by itself is unable to account for the large values of the anomalous scattering.

The observed scattering at 10° and 15° is in general agreement with previous measurements[*] of the scattering at these angles. Divergences occur at shorter ranges where the earlier experiments were in error due to the effects of straggling, etc. For the lower velocities of α-particles used, the observed scattering at 10°, 15° and 27° approaches closely to that predicted by Mott for inverse square forces.

Curves giving the values of K_0 calculated from the scattering at 27° are shown in fig. 6. It will be observed that there are two values of K_0 corresponding to each value of the range or velocity. Now, at low velocities the scattering is Coulombian, hence K_0 must tend to zero as the velocity diminishes.
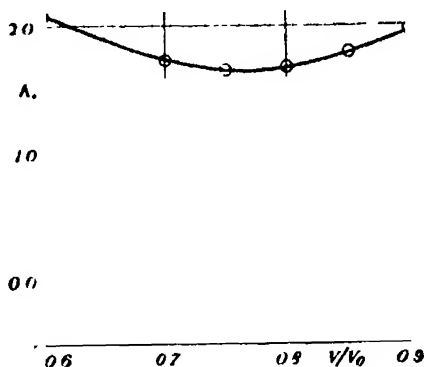
Fig. 6.—Values of K_0 calculated from scattering at 27°. v = velocity of incident α-particles, v_0 = velocity of α-particles from Ra C, $1 \cdot 922 \times 10^9$ cm./sec.

Again, for large values of the velocity, K_0 must be positive since the divergence of the potential field from a Coulomb one is such as to make the wave-length of the wave function for $r < a$, where r is distance from the centre of the nucleus and a is the radius within which the forces are no longer inverse square, less than the wave-length in the Coulomb field. Hence it becomes necessary to suppose that the two sets of values of K_0 are in reality cross connected. Such a procedure is more dubious here than in the case where the curves for K_0 are calculated from the scattering at 45°, and it would be futile to attempt to use

---

[*] ' Phil. Mag.,' vol. 4, p. 605 (1927).

values of K_0 thus determined to deduce values of K_2 from the observed scattering at another angle. Values of K_2 were calculated, however, from the lower curve for K_0 and the observed scattering at 45°, though there are objections to this procedure. The scattering at other angles calculated by using the two parameters K_0 and K_2 was found to differ very widely from the observed scattering.

It is evident that the analysis cannot be extended to a consideration of more than one parameter K_0. The fact that the observed scattering at 27° does not provide a set of values of K_0, which can be used to deduce values of the second parameter K_2, would appear to indicate that the remaining terms of the series are of some importance. At the same time, the scattering deduced by using the approximate values of K_0, determined from the observed scattering at 45°, is in fair agreement with experiment. It must be concluded, therefore, that if more than one parameter is to be used then it is necessary to consider not only K_2 but also the remaining terms of the series.

The agreement between the scattering deduced using a single parameter, and the observed scattering at angles 45° to 10°, is sufficiently close to support the general explanation put forward by Taylor, namely, that the phenomenon is a consequence of the wave mechanical scattering by the region of the helium nucleus where the forces differ from inverse square forces.

Summary.

Earlier work by Rutherford and Chadwick on the collisions of α-particles with helium nuclei seemed to point to some asymmetry of the helium nucleus, whereas we know now, both from spectroscopic evidence and studies of collisions of certain types, that the helium nucleus is perfectly symmetrical. The present experiments have in general confirmed and extended the older work. The results thus suggested a contradiction in our ideas. Before the work was completed, however, a satisfactory explanation of the anomalous scattering was given by H. M. Taylor on the basis of the wave mechanics.

The experimental arrangement used in this investigation was the annular ring method as adapted by Rutherford and Chadwick for the observation of scattering of α-particles in a gas. The scattered particles were recorded by means of a Geiger proportional counter used in conjunction with a valve amplifier. The agreement between the observed scattering at angles 10°, 15° and 27°, and the scattering predicted by Taylor's theory was sufficiently close to support the general explanation put forward by Taylor, namely, that

the phenomenon is a consequence of the wave mechanical scattering by the region of the helium nucleus where the forces differ from inverse square forces. The present paper shows that the collisions of α-particles with helium nuclei can only be explained on the wave mechanics and it indicates also how far such calculations can give an accurate picture of the collision processes.

It is a pleasure to express my thanks to Lord Rutherford for his interest in this research and to Dr J. Chadwick, who suggested the problem, for much valuable advice. I also wish to acknowledge my indebtedness to Mr. J. P. Gott who collaborated with me in the earlier stages of the work, and to Mr. H. M. Taylor for many helpful discussions.

The Scattering of Fast β-Particles by Electrons.

By F. C. CHAMPION, Ph.D., Cavendish Laboratory, Cambridge.

[PLATE 22]

1. *Introduction.*

In a recent paper,† it has been shown, using the expansion method, that the simple relativistic expressions govern the transfer of momentum and energy during the close collisions of fast β-particles with electrons. The present paper gives an account of an investigation of the scattering of fast β-particles by electrons, using the expansion method.

Among the many formulæ‡ which have been proposed to express the interaction of two electrons, the relativistically invariant expression due to Moller§ appears to be the most satisfactory theoretically.‖ Moller has referred the scattering for all velocities¶ to a Lorentz frame of co-ordinates in which the

† Champion, ' Proc. Roy Soc.,' A, vol. 136, p. 630 (1932).

‡ Gaunt, ' Proc. Roy. Soc.,' A, vol. 122, p. 513 (1929) ; ' Phil. Trans.,' A, vol. 228, p. 151 (1929) ; Breit, ' Phys. Rev.,' vol. 34, p. 553 (1930) ; Wolfe, ' Phys. Rev.,' vol. 37, p. 591 (1931) ; Inglis, ' Phys. Rev.,' vol. 37, p. 795 (1931).

§ ' Z. Physik,' vol. 70, p. 786 (1931).

‖ Dirac, ' Proc. Roy. Soc.,' A, vol. 135, p. 453 (1932) ; Heisenberg, 'Ann. Physik,' vol. 13, p. 430 (1932).

¶ The writer is indebted to Dr. Möller for communicating these results by letter.

momenta of the two electrons are equal and opposite. The observed angle of scattering θ is connected with θ^*, the angle of scattering in the Lorentz frame, by the relation

$$x = \cos \theta^* = \frac{2 - (\gamma + 3) \sin^2 \theta}{2 + (\gamma - 1) \sin^2 \theta}, \tag{1}$$

where $\gamma = 1/(1 - \beta^2)^{\frac{1}{2}}$ and $\beta = v/c$, v being the relative velocity of the two particles before collision and c the velocity of light.

The expression for the scattering is

$$dQ(\theta) = 4\pi \left(\frac{e^2}{m_0 v^2}\right)^2 \frac{(\gamma + 1)}{\gamma^2} dx \left\{ \frac{4}{(1-x^2)^2} - \frac{3}{(1-x^2)} + \frac{(\gamma - 1)^2}{4\gamma^2} \left[1 + \frac{4}{(1-x^2)} \right] \right\}. \tag{2}$$

It is interesting to note that the formula contains no terms in Planck's constant h. At low velocities, equation (2) becomes

$$dQ(\theta) = \left(\frac{e^2}{m_0 v^2}\right)^2 \sin 2\theta \; 2d\theta \; d\phi \left\{ (\operatorname{cosec}^4 \theta + \sec^4 \theta - \operatorname{cosec}^2 \theta \sec^2 \theta) \right.$$
$$\left. - \frac{\beta^2}{4} \left[4 \operatorname{cosec}^4 \theta + 3 \sec^4 \theta - 2 \operatorname{cosec}^2 \theta \sec^2 \theta - 3 \sec^2 \theta \right] \right\}. \tag{3}$$

Now Mott[†] has obtained the following formula for the scattering of slow β-particles[‡] by electrons :—

$$dQ(\theta) = \left(\frac{e^2}{m_0 v^2}\right)^2 \{ \operatorname{cosec}^4 \theta + \sec^4 \theta - \operatorname{cosec}^2 \theta \sec^2 \theta \cos U \} \sin 2\theta \; 2d\theta \; d\phi \tag{4}$$

where

$$U = \frac{2}{137} \cdot \frac{c}{v} \cdot \log \cot \theta.$$

It is clear that the first two terms in the first bracket of (3) and (4) represent the β-particles scattered and the electrons projected through θ respectively according to classical non-relativistic theory.[§] Further, when U is nearly

[†] 'Proc. Roy. Soc.,' A, vol 126, p 259 (1930).

[‡] This formula has been confirmed experimentally for slow β-particles by Williams, 'Proc. Roy. Soc.,' A, vol. 128, p 459 (1930), using the expansion method

[§] The term "classical non-relativistic theory" is used here and throughout this paper to refer to the case where the mass of the moving particles is assumed to be invariant and equal to the rest mass of the electron   Such a case does not occur in reality but we wish to compare the scattering laws in the regions where the relativity effects are appreciable, with those obtained by a complete neglect of relativity. Further, we wish to see what empirical changes we must make in a completely non-relativistic formula in order that the new formula may agree with experiment. The rest mass, in this paper, is always denoted by m_0, but it should be observed that in much of the existing literature, especially on the theoretical side, the symbol m without the suffix often stands for the rest mass

zero, that is when the velocity is not too small, Mott's formula (4) reduces to the first bracket of (3). The term in β^2 in (3), which is not given in Mott's expression, clearly represents the "relativity effect" for velocities which are not too great. For small angles of scattering this term becomes $\beta^2 \csc^4 \theta$, the exchange term of Mott and the $\sec^4 \theta$ term may be neglected, and the expression reduces to the classical non-relativistic formula with $m_0/(1 - \beta^2)^{\frac{1}{2}}$ in place of m_0.†

Mott's formula predicts, at large angles of scattering and large velocities, considerably less scattering than that predicted classically, the ratio being one half for all velocities when θ is 45°. Equation (3) predicts even less scattering than Mott's formula; hence both the exchange effect suggested by Mott and the effect of relativity combine to reduce the scattering much below that predicted classically for the interaction of two point charges obeying Coulomb's law of electro-static repulsion.

2. *Experimental Method.*

The great advantage of the expansion method in investigating the present problem lies in the fact that it is the only method that separates the nuclear scattering clearly and definitely from the electron scattering. Williams and Terroux‡ have considered the scattering of fast β-particles by electrons up to angles of about 12°, actually measuring not the angles of scattering, but the ranges of the recoil electrons. In a total track length of about 18 metres, with β varying from 0·60 to 0·97, they obtained about 70 branches with energies from 7500 to 40,000 volts. This number they compared with the values deduced from Bohr's formula,§

$$P(Q) = \frac{2\pi e^2 n}{m_0 v^2} \bigg/ Q^2,$$

where $P(Q)$ is the probability of formation of a branch track having an energy between Q and $Q + dQ$, v being the velocity of the incident particle. In obtaining this formula the electrons were treated classically as particles but the effects of relativity were considered. At higher velocities the observed scattering was about twice that predicted theoretically but the ratio decreased with decreasing velocity.

† It should be observed that we cannot call the formula so obtained, with m (where $m = m_0/(1 - \beta^2)^{\frac{1}{2}}$) in place of m_0, the *classical relativistic* formula, for it presumes that the mass of the electron in the atom is equal to that of the incident β-particle.

‡ 'Proc. Roy. Soc.,' A, vol. 126, p. 289 (1930).

§ 'Phil. Mag.,' vol. 30, p. 581 (1915).

The use of an automatic expansion chamber for the production of a large number of photographs of fast β-ray tracks has been described in a previous paper.† The two cameras are arranged with their axes mutually at right angles, and the angles of scattering are computed from measurements of the projected angles on the two films. The velocities of the particles are deduced from the curvatures of the tracks in a magnetic field, the latter being perpendicular to the plane of the chamber

The present results are from the analysis of 4000 photographs, giving about 30,000 tracks of fast β-particles in nitrogen Summing the small lengths of track, a total track length of nearly 2 kilometres was obtained which was homogeneous in β to within 10 per cent In order, however, to measure the curvature of a track with reasonable accuracy for the purpose of deducing the velocity of the particle, it is necessary that the first half of the track should be free from nuclear or electronic deflections. The effective track length available for the actual observation of collisions is thus reduced immediately by one-half. The effective track length for a single particle was estimated at 5 cm. although the total track length visible in the chamber was often about 12 cm. In contrast to previous experiments, the ranges of the ejected electrons were not considered, the actual angle of scattering being measured. The use of relations connecting range and energy was thus avoided

3. *The Results.*

In 650 metres of track, 250 collisions have been obtained with angles of scattering θ greater than 10`, and with β varying from 0·82 to 0·92. It was not feasible to count values of θ less than 10° owing partly to the comparatively large percentage error which would be introduced and partly to the greatly increased number of measurements it would entail.

For each collision, a dot corresponding to the observed values of θ and β was placed on a diagram with these quantities as co-ordinates, fig. 1. The density of the dots is then a measure of the scattered intensity. The scattering is no longer symmetrical about θ = 45° owing to the fact that the angle between the two arms of a fork is not now equal to 90° but becomes a function of θ and γ as given by equation (6) in a previous paper.‡ The broken line in fig. 1 indicates the maximum possible angle of scattering for the range of velocities considered here ; it is therefore the line $x = 0$, where x is defined as in equation (1).

† Champion, *loc. cit.*
‡ Champion, *loc. cit.*

F. C. Champion.

The number of collisions is observed to fall off extremely rapidly with increasing values of θ. For the purpose of numerical comparison with theory, another diagram (not shown) was plotted with x and γ as co-ordinates, the integration boundaries being taken from $\gamma = 1 \cdot 74$ to the end of the β-ray spectrum of radium E at about $\gamma = 3 \cdot 0$. These limits correspond to a range
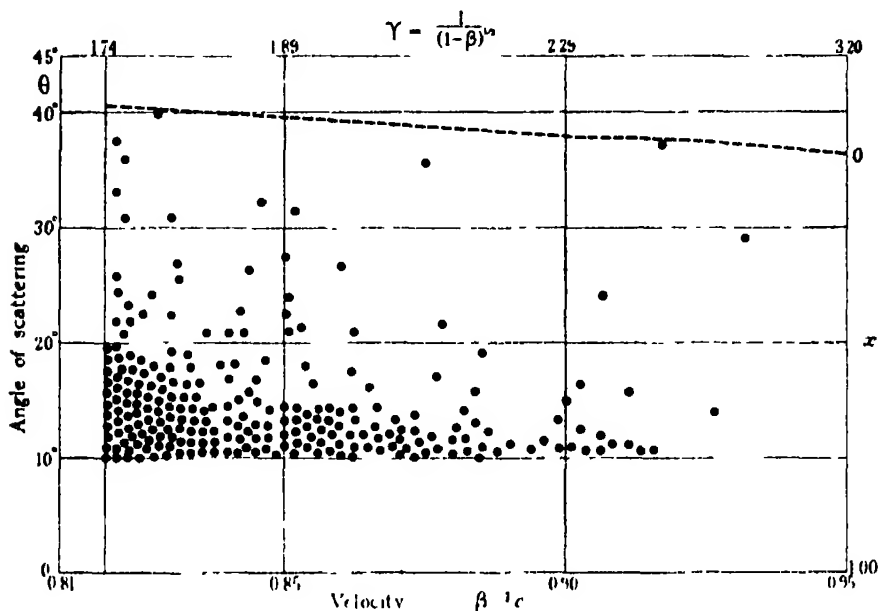
Fig. 1.

in velocity of $\beta = 0 \cdot 82 - 0 \cdot 92$, of $H\rho$ from 2400–5000 and of energies from 400,000 to 1,100,000 volts. The number of particles with energies greater than 800,000 volts, however, has been shown in a previous paper[†] to be only about 5 per cent. of the total number of particles considered. For the integration limits of x those values corresponding to θ equal to 10°, 20°, 30° and maximum, were taken It may be observed that x, besides being a function of θ, depends also on γ

The number of particles with velocities lying between values corresponding to γ and $\gamma + d\gamma$, scattered through angles corresponding to x lying between x and $x + dx$, in going a distance dr in the gas is from (2) :—

$$dq = 4\pi \left(\frac{e^2}{m_0 c^2} \right)^2 N_0 f(\gamma, x) \, dx \, dn \, dr, \qquad (5)$$

where N_0 is the number of scattering electrons per cubic centimetre of the

† Champion, ' Proc. Roy. Soc ,' A, vol. 134, p. 672 (1932).

gas and *dn* is the number of β-particles with velocities lying between γ and γ + *d*γ, while $f(\gamma, x)$ is given by :—

$$f(\gamma, x) = \frac{\gamma^2}{(\gamma^2 - 1)(\gamma - 1)} \cdot \left\{ \frac{4}{(1 - x^2)^2} - \frac{3}{(1 - x^2)} + \frac{(\gamma - 1)^2}{4\gamma^2} \left[1 + \frac{4}{(1 - x^2)} \right] \right\} \quad (6)$$

The quantity *dn* was obtained from data previously given by the writer.[†] It is clear that the chief factor influencing the decrease in the number of dots as we pass from left to right across the scattering diagram is the distribution of γ in the β-ray spectrum of radium E and not simply the smaller chance of scattering for a higher value of γ.

The integrations had, of course, to be carried out graphically. The final results are shown in Table 1 Column 1 contains the angular limits of θ, and column 2 contains the observed numbers of dots in the three cells. The numbers predicted by Moller's theory are given in the next column, while column 4 contains the values deduced from classical non-relativistic theory. Column 5 contains the values deduced from Mott's equation (4) ; in the next column are given the values obtained by substituting $m_0/(1 - \beta^2)^{\frac{1}{2}}$ for m_0 in Mott's formula. Column 7 gives the values obtained by treating the classical non-relativistic formula in the same way, while the last column gives the values obtained from this formula with T^2 in the denominator in place of $(\frac{1}{2}.m_0 v^2)^2$, where T is the initial kinetic energy of the incident β-particle.

Table 1

1	2	3	4	5	6	7	8
θ-	Observed	Möller.	C	M (Mott)	M(1 β²).	C(1 - β²)	C/T²
30-max	10	13	57	28	7	15	9
20-30	26	30	148	105	26	37	21
10-20	214	230	761	650	162	190	108
Total	250	273	966	783	195	242	138

4. *Discussion.*

First comparing the total scattering for θ greater than 10°, it will be seen that the observed values and those calculated from Moller's formula are in

† Champion, ' Proc. Roy. Soc.,' A, vol 134, p 672 (1932).

good agreement.† The classical non-relativistic formula predicts about $3\frac{1}{2}$ times as much total scattering, but if corrected by writing T^2 in the denominator for $(\frac{1}{2}m_0v^2)^2$, it gives about half the observed value. Writing $m_0/(1 - \beta^2)^{\frac{1}{2}}$ for m_0 gives a value of the right order. It is worth noting that this treatment of the classical formula gives also to a first approximation the formula deduced by Mott‡ on quantum principles for the *nuclear* scattering of β-particles. Mott's formula for electron scattering gives about three times as much as that observed and when modified by the above treatment gives too little as shown in the next column.

Examining the distribution of the scattering with varying θ we observe good agreement with Moller's formula. The non-relativistic formulae are all inapplicable but either $M(1 - \beta^2)$ or C/T^2 give good agreement for angles greater than 20°. For angles less than 20° both these corrections give values which are too low, $C(1 - \beta^2)$ being more satisfactory. This is to be expected, for we have shown that equation (3) reduces to $C(1 - \beta^2)$ for small angles of scattering. The fact that the observed scattering falls so much below that predicted classically for angles greater than 10° indicates that the scattering below this angle must, in some region, be considerably greater than the classical values. This may account for the excess scattering found by Williams and Terroux for the branch tracks up to an angle of scattering of about 10°.

The only other experiment so far performed on the scattering of fast β-particles by electrons is that of Henderson,§ who used the annular ring method. With angles of scattering between 10° and 30°, the results showed that hydrogen and helium possessed a scattering power for fast β-particles considerably in excess of that to be expected from classical considerations of the nuclear and electronic scattering powers of these elements. The conclusion that the observed electronic scattering was about three times that to be expected classically, after a certain correction had been made for the effects of relativity, cannot be said to be in good agreement with the present results, for Henderson's correction was essentially that adopted in column 7 of Table I and the present

---

† It should be remarked that the experimental difficulties encountered in determining the numbers of dots in the lowest cells of the scattering diagram for the scattering of slow α-particles by helium (Blackett and Champion, ' Proc. Roy. Soc.,' A, vol 130, p 380, 1931) are not encountered in the corresponding process in the scattering of fast β-particles by electrons. This is because it is very *difficult* to miss a small angle collision of a fast β-particle with an electron, for the ionisation along the slow branch is much denser than that of the parent track or any general background of cloud that may be present.

‡ ' Proc. Roy. Soc.,' A, vol. 124, p. 425 (1929) ; *ibid*, vol. 135, p. 429 (1932).

§ ' Phil. Mag.,' vol. 8, p. 847 (1929).

Champion.

Proc. Roy. Soc., A, vol 137, Pl. 22.

results are observed to indicate a total scattering only slightly in excess of that calculated theoretically on this basis. Both experiments, however, show that the observed values are much less than those to be expected if the electron behaved *classically* as a small magnet with a magnetic moment equal to one Bohr magneton. It is now clear that since the de Broglie wave-lengths associated with the β-particles of the energies considered here are about 100 times the closest distance of approach as calculated classically, classical conceptions are inapplicable. It is concluded that Moller's formula gives the best account of the scattering of electrons by electrons.

Summary.

From the analysis of over half a kilometre of track of fast β-particles in nitrogen, photographed by the expansion method, 250 collisions with atomic electrons have been obtained in which the angle of scattering is greater than 10°. The velocities of the incident particles lay between 0·82 and 0·92 that of light.

The absolute numbers scattered and the distribution with angle were in good agreement with a formula of Moller, based on quantum mechanics.

PLATE 22.

Description of Photographs (about one-and-a-quarter times natural size).

(1) This shows a collision near the lower limit of angle measured, having θ – 12°. The recoil electron is observed to make another collision near the end of its range

(2) Two close collisions occur here on the same photograph. For the right-hand fork β – 0 82, and it was therefore just included in the measurements. For this fork θ = 30°. The left-hand fork has β – 0·90 and θ – 18°. In this case the collision occurred in the plane of the chamber and consequently the arms of the branch remain in the illuminating beam and also in focus.

(3) Two collisions, one just below the angular limit of measurement and the other having β – 0·88 and θ = 14°.

(4) A close collision with β – 0·83 and θ = 31°.

Non-Adiabatic Crossing of Energy Levels.

By CLARENCE ZENER, National Research Fellow of U.S.A.

(Communicated by R H Fowler, F.R S.—Received July 19, 1932.)

1. Introduction.

The crossing of energy levels has been a matter of considerable discussion.[*] The essential features may be illustrated in the crossing of a polar and homopolar state of a molecule.
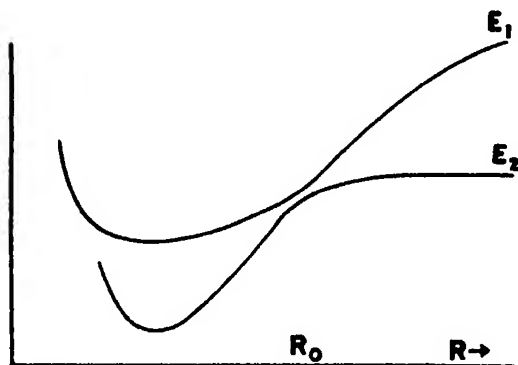
FIG. 1.—Crossing of polar and homopolar states.

Let $\psi_1(x/R)$, $\psi_2(x/R)$ be two electronic eigenfunctions of a molecule with stationary nuclei. Let these eigenfunctions have the property that for $R \gg R_0$, ψ_1 has polar characteristics, ψ_2 homopolar; while at $R \ll R_0$, ψ_2 has polar characteristics, ψ_1 homopolar. In the region $R = R_0$ these two eigenfunctions may be said to exchange their characteristics.

The adiabatic theorem tells us that if the molecule is initially in state ψ_2, and R changes infinitely slowly from $R \gg R_0$ to $R \ll R_0$, then the molecule will remain in state ψ_2. However, if R changes with a finite velocity, the final state $\psi(x/R)$ will be a linear combination

$$\psi(x/R) = A_1(R)\,\psi_1(x/R) + A_2(R)\,\psi_2(x/R). \tag{1}$$

Neumann and Wigner (loc. cit.) have found the conditions for which

$$A_1 \sim 0, \qquad |A_2| \sim 1$$

and

$$|A_1| \sim 1, \qquad A_2 \sim 0,$$

* Hund, ' Z. Physik,' vol. 40, p. 742 (1927) ; Neumann and Wigner, ' Phys. Z.,' vol. 30, p. 467 (1929) ; Kemble and Zener, ' Phys. Rev.,' vol. 33, p. 536 (1929).

respectively, without however obtaining the explicit dependence of the A's upon the parameters of the system.

In order that the problem of obtaining this explicit dependence may be reduced to a precise soluble mathematical problem, it is desirable to specify the conditions of the transition as simply as possible, at the same time retaining the essential features.

Let ϕ_1, ϕ_2 be such linear combinations of ψ_1, ψ_2, that for all values of R, ϕ_1 has the characteristics which ψ_1 has at $R \gg R_0$, while ϕ_2 has the characteristics which ψ_2 has at $R \gg R_0$. In our molecular example, ϕ_1 will be a pure polar state, ϕ_2 a pure homopolar state for all internuclear distances. While ϕ_1, ϕ_2 can be made orthogonal, they will not satisfy the wave equation for fixed nuclei, rather

$$\left. \begin{array}{l} H\phi_1 = \varepsilon_1 \phi_1 + \varepsilon_{12} \phi_2 \\ H\phi_2 = \varepsilon_{12} \phi_1 + \varepsilon_2 \phi_2 \end{array} \right\} \tag{2}$$

The simplifications which will be made in order to obtain the explicit functions A_1, A_2, are the following :—

(a) $\varepsilon_{12}(R_0) \ll$ the relative kinetic energy of the two systems. Under this condition the motion of the centres of gravity of the two atoms, or in general of the two systems, may be treated as external parameters. That is, the variable R becomes a known function of time.

(b) The transition region is so small that in it we may regard $\varepsilon_1 - \varepsilon_2$ as a linear function of time, and $\varepsilon_{12}(R)$, $\phi_1(x/R)$, $\phi_2(x/R)$ as independent of time. This condition is satisfied provided $\varepsilon_{12}(R_0)$ is sufficiently small. Since only the characteristics in the transition region are of importance, this condition enables us to replace the physical problem by an ideal problem in which

$$\left. \begin{array}{l} \dfrac{2\pi}{h} (\varepsilon_1 - \varepsilon_2) = \alpha t \\[2mm] \dot{\varepsilon}_{12} = \dot{\phi}_1 = \dot{\phi}_2 = 0 \end{array} \right\} \tag{3}$$

for all time.

If the relative velocity of the atoms is constant, assumption (b) leads to the relationship shown in fig. 2 between $\varepsilon_1(R)$, $\varepsilon_2(R)$ and the eigenwerte of ψ_1, ψ_2, namely $E_1(R)$, $E_2(R)$.

$E_1(R)$, $E_2(R)$ are hyperbolæ having $\varepsilon_1(R)$, $\varepsilon_2(R)$ as asymptotes. The closest distance between E_1 and E_2, *i.e.*, $E_1(R_0) - E_2(R_0)$, is given by $2\varepsilon_{12}(R_0)$.

C. Zener.

2. *Analysis.*

In the analysis it has been found more convenient to use the linear combinations ϕ_1, ϕ_2 of the exact adiabatic solutions ψ_1, ψ_2 rather than these
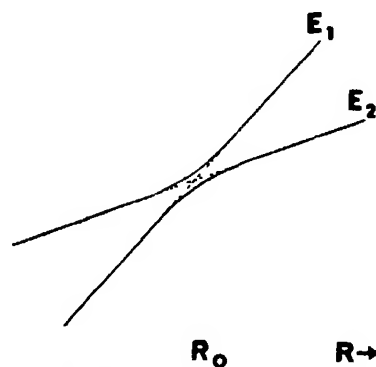
Fig 2 —Crossing of energy levels in idealised problem. Full lines are adiabatic eigenwerte.

solutions themselves. Further, it has been found advantageous to start from the wave equation in the form

$$\left(H - \frac{h}{2\pi i}\frac{\delta}{\delta t}\right)\left\{C_1(t)\, e^{\frac{2\pi i}{h}\int \epsilon_1\, dt}\, \phi_1(r) + C_2(t)\, e^{\frac{2\pi i}{h}\int \epsilon_2\, dt}\, \phi_2(x)\right\} = 0$$

The relations (2) reduce this wave equation to two simultaneous first order differential equations in the C's.

$$\left. \begin{aligned} \frac{h}{2\pi i}\frac{\delta C_1}{\delta t} &= \epsilon_{12}\, e^{\frac{2\pi i}{h}\int (\epsilon_1 - \epsilon_2)\, dt}\, C_2. \\[2mm] \frac{h}{2\pi i}\frac{\delta C_2}{\delta t} &= \epsilon_{12}\, e^{\frac{2\pi i}{h}\int (\epsilon_1 - \epsilon_2)\, dt}\, C_1 \end{aligned} \right\} \tag{4}$$

The boundary conditions under which these equations are to be solved must correspond to our knowledge that initially the system is in state ψ_2 or ϕ_2, which are equivalent when $R \gg R_0$. These conditions are thus

$$C_1(-\infty) = 0. \tag{5A}$$

$$|C_2(-\infty)| = 1. \tag{5B}$$

If we call $|A_1(R \ll R_0)|^2$ of (1) the probability P of a non-adiabatic transition, then

$$P = |C_2(\infty)|^2 = 1 - |C_1(\infty)|^2.$$

We thus need know only the asymptotic values of the solutions of (4).

Elimination of C_2 from (4) leads to the single equation

$$\frac{d^2C_1}{dt^2} + \left\{\frac{2\pi i}{h}\left(\varepsilon_1 - \varepsilon_2\right) - \frac{\dot{\varepsilon}_{12}}{\varepsilon_{12}}\right\}\frac{dC_1}{dt} + \left(\frac{2\pi\varepsilon_{12}}{h}\right)^2 C_1 = 0. \tag{6}$$

Substitution of the assumption (3), together with the definition

$$f = \frac{2\pi\varepsilon_{12}}{h}$$

and the substitution

$$C_1 = e^{-\frac{\pi i}{h}\int(\varepsilon_1 - \varepsilon_2)\,dt}\, U_1$$

reduces (6) to the Weber* equation

$$\frac{d^2U_1}{dt^2} + \left(f^2 - \frac{i\alpha}{2} + \frac{\alpha^2}{4}t^2\right)U_1 = 0.$$

This is thrown into the standard form

$$\frac{d^2U_1}{dz^2} + \left(n + \tfrac{1}{2} - \tfrac{1}{4}z^2\right)U_1 = 0,$$

by the substitutions

$$z = \alpha^{\frac{1}{2}}\,e^{i\pi/4}\,t$$

$$n = if^2/\alpha.$$

The Weber function $D_{-n-1}(iz)$ is a particular solution of this equation which vanishes for infinite z along the directions $\infty\exp(-\tfrac{3}{4}\pi i)$ and $\infty\exp(-\tfrac{1}{4}\pi i)$. Hence the solution

$$U_1(z) = A_\pm\, D_{-n-1}(\mp iz), \qquad \alpha \gtrless 0,$$

satisfies the first boundary condition (5A).

The constants $A_\pm$ are determined from the asymptotic values

$$D_{-n-1}(iR\,e^{-i\pi i}) \xrightarrow{R\to\infty} e^{\frac{\pi}{4}(n+1)i}\, e^{iR^2/4}\, R^{-n-1},$$

$$D_{-n-1}(iR\,e^{i\pi i}) \xrightarrow{R\to\infty} e^{-\frac{\pi}{4}(n+1)i}\, e^{-iR^2/4}\, R^{-n-1},$$

by means of the second boundary condition (5B). We find

$$|A_+| = |A_-| = \gamma^{\frac{1}{2}}\, e^{-\pi\gamma/4},$$

where

$$\gamma = f^2/|\alpha|.$$

---

* Those properties of this equation, and of its solutions, which are used in this analysis are fully discussed in Whitaker and Watson's "Modern Analysis," pp. 347-349, 4th ed.

Summarising,

$$e^{i\frac{\pi\alpha t}{h}} \underset{t \to \infty}{L} C_1(t) = \underset{z \to e^{1/4}\infty \exp(-i\frac{1}{4}\pi)}{L} U_1(z) = \begin{cases} \gamma^{\frac{1}{2}}e^{-\pi\gamma/4} \underset{R \to \infty}{L} D_{-n-1}(iRe^{\frac{1}{4}\pi i}), & \alpha > 0. \\ \gamma^{\frac{1}{2}}e^{-\pi\gamma/4} \underset{R \to \infty}{L} D_{n-1}(iRe^{\frac{1}{4}\pi i}), & \alpha < 0. \end{cases}$$

By use of the asymptotic values

$$\underset{R \to \infty}{L} D_{-n-1}(iRe^{\frac{1}{4}\pi i}) = e^{\frac{1}{4}\pi(n+1)i} e^{-iR^2/4} R^{-n-1} + \frac{\sqrt{2\pi}}{\Gamma(n+1)} e^{\frac{1}{4}\pi n i} e^{iR^2/4} R^n,$$

$$\underset{R \to \infty}{L} D_{n-1}(iRe^{\frac{1}{4}\pi i}) = e^{-\frac{1}{4}\pi(n+1)i} e^{iR^2/4} R^{-n-1} + \frac{\sqrt{2\pi}}{\Gamma(n+1)} e^{\frac{1}{4}\pi n i} e^{-iR^2/4} R^n$$

we obtain

$$|C_1(\infty)|^2 = \frac{2\pi\gamma e^{-\pi\gamma}}{\Gamma(i\gamma+1)\Gamma(-i\gamma+1)} = 2e^{-\pi\gamma}\sinh\pi\gamma$$

$$= 1 - e^{-2\pi\gamma}.$$

Therefore

$$P = e^{-2\pi\gamma}, \qquad \gamma = \frac{2\pi}{h}\epsilon_{12}^2 \Big/ \left| \frac{d}{dt}(\epsilon_1 - \epsilon_2) \right|$$

Rosenkewitsch* states that Landau has obtained the formula

$$P \sim e^{-\frac{\pi}{2hv}\frac{\Delta^2}{F_1 - F_2}}$$

where $\Delta = 2\epsilon_{12}$, v is the relative velocity, and F_1, F_2 are the "forces" acting upon the two states. If the identification $\frac{d}{dt}(\epsilon_1 - \epsilon_2) = v(F_1 - F_2)$ can be made, the exponent of Landau's formula is too small by a factor of 2π.

3. Discussion.

Equation (6), with ϵ_1, ϵ_2, ϵ_{12}, as arbitrary functions of time, is the general equation for a transition probability between two electronic states, provided (a) all other states may be neglected; (b) the motion of the atoms may be taken as external parameters; (c) changes in the "unperturbed" wave functions ϕ_1, ϕ_2 may be neglected. Two cases are of particular interest. In one $\epsilon_1 - \epsilon_2 = \Delta E$, a constant, and ϵ_{12} is a function having the general form of curve a, fig. 3. In the other $\epsilon_1 - \epsilon_2$ is a linear function, and ϵ_{12} is a constant.

* 'Phys. Z. U.S.S.R.,' vol. 1, p. 426 (1932).

An investigation[*] of the first case has revealed that the transition probability P satisfies the inequality

$$P \leqslant \left| \frac{\int_{-\infty}^{\infty} \varepsilon_{12}(t)\, e^{\frac{2\pi i}{h} \Delta E t}\, dt}{\int_{-\infty}^{\infty} \varepsilon_{12}(t)\, dt} \right|^2 .$$

A more instructive form is obtained by introducing the variable $\xi = t/\tau$, where τ is the time of collision defined by

$$\tau \varepsilon_{12}(0) = \int_{-\infty}^{0} \varepsilon_{12}(t)\, dt.$$

Then

$$P \leqslant \left| \frac{\int_{-\infty}^{\infty} \varepsilon_{12}(\xi)\, e^{2\pi i \frac{\tau \Delta E}{h} \xi}\, d\xi}{\int_{-\infty}^{\infty} \varepsilon_{12}(\xi)\, d\xi} \right|^2 \tag{7}$$

When $\tau \Delta E/h > 1$, P is much smaller when ε_{12} is an analytic function than of the type of curve b, fig. 2. The question arises, would this difference in the two P's be eliminated merely by rounding off the corners of curve b, or must all
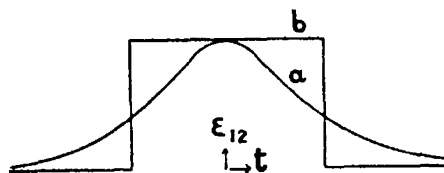
Fig. 3.—ε_{12} when ε_1 ε_2 a constant

derivatives of ε_{12} be continuous ? We find the answer when we integrate the numerator of (7) by parts. Since ε_{12} vanishes at $\xi = \pm \infty$, an expansion of P in inverse powers of $(2\pi\tau\Delta E/h)$ is seen to start with the $-2n'$th power, where n is the order of the first discontinuous derivative of ε_{12} [†]

The second case has been solved in the preceding section The problem is illustrated in fig. 2.

It was found that the transition probability P was

$$P = e^{-\frac{\pi^2}{h} \Delta^2 / \left| \frac{d}{dt}(\varepsilon_1 - \varepsilon_2) \right|}$$

[*] N. Rosen and C. Zener, 'Phys Rev.,' vol 40, p 502 (1932)
[†] The author is indebted to Professor Norbert Wiener for pointing out this relation.

where $\Delta = 2\varepsilon_{12}(0) = $ closest distance between the adiabatic eigenwerte E_1, E_2 of the system.

In both cases P depends upon the relative velocity v in nearly the same manner, namely

$$P \sim e^{-r_0/r}.$$

In collisions one measures an effective cross section Q. Let the transitional region occur about the interatomic distance R_0, then since v refers to the component of the relative velocity along the internuclear line, Q will be given by approximately

$$Q = \pi R_0^2 \int_0^{\pi/2} e^{-v_0/v \cos \theta} \sin \theta \, d\theta$$

$$= \pi R_0^2 \left\{ e^{-v_0/r} + \frac{v_0}{v} \, Ei \, (-v_0/v) \right\}.$$

Summary.

When a single parameter is varied adiabatically, two eigenwerte of a system may approach each other, and then recede, the corresponding eigenfunctions having exchanged their characters. If the parameter is varied with a finite velocity, the system may jump from one state to the other, thus not suffering a change of character. This transition probability has been rigorously calculated provided the system satisfies certain reasonable restrictions.

Energy Exchange between Inert Gas Atoms and a Solid Surface.

By J. M. JACKSON, Department of Mathematics, University of Manchester, and N. F. MOTT, M.A., Gonville and Caius College, Cambridge.

§ 1. *Introduction.*—If gas atoms, having energy corresponding to a temperature T_2, are incident on a solid surface at a temperature T_1, then the reflected atoms will have a mean energy corresponding to some new temperature T_2', which is a function of T_1 and T_2. For simplicity it is convenient to define Knudsen's thermal accommodation coefficient as

$$\alpha = \lim_{T_1 \to T_2 \to T} \frac{T'_2 - T_2}{T_1 - T_2}.$$

The accommodation coefficient depends on the nature of the gas atom, the nature of the solid surface, and the temperature T

Accommodation coefficients have been measured by various workers, and the present paper is an attempt to give a theoretical explanation of the results of Roberts,* who has measured the accommodation coefficient for helium on tungsten at various temperatures, taking particular precautions to obtain a clean surface.

The first step in the calculation of the accommodation coefficient is the calculation of the probability that when a gas atom with energy W hits an atom of the solid in the quantum state i, a transition will take place to the state n. We denote this probability by $p_i{}^n$ (W). One must then assume some energy distribution for the vibrating solid atoms. We assume that they are all independent, so that the number in the state with energy W_n is proportional to exp. $(- W_n/KT)$, as in the Einstein specific heat theory. The accommodation coefficient is then found by averaging $p_i{}^n$ for all W and all i, n.

A theory of the accommodation coefficient has already been given by one of us,† the interaction energy between the solid and the gas being taken to be of the form $V = C$ for $r > 0$, $V = 0$ for $r < 0$, where r denotes the distance between the two atoms. With a suitable choice of C it was possible to obtain a fairly good fit with the experimental curve. This type of field has, however, little resemblance to the actual field between the gas atom and the solid surface.

* 'Proc. Roy. Soc.,' A, vol. 129, p. 146 (1930), vol. 135, p 192 (1932).

† J. M. Jackson, 'Proc. Camb. Phil. Soc.,' vol 28, p. 136 (1932).

The method of calculating the accommodation coefficient given in this paper will be followed, except that we shall take the interaction energy between the gas atom and the solid atom to be of the form

$$C \exp. (-ar).$$

Zener* has calculated the accommodation coefficient using a field of this type, but in calculating the transition probabilities he approximates to the exponential by means of an inverse square term $A (r - b)^{-2}$ adjusted to fit on smoothly to the exponential at the classical distance of closest approach. This approximation appears to affect the answer by a factor of about 6. Good agreement with experiment was only obtained by giving a the somewhat large value 65×10^8 cm $^{-1}$

In the present paper we have been able to evaluate the integrals involved in the transition probabilities exactly without making any approximations. Quite a simple formula is obtained, and good agreement with experiment, with a more reasonable value of a (8×10^8 cm $^{-1}$) We also discuss the validity of the perturbation method used, and come to the conclusion that this is almost the only collision problem in which the terms neglected in a first order perturbation theory are certainly small

§ 2. *The Probabilities of Energy Transfer* —In this section we shall treat the solid surface as consisting of an assembly of independent atoms each free to vibrate about a position of equilibrium with the same frequency v The problem is to calculate the probability that, when a gas atom of given energy collides with an atom of the solid vibrating in the nth stationary state, the solid atom will make a transition to the n'th state. The model used is one dimensional, both atoms being supposed to move only at right angles to the surface of the solid.

Let X denote the displacement at any time of the solid atom from its mean position. The Schrodinger equation for the unperturbed solid atom is then

$$(H - W_n) \psi_n (X) = 0, \tag{1}$$

where H denotes

$$-\frac{h^2}{8\pi^2 M} \frac{d^2}{dX^2} + 2\pi^2 M v^2 X^2,$$

M being the mass of the solid atom. Equation (1) has the usual series of oscillator eigenfunctions $\psi_n (X)$ and eigenvalues $W_n = (n + \frac{1}{2}) hv$. We assume that the oscillator wave functions $\psi_n (X)$ are normalised to unity.

* 'Phys. Rev.,' vol. 37, p. 557 (1931) ; vol. 40, pp. 178, 335 (1932).

Let us denote by ψ_i the wave function of the initial state and ψ_n the wave function of the final state of the solid atom. Let m denote the mass of the gas atom and x its distance from the mean position of the solid atom.

We take for the interaction energy $V(x, X)$ between the two atoms

$$V(x, X) = C \exp\left[-a(x - X)\right]. \tag{2}$$

Let $\Psi(x, X)$ be the wave function which describes the collision and satisfies the wave equation

$$\left[-H + \frac{h^2}{8\pi^2 m} \frac{d^2}{dx^2} + \frac{8\pi^2 m}{h^2}(W - Ce^{-a(x-X)})\right]\Psi = 0. \tag{3}$$

We require a solution with the following property; if it is expanded in a series

$$\Psi(x, X) = \sum_n \psi_n(X) f_n(x) \tag{4}$$

then for large x we must have

$$f_i(x) \sim \exp(-ik_i x) + A_i \exp(ik_i x)$$
$$f_n(x) \sim \qquad\qquad A_n \exp(ik_n x) \qquad n \neq i. \tag{5}$$

Here

$$k_i = 2\pi m v_i/h, \qquad k_n = 2\pi m v_n/h,$$

v_i being the velocity of the gas atom before collision, and v_n its velocity after it has excited the solid atom to the state n.

The solution (5) represents a wave of unit amplitude falling on the solid atom together with a number of reflected waves. The probability per collision that the transition $i \rightarrow n$ will take place is

$$p_i{}^n = \frac{k_n}{k_i} |A_n|^2. \tag{6}$$

The method appropriate to the solution of equation (3) depends on the value of the constant a in the expression (2) for the interaction energy. If a^{-1} is small compared with the amplitude of oscillations of the solid atom, the atoms may be treated as rigid elastic spheres. In § 3 a method of solution suited to this case is given. If a^{-1} is large compared with this amplitude, the method employed by Zener is appropriate. This is discussed in § 4.

From the two formulæ one can obtain transition probabilities for all values of a by interpolation. We may remark here that if a^{-1} is large compared to the wave-length of the incident atoms, the collision is adiabatic and no energy transfer takes place.

§ 3. *Rigid Elastic Spheres as a Model for the Atoms.*—In this section the atoms are treated as rigid elastic spheres; that is to say, we write the interaction energy in the form

$$V(x, X) = C' e^{-a(x-X-\xi)} \tag{7}$$

and let $a \to \infty$. ξ may be interpreted as the sum of the radii of the spheres. Then

$$V(x, X) = 0 \qquad x - X > \xi$$
$$= \infty \qquad x - X < \xi$$

We have therefore to find a solution of

$$\left[-H + \frac{h^2}{8\pi^2 m} \frac{d^2}{dx^2} + W \right] \Psi(x, X) = 0,$$

which vanishes along the line $x - X = \xi$. Such a solution, having the asymptotic form required in (4) and (5), is

$$\Psi(x, X) = \psi_i(X) 2i \sin k_i(x - \xi) + \sum_n A_n \psi_n(X) \exp[ik_n x],$$

the A_n being chosen in such a way that

$$\psi_i(X) 2i \sin k_i X + \sum_n A_n \psi_n(X) \exp[ik_n(X + \xi)] = 0 \tag{8}$$

for all values of X.

Now the wave-length of the incident helium atoms is large compared with the amplitude through which the solid atoms vibrate; hence $\psi_n(X)$ is only finite in a region in which $k_i X$, $k_n X$, etc., are small. We may therefore replace $\exp ik_n X$ in (8) by unity. We obtain

$$\psi_i(X) 2ik_i X + \sum_n A_n \psi_n(X) \exp[ik_n \xi] = 0$$

for all X.

Hence multiplying by $\psi_n(X)$ and integrating over all X, we obtain

$$A_n = -2ik_i X_{in} \exp(-ik_n \xi),$$

where

$$X_{in} = \int_{-\infty}^{\infty} X \psi_i \psi_n \, dX. \tag{9}$$

Hence from (6) the probability that the transition will take place is

$$p_i^n = 4k_i k_n |X_{in}|^2. \tag{10}$$

§ 4. In this section we suppose that a^{-1} is large compared with the amplitude of vibrations of the solid atom. (This is in fact the case, since for tungsten at ordinary temperatures this amplitude is of order 2×10^{-10} cm.) The method

is that used by Zener. It is similar to the Born method in collision problems, differing from it in that distorted zero order wave functions must be used.

We substitute the solution (4) in equation (3) and obtain

$$\sum_n \left[\frac{d^2}{dx^2} + k_n^2 - \frac{8\pi^2 mC}{h^2} e^{-a(x-X)} \right] f_n(x)\, \psi_n(X) = 0. \tag{11}$$

We now write

$$V_{ns}(x) = \frac{8\pi^2 mC}{h^2} \int_{-\infty}^{\infty} e^{-a(x-X)}\, \psi_n(X)\, \psi_s(X)\, dX,$$

which is equal to

$$U(x)\, Y_{ns},$$

where

$$U(x) = 8\pi^2 mC e^{-ax}/h^2, \tag{11.1}$$

$$Y_{ns} = \int e^{aX} \psi_n(X)\, \psi_s(X)\, dX. \tag{11.2}$$

Expanding e^{aX}, and remembering that aX is small in the region[*] (denoted by τ) where ψ_n is finite, we have to a very good approximation

$$Y_{nn} = 1.$$

We thus have approximately

$$V_{nn}(x) = U(x). \tag{12}$$

Further, we see that

$$Y_{n,\, n\pm 1} \text{ is of order } a\tau,$$

$$Y_{n,\, n\pm 2} \text{ is of order } (a\tau)^2.$$

From equation (11), multiplying by $\psi_s(X)$ and integrating with respect to X from $-\infty$ to $+\infty$,

$$\left(\frac{d^2}{dx^2} + k_s^2 \right) f_s(x) + \sum_n V_{sn}(x) f_n(x) = 0. \tag{13}$$

This equation is exact.

We have just seen that the non diagonal terms V_{ns} are small compared with the diagonal terms V_{nn}. We may therefore solve (13) by the method of successive approximations. We set for the waves representing the incident and elastically reflected particles

$$f_i(x) = f_i^{(0)} + f_i^{(1)} + \cdots, \tag{14.1}$$

and for the particles reflected after causing a transition

$$f_n(x) = f_n^{(1)} + \cdots \tag{14.2}$$

[*] τ is equal to about 10^{-10} cm.

Substituting in (13) we obtain

$$\left[\frac{d^2}{dx^2} + k_i{}^2 - V_{ii}\right] f_i{}^{(0)} = 0, \tag{15}$$

$$\left[\frac{d^2}{d^2} + k_n{}^2 - V_{nn}\right] f_n{}^{(1)} = Y_{in} U(x) f_i{}^{(0)}(x), \qquad n \neq i. \tag{16}$$

We note that $V_{ii} = V_{nn} = U(x)$.

Let now $F_n(x)$ denote that solution of the equation

$$\left[\frac{d^2}{dx^2} + k_n{}^2 - U(x)\right] F_n(x) = 0, \tag{17}$$

which tends to zero as $x \to -\infty$, and is normalised so as to have the asymptotic form

$$F_n \sim \cos(k_n x + \eta) \qquad x \to +\infty, \tag{18}$$

where η is a constant. Then we must take

$$f_i{}^{(0)} = 2F_i(x), \tag{18.1}$$

representing an incident and reflected wave each of unit amplitude, as demanded by (5).

We may solve (16) by the substitution

$$f_n{}^{(1)}(x) = y F_n(x).$$

This gives

$$\frac{d}{dx}\left(F_n{}^2 \frac{dy}{dx}\right) = 2Y_{in} U(x) F_n F_i.$$

Integrating, and remembering that f_n must vanish as $x \to -\infty$ we have

$$F_n{}^2 \frac{dy}{dx} = 2Y_{in} \int_{-\infty}^{x} U(x) F_n F_i \, dx.$$

Integrating this equation, we have, for large values of x,

$$y \sim \left[\frac{1}{k_n}\tan(k_n x + \eta) + \text{const}\right] 2Y_{in} \int_{-\infty}^{\infty} U(x) F_n F_i \, dx.$$

Choosing the constant so that f_n shall have the asymptotic form (5), we find

$$f_n{}^{(1)} \sim \exp\left[-i(k_n x + \eta)\right] \frac{2Y_{in}}{k_n} \int_{-\infty}^{+\infty} U(x) F_n F_i \, dx.$$

Hence we have (cf. equation (5))

$$|A_n| = \frac{2Y_{in}}{k_n} \int_{-\infty}^{\infty} U(x) F_n F_i \, dx,$$

and from (6) the probability per collision that the solid atom of energy W will make a transition from the state i to the state n is

$$p_i{}^n = \frac{4\,(Y_{in})^2}{k_i k_n}\left[\frac{8\pi^2 mC}{h^2}\int_{-\infty}^{\infty} e^{-ax}\,F_i F_n\,dx\right]^2. \tag{19}$$

Zener obtains the result (19) without the factor 4. This is due to the omission of a factor 2 in the equation corresponding to (18.1).

§ 5. We now require the exact solutions of (17) which tend to zero as $x \to -\infty$, and which have the asymptotic form (18) as $x \to \infty$. Writing

$$U(x) = B^2 e^{\,ax},$$

we can transform (17) by means of the substitution

we obtain
$$y = 2B/a\,.\,\exp\left(-\tfrac{1}{2}ax\right);$$

$$F''_n + y^{-1}F'_n + (q_n{}^2 y^{-2} - 1)F_n = 0,$$

where the dashes denote differentiation with respect to y, and

$$q_n = 2k_n/a.$$

This is Bessel's equation of imaginary order iq_n and imaginary argument iy. In the usual notation of Bessel functions* the solution of this equation which tends to zero as x tends to $-\infty$ is

$$K_{iq}(y), \qquad q = q_n.$$

This function can be represented by the integral*

$$K_{iq}(y) = \int_0^\infty e^{-y\cosh u}\cos q_n u\,du. \tag{20}$$

It is clear from (20) that as $x \to -\infty$ and $y \to +\infty$, $K_{iq}(y) \to 0$. In order to show that it behaves like $\cos(kx + \eta)$ as $x \to +\infty$, $y \to 0$, we proceed as follows. Making the substitution $q\cosh u = z$, and assuming that y is small, the integral (20) becomes

$$\int_0^\infty e^{-z}\,\tfrac{1}{2}\left[\left(\frac{2z}{y}\right)^{iq} + \left(\frac{2z}{y}\right)^{-iq}\right]\frac{dz}{z},$$

which reduces to

$$\left(\frac{\pi}{q\sinh \pi q}\right)^{\tfrac{1}{2}}\cos(kx + \eta).$$

Thus for $F_n(x)$ we must take

$$F_n(x) = \left(\frac{q\sinh \pi q}{\pi}\right)^{\tfrac{1}{2}} K_{iq}(x). \tag{21}$$

* G. N. Watson, " Bessel Functions," pp. 73, 181.

§ 6. *Calculation of the Transition Probabilities.*—In §§ 3 and 4, equations (10) and (19), we have obtained expressions for the transition probabilities per collisions for gas atoms incident on the solid with definite energy. It is readily found that*

$$Y_{n,\,n\pm1} = a \left(\frac{n + \frac{1}{2} \pm \frac{1}{2}}{8\pi^2 Mh\nu/h^2}\right)^{\frac{1}{2}} \tag{22}$$

$$Y_{n,\,n\pm2} = a^2 \frac{[(n+1\pm1)(n\pm1)]^{\frac{1}{2}}}{16\pi^2 Mh\nu/h^2}. \tag{23}$$

We have further

$$X_{in} = 0 \qquad i \neq n \pm 1$$

$$= Y_{in}/a \qquad i = n \pm 1.$$

From (10) we have, therefore, for elastic spheres,

$$p_n^{n\,\pm\,1} = 4\,\frac{m}{M}\,(n + \tfrac{1}{2} \pm \tfrac{1}{2})\,[E\,(E \mp 1)]^{\frac{1}{2}} \tag{24}$$

where

$$E = W/h\nu.$$

The evaluation of (19) depends on the integral

$$\int_{-\infty}^{\infty} e^{-ax}\,F_i F_n\,dx.$$

Changing the variable of integration to y as before we find for this integral

$$\frac{ah^2}{16\pi^2 mC}\,\frac{(qq'\,\sinh\pi q'\,\sinh\pi q)^{\frac{1}{2}}}{\pi}\int_0^{\infty} K_{iq}K_{iq'}\,y\,dy,$$

here q is written for q_i, q' for q_n.

Using (20) we can write the integral on the right as a repeated integral, namely

$$\int_0^{\infty}\int_0^{\infty}\int_0^{\infty} ye^{-y(\cosh t\,+\,\cosh u)}\cos qu\,\cos q't\,du\,dt\,dy.$$

Putting the lower limit of the y integration equal to y_0, and interchanging the order of integration so that the y integration is performed first, afterwards allowing y_0 to tend to zero, we find that this integral reduces to

$$\tfrac{1}{2}\int_{-\infty}^{\infty}\int_{-\infty}^{\infty}\frac{\cos q't\,\cos qt}{(\cosh t + \cosh u)^2}\,du\,dt.$$

* Sommerfeld, 'Wellenmekanik,' p. 61.

Making the substitution* $t + u = 2\mathrm{T}$, $t - u = 2\mathrm{U}$, we find that this integral becomes

$$\tfrac{1}{2} \int_0^\infty \frac{\cos{(q + q')}\,\mathrm{T}}{\cosh^2 \mathrm{T}}\, d\mathrm{T} \int_0^\infty \frac{\cos{(q' - q)}}{\cosh^2 \mathrm{U}}\, d\mathrm{U}.$$

By integrating $e^{ipz}/\cosh^2 z$ round the closed rectangular contour $-\infty$, $+\infty$, $+\infty + \pi i$, $-\infty + \pi i$, enclosing the point $z = \tfrac{1}{2} i \pi$, we find that

$$\int_0^\infty \frac{\cos px}{\cosh^2 x}\, dx = \tfrac{1}{2} \pi p / \sinh \tfrac{1}{2} \pi p.$$

Therefore we have

$$\int_0^\infty y\, dy\, \mathrm{K}_{iq} \mathrm{K}_{iq'} = \tfrac{1}{4} \pi^2 (q'^2 - q^2) \,/\, (\cosh \pi q' - \cosh \pi q).$$

The transition probability $p_i{}^n$ is therefore

$$p_i{}^n = \frac{a^2}{\pi^3} \frac{\mathrm{Y}_{in}{}^2}{\mathrm{K}_i \mathrm{K}_n}\, qq' \left[\frac{\tfrac{1}{4} \pi^2 (q'^2 - q^2)}{\cosh \pi q' - \cosh \pi q} \right]^2 \sinh \pi q \sinh \pi q'. \tag{25}$$

In particular

$$p_n{}^{n \pm 1} = \frac{32 \pi^4}{h^2} \frac{m}{\mathrm{M}} \frac{mh\nu}{a^2} \left(n + \tfrac{1}{2} \pm \tfrac{1}{2} \right) \frac{\sinh q \sinh q'}{(\cosh \pi q - \cosh \pi q')^2} \tag{25.1}$$

and

$$p_n{}^{n \pm 2} = 4 \pi^2 \left(\frac{m}{\mathrm{M}} \right)^2 (n + 1 \pm 1)(n \pm 1) \frac{\sinh \pi q' \sinh \pi q,}{(\cosh \pi q - \cosh \pi q')^2} \tag{25.2}$$

etc.

Here q, q' are $4\pi mv/ah$, $4\pi mv'/ah$ where v, v' are the velocities of the gas atom before and after the collision.

It is interesting to note that if we allow a to become very large in equation (25.1), the formula (25.1) tends to the form (24) obtained for hard spheres. Thus, although there is no theoretical justification for using this perturbation method for large a (as the non-diagonal elements are not small), the result obtained seems to be valid for all a.

§ 7. *Calculation of the Thermal Accommodation Coefficient.*—The thermal accommodation coefficient α is defined at the beginning of § 1. Using this definition it has been shown by one of us† that α can be expressed as a double series of partial accommodation coefficients $\alpha(n|n')$, one for each particular quantum transition $n \to n'$; it was found that

$$\alpha = \sum_{n=0}^\infty \sum_{n'=0}^\infty \alpha(n|n'), \tag{26}$$

---

* G. N. Watson, *loc. cit.*, p. 440.

† Jackson, *loc. cit.*

where

$$\alpha\,(n\,|\,n') = \tfrac{2}{7}\,\mu^3\,(1 - e^{-\mu})\,(n - n')^2\,e^{-n\mu}\,P_n^{\,n'}\,(\mu). \qquad (27)$$

In this expression $\mu = \Theta/T$ where Θ is the characteristic temperature of the solid, and

$$P_n^{\,n'}\,(\mu) = \int_0^\infty p_n^{\,n'}\,(E)\,e^{-\mu E}\,dE. \qquad (28)$$

Expressions for $p_n^{\,n'}$ have been given in the previous section (equations (25)). To calculate the accommodation coefficient we must therefore evaluate the integral (28).

We write

$$\alpha = \alpha\,(1) + \alpha\,(2) + \dots \qquad (29)$$

where $\alpha(s)$ is a partial accommodation coefficient corresponding to change of quantum number by s.

We obtain, summing over all n, n' which differ by unity and by two

$$\alpha\,(1) = \tfrac{2}{1}\,\mu^3\,(e^{-\mu} - 1)^{-1}\,P\,(1,\,\mu) \qquad (30)$$

$$\alpha\,(2) = \tfrac{1}{14}\,\mu^3\,(e^{\mu} - 1)^{-2}\,P\,(2,\,\mu), \qquad (31)$$

where $P\,(1,\,\mu)$, $P\,(2,\,\mu)$ are to be obtained from (28), for the cases $n' = n \pm 1$, $n' = n \pm 2$, by omitting the factor $(n + \tfrac{1}{2} \pm \tfrac{1}{2})$ from (25.1) and (24), and the factor $(n \pm 1)\,(n + \pm 1)$ from (25.2).

Further terms of the series (26) have not been investigated, as in the case of helium on tungsten $\alpha(2)$ is never more than 5 per cent. of $\alpha(1)$. The convergence seems sufficiently good to justify the neglect of further terms of the series.

Only in the case of rigid elastic spheres [§ 3 and § 6, equation (24)] is it possible to evaluate the integral (28) analytically. In this case, we have from (24)

$$P\,(1,\,\mu) = 4\,\frac{m}{M}\int_0^\infty [E\,(E + 1)]^{\frac{1}{2}}\,e^{-\mu E}\,dE.$$

Changing the variable of integration to u, where $u = 2E + 1$, this integral reduces to

$$\tfrac{1}{2}\,\frac{m}{M}\,[K_2\,(\tfrac{1}{2}\mu) - K_0\,(\tfrac{1}{2}\mu)]\,e^{\frac{1}{2}\mu},$$

where K_2 and K_0 are Bessel functions of the third kind. We find from (29) and (30)

$$\alpha = \alpha\,(1) = \tfrac{1}{6}\mu^3\,\frac{m}{M}\,\mathrm{cosech}\,\tfrac{1}{2}\mu\,\{K_2\,(\tfrac{1}{2}\mu) - K_0\,(\tfrac{1}{2}\mu)\}. \qquad (32)$$

This is the result for a molecular model of rigid elastic spheres. With such a model the nature of the gas only enters into the result in the mass-ratio factor m/M and thus the accommodation coefficients of various monatomic gases at the same temperature on a clean tungsten surface would be proportional to their atomic weights.

With the exponential interaction energy Ce^{-ar}, the transition probabilities per collision are given by (25).

We obtain, from (25) and (30)

$$\alpha\,(1) = \tfrac{2}{3}\,\mu^3\,(e^\mu - 1)^{-1}\,\frac{32\pi^4}{h^2}\,\frac{M}{m}\,\frac{mh\nu}{a^2}\int_0^\infty \frac{\sinh\frac{\gamma}{a}\,(E+1)^{\frac12}\sinh\frac{\gamma}{a}\,E^{\frac12}\,.\,e^{-\mu E}\,dE}{\left[\cosh\frac{\gamma}{a}\,(E+1)^{\frac12} - \cosh\frac{\gamma}{a}\,E^{\frac12}\right]^2}$$

and

$$\alpha\,(2) = \tfrac{1}{3}\,\mu^3\,(e^\mu - 1)^{-2}\,.\,4\pi^2\left(\frac{m}{M}\right)^2\int_0^\infty \frac{\sinh\frac{\gamma}{a}\,(E+2)^{\frac12}\sinh\frac{\gamma}{a}\,E^{\frac12}\,.\,e^{-\mu E}\,dE}{\left[\cosh\frac{\gamma}{a}\,(E+2)^{\frac12} - \cosh\frac{\gamma}{a}\,E^{\frac12}\right]^2}$$

where $\gamma^2 = 32\pi^4\,mh\nu/h^2$.

The integrals were evaluated numerically for various values of μ, a. The results are given in § 8.

§ 8. *Modification of the Theory when an Attractive Potential is included in the Field of the Solid.*—In order to take some account of the possibility of adsorption it is interesting to include in some way the long range attractive field of the solid (van der Waals forces). The simplest method of doing this is to include a small attractive potential step of magnitude Φ situated at a constant distance d from the mean position of the oscillating surface atom. For d we have taken about 5 A.U.

With this very approximate representation of the attractive field of the solid, the only modifications[*] which must be made in the analysis of the preceding section are that instead of $P\,(1)$ one must write

$$P\,(1,\chi) = \int_\chi^\infty p\,(1)\,e^{-\mu E}\,dE, \qquad \chi = \Phi/h\nu.$$

(1) and (2) must also be multiplied by the factor $\exp \Phi/kT$.

The expressions for $\alpha\,(1)$ and $\alpha\,(2)$ now become

$$\tfrac{2}{3}\,\mu^3\,(e^\mu - 1)^{-1}\,e^{\mu\chi}\,P\,(1,\chi)$$

$$\tfrac{1}{3}\,\mu^3\,(e^\mu - 1)^{-2}\,e^{\mu\chi}\,P\,(2,\chi).$$

[*] Jackson, *loc. cit.*, p. 156.

The factor $e^{\mu\chi}$ increases as the temperature decreases, but the integral P (1, χ) decreases with the temperature more rapidly than P (1). The effect of the factor $e^{\mu\chi}$ is predominant, but the alterations in the integrals P are not negligible and are more marked for low temperatures.

§ 9. *Numerical Results.*—The experiments of Roberts (*loc. cit.*) provide the only available data with which the theory may be compared. The experimental results for tungsten and helium are

$$295° \text{ K}, \alpha = 0·057 \text{ ; } 195° \text{ K}, \alpha = 0·046 \text{ ; } 79° \text{ K}, \alpha = 0·025.$$

Calculations have been made for values of a equal to $4·02$, $8·05$, $9·00 \times 10^8$ cm.$^{-1}$, and also for the hard sphere model. The value of the characteristic temperature Θ of tungsten is 205° K, if we take the atomic frequency to be $4·3 . 10^{12}$. sec.$^{-1}$. This frequency is determined from Lindemann's melting point formula, which gives good agreement with the values of Θ determined from specific heat data, particularly in the case of metals. The accommodation coefficient was computed for the above values of a, and for the following values of μ

$$\mu = 0·7, \ 1·0, \ 1·4, \ 2·0, \ 3·0$$

or

$$T = 293°, \ 205°, \ 147°, \ 102·5°, \ 68·4°.$$

For the attractive potential step we have taken $\chi = 0·20$, $0·25$, and also zero. The two former values correspond to $\Phi = 3·54$ and $4·43 . 10^{-3}$ electron volts, or heats of adsorption[*] of helium on tungsten of the order of 80–100 cals./gm. atom. These are probably of the correct order of magnitude.

The variation of the accommodation coefficient with temperature for various values of a and Φ is shown in fig. 1. In fig. 2 the results are shown multiplied by an arbitrary factor to fit them to the experimental curve at T = 205° K. We do this for two reasons : firstly it is possible that the use of a one dimensional model may have introduced a constant factor in our results ; and secondly the experimental values are probably too large, owing to the roughness of the solid surface. The best agreement is obtained with $a = 9 \times 10^8$ cm.$^{-1}$, which is rather large.

The value $a = 4 \times 10^8$ cm.$^{-1}$ is probably approximately correct. The theoretical curve for this value is shown in fig. 1. With this value of a one

---

[*] Lennard-Jones, ' Trans. Faraday Soc.,' vol. 28, p. 340 (1932).

has to multiply the theoretical curve by 2 in order to fit it to the experimental curve. This factor 2 may well be accounted for by the roughness of the surface. The agreement, fig. 2, between the fitted curve and the experimental is not quite so good as for $a = 9 \times 10^8$ cm.$^{-1}$, but is nevertheless satisfactory
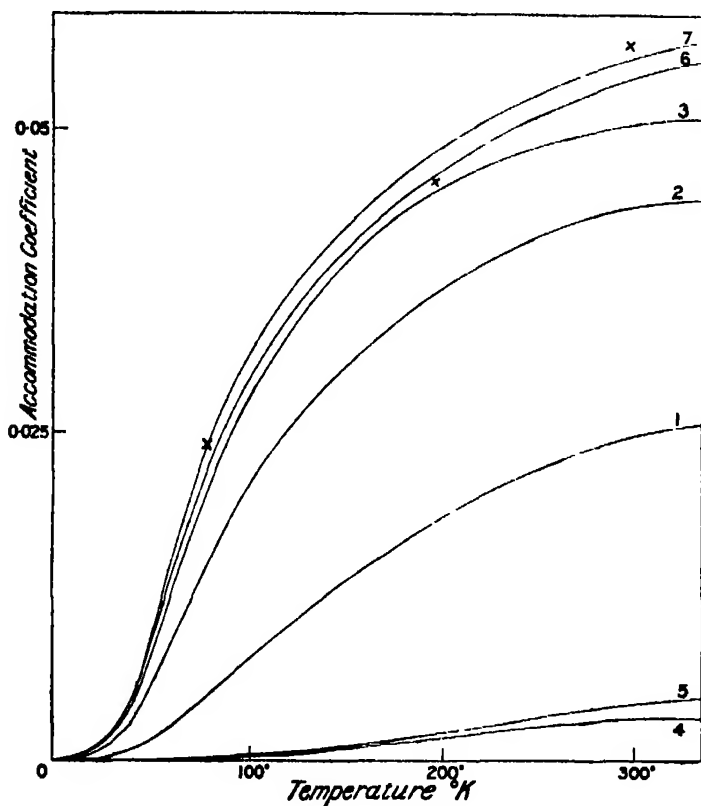
FIG. 1.—Calculated values of the thermal accommodation coefficient for tungsten/helium, with interaction energy e^{-ar}.

Curve 1, $a = 4 \cdot 02 \times 10^8$ cm.$^{-1}$ ⎫
Curve 2, $a = 9 \cdot 0 \times 10^8$ cm.$^{-1}$ ⎬ One quantum transitions only.
Curve 3, rigid elastic sphere model ⎭
Curve 4, $a = 9 \cdot 0 \times 10^8$ cm.$^{-1}$, two quantum transitions only.
Curve 5, $a = 9 \cdot 0 \times 10^8$ cm.$^{-1}$, two quantum transitions only, but including an attractive potential step $\chi = 0 \cdot 2$. [$\Phi = 3 \cdot 54 \cdot 10^{-3}$ electron volts.]
Curve 6, $a = 9 \cdot 0 \times 10^8$ cm.$^{-1}$, $\chi = 0 \cdot 2$ including both one- and two-quantum transitions.
Curve 7, $a = 9 \cdot 0 \times 10^8$ cm.$^{-1}$, $\chi = 0 \cdot 25$ including both one- and two-quantum transitions.
The experimental values are marked with a cross.
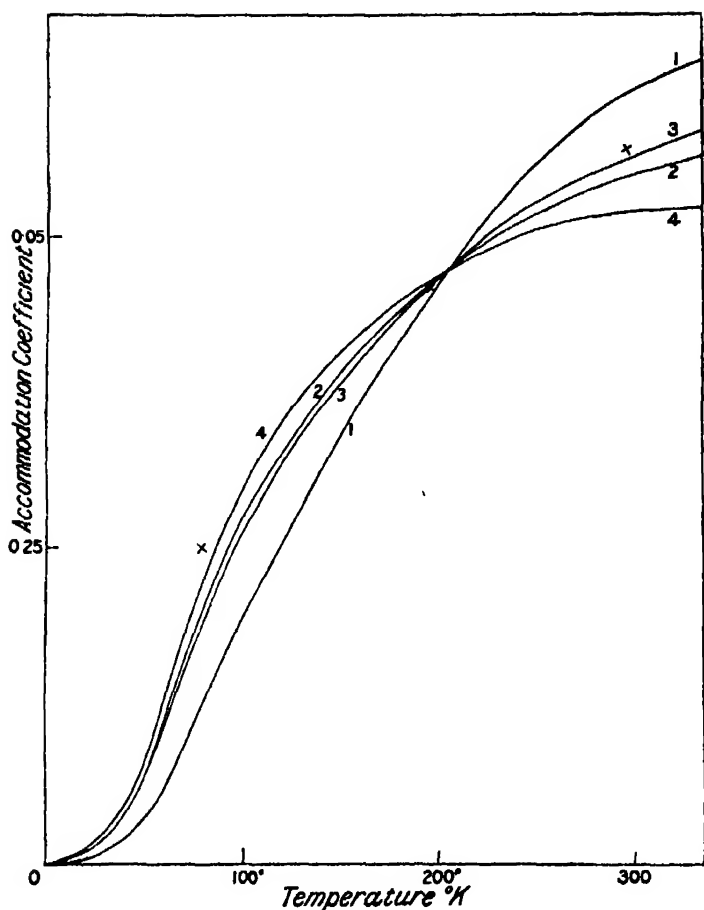
Fig. 2.—Thermal accommodation coefficients : helium/tungsten fitted to the experimental value at 205° K.

Curve 1, $a = 4 \cdot 02 \times 10^8$ cm.$^{-1}$, one quantum transitions only.
Curve 2, $a = 9 \cdot 00 \times 10^8$ cm.$^{-1}$, one quantum transitions only.
Curve 3, $a = 9 \cdot 00 \times 10^8$ cm.$^{-1}$, including two quantum transitions.
Curve 4, rigid elastic sphere model.

The experimental values are marked with a cross.

in view of the difficult nature of the experiments, and the simple model used in the theory.

In fig. 3 some transition probabilities are drawn plotted against $E = W/h\nu$, where W is the translational energy of a gas atom normal to the surface. They are also plotted against T, where $W = \frac{1}{2}KT$.
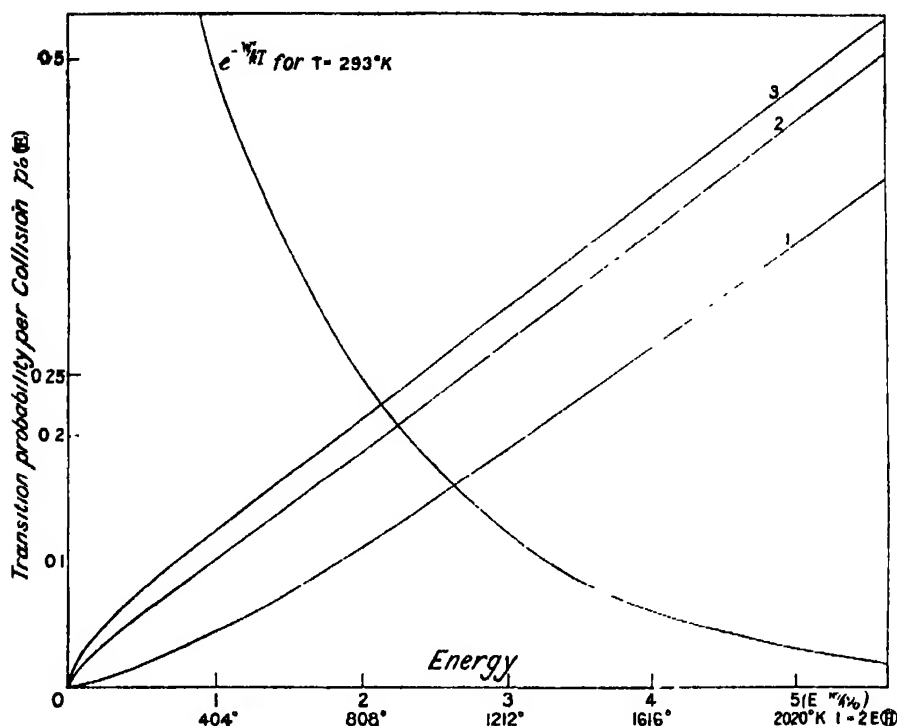
Fig. 3.—Transition probabilities p_0' (E) per collision. The energy scale is in terms of oscillator quanta, $E = W/h\nu$; alternatively it is expressed in terms of the temperature $T = \frac{1}{2}W/K$.

Curve 1, $a = 4\cdot02 \times 10^8$ cm.$^{-1}$.

Curve 2, $a = 9\cdot00 \times 10^8$ cm $^{-1}$.

Curve 3, rigid elastic sphere model.

The curve $e^{-W/kT}$ is drawn on the same scale for $T = 293°$ K.

Summary.

A theory of the accommodation coefficient for helium on tungsten is given, using an exponential field between the gas atom and a surface atom of the solid. Good agreement is obtained with the experimental results of Roberts.

In conclusion, we would like to thank Mr. J. K. Roberts for his interest in this work.

INDEX to VOL. CXXXVII. (A.)

END OF THE ONE HUNDRED AND THIRTY-SEVENTH VOLUME (SERIES A).